

# ***Thermophysical properties database of materials for light water reactors and heavy water reactors***

*Final report of a coordinated research project  
1999–2005*



**IAEA**

International Atomic Energy Agency

June 2006

# ***Thermophysical properties database of materials for light water reactors and heavy water reactors***

*Final report of a coordinated research project  
1999–2005*



**IAEA**

International Atomic Energy Agency

June 2006

The originating Section of this publication in the IAEA was:

Nuclear Power Technology Development Section  
International Atomic Energy Agency  
Wagramer Strasse 5  
P.O. Box 100  
A-1400 Vienna, Austria

THERMOPHYSICAL PROPERTIES DATABASE OF MATERIALS FOR LIGHT WATER  
REACTORS AND HEAVY WATER REACTORS

IAEA, VIENNA, 2006  
IAEA-TECDOC-1496  
ISBN 92-0-104706-1  
ISSN 1011-4289

© IAEA, 2006

Printed by the IAEA in Austria  
June 2006

## FOREWORD

The IAEA Coordinated Research Project (CRP) on the Establishment of a Thermo-physical Properties Database for Light Water Reactors (LWRs) and Heavy Water Reactors (HWRs) started in 1999. It was included in the IAEA's Nuclear Power Programme following endorsement in 1997 by the IAEA's Technical Working Groups on Advanced Technologies for LWRs and HWRs (the TWG-LWR and the TWG-HWR). Furthermore, the TWG on Fuel Performance and Technology (TWG-FPT) also expressed its support. This CRP was conducted as a joint task within the IAEA's project on technology development for LWRs and HWRs in its nuclear power programme.

Improving the technology for nuclear reactors through better computer codes and more accurate materials property data can contribute to improved economics of future plants by helping to remove the need for large design margins, which are currently used to account for limitations of data and methods. Accurate representations of thermo-physical properties under relevant temperature and neutron fluence conditions are necessary for evaluating reactor performance under normal operation and accident conditions.

The objective of this CRP was to collect and systematize a thermo-physical properties database for light and heavy water reactor materials under normal operating, transient and accident conditions and to foster the exchange of non-proprietary information on thermo-physical properties of LWR and HWR materials. An internationally available, peer reviewed database of properties at normal and severe accident conditions has been established on the Internet.

This report is intended to serve as a useful source of information on thermo-physical properties data for water cooled reactor analyses. The properties data have been initially stored in the THERSYST data system at the University of Stuttgart, Germany, which was subsequently developed into an internationally available Internet database named THERPRO at Hanyang University, Republic of Korea.

Appreciation is expressed to the institutes participating in the CRP. In particular, appreciation is expressed to P.M. Mathew, Atomic Energy of Canada Ltd, for serving as chairman of the CRP and to J.K. Fink who has been working closely with the IAEA during the past several years as a consultant from Argonne National Laboratory on the planning and conduct of this CRP. The IAEA is particularly grateful to the Government of the Republic of Korea for extra-budgetary funds to prepare and maintain the Internet database.

The IAEA staff members responsible for this publication were Y.-E. Kim, J.-W. Park and J. Cleveland of the Division of Nuclear Power.

### *EDITORIAL NOTE*

*The use of particular designations of countries or territories does not imply any judgement by the publisher, the IAEA, as to the legal status of such countries or territories, of their authorities and institutions or of the delimitation of their boundaries.*

*The mention of names of specific companies or products (whether or not indicated as registered) does not imply any intention to infringe proprietary rights, nor should it be construed as an endorsement or recommendation on the part of the IAEA.*

## CONTENTS

1. INTRODUCTION .....	1
2. OBJECTIVE AND SCOPE .....	3
3. ACTIVITIES AND CONTRIBUTIONS OF PARTICIPATING INSTITUTES .....	4
3.1. Atomic Energy of Canada Limited .....	4
3.2. Nuclear Power Institute, China .....	4
3.3. University of West Bohemia, Czech Republic .....	4
3.4. CEA Cadarache, France .....	4
3.5. Bhabha Atomic Research Centre, India .....	4
3.6. Seoul National University, Republic of Korea .....	5
3.7. Hanyang University, Republic of Korea .....	5
3.8. Institute for High Energy Densities, Russian Federation .....	5
3.9. Institute of Physics and Power Engineering, Russian Federation .....	5
3.10. J.K. Fink (Argonne National Laboratory, USA) .....	5
4. PROCEDURE FOR ASSESSMENT AND PEER REVIEW .....	6
4.1. Assessment guidelines .....	6
4.1.1. Collect data .....	6
4.1.2. Convert to ITS-90 temperature scale .....	6
4.1.3. Review data for consistency, reliability, and systematic errors .....	7
4.1.4. Review all available equations from other assessments .....	7
4.1.5. Statistical analysis of all data .....	7
4.1.6. Error analysis and uncertainties .....	8
4.1.7. Submit assessment for peer review .....	8
4.2. Temperature conversion .....	9
4.2.1. Comparison between ITS-27 and IPTS-48 .....	9
4.2.2. Comparison between IPTS-48 and IPTS-68 .....	10
4.2.3. Comparison between IPTS-68 and ITS-90 .....	14
4.2.4. Conversion of the thermo-physical property values to the new temperature scale ITS-90 .....	19
4.2.5. Graphic representation of temperature differences and derivatives .....	20
4.2.6. General recommendations .....	21
5. SUMMARY OF DATA USED IN ASSESSMENT .....	23
6. THERMO-PHYSICAL PROPERTIES OF MATERIALS .....	25
6.1. Fuel materials .....	25
6.1.1. Uranium dioxide ( $\text{UO}_2$ ) .....	25
6.1.2. Thermal conductivity of irradiated $\text{UO}_2$ .....	143
6.1.3. Thermal properties of $(\text{U}, \text{Gd})\text{O}_2$ .....	152
6.1.4. $\text{ThO}_2$ , $(\text{Th}_{1-y}\text{U}_y)\text{O}_2$ and $(\text{Th}_{1-y}\text{Pu}_y)\text{O}_2$ properties .....	182
6.2. Cladding and pressure tube materials .....	225
6.2.1. Zircaloy .....	225
6.2.2. Thermal conductivity of $\text{Zr-1\%Nb}$ .....	289
6.2.3. Thermal conductivity of $\text{Zr-2.5\%Nb}$ .....	293
6.3. Absorber materials and their oxides .....	296
6.3.1. Hafnium .....	296
6.3.2. Hafnium dioxide .....	307

6.4.	Structural materials .....	314
6.4.1.	Russian steels .....	314
6.4.2.	Thermal conductivity of alloy 600 and 800 .....	324
6.5.	Zirconium .....	328
6.5.1.	Enthalpy and heat capacity .....	328
6.5.2.	Thermal conductivity .....	334
6.5.3.	Enthalpy of fusion .....	336
6.5.4.	Surface tension .....	340
6.5.5.	Viscosity .....	343
7.	THERMO-PHYSICAL PROPERTIES OF LIGHT AND HEAVY WATER .....	345
7.1.	Introduction .....	345
7.2.	Thermo-physical properties of light water .....	345
7.2.1.	The IAPWS formulation 1997 for the thermodynamic properties of water and steam for industrial use .....	346
7.2.2.	Transport properties .....	347
7.2.3.	Other properties .....	348
7.2.4.	Steam tables and software based on the IAPWS-IF97 .....	349
7.3.	Thermo-physical properties of heavy water .....	351
7.3.1.	Thermodynamic properties .....	351
7.3.2.	Transport properties .....	351
7.3.3.	Other properties of heavy water .....	351
8.	THERMO-PHYSICAL PROPERTIES OF CORIUM UNDER SEVERE ACCIDENT CONDITIONS (CEA, CADARACHE) .....	376
8.1.	Thermo-physical properties for severe accident analysis .....	376
8.1.1.	Experimental approach .....	376
8.1.2.	Database approach .....	377
8.1.3.	Theoretical approach .....	378
8.2.	Modelling of corium properties .....	378
8.2.1.	Density .....	378
8.2.2.	Thermal conductivity .....	381
8.2.3.	Viscosity .....	383
9.	THERPRO: ON-LINE NUCLEAR MATERIALS THERMO-PHYSICAL PROPERTIES DATABASE .....	388
9.1.	Introduction to THERPRO database .....	388
9.2.	Structure of THERPRO database .....	388
9.2.1.	Overall structure of database .....	388
9.2.2.	Structure of standard data set .....	391
9.2.3.	Data retrieval schemes .....	392
9.2.4.	User registration/authorization and database security .....	394
9.2.5.	THERPRO database management: data update and upgrade .....	395
	CONTRIBUTORS TO DRAFTING AND REVIEW .....	397

## 1. INTRODUCTION

The IAEA's Nuclear Power Programme includes a sub-programme on Nuclear Power Reactor Technology Development. The sub-programme's objective is to increase the exchange of non-commercial information and to foster cooperative research in nuclear power technology development and its applications. A project on technology development for advanced water cooled nuclear power plants is carried out within this sub-programme to foster international information exchange and collaboration in achieving technology advances for improving reliability, economics and safety. The activities are formulated with the advice, and carried out with the support, of the IAEA Department of Nuclear Energy's Technical Working Groups on Advanced Technologies for Light Water Reactors and for Heavy Water Reactors (the TWG-LWR and the TWG-HWR).

Evaluation of reactor performance under normal operation and severe accident conditions are important for current and future water cooled reactors and require accurate representations of thermo-physical properties under relevant temperature and neutron fluence conditions. Assuring that the needed thermo-physical properties are sufficiently accurate requires evaluation, documentation, peer review of existing data and selective measurements to obtain new data at conditions for which data are currently lacking or highly inadequate.

Moreover, improving the technology base through better codes and databases can contribute to improved economics of future plants by helping to remove the need for large design margins, which are currently used to account for limitations of data and methods. Accurate representations of thermo-physical properties under relevant temperature and neutron fluence conditions are necessary for evaluating reactor performance under normal operation and accident conditions.

From 1990 to 1994 the IAEA carried out a CRP on thermo-physical properties of materials for water cooled reactors. The objective of this activity was to collect and systematize a thermo-physical properties database for light and heavy water reactor materials. Data already existing at the participating institutes, and new data from some additional measurements carried out within the CRP, were collected. The data were then independently reviewed by Argonne National Laboratory and Atomic Energy of Canada Limited and additional data was provided by these organizations. Subsequently this database was published in 1997 [1], and the data stored in electronic format in the THERSYST system at the Institute for Nuclear Technology and Energy Systems, University of Stuttgart, Germany.

The results of the work carried out from 1990 to 1994 showed a large "spread" in some openly available thermo-physical properties data in use at that time. For this reason, a new IAEA CRP was established to critically assess and peer review selected property data and correlations, to extend the database to include properties at severe accident conditions, and to recommend the most appropriate data, if warranted. Critical steps in establishing recommended, "most appropriate", data with known uncertainties, including peer review of the data, review of the measurement techniques, and selected new measurements which were beyond the scope of the 1990–1994 CRP, were included in this new CRP on Establishment of a Thermo-physical Properties Database for LWRs and HWRs.

Nine institutes from 7 countries participated in this CRP; Atomic Energy of Canada Ltd (Canada); the Nuclear Power Institute of China (China); the University of West Bohemia (Czech Republic); the Institute of Physics and Power Engineering, and the Institute of High Densities of the Russian Academy of Sciences (Russian Federation); the Bhabha Atomic Research Centre (India); Commissariat à l'Énergie Atomique, Grenoble (France); and Hanyang University and Seoul National University (Rep. Of Korea). Significant contributions were also made by the Argonne National Laboratory (USA), through its work in establishing a thermo-physical properties database within the International Nuclear Safety Programme. Participants collaborated to establish an internationally available, peer reviewed database of properties at normal and severe accident conditions on the Internet. New measurements of thermo-physical properties of Zirconium liquid, Hf, Zr-2.5%Nb and  $\text{UO}_2\text{-Gd}_2\text{O}_3$  were completed. Assessments of thermo-physical properties of materials including Zircaloy, Zr-2.5% Nb, Zr-1% Nb, Zr liquid,  $\text{ThO}_2$  - $\text{UO}_2$ ,  $\text{ThO}_2$ ,  $\text{UO}_2\text{-Gd}_2\text{O}_3$ ,  $\text{UO}_2$ , Russian steels, Hafnium, Corium and Inconel were carried out by the participants, and they were peer reviewed by designated institutes. To support this effort, the THERSYST system was obtained from the University



of Stuttgart by the IAEA in December 2000. This system was converted to a web-based system, called THERPRO, for data storage and retrieval by Hanyang University [2], which is the database manager. The THERPRO database contains over 13,000 data files for 250 reactor materials, descriptions of experiments, and bibliographic information.

To coordinate this CRP, three Research Coordination Meetings were convened at the IAEA Headquarters in Vienna, Austria, in 1999, 2001 and 2003, respectively. At the first meeting the contribution of thermo-physical properties data by institutes to the CRP was planned. Further, the procedures for data assessment and assessment guidelines as well as activities to achieve the output expected from the CRP were established. At the second meeting, the status of CRP contributions from the participating institutes covering thermo-physical property assessments, peer reviews, research and new measurements, including planned future contributions was presented and the work conducted by the participating institutes on the assessments and peer reviews was confirmed. At the third meeting, the status of contributions to the CRP from the participating institutes covering thermo-physical property assessments, peer reviews, research and new measurements was presented, which was followed by technical discussions among the participants. The tasks to be conducted by participating institutes were confirmed and discussed. A demonstration of the THERPRO database on the Internet was performed. The Hanyang University was designated by the IAEA as the responsible organization for the management and update of the database.

## REFERENCES TO SECTION 1

- [1] INTERNATIONAL ATOMIC ENERGY AGENCY, Thermo-physical Properties of Materials for Water Cooled Reactors, IAEA-TECDOC-949, Vienna (1997).
- [2] KIM, Y.S., et al., Web-THERSYST: A Compilation of Thermo-physical Properties of Nuclear Materials on the Internet Proceedings of the International Conference on Nuclear Fuel for Today and Tomorrow : Experience and Outlook – TOPFUEL 2003, Würzburg, Germany, March 16–19, 2003.

## 2. OBJECTIVE AND SCOPE

The objective of the CRP was to collect and systematize a thermo-physical properties database for light and heavy water reactor materials under normal operating, transient and accident conditions. The materials properties considered include those needed for light and heavy water reactor operational and safety assessments. The materials have been grouped within the following categories:

- Nuclear Fuel Materials
- Cladding and Pressure Tube Materials
- Absorber Materials and their Oxides
- Structural Materials
- Coolants (light and heavy water)

The thermo-physical properties included in the database are:

- Thermal Conductivity
- Thermal Diffusivity
- Thermal Expansion
- Enthalpy
- Heat Capacity
- Enthalpy of Fusion
- Melting Point
- Coefficient of Thermal Expansion
- Emissivity
- Density
- Viscosity
- Vapour Pressure
- Surface Tension

The THERSYST database system established at the University of Stuttgart in Germany was adopted as the system for maintaining the reactor materials thermo-physical properties database. The database on reactor materials documented in this document is included in the THERSYST system, which has been converted to a web-based system for data storage and retrieval by Hanyang University called THERPRO. The Hanyang University serves as the database manager.

The CRP was carried out through research agreements with institutes in the United States, Canada and France and research contracts with the Russian Federation, Czech Republic, China, India and Republic of Korea. The following Chief Scientific Investigators participated from various countries and institutes:

P.M. Mathew	AECL/Canada
Y. Jiang	NPIC/China
R. Mares	Univ. of West Bohemia/Czech Republic
K. Froment	CEA /France
A.K. Sengupta	BARC/India
I.S. Hwang	Seoul National University/Rep. of Korea
Y.S. Kim	Hanyang University/Rep. of Korea
V. Fortov	Inst. of High Energy Densities/Russian Federation
A. Efanov	IPPE/Russian Federation
J.K. Fink	Argonne National Laboratory(ANL)/United States of America
G. Jaroma-Weiland	University of Stuttgart / Germany

### **3. ACTIVITIES AND CONTRIBUTIONS OF PARTICIPATING INSTITUTES**

This section contains a summary of activities and contributions of the participating institutes.

#### **3.1. Atomic Energy of Canada Limited**

- Assessment of Ni-Cr alloys (Alloy 600 & 800, Thermal Conductivity);
- Peer reviews of Zircaloy, Zr-1%Nb, Zr-2.5%Nb (Thermal Conductivity), Zirconium, Corium  $\text{UO}_2$  and Irradiated  $\text{UO}_2$ ;
- Provided Ni-Cr alloy (Thermal Conductivity) data, Zircaloy-O Phase Diagram data and Zr-2 Heat capacity that were not in IAEA THERSYST database;
- P. M. Mathew, chief investigator of AECL, chaired the 3<sup>rd</sup> Research Coordination Meeting and contributed to the completion of the TECDOC.

#### **3.2. Nuclear Power Institute, China**

- Assessment of  $\text{UO}_2\text{-Gd}_2\text{O}_3$  (Heat Capacity, Thermal Conductivity and Thermal Expansion)

#### **3.3. University of West Bohemia, Czech Republic**

- Provides information on the current internationally accepted formulations for thermo-physical properties for ordinary (light) and heavy water substance with regard to their applications in power engineering and related fields;
- Advises IAEA working group on conversion of thermo-physical property values of material for LWRs from temperature scale IPTS-48 and IPTS-68 to ITS-90 and provides the method for temperature conversion;
- Complement of new products of IAPWS to IAEA database;
- Harmonization of the new IAPWS industrial formulation IAPWS-IF97 to IAEA database;
- Complement of current IAPWS papers of references on the thermo-physical properties of heavy water to the IAEA database;
- Provides new products of IAPWS;
- Provides the IAEA link to the IAPWS website and statement for the link.

#### **3.4. CEA Cadarache, France**

- Provides a methodology to estimate the corium physical properties as a function of composition and temperature for experimental interpretation, modeling/code calculations for severe accident applications;
- Assessment of corium (Density, Thermal conductivity and Viscosity) and Hafnium dioxide (Enthalpy and Heat Capacity);
- Peer reviews  $\text{ThO}_2\text{-UO}_2$ ,  $\text{ThO}_2$ ,  $\text{ThO}_2\text{-PuO}_2$ , Hafnium and Hafnium dioxide (Thermal Conductivity);
- Provides IAEA link to THERMADATA website and statement for link.

#### **3.5. Bhabha Atomic Research Centre, India**

- Provided information on the database on thermo physical properties for  $(\text{Th,U})\text{O}_2$  and  $(\text{Th,Pu})\text{O}_2$  fuel systems which included thermal diffusivity, conductivity, specific heat, thermal expansion, density and melting point. The data were presented as a function of  $\text{UO}_2$  and  $\text{PuO}_2$  content and temperature. Recommendations were made on the basis of assessments;
- Provides new experimental data of  $\text{ThO}_2\text{-UO}_2$ ,  $\text{ThO}_2\text{-PuO}_2$ ;

- Measurement of  $\text{ThO}_2\text{-UO}_2(\Delta L/L, H, Cp)$ ,  $\text{ThO}_2\text{-PuO}_2(\Delta L/L, k)$  and  $\text{UO}_2+4\%\text{PuO}_2$  with varying  $\text{Gd}_2\text{O}_3$ ;
- Assessment of  $\text{ThO}_2\text{-UO}_2$ ,  $\text{ThO}_2$  and  $\text{ThO}_2\text{-PuO}_2$ ;
- Assessment of Hafnium dioxide (Enthalpy and Specific Heat);
- Peer reviews  $\text{UO}_2\text{-Gd}_2\text{O}_3$ .

### **3.6. Seoul National University, Republic of Korea**

- Peer reviews Ni-Cr alloys (Alloy 600 & 800, Thermal conductivity) and Russian Steel (Thermal conductivity).

### **3.7. Hanyang University, Republic of Korea**

- Assessment of the Thermal conductivity of Irradiated  $\text{UO}_2$ ;
- Provides new experimental data on mechanical properties of Zr, Zr-4, Zr(O) and Zr-4(O);
- Development of web-based THERPRO database, redesign and reconstruction.

### **3.8. Institute for High Energy Densities, Russian Federation**

- Assessment of Zirconium, and Hafnium (solid);
- Peer reviews of Zirconium (liquid and mixture);
- Measurement of the Thermal conductivity of Zr-2.5%Nb alloy at 400~1600K and provides new experiment data (Zr-2.5%Nb);
- Measurement of Thermal expansion of Hafnium (solid) and Zirconium;
- Measurement of Enthalpy and Heat capacity of Hafnium dioxide.

### **3.9. Institute of Physics and Power Engineering, Russian Federation**

- Assessment of Russian steel and Zr-2.5%Nb;
- Peer reviews  $\text{UO}_2$ , Zr-1%Nb and Zr(solid);
- Feasibility study and cooperation of converting THERSYST to web database with HYU.

### **3.10. J.K.Fink (Argonne National Laboratory, USA)**

- Provides data that have been used in assessment, which were not available on the THERSYST database;
- Assessment of  $\text{UO}_2$ , Zircaloy, Zr-1%Nb, Zirconium;
- Peer reviews  $\text{UO}_2$  (Thermal conductivity), Zr-2.5%Nb, Zr(liquid),  $\text{ThO}_2\text{-UO}_2$ ,  $\text{ThO}_2\text{-PuO}_2$ , Russian steel, Hafnium, Hafnium dioxide, Ni-Cr alloys,  $\text{UO}_2\text{-Gd}_2\text{O}_3$ ;
- J.K. Fink, as a consultant from ANL, chaired the 1<sup>st</sup> and 2<sup>nd</sup> Research Coordination Meetings and ANL contributed significantly to this CRP through its work in establishing a thermo-physical properties database within the International Nuclear Safety Programme.

## 4. PROCEDURE FOR ASSESSMENT AND PEER REVIEW

Most of the data assessments completed as part of this CRP consisted of a review and analysis of data from experimental measurements of a given thermo-physical material property. To finalize the assessments and peer reviews for the thermo-physical properties database, the following procedure was established. This assessment document followed the general format: Recommendation / Uncertainty / Discussion / References.

- When an assessment was complete, it was forwarded to the peer reviewers directly and the peer reviewers forwarded their comments to the author;
- The author addressed the comments and obtained consensus;
- Final assessments and data were sent to IAEA.

The detailed procedure used in those assessments is described in Section 1 of this chapter. One step of this procedure is the conversion of all temperatures to the current International Temperature Scale (ITS-90). Section 2 of this chapter discusses the international temperature scales that have been in effect from 1927 to the present and the relationship between the temperature scales. It also provides tables, graphs, and equations for converting data from one temperature scale to another.

In the review of data on Russian Steels, the data were classified according to the categories, whether they were from (1) experimental measurements, (2) a data compilation, (3) an evaluation of experimental data, or (4) from a recommendation

### 4.1. Assessment guidelines

The following guidelines were used to perform the assessment.

#### 4.1.1. Collect data

For solid reactor materials, obtain data that are in the THERSYST database, which is available in English. Data may be obtained by sending an electronic mail request to the International Atomic Energy Agency. For liquids and materials not included in the THERSYST database, a comprehensive literature search must be made to locate data in the open literature. Computerized literature searches using key words that search journal abstracts and journal key word lists are an ideal starting point of a comprehensive literature search.

#### 4.1.2. Convert to ITS-90 temperature scale

Temperatures for experimental data obtained before 1969 were measured using thermocouples, and optical pyrometers that had been calibrated according to the International Practical Temperature Scale (IPTS) of 1948. Measurements made between 1969 and 1990 were made relative to the IPTS of 1968. Temperature measurements for experimental data obtained after 1990 were measured using instruments calibrated according to the International Temperature Scale of 1990 (ITS-1990). Comparison of IPTS 1968 and ITS 1990 shows that the difference in calculated values between these temperature scales is small - often less than the experimental uncertainty in the temperature measurements. Thus the need to convert from IPTS 1968 to ITS 1990 may be determined by the uncertainty in the temperature measurements. If the difference between the temperature scales is less than the temperature uncertainty, such a conversion is not warranted. However, the difference in calculated values between IPTS 1948 and IPTS 1968 is significant. Thus the temperatures of the data obtained prior to 1968 must be converted to the IPTS 1968 scale for the analysis of those data for comparison with measurements made since 1968. Open literature papers provide tables and equations for conversion of the temperatures measured relative to the IPTS 1948 to the IPTS 1968 [1] and for conversion of the temperatures measured relative to the IPTS 1968 to ITS 1990 [2].

#### **4.1.3. Review data for consistency, reliability, and systematic errors**

With the collection of the experimental data, the experimental technique must be examined to determine its reliability. Data from different measurements are compared for consistency and inconsistent data are discarded. When sufficient data are available, inconsistent data are identified using standard statistical methods to determine outliers and to determine if the data belong to the same set and can therefore be analysed together. For example, properties of zirconium alloys are dependent on direction. Thus, data on axial thermal expansion cannot be analysed with data on circumferential thermal expansion. These data belong to two different sets. This may be determined either from knowledge about zirconium alloys or from a statistical analysis. If experimental data from different sources disagree and insufficient data are available for a statistical analysis, data selections are based on

- (1) the reliability of the experimental techniques,
- (2) agreement between two or more independent measurements, and
- (3) examination of each experimenter's results for reference standards and for materials for which more data are available.

Systematic errors in an experiment can often be detected from comparison of data from different samples and from different investigators. Some systematic errors, such as a zero reference point, can be corrected, as was done for thermal expansion measurements by Martin [3]. In other cases, the data must be excluded because of inconsistency.

If data are not included in the analysis, the reason the data have been excluded must be stated as part of the assessment. Examples of excluded data such as outliers resulting from misprints and inconsistent data are given in the analysis of zirconium thermal conductivity [4].

#### **4.1.4. Review all available equations from other assessments**

If peer review of an existing critical assessment indicates that it is complete and reliable and no new data are available since that review, then that recommendation may be adopted. If new data exist or data were not included in the existing assessment, then the recommendation from the existing assessment must be compared with these additional data to determine if it is appropriate for these additional data. Frequently, new data are not consistent with existing equations, indicating that a new analysis of all the data must be made.

#### **4.1.5. Statistical analysis of all data**

When possible, experimental errors are obtained from the paper describing the measurements. If experimental errors are known, they may be used to weight the data in the statistical regression analysis or the chi-square minimization procedure. The weight is the inverse of the square of experimental error. Usually, there is insufficient information to weight the data in the statistical analysis.

In determining the form of equation to fit the data, theoretically based functional forms are used, when possible, because these forms are more reliable than polynomials if they are extrapolated beyond the range of the data. For example, theoretically based forms have been used in the analysis of the thermal conductivity of  $\text{UO}_2$  [5]. However, use of theoretical forms for equations often requires forms that require nonlinear regression analysis or a chi-square minimization procedure. If theoretically-based forms are not available, then a linear regression analysis is used to fit the data to a polynomial. Statistical analysis provides, based on the number of tests and goodness of fit, the number of terms in the polynomial that are justified based on the data being analysed. Although reactor-safety code developers prefer polynomial equations to the more complex theoretically-based equations, polynomial equations should not be extrapolated beyond the range of the data analysed because such extrapolation can give unphysical values. Thus, if a polynomial equation is used, the equation derived in the assessment should not be extrapolated beyond the range of the experimental data.

Note that the Microsoft Excel Data Analysis package in Tools includes statistical analysis functions such as linear regression analysis and solver, which may be used for doing chi-squared minimizations of non-linear equations with constraints.

The property data must be analysed so that recommendations of related properties are consistent and that all thermodynamic relationships between properties are maintained. For example, enthalpy data and heat capacity data must be analysed together because heat capacities are the temperature derivative of enthalpy. Similarly, thermal conductivity ( $k$ ) is related to thermal diffusivity ( $D$ ), heat capacity ( $C_p$ ) and density ( $\rho$ ) by:

$$k = D \rho C_p$$

Recommended values for all these properties must be consistent so that the above relationship holds.

#### **4.1.6. Error analysis and uncertainties**

When possible, errors in the property measurements are obtained from the paper that describes the measurements. Unfortunately, often the experimenters fail to estimate the errors and insufficient information is given relative to results for standards for the reader to estimate the experimental uncertainty. If experimental errors are available, then the total error may be determined from a statistical error analysis, where the total error is the root mean square of all the sum of the squares of all the contributing errors (Contributing errors include: errors in the measurements, errors in fitting of the data, uncertainties in the theories on which the fitting equations have been based, etc.).

When rigorous statistical error analysis is not possible, an uncertainty estimate or an estimate of the reliability of the recommended equations and/or values must be made. The uncertainty (reliability) is estimated from deviations in the data obtained from different measurements, deviations of the data from the recommendation, and deviations between the recommended equations and equations given in other assessments.

An explanation of what criteria was used to determine the uncertainty or reliability estimate should be included in the documentation of the assessment.

#### **4.1.7. Submit assessment for peer review**

Send Microsoft Word or Word Perfect document of the assessments with equations, tables, and graphs by electronic mail to the International Atomic Energy Agency. The tables and graphs may be included as separate files or included as part of the document.

### **REFERENCES TO SECTION 4.1**

- [1] DOUGLAS, T.B., Conversion of existing calorimetrically determined thermodynamic properties to the basis of the International Practical Temperature Scale of 1968, J. of Research of the national Bureau of Standards 73A, 451-470, see Section 3 pp. 461-470 (1969).
- [2] RUSBY, R.L., Revised values for (T(90)-T(68)) from 630°C to 1064°C, Metrologia 31, 149-153 (1994).
- [3] MARTIN, D.G., The thermal expansion of solid UO<sub>2</sub> and (U, Pu) mixed oxides — a review and recommendations, J. Nuc. Mat. 152, 94-101 (1988).
- [4] FINK, J.K. and LEIBOWITZ, L., "Thermal conductivity of zirconium", J. Nuc. Mat. 266, 44-50 (1995); J.K. Fink, T. Softi, and H. Ley, International Nuclear Safety Center Database on thermophysical properties of reactor materials," Int. J. Thermophys. 20, 279-287 (1999).
- [5] RONCHI, C. et al., "Thermal conductivity of uranium dioxide up to 2900 K from simultaneous measurement of the heat capacity and thermal diffusivity", J. Applied Phys. 85, 776-789 (1999); see also the INSC database.

## 4.2. Temperature conversion

Contemporary science and technology have brought with them the need for more accurate data on material properties. These temperature dependent data come from new measurements or from older ones given in literature and compilations. Thus at the critical evaluation of data we should be aware of the differences in temperature standards by which the data were determined. The temperature scales differ from each other by detectable amounts. These differences are generally small and sometimes not even significant. However, in some cases - measurements of high accuracy, and in thermodynamics where first and second derivatives with respect to temperature are applied to calculate derived properties - comparison of data should be made on a common temperature scale.

A brief survey of used temperature scales is given in the article by Hust [1].

In 1854 Kelvin [2] proposed a thermodynamic temperature scale based on the Carnot cycle. This scale is independent of the properties of the substance used for the measurement. The first internationally acceptable practical temperature standard was adopted in 1927 as the International Temperature Scale of 1927 (ITS-27). The ITS-27 was defined in order to approximate the thermodynamic scale as close as experimentally possible. The ITS-27 [3] was changed in 1948 [4] to the International Temperature Scale of 1948 (Amended Edition of 1960) (IPTS-48) [5]. In as much as the numerical values of temperature on the IPTS-48 were the same as on the ITS-48, the former was not a revision of the 1948 scale but only an amended form of it.

Very extensive changes led to the International Practical Temperature Scale of 1968 [6] (IPTS-68). It was amended in 1975, but without influence on temperature values. Additionally to the ITS-68, the 1976 Provisional 0.5 K to 30 K Temperature Scale (EPT-76) was introduced.

The International Temperature Scale of 1990 [7] (ITS-90) is valid now. This scale superseded the International Practical Temperature Scale of 1968 (amended edition of 1975) and the 1976 Provisional 0.5 K to 30 K Temperature Scale. The thermodynamic bases of the ITS-90 are described in [8].

The unit of the thermodynamic scale is kelvin. It is defined as the fraction  $1/273.15$  of the thermodynamic temperature of the triple point of water. The Celsius temperature is defined by:

$$t [^{\circ}\text{C}] = T [\text{K}] - 273.15 \quad (1)$$

### 4.2.1. Comparison between ITS-27 and IPTS-48

The comparison of ITS-27 and IPTS-48 shows good agreement in the platinum thermometer range - 183 to 600°C [1].

In the IPTS-48 the Wien formula for temperatures above the gold point was replaced by the Planck radiation formula. In this range it is difficult to determine exact differences of the ITS-27 and the IPTS-48 due to the variability of  $\lambda$ . The wavelength of the radiation on the ITS-27 is restricted to the visible spectrum and is not restricted at all on the 1948 scale. The differences calculated at  $\lambda_1 = 0.4738 \times 10^{-4} \text{ cm}$  and  $\lambda_2 = 0.65 \times 10^{-4} \text{ cm}$  according to Corrucini [9] are presented in Table 1 and Fig.1.



Table 1. Differences between ITS-27 and IPTS-48

STANDARD THERMOCOUPLE		RADIATION LAW	RANGE	
$t (^{\circ}\text{C})$	$\Delta t$	$t (^{\circ}\text{C})$	$\Delta t \text{ }^{\circ}\text{C}(\text{IPTS-48}) - ^{\circ}\text{C}(\text{ITS-27})$	
$^{\circ}\text{C}(\text{IPTS-48})$	$^{\circ}\text{C}(\text{IPTS-48}) - ^{\circ}\text{C}(\text{ITS-27})$	$^{\circ}\text{C}(\text{IPTS-48})$	$\lambda_1$	$\lambda_2$
630.5	0.00*	1063	0	0
650	0.08*	1500	-2	-2
700	0.24	2000	-6	-6
750	0.35	2500	-12	-12
800	0.42	3000	-19	-20
850	0.43	3500	-28	-30
900	0.40	4000	-39	-43
950	0.32			
1000	0.20			
1050	0.05			
1063	0.00			

\* These values are uncertain since Pt thermometers are only defined up to 630.5°C on IPTS-48.

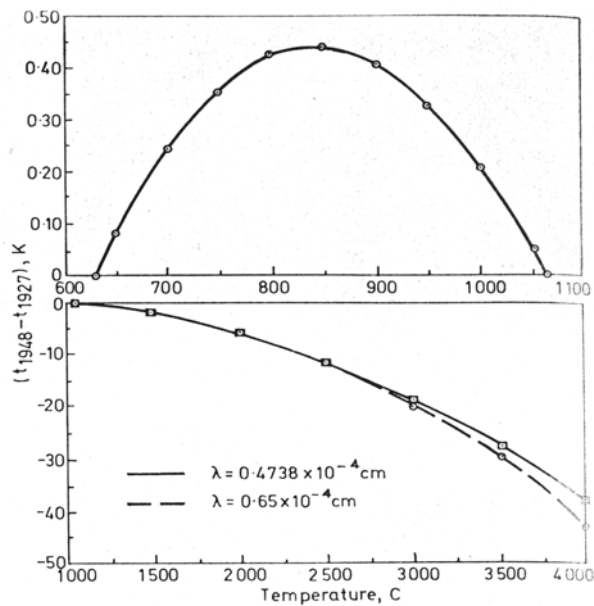


FIG. 1. Temperature differences between the ITS-27 and IPTS-48 [1] after Corrucini [9].

#### 4.2.2. Comparison between IPTS-48 and IPTS-68

Approximate differences  $(t_{68} - t_{48})$ , in kelvin, between the values of temperature given by IPTS-68 and IPTS-48, covering the range -180 to 4000°C, are tabulated in [6] and [1] and reproduced in Table 2.

Table 2. Approximate differences ( $t_{68} - t_{48}$ ), in kelvins, between the values of temperature given by IPTS-68 and IPTS-48

$t_{68} \text{ }^{\circ}\text{C}$	0	-10	-20	-30	-40	-50	-60	-70	-80	-90	-100
-100	0.022	0.013	0.003	-0.006	-0.013	-0.013	-0.005	0.007	0.012		
- 0	0.000	0.006	0.012	0.018	0.024	0.029	0.032	0.034	0.033	0.029	0.022
$t_{68} \text{ }^{\circ}\text{C}$	0	10	20	30	40	50	60	70	80	90	100
0	0.000	-0.004	-0.007	-0.009	-0.010	-0.010	-0.010	-0.008	-0.006	-0.003	0.000
100	0.000	0.004	0.007	0.012	0.016	0.020	0.025	0.029	0.034	0.038	0.043
200	0.043	0.047	0.051	0.054	0.058	0.061	0.064	0.067	0.069	0.071	0.073
300	0.073	0.074	0.075	0.076	0.077	0.077	0.077	0.077	0.077	0.076	0.076
400	0.076	0.075	0.075	0.075	0.074	0.074	0.074	0.075	0.076	0.077	0.079
500	0.079	0.082	0.085	0.089	0.094	0.100	0.108	0.116	0.126	0.137	0.150
600	0.150	0.165	0.182	0.200	0.23	0.25	0.28	0.31	0.34	0.36	0.39
700	0.39	0.42	0.45	0.47	0.50	0.53	0.56	0.58	0.61	0.64	0.67
800	0.67	0.70	0.72	0.75	0.78	0.81	0.84	0.87	0.89	0.92	0.95
900	0.95	0.98	1.01	1.04	1.07	1.10	1.12	1.15	1.18	1.21	1.24
1000	1.24	1.27	1.30	1.33	1.36	1.39	1.42	1.44			
$t_{68} \text{ }^{\circ}\text{C}$	0	100	200	300	400	500	600	700	800	900	1000
1000		1.5	1.7	1.8	2.0	2.2	2.4	2.6	2.8	3.0	3.2
2000	3.2	3.5	3.7	4.0	4.2	4.5	4.8	5.0	5.3	5.6	5.9
3000	5.9	6.2	6.5	6.9	7.2	7.5	7.9	8.2	8.6	9.0	9.3

Differences between the IPTS-68 and the low temperature national scales, NBS-55, NPL-61, PRIM-54 and PSU-54 are published in [10]. This allows giving a close approximation to the IPTS-68.

Douglas [11] derived formulas for converting the selected thermodynamic properties derived from calorimetric data - enthalpy, heat capacity, entropy and Gibbs free energy - from IPTS-48 to IPTS-68. Four temperature ranges, namely 90.188 K to 273.15 K, 273.15 K to 903.89 K, 903.89 K to 1337.58 K and 1337.58 K to 10000 K, have been treated individually. Equations giving the differences between the two temperature scales have been derived

$$\mu(T_{68}) = T_{68} - T_{48} = t_{68} - t_{48}. \quad (2)$$

They are applicable with sufficient accuracy for most practical purposes.

From the derived equations Douglas calculated and tabulated values of  $\mu = T_{68} - T_{48}$  and  $d(T_{68} - T_{48})/dT_{68}$  at rounded temperatures  $T_{68}$  from 90 to 10000 K. They are reprinted in Table 3. Presented values are in agreement with [6].

Table 3. Approximate difference in the value of temperature, and its temperature derivative, given by the IPTS-68 and IPTS-48

$T_{68}$	$T_{68} - T_{48}$	$d(T_{68} - T_{48})/dT_{68}$	$T_{68}$	$T_{68} - T_{48}$	$d(T_{68} - T_{48})/dT_{68}$	$T_{68}$	$T_{68} - T_{48}$	$d(T_{68} - T_{48})/dT_{68}$
90	+0.0076	+0.0022	128	-0.0135	0.00000	220	+0.0299	-0.00038
90.188	.0080	.0021	130	-.0134	+.00015	225	.0278	-.00045
91	.0095	.0017	132	-.0129	.00028	230	.0254	-.00051
92	.0110	.0013	134	-.0122	.00041	235	.0227	-.00056
93	.0121	.0008	136	-.0113	.00052	240	.0198	-.00059
94	.0127	.0005	138	-.0102	.00062	245	.0168	-.00061
95	.0130	.0002	140	-.0088	.00071	250	.0137	-.00062
96	.0130	-.0001	142	-.0073	.00079	255	.0105	-.00062
97	.0128	-.0004	144	-.0057	.00086	260	.0074	-.00061
98	.0123	-.0006	146	-.0039	.00092	265	.0044	-.00058
99	.0116	-.0008	148	-.0020	.00096	270	.0016	-.00054
100	.0108	-.00089	150	.0000	.00100	273.15	.0000	-.00050
102	.0088	-.00112	155	+.0050	.00103	275	-.0009	-.00047
104	.0064	-.00124	160	.0102	.00102	280	-.0031	-.00041
106	.0038	-.00130	165	.0152	.00096	285	-.0050	-.00035
108	.0012	-.00130	170	.0197	.00087	290	-.0066	-.00029
110	-.0013	-.00125	175	.0238	.00075	295	-.0079	-.00023
112	-.0038	-.00116	180	.0272	.00061	298.15	-.0085	-.00020
114	-.0060	-.00106	185	.0299	.00047	300	-.0089	-.00018
116	-.0080	-.00092	190	.0318	.00032	305	-.0096	-.00013
118	-.0097	-.00078	195	.0331	.00017	310	-.0101	-.00008
120	-.0111	-.00063	200	.0336	.00005	315	-.0104	-.00003
122	-.0122	-.00046	205	.0335	-.00009	320	-.0105	+.00001
124	-.0129	-.00030	210	.0328	-.00020	325	-.0103	.00006
126	-.0134	-.00015	215	.0316	-.00029	330	-.0099	.00009

Table 3. Approximate difference in the value of temperature, and its temperature derivative, given by the IPTS-68 and IPTS-48 (continued)

$T_{68}$	$T_{68} - T_{48}$	$d(T_{68} - T_{48})/dT_{68}$	$T_{68}$	$T_{68} - T_{48}$	$d(T_{68} - T_{48})/dT_{68}$	$T_{68}$	$T_{68} - T_{48}$	$d(T_{68} - T_{48})/dT_{68}$
335	-0.0093	+0.00013	700	+0.075	0.0000	1320	+1.378	+0.0029
340	-.0086	.00016	710	.074	.0000	1337.58	1.430	<sup>b</sup> .0030
345	-.0077	.00020	720	.074	.0000			<sup>c</sup> .0016
350	-.0066	.00023	730	.074	.0000	1350	1.45	.0016
355	-.0054	.00026	740	.075	+ .0001	1375	1.49	.0016
360	-.0041	.00028	750	.076	.0001	1400	1.53	.0016
365	-.0026	.00030	760	.077	.0001	1425	1.57	.0017
370	-.0010	.00033	770	.079	.0002	1450	1.61	.0017
373.15	.0000	.00034	780	.081	.0003	1475	1.66	.0017
375	+ .0006	.00035	790	.084	.0003	1500	1.70	.0017
380	.0024	.00036	800	.088	.0004	1525	1.74	.0017
385	.0043	.00038	810	.093	.0005	1550	1.78	.0017
390	.0062	.00039	820	.098	.0006	1575	1.83	.0018
395	.0082	.00041	830	.105	.0007	1600	1.87	.0018
400	.0103	.00042	840	.113	.0009	1625	1.92	.0018
410	.0146	.00044	850	.123	.0010	1650	1.96	.0018
420	.0190	.00045	860	.134	.0012	1675	2.01	.0018
430	.0235	.00045	870	.146	.0013	1700	2.05	.0019
440	.0280	.00045	880	.160	.0015	1725	2.10	.0019
450	.0325	.00045	890	.176	.0017	1750	2.15	.0019
460	.0369	.00044	900	.194	.0019	1775	2.20	.0019
470	.0413	.00043	903.89	.202	<sup>a</sup> .0020	1800	2.24	.0019
480	.0454	.00041			<sup>b</sup> .0027	1825	2.29	.0020
490	.0494	.00039	910	.218	.0027	1850	2.34	.0020
500	.0532	.00037	920	.245	.0027	1875	2.39	.0020
510	.057	.0003	940	.300	.0027	1900	2.44	.0020
520	.060	.0003	960	.354	.0027	1925	2.49	.0020
530	.063	.0003	980	.409	.0027	1950	2.54	.0021
540	.066	.0003	1000	.464	.0028	1975	2.60	.0021
550	.068	.0002	1020	.519	.0028	2000	2.65	.0021
560	.070	.0002	1040	.575	.0028	2050	2.75	.0021
570	.072	.0002	1060	.631	.0028	2100	2.86	.0022
580	.074	.0001	1080	.687	.0028	2150	2.97	.0022
590	.075	.0001	1100	.743	.0028	2200	3.08	.0022
600	.076	.0001	1120	.800	.0028	2250	3.19	.0023
610	.076	.0001	1140	.857	.0028	2300	3.31	.0023
620	.077	.0000	1160	.914	.0029	2350	3.43	.0024
630	.077	.0000	1180	.971	.0029	2400	3.55	.0024
640	.077	.0000	1200	1.029	.0029	2450	3.67	.0024
650	.077	.0000	1220	1.086	.0029	2500	3.79	.0025
660	.076	.0000	1235.08	1.130	.0029	2600	4.0	.003
670	.076	.0000	1240	1.144	.0029	2700	4.3	.003
680	.076	.0000	1260	1.202	.0029	2800	4.6	.003
690	.075	.0000	1280	1.261	.0029	2900	4.8	.003
692.73	.075	.0000	1300	1.319	.0029	3000	5.1	.003

### 4.2.3. Comparison between IPTS-68 and ITS-90

Differences between ITS-90 and EPT-67 (provisional 0.5 to 30 K temperature scale 1976), and ITS-90 and IPTS-68 for specified values of  $T_{90}$  and  $t_{90}$  according to [7] were revised by Rusby [12]. The revision affects only the range 630 to 1064 °C, where the IPTS-68 specified the use of Pt -Pt 10% Rh thermocouples. It follows from new intercomparisons of thermocouples carrying IPTS-68 calibrations with Pt resistance thermometers and radiation thermometers calibrated in accordance with the ITS-90. The revised tables are reprinted in Table 4.

Table 4. Revised differences between the ITS-90 and the IPTS-68, and the differences between the ITS-90 and the EPT-76

$(T_{90} - T_{76})/\text{mK}$										
$T_{90}/\text{K}$	0	1	2	3	4	5	6	7	8	9
0						-0,1	-0,2	-0,3	-0,4	-0,5
10	-0,6	-0,7	-0,8	-1,0	-1,1	-1,3	-1,4	-1,6	-1,8	-2,0
20	-2,2	-2,5	-2,7	-3,0	-3,2	-3,5	-3,8	-4,1		
$(T_{90} - T_{68})/\text{K}$										
$T_{90}/\text{K}$	0	1	2	3	4	5	6	7	8	9
10					-0,006	-0,003	-0,004	-0,006	-0,008	-0,009
20	-0,009	-0,008	-0,007	-0,007	-0,006	-0,005	-0,004	-0,004	-0,005	-0,006
30	-0,006	-0,007	-0,008	-0,008	-0,008	-0,007	-0,007	-0,007	-0,006	-0,006
40	-0,006	-0,006	-0,006	-0,006	-0,006	-0,007	-0,007	-0,007	-0,006	-0,006
50	-0,006	-0,005	-0,005	-0,004	-0,003	-0,002	-0,001	0,000	0,001	0,002
60	0,003	0,003	0,004	0,004	0,005	0,005	0,006	0,006	0,007	0,007
70	0,007	0,007	0,007	0,007	0,007	0,008	0,008	0,008	0,008	0,008
80	0,008	0,008	0,008	0,008	0,008	0,008	0,008	0,008	0,008	0,008
90	0,008	0,008	0,008	0,008	0,008	0,008	0,008	0,009	0,009	0,009
$T_{90}/\text{K}$	0	10	20	30	40	50	60	70	80	90
100	0,009	0,011	0,013	0,014	0,014	0,014	0,014	0,013	0,012	0,012
200	0,011	0,010	0,009	0,008	0,007	0,005	0,003	0,001		
$(t_{90} - t_{68})/^{\circ}\text{C}$										
$t_{90}/^{\circ}\text{C}$	0	-10	-20	-30	-40	-50	-60	-70	-80	-90
-100	0,013	0,013	0,014	0,014	0,014	0,013	0,012	0,010	0,008	0,008
0	0,000	0,002	0,004	0,006	0,008	0,009	0,010	0,011	0,012	0,012
$t_{90}/^{\circ}\text{C}$	0	10	20	30	40	50	60	70	80	90
0	0,000	-0,002	-0,005	-0,007	-0,0010	-0,013	-0,016	-0,018	-0,021	-0,024
100	-0,026	-0,028	-0,030	-0,032	-0,034	-0,036	-0,037	-0,038	-0,039	-0,039
200	-0,040	-0,040	-0,040	-0,040	-0,040	-0,040	-0,040	-0,039	-0,039	-0,039
300	-0,039	-0,039	-0,039	-0,040	-0,040	-0,041	-0,042	-0,043	-0,045	-0,046
400	-0,048	-0,051	-0,053	-0,056	-0,059	-0,062	-0,065	-0,068	-0,072	-0,075
500	-0,079	-0,083	-0,087	-0,090	-0,094	-0,098	-0,101	-0,105	-0,108	-0,112
600	-0,115	-0,118	-0,122	-0,125	-0,11	-0,10	-0,09	-0,07	-0,05	-0,04
700	-0,02	-0,01	0,00	0,02	0,03	0,03	0,04	0,05	0,05	0,05
800	0,05	0,05	0,04	0,04	0,03	0,02	0,01	0,00	-0,02	-0,03
900	-0,05	-0,06	-0,08	-0,10	-0,11	-0,13	-0,15	-0,16	-0,18	-0,19
1 000	-0,20	-0,22	-0,23	-0,23	-0,24	-0,25	-0,25	-0,25	-0,26	-0,26
$t_{90}/^{\circ}\text{C}$	0	100	200	300	400	500	600	700	800	900
1 000		-0,026	-0,30	-0,35	-0,39	-0,44	-0,49	-0,54	-0,60	-0,66
2 000	-0,72	-0,79	-0,85	-0,93	-1,00	-1,07	-1,15	-1,24	-1,32	-1,41
3 000	-1,50	-1,59	-1,69	-1,78	-1,89	-1,99	-2,10	-2,21	-2,32	-2,43

In [13] Rusby discussed the conversion of thermal reference values to the ITS-90 and provided analytical equations representing the differences between the ITS-90 and IPTS-68. Analytical representations for individual temperature ranges are as follows, where temperature is in [K]:

Temperature range  $T_{68} = 13.81 \text{ K to } 83.8 \text{ K}$

$$(T_{90} - T_{68}) = \sum_{i=0}^{12} a_i \left[ \{(T_{68}) - 40\} / 40 \right]^i \quad (3)$$

Temperature range  $T_{68} = 73.15 \text{ K to } 903.89 \text{ K}$

$$(T_{90} - T_{68}) = \sum_{i=1}^8 b_i \left[ \{(T_{68}) - 273.15\} / 630 \right]^i \quad (4)$$

For the limited temperature range  $T_{68} = 260 \text{ K to } 400 \text{ K}$  the differences may be represented by the equation

$$(T_{90} - T_{68}) = -0.00025 \{(T_{68}) - 273.15\}, \quad (5)$$

with an accuracy of  $\pm 0.001 \text{ K}$ .

Table 5. Coefficients  $a_i$ ,  $b_i$  and  $d_i$  of equations (3), (4) and (7)

$i$	$a_i$	$b_i$	$d_i$
0	-0.005903	—	—
1	0.008174	-0.148759	7.8687209 E+1
2	-0.061924	-0.267408	-4.7135991 E-1
3	-0.193388	1.080760	1.0954715 E-3
4	1.490793	1.269056	-1.2357884 E-6
5	1.252347	-4.089591	6.7736583 E-10
6	-9.835868	-1.871251	-1.4458081 E-13
7	1.411912	7.438081	—
8	25.277595	-3.536296	—
9	-19.183815	—	—
10	-18.437089	—	—
11	27.000895	—	—
12	-8.716324	—	—

Temperature range  $T_{68} = 903.89 \text{ K to } 1337.58 \text{ K}$

In [13] the analytical representation of the differences was originally given by the following equation, where temperature is in [K].

$$(T_{90} - T_{68}) = \sum_{i=0}^7 c_i \left[ \{(T_{68}) - 1173.15\} / 300 \right]^i. \quad (6)$$

However, in 1994 a new revised equation was published for this temperature range [12], where temperature is in [ $^{\circ}\text{C}$ ], which superseded the equation given above

$$(t_{90} - t_{68}) = \sum_{i=1}^6 d_i (t_{90})^{i-1}. \quad (7)$$

Temperature range  $T_{68} > 1337.58 \text{ K}$

$$(T_{90} - T_{68}) = -0.25 \left( \frac{T_{68}}{1337.58} \right)^2 \frac{\{1 - \exp(-c_2 / \lambda T_{68})\}}{\{1 - \exp(-c_2 / \lambda 1337.58)\}} \quad (8)$$

Weir and Goldberg [14] revised the Douglas equations [11] and after discarding higher-order terms, they obtained simplified equations for conversion of values in IPTS-68 to ITS-90. They presented tables of differences:  $(T_{90} - T_{76})$  in [K] (differences between ITS-90 and EPT-76) and the derivatives  $d(T_{90} - T_{76})/dT$  as a function of  $T_{76}$ , which are reprinted in Table 6. The differences  $(T_{90} - T_{68})$  in [K], (differences between ITS-90 and IPTS-68) taken from [14] and the corresponding derivatives  $d(T_{90} - T_{68})/dT$  as a function of  $T_{68}$  are reprinted in Table 7.

Table 6. Differences  $\Delta T / K = (T_{90} - T_{76})$  between the ITS-90 and EPT-76 and derivatives  $d\Delta T/dT$  as a function of  $T_{76}$  [K]

$\frac{T_{76}}{K}$	$\frac{\Delta T}{K}$	$d\Delta T/dT$
5	-0.0001	-0.00010
6	-0.0002	-0.00010
7	-0.0003	-0.00010
8	-0.0004	-0.00010
9	-0.0005	-0.00010
10	-0.0006	-0.00010
11	-0.0007	-0.00010
12	-0.0008	-0.00013
13	-0.0010	-0.00013
14	-0.0011	-0.00013
15	-0.0013	-0.00013
16	-0.0014	-0.00013
17	-0.0016	-0.00020
18	-0.0018	-0.00020
19	-0.0020	-0.00020
20	-0.0022	-0.00024
21	-0.0025	-0.00024
22	-0.0027	-0.00024
23	-0.0030	-0.00024
24	-0.0032	-0.00024
25	-0.0035	-0.00030
26	-0.0038	-0.00030
27	-0.0041	-0.00030

Table 7. Differences  $\Delta T / K = (T_{90} - T_{68}) [K]$  between the ITS-90 and the IPTS-68 as a function of  $T_{68}$  and derivatives of these differences  $d\Delta T / dT$  as a function of  $T_{68} [K]$

$\frac{T_{68}}{K}$	$\frac{\Delta T}{K}$	$d\Delta T/dT$	$\frac{T_{68}}{K}$	$\frac{\Delta T}{K}$	$d\Delta T/dT$	$\frac{T_{68}}{K}$	$\frac{\Delta T}{K}$	$d\Delta T/dT$
14	-0.006	+0.0050	51	-0.005	+0.0000	88	+0.008	+0.0000
15	-0.003	+0.0000	52	-0.005	+0.0000	89	+0.008	+0.0000
16	-0.004	-0.0013	53	-0.004	+0.0010	90	+0.008	+0.0000
17	-0.006	-0.0020	54	-0.003	+0.0010	91	+0.008	+0.0000
18	-0.008	-0.0013	55	-0.002	+0.0010	92	+0.008	+0.0000
19	-0.009	+0.0000	56	-0.001	+0.0010	93	+0.008	+0.0000
20	-0.009	+0.0000	57	+0.000	+0.0010	94	+0.008	+0.0000
21	-0.008	+0.0010	58	+0.001	+0.0010	95	+0.008	+0.0000
22	-0.007	+0.0000	59	+0.002	+0.0010	96	+0.008	+0.0000
23	-0.007	+0.0000	60	+0.003	+0.0000	97	+0.009	+0.0000
24	-0.006	+0.0010	61	+0.003	+0.0000	98	+0.009	+0.0000
25	-0.005	+0.0010	62	+0.004	+0.0000	99	+0.009	+0.0000
26	-0.004	+0.0000	63	+0.004	+0.0000	100	+0.009	+0.0000
27	-0.004	+0.0000	64	+0.005	+0.0000	110	+0.011	+0.00020
28	-0.005	-0.0010	65	+0.005	+0.0000	120	+0.013	+0.00013
29	-0.006	+0.0000	66	+0.006	+0.0000	130	+0.014	+0.00000
30	-0.006	+0.0000	67	+0.006	+0.0000	140	+0.014	+0.00000
31	-0.007	-0.0010	68	+0.007	+0.0000	150	+0.014	+0.00000
32	-0.008	+0.0000	69	+0.007	+0.0000	160	+0.014	+0.00000
33	-0.008	+0.0000	70	+0.007	+0.0000	170	+0.013	-0.00010
34	-0.008	+0.0000	71	+0.007	+0.0000	180	+0.012	+0.00000
35	-0.007	+0.0000	72	+0.007	+0.0000	190	+0.012	+0.00000
36	-0.007	+0.0000	73	+0.007	+0.0000	200	+0.011	-0.00010
37	-0.007	+0.0000	74	+0.007	+0.0000	210	+0.010	-0.00010
38	-0.006	+0.0000	75	+0.008	+0.0000	220	+0.009	-0.00010
39	-0.006	+0.0000	76	+0.008	+0.0000	230	+0.008	-0.00010
40	-0.006	+0.0000	77	+0.008	+0.0000	240	+0.007	-0.00013
41	-0.006	+0.0000	78	+0.008	+0.0000	250	+0.005	-0.00020
42	-0.006	+0.0000	79	+0.008	+0.0000	260	+0.003	-0.00020
43	-0.006	+0.0000	80	+0.008	+0.0000	270	+0.001	-0.00026
44	-0.006	+0.0000	81	+0.008	+0.0000	273.15	+0.000	-0.00021
45	-0.007	+0.0000	82	+0.008	+0.0000	280	-0.001	-0.00019
46	-0.007	+0.0000	83	+0.008	+0.0000	290	-0.004	-0.00024
47	-0.007	+0.0000	84	+0.008	+0.0000	300	-0.006	-0.00024
48	-0.006	+0.0000	85	+0.008	+0.0000	310	-0.009	-0.00030
49	-0.006	+0.0000	86	+0.008	+0.0000	320	-0.012	-0.00030
50	-0.006	+0.0000	87	+0.008	+0.0000	330	-0.015	-0.00024



Table 7. Differences  $\Delta T / K = (T_{90} - T_{68}) [K]$  between the ITS-90 and the IPTS-68 as a function of  $T_{68}$  and derivatives of these differences  $d\Delta T / dT$  as a function of  $T_{68} [K]$  (continued)

$T_{68}$ K	$\Delta T$ K	$d\Delta T/dT$	$T_{68}$ K	$\Delta T$ K	$d\Delta T/dT$	$T_{68}$ K	$\Delta T$ K	$d\Delta T/dT$
340	-0.017	-0.00024	800	-0.089	-0.00034	1240	-0.16	-0.0016
350	-0.020	-0.00030	810	-0.093	-0.00040	1250	-0.17	-0.0015
360	-0.023	-0.00024	820	-0.097	-0.00034	1260	-0.19	-0.0014
370	-0.025	-0.00020	830	-0.100	-0.00034	1270	-0.20	-0.0013
380	-0.027	-0.00020	840	-0.104	-0.00034	1280	-0.21	-0.0011
390	-0.029	-0.00020	850	-0.107	-0.00034	1290	-0.22	-0.00098
400	-0.031	-0.00020	860	-0.111	-0.00034	1300	-0.23	-0.00082
410	-0.033	-0.00020	870	-0.114	-0.00030	1310	-0.24	-0.00064
420	-0.035	-0.00020	880	-0.117	-0.00034	1320	-0.25	-0.00045
430	-0.037	-0.00013	890	-0.121	-0.00034	1330	-0.25	-0.00026
440	-0.038	-0.00010	900	-0.124	+0.00000	1337.58	-0.25	-0.00010
450	-0.039	+0.00000	903.89	-0.125	—	1340	-0.25	-0.00037
460	-0.039	+0.00000	910	-0.12	+0.0012	1350	-0.26	-0.00038
470	-0.040	+0.00000	920	-0.10	+0.0014	1360	-0.26	-0.00038
480	-0.040	+0.00000	930	-0.09	+0.0015	1400	-0.27	-0.00039
490	-0.040	+0.00000	940	-0.07	+0.0016	1500	-0.31	-0.00042
500	-0.040	+0.00000	950	-0.06	+0.0016	1600	-0.36	-0.00045
510	-0.040	+0.00000	960	-0.04	+0.0016	1700	-0.40	-0.00048
520	-0.040	+0.00000	970	-0.03	+0.0015	1800	-0.45	-0.00050
530	-0.040	+0.00000	980	-0.01	+0.0014	1900	-0.50	-0.00053
540	-0.039	+0.00000	990	+0.00	+0.0013	2000	-0.56	-0.00056
550	-0.039	+0.00000	1000	+0.01	+0.0012	2100	-0.62	-0.00059
560	-0.039	+0.00000	1010	+0.02	+0.0010	2200	-0.68	-0.00061
570	-0.039	+0.00000	1020	+0.03	+0.00083	2300	-0.74	-0.00064
580	-0.039	+0.00000	1030	+0.04	+0.00065	2400	-0.81	-0.00067
590	-0.039	+0.00000	1040	+0.05	+0.00047	2500	-0.87	-0.00070
600	-0.040	+0.00000	1050	+0.05	+0.00027	2600	-0.95	-0.00073
610	-0.040	+0.00000	1060	+0.05	+0.00008	2700	-1.02	-0.00075
620	-0.041	-0.00010	1070	+0.05	-0.00011	2800	-1.09	-0.00078
630	-0.042	-0.00010	1080	+0.05	-0.00031	2900	-1.17	-0.00081
640	-0.043	-0.00010	1090	+0.04	-0.00049	3000	-1.26	-0.00084
650	-0.044	-0.00013	1100	+0.04	-0.00067	3100	-1.34	-0.00087
660	-0.046	-0.00013	1110	+0.03	-0.00084	3200	-1.43	-0.00089
670	-0.047	-0.00015	1120	+0.02	-0.00099	3300	-1.52	-0.00092
680	-0.050	-0.00024	1130	+0.01	-0.0011	3400	-1.62	-0.00095
690	-0.052	-0.00024	1140	+0.00	-0.0013	3500	-1.71	-0.00098
700	-0.055	-0.00030	1150	-0.01	-0.0014	3600	-1.81	-0.0010
710	-0.058	-0.00030	1160	-0.03	-0.0015	3700	-1.92	-0.0010
720	-0.061	-0.00030	1170	-0.04	-0.0016	3800	-2.02	-0.0011
730	-0.064	-0.00030	1180	-0.06	-0.0016	3900	-2.13	-0.0011
740	-0.067	-0.00034	1190	-0.08	-0.0017	4000	-2.24	-0.0011
750	-0.071	-0.00034	1200	-0.09	-0.0017	4100	-2.35	-0.0012
760	-0.074	-0.00034	1210	-0.11	-0.0017	4200	-2.46	-0.0012
770	-0.078	-0.00040	1220	-0.13	-0.0017	4300	-2.58	-0.0012
780	-0.082	-0.00040	1230	-0.14	-0.0016			
790	-0.086	-0.00034	1235.08	-0.15	-0.0016			

#### 4.2.4. Conversion of the thermo-physical property values to the new temperature scale ITS-90

This section is limited to temperature conversion of experimental values. It provides guidance to make conversion to a fixed-point temperature, for which the values are different on two different temperature scales. Conversion procedures are demonstrated on examples.

- a) Experimental values with the exception of such values as mentioned in paragraphs (b) and (c) are dependent on the thermal state only. Thus the conversion involves merely associating them with a different temperature. Density can serve as an example.

*Example 1:*

Convert an experimental value of density  $\rho=810.52 \text{ kg/m}^3$  at  $p=1.011 \text{ MPa}$  and  $t_{68}=230.00^\circ\text{C}$  (temperature in IPTS-68) to the ITS-90. The tabulated value of temperature difference is  $(t_{90}-t_{68}) = -0.040 \text{ K}$  (see Table 4 or Table 7). Then temperature in ITS-90 is  $t_{90} = 229.96^\circ\text{C}$ .

Result: The 'converted' value to the ITS=90 is:  $\rho=810.52 \text{ kg/m}^3$  at  $p=1.011 \text{ MPa}$  and  $t_{90} = 229.96^\circ\text{C}$ .

- b) Thermodynamic properties such as enthalpy cannot be assigned absolute values and therefore are usually expressed numerically as the magnitude in excess of the enthalpy at a reference temperature. Thus the correction to be applied to an enthalpy increment involves merely associating it with different boundary temperatures [11].
- c) Compound quantities, which involve temperature intervals, such as heat capacity, thermal conductivity, and thermal expansion, are affected as values mentioned above, and also by virtue of their correspondence on the derivative  $d\Delta T/dT$  [15].

*Example 2:*

Convert an experimental value of the coefficient of thermal conductivity  $\lambda_{68} = 0.09124 \text{ W}\cdot\text{m}^{-1}\cdot\text{K}^{-1}$  at  $p = 1 \text{ MPa}$  and  $T_{68} = 950.00 \text{ K}$  (temperature in IPTS-68) to the ITS-90.

Coefficient of thermal conductivity,  $\lambda$ , is defined by the Fourier equation for the heat flux:

$$q = -\lambda \cdot \text{grad}(t) \quad (9)$$

For one-dimensional heat transfer the equation (9) is expressed with the derivative

$$q = -\lambda \cdot \frac{dt}{dx} \quad (10)$$

For the temperature scale ITS-90 the equation (10) becomes

$$q = -\lambda_{90} \cdot \frac{dt_{90}}{dx} \quad (11)$$

and for the IPTS-68

$$q = -\lambda_{68} \cdot \frac{dt_{68}}{dx} \quad (12)$$

Comparing equations (11) and (12) we get

$$\lambda_{90} = \lambda_{68} \cdot \frac{dt_{68}}{dt_{90}} \quad (13)$$

The derivative of the temperature difference may be expressed as

$$\frac{d(t_{90}-t_{68})}{dt_{90}} = 1 - \frac{dt_{68}}{dt_{90}} \quad (14)$$

and hence

$$\frac{dt_{68}}{dt_{90}} = 1 - \frac{d(t_{90} - t_{68})}{dt_{90}} \quad (15)$$

*Numerical solution:*

From Table 7 the temperature difference and its derivative are  $\Delta T = T_{90} - T_{68} = -0.06 \text{ K}$  and  $d\Delta T/dT = +0.0016$ .

Then  $T_{90} = T_{68} + \Delta T = 950.00 - 0.06 = 949.94 \text{ K}$

From (15)

$$\frac{dt_{68}}{dt_{90}} = 1 - \frac{\Delta T}{dT} = 1 - 0.0016 = 0.9984$$

Then the converted value according to (13) is

$$\lambda_{90} = \lambda_{68} \cdot \frac{dt_{68}}{dt_{90}} = 0.09124 \cdot 0.9984 = 0.09109 \text{ W.m}^{-1}.\text{K}^{-1}.$$

Result: The converted value is  $\lambda_{90} = 0.09109 \text{ W.m}^{-1}.\text{K}^{-1}$  at  $p = 1 \text{ MPa}$  and  $T_{90} = 949.94 \text{ K}$ .

#### 4.2.5. Graphic representation of temperature differences and derivatives

The temperature differences and their derivatives were calculated in the temperature range  $903.765 \text{ K} < T_{90} < 1337.33 \text{ K}$ . The diagrams were taken from [15].

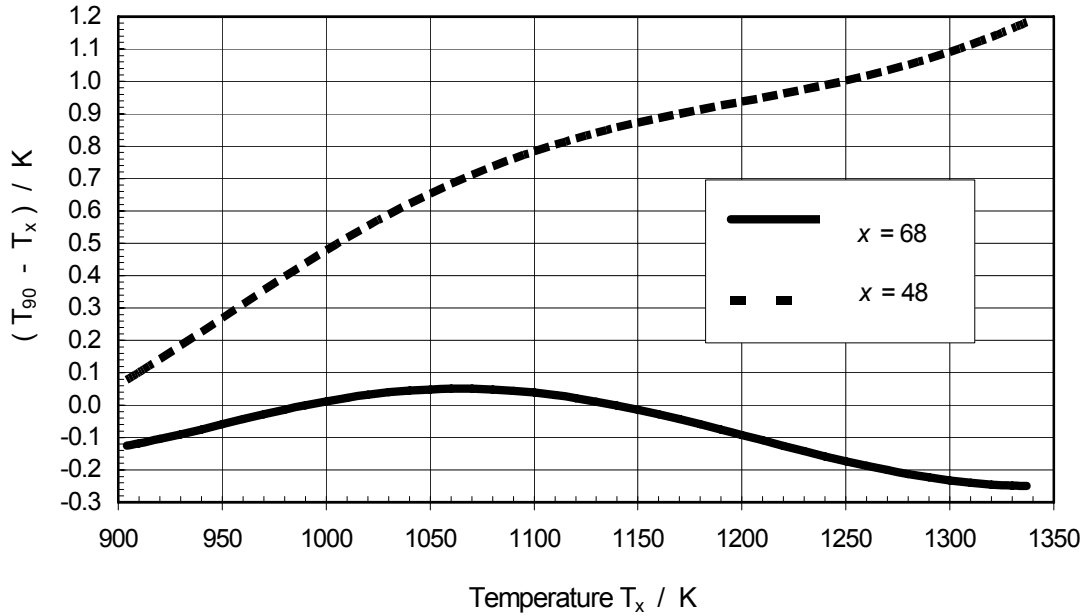


FIG .2. Temperature differences [15]:  $(T_{90} - T_{68})/[K]$  calculated from the revised equation (7) and  $(T_{90} - T_{48}) / K$  calculated from (7) and from the equation (85) of [11].

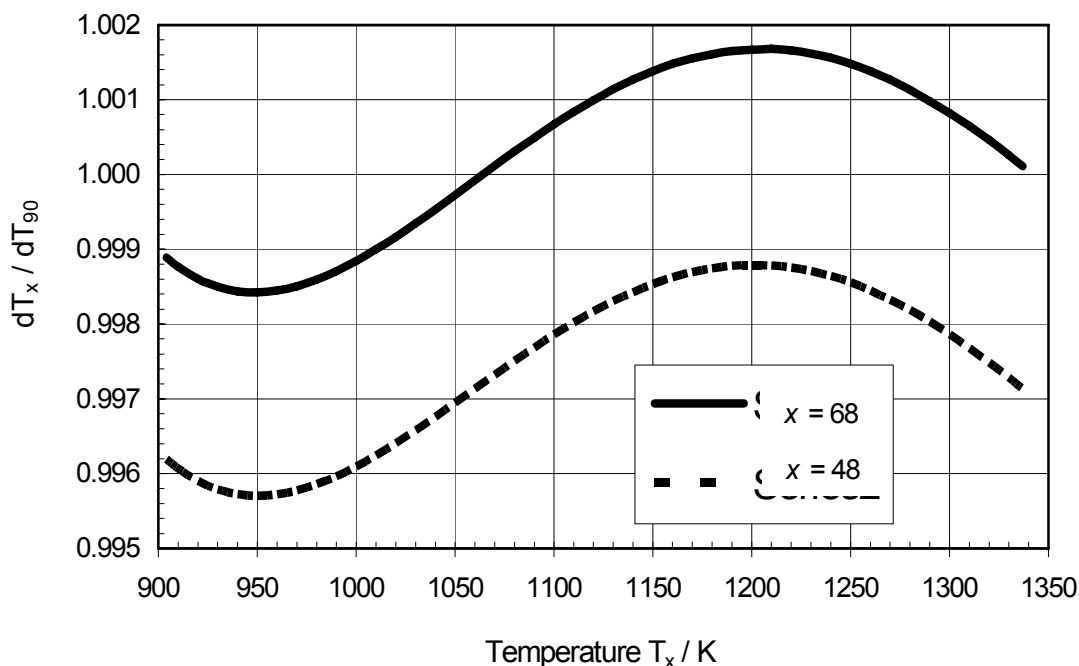


FIG. 3. Temperature derivatives [15]:  $dT_{68}/dT_{90}$  calculated from the derivative equation (7) and  $dT_{48}/dT_{90}$  calculated from the derivative equation (7) and equation (86) of [11].

#### 4.2.6. General recommendations

For a critical evaluation of temperature dependent high accurate property data the following procedure is recommended:

- Read carefully the particular document, assess the accuracy of reported data and determine the temperature scale that the author used.
- For measurements carried out before 1930 there may appear a problem in determination of the temperature scale. Then an investigator may use other techniques, e.g. comparing values for a given property, which is a reasonable approach, if the differences in property value are caused primarily by the difference in the temperature scale.
- Use the appropriate temperature conversion tables (1927→1948), (1948→1968), (1968→1990) or appropriate conversion equations, if available. A user should take into consideration the revised tables of temperature differences ( $t_{90} - t_{68}$ ) and corresponding revised equation, which have been published for the range 630°C to 1064°C [12]. In this temperature range the largest change occurs at 760°C, where the formerly tabulated difference 0.36°C is now 0.04°C.

## REFERENCES TO SECTION 4.2

- [1] HUST, J.G., A compilation and historical review of temperature scales differences. Cryogenics 9, No.12 (1969) 443-455.
- [2] THOMSON, K. (Lord Kelvin), On an absolute thermometric scale founded on Cartont's theory of the motive power of heat, and calculated from Regnault's observations. Proc. Cambridge Phil. Soc. June 1848.
- [3] BURGESS, G.K., Bureau of Standards Journal of Research 1(1928) 635, Research Report 22.

- [4] STIMSON, H.F., The International Temperature Scale of 1948. Jour. of Res. NBS 42 (1949) 209-217, Research Paper RP 1962.
- [5] STIMSON, H.F., In: Temperature, its measurement and control in science and industry Vol. 3. Part 1, 59-66 (Renumber 4a to 5 etc.)
- [6] The International Practical temperature Scale of 1968. Metrologia 5 (1969) 35, also NPL: The International Practical Temperature Scale of 1968. National Physical Laboratory, Ministry of Technology. London HMSO 1969.
- [7] PRESTON, Thomas H., The International Temperature Scale of 1990 (ITS-90). Metrologia 27 (1990) 3-10.
- [8] RUSBY, R.L. et al., Thermodynamic bases of the ITS-90. Metrologia 28 (1991) 9-18.
- [9] CORRUCINI, J.R.: J. Res. NBS 43 (1949) 133-136.
- [10] Relationship between the IPTS-68 and NBS-55, NPL-61, PRIM-54 and PSU-54 temperature scales in the range from 13.81 to 90.188 K. Metrologia 5 (1969) 47.
- [11] DOUGLAS, T. B., Conversion of existing calorimetrically determined thermodynamic properties to the bases of the International Practical Scale of 1968. Jour. of Res. NBS - A: Physics and Chemistry, 73A, No.5, (1969) 451 - 470.
- [12] RUSBY, R.L. et al., Revised values for (t<sub>90</sub> - t<sub>68</sub>) from 630°C to 1064°C . Metrologia 31 (1994), 149-153.
- [13] RUSBY, R.L., The conversion of thermal reference values to the ITS-90. Jour. Chem. Thermodynamics 23 (1991) 1153-1161.
- [14] WEIR, Ron D., GOLDBERG, R.N., On the conversion of thermodynamic properties to the bases of the International Temperature Scale of 1990. Jour. Chem. Thermodynamics 28 (1996) 261-276.
- [15] MARES, R., SIFNER, O., Temperature Conversion of Coefficient of Thermal Conductivity Proceedings of the University of West Bohemia in Pilsen (2003).

## 5. SUMMARY OF DATA USED IN ASSESSMENT

Table 1 lists a summary of the assessments completed in the CRP, which includes new data and previous unpublished data. New data are data obtained from new measurements during the CRP and contributed for the assessment, which are marked by an asterisk. Unpublished data are marked with two asterisks. Those are data, which were made available for the assessment by the various countries, but were not published in the open literature. Table 1 also identifies the thermo-physical property as well as the organizations who carried out the assessments and peer-reviews.

Table 1. Summary of assessments and peer reviews performed during the CRP, including new data and previously unpublished data

MATERIAL	PROPERTIES	ASSESSMENT	PEER REVIEW	REMARK
UO <sub>2</sub>	Enthalpy & Heat capacity (solid)	Fink	AECL	
	Emissivity & Optical constants	Fink	AECL	
	Thermal expansion (solid)	Fink	AECL	
	Enthalpy & Heat capacity (liquid)	Fink	AECL	
	Enthalpy of Fusion	Fink	AECL	
	Thermal Conductivity & Diffusivity (liquid)	Fink	AECL	
	Thermal Conductivity & Diffusivity (solid)	Fink	AECL	
	Density (Liquid)	Fink	AECL	
	Thermal expansion coeff. (liquid)	Fink	AECL	
	Density (solid)	Fink	AECL	
	Surface tension & surface energy	Fink	AECL	
	Melting point	Fink	AECL	
	Viscosity (liquid)	Fink	AECL	
	Vapor pressure	Fink	AECL	
Irradiated UO <sub>2</sub>	Thermal Conductivity	HYU	AECL	
(U,Gd)O <sub>2</sub>	Heat capacity (solid) Thermal conductivity (solid) Thermal expansion (solid)	NPIC	Fink, BARC	New data (NPIC) New data (NPIC) New data (NPIC)
ThO <sub>2</sub> , (Th <sub>1-y</sub> U <sub>y</sub> )O <sub>2</sub> and (Th <sub>1-y</sub> Pu <sub>y</sub> )O <sub>2</sub>	Melting point of ThO <sub>2</sub>	BARC	Fink, CEA	New data (BARC)
	Density of ThO <sub>2</sub> and (Th,U)O <sub>2</sub>	BARC	Fink, CEA	
	Enthalpy increments and heat capacities of ThO <sub>2</sub> and (Th <sub>y</sub> U <sub>1-y</sub> )O <sub>2</sub>	BARC	Fink, CEA	
	Thermal conductivity of (Th <sub>1-y</sub> U <sub>y</sub> )O <sub>2</sub> fuels	BARC	Fink, CEA	New data (BARC)
	Thermal conductivity of (Th <sub>1-y</sub> Pu <sub>y</sub> )O <sub>2</sub>	BARC	Fink, CEA	New data (BARC)
	Thermal expansion of ThO <sub>2</sub> -UO <sub>2</sub> and ThO <sub>2</sub> -PuO <sub>2</sub>	BARC	Fink, CEA	New data (BARC)
Zircaloy	Heat capacity	Fink	AECL	Unpublished data (AECL)
	Viscosity	Fink	AECL	Unpublished data (AECL)
	Zircaloy-4(O) solidus temperatures	Fink	AECL	
	Thermal conductivity	Fink	AECL	
	Thermal expansion	Fink	AECL	

(continued)

MATERIAL	PROPERTIES	ASSESSMENT	PEER REVIEW	REMARK
Zirconium	Surface tension Thermal conductivity(liquid zirconium) Viscosity(zirconium) Enthalpy & Heat capacity Enthalpy of fusion	Fink Fink  Fink IHED Fink	AECL AECL  AECL Fink AECL	New data (IHED)
Zr-1%Nb	Thermal conductivity	Fink	AECL,IPPE	New data(IPPE)
Zr-2.5%Nb	Thermal conductivity	IPPE	AECL,Fink	Unpublished data (IHED,AECL,NPIC)
Hafnium	Thermal expansion Enthalpy & Heat capacity Emissivity	IHED IHED IHED	Fink,CEA Fink,CEA Fink,CEA	New data(IHED)
Hafnium dioxide	Enthalpy & Heat capacity	BARC	Fink,CEA	
Russian steel	Solids/Liquids temperature Enthalpy Density Thermal conductivity Thermal Diffusivity Specific heat Thermal expansion	IPPE IPPE IPPE IPPE IPPE IPPE	Fink,SNU Fink,SNU Fink,SNU Fink,SNU Fink,SNU	Unpublished data (IPPE)
Alloy 600 & 800	Thermal conductivity	AECL	Fink	Unpublished data(AECL)
Light & Heavy water	Viscosity Thermal conductivity Dielectric constant Refractive index Surface tension	UWB	AECL	
Corium	Density Thermal conductivity Viscosity	CEA	AECL	

- [1] New data are data, obtained from new measurements during the CRP and contributed for the assessment.
- [2] Unpublished data are data which were made available for assessment but were not published in open literature.

## 6. THERMO-PHYSICAL PROPERTIES OF MATERIALS

### 6.1. Fuel materials

#### 6.1.1. Uranium dioxide (UO<sub>2</sub>)

##### 6.1.1.1. Enthalpy and heat capacity of solid UO<sub>2</sub>

##### *Summary and recommended equations*

Recommended equations for the enthalpy and heat capacity of solid UO<sub>2</sub> are based on a combined analysis of the available enthalpy data [1–6] from 483 to 3100 K, the heat capacity data from 293 to 1006 K [7–8] and the heat capacity data from 1997–2873 K from recent measurements by Ronchi et al.[9]. Heat capacity data reported by Affortit and Marcon [10], Affortit [11], Popov et al. [12] and Engel [13] were not included in the combined fit because the data which they reported was not in agreement with the consensus and showed systematic errors. Although the  $\lambda$ -phase transition at 2670 K has been confirmed by high-temperature neutron diffraction and scattering experiments reported by Hutchings et al. [14–15] and by thermal analysis of UO<sub>2+x</sub> cooling curves from 2300 to 3000 K by Hiernaut et al. [16], single equations for the enthalpy and heat capacity are recommended from 298 to 3120 K to provide the best fit to the high-temperature heat capacity data of Ronchi et al. Heat capacity data above and below the  $\lambda$ -phase transition show similar temperature behavior. The best fit to the enthalpy data was obtained with the equation:

for  $298.15 \text{ K} \leq T \leq 3120 \text{ K}$

$$\begin{aligned} H(T) - H(298.15 \text{ K}) = & C_1 \theta \left[ (e^{\theta/T} - 1)^{-1} - (e^{\theta/298.15} - 1)^{-1} \right] \\ & + C_2 \left[ T^2 - (298.15)^2 \right] \\ & + C_3 e^{-E_a/T} \end{aligned} \quad (1)$$

where  $C_1 = 81.613$ ,  
 $\theta = 548.68$ ,  
 $C_2 = 2.285 \times 10^{-3}$ ,  
 $C_3 = 2.360 \times 10^7$ ,  
 $E_a = 18531.7$ ,

T is the temperature in K and the enthalpy increment,  $H(T) - H(298.15 \text{ K})$ , is in  $\text{J} \cdot \text{mol}^{-1}$ .

The temperature derivative of Eq.(1) gives the heat capacity,  $C_p$ , in  $\text{J} \cdot \text{mol}^{-1} \cdot \text{K}^{-1}$ :

for  $298.15 \text{ K} \leq T \leq 3120 \text{ K}$

$$C_p = \frac{C_1 \theta^2 e^{\theta/T}}{T^2 (e^{\theta/T} - 1)^2} + 2 C_2 T + \frac{C_3 E_a e^{-E_a/T}}{T^2} \quad (2)$$

where the constants are identical to those for Eq.(1). The enthalpy data were fit with the 7-term polynomial:

for  $298.15 \text{ K} \leq T \leq 3120 \text{ K}$

$$\begin{aligned} H(T) - H(298.15 \text{ K}) = & -21.1762 + 52.1743 \tau + 43.9753 \tau^2 \\ & - 28.0804 \tau^3 + 7.88552 \tau^4 - 0.52668 \tau^5 \\ & + 0.71391 \tau^{-1} \end{aligned} \quad (3)$$

where  $\tau = T/1000$ , T is the temperature in K, and the enthalpy increment,  $H(T) - H(298.15 \text{ K})$ , is in  $\text{kJ} \cdot \text{mol}^{-1}$ . The corresponding heat capacities were calculated from the temperature derivative of Eq.(3), which is:



$$C_p(T) = +52.1743 + 87.951\tau - 84.2411\tau^2 + 31.542\tau^3 - 2.6334\tau^4 - 0.71391\tau^{-2} \quad (4)$$

for  $298.15 \text{ K} \leq T \leq 3120 \text{ K}$

where  $\tau = T/1000$ ,  $T$  is the temperature in K, and the heat capacity,  $C_p$ , is in  $\text{J} \cdot \text{mol}^{-1} \cdot \text{K}^{-1}$ .

The enthalpy values from these two fits agree within 0.5% and cannot be distinguished in the graph in Figure 1, which compares these fits with the enthalpy data. Figure 2, which compares the heat capacity data with values calculated from Eq. (2) and Eq. (4), shows that the values obtained from these two equations are almost identical. They deviate by at most 1%, which is less than the scatter in the data. The  $\lambda$ -phase transition at 2670 K has been included in Figure 2. Because the fits by both functional forms are almost identical both equations are recommended. However, because the individual terms of Eq.(1–2) are not related to the contributions from the physical processes, which can now be calculated from first principles [17, 18] and because polynomial forms are simpler for inclusion in large computer codes that are used in reactor-safety calculations, the polynomials given in Eqs (3–4) may be preferred. Recommended values of the enthalpy and heat capacity calculated from Eqs (1) and (2) are tabulated as a function of temperature in Table 1. Values calculated using the polynomial equations, Eq.(3) and Eq.(4), are tabulated in Table 2. Table 3 gives values per kg of  $\text{UO}_2$  obtained from Eqs (1) and (2). Table 4 gives values per kg of  $\text{UO}_2$  obtained from the polynomial equations, Eq.(3) and Eq.(4).

### ***Uncertainties***

The uncertainty in the recommended enthalpy increments is  $\pm 2\%$  from 298.15 K to 1800 K and  $\pm 3\%$  from 1800 K to the melting point (3120K). The heat capacity uncertainty is  $\pm 2\%$  from 298.15 to 1800 K;  $\pm 13\%$  from 1800 to 3120 K. These uncertainties, shown in Figure 2, are based on the scatter in the data and the percent deviations of the data from the recommended equations. Because no attempt has been made to calculate the heat capacity peak in the vicinity of the  $\lambda$ -phase transition, as was done in the detailed analysis by Ronchi and Hyland [17], the heat capacity equation and uncertainties are not valid for temperatures close to the phase transition.

Table 1. Enthalpy and heat capacity of  $\text{UO}_2$  per mole of  $\text{UO}_2$  calculated from equations (1) and (2)

TEMPERATURE K	ENTHALPY $H(T)-H(298.15\text{ K})$ kJ/mol	HEAT CAPACITY $C_p$ J/(mol K)
298.15	0.00	63.4
300	0.12	63.6
400	6.93	71.8
500	14.3	76.2
600	22.1	78.9
700	30.1	80.8
800	38.2	82.1
900	46.5	83.2
1000	54.9	84.2
1100	63.3	85.0
1200	71.9	85.7
1300	80.5	86.5
1400	89.2	87.4
1500	98.0	88.4
1600	106.9	89.7
1700	115.9	91.5
1800	125.2	93.8
1900	134.7	96.8
2000	144.6	100.6
2100	154.9	105.3
2200	165.7	111.1
2300	177.1	117.9
2400	189.3	125.9
2500	202.3	134.9
2600	216.3	145.1
2700	231.4	156.4
2800	247.6	168.6
2900	265.2	181.9
3000	284.0	196.0
3100	304.4	210.9
3120	308.6	214.0

Table 2. Enthalpy and heat capacity of  $\text{UO}_2$  per mole of  $\text{UO}_2$  calculated from polynomial equations (3) and (4)

TEMPERATURE  K	ENTHALPY H(T)-H(298.15 K)  kJ/mol	HEAT CAPACITY Cp  J/(mol K)
298.15	0.00	63.7
300	0.12	63.9
400	6.91	71.4
500	14.3	76.0
600	22.1	79.1
700	30.1	81.2
800	38.3	82.6
900	46.6	83.5
1000	55.0	84.1
1100	63.4	84.5
1200	71.9	85.0
1300	80.4	85.5
1400	89.0	86.3
1500	97.7	87.4
1600	106.5	88.9
1700	115.5	91.0
1800	124.7	93.6
1900	134.2	97.0
2000	144.1	101.1
2100	154.5	106.1
2200	165.4	112.0
2300	176.9	118.8
2400	189.1	126.6
2500	202.2	135.4
2600	216.3	145.3
2700	231.3	156.3
2800	247.6	168.4
2900	265.1	181.7
3000	283.9	196.1
3100	304.3	211.7
3120	308.6	214.9

Table 3. Enthalpy and heat capacity of  $\text{UO}_2$  per kg of  $\text{UO}_2$  calculated from equations (1) and (2)

TEMPERATURE  K	ENTHALPY H(T)-H(298.15 K)  kJ/kg	HEAT CAPACITY Cp J/(kg K)
298.15	0.00	235
300	0.43	235
400	25.7	266
500	53.1	282
600	81.9	292
700	111	299
800	142	304
900	172	308
1000	203	312
1100	235	315
1200	266	318
1300	298	320
1400	330	324
1500	363	327
1600	396	332
1700	429	339
1800	464	347
1900	499	358
2000	535	373
2100	574	390
2200	614	411
2300	656	437
2400	701	466
2500	749	500
2600	801	537
2700	857	579
2800	917	625
2900	982	674
3000	1052	726
3100	1127	781
3120	1143	792

Table 4. Enthalpy and heat capacity of  $\text{UO}_2$  per kg of  $\text{UO}_2$  calculated from polynomial equations (3) and (4)

TEMPERATURE  K	ENTHALPY H(T)-H(298.15 K)  kJ/kg	HEAT CAPACITY Cp  J/(kg K)
298.15	0.00	236
300	0.44	237
400	25.6	264
500	53.0	281
600	81.7	293
700	111	301
800	142	306
900	173	309
1000	204	311
1100	235	313
1200	266	315
1300	298	317
1400	330	319
1500	362	324
1600	394	329
1700	428	337
1800	462	347
1900	497	359
2000	534	375
2100	572	393
2200	612	415
2300	655	440
2400	700	469
2500	749	501
2600	801	538
2700	857	579
2800	917	624
2900	982	673
3000	1052	726
3100	1127	784
3120	1143	796

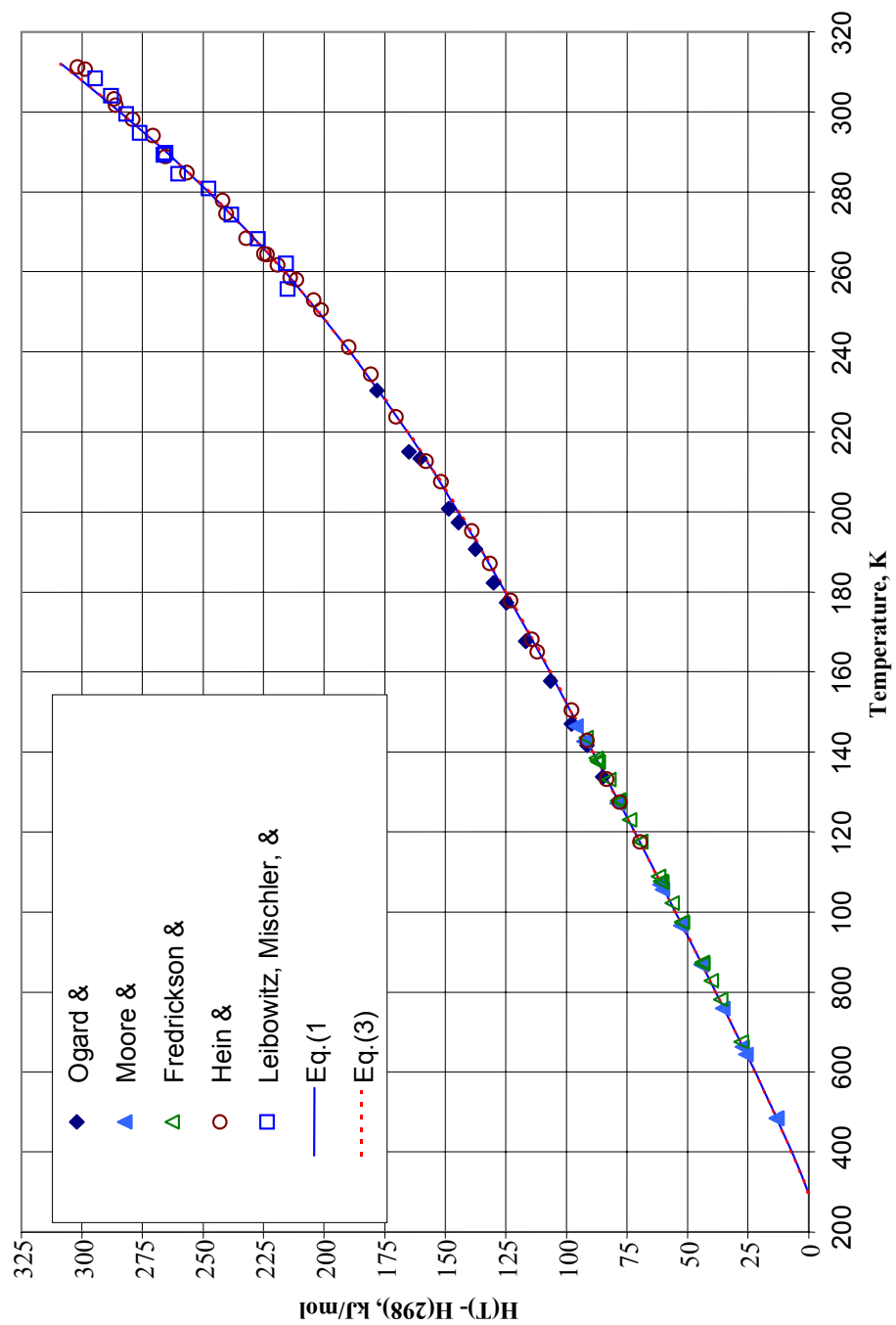


FIG. 1. Enthalpy of solid  $\text{UO}_2$

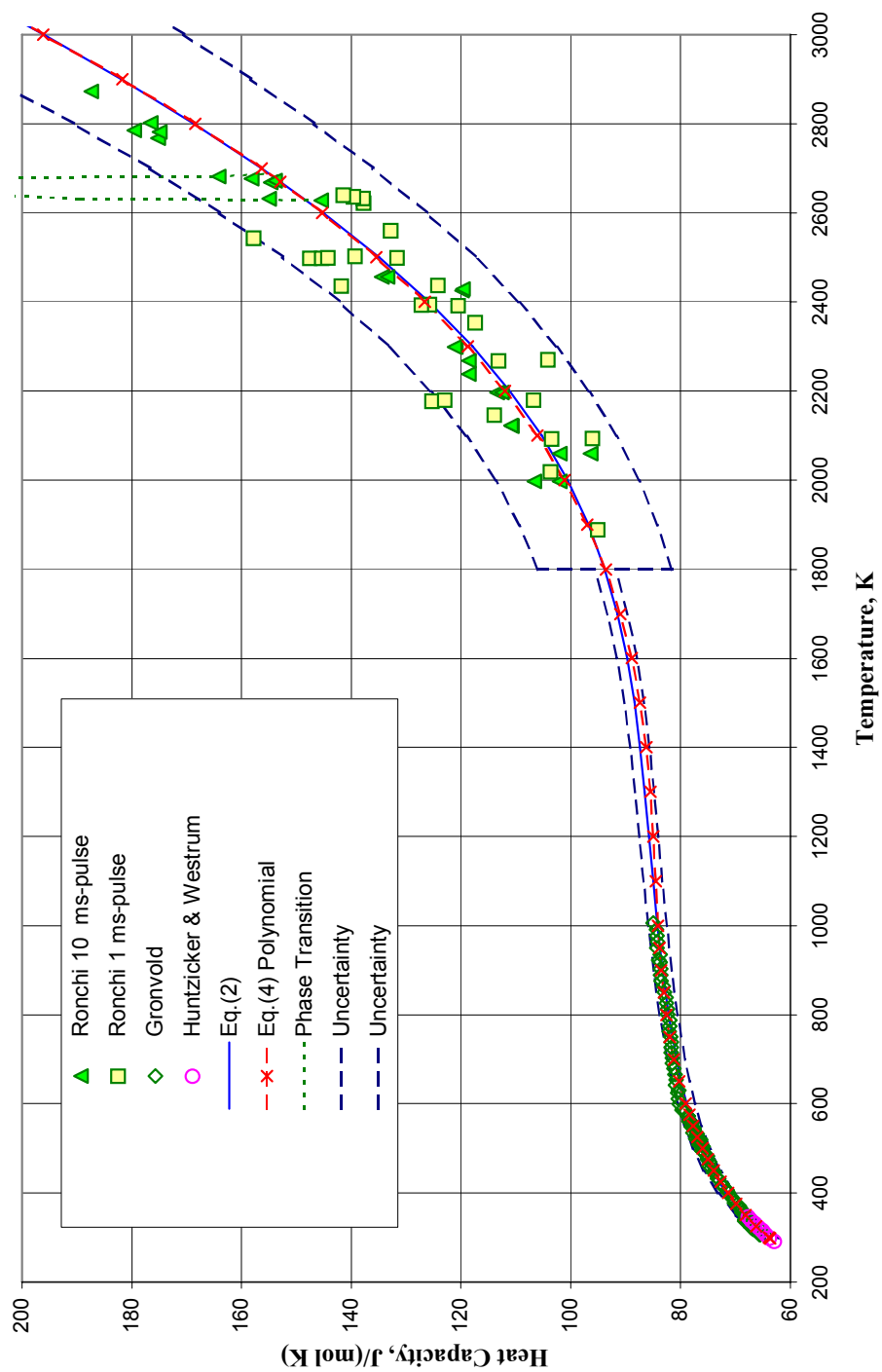


FIG. 2. Heat capacity of  $UO_2$

## Discussion

### Background and theory

The existence of the  $\lambda$ -phase transition in solid  $\text{UO}_2$  at 2670 K that had been suggested by Bredig [19] and included in the enthalpy equations recommended by Fink [20, 21] and of Harding et al. [22] has been confirmed by Hutchings et al. [14, 15] using neutron scattering experiments to study the oxygen defects and by Hiernaut et al. [16] from the analysis of cooling curves of  $\text{UO}_{2\pm x}$ . Hiernaut et al. [16] reported a  $\lambda$ -phase transition at  $2670 \pm 30$  K in  $\text{UO}_{2.00}$  and developed a model for the transition as a function of stoichiometry and temperature.

High-temperature neutron diffraction and inelastic scattering experiments on  $\text{UO}_2$  and  $\text{ThO}_2$  at temperatures from 293 to 2930 K reported by Hutchings et al. [14, 15] provide direct evidence for thermally induced Frenkel oxygen lattice disorder at temperatures above 2000 K. The disorder has been identified as dynamic Frenkel type similar to that in halide fluorites with a Frenkel pair formation energy of  $4.6 \pm 0.5$  eV. Hutchings [15] suggests that the high oxygen vacancy concentrations and their mobility at high temperatures may be related to the observed high creep rate [23] and softening or plasticity of  $\text{UO}_2$  above 2500 K. He also reported that inelastic magnetic scattering on lowest magnetic energy levels of  $\text{U}^{4+}$  indicate that excitation of these levels make a significant contribution to the heat capacity in  $\text{UO}_2$ .

Hiernaut et al. [16] determined that the transition temperature in nominally stoichiometric  $\text{UO}_{2.00}$  is at  $2670 \pm 30$  K, which is coincident with the transition temperature proposed by Bredig [19] but higher than the 2610 K value proposed by Ralph and Hyland [24]. The scatter in the data of Hiernaut et al. was approximately twice the precision of the temperature measurement. The transition was identified as a first-order phase transition from cooling curves in the temperature range of 2300 to 3000 K. The transition temperature for substoichiometric urania ( $\text{UO}_{2-x}$ ) increased with increasing  $x$  (i.e. reduction of the sample in a 3% hydrogen atmosphere) and the cooling curves exhibit undercooling indicative of a first-order transition. No transition was detected in  $\text{UO}_{2+x}$ .

Hiernaut et al. [16] found that the phase transition in stoichiometric  $\text{UO}_{2.00}$  was consistent with that in stoichiometric non-actinide fluorites (e.g.  $\text{SrCl}_2$ ), where the high-temperature phase is established rapidly but continuously. They modeled the  $\lambda$ -like phase transition in  $\text{UO}_{2.00}$  as a second-order transition involving oxygen Frenkel disorder. Their model is consistent with the second-order  $\lambda$ -transition in  $\text{UO}_{2.00}$  converting to a first-order phase transition in  $\text{UO}_{2-x}$ . Although no transition was detected in  $\text{UO}_{2+x}$ , their model is consistent with a second-order transition that decreases with increasing  $x$  from  $T=2670$  K at  $x = 0$  to cross the  $\text{U}_4\text{O}_9$  phase boundary near 973 K, where a diffuse order-disorder transition is observed in the  $\text{U}_4\text{O}_9$  oxygen sublattice. They suggest that the second-order  $\lambda$ -transition in  $\text{UO}_{2.00}$  is the stoichiometric counterpart of the interstitial superlattice transition in  $\text{U}_4\text{O}_9$ . Hiernaut et al. [16] conclude that they did not detect a transition in  $\text{UO}_{2+x}$  because the transition rapidly decreases in peak height and increases in peak width with  $x$ . Based on their experimental results and their model, they have modified the U-O phase diagram to include these transitions.

From interpretation of these experimental data, Ronchi and Hyland [17] calculated the contributions from each process to compare with available data and provided an excellent description of the theoretical understanding of the contributions from each physical process to the heat capacity. The dominant contributions in each of four temperature intervals for the solid discussed in detail by Ronchi and Hyland [17] are summarized below.

- 1) From room temperature to 1000 K, the increase in heat capacity is governed by the harmonic lattice vibrations, which may be approximated by a Debye model. By 1000 K, this contribution becomes constant. A smaller contribution is provided by thermal excitation of localized electrons of  $\text{U}^{4+}$  ( $5f$ )<sup>2</sup> in the crystal field levels. This crystal field contribution is proportional to  $T$  at low temperatures but becomes temperature independent at high temperatures where the concentration of  $\text{U}^{4+}$  decreases as the concentrations of  $\text{U}^{3+}$  and  $\text{U}^{5+}$  increase;
- 2) From 1000 to 1500 K, the heat capacity increases due to increases in the anharmonicity of the lattice vibrations as evidenced in the thermal expansion. This contribution has been previously referred to as the thermal expansion or dilation contribution;



- 3) From 1500 to 2670 K, the increase in heat capacity is due to formation of lattice and electronic defects. The peak in the heat capacity at 2670 K (85.6% of the melting point) has been attributed to Frenkel defects both from theoretical considerations and neutron scattering measurements of the oxygen defect concentration as a function of temperature. A similar discontinuity and anion behavior was observed for ThO<sub>2</sub> [14, 15]. Harding et al. [22] comment that because no excess enthalpy is evident in ThO<sub>2</sub> below the corresponding transition, it is reasonable to suggest that the increase in UO<sub>2</sub> below the phase transition is due to coupling between electronic disorder and Frenkel disorder. Ronchi and Hyland [17] point out that the increase in the electrical conductivity in this temperature interval indicates a contribution from electronic defects but the small polaron contribution from electron-hole interactions is minor compared to contributions due to Frenkel defects;
- 4) Above the phase transition temperature, the peak of the heat capacity drops sharply due to rapid saturation of the defect concentration. From 2700 K to the melting point, Schottky defects become important.

#### *Review and analysis of experimental data*

Recently, Ronchi et al. [9] made simultaneous measurements of the heat capacity and thermal diffusivity from 2000 to 2900 K. Although these measurements lacked the sensitivity required to detect the phase transition peak, they showed that above the  $\lambda$ -phase transition, the heat capacity has a temperature dependence that is similar to that prior to the phase transition. Figure 3 shows that the heat capacity data of Ronchi et al. [9] at temperatures higher than the  $\lambda$ -phase transition are inconsistent with the constant heat capacity that was recommended by Fink et al. [20, 21] and by Harding et al. [22], and with the theoretical calculation of Ronchi and Hyland [17]. The heat capacity equation in the MATPRO database [25], also shown in Figure 3, does not provide a good representation of these high-temperature data even though this equation gives heat capacity values that increase with temperature. Therefore, all available heat capacity and enthalpy data for solid UO<sub>2</sub> have been reviewed and a combined analysis of enthalpy and heat capacity data has been made to obtain equations for the enthalpy increments and heat capacities that are consistent with each other and with the experimental data.

Comparison of the available enthalpy data, shown in Figure 1, indicates that the data from 1174 to 3112 K of Hein and Flagella [3, 4] are in good agreement with the data of Leibowitz, Mishler and Chasanov [1] from 2561 to 3088 K and with the data of Fredrickson and Chasanov [2] from 674 to 1436 K. Data given by Hein, Sjodahl and Szwarc [4] is identical to that reported by Hein and Flagella [3]. Data reported by Conway and Hein [26] in 1965 are preliminary results of the data published in 1968. Therefore, these preliminary data have not been included in this analysis. The 1947 measurements by Moore and Kelley [5] from 483 to 1464 K tend to be slightly high relative to the data of Fredrickson and Chasanov [2]. The data of Ogard and Leary (from 1339 to 2306 K) [6] are consistently high relative to the data of Hein and Flagella [3] and that of Fredrickson and Chasanov [2].

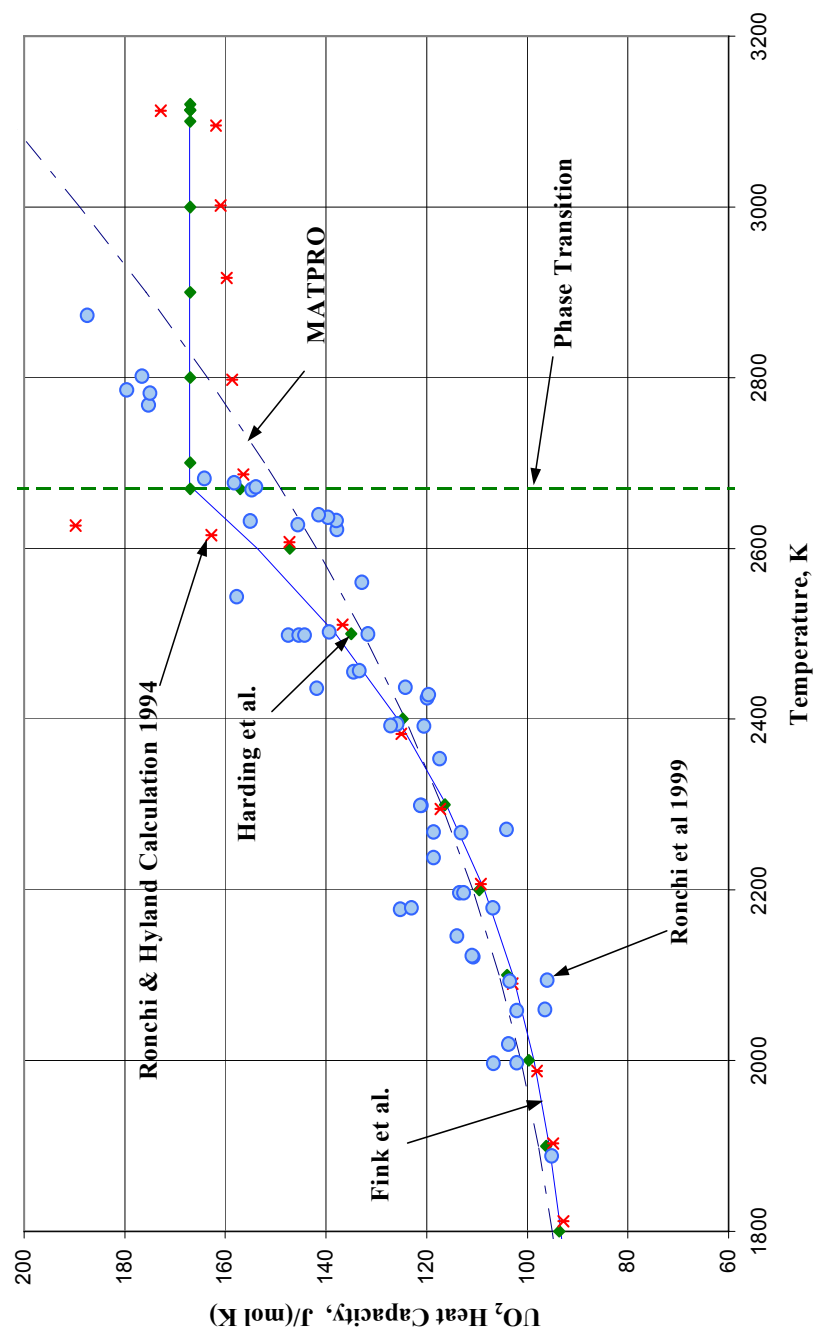


FIG. 3.  $UO_2$  heat capacity data of Ronchi et al. compared with equations.

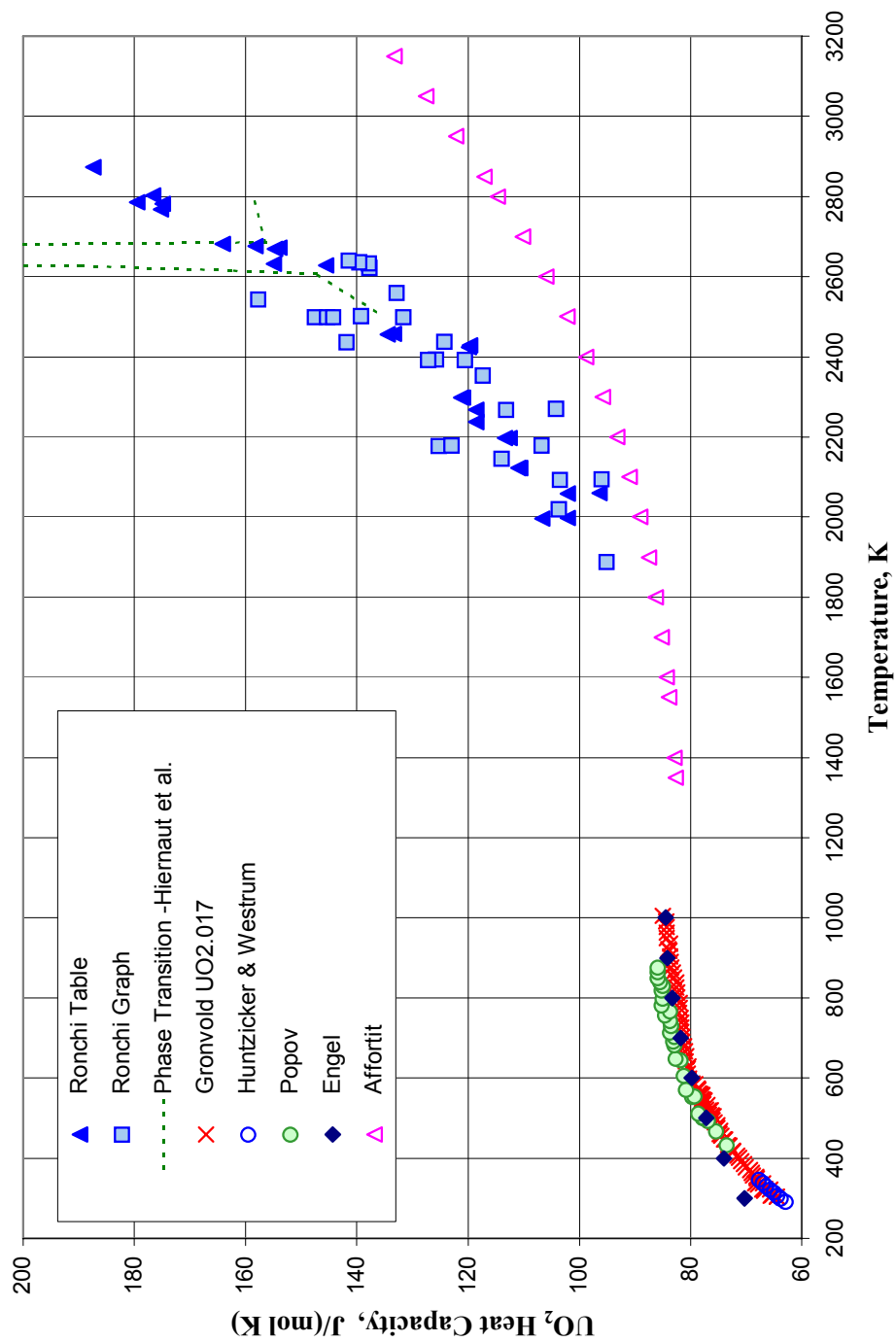


FIG. 4. Solid  $\text{UO}_2$  heat capacity data.

Figure 4 shows all the available heat capacity data. The heat capacity data of Affortit and Marcon [10] and of Affortit [11], that are labeled “Affortit” in Figure 4, clearly disagree with other data. Therefore these data were not included in the combined analysis. The variances (square of the standard deviations) of these data from a smooth curve through all the data are 100 to 1000 times larger than variances of data included in the analysis. Figure 5, which shows the low-temperature heat capacity data, indicates that the heat capacity data from 5 to 346 K of Hunzicker and Westrum [7] and that of Gronvold et al. [8] (304-1006 K) are in good agreement in the temperature range of overlap. However, between 500 and 800 K, the data of Gronvold et al. [8] are high because of contamination of the sample by  $U_4O_9$ . Data from 433 to 876 K of Popov et al. [12] were excluded from the combined analysis because they are consistently higher than the data of Gronvold et al. Figure 5 shows that the data of Engel [13] (300 to 1000 K) appear to have a systematic error because they differ from other data by a normalization. Thus the data of Engel have not been included in the combined analysis. The variances for the data of Popov et al. and that of Engel from a smoothed curve through all the data are about a factor of 20 higher than the variances for data included in this analysis.

A combined fit of the enthalpy and heat capacity data [1-9], which are listed in Table 5, has been made using a nonlinear weighted  $\chi^2$  minimization procedure. Data from each experiment was weighted by the inverse of the square of the standard deviation of that set of data from a smooth curve through all the data in that temperature range. The smooth curves used for the enthalpy data and the low-temperature heat capacity data were those defined by the polynomials of Harding et al. [21], which are identical with the values from the equations of Fink et al. [19,20]. For the two sets of data of Ronchi et al. [9], the standard deviations from the curve given by Ronchi et al. were used to determine appropriate weights. The temperatures of data obtained prior to 1969 were converted from the 1948 International Practical Temperature Scale (IPTS) to the 1968 IPTS.

The combined fits of the enthalpy and heat capacity data were constrained by:

$$H(T) - H(298.15K) = 0 \text{ at } 298.15 \text{ K and}$$

$$(\partial H / \partial T)_P = C_P$$

where  $H(T) - H(298.15K)$  is the enthalpy increment and  $C_P$  is the heat capacity. Some of the functional forms considered are listed in Table 6. Forms included polynomials as well as functional forms that approximated the physical processes that were shown to be important by the theoretical work of Ronchi and Hyland [17]. The lattice term, which was used in the equation of Kerrisk and Clifton [27] and in the low-temperature equation of Fink et al. [20, 21], approximates the harmonic lattice contribution. The  $T^2$  term accounts for the anharmonicity of the lattice as given by dilation. An exponential term,  $C e^{-E/T}$ , and a term with temperature times the exponential,  $C T e^{-E/T}$ , were considered for describing the contributions from defects. Frenkel defects are more appropriately described by the term  $C e^{-E/T}$ . The electronic small polaron contribution is better described by the functional form  $C T e^{-E/T}$ . The combined data were fit better using  $C e^{-E/T}$  to describe the defect contribution, which is consistent with calculations by Ronchi and Hyland [17] that indicated that contributions to the heat capacity due to Frenkel defects are larger than the electronic small polaron contribution.

Browning et al. [18] have commented that the ability to calculate the magnitude of each contribution to the enthalpy from physical principles, as has been done by Ronchi and Hyland [17], makes analysis of the enthalpy data based on a least squares fitting procedures using approximate functional forms obsolete because the fitting procedure does not account for all physical processes and therefore gives values for parameters in each functional term that differ from the known physical values. For example, the Debye and Einstein temperatures of  $UO_2$  are well known and different from the values obtained in such a fitting procedure. However, Browning et al. [18] concur that functional forms that approximate physical processes provide a better fit to the experimental data than do fits using polynomials.

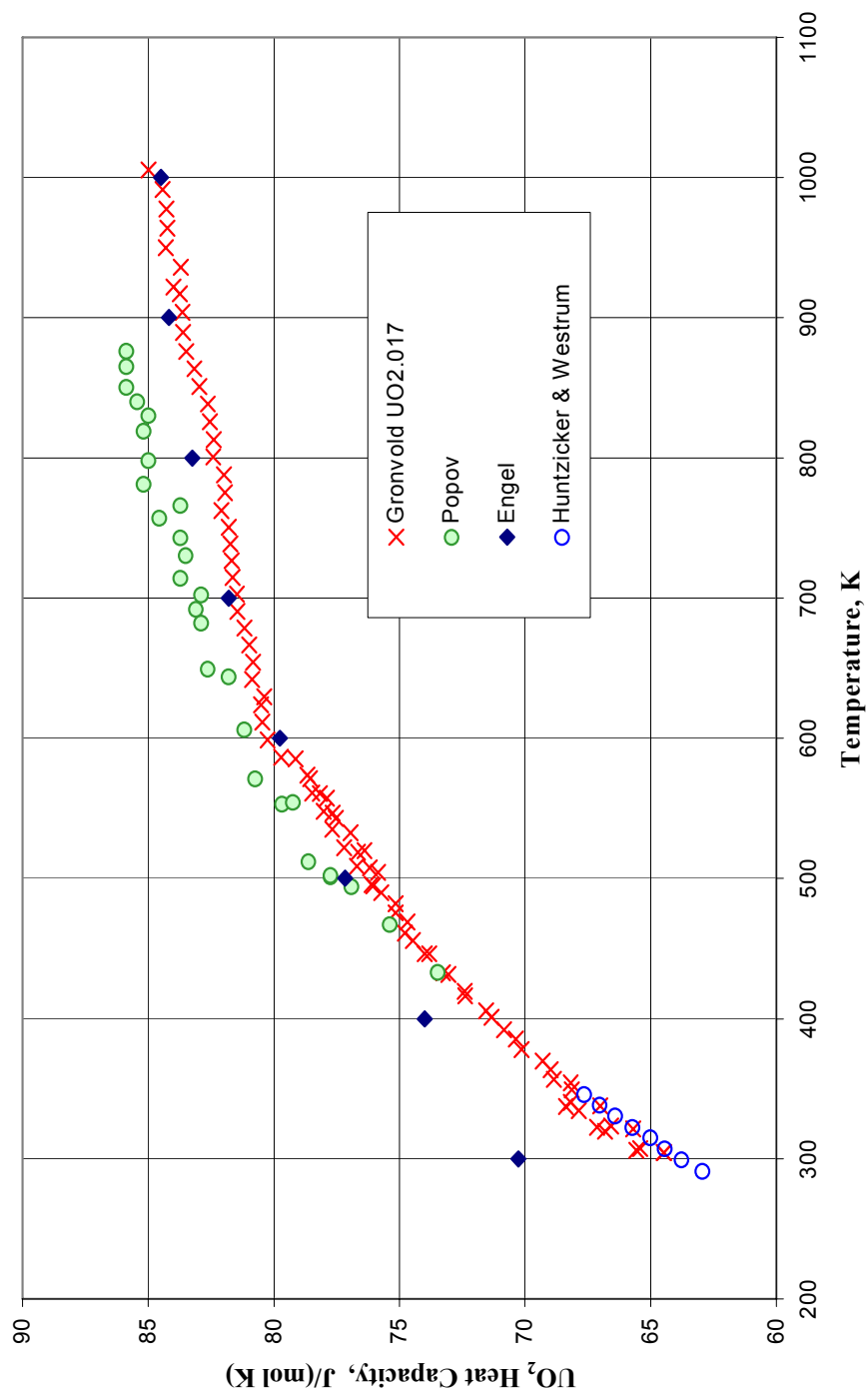


FIG. 5. Low temperature solid  $\text{UO}_2$  heat capacity data.

Table 5. Percent standard deviations of data from the best combined fits of the enthalpy and heat capacity of solid UO<sub>2</sub>

DATA REFERENCE	TEMPERATURE RANGE (K)	N	% STANDARD DEVIATIONS	
			POLYNOMIAL	Eq.(1-2)
Enthalpy				
Ogard & Leary 1968 [6]	1339-2306	13	3.04	2.25
Moore & Kelly 1947 [5]	483-1464	14	1.80	1.50
Fredrickson & Chasanov 1970 [2]	674-1436	24	0.73	0.62
Hein and Flagella 1968 [3,4]	1174-3112	33	0.90	0.86
Leibowitz et al. 1969 [1]	2561-3088	12	1.85	1.60
Heat Capacity				
Huntzicker & Westrum 1971 [7]	293-346	9	0.72	0.57
Gronvold et al. 1970 [8]	304-1006	88	0.64	0.77
Ronchi et al. 1999 [9]	1997-2873	54	5.96	4.58

$$\% \text{ Standard Deviation} = \left( \frac{\sum \left[ \frac{(\text{Fit} - \text{Data})}{\text{Data}} 100\% \right]^2}{N - \text{free parameters}} \right)^{1/2}$$

N = number of data

Table 6. Variances,  $\sigma^2$ , of weighted fits for different equation forms

ENTHALPY FUNCTIONAL FORM	# of PARAMETERS	TOTAL $\sigma^2$	H $\sigma^2$	C <sub>p</sub> $\sigma^2$
Lattice +T <sup>2</sup> + exponential, Eq.(1)	5	0.34	0.25	0.47
Polynomial, Eq.(3)	7	0.32	0.28	0.38
Lattice +T <sup>2</sup> +T exponential	5	0.55	0.40	0.73
T<2670 K: Lattice+T <sup>2</sup> +exponential T>2670K: Quadratic	8	0.36	0.31	0.38
T<2670 K: Lattice+T <sup>2</sup> +exponential T>2670K, quadratic+exponential	10	0.35	0.29	0.45

$$\sigma^2 = \frac{\frac{1}{N - \text{free}} \sum \frac{1}{\sigma_i^2} [y_i - y(T_i)]^2}{\frac{1}{N} \sum \frac{1}{\sigma_i^2}}$$

where N= number of data, free = # of free parameters,  $(1/\sigma_i)^2$  = weight,

$y_i$  = datum,  $y(T_i)$  = fit at temperature  $T_i$

$$\text{Lattice} = \frac{C_1 \theta}{(e^{\theta/T} - 1)}$$

where  $C_1$  and  $\theta$  are parameters.

This combined least squares analysis showed that the combined enthalpy and heat capacity data could not be well fit by a polynomial using the  $\chi^2$  minimization procedure unless the first guess of the coefficients was very close to the final values. The recommended polynomial equation was obtained by using a linear regression to obtain a polynomial approximation to closely spaced enthalpy increments calculated from Eq.(1) and using the terms of that polynomial as a first guess for the nonlinear least squares fit of the enthalpy and heat capacity data

Both single equations for the entire temperature range and two equations (one below and one above the transition at 2670 K) were considered. Table 6, which tabulates the values of the variances for the enthalpy data, the heat capacity data, and the combined enthalpy and heat capacity data for the functional forms evaluated, shows that the use of two equations did not improve the fit to the combined data. The reason for this is clear from examination of the fits to the high-temperature heat capacity data in Figure 6 and the enthalpy data in Figure 7. The linear heat capacity equation that is the best fit to the heat capacity data above 2670 K results in a quadratic equation for the enthalpy increments, which is high relative to the enthalpy data. The heat capacity increase above the  $\lambda$ -phase transition seems inconsistent with the enthalpy data above this transition, because the slope of the enthalpy data above 3000 K is less than the slope below the transition. Further, enthalpy and heat capacity data are needed above the  $\lambda$ -phase transition to resolve this apparent inconsistency. Thus, the best fit to the combined data is a single equation that is a compromise between the best fit to the high-temperature enthalpy data and the best fit to the high-temperature heat capacity data.

Table 6 shows that the smallest total variance was obtained for the 7-term polynomial because it gives the best fit to the low-temperature heat capacity data, which have large weights and a large number of points. However, Eq.(1), containing lattice,  $T^2$ , and exponential terms, fits most data sets better than the polynomial, as shown in Table 5. The variances shown in Table 6 indicate that the best fit to the enthalpy data was with Eq.(1). The enthalpy values from these two fits agree within 0.5% and cannot be distinguished in the graph in Figure 1. The closeness of these two fits to the enthalpy data is indicated by the percent deviations of the enthalpy data from each equation, which are plotted in Figure 8. The percent deviation is defined as:

$$\% \text{ Deviation} = \frac{(\text{Equation} - \text{Data})}{\text{Data}} 100\%$$

Figure 2, which compares the heat capacity data with values calculated from Eq.(2) and Eq.(4), shows that the values obtained from these two equations are almost identical. They deviate by at most 1%, which is less than the scatter in the data, as shown by the deviation plot in Figure 9. Because the fits by both functional forms are almost identical both equations are recommended. However, because the individual terms of Eq.(1–2) are not related to the contributions from the physical processes, which can now be calculated from first principles [17,18] and because polynomial forms are simpler for inclusion in large computer codes that are used in reactor-safety calculations, the polynomials given in Eqs (3–4) may be preferred.

0 K

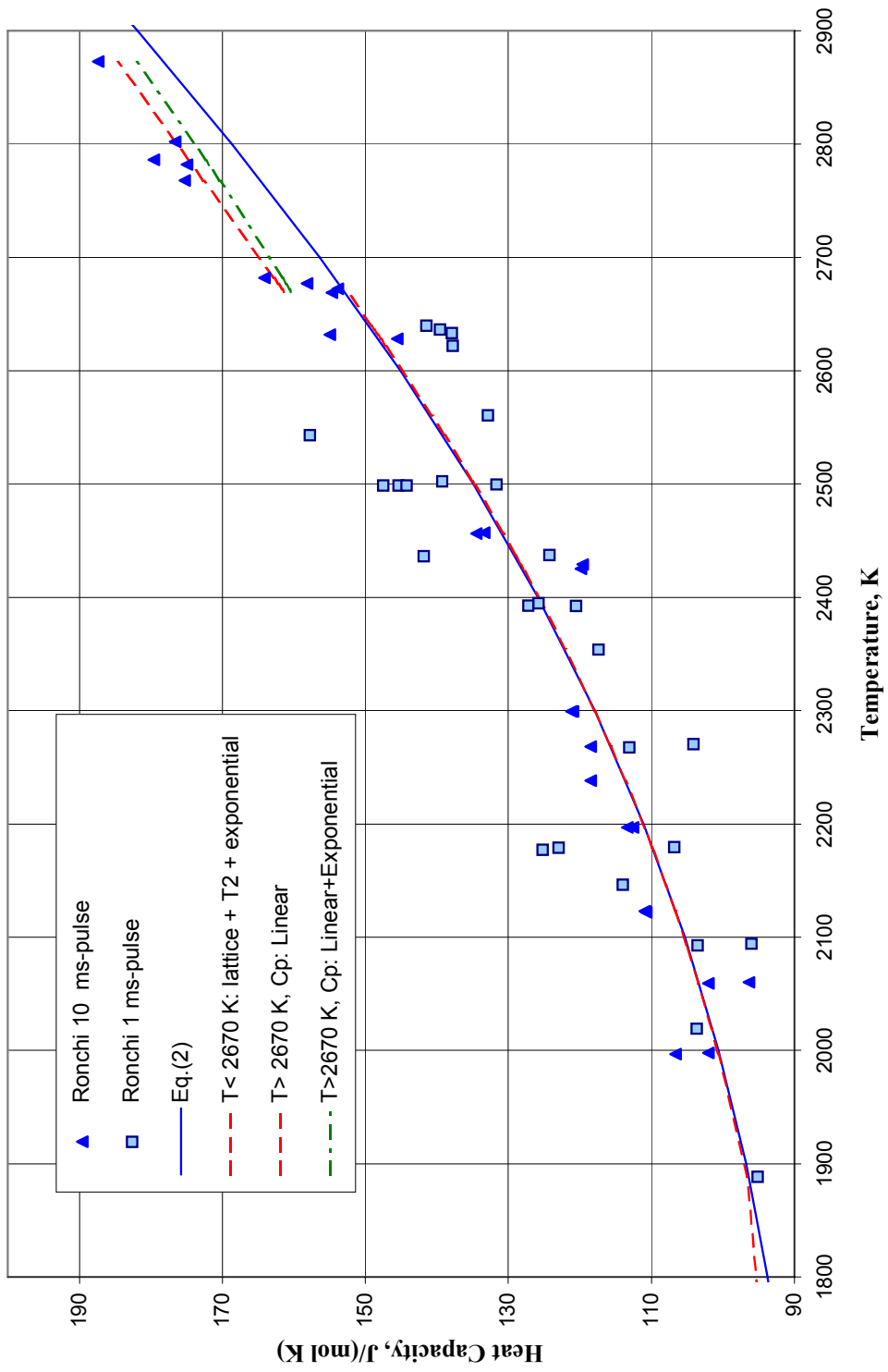


FIG. 6.  $UO_2$  heat capacity forms with and without break at 2670 K.



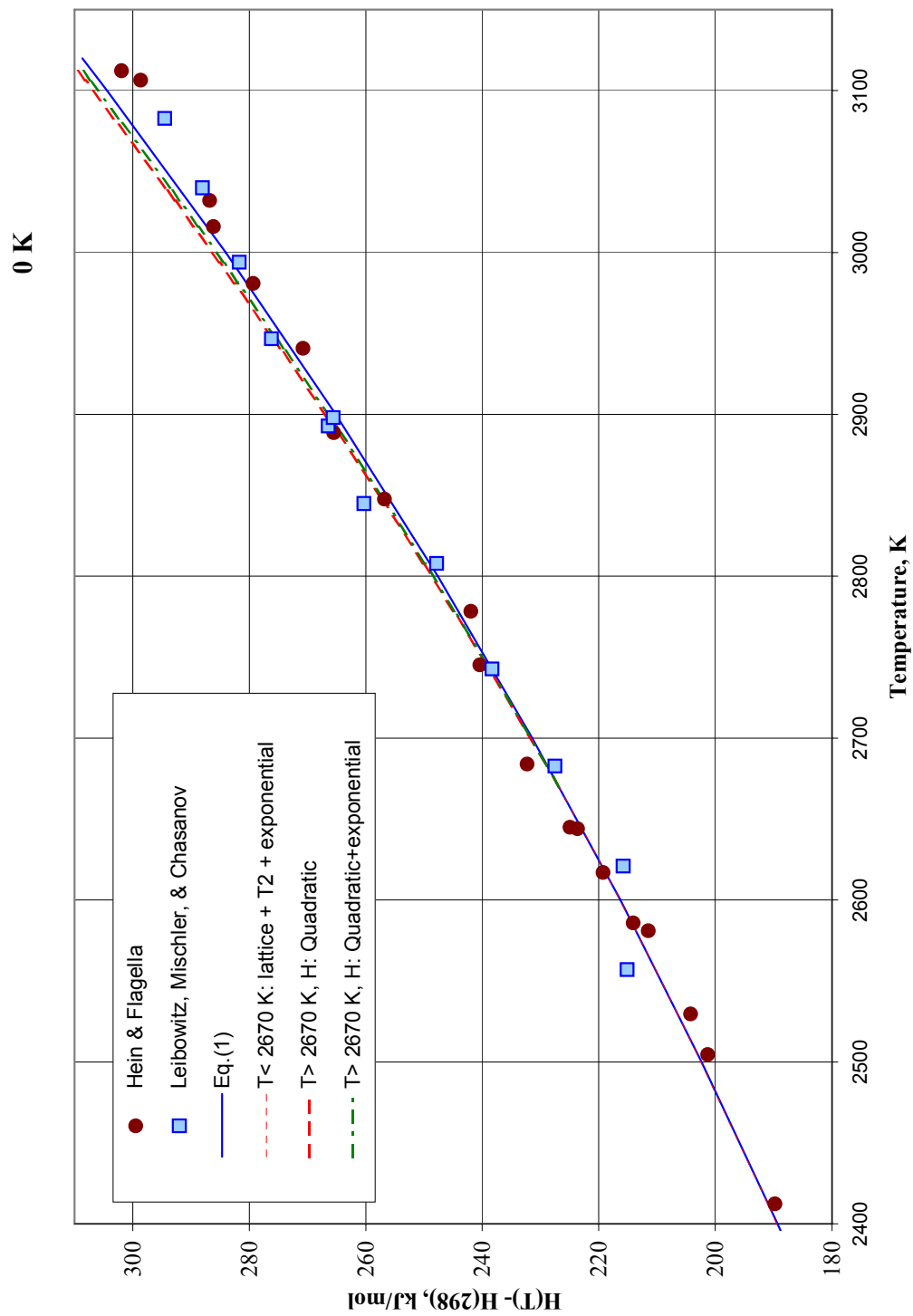


FIG. 7.  $\text{UO}_2$  enthalpy equations with and without break at 2670 K.

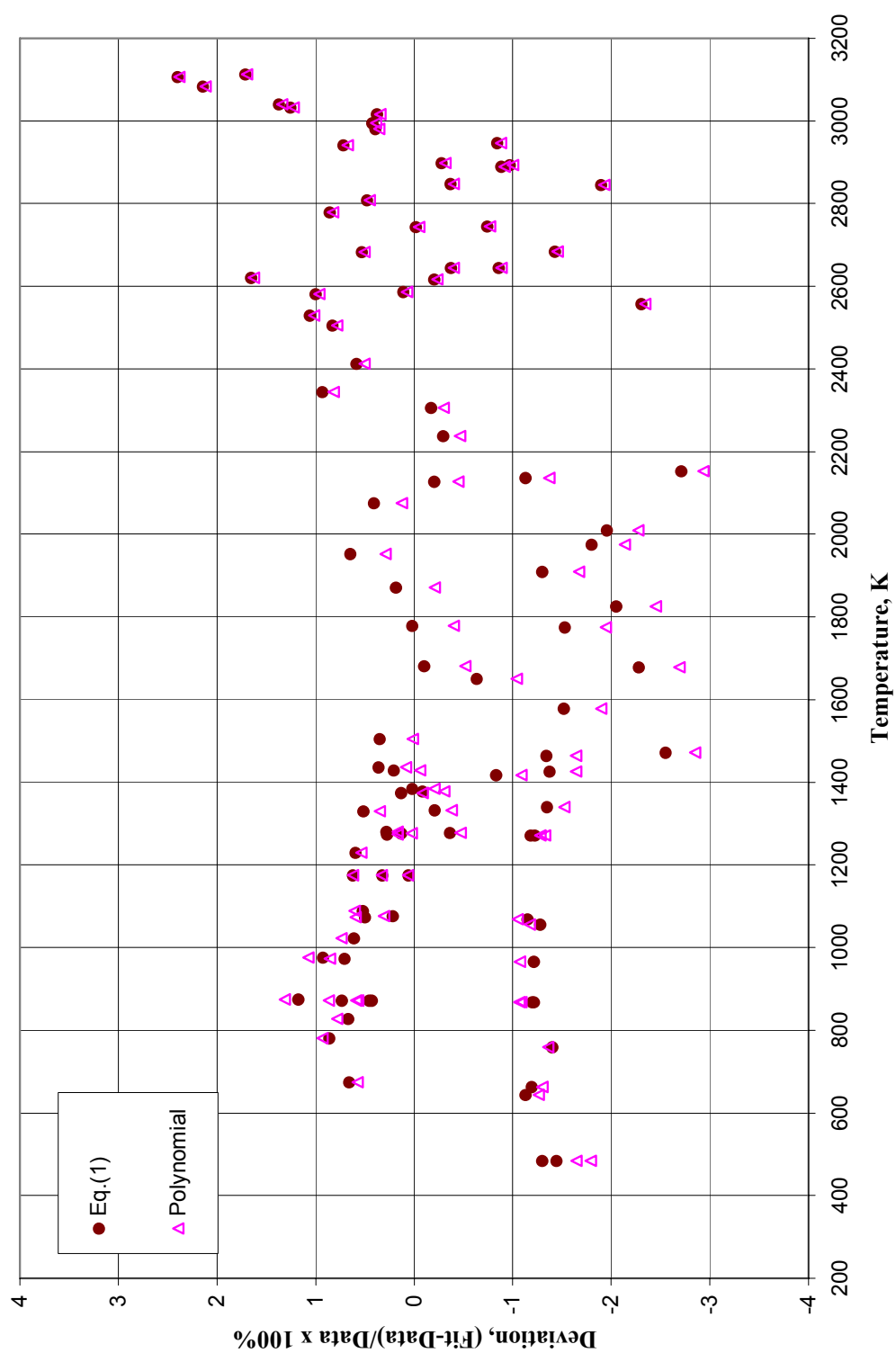


FIG. 8. Percent deviations of enthalpy data from the recommended equations.

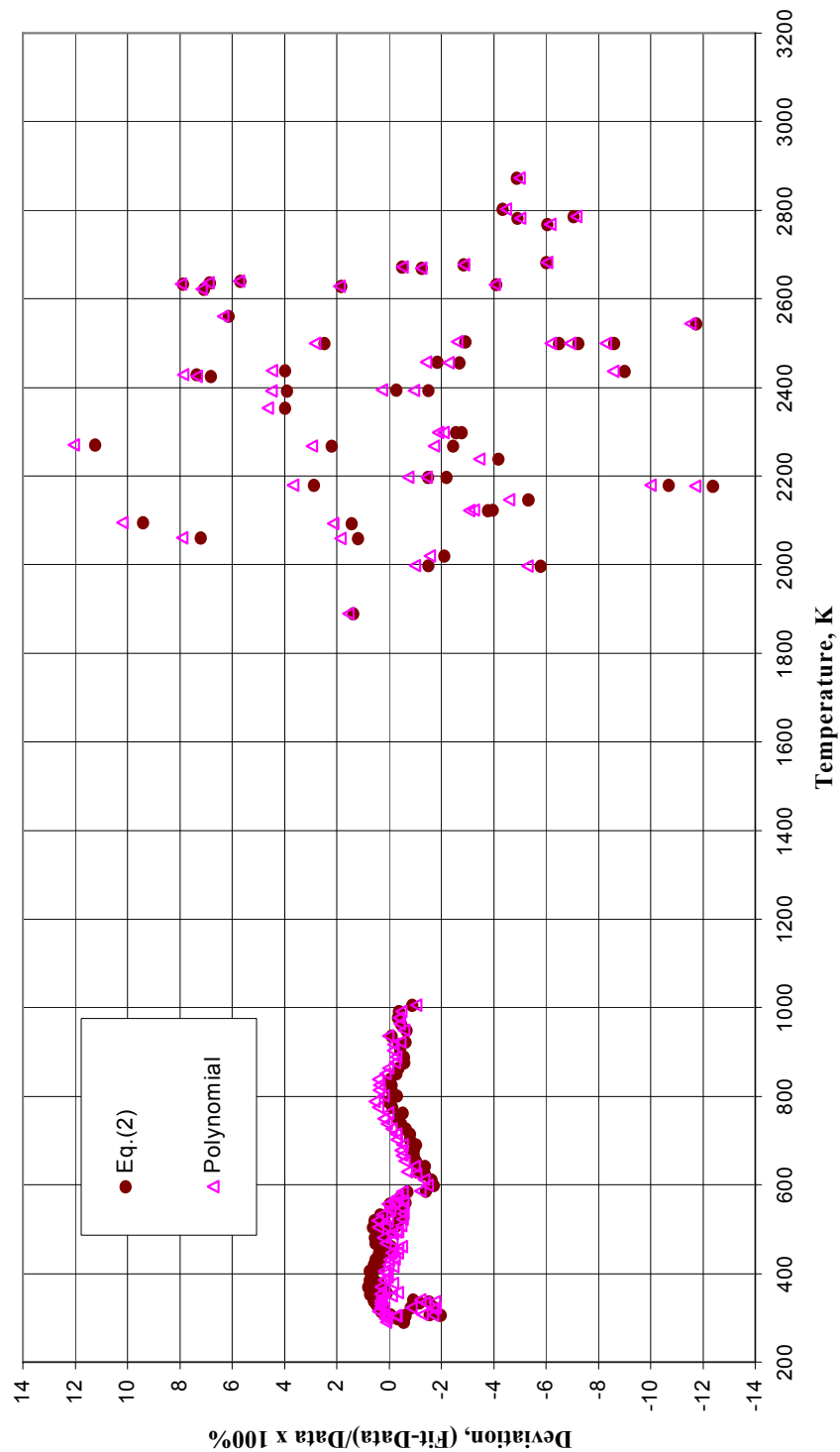


FIG. 9. Enthalpy of solid  $UO_2$

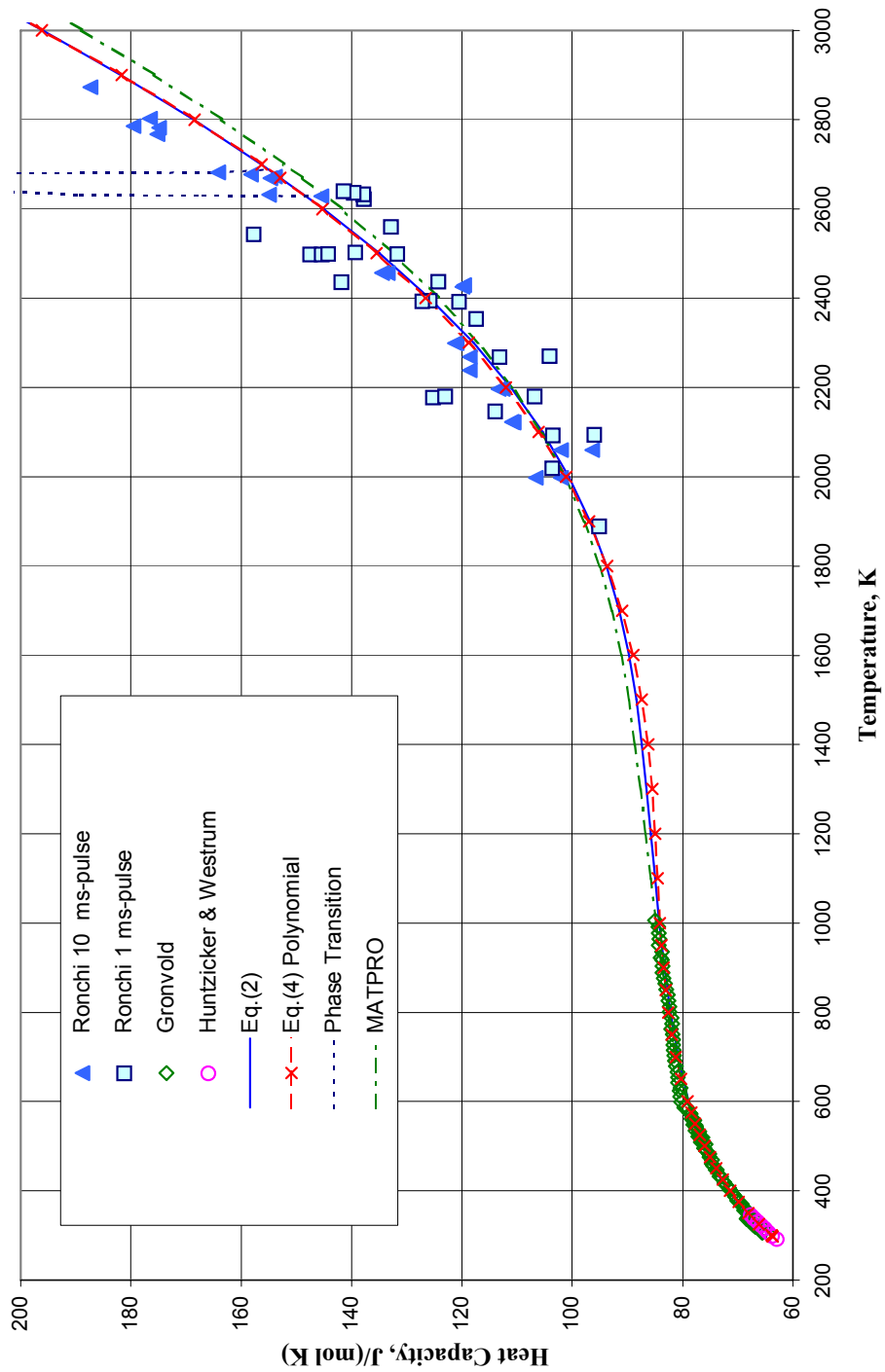


FIG. 10. Comparison of recommended equation and data with MATPRO equation.

### *Comparison with existing equations*

Previously recommended [28] equations developed by Fink et al. [20,21] and Harding et al. [22], which give a constant heat capacity above 2670 K are not consistent with the heat capacity data of Ronchi et al. [9] above 2670 K. Figure 10 shows that the MATPRO [25] single equation does not provide as good a fit to these data as the recommended equations.

### **REFERENCES TO SECTION 6.1.1.1**

- [1] LEIBOWITZ, L., MISHLER, L.W., and CHASANOV, M.G., J. Nucl. Mater. 29, 356 (1969).
- [2] FREDRICKSON, D.R., and CHASANOV, M.G., J. Chem. Thermodynamics 2, 263 (1970).
- [3] HEIN, R.A., and FLAGELLA, P.N., Enthalpy measurements of UO<sub>2</sub> and Tungsten to 3260 K, GE Report GEMP-578, General Electric, February 16, 1968.
- [4] HEIN, R.A., SJODAHN, L.A., and SZWARC, R., J. Nucl. Mater. 25, 99 (1968).
- [5] MOORE, G.E., and KELLY, K.K., J. Am. Chem. Soc. 69, 2105 (1947).
- [6] OGARD, A.E., and LEARY, J.A., High-temperature heat content and heat capacity of uranium dioxide and uranium dioxide-plutonium dioxide solid solutions, in Thermodynamics of Nuclear Materials 1967, IAEA, Vienna, p. 651 (1969).
- [7] HUNZICKER, J.J., and WESTRUM, E.F., J. Chem. Thermodynamics 3, 61 (1971).
- [8] GRONVOLD, F., KVSETH, N.J., SVEEN, A., and TICHY, J., J. Chem. Thermo. 2, 665 (1970).
- [9] RONCHI, C., SHEINDLIN, M., MUSELLA, M., and HYLAND, G.J., J. Applied Phys. 85, 776-789 (1999).
- [10] AFFORTIT, C., and MARCON, J., Rev. Int. Hautes Temp. et Refract. 7, 236 (1970).
- [11] AFFORTIT, C., High Temperatures-High Pressures 1, 27-33 (1969).
- [12] POPOV, M.M., GALCHENKO, G.L., and SENIV, M.D., ZH. NEORG. Kim. 3, 1734 (1958) [English translation of J. Inorganic Chem USSR 3, 18 (1958)].
- [13] ENGEL, T.K., J. Nucl. Mater. 31, 211 (1969).
- [14] HUTCHINGS, M.T., High-temperature studies of UO<sub>2</sub> and ThO<sub>2</sub> using neutron scattering techniques, J. Chem. Soc. Faraday Trans. II 83, 1083-1103 (1987).
- [15] HUTCHINGS, M.T., CLAUSEN, K., DICKEN, M.H., HAYES, W., KJEMS, J.K., SCHNABEL, P.G., and SMITH, C., J. Phys. C 17, 3903 (1984).
- [16] HIERNAUT, J.P., HYLAND, G.J. and RONCHI, C., Premelting transition in uranium dioxide, Int. J. Thermophys. 14(2), 259-283 (1993).
- [17] RONCHI, C. and HYLAND, G.J., Analysis of recent measurements of the heat capacity of uranium dioxide, J. of Alloys and Compounds 213/214, 159-168 (1994).
- [18] BROWNING, P., HYLAND, G.J., and RALPH, J., The origin of the specific heat anomaly in solid Urania, High Temperatures-High Pressures 15, 169-178 (1983).
- [19] BREDIG, M.A., L'étude des transformations cristalline a hautes temperatures, Proceedings of a Conference held in Odeillo, France, 1971 (CNRS, Paris, 1972), p. 183
- [20] FINK, J.K., Enthalpy and heat capacity of the actinide oxides, Int. J. Thermophys. 3(2), 165-200 (1982).
- [21] FINK, J.K., CHASANOV, M.G., and LEIBOWITZ, L., Thermophysical properties of uranium dioxide, J. Nucl. Mater. 102, 17-25 (1981); also as ANL Report ANL-CEN-RSD-80-3, Argonne National Laboratory (April 1981).
- [22] HARDING, J.H., MARTIN, D.G., and POTTER, P.E., Thermophysical and thermochemical properties of fast reactor materials, Commission of the European Communities Report EUR 12402 EN (1989).
- [23] LEIBOWITZ, L., FINK, J.K., and SLAGLE, O.D., Phase transitions, creep, and fission gas behavior in actinide oxides, J. Nucl. Mater. 116, 324-325 (1983).
- [24] RALPH, J., and HYLAND, G.J., Empirical confirmation of a Bredig transition in UO<sub>2</sub>, J. Nucl. Mater. 132, 76 (1985).
- [25] HAGRMAN, D.T., ed., SCADAP/RELAP5/MOD 3.1 Code Manual Vol. 4: MATPRO - a library of materials properties for light water reactor accident analysis, NUREG/CR-6150 (1995).
- [26] CONWAY, J.B., and HEIN, R.A., J. Nucl. Mater. 15, 149 (1965).

- [27] KERRISK, J.F., and CLIFTON, D.G., Smoothed values of the enthalpy and heat capacity of  $\text{UO}_2$ , Nucl. Technol. **16**, 531 (1972).
- [28] FINK, J.K., and PETRI, M.C., *Thermophysical Properties of Uranium Dioxide*, Argonne National Laboratory Report ANL/RE-97/2 (February 1997).

#### 6.1.1.2. Emissivity and optical constants of $\text{UO}_2$

##### **Summary of recommendations**

###### *Emissivity*

The experiments of Bober et al. [1-6] for the emissivity, reflectivity, and optical constants of  $\text{UO}_2$  in the solid and liquid phases provide the most reliable data for these properties. Bober, Karow, and Mueller [3] commented that, within the limits of experimental error, their data for solid  $\text{UO}_2$  agree with earlier emissivity measurements by Cabannes et al. [7], Held and Wilder [8], and Schoenes [9]. The data in the range of 1000 K to the melting temperature (3120 K) indicate that the emissivity of both sintered and premelted solid  $\text{UO}_2$  varies little with temperature and is only a weak function of wavelength. Thus, the constant total hemispherical emissivity ( $\epsilon^h$ ) that was suggested by Gentry [10] and also by Harding et al. [11] is recommended:

$$\epsilon^h = 0.85 \pm 0.05 \quad (1)$$

The equation given by Bober, Karow, and Muller [3] for the normal spectral emissivity of premelted solid  $\text{UO}_2$  at the wavelength of 630 nm is recommended for wavelengths in the visible range:

$$\epsilon(\lambda = 630\text{nm}) = 0.836 + 4.321 \times 10^{-6} (T - 3120) \quad (2)$$

For  $1000 \text{ K} \leq T \leq 3120 \text{ K}$  and  $400 \text{ nm} \leq \lambda \leq 700 \text{ nm}$ ,

where  $T$  is in K. Values from this equation are given in Table 1 and shown in Figure 1.

The emissivity of liquid  $\text{UO}_2$  is a function of both wavelength and temperature. For wavelengths in the visible range, however, the normal spectral emissivity of liquid  $\text{UO}_2$  is approximately independent of wavelength. The recommended values as a function of temperature for this wavelength range are those calculated from an equation for a wavelength of 630 nm determined by Fink et al. [12]:

$$\epsilon(\lambda = 630\text{nm}) = 1 - 0.16096 \exp \left[ -3.7897 \times 10^{-4} \Delta T - 3.2718 \times 10^{-7} (\Delta T)^2 \right] \quad (3)$$

For  $3120 \text{ K} \leq T \leq 6000 \text{ K}$  and  $400 \text{ nm} \leq \lambda \leq 700 \text{ nm}$ ,

where  $\Delta T = T - 3120 \text{ K}$ .

Normal spectral emissivities calculated with this equation are tabulated in Table 2 and are included in Figure 1. Although Eq.(3) was derived to fit the data of Bober, Karow, and Muller [3] at a wavelength of 630 nm, it also gives a good fit to more recent data [1, 2] at wavelengths of 548, 514.5, 647, and 752.5 nm. However, the behavior of the emissivity in the infrared region differs considerably from Eq.(3). Bober et al. [3,6] found that the normal spectral emissivity at a wavelength of 10600 nm falls from 0.85 at 3120 K to 0.64 at 3670 K and to 0.4 at 4000 K. Further emissivity measurements of liquid  $\text{UO}_2$  are needed in the infrared and far infrared region to confirm these results.

Table 1. Normal spectral emissivity of premelted  $\text{UO}_2$  at  $\lambda = 630 \text{ nm}$

TEMPERATURE, K	EMISSIONITY ( $\lambda = 630 \text{ nm}$ )
300	0.82
500	0.82
1000	0.83
1500	0.83
2000	0.83
2500	0.83
3000	0.84
3120 (s)	0.84

Table 2. Normal spectral emissivity of liquid  $\text{UO}_2$  at  $\lambda = 630 \text{ nm}$

TEMPERATURE , K	EMISSIONITY ( $\lambda = 630 \text{ nm}$ )
3120	0.84
3500	0.87
4000	.91
4500	(0.95)*
5000	(0.98)*
5500	(0.99)*
6000	(0.99)*

\* Extrapolated beyond the range of experimental data

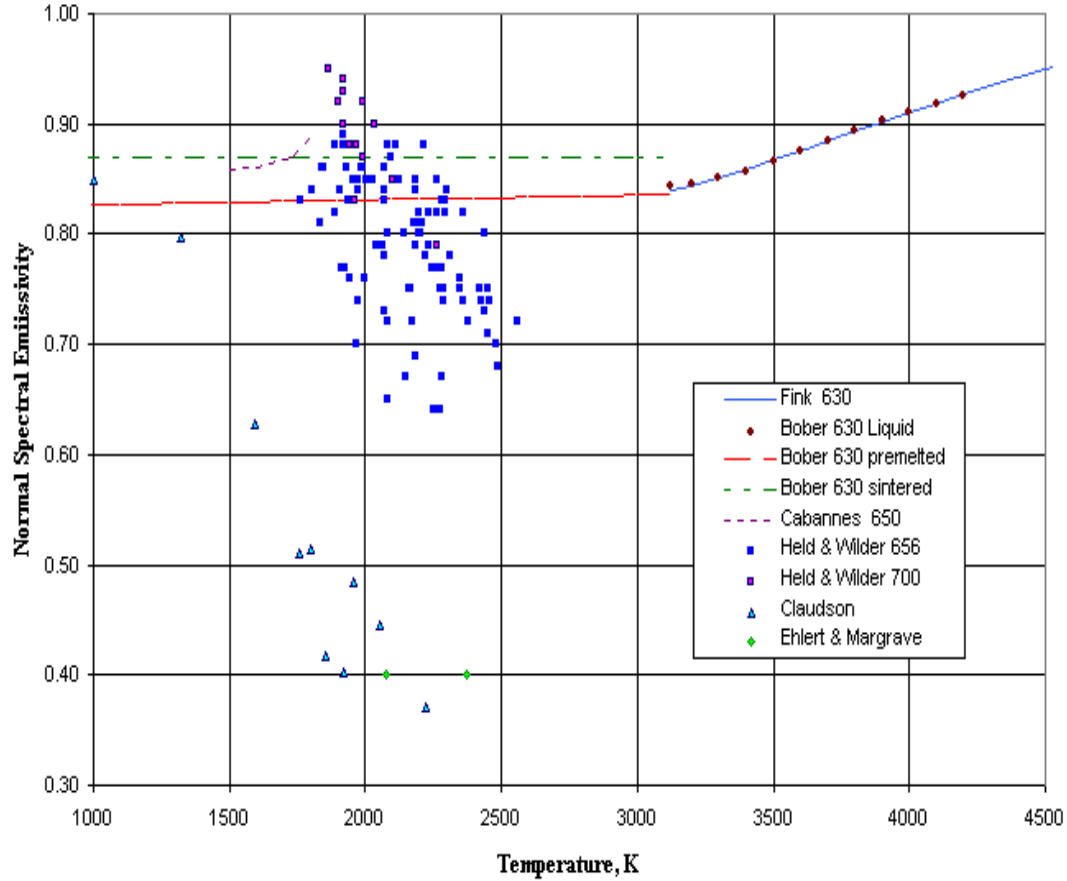


FIG. 1.  $UO_2$  emissivity.

### Optical constants

Provisional recommendations are available from measurements by Bober, Singer, and Wagner [1,2]. They determined the optical constants for liquid  $UO_2$  from 3100 to 3600 K and for single-crystal  $UO_2$  at room temperature from reflectivity measurements in the spectral range of 450 to 750 nm. Their room temperature index of refraction values confirm the values of Ackermann et al. [13]. The average values for the index of refraction ( $n$ ) and absorption coefficient ( $k$ ) of  $UO_2$  at room temperature and in the liquid region are

$$n = 2.2; k = 0.7. \quad (4)$$

For  $T = 300$  K,

$$n = 1.7; k = 0.8. \quad (5)$$

For  $3100 < T \leq 3600$  K,

### Uncertainties

The uncertainty in the total hemispherical emissivity is  $\pm 0.05$ . [10, 11] Experimental uncertainties given by Karow and Bober [6] for the normal spectral emissivity of premelted solid  $UO_2$  at the wavelength of 630 nm increase from  $\sim 1\%$  at 1500 K to  $2\%$  at 3000 K. In the liquid region, their uncertainties are 2.5 to 3%. Uncertainties of  $+3\%/-10\%$  are suggested [12] for extrapolation of Eq.(2) above 4200 K. Large scatter in the reflectivity data from which the optical constants are derived lead to uncertainties in the refractive index ( $n$ ) of  $\pm 10\%$  and in the absorption constant ( $k$ ) of  $\pm 20\%$ .



## Discussion

### *Emissivity of solid UO<sub>2</sub>*

Data of Bober et al. [1–6] provide normal spectral emissivities of solid and molten UO<sub>2</sub> from 1000 to 4200 K and optical constants of molten UO<sub>2</sub> from 3000 to 4000 K. These are the most recent and reliable data and cover the largest temperature range. The normal spectral emissivities at a wavelength of 630 nm determined by Bober et al. [3, 6] are in reasonable agreement with normal spectral emissivities of Cabannes et al. [7] at a wavelength of 650 nm, and of Held and Wilder [8] at wavelengths of 656 and 700 nm but disagree with earlier data of Claudson [14, 15] and of Ehlert and Margrave, [15, 16] as shown in Figure 1. The data of Claudson, [14, 15] which show a decrease in the emissivity in the temperature range of 1000 to 2000 K, have been rejected in reviews by Fink et al., [12] Gentry, [10, 11] and Harding et al. [11] Cabannes et al. [7] have suggested that the decrease with temperature observed by Claudson [14, 15] was due to errors in the experimental technique. Unlike the data of Held and Wilder, [8] which decrease with temperature above 2000 K, the data of Bober et al. [3, 6] show little temperature dependence and no decrease with temperature above 2000 K.

Bober, Karow, and Muller [3] found that the normal spectral emissivity of sintered UO<sub>2</sub> at a wavelength of 630 nm is slightly higher than that for premelted UO<sub>2</sub>. From 1000 to 3120 K, they obtained an emissivity of 0.87 for sintered UO<sub>2</sub> and recommended Eq.(1) to represent the emissivity of premelted UO<sub>2</sub>. Their data are supported by the measurements of Babelot et al. [17] who obtained an emissivity of 0.84 at a wavelength of 650 nm at the melting point, 3120 K.

Cabannes et al. [7] determined emissivities at 300, 1200, and 1600 K for wavelengths ranging from 500 nm to the infrared region (10000 nm). They found little variation in emissivity with wavelength or temperature. From these data, they obtained total emissivities of 0.86, 0.90, and 0.90 at 300, 1200 and 1600 K, respectively. These total emissivities are consistent with the recommendation of Gentry [10, 11] for a total emissivity of  $0.85 \pm 0.05$ . The temperature-dependent total emissivity for solid UO<sub>2</sub> determined by Mason [18] is given in MATPRO [19]:

$$\varepsilon = 0.7856 + 1.5263 \times 10^{-5} T \quad (6)$$

Total emissivities calculated with Eq.(6) increase from 0.79 at 300 K to 0.80 at 1000 K and 0.83 at 3120 K. These emissivities are consistently lower than the value given by Gentry. [10, 11]. However, above 700 K, they are within the uncertainty for the total emissivity recommended by Gentry.

### *Emissivity of liquid UO<sub>2</sub>*

Bober, Karow, and Muller [3] fit their data for the normal spectral emissivity of liquid UO<sub>2</sub> at a wavelength of 630 nm to a quadratic equation:

$$\varepsilon(\lambda = 630\text{nm}) = 0.843 + 1.4465 \times 10^{-4} \Delta T + 1.6497 \times 10^{-7} \Delta T^2 - 1.3136 \times 10^{-10} \Delta T^3 + 2.899 \times 10^{-14} \Delta T^4 \quad (7)$$

where  $\Delta T = T - 3120\text{K}$ , and  $T$  is in K. Although Eq.(7) represents the experimental data of Bober, Karow, and Muller [3]. This equation should not be used to extrapolate beyond 4200 K because it goes through an inflection point at 4831 K followed by an increasing slope that results in values greater than unity for temperatures above 5668 K. Consequently, Fink et al. [12] fit the data of Bober, Karow, and Muller [3] to an equation with a functional form appropriate for extrapolation beyond the range of experimental data without introducing unphysical behavior. That equation is the recommended equation, Eq.(3). In the temperature range of experimental data, Eq.(3) reproduces the values given by Eq.(7) to within 0.14%. Equation (3) also provides a good fit to liquid emissivity data for other wavelengths in the visible range ( $\lambda = 459, 514.5, 647, \text{ and } 752.5 \text{ nm}$ ).

The normal spectral emissivity of liquid UO<sub>2</sub> at wavelengths in the far infrared range shows an entirely different temperature behavior from that at wavelengths in the visible range. Data of Karow and Bober [3,6] show that for  $\lambda = 10600 \text{ nm}$  the normal spectral emissivity of liquid UO<sub>2</sub> falls from 0.85 at 3120 K to 0.64 at 3670 K and to 0.4 at 4000 K. Further data are required at wavelengths in the infrared region to confirm these results and determine total emissivities for the liquid.

### *Optical constants*

Optical constants of single-crystal  $\text{UO}_2$  were determined at 300 K by Bober et al. [1, 2, 4] for comparison with values obtained by Ackermann et al. [13]. Ackermann et al. determined the index of refraction at room temperature in the ultraviolet region (at the wavelength of 260 nm) and in the visible range (at wavelengths from 450 to 800 nm). Figure 2 shows refractive indices obtained from these measurements at wavelengths in the visible range. Room temperature values obtained from measurements by Ackermann et al. are consistently higher than those given by Bober et al.; but these data are usually within the estimated 10% experimental uncertainty. The average of the values for the room temperature index of refraction from the data of Bober et al. [1] is 2.24. The average index of refraction from the values of Ackermann et al. [13] is 2.45. These averages are within the 10% uncertainty given by Bober et al. [1, 2]. They are both higher than the room temperature index of refraction at a wavelength of 260 nm given by Ackermann et al. (1.95). Figure 2 shows that they are also consistently higher than values for liquid  $\text{UO}_2$  at wavelengths in the visible spectrum. Absorption coefficients for  $\text{UO}_2$  at room temperature, determined by Bober et al., decreased from 0.84 at a wavelength of 458 nm to 0.60 at a wavelength of 752.5 nm with an average value of 0.7.

Bober, Singer, and Wagner [1, 2] determined the optical constants for liquid  $\text{UO}_2$  from reflectivity measurements with polarized light in the temperature range of 3000 to 4000 K at four visible wavelengths (458, 514.5, 647, and 752.5 nm) and at three angles of incidence ( $45^\circ$ ,  $58^\circ$ , and  $71^\circ$ ). Reflectivities measured as a function of temperature and wavelength showed considerable scatter with angle of incidence. Optical constants were calculated from the reflectivities at each temperature and wavelength for each of the three possible pairs of measurement angles ( $45^\circ$  and  $58^\circ$ ,  $45^\circ$  and  $71^\circ$ ,  $58^\circ$  and  $71^\circ$ ). Then these three sets of values were averaged to obtain optical constants for each wavelength and temperature. Figures 3 and 4 show, respectively, the average refractive index and average absorption coefficient for liquid  $\text{UO}_2$  for four visible wavelengths as a function of temperature. Both optical constants decrease with increasing temperature. Based on these data, Bober et al. [1, 2] proposed average values for the refractive index and absorption coefficient for wavelengths in the visible range and temperatures from 3100 to 3600 K. Their average values are:  $n = 1.7$  and  $k = 0.8$ .

From the scatter in their reflectance data, Bober et al. [1,2] estimated the uncertainty in the refractive index,  $n$ , as  $\pm 10\%$  and the uncertainty in the absorption coefficient,  $k$ , as  $\pm 20\%$ . Bober et al. [1] commented that the accuracy of the absorption coefficient,  $k$ , is influenced more by measurement errors than that of the refractive index,  $n$ . The equations used to calculate the optical constants are based on the assumption of an ideal optically smooth surface, which is difficult to attain. Scatter in the experimental data was attributed to imperfections of the reflecting surface, variations in the angle of incidence arising from oscillations of the liquid surface, and the formation of a meniscus. With increased temperature, surface disturbances from vaporization and gas bursts added to the difficulty of the measurements. The increased difficulty is apparent in the decreased consistency in the reflectance data above 3500 K.

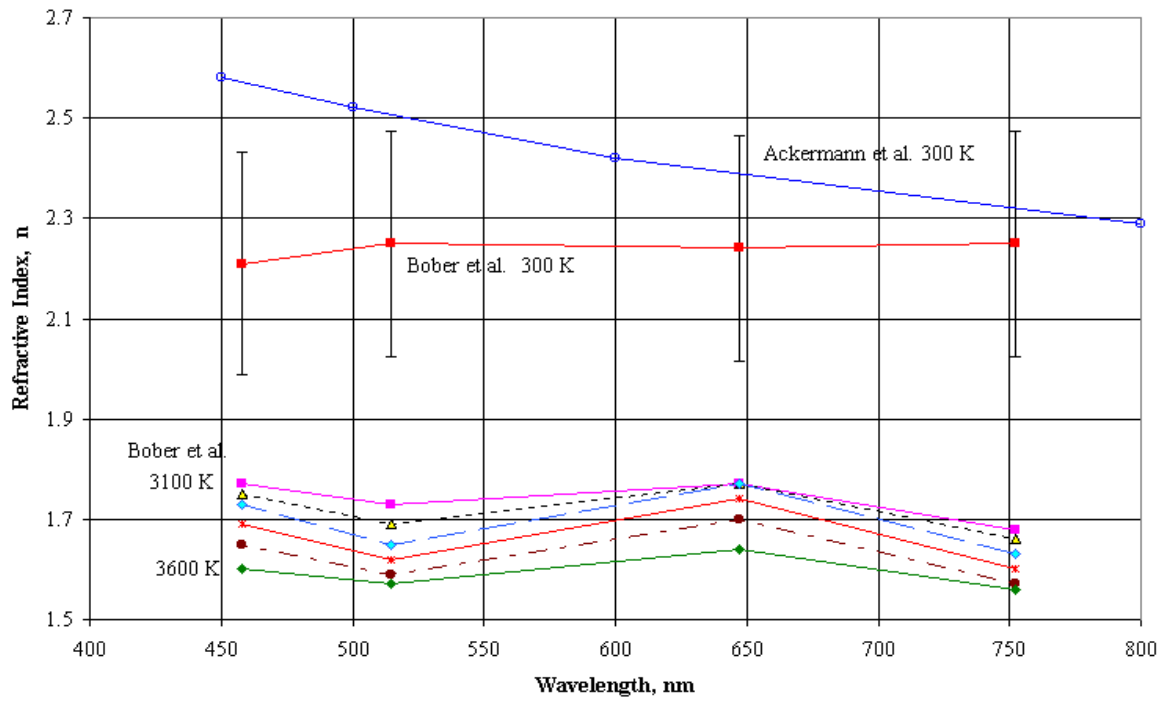


FIG. 2. Average refractive index of  $\text{UO}_2$

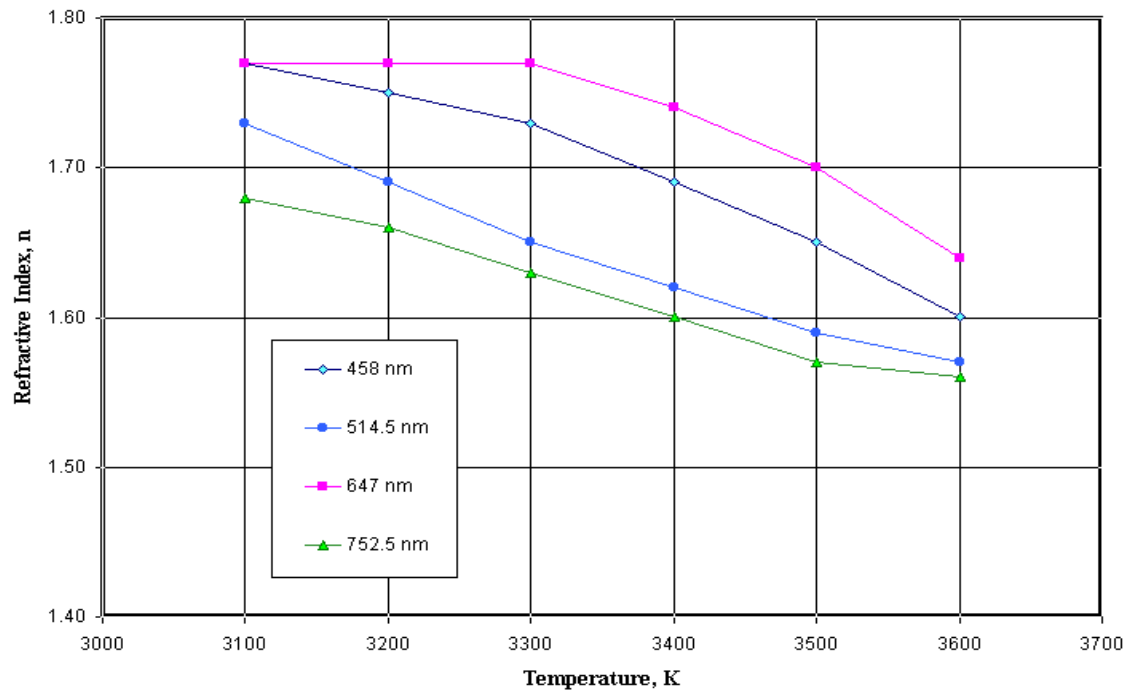


FIG. 3. Average refractive index of  $\text{UO}_2$  from measurements of Bober et al.

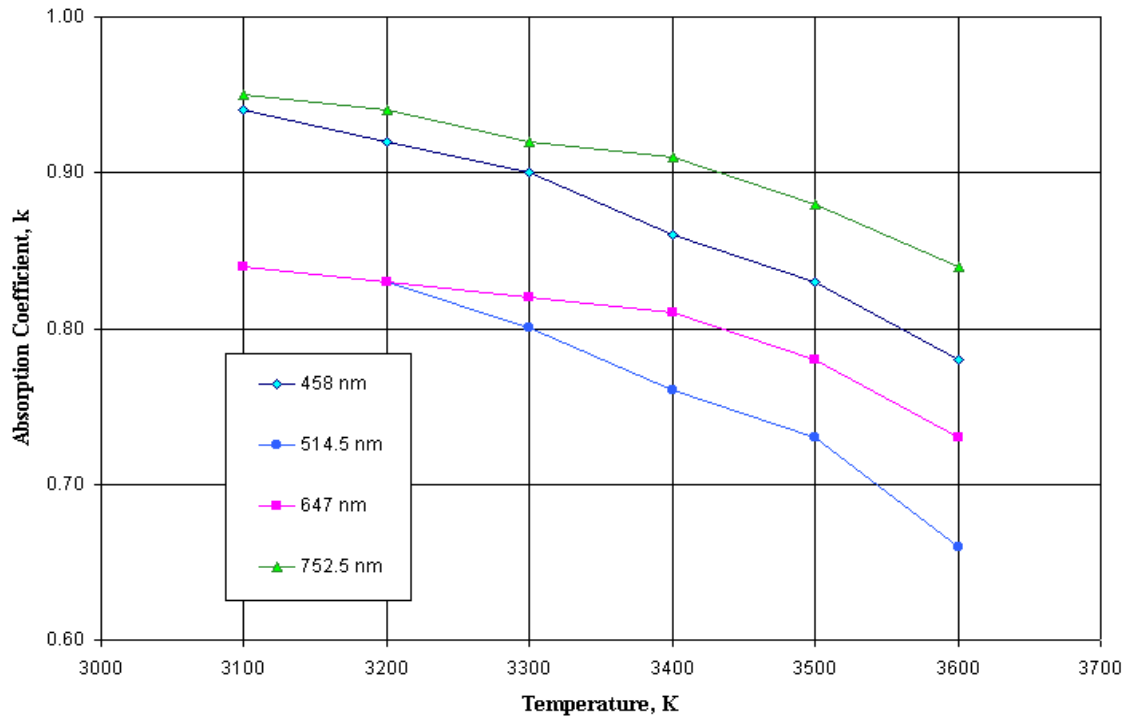


FIG. 4. Average  $\text{UO}_2$  absorption coefficient from measurements of Bober et al.

#### REFERENCES TO SECTION 6.1.1.2

- [1] BOBER, M., SINGER, J., and WAGNER, K., Determination of the optical constants of liquid  $\text{UO}_2$  from reflectivity measurements, Proc. Eighth Symp. on Thermophysical Properties, Gaithersburg, MD, 1981, Vol II, pp. 234-244, ASME (1982).
- [2] BOBER, M., SINGER, J., and WAGNER, K., Bestimmung der optischen Konstanten von geschmolzenen Kernbrennstoffen, J Nucl. Mater. 124, 120-128 (1984).
- [3] BOBER, M., KAROW, H.U., and MULLER, K., Study of the spectral reflectivity and emissivity of liquid ceramics, High Temp. - High Pressures 12, 161-168 (1980).
- [4] BOBER, M., Spectral reflectivity and emissivity of solid and liquid  $\text{UO}_2$  as a function of wavelength, angle of incidence, and polarization, High Temp. - High Pressures 12, 297-306 (1980).
- [5] BOBER, M. and KAROW, H.U., Measurements of spectral emissivity of  $\text{UO}_2$  above the melting point, Proc. Seventh Symp. on Thermophysical Properties, Gaithersburg, MD, 1977, pp. 344-350, ASME (1978).
- [6] KAROW, H.U. and BOBER, M., Experimental investigations into the spectral relectivities and emissivities of liquid  $\text{UO}_2$ , UC,  $\text{ThO}_2$ , and  $\text{Nd}_2\text{O}_3$ , Thermodynamics of Nuclear Materials 1979 Vol I, Proc. Symp. Julich, 1979, pp. 155-169, IAEA (1980).
- [7] CABANNES, F., STORA, J.P. and TSAKIRIS, J., Facteurs de reflexion et d'emission de  $\text{UO}_2$  a haute temperature, C. R. Acad. Sc. Paris, 264B, 45-48 (1967).
- [8] HELD, P.C. and WILDER, D.R., High-temperature hemispherical spectral emittance of uranium oxides at 0.65 and 0.70  $\mu\text{m}$ , J. Am. Ceramic Society 52, 152-185 (1969).
- [9] SCHOENES, J., Optical properties and electronic structure of  $\text{UO}_2$ , J. Appl. Phys. 49 1463-1465 (1978).
- [10] GENTRY, P.J., Report ND-P-6887 (W) (1981), as referenced by J.H. Harding, D.G. Martin, and P.E. Potter, Thermophysical and thermochemical properties of fast reactor materials, Commission of the European Communities Report EUR 12402 EN (1989).
- [11] HARDING, J.H., MARTIN, D.G. and POTTER, P.E., Thermophysical and thermochemical properties of fast reactor materials, Commission of the European Communities Report EUR 12402 EN (1989).

- [12] FINK, J.K., CHASANOV, M.G. and LEIBOWITZ, L., Transport properties of uranium dioxide, NL-CEN-RSD-80-4, Argonne National Laboratory (April 1981).
- [13] ACKERMANN, R.J., THORN, R.J. and WINSLOW, G.H., Visible and ultraviolet absorption properties of uranium dioxide films, J. Opt. Soc. Am. 49, 1107 (1959).
- [14] CLAUDSON, T.T., Emissivity data for uranium dioxide, Report AW-55414 (Nov. 1958), as referenced in *Uranium Dioxide Properties and Nuclear Applications*, J. Belle, Ed., pp. 196-197, US AEC (1961)
- [15] BELLE, J. (Ed.), Uranium dioxide properties and nuclear applications, pp. 196-197, US AEC (1961)
- [16] EHLERT, T.C. and MARGRAVE, J.L., Melting point and spectral emissivity of uranium dioxide, J. Am. Ceram. Soc. 41, 330 (1958), as referenced in *Uranium Dioxide Properties and Nuclear Applications*, J. Belle, Ed., pp. 196-197, USAEC (1961).
- [17] BABELOT, J.F., BRUNNE, G.D., KINSMAN, P.R. and OHSE, R.W., Atomwirt-Atomtech 22, (No. 7-8), 387 (1977).
- [18] MASON, R.E., Fuel emissivity, CDAP-TR-78-039, Idaho Engineering Laboratory (1978).
- [19] HOHORST, J.K. (Ed.), *SCADAP/RELAP5/MOD2 Code Manual, Vol. 4: MATPRO - a library of materials properties for light-water-reactor accident analysis*, NUREG/CR-5273 (1990).

### 6.1.1.3. Thermal expansion of solid $UO_2$

#### **Summary and recommended equations**

The recommended equations for the thermal expansion of solid uranium dioxide are from the 1988 assessment by D.G. Martin [1], which included the high temperature neutron diffraction data of Hutchings [2] that were not available to previous assessments [3, 4]. Martin compared data from lattice parameter measurements and macroscopic length changes from 15 references [2, 5–18], made corrections to macroscopic thermal expansion measurements that exhibited a zero error, and excluded data that did not agree with the common consensus. Martin fit the remaining data to two cubic polynomials. Refitting the data fit by Martin plus new data by Momin et al. [19] and the data of Christensen [11], which was not included in the fit by Martin, gave equations that differed little from those of Martin. Thus, the equations of Martin are recommended. The recommended equations for the linear thermal expansion of solid  $UO_2$  are:

for  $273\text{ K} \leq T \leq 923\text{ K}$ ,

$$L = L_{273} (9.9734 \times 10^1 + 9.802 \times 10^6 T - 2.705 \times 10^{10} T^2 + 4.391 \times 10^{-13} T^3); \quad (1)$$

for  $923\text{ K} \leq T \leq 3120\text{ K}$ ,

$$L = L_{273} (9.9672 \times 10^1 + 1.179 \times 10^5 T - 2.429 \times 10^9 T^2 + 1.219 \times 10^{-12} T^3) \quad (2)$$

where  $L$  and  $L_{273}$  are the lengths at temperatures  $T(K)$  and  $273\text{ K}$ , respectively. The fractional change in the linear thermal expansion of  $UO_2$ ,  $\Delta L/L_{273} = (L - L_{273})/L_{273}$ , expressed as a percent, is shown in Figure 1 with the recommended uncertainties, the data fit by Martin and new data by Momin et al. [19]. Recommended values for the fractional change in linear thermal expansion,  $\Delta L/L_{273}$ , are tabulated in Table 1. Values for the fractional change in volumetric thermal expansion of  $UO_2$ ,  $\Delta V/V_{273}$ , are given in Table 2.

From assessment of the available data on hyperstoichiometric uranium dioxide ( $UO_{2+x}$ ), Martin recommends using these equations for the linear thermal expansion of  $UO_{2+x}$  for  $x$  in the ranges 0 to 0.13 and 0.23 to 0.25.

The recommended equations for the instantaneous linear thermal expansion coefficients,

$$\alpha_P(l) = \frac{l}{L} \left( \frac{\partial L}{\partial T} \right)_P \quad (3)$$

$\alpha_P(l)$ , are cubic polynomial approximations<sup>1</sup> to the exact partial differentials of Eqs.(1) and (2). These approximations do not differ by more than 0.6% from the exact differentials over the given temperature range. Martin recommends:

for  $273 \text{ K} \leq T \leq 923 \text{ K}$ ,

$$\alpha_P(l) = 9.828 \times 10^6 - 6.930 \times 10^{10} T + 1.330 \times 10^{12} T^2 - 1.757 \times 10^{17} T^3; \quad (4)$$

for  $923 \text{ K} \leq T \leq 3120 \text{ K}$ ,

$$\alpha_P(l) = 1.1833 \times 10^5 - 5.013 \times 10^9 T + 3.756 \times 10^{12} T^2 - 6.125 \times 10^{17} T^3; \quad (5)$$

where  $\alpha_P(l)$  is the coefficient of thermal expansion in  $\text{K}^{-1}$ . Recommended values of the instantaneous linear thermal expansion coefficient of  $\text{UO}_2$  are shown in Figure 2, and tabulated as a function of temperature in Table 1. Dotted lines in Figure 2 represent the recommended uncertainties, which are larger than those suggested by Martin. Values for the instantaneous volumetric thermal expansion coefficient, the thermodynamic quantity,  $\alpha_P$ , are given in Table 2. Equations relating the linear and volumetric thermal expansion coefficients and fractional changes in length, volume, and density with temperature are given in the Appendix (A.1.1.) entitled “Density and thermal expansion relations”.

### **Uncertainties**

From 293 through 535 K, the recommended uncertainty in the fractional linear expansion ( $L/L_{273} - 1$ ) is  $\pm 2.6 \times 10^{-4}$ , which is the uncertainty given by Martin. In terms of the percent of the linear expansion,  $\Delta L/L_{273}$ , this constant uncertainty decreases from 105% at 298 K to 10% at 535K. The percent uncertainty is 10% from 600 to 1000 K and 7% from 1400 to 3120 K with a linear percent decrease from 535 to 600 K and from 1000 to 1400 K. Above 535 K, larger uncertainties are recommended than those given by Martin so that most of the new data by Momin et al.[19] and some of the high-temperature data of Baldcock [17] and Christensen [11] fall between the recommended values and the uncertainty limits.

The uncertainties in the instantaneous linear thermal expansion,  $\alpha_P(l)$ , are:  $\pm 0.11 \times 10^{-6}$ ,  $\pm 0.22 \times 10^{-6}$ , and  $\pm 1.1 \times 10^{-6}$  for the temperature ranges 293–1273 K, 1273–2273 K, and 2273–2929 K, respectively.

Table 1. Recommended linear thermal expansion of  $\text{UO}_2$

T, K	$\Delta L/L$ , %	$\alpha_p(l) \times 10^6$ , $\text{K}^{-1}$
273	0.000	9.74
298	0.025	9.74
300	0.027	9.74
400	0.125	9.76
500	0.223	9.81
600	0.322	9.89
700	0.422	9.99
800	0.523	10.12
900	0.626	10.27
1000	0.730	10.51
1100	0.837	10.78
1200	0.948	11.12
1300	1.062	11.53
1400	1.181	12.01
1500	1.305	12.56
1600	1.436	13.18
1700	1.573	13.86
1800	1.718	14.62
1900	1.871	15.45
2000	2.034	16.34
2100	2.206	17.30
2200	2.388	18.33
2300	2.582	19.43
2400	2.788	20.59
2500	3.006	21.82
2600	3.238	23.11
2700	3.484	24.47
2800	3.745	25.90
2900	4.021	27.39
3000	4.314	28.94
3100	4.624	30.56
3120	4.688	30.89

Table 2. Recommended volumetric thermal expansion of  $\text{UO}_2$

T, K	$\Delta V/V$ , %	$\alpha_p \times 10^6$ , $\text{K}^{-1}$
298	0.075	29.22
300	0.080	29.22
400	0.374	29.29
500	0.670	29.44
600	0.969	29.66
700	1.271	29.97
800	1.578	30.35
900	1.891	30.81
1000	2.206	31.54
1100	2.533	32.35
1200	2.870	33.36
1300	3.220	34.59
1400	3.585	36.03
1500	3.968	37.67
1600	4.370	39.53
1700	4.794	41.59
1800	5.243	43.87
1900	5.720	46.34
2000	6.226	49.02
2100	6.764	51.91
2200	7.337	54.99
2300	7.947	58.28
2400	8.598	61.77
2500	9.292	65.46
2600	10.032	69.34
2700	10.820	73.42
2800	11.660	77.70
2900	12.556	82.17
3000	13.509	86.83
3100	14.524	91.69
3120	14.734	92.68

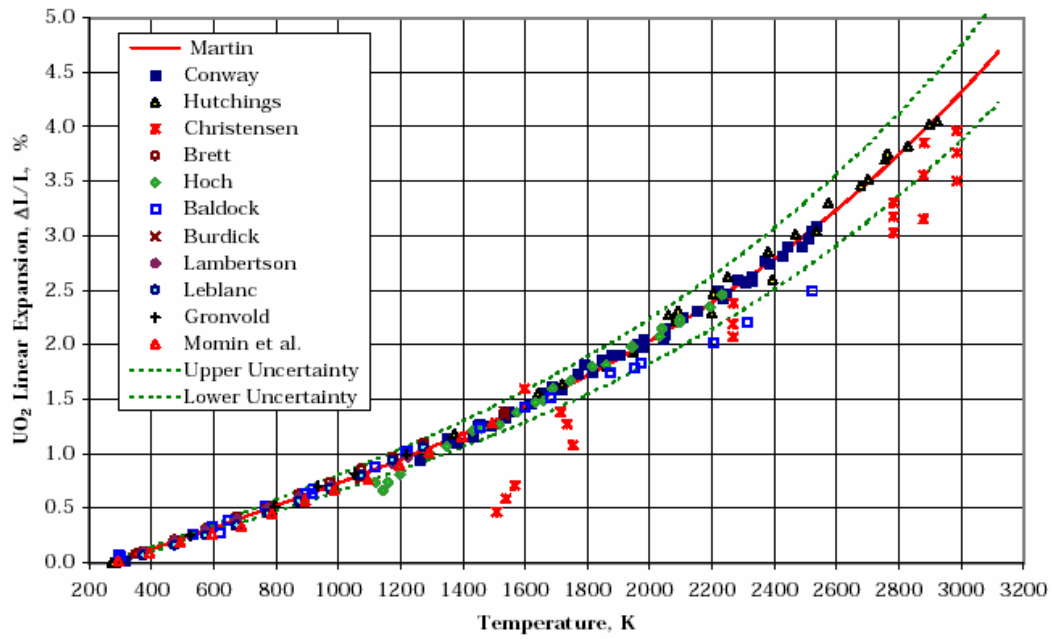


FIG. 1. Recommended  $UO_2$  linear thermal expansions.

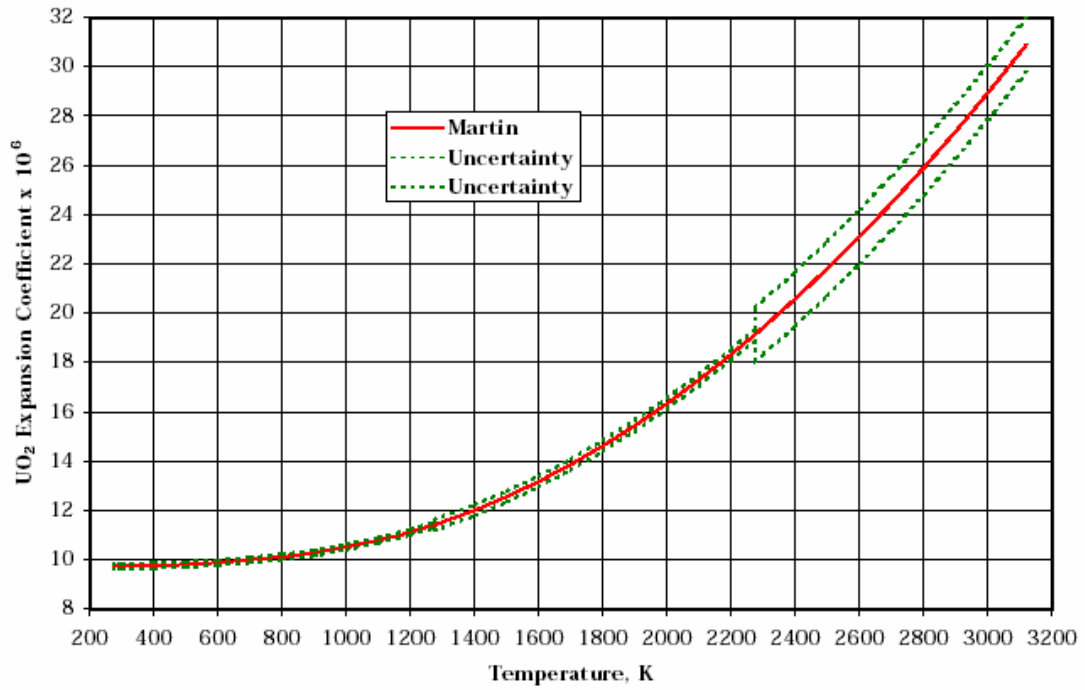


FIG. 2.  $UO_2$  Instantaneous linear thermal expansion coefficient.



### *Discussion of recommended equations for UO<sub>2</sub>*

Martin [1] reviewed and compared UO<sub>2</sub> thermal expansion data from macroscopic length changes [5–13], neutron diffraction [2, 18], and X-ray diffraction measurements [17] except for the recent X-ray diffraction results by Momin et al. [19]. In his thorough data assessment, Martin examined the macroscopic expansion data for possible zero errors and made corrections to the data of Lambertson and Hanwerk [6], the data of Brett and Russell [9], and the data of Murray and Thackery [10]. He found good agreement between the data from macroscopic length changes and lattice parameter measurements so that these data could be combined in the final analysis. The good agreement between data from macroscopic measurements by Conway et al. and the lattice parameter measurements of Hutchings [2] led Martin to conclude that at least up to 2523 K, the contribution to the macroscopic expansion due to Schottky defects is negligible. In formulating equations to represent the linear thermal expansion of UO<sub>2</sub>, Martin excluded data that did not agree with the common consensus. Data excluded by Martin are: data of Bell et al.[5], data of Christensen [11], data of Halden et al.[12], data above 1871 K from measurements by Baldock et al.[17], and data from 1118 to 1200 K from measurements by Hoch and Momin [15].

The analysis of Martin [1] has been re-examined because it excluded the data of Christensen [11], which are still being used in determining density equations [20] and because the recent data of Momin et al.[19] fall outside the errors given by Martin. A weighted least squares minimization procedure has been used to fit the thermal expansion data that were fit by Martin, the data of Christensen [11], and the data of Momin et al.[19]. The weights used for the data fit by Martin and the data of Momin et al. are the inverse of the squares of the standard deviations from the equations recommended by Martin. The deviation of the data of Christensen near 1700 K from the common data was used to weight the data of Christensen. The least squares fit to these data gave equations that differed from those given by Martin by less than 1%. Thus, the equations given by Martin are consistent with this larger data set and are therefore recommended. This larger set of data has been included in Figure 1, which shows the recommended equations of Martin, expressed as the percent change in length relative to the length at 273 K, ie. ( $\Delta L/L_{273}$ , %).

Percent deviations of the data from the recommended equations of Martin are shown in Figure 3. Percent deviations in Figure 3 are defined as:

$$Deviation(\%) = \frac{\frac{\Delta L(Data)}{L} - \frac{\Delta L(Martin)}{L}}{\frac{\Delta L(Martin)}{L}} \bullet 100\% \quad (6)$$

The recommended uncertainties are included in Figure 3 for comparison with the deviations of Martin's equations from the analysed data. Figure 3 shows that most of the data fall within the uncertainty limits. However, the data of Christensen [11] show considerable scatter with significant numbers of deviations greater than the uncertainty. Figure 3 shows that the data of Momin et al. [19], based on X-ray diffraction measurements, are consistently lower than the recommended values. Deviations of the data of Momin et al. calculated from Eq. (6) range from -24% at 298 K to -0.5% at 1600 K. Momin et al. report 0.5469 nm for the lattice parameter of UO<sub>2</sub> at room temperature, which is slightly lower than the 0.54704 nm at 293 K obtained by Gronvold [16] and the 0.5470 nm at 293 K obtained by Hutchings [2]. Thus, the results reported by Momin et al. appear to be low relative to other data as well as compared to the recommendation of Martin.

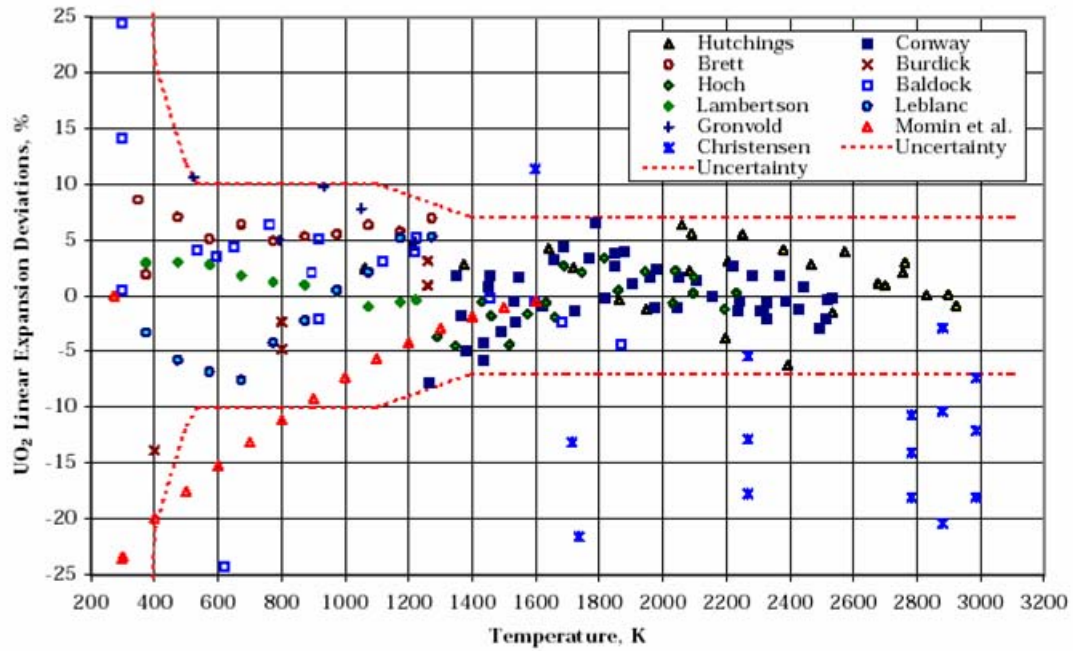


FIG. 3. Deviation of  $UO_2$  thermal expansion data from recommendation.

#### Comparison of $UO_2$ recommendation with previous recommendations

The 1981 recommendation of Fink, Chasanov, and Leibowitz [3] and the recommendation of MATPRO [4] were based on an analysis by Olsen [4], which used the data of Conway et al. [13] from 1263 to 2535 K and that of Christensen [11] from 1473 to 3073 K. Although the data of Christensen showed much scatter, they were the only data available in 1981 above 2535 K. The current version of MATPRO [20] gives an equation that is a function of stoichiometry from analysis of data in references [6, 8, 9, 11, 13–17]. This set of data is the same as that included in the final analysis by Martin except the MATPRO analysis included the data of Christensen but did not include the data of Hutchings. The recent data of Hutchings [2] are in much better agreement with that of Conway et al. than the data of Christensen and show that the data of Christensen are not reliable. Figure 4 compares  $\Delta L/L_{273}$  from data of Hutchings, Conway, and Christensen with the recommended equations of Martin, the 1981 recommendation of Fink et al. [3] and the MATPRO values [20]. Differences are significant at high temperatures where the fits are based on different sets of data. From 2800 through 3120, deviations of the equation of Fink et al. from the recommended one increase from 3% to 6.5%. These deviations are greater than the uncertainties given by Martin but are within the 7% uncertainty that is recommended. Deviations of the MATPRO values from those of Martin increase from 7% at 2400 K to 22% at 3100 K.

The recommended instantaneous linear thermal expansion coefficient given by Martin [1] is compared in Figure 5 with the 1981 recommended values [3]. Deviations between these instantaneous linear thermal expansion coefficients are even greater than the deviations between the fractional changes in linear thermal expansion ( $\Delta L/L_{273}$ ) because the linear instantaneous thermal expansion coefficient is the temperature derivative of the linear thermal expansion.

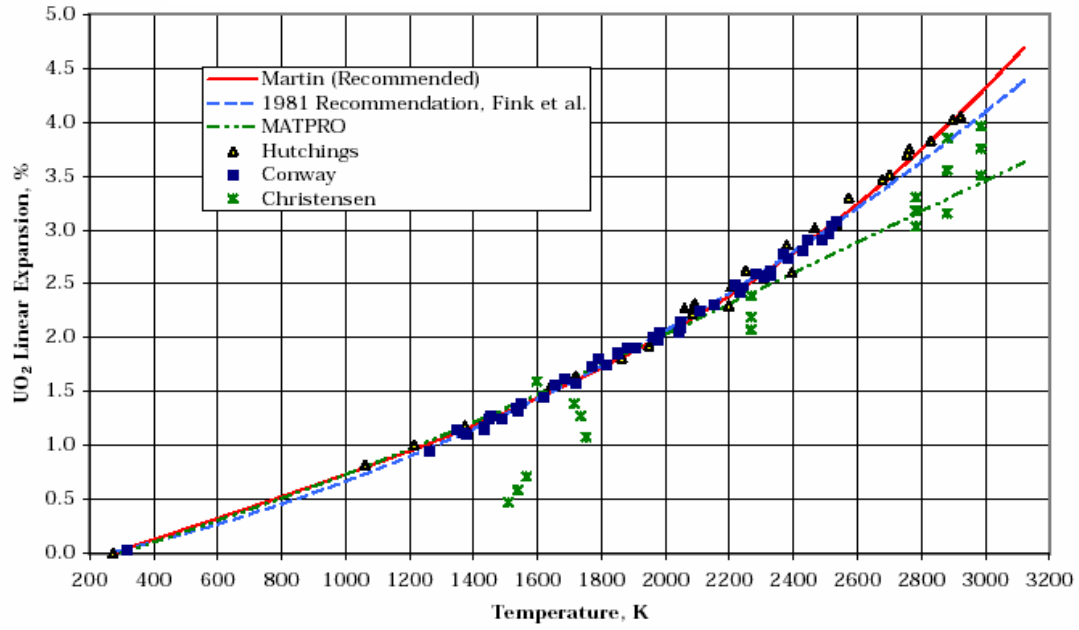


FIG. 4. Comparison of recommended  $UO_2$  thermal expansion with previous recommendations and data of Christensen, Conway, and Hutchings.

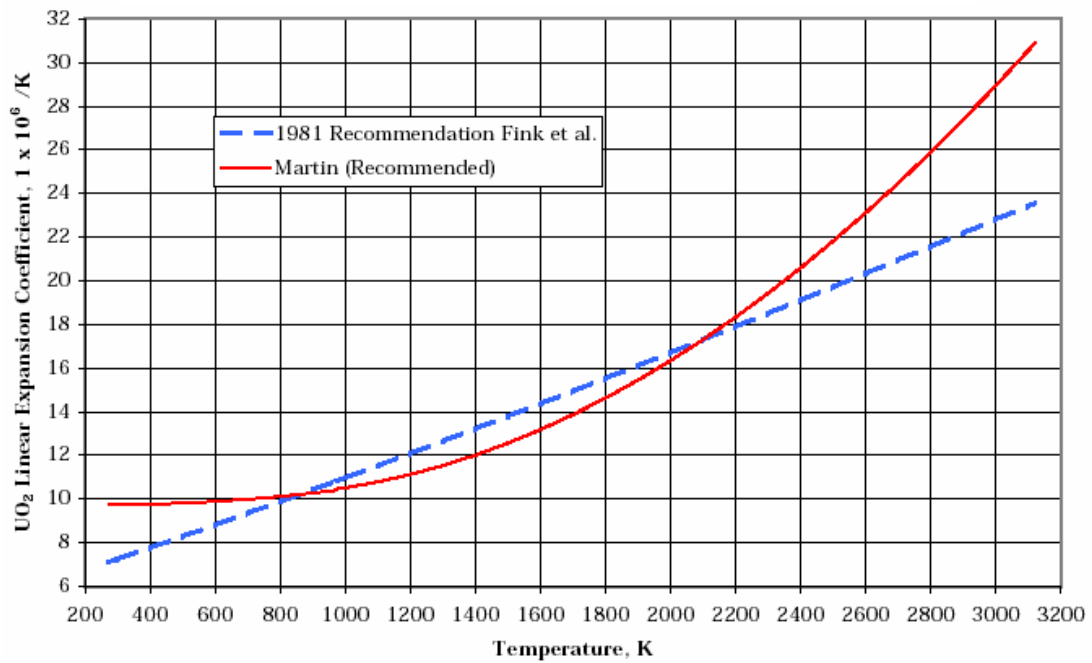


FIG. 5. Comparison of recommended  $UO_2$  linear thermal expansion coefficient of Martin with previous recommendation.

### Discussion of hyperstoichiometric uranium dioxide ( $\text{UO}_{2+x}$ )

Martin has examined the X-ray lattice parameter measurements of  $\text{UO}_{2+x}$  of Gronvold [16] for O/M ratios of 2.00, 2.10, 2.25, and 2.60; of Roth et al. [21] for O/M ratios of 2.08, and 2.24; of Fergusson et al. [22] for O/M = 2.235; and the macroscopic expansion studies on  $\text{UO}_{2+x}$  by Murray and Thackery [10] for O/M = 2.00 and 2.13 and those by Leblanc and Andriessen [7] for O/M = 2.00, 2.10, and 2.21. He made a zero error correction to the data of Murray and Thackery. He excluded the data of Gronvold with an O/M ratio of 2.60 on the basis that these data relate to an orthorhombic ( $\text{U}_3\text{O}_8$ ) structure not a fluorite structure. From comparison of the remaining data to his equations for the thermal expansion of  $\text{UO}_{2.00}$ , Martin concluded that the thermal expansion of  $\text{UO}_{2+x}$  is the same as that of  $\text{UO}_{2.00}$  for x values of 0–0.13 and 0.235–0.25 up to 1520 K. Figure 6, which compares some of the  $\text{UO}_{2+x}$  data with Martin's recommended percent change in the linear thermal expansion of  $\text{UO}_{2.00}$ , shows that Martin's conclusion is justified. The data for  $\text{UO}_{2+x}$  are very close to the recommendation for  $\text{UO}_{2.00}$  with deviations and scatter similar to that for the  $\text{UO}_{2.00}$  thermal expansion data. Because no data for  $\text{UO}_{2+x}$  exists above 1520 K, Martin speculates that his conclusion for thermal expansion at lower temperatures may be extended to the melting point.

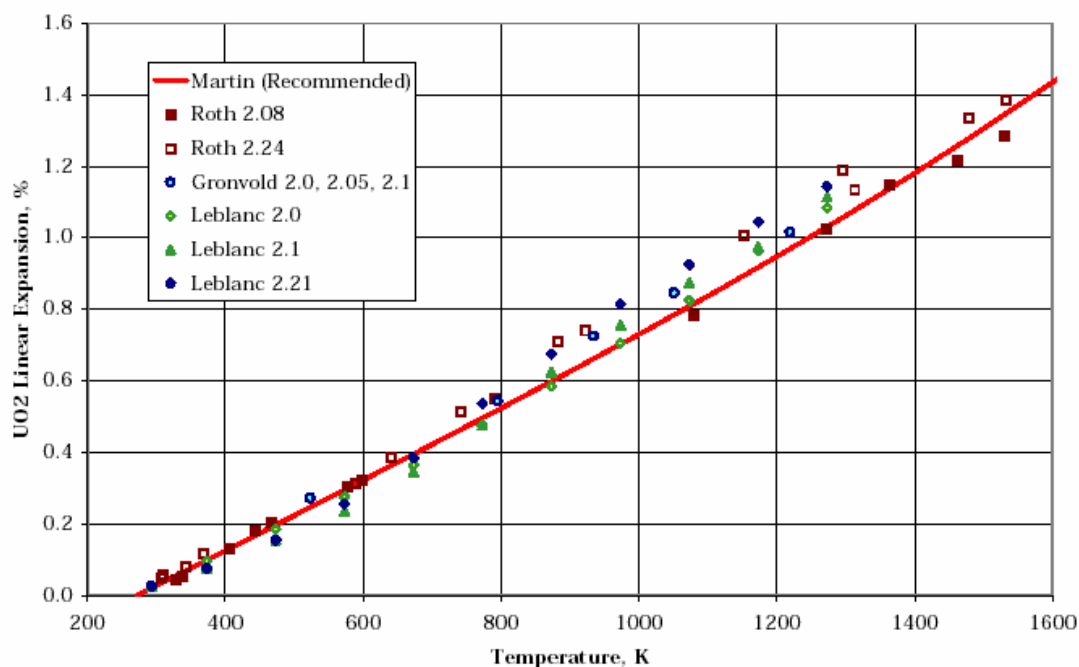


FIG. 6.  $\text{UO}_{2+x}$  thermal expansion data compared with recommendation.

### REFERENCES TO SECTION 6.1.1.3

- [1] MARTIN, D.G., The Thermal expansion of solid  $\text{UO}_2$  and (U,Pu) mixed oxides - A review and recommendations, J. Nucl. Mater. 152 94-101 (1988).
- [2] HUTCHINGS, M.T., High-temperature studies of  $\text{UO}_2$  and  $\text{ThO}_2$  using neutron scattering techniques, J. Chem. Soc. Faraday Trans. II 83, 1083-1103 (1987).
- [3] FINK, J.K., CHASANOV, M.G. and LEIBOWITZ, L., Thermophysical properties of uranium dioxide, J. Nucl. Mater. 102 17-25 (1981).
- [4] OLSEN, C.S., Fuel thermal expansion (FTHEXP) in MATPRO- Version 11: A handbook of materials properties for use in the analysis of light water reactor fuel rod behavior, ed. D. R. Hagraman and G. A. Reymann, US Nuclear Regulatory Commission Rep. NUREG/CR-0497 (February 1979); also revision (1981).
- [5] BELL, I.P. and MAKIN, S.M., R. and D. B. (C), Tech. Note No. 70, Culcheth Laboratories, UK (1954), as referenced by D. G. Martin, The thermal expansion of solid  $\text{UO}_2$  and (U,Pu) mixed oxides - A review and recommendations, J. Nucl. Mater. 152 94-101 (1988).
- [6] LAMBERTSON, W.A. and HANWERK, J.H., The fabrication and physical properties of urania bodies, Argonne National Laboratory Report ANL-5053 (1963).
- [7] LEBLANC, J.M. and ANDRIESSEN, H., EURATOM/USA Report EURAEC-434 (1962).
- [8] BURDICK, M.D. and PARKER, H.S., J. AM. CERAM. Soc. 39, 181-187 (1956).
- [9] BRETT, N.H. and RUSSELL, L.E., The thermal expansion of  $\text{PuO}_2$  and some other actinide oxides between room temperature and  $1000^\circ\text{C}$ , in Plutonium 1960, p. 397-410, E. Grison, W. B. H. Lord, and R. D. Fowler, eds., Cleaver Hyne Oress Ltd., London (1961).
- [10] MURRAY, P. and THACKRAY, R.W., *The Thermal Expansion of Sintered  $\text{UO}_2$* , Harwell memo AERE M/M22 (1950).
- [11] CHRISTENSEN, J.A., Thermal expansion and change in volume of uranium dioxide on melting, J. Am. Ceram. Soc. 46, 607-608 (1963).
- [12] HALDEN, F.A., WOHLERS, H.C., and REINHART, R.H., Thermal expansion of uranium dioxide, Stanford Research Institute Report No. SRI A-6, available from Technical Information Services Oak Ridge National Laboratory Report TID 5722 (1959).
- [13] CONWAY, J.B., FINCEL, R.M. and HEIN, R.A., *The Thermal Expansion and Heat Capacity of  $\text{UO}_2$  to  $2200^\circ\text{C}$* , Trans. Am. Nucl. Soc. 6, 153 (1963).
- [14] KEMPTER, C.P. and ELLIOT, R.O., J. CHEM. Phys. 30, 1524 (1959), as referenced by D. G. Martin, The thermal expansion of solid  $\text{UO}_2$  and (U,Pu) mixed oxides - A review and recommendations, J. Nucl. Mater. 152 94-101 (1988).
- [15] HOCH, M. and MOMIN, A.C., High temperature thermal expansion of  $\text{UO}_2$  and  $\text{ThO}_2$ , High Temp.-High Press. 1, 401-407 (1969).
- [16] GRONVOLD, F., J. INORG. Nucl. Chem. 1, 357 (1955).
- [17] BALDOCK, P.J., SPINDLER, W.E. and BAKER, T.W., The X-ray thermal expansion of near - stoichiometric  $\text{UO}_2$ , J. Nucl. Mater. 18 305-313 (1966).
- [18] ALBINATI, A., COOPER, M. J., ROUSE, K.D., THOMAS, M.W. and WILLIS, B.T.M., Acta Crystallogr. A36, 265 (1980).
- [19] MOMIN, A.C., MIZA, E.B. and MATHEWS, M.D., High temperature X-ray diffractometric studies on the lattice thermal expansion behaviour of  $\text{UO}_2$ ,  $\text{ThO}_2$ , and  $(\text{U}_{0.2}\text{Th}_{0.8})\text{O}_2$  doped with fission product oxides, J. Nucl. Mater. 185, 308-310 (1991).
- [20] HAGRMAN, D.T. (Ed.), SCDAP/RELAP5/Mod3.1 Code Manual, MATPRO - A library of materials properties for light-water-reactor accident analysis, US Nuclear Regulatory Commission Report NUREG/CR-6150 Vol. 4 (June 1995).
- [21] ROTH, J. and HALTEMAN, E.K., Nuclear Materials and Equipment Corp. Report NUMEC-389-9 (1965).
- [22] FERGUSON, I.F. and STREET, R.S., Harwell memo AERE M 1192 (1963) as referenced by D.G. Martin, The thermal expansion of solid  $\text{UO}_2$  and (U,Pu) mixed oxides - A review and recommendations, J. Nucl. Mater. 152 94-101 (1988).

### APPENDIX TO SECTION 6.1.1.3

#### DENSITY AND THERMAL EXPANSION RELATIONS

The thermal-expansion coefficient( $\alpha_P$ ) is a thermo-dynamic quantity defined as

$$\alpha_P = \frac{1}{V} \left( \frac{\partial V}{\partial T} \right)_P \quad (1)$$

where P, V, and T are respectively, pressure, volume, and temperature. We will refer to ( $\alpha_P$ ) as the instantaneous volumetric thermal-expansion coefficient. For simplicity, the subscript P has been eliminated from the thermal-expansion coefficients in the following discussion with the understanding that constant pressure is implied in all the following equations.

$$\bar{\alpha} = \frac{1}{V_o} \left( \frac{V - V_o}{T - T_o} \right) \quad (2)$$

where V and V<sub>0</sub> are the volumes at temperatures T and T<sub>0</sub> respectively. Because many measurements of thermal expansion involve measurement of a length change, it is common to find tabulations of the fractional (or percent) change in length,

$$\frac{\Delta L}{L_o} = \left( \frac{L - L_o}{L_o} \right) \quad (3)$$

where L and L<sub>0</sub> are respectively the sample lengths at temperatures T and T<sub>0</sub>. The instantaneous linear thermal-expansion coefficient is

$$\alpha_l = \frac{1}{L} \left( \frac{\partial L}{\partial T} \right) \quad (4)$$

The mean linear thermal-expansion coefficient is:

$$\bar{\alpha}_l = \frac{1}{L_o} \left( \frac{L - L_o}{T - T_o} \right) = \frac{1}{\Delta T} \left( \frac{L}{L_o} - 1 \right) \quad (5)$$

The instantaneous volumetric thermal-expansion coefficient is just three times the instantaneous linear thermal-expansion coefficient; i.e.,  $\alpha = 3 \times \alpha_l$ . The same relation does not hold for the mean thermal-expansion coefficients, as the following considerations show. The mean volumetric thermal-expansion coefficient may be written as:

$$\bar{\alpha} = \frac{1}{\Delta T} \left( \frac{V}{V_o} - 1 \right) \quad (6)$$

Since  $V = L^3$  the definition of the mean linear thermal-expansion coefficient in Eq. (4) gives

$$\frac{V}{V_o} = (1 + \bar{\alpha}_l \Delta T)^3 \quad (7)$$

when this is substituted in Eq. (6) and expanded, the relationship between the mean volumetric and mean linear coefficient is

$$\bar{\alpha} = 3\bar{\alpha}_l + 3\Delta T \bar{\alpha}_l^2 + \Delta T^2 \bar{\alpha}_l^3 \quad (8)$$

The error introduced by taking only the first term in this equation will generally be small in many applications. For example for  $\Delta T = 1000$  and  $\alpha = 1 \times 10^{-5}$ , only a 1% error will be introduced by ignoring the last two terms. The relation between linear thermal-expansion and density is

$$\frac{\Delta \rho}{\rho_o} = \frac{1 - (1 + \Delta L/L_o)^3}{(1 + \Delta L/L_o)^3} \quad (9)$$

where  $\Delta \rho = \rho - \rho_o$  is the difference between densities at temperatures  $T$  and  $T_o$ . Equation (9) may be derived from the definition of density

$$\rho = \frac{m}{V} = \frac{m}{V_o \left(1 + \frac{\Delta V}{V_o}\right)} \quad (10)$$

giving

$$\frac{\Delta \rho}{\rho_o} = \frac{\frac{-\Delta V}{V_o}}{\left(1 + \frac{\Delta V}{V_o}\right)} \quad (11)$$

and the relation between fractional change in volume and fractional change in length

$$1 + \frac{\Delta V}{V_o} = \left(1 + \frac{\Delta L}{L_o}\right)^3 \quad (12)$$

#### 6.1.1.4. Enthalpy and heat capacity of liquid $UO_2$

##### **Recommendation**

The recommended equations for the enthalpy and heat capacity of liquid  $UO_2$  are a least squares fit to the combined enthalpy data from 3173 to 3523 K of Leibowitz et al. [1], the enthalpy data from 3123 to 3260 K of Hein and Flagella [2] and the heat capacity data from 3100 to 4500 K of Ronchi et al. [3]. The data were weighted according to their uncertainties. Although Ronchi et al. made measurements to 8000 K, the data fit were limited to the 3100 to 4500 K temperature range because this is the range of interest for reactor safety calculations and the uncertainties in the determined heat capacities increase significantly with temperature above 4500 K.

For the temperature range 3120 to 4500 K, the recommended equation for the enthalpy increment of liquid  $UO_2$  in  $J mol^{-1}$  is:

$$H(l,T) - H(s,298.15K) = 8.0383 \times 10^5 + 0.25136T - \frac{1.3288 \times 10^9}{T} \quad (1)$$

The heat capacity at constant pressure is the temperature derivative of the enthalpy. For 3120 to 4500 K, the recommended equation for the heat capacity,  $C_P$ , in  $\text{J mol}^{-1} \text{K}^{-1}$  is:

$$C_P = +0.25136 + \frac{1.3288 \times 10^9}{T^2} \quad (2)$$

In Eqs. (1) and (2), the temperature,  $T$ , is in K. Recommended values of the enthalpy increment in  $\text{J mol}^{-1}$  and the heat capacity in  $\text{J mol}^{-1} \text{K}^{-1}$  are tabulated in Table 1 and shown in Figures 1 and 2.

Table 1. Enthalpy and heat capacity of liquid  $\text{UO}_2$  per mole of  $\text{UO}_2$

TEMPERATURE	ENTHALPY	HEAT CAPACITY
K	$H(T)-H(298.15 \text{ K})$ $\text{kJ mol}^{-1}$	$C_P$ $\text{J mol}^{-1} \text{K}^{-1}$
3120	379	137
3150	383	134
3200	389	130
3250	396	126
3300	402	122
3350	408	119
3400	414	115
3450	420	112
3500	425	109
3550	430	106
3600	436	103
3650	441	100
3700	446	97.3
3750	450	94.7
3800	455	92.3
3850	460	89.9
3900	464	87.6
3950	468	85.4
4000	473	83.3
4050	477	81.3
4100	481	79.3
4150	485	77.4
4200	488	75.6
4250	492	73.8
4300	496	72.1
4350	499	70.5
4400	503	68.9
4450	506	67.4
4500	510	65.9



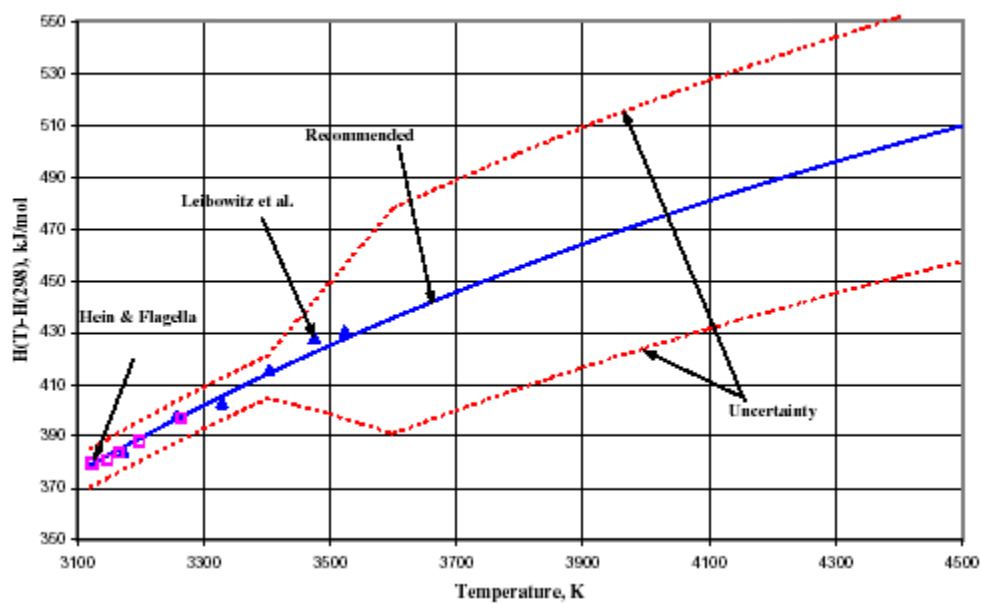


FIG. 1. Recommended values for the enthalpy of liquid  $\text{UO}_2$ .

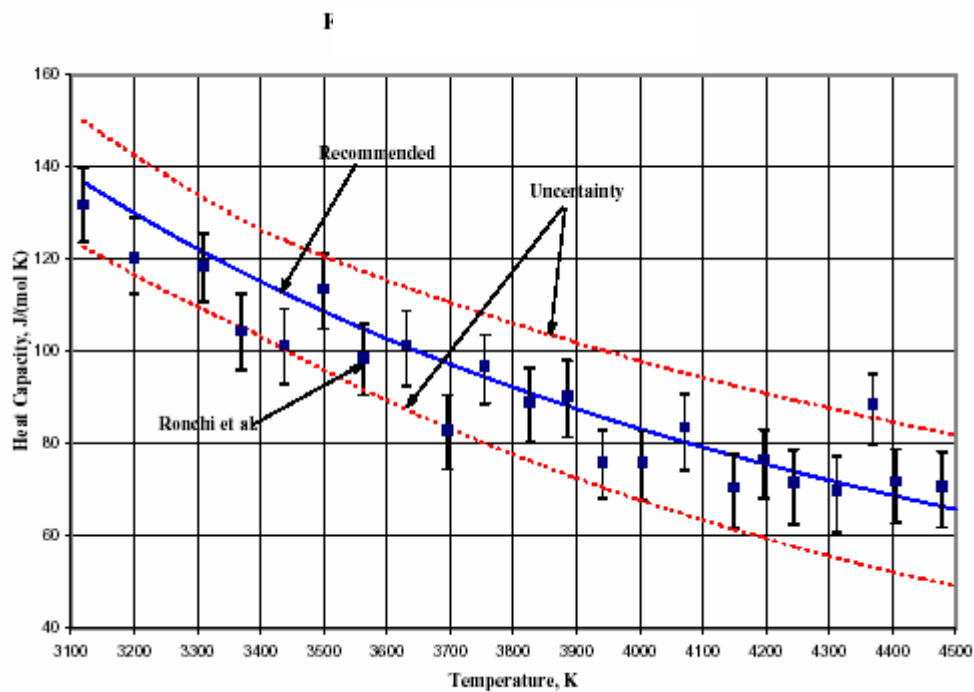


FIG. 2. Liquid  $\text{UO}_2$  heat capacity.

The recommended equations for the enthalpy increment in J kg<sup>-1</sup> and the heat capacity at constant pressure in J kg<sup>-1</sup>K<sup>-1</sup> are:

$$H(T) - H(298.15K) = 2.9768 \times 10^6 + 0.93087T - \frac{4.9211 \times 10^9}{T} \quad (3)$$

where temperature, T, is in K. Table 2 gives values for the enthalpy increment in J kg<sup>-1</sup> and the heat capacity in J kg<sup>-1</sup>K<sup>-1</sup>.

$$C_p = +0.93087 + \frac{4.9211 \times 10^9}{T^2} \quad (4)$$

### **Uncertainty**

The uncertainty in the recommended values for the enthalpy of liquid UO<sub>2</sub> is 2% from 3120 to 3500 K. It is based on the scatter in the data and deviation of the data from the fit. A 10% uncertainty is estimated for the extrapolated range from 3500 to 4500 K. The uncertainty in the recommended values for the heat capacity of liquid UO<sub>2</sub> is 10% from 3120 through 3400 K and increases linearly from 10% at 3400 K to 25% at 4500 K. Uncertainties have been included in Figure 2, which shows that all the heat capacity data are within the uncertainties except for data at 3370, 3700, and 4370 K.

### **Discussion**

#### *Enthalpy experiment*

Both Leibowitz et al.[1] and Hein and Flagella [2] used drop calorimetry to measure the enthalpy increments of molten UO<sub>2</sub> encapsulated in tungsten. Leibowitz et al. made 6 measurements from 3173 to 3523 K; Hein and Flagella made 6 measurements in the temperature range from 3123 to 3264 K but the datum at 3124 K was low relative to other data and discarded by Hein and Flagella. These two sets of data are in excellent agreement even though the samples differed in stoichiometry. The sample of Hein and Flagella had an O/M = 2.003 ± 0.003 at the start of the measurements and an O/M = 2.000 ± 0.003 at the end of the experiments whereas the sample of Leibowitz et al. had an O/M = 2.015 at the start and an O/M = 1.98 at the end of the experiments. Although the change in O/M was greater in the experiments of Leibowitz et al. than in those of Hein and Flagella, the range in O/M is well within the range expected for variations of O/M in reactor fuel. The greater variation in the O/M in the experiments of Leibowitz et al. is most likely due to reduction from tungsten at high temperatures (~3500 K) because the effect of tungsten would increase as the melting point of tungsten (3685 K) is approached. Four of the six measurements of Leibowitz et al. were above the highest temperature measured by Hein and Flagella.

Table 2. Enthalpy and heat capacity of liquid UO<sub>2</sub> per kg of UO<sub>2</sub>

TEMPERATURE K	ENTHALPY H(T)-H(298.15 K) kJ kg <sup>-1</sup>	HEAT CAPACITY C <sub>p</sub> J kg <sup>-1</sup> K <sup>-1</sup>
3120	1403	507
3150	1418	497
3200	1442	482
3250	1466	467
3300	1489	453
3350	1511	439
3400	1533	427
3450	1554	414
3500	1574	403
3550	1594	391
3600	1613	381
3650	1632	370
3700	1650	360
3750	1668	351
3800	1686	342
3850	1702	333
3900	1719	325
3950	1735	316
4000	1750	309
4050	1766	301
4100	1781	294
4150	1795	287
4200	1809	280
4250	1823	273
4300	1837	267
4350	1850	261
4400	1863	255
4450	1875	249
4500	1888	244

Rand et al. [4] fit the data of Leibowitz et al.[1] and of Hein and Flagella[2] and the linear equation:

$$H(T) - H(298.15K) = 130.95 T - 3091 \quad (5)$$

where the enthalpy increment is in J mol<sup>-1</sup> and temperature (T) is in K. This equation fits the data with a standard deviation of 0.41%. This equation has been recommended for the enthalpy of liquid UO<sub>2</sub> by Fink et al.[5] and by Harding, Martin, and Potter [6]. The data of Leibowitz et al.[1] and of Hein and Flagella [2] and the linear equation of Rand et al. [4] are shown in Figure 3.

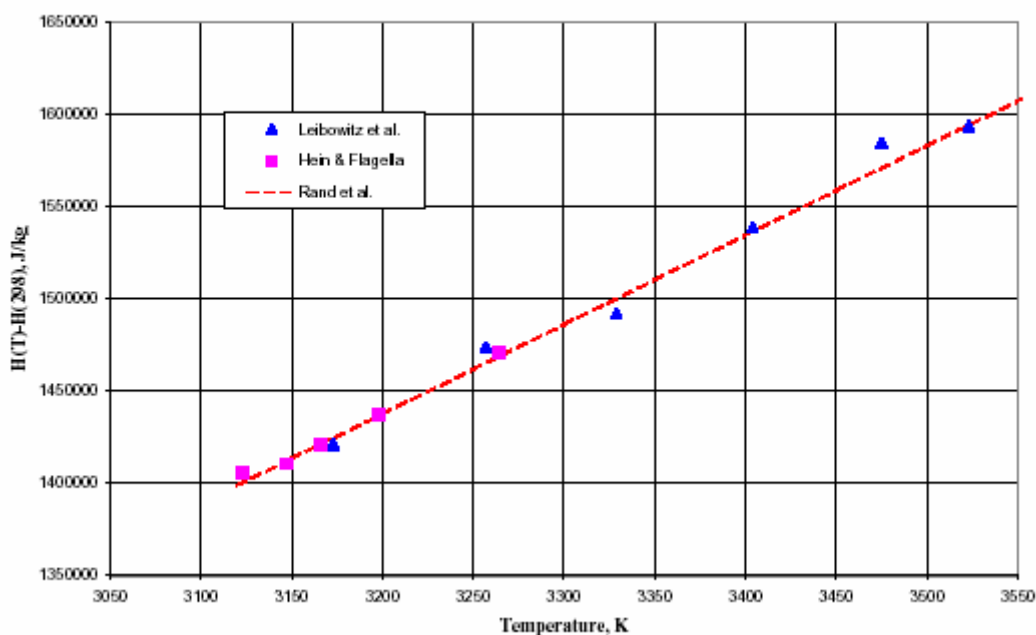


FIG. 3. Fit of the enthalpy of liquid  $\text{UO}_2$  by linear equation of Rand et al.

#### Heat capacity experiments

The heat capacity of molten  $\text{UO}_2$  has been determined by Ronchi et al. [3] from the analysis of cooling curves of 0.5- to 1-mm-diameter  $\text{UO}_2$  microspheres heated to 3100-8000 K by four tetrahedrally oriented Nd:YAG lasers. The sintered  $\text{UO}_2$  microspheres were suspended on a tungsten needle in an inert atmosphere autoclave at pressures up to 1000 bar (100 MPa). Analysis of the experiments was based on an energy balance of the rate of input energy and the enthalpy increase of the sample. The determination of the heat capacity is based on the measurement of the sample surface-temperature history during heating and cooling. Since in most cases, the laser-energy deposition rate cannot be assessed with precision, the cooling branch of the curve is used preferentially [7]. Consequently, these difficult experiments required accurate (1) measurements of the sample temperature during and after laser pulse heating, (2) evaluation of energy loss rates and (3) determination of the heat transport in the sample.

The experimenters took great care to minimize measurement errors as much as possible and to assess all energy losses. In an effort to reduce the errors due to optical absorption by the vapor surrounding the sample [8], temperatures were measured using a six-wavelength optical pyrometer. Melting experiments of oxides and refractory metals, including tungsten, indicated that the accuracy of the temperature measurement was within  $\pm 10$  K. Measurements of the freezing temperature of  $\text{UO}_2$  for various samples indicated that it was in the interval  $3070 \pm 20$  K for samples heated in an inert atmosphere with up to 0.1 bar (0.01 MPa) of oxygen. Higher melting temperatures ( $3140 \pm 20$  K) were obtained for samples in an inert atmosphere without oxygen. This trend is consistent with the effect of change of O/U ratio on the melting temperature. The melting point of stoichiometric  $\text{UO}_2$  is  $3120 \pm 30$  K. This value, recommended by Rand et al.[4] from their analysis of fourteen experimental studies (over a period of 20 years), has been accepted internationally. Although Ronchi et al. [3] cite accurate measurements of lower values [9] ( $3075 \pm 30$  K); Adamson et al.[10] found in their examination of melting behavior of  $\text{UO}_2$  and  $(\text{U,Pu})\text{O}_2$  as a function of stoichiometry and irradiation that these measurements used a V-filament method which yields consistently low melting temperatures. The V-filament method is a measurement on uncontained samples supported on a tungsten needle analogous to the method used for heat capacity measurements by Ronchi et al. [3]. Adamson et al. [10] state that in the V-filament method pronounced compositional changes occur in the small uncontained samples as a result of rapid incongruent vaporization and in some cases

interactions involving oxygen exchange between either the atmosphere or the tungsten support. These changes lead to surface emissivity changes, which cause an error in the temperature measurement. Ronchi et al. did not determine the stoichiometry of the microspheres before or after the heat capacity measurements because of the small size of the samples. They comment that oxidation to stoichiometries of O/U  $\approx$  2.03 cannot be excluded but no evidence of the formation of U<sub>4</sub>O<sub>9</sub> was observed in x-ray analysis. Although increases in stoichiometry may have occurred during heating at high pressure in an atmosphere of an inert gas plus oxygen, reductions could have occurred from heating in contact with tungsten in an inert atmosphere. Diffusion of tungsten from the supporting needle into the UO<sub>2</sub> was observed above 3000 K. The thickness of the UO<sub>2</sub>/tungsten interaction region was a function of the pulse time. For a 20 ms pulse creating central melting, the chemical interaction only effected a 10 to 20  $\mu$ m region near the tungsten needle and was, therefore, negligible. With repeated pulses, the tungsten precipitates migrated to the outside of the microsphere.

Heat losses taken into account during the pulse included radiation losses, evaporation losses, and convective losses. The experimenters observed that the plasma that surrounded their samples was significantly affected by laser excitation (inverse bremsstrahlung and photoeffects). Because the vapor partial pressure of liquid UO<sub>2</sub> is high and evaporation of atoms presented a serious experimental complication, the experiments had to be done under high pressures to prevent significant vaporization and mass loss. The type and pressure of the gas in the autoclave was selected based on the equation of state of Fischer [11] to reduce losses from vaporization to <1% of the radiative losses. Heat losses due to heat conduction and convection in the buffer gas were determined from similar experiments using tungsten, which has a well known heat capacity. Convective losses were dominant up to 4000 K.

In analysis of the experiments, Ronchi et al. used an iterative numerical method to find the unique heat capacity  $C_p(T)$  that satisfies at any time the heat transport equation with the measured temperature boundary conditions and the one-dimensional unsteady energy conservation equation,

$$\frac{dH}{dt} = \int_0^{r_0} 4\pi r^2 \rho(T) C_p(T) \frac{\delta T(r)}{\delta t} dr = \text{losses} \quad (6)$$

where H is the enthalpy,  $\rho(T)$  is the density as a function of temperature,  $C_p(T)$  is the heat capacity at constant pressure as a function of temperature, T is the temperature, t is the time, and  $r_0$  is the radius of the UO<sub>2</sub> microsphere. The losses in Eq.(6) are defined by the boundary condition:

for  $r = r_0$  and  $t > 0$ ,

$$-k \frac{\partial T}{\partial r} = \varepsilon \sigma (T_s^4 - T_A^4) + D(T_s - T_A) - \phi_L(t) \quad (7)$$

where

- k = thermal conductivity of the sphere,
- $T_s$  = sphere surface temperature,
- $T_A$  = ambient temperature,
- $\sigma$  = Stefan-Boltzmann constant,
- $\varepsilon$  = total hemispherical emissivity,
- $r_0$  = outer radius of the sphere,
- D = coefficient of convective and conductive heat losses to the environment,
- and  $\phi_L$  = laser energy flux deposited onto the surface.

The quality of the experiments and selection of analysed pulses was based on posttest metallographic examination of the microsphere to determine the integrity of the zone beneath the measured area. Because severe cracking and large voids influenced temperature measurements, data from samples

with defects in the vicinity of the measured area were discarded. Of 120 laser shots, only 20 were considered of sufficient quality for data analysis. Figure 4 shows the heat capacity data and uncertainties, which have been obtained from the graph in Figure 14 of reference 3 because the experimenters have not published their tabulated data points. The points designated as “Ronchi (Not Used)” in the legend of Figure 4 indicate data that the experimenters considered to be in error and were discarded in their data analysis. They fit their data to the equation:

$$C_P = 277 + \frac{1.1 \times 10^7}{T^2} \exp\left(\frac{15500 \pm 1000}{T}\right) + \frac{1.0 \times 10^{12}}{T^2} \exp\left(-\frac{35500 \pm 4000}{T}\right) \quad (8)$$

where  $T$  is the temperature in K and  $C_P$  is the heat capacity in  $\text{J kg}^{-1} \text{K}^{-1}$ . Heat capacities calculated with this equation are shown in Figure 4 as the curve labeled “RSHS”.

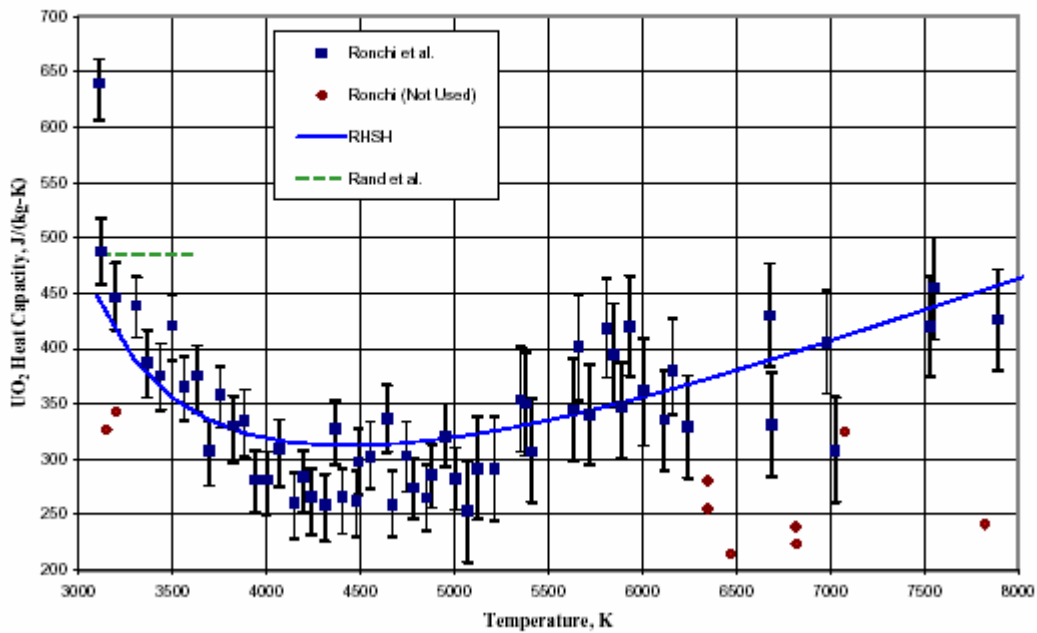


FIG. 4. Liquid  $\text{UO}_2$  heat capacity measurements of Ronchi et al.

The experimenters comment [3] that the accuracy of the heat capacities obtained from their data analysis depends on the spherical symmetry and the precision of the physical properties used in the analysis. The data reduction and analysis by Ronchi et al. [3] assumed spherical symmetry of the heat pulse, spherical symmetry of the temperature distribution in the microsphere, and maintenance of the spherical shape of the microsphere throughout the measurement. Because the surface temperature was measured on only a small area of the sample, the analysis is only viable if this temperature can be assumed to be homogeneous and if the internal temperature field can be considered spherically symmetric [7]. Although the experimenters commented that posttest examination of their samples showed that the melting front was approximately circular, it is not clear from the paper that all the necessary spherical symmetries were always maintained throughout the measurements. The laser pulse duration ranged from 153 to 10 ms depending on the desired peak surface temperature (3100 to 7850 K) and the input power of the laser. The experimenters commented that the pulse duration was limited because the liquid adheres to the supporting tungsten needle for only a few tens of milliseconds before dropping. It is not clear how long the spherical symmetry of the liquid was maintained because the liquid drop must deform prior to dropping from the needle in tens of milliseconds. The plume of hot gas around the sample during the laser heating, shown in photographs

in Figure 6 of Reference 3 and Figure 4 of Reference 7 are not spherical. It is not clear if this departure from spherical symmetry is due to (1) gas flow in the autoclave, (2) nonspherical energy input and heat transfer, (3) change in the sample shape from that of a sphere, or some combination of these mechanisms.

Because the reliability of the calculated heat capacities depends on the accuracy of the physical properties used in the data analysis, the equations used for thermal conductivity and density have been compared with literature recommendations. Ronchi et al. [3] calculated the density of solid  $\text{UO}_2$  from:

$$\rho^s(T) = 10970 [1 + 2.04 \times 10^{-5}(T - 273) + 8.7 \times 10^{-9}(T - 273)^2] \text{ J}^{-1} \quad (9)$$

where density  $\rho^s$  is in  $\text{kg m}^{-3}$  and  $T$  is in K. Densities calculated with this equation agree within 2% with values recommended in the recent assessment by Martin [12]. The thermal conductivity of solid  $\text{UO}_2$  in  $\text{W m}^{-1} \text{K}^{-1}$  was obtained from the equation of Hyland [13] for  $T > 2000 \text{ K}$ ;

$$k(T) = (2.3 \pm 0.4) + \frac{2.25 \times 10^5}{T} \exp\left(-\frac{12410}{T}\right) \quad (10)$$

where  $T$  is in K. Melting point values calculated with this equation agree within 8% with the values recommended by Harding and Martin [14] but are 14% higher than the melting point value recommended in this INSC Material Properties Database assessment and analysis that includes the 1999 high-temperature heat capacity and thermal diffusivity data of Ronchi et al. [15].

Ronchi et al. [3] calculated the liquid density of  $\text{UO}_2$  from their least-squares fit to the data of Christensen [16] and Drotning [17]

$$\rho^l(T) = 10970 [1 + 9.30 \times 10^{-5}(T - 273)] \text{ J}^{-1} \quad (11)$$

where density is in  $\text{kg m}^{-3}$  and  $T$  is in K. The form selected for this equation is the same as that for the solid density. Values calculated with this equation differ significantly from those obtained from the equation recommended by Drotning and the recent equation of Breitung and Reil [18] which is based on in reactor measurements of the density and thermal expansion from the melting point to 8000 K. The equation of Breitung and Reil [18] is:

$$\rho = 8860 - 0.9285(T - 3120)$$

where density ( $\rho$ ) is in  $\text{kg m}^{-3}$  and  $T$  is in K. Densities obtained from the equation by Breitung and Reil are in good agreement with values recommended by Drotning (within 1.2% from 3120 to 7600 K), and within 2.5% of the densities recommended from the melting point to 7600 K in an independent assessment by Harding, Martin, and Potter [6]. In Figure 5, densities calculated with the equation given by Ronchi et al. [3] are compared with the experimental data of Drotning and of Christensen, and with the equation recommended by Breitung and Reil. Densities calculated with the equation used by Ronchi et al. show a systematic deviation compared to densities calculated from the equation of Breitung and Reil. They deviate by -2% at the melting point, +4% at 4500 K, +16% at 6000 K, and +40% at 7600 K. Although the analytical form of equation selected by Ronchi et al. gives decreasing densities with increasing temperature, they do not decrease as fast as the linear equations recommended by Breitung and Reil and by Christensen. Fischer [11] comments that the linear decrease with temperature of the liquid density is well established by existing experiments and the only physical reason for the liquid density to deviate from a straight line is due to the approach of the critical point where the deviation is more negative. The critical temperature and density given by Fischer [11] are respectively 10600 K and 1560  $\text{kg m}^{-3}$ . The possibility exists that the density equation used by Ronchi et al. includes the increase of density with pressure since experiments at higher temperatures were performed at high pressure. However, Ronchi et al. make no mention of including the effects of pressure in their equation for the liquid density. They simply state that the data of Drotning and of Christensen were fit to Eq. (11). Breitung and Reil have commented that along the saturation line, the change in density due to increasing pressure is much smaller than the change in density due to thermal expansion [18]. Even at 8000 K, the correction of density for saturation pressure is only a few percent [18] so the effects of pressure can be ignored. Thus, it is unclear why

the equation given by Ronchi et al. [3] for the liquid density of  $\text{UO}_2$  deviates so greatly from the expected liquid density behavior and recommended densities at high temperatures.

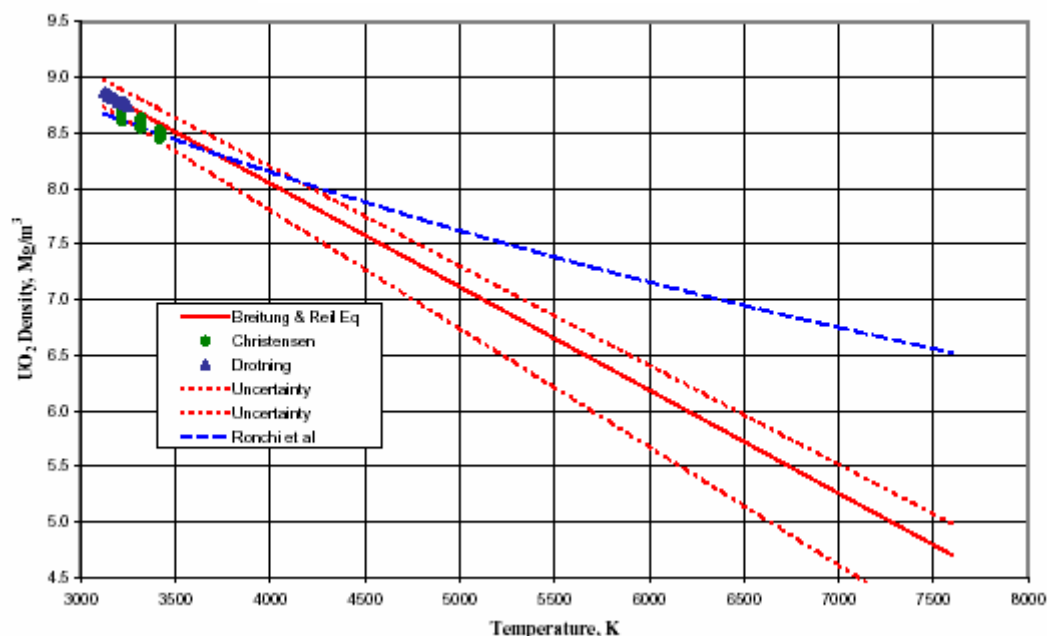


FIG. 5. Liquid density of  $\text{UO}_2$ .

For the thermal conductivity of liquid  $\text{UO}_2$ , Ronchi et al. used  $2.5 \text{ W m}^{-1} \text{ K}^{-1}$ , which is the value obtained just above the melting point in recent measurements by Tasman [19] at the Institute for Transuranium Elements. This value is in agreement with the average value of  $2.2 \text{ W m}^{-1} \text{ K}^{-1}$  previously obtained by Tasman et al. [20] for the temperature range 3103–3473 K. In these earlier measurements, a thermal conductivity of  $2.4 \text{ W m}^{-1} \text{ K}^{-1}$  was obtained in an experiment in which the maximum top center temperature of the molten pool was 3473 K. In addition to the thermal conductivity measurements of Tasman et al. [19, 20],  $\text{UO}_2$  thermal diffusivity measurements were made by Kim et al. [21] from 3187 to 3310 K and by Otter and Damien [22] in the temperature range of 3133 to 3273 K. The available experimental data on the thermal diffusivity and thermal conductivity [19] of  $\text{UO}_2$  were reassessed in 1985 by Fink and Leibowitz [23] who recommended  $5.6 \text{ W m}^{-1} \text{ K}^{-1}$  for the thermal conductivity from the melting point to 3500 K. In this reassessment, Fink and Leibowitz used  $131 \text{ J mol}^{-1} \text{ K}^{-1}$  ( $485 \text{ J kg}^{-1} \text{ K}^{-1}$ ), the constant heat capacity given by the enthalpy equation of Rand et al. [4]. If the heat capacities given by Ronchi et al. had been used in the reassessment, lower thermal conductivity values ( $3.3$  to  $5.8 \text{ W m}^{-1} \text{ K}^{-1}$ ) would have been obtained in the assessment of these data. Ronchi et al. comment that the existence of a systematic error in the experimental measurements of Tasman et al. cannot be excluded. At low temperatures, their calculated heat capacity is approximately inversely proportional to the thermal conductivity. Thus, selection of a higher thermal conductivity in this low temperature region would give lower heat capacities.

Ronchi et al. have assumed a constant thermal conductivity based on the assumption that thermal conductivity of liquids obey the Lorenz rule and are therefore only a weak function of temperature. Because no temperature dependence was evident in any of the thermal diffusivity data and no information is available on variation of thermal conductivity with temperature from the measurements of Tasman et al., there is no basis to assess this assumption. Wakeham [24] comments that the thermal conductivities of a number of liquids at high pressure are stronger functions of density change with pressure than functions of temperature. In their analysis, Ronchi et al. have not considered the effects of changes in pressure on the thermal conductivity although the high temperature measurements were done at pressures on the order of 100 MPa (1000 bar). Wakeham [23] found that for pressure variation



from 0.1 to 700 MPa, the reduced thermal conductivity decreased as a function of increasing reduced molar volume (inverse reduced density).

#### *Relationship between enthalpy and heat capacity measurements, $C_P$ , and $C_\sigma$*

The enthalpy measurements by Leibowitz et al. [1] and by Hein and Flagella [2] were performed on encapsulated samples so that the liquid was maintained in equilibrium with a small amount of vapor giving the enthalpy along the saturation curve. The temperature derivative of these enthalpies is the heat capacity along the saturation curve,  $C_\sigma$ , which is related to the heat capacity at constant pressure,  $C_P$ , by:

$$\left(\frac{\partial H}{\partial T}\right)_\sigma = C_\sigma = C_P - \frac{(T\alpha_P - 1)}{\rho} \left(\frac{\partial P}{\partial T}\right)_\sigma \quad (13)$$

where  $P$  is the vapor pressure,  $\rho$  is the density,  $\alpha_P$  is the instantaneous thermal expansion coefficient,  $T$  is the temperature, and the subscript  $\sigma$  designates the saturation curve. For most liquids, the difference between  $C_P$  and  $C_\sigma$  is not significant at temperatures below 75% of the critical temperature. Recent vapor pressure measurements by Breitung and Reil [18] and equation of state calculations by Fischer [11] indicate that the critical temperature for  $\text{UO}_2$  is 10600 K. Thus, differences between  $C_P$  and  $C_\sigma$  are not significant below 7950 K. Therefore, for the temperature range of the  $\text{UO}_2$  enthalpy data, the temperature derivative of the equation that fits the enthalpy measurements may be considered as the heat capacity at constant pressure.

The heat capacity measurements of Ronchi et al. were not done at constant pressure because measurements at constant pressure would have resulted in complete vaporization of the sample as the temperature was increased. Ronchi et al. used the saturated and total pressures from the equation of state of Fischer [11] to determine the pressure needed to prevent large losses from vaporization. However, the extent of increase from the saturation pressure is not clear from the description of the experiment. In the analysis of Ronchi et al. and the analysis below, the heat capacities reported by Ronchi et al. are assumed to be equivalent to  $C_P$ .

#### *Combined analysis of enthalpy and heat capacity data*

Ronchi et al. [3] state that the enthalpy data of Hein and Flagella and of Leibowitz et al. are consistent with their equation 20, which will subsequently be referred to as "RHS Eq. 20":

$$C_P(T) = 277 + \frac{(2370 \pm 290)}{(T/1000)^2} \quad (14)$$

where heat capacity is in  $\text{J kg}^{-1} \text{K}^{-1}$  and temperature is in K. The first term of this equation is the Neumann-Kopp heat capacity value for a harmonic triatomic lattice (9R) which was fixed so that the only free parameter in the fitting procedure was the coefficient for the second term.

They fit their heat capacity data from 3200 to 4500 K to an equation of the same form allowing both parameters to vary giving their equation 21, which will be referred to as "RHS Eq. 21":

$$C_P(T) = 67.7 + \frac{(3831 \pm 300)}{(T/1000)^2} \quad (15)$$

where heat capacity is in  $\text{J kg}^{-1} \text{K}^{-1}$  and temperature is in K.

A weighted chi-squared minimization analysis of has been made of the combined enthalpy and heat capacity data. This analysis included the enthalpy data of Leibowitz et al. [1] from 3173 to 3523 K and of Hein and Flagella [2] from 3123 to 3260 K and the heat capacity data of Ronchi et al. [3] from 3100 to 4500 K. Only the heat capacity at or below 4500 K have been included in this combined analysis because:

- 1) above 4500 K, the deviations of the densities used by Ronchi et al. increases above 4% from accepted liquid densities;
- 2) at higher temperatures, the pressure in the autoclave was increased significantly to prevent sample vaporization;

- 3) at 4500 K and above, oxygen was added to the gas in an attempt to control the change in sample stoichiometry arising from vaporization so greater uncertainty exists in the stoichiometry of the sample and in the temperature measurements;
- 4) as the temperature increases, sample loss due to laser ablation and ionization effects from the laser heating become more pronounced;
- 5) data above 4500 K are not needed for light water nuclear reactor severe accident analysis because higher temperatures are unlikely in these accident scenarios.

The form of the equation for the heat capacity used in this combined analysis is that suggested by Ronchi et al. in their data analysis in this temperature range. A weighted chi-squared minimization was used to determine the coefficients. In a previous assessment [25], the value of the enthalpy at the melting point had been constrained to equal that given by the enthalpy equation of Rand et al. [4] in order for that analysis to be consistent with the heat of fusion of Rand et al. [4]. No constraint has been made on the enthalpy increment at the melting point in this analysis because the enthalpy of fusion must be redetermined because of changes to the enthalpy and heat capacity of the solid at the melting point. The data have been weighted by the inverse of their uncertainties. Because the enthalpy data are in excellent agreement in the two independent experiments [1, 2] which used standard techniques with calibration standards and the stoichiometry change in these enthalpy experiments were within the variation for reactor fuel, these data were considered to be of higher quality than the heat capacity data. The uncertainty in the enthalpy data has been estimated as 2%. Ronchi et al. state that the uncertainty in the heat capacity data is on the order of 15 to 20% from 3000 to 5000 K. A 15% uncertainty has been assumed for the heat capacity data. Thus, the enthalpy chi-squared has been weighted by a factor of 50 relative to the heat capacity chi-squared in the combined chi-squared minimization.

Equations (1) and (2) are, respectively, the enthalpy and heat capacity equations obtained from this weighted chi squared minimization. In Figure 6, the enthalpy data are compared with Eq. (1) from this weighted fit, the linear equation of Rand et al., the enthalpies obtained from integration of the heat capacity equation of Ronchi et al. using a constant of integration that gives the enthalpy of Rand et al. at 3120 K (RHSR rel 3120), and the 1997 constrained fit to the enthalpy and heat capacity data [25]. The main difference between this weighted fit and the 1997 constrained fit is the value of the enthalpy increment at 3120 K. Enthalpy increments from these two analyses are within 0.3%, which is less than the uncertainty in the data. Equation (1) fits the data to within 0.7% except for the datum at 3475 K, which is fit to 1.3%. Greater deviation for the higher data may be expected because the stoichiometry variation detected by Leibowitz et al. most likely occurred during these high temperature measurements.

Figure 7 compares the heat capacity data of Ronchi et al. with a number of equations as a function of the square of the inverse temperature. Equations in Figure 7 are the constant heat capacity of Rand et al., RHSR Eq. 20 (the one-parameter enthalpy data fit of Ronchi et al.), RHSR Eq. 21 (the two parameters heat capacity fit of Ronchi et al.), RHSR (the fit by Ronchi et al. to all the heat capacity data) and the recommended equation, Eq. (2), which is the weighted combined fit to the enthalpy and heat capacity data. The equation obtained from this weighted combined analysis fits the heat capacity data as well as the equation suggested by Ronchi et al. for the entire temperature range (RHSR).

Figure 8 shows the heat capacity data with the error bars given by Ronchi et al., the fit by Ronchi et al. to data up to 4500 K (RHSR Eq. 21), the fit by Ronchi et al to the heat capacities for the entire temperature range (RHSR) and the weighted combined fit to the enthalpy and heat capacities. All but four data are fit to within 10%. Data with error bars that do not intersect this combined fit are also not well represented by the RHSR Eq. 21 indicating that they are not consistent with other heat capacity data in this temperature range.

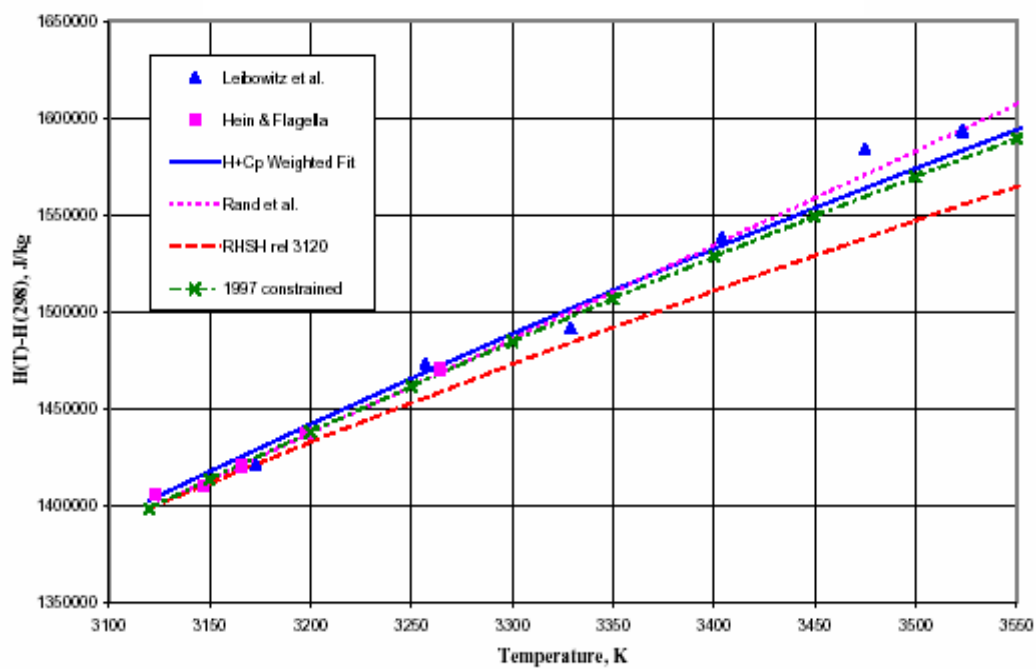


FIG. 6. Comparison of equations for the enthalpy of liquid  $\text{UO}_2$

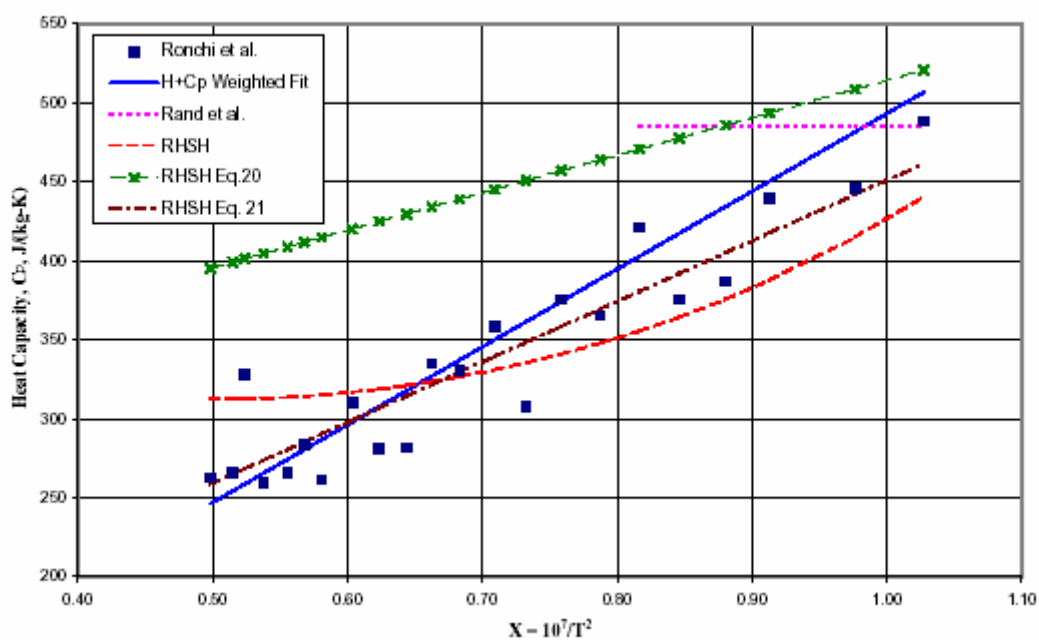


FIG. 7. Comparison of equations for the heat capacity of liquid  $\text{UO}_2$

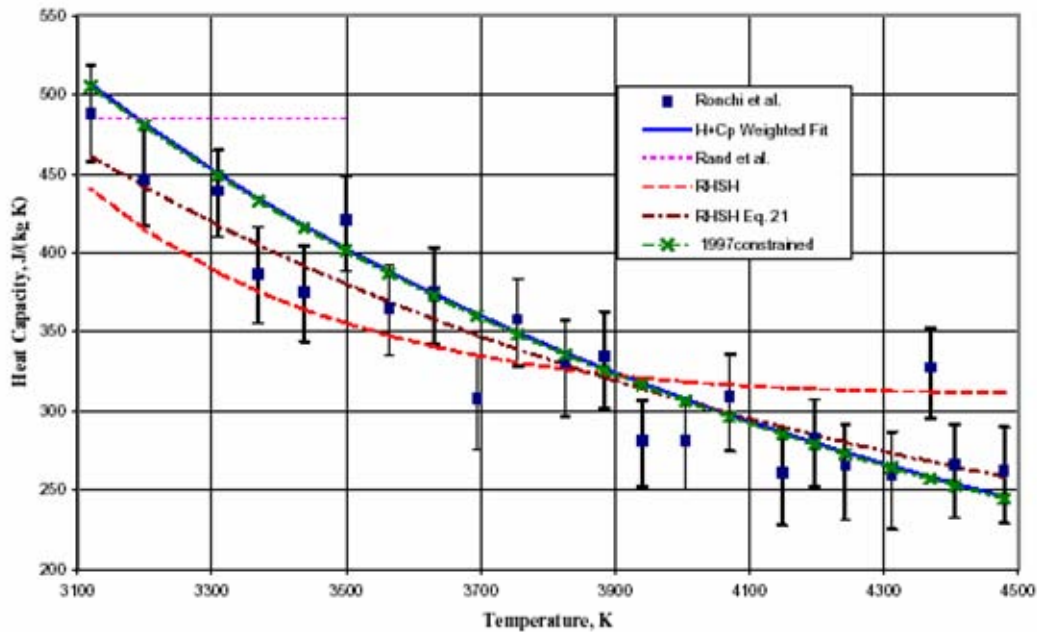


FIG. 8. Liquid  $\text{UO}_2$  heat capacity.

#### REFERENCES TO SECTION 6.1.1.4

- [1] LEIBOWITZ, L., CHASANOV, M.G., MISHLER, L.W. and FISCHER, D.F., Enthalpy of liquid uranium dioxide to 3500 K, J. Nucl. Mater. 39 115-116 (1971).
- [2] HEIN, R.A. and FLAGELLA, P.N., Enthalpy measurements of  $\text{UO}_2$  and Tungsten to 3260 K, General Electric Report GEMP-578 (February 16, 1968).
- [3] RONCHI, C., HIERNAUT, J.P., SELFSLAG, R. and HYLAND, G.J., Laboratory measurement of the heat capacity of Urania up to 8000 K: I. Experiment, Nuclear Science and Engineering 113, 1-19 (1993).
- [4] RAND, M.H., ACKERMANN, R.J., GRONVOLD, F., OETTING, F.L., PATTORET, A., The thermodynamic properties of the Urania phase, Rev. Int. Hautes Temp. Refract. 15, 355-365 (1978).
- [5] FINK, J.K., CHASANOV, M.G., and LEIBOWITZ, L., Thermo-physical properties of uranium dioxide, J. Nucl. Mater. 102, 17-25 (1981); also as ANL Report ANL-CEN-RSD-80-3, Argonne National Laboratory (April 1981).
- [6] HARDING, J.H., MARTIN, D.G. and POTTER, P.E., Thermo-physical and thermo-chemical properties of fast reactor materials, Commission of the European Communities Report EUR 12402 EN (1989).
- [7] HIERNAUT, J.-P., and RONCHI, C., Calorimetric measurements with acoustic levitation high-temperature heating experiments with pulsed laser beams, High Temps-High Pressures 21, 119-130 (1989).
- [8] RONCHI, C., BEUKERS, R., HEINZ, H., HIERNAUT, J.P. and SELFSLAG, R., Graphite melting under laser pulse heating, Int. J. Thermo-phys. 13 (1) 107-129 (1992).
- [9] BATES, J.L., Proc. IAEA Symp. Thermodynamics, Vienna, July 22-27 1965, Vol. II, p. 73, International Atomic Energy Agency, Vienna (1966); as referenced by C. Ronchi, J. P. Hiernaut, R. Selfslag, and G. J. Hyland, Laboratory measurement of the heat capacity of Urania up to 8000 K: I. Experiment, Nuclear Science and Engineering 113, 1-19 (1993).
- [10] ADAMSON, M.G., AITKEN, E.A. and CAPUTI, R.W., Experimental and thermo-dynamic evaluation of the melting behavior of irradiated oxide fuels, J. Nucl. Mater. 130, 349-365 (1985).
- [11] FISCHER, E.A., Evaluation of the Urania equation of state based on recent vapour pressure measurements, Kernforschungszentrum Karlsruhe GmbH Report KfK 4084 (September 1987); Nuclear Science and Engineering 101, 97-116 (1989).

- [12] MARTIN, D.G., The thermal expansion of solid UO<sub>2</sub> and (U,Pu) mixed oxides - A review and recommendations, J. Nucl. Mater. 152, 94-101 (1988).
- [13] HYLAND, G.J., Thermal conductivity of solid UO<sub>2</sub>: critique and recommendation, J. of Nucl. Mater. 113, 125-132 (1983).
- [14] HARDING, J.H. and MARTIN, D.G., A recommendation for the thermal conductivity of UO<sub>2</sub>, J. of Nucl. Mater. 166, 223-226 (1989).
- [15] RONCHI, C., SHEINDLIN, M., MUSELLA, M. and HYLAND, G.J., Thermal conductivity of uranium dioxide up to 2900 K from simultaneous measurement of the heat capacity and thermal diffusivity, J. Appl. Phys. 85, 776-789 (1999).
- [16] CHRISTENSEN, J.A., Thermal expansion and change in volume of uranium dioxide on melting, J. Am. Ceram. Soc. 46, 607-608 (1963).
- [17] DROTNING, W.D., Thermal expansion of molten uranium dioxide, Proceedings of the Eighth Symp. On Thermo-physical Properties, Gaithersburg, Maryland, June 15-18, 1981, J. V. Sengers, Ed., ASME, New York, Vol. II, pp 245-249 (1981).
- [18] BREITUNG, W. and REIL, K.O., The density and compressibility of liquid (U,Pu)-mixed oxide, Nuclear Science and Engineering 105, 205-217 (1990).
- [19] TASMAN, H.A., Thermal conductivity of liquid UO<sub>2</sub>, Commission of the European Communities Joint Research Centre Annual Report TUAR88, Karlsruhe, Germany EUR-12385, p. 80 (1989), as referenced by C. Ronchi in *On the Thermal Conductivity and Diffusivity of Solid and Liquid Uranium Dioxide*, J. Phys. Condens. Matter 6, L561-L567 (1994).
- [20] TASMAN, H.A., PEL, D., RICHTER, J. and SCHMIDT, H.E., Measurement of the thermal conductivity of liquid UO<sub>2</sub>, High Temp.-High Pressures 15, 419-431 (1983).
- [21] KIM, C.S., HALEY, R.A., FISCHER, J., CHASANOV, M.G. and LEIBOWITZ, L., Measurement of thermal diffusivity of molten UO<sub>2</sub>, Proc. Seventh Symp. On Thermo-physical Properties, A. Cezairliyan, Ed., ASME, New York, p. 338-343 (1977).
- [22] OTTER, C. and DAMIEN, D., Mesure de la diffusivite thermique de UO<sub>2</sub> fondu, High Temp.-High Pressures 16, 1-6 (1984).
- [23] FINK, J.K. and LEIBOWITZ, L., An analysis of measurements of the thermal conductivity of liquid urania, High Temp.- High Pressures 17, 17-26 (1985).
- [24] WAKEHAM, W.A., Thermal conductivity of liquids under pressure, High Temp.- High Pressures 21, 249-259 (1989).
- [25] FINK, J.K. and PETRI, M.C., Thermo-physical properties of uranium dioxide (Version 0 for Peer Review), Argonne National Laboratory Report ANL/RE-97/2 (February 1997).

#### 6.1.1.5. Enthalpy of fusion of UO<sub>2</sub>

##### **Recommendation**

The recommended value for the enthalpy of fusion of UO<sub>2,00</sub> is:

$$\Delta H_f = 70 \pm 4 \text{ kJ} \cdot \text{mol}^{-1}$$

or  $259.3 \pm 14.8 \text{ kJ} \cdot \text{kg}^{-1}$ . The enthalpy of fusion was calculated from the following equations for the enthalpy of solid and of liquid UO<sub>2</sub> at the melting point of 3120 K:

$$\begin{aligned} H(T) - H(298.15 \text{ K}) = & C_1 \theta \left[ (e^{\theta/T} - 1)^{-1} - (e^{\theta/298.15} - 1)^{-1} \right] \\ & + C_2 \left[ T^2 - (298.15)^2 \right] \\ & + C_3 e^{-E_a/T} \end{aligned} \quad (1)$$

Solid UO<sub>2</sub>;  $298.15 \text{ K} \leq T \leq 3120 \text{ K}$ ,

where  $C_1 = 81.613$ ,  
 $\theta = 548.68$ ,  
 $C_2 = 2.285 \times 10^{-3}$ ,  
 $C_3 = 2.360 \times 10^7$ ,  
 $E_a = 18531.7$ ,

T is the temperature in K and the enthalpy increment,  $H(T) - H(298.15 \text{ K})$ , is in  $\text{J} \cdot \text{mol}^{-1}$ .

$$H(l, T) - H(s, 298.15 K) = 8.0383 \times 10^5 + 0.25136T - \frac{1.3288 \times 10^9}{T} \quad (2)$$

Liquid  $\text{UO}_2$ ;  $3120 \text{ K} \leq T \leq 4500 \text{ K}$ ,

where  $T$  is the temperature in K and the enthalpy increment  $H(l, T) - H(s, 298.15 \text{ K})$ , is in  $\text{J} \cdot \text{mol}^{-1}$ .

### **Discussion of recommendation**

Equation (1) for the enthalpy of solid  $\text{UO}_2$  is a weighted least squares analysis of the enthalpy data of Leibowitz et al. [1], Fredrickson and Chasanov [2], Hein and Flagella [3, 4], Ogard and Leary [5], and Moore and Kelly [6] and the heat capacity data from 293 to 1006 K of Huntzicker and Westrum [7] and Gronvold et al. [8] and the heat capacity data from 1997–2873 K from recent measurements by Ronchi et al. [9]. Equation (2) for the enthalpy of liquid  $\text{UO}_2$ , is a combined fit of the liquid  $\text{UO}_2$  heat capacity data of Ronchi et al. [10] and the enthalpy data of Leibowitz et al. [11] and of Hein and Flagella [3, 4]. No constraint on the value of the liquid enthalpy at the melting point has been included in this analysis of the liquid data.

The recommended value for the enthalpy of fusion is less than the previously recommended value,  $74.8 \text{ kJ} \cdot \text{mol}^{-1}$  [12, 13]. The enthalpy of fusion given in MATPRO [14] is:  $274.0 \text{ kJ} \cdot \text{kg}^{-1}$ , which is  $74.0 \text{ kJ} \cdot \text{mol}^{-1}$ .

### **Uncertainty**

The uncertainty in the recommended enthalpy of fusion of  $\text{UO}_2$  is  $\pm 6\%$ .

## **REFERENCES TO SECTION 6.1.1.5**

- [1] LEIBOWITZ, L., MISHLER, L.W. and CHASANOV, M.G., J. Nucl. Mater. 29, 356 (1969).
- [2] FREDRICKSON, D.R. and CHASANOV, M.G., J. Chem. Thermodynamics 2, 263 (1970).
- [3] HEIN, R.A. and FLAGELLA, P.N., *Enthalpy Measurements of  $\text{UO}_2$  and Tungsten to 3260 K*, GE Report GEMP-578, General Electric, February 16, 1968.
- [4] HEIN, R.A., SJODAHL, L.A. and SZWARC, R., J. Nucl. Mater. 25, 99 (1968).
- [5] MOORE, G.E. and KELLY, K.K., J. Am. Chem. Soc. 69, 2105 (1947).
- [6] OGARD, A.E. and LEARY, J.A., *High-Temperature Heat Content and Heat Capacity of Uranium Dioxide and Uranium Dioxide-Plutonium Dioxide Solid Solutions*, in Thermodynamics of Nuclear Materials 1967, IAEA, Vienna, p. 651 (1969).
- [7] HUNZICKER, J.J. and WESTRUM, E.F., J. Chem. Thermodynamics 3, 61 (1971).
- [8] GRONVOLD, F., KVSETH, N.J., SVEEN, A. and TICHY, J., J. Chem. Thermo. 2, 665 (1970).
- [9] RONCHI, C., SHEINDLIN, M., MUSELLA, M. and HYLAND, G.J., J. Applied Phys. 85, 776-789 (1999).
- [10] RONCHI, C., HIERNAUT, J.P., SELFSLAG, R. and HYLAND, G.J., *Laboratory Measurement of the Heat Capacity of Urania up to 8000 K: I. Experiment*, Nuclear Science and Engineering 113, 1-19 (1993).
- [11] LEIBOWITZ, L., CHASANOV, M.G., MISHLER, L.W. and FISCHER, D.F., *Enthalpy of Liquid Uranium Dioxide to 3500 K*, J. Nucl. Mater. 39 115-116 (1971).
- [12] FINK, J.K. and PETRI, M.C., *Thermophysical Properties of Uranium Dioxide*, Argonne National Laboratory Report ANL/RE-97/2 (February 1997).
- [13] FINK, J.K., CHASANOV, M.G. and LEIBOWITZ, L., *Thermophysical Properties of Uranium Dioxide*, J. Nucl. Mater. 102 17-25 (1981).
- [14] HORHORST, J.K. (Ed.), *SCADAP/RELAP5/MOD2 Code Manual Vol. 4: MATPRO - a library of materials properties for light-water reactor accident analysis*, Eg&G Idaho Report NUREG/CR-5273 (1990).

#### 6.1.1.6. Thermal conductivity and diffusivity of liquid $\text{UO}_2$

##### **Recommendation**

Based on an initial review of the limited data [1-4] on the thermal conductivity and thermal diffusivity of liquid  $\text{UO}_2$ , the liquid thermal conductivity is in the range of 2.5 to 3.6  $\text{W m}^{-1} \text{K}^{-1}$ . Liquid thermal diffusivities range from  $6 \times 10^{-7}$  to  $11 \times 10^{-7} \text{m}^2 \text{s}^{-1}$ .

##### **Experiments**

The available data on the thermal conductivity ( $k$ ) and thermal diffusivity ( $\alpha$ ) of liquid  $\text{UO}_2$  are summarized in Table 1. Measurements of thermal diffusivity were made by Kim et al. [1] and by Otter and Damien [2]. Tasman et al. [3,4] measured thermal conductivity. The measurements by Kim et al. [1] and by Otter and Damien were based on standard methods for obtaining the thermal diffusivity.

Kim et al. [1] used a modulated electron beam technique to measure the thermal diffusivity of  $\text{UO}_2$  in the temperature range of 3187 to 3310 K. A thin  $\text{UO}_2$  sample clad in tungsten was heated by two electron beams. The top beam was modulated sinusoidally and the difference in phase between the top and bottom temperatures was measured. The thermal diffusivity was determined from the phase changes. Measurements were made on two thicknesses of  $\text{UO}_2$  (0.813 and 1.219 mm) and three modulated frequencies: 0.25 Hz ( $\pi/2 \text{ rad s}^{-1}$ ), 0.50 Hz ( $\pi \text{ rad s}^{-1}$ ), and 0.75 Hz ( $3\pi/2 \text{ rad s}^{-1}$ ). The tungsten above and below the  $\text{UO}_2$  layer was 1.397 and 1.016 mm thick. In the reanalysis [5] of the data of Kim et al. [1], an error was found in the original analysis by Kim et al. [1]. The reanalysis included (1) the ideal calculation done by Kim et al., (2) an ideal model using a three-dimensional unsteady-state heat transfer code that assumed infinite slabs with no sidewalls, and (3) the real case accounting for heat transfer in the tungsten sidewalls using a transient 3-dimensional unsteady-state heat transfer code. No radiative heat transfer within the liquid was modeled based on the comment of Bober [7] that radiative heat transfer in the liquid would be small and could not account for the increase in thermal conductivity of the liquid. The heat transfer analysis using ideal and real models of the  $\text{UO}_2$  in the tungsten cell showed that if the thermal conductivity was low, then the ideal model was not a good approximation because wall conductivity becomes important as the conductivity of the liquid layer decreases. As shown in Table 1, statistically significant difference was found between the thermal conductivities of the thick and thin layers. Although tungsten contamination of the samples could affect the conductivity, it would have a greater effect in the thin cell than in the thick cell and give the larger conductivity for the thin cell. Lack of good contact between the tungsten and the liquid could also affect the experimental results. The difference between the thin and thick cell results is analogous to differences observed in diffusivity measurements of materials in which radiation is important and cannot be neglected [8, 9]. The main uncertainties in this experiment are effects from radiative heat transfer in the liquid and effects from changes in the O/M ratio in the  $\text{UO}_2$  due to tungsten contamination in the liquid  $\text{UO}_2$  sample.

Otter and Damien [2] measured the thermal diffusivity of a 0.7-mm layer of liquid  $\text{UO}_2$  encased in tungsten using a laser flash method in the temperature range of 3133 to 3273 K. Although this method is well established, analysis of the data becomes more complex at high temperatures with liquids encased in metal cells because of the necessity of including thermal losses to the environment and the need for the use of properties such as heat capacity, density, and thermal conductivity of the metal containment [10]. The reanalysis [5] of their experiment gave lower thermal conductivities than those originally reported by Otter and Damien. Insufficient information is available regarding their experiment and heat losses to determine if the differences are due to different treatment of heat losses in the reanalysed three-dimensional transient heat transfer calculation. Radiation within the sample was not included in the reanalysis. If radiative heat transfer was significant in the experiments of Kim et al., it would also affect the experiment of Otter and Damien. In addition, errors from tungsten contamination of the sample cannot be ruled out.

Table 1. Thermal conductivity of liquid  $\text{UO}_2$  from measurements of thermal diffusivity and thermal conductivity

EXPERIMENT	KIM et al. [1]	OTTER & DAMIEN [2]	TASMAN et al. [3, 4]
Property Measured	Thermal Diffusivity	Thermal Diffusivity	Thermal Conductivity
Method	Periodic Heat Flow	Laser Flash	Laser Heating - Melt & Ablate $\text{UO}_2$ self-contained sample
Sample	$\text{UO}_2$ in tungsten 3 -layers; $\text{UO}_2$ layer: 0.8 mm, 1.2 mm	$\text{UO}_2$ in tungsten 3 -layers; $\text{UO}_2$ layer: 0.7 mm	$\text{UO}_2$ 6-mm diam. disc partially molten; molten layer: 0.2 mm
k reported, $\text{W m}^{-1} \text{K}^{-1}$	11	8.5	2.0-2.4; mean 2.2 [3]
Re-evaluated 3-dim. transient heat transfer model [5] k, $\text{W m}^{-1} \text{K}^{-1}$	5.5 (mean) 4.8 (thin 0.8 mm) 6.2 (thick 1.2 mm)	6.7	4.5
Corrected 3-dim transient heat transfer calculation using $C_p$ of Ronchi et al. [6] k, $\text{W m}^{-1} \text{K}^{-1}$	3.9 (thin) 5.1 (thick)	5.8	3.3
Re-measurement & f.e.m**. analysis under unsteady conditions; k, $\text{W m}^{-1} \text{K}^{-1}$ [4]			2.5 [4]

\* f.e.m. stands for finite element method

Tasman et al. [3] determined the thermal conductivity of liquid  $\text{UO}_2$  from a steady-state finite element analysis of the heat transfer in a partially molten, self-contained sample. A  $\text{UO}_2$  disc (6 mm in diameter by 1.2- to 3-mm thick) was heated in an argon atmosphere at 4 bar (0.4 MPa) using three continuous-wave  $\text{CO}_2$  laser beams. One laser beam was focused on a 4-mm diameter area on the bottom of the disc; two laser beams were focused on an area 2-mm in diameter on the top of the disc. The sample was heated with only the bottom beam until it reached  $1800^\circ\text{C}$  (2073 K). Then the upper beams were turned on and a molten pool was formed on the top of the sample. Temperatures were measured with optical pyrometers and a fast scanning device. During heating, only the bottom temperature was measured. The peak top temperature was  $3200^\circ\text{C}$  (3473 K). Because of extensive vaporization of the sample, the top of the sample could be heated for only 4–5 sec. When heated longer, extensive evaporation created a deep pit in the top center of the sample and part of the ejected material was deposited in crystalline form along the center crater edge. Even on short (5-sec) exposures, recondensed crystals were found. Sample loss from evaporation was limited to less than 2 mg (0.5%) if the exposure to the upper beams was limited to 5 sec. However, it is not clear how much sample mass was redistributed by vaporization and condensation on cooler parts of the sample during the 5 sec exposure to the upper beam. Significant vaporization of  $\text{UO}_2$  began at  $2300^\circ\text{C}$  (2573 K), which is well below the melting point, 3120 K. Tasman et al. [3] stated that the largest uncertainty in their experiment was the temperature measurement and temperature profile of the top and bottom faces. Because these profiles are critical input in the analysis of the experiment, there is significant uncertainty in the calculated results. The precision of the experiment is limited by the presence of very high radial temperature gradients and axial asymmetries. However, the error is bounded by the depth of the molten layer, which was determined after solidification from examination



of cross sections of the sample. The reliability of visual observation of the liquid depth was questioned [5] based on (1) low melting points (2661 and 2699 K) obtained by early investigators [11] from the appearance of residues and (2) the observed [12] softening and plasticity of  $\text{UO}_2$  above about 2500 K where the Frenkel oxygen lattice disorder increases as the phase transition is approached. Above 2670 K, the creep rate also increases significantly [12, 13], so  $\text{UO}_2$  readily deforms to the shape of its container. Ronchi [14] commented that in the short duration of the experiment of Tasman et al. (~10 sec), the grain growth is approximately 10  $\mu\text{m}$  at 2700 K [13] and is estimated to be only 5 times larger at 3050 K. He, therefore, concluded that the solid grains are still recognizable at temperatures near the melt front so that the liquid phase is readily distinguished. The reanalysis of this experiment by Fink and Leibowitz [5] indicated that the assumption of steady state conditions made by Tasman et al.[3] makes a significant difference in the resulting thermal conductivity.

Tasman [4] repeated his experiment using a rapid 2D temperature-scanning device and included unsteady transport in the 2D finite-element method analysis. His correction was less than that reported by Fink and Leibowitz [5]. He claimed that perturbations that cannot be accounted for in his analysis would lead to lower values in the thermal conductivity [14]. He concluded that the thermal conductivity of liquid  $\text{UO}_2$  is  $2.5 \pm 1 \text{ W m}^{-1} \text{ K}^{-1}$ , which is lower than the thermal conductivity of the solid at the melting point given by Harding and Martin [15] ( $3.95 \text{ W m}^{-1} \text{ K}^{-1}$ ) and by Hyland [16] ( $3.65 \text{ W m}^{-1} \text{ K}^{-1}$ ). The thermal conductivity equation for solid  $\text{UO}_2$  of Harding and Martin includes a phonon lattice contribution and an electronic contribution from small polarons, whereas Hyland also included a radiation contribution. At the melting point, the electronic contribution calculated by Harding and Martin is  $2.56 \text{ W m}^{-1} \text{ K}^{-1}$ , which is slightly higher than the value for the thermal conductivity of the liquid obtained by Tasman. The electronic, radiation, and lattice contributions to the solid thermal conductivity at the melting point determined by Hyland are  $1.55 \text{ W m}^{-1} \text{ K}^{-1}$ ,  $0.2 \text{ W m}^{-1} \text{ K}^{-1}$ , and  $2.1 \text{ W m}^{-1} \text{ K}^{-1}$ , respectively. The radiative contribution calculated by Hyland was  $0.48 \text{ W m}^{-1} \text{ K}^{-1}$ , but he assumed a 50% uncertainty because this value was higher than needed for good agreement with experimental total thermal conductivities. Differences in the lattice and electronic contributions to the thermal conductivity of the solid in these two calculations are related to the different data used in the models. Because of these differences, no conclusions with regard to the reliability of the measurement of Tasman can be made from comparison with contributions to the solid thermal conductivity at the melting point.

## Discussion

Ronchi et al. [6] determined the heat capacity of liquid  $\text{UO}_2$  from the melting point to 8000 K by heating sintered 0.5- to 1-mm diameter microspheres by four tetrahedrally oriented laser beams in an inert autoclave at pressures up to 1000 bar. The samples were suspended by a tungsten needle during pulses of a few milliseconds duration. The heat capacity was calculated numerically from the energy input, the sample temperature during and after laser pulse heating, the energy loss rates, the cooling mechanisms (radiation and convection), and the heat transport within the sample. The accuracy of the calculation depended on the symmetry (of the temperature field from the lasers and the sample shape) and the accuracy of the physical properties (density and thermal conductivity) used in the heat transport analysis. In the calculations, Ronchi et al. [6] used  $2.5 \text{ W m}^{-1} \text{ K}^{-1}$  for the thermal conductivity of liquid  $\text{UO}_2$ . However, they commented that selection of a higher value for the thermal conductivity of the liquid would result in a lower heat capacity. The thermal conductivity values in the next to the last row of Table 1 are the values of thermal conductivity from the reanalysis of Fink and Leibowitz [5] adjusted for the heat capacities of Ronchi et al. Although the new heat capacity values reduce the thermal conductivities calculated by Fink and Leibowitz [5], the calculated thermal conductivities are not as low as the value reported by Tasman [4]. However, the corrected value calculated for the experiment of Tasman et al.[3] is within the original uncertainty given by Tasman et al. [3, 4].

Because the heat capacities obtained by Ronchi et al. [6] are a function of the value selected for the thermal conductivity and are consistent with the value reported by Tasman [4] and all other data in Table 1 are from thermal diffusivity measurements, thermal diffusivities should be compared instead of thermal conductivities. The temperature at which the thermal conductivity of liquid  $\text{UO}_2$  was remeasured by Tasman [4] has not been reported by Ronchi et al. [6, 14]. In their analysis of their heat capacity data, Ronchi et al. [13] assumed that the liquid thermal conductivity is constant at  $2.5 \text{ W m}^{-1}$

K<sup>-1</sup> for the liquid temperature range (3120 - 8000 K). It is not clear if their observed variation in heat capacity with temperature is real or is due, in part, to this assumption of constant thermal conductivity. In any case, the thermal diffusivity calculated using the heat capacities ( $C_p$ ) of Ronchi et al. [6, 13] and constant thermal conductivity ( $k$ ) of 2.5 W m<sup>-1</sup> K<sup>-1</sup> is consistent with the analytical treatment of the heat capacity data of Ronchi et al. [6, 13]. The liquid UO<sub>2</sub> densities ( $\rho$ ) of Breitung and Reil [17], which agree with the values of Drotning [18], have been used in the conversion to thermal diffusivity ( $\alpha$ ) via the relationship:

$$\alpha = \frac{k}{C_p \rho}$$

Thermal diffusivities from the most recent measurements of Tasman [4] and the thermal diffusivity experiments of Otter and Damien [2] and Kim et al. [1] are given in Table 2.

Ronchi [14] commented that diffusivity in crystals decreases with temperature due to increased anharmonic vibrations caused by defects, impurities, and lattice strains. Below 2500 K, the behavior of the thermal diffusivity of UO<sub>2</sub> is in accord with this crystalline behavior. As the  $\lambda$  phase transition at 2670 K is approached, the number of phonon scattering centers increases. Above the  $\lambda$  phase transition, the concentration of Frenkel pairs in the oxygen sublattice approaches 0.2 [13], so the lattice has a very high degree of disorder similar to an amorphous or glassy material. Ronchi [14] commented that materials that have both crystalline and glassy forms (e.g., SiO<sub>2</sub>) have a different temperature dependence for the thermal diffusivity in the two forms (decreasing for the crystal; increasing for the glassy phase) [14]. In metals and alloys that undergo order/disorder  $\lambda$  transitions, the slope of thermal diffusivity changes at the  $\lambda$  transition from decreasing to increasing. If no transition exists, the reversal of slope normally occurs at the melting point and is often accompanied by a discontinuity in thermal diffusivity upon melting. For materials with a premelting order/disorder transition, the thermal diffusivity typically increases continuously across the melting point [14]. In Figure 1, the thermal diffusivities of liquid UO<sub>2</sub> from the measurements of Kim et al. [1], Otter and Damien [2] and Tasman [4] are compared with thermal diffusivities of solid UO<sub>2</sub> near the melting point. The solid values are from thermal diffusivity measurements by Weilbacher [19,20] and the thermal conductivity equations of Harding and Martin [15] and of Hyland [16]. The thermal conductivities were converted to thermal diffusivities using Eq. (1) and the heat capacities from the assessment by Fink [21] and the densities from the assessment of Martin [22]. Thermal diffusivities, calculated from the thermal conductivity of Tasman [4], are between the solid values of Martin and of Hyland. Based on the behavior of other materials with premelting transitions, Ronchi [14] concluded that the thermal diffusivity obtained from the thermal conductivity measurement of Tasman is the most consistent with the thermal diffusivities of solid UO<sub>2</sub>.

Table 2. Thermal diffusivity of liquid  $\text{UO}_2$  from measurements of thermal diffusivity and thermal conductivity

EXPERIMENT	KIM et al. [1]	OTTER & DAMIEN [2]	TASMAN et al. [3,4]
Property Measured	Thermal Diffusivity	Thermal Diffusivity	Thermal Conductivity
Method	Periodic Heat Flow	Laser Flash	Laser Heating - Melt & Ablate $\text{UO}_2$ self-contained sample
Sample	$\text{UO}_2$ in tungsten 3 -layers; $\text{UO}_2$ layer: 0.8 mm, 1.2 mm	$\text{UO}_2$ in tungsten 3 -layers; $\text{UO}_2$ layer: 0.7 mm	$\text{UO}_2$ 6-mm diam. disc partially molten; molten layer: 0.2 mm
Reported $\alpha$ , $\text{m}^2 \text{s}^{-1}$	$19 \times 10^{-7}$ - $33 \times 10^{-7}$ *	$16 \times 10^{-7}$ - $25 \times 10^{-7}$	-
Re-evaluated 3 -dim. transient heat transfer model [5]	$11 \times 10^{-7}$ (thin) $15 \times 10^{-7}$ (thick)	$16 \times 10^{-7}$	
Re-measurement & f.e.m.** analysis under unsteady conditions; $\alpha$ , $\text{m}^2 \text{s}^{-1}$ [4]			$6 \times 10^{-7}$ - $8 \times 10^{-7}$

\* In the assessment by Fink and Leibowitz, an error was found in the original analysis by Kim et al. that indicated that these values reported by Kim et al. are high by about a factor of two.

\*\* f.e.m. stands for finite element method

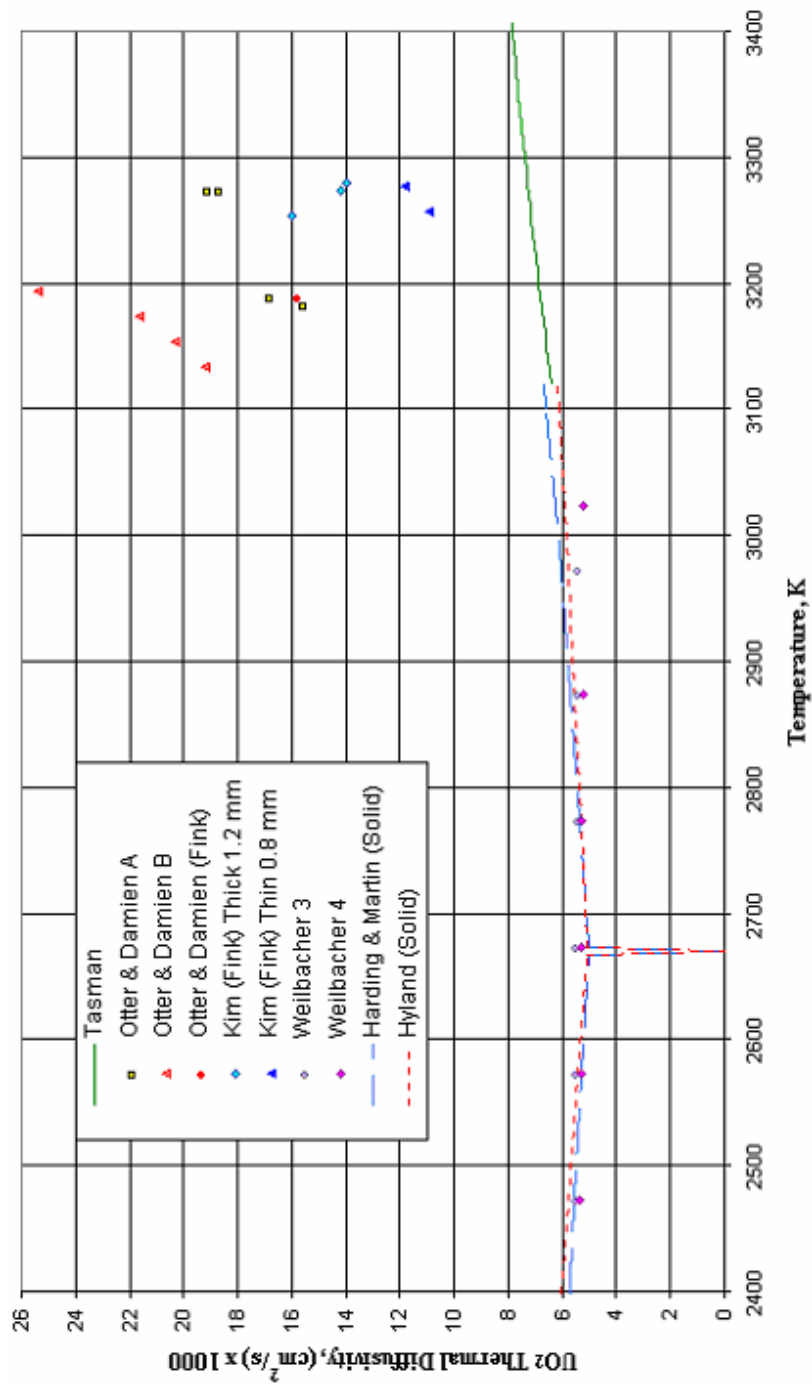


FIG. 1. Thermal conductivity and diffusivity of liquid UO<sub>2</sub>; UO<sub>2</sub> thermal diffusivity.

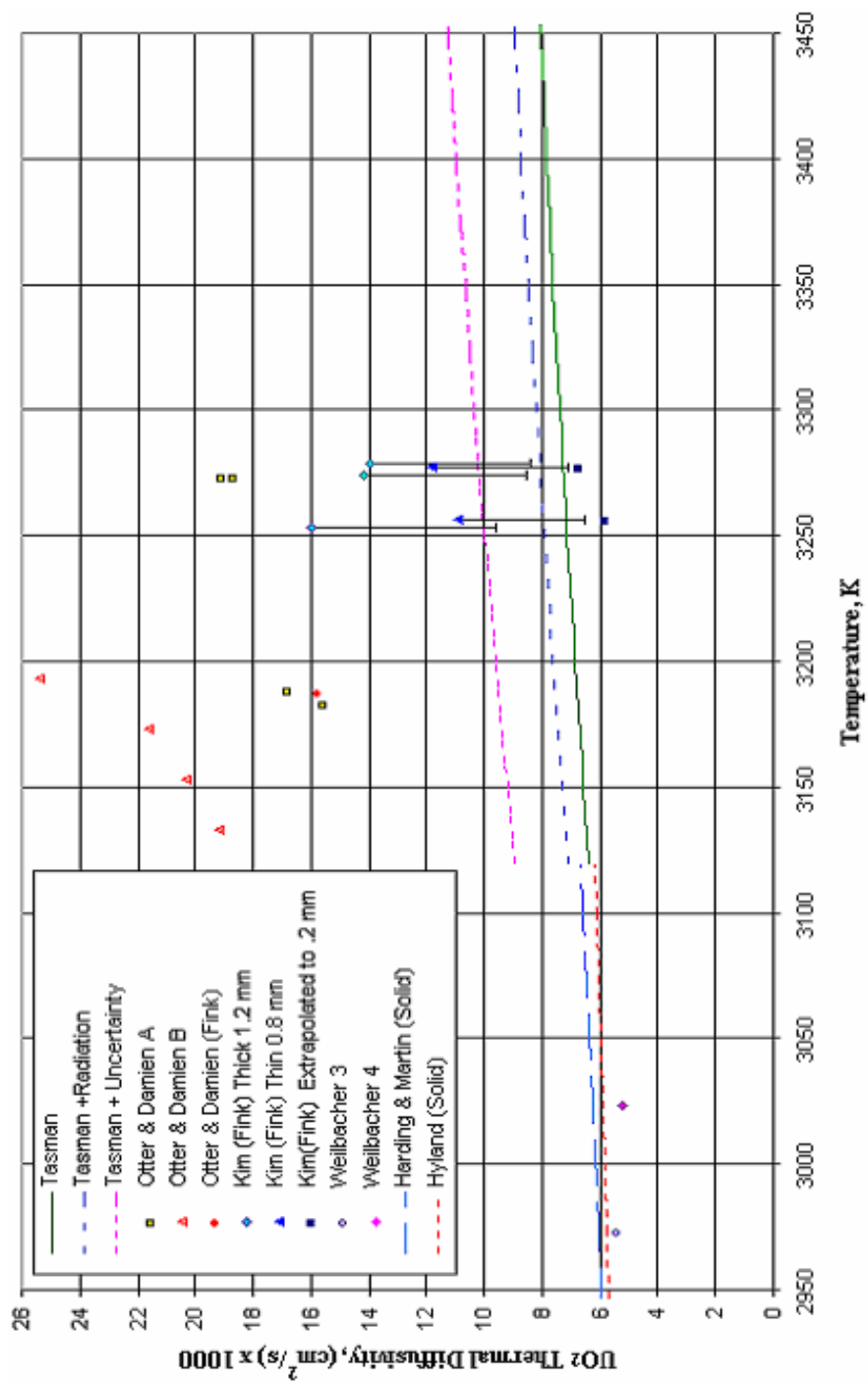


FIG. 2. Thermal diffusivity of liquid  $UO_2$ :  $UO_2$  thermal diffusivity.

If the  $\lambda$  transition at 2670 K results in sufficient disorder for the thermal diffusivity to follow glassy behavior, then internal radiation, which is important for glassy materials, must also be considered for  $\text{UO}_2$  above this transition. In his critical analysis of the thermal conductivity of solid  $\text{UO}_2$ , Hyland [16] included a contribution from radiation. At the melting point,  $0.48 \text{ W m}^{-1} \text{ K}^{-1}$  is the radiative contribution to the thermal conductivity of solid  $\text{UO}_2$  calculated by Hyland [16] using the method given by Browning [23] and the optical property data for solid  $\text{UO}_2$  measured by Bober et al. [7]. This result for the solid and the statistically significant difference between the thermal diffusivities of the thin and thick  $\text{UO}_2$  layers, which is indicative of internal radiation [8, 9], imply that the radiative contribution should also be considered for the liquid. The radiative contribution to the thermal conductivity for an optically thick sample is:

$$k_r = \frac{16 n^2 \sigma T^3}{3K_R}$$

where  $n$  is the refractive index (1.72 for liquid  $\text{UO}_2$ ) [7],  $K_R$  is the Rosseland absorption coefficient, and  $\sigma$  is the Stephan-Boltzmann constant. Following Hyland [16], the value of  $K_R$  was obtained from Figure 4 of Browning [23], which includes the contributions beyond the absorption edge of the material. For the liquid at the melting point, the radiative contribution to the thermal conductivity in the optically thick limit is  $0.28 \text{ W m}^{-1} \text{ K}^{-1}$ . This corresponds to corrections to the thermal diffusivity of  $0.7 \times 10^{-7}$  to  $0.9 \times 10^{-7} \text{ m}^2 \text{ s}^{-1}$  between 3120 and 3400 K, assuming constant thermal conductivity and thermal diffusivity variations with temperature in accord with changes in density and heat capacity. In Figure 2, the curve labeled “*Tasman + Radiation*” includes the optically thick radiative contribution to the thermal conductivity of Tasman. If the assumption is made that the difference in thermal diffusivities between the thick and thin layers of  $\text{UO}_2$  in the experiment of Kim et al. arises from failure to include the radiative term in the analysis, and the radiative contribution scales according to the thickness of the  $\text{UO}_2$  layer, the experimental thermal diffusivity of a 0.2 mm thickness of  $\text{UO}_2$  (thickness of the molten layer in the experiment of Tasman [3]) can be estimated. For the temperatures of 3250 and 3277 K, this estimate gives thermal diffusivities in the range of  $5.8 \times 10^{-7} \text{ m}^2 \text{ s}^{-1}$  to  $6.7 \times 10^{-7} \text{ m}^2 \text{ s}^{-1}$ . These values, shown in Figure 2, are slightly lower than the values calculated from the thermal conductivity of Tasman [4] using the heat capacities of Ronchi et al. [6] and densities of Breitung and Reil [17]. This scaled correction is larger than the calculated radiative contribution due to an optically thick layer. Figure 2 includes the positive uncertainty of Tasman and a corresponding negative uncertainty (-40%) in the thermal diffusivities from the 0.813 mm layer measurements of Kim et al. These uncertainty bands overlap.

## Conclusion

From these comparisons, it is reasonable to assume that  $2.5 \text{ W m}^{-1} \text{ K}^{-1}$  (the new value reported by Tasman [4]) represents a lower limit of the thermal conductivity of liquid  $\text{UO}_2$ . An upper limit of  $3.6 \text{ W m}^{-1} \text{ K}^{-1}$  is consistent with the error limit given by Tasman and with the lower value obtained from the experiments of Kim et al. with the optically thick radiative contribution ( $0.3 \text{ W m}^{-1} \text{ K}^{-1}$ ) subtracted. Clearly, the data of Kim et al. must be reanalysed with radiative contributions for the thickness of the  $\text{UO}_2$  layers included. Although the data of Kim et al. show systematic differences between the thick and thin layers of  $\text{UO}_2$  and the data of Otter and Damien appear to be high, these measurements are consistent in that they show little variation in thermal diffusivity with temperature. However, thermal diffusivities calculated using the constant thermal conductivity of Tasman [4] and the heat capacities of Ronchi et al. [6] show significant increases with temperature. From the experiments of Ronchi et al. [6] it is unclear how much of the temperature variation in  $C_p$  arises from the change in thermal conductivity with temperature. (Thermal conductivity was assumed to be constant in their analysis.) Ronchi [14] states that glassy ceramics show a slight increase in the thermal diffusivity with temperature and the thermal diffusivity usually increases continuously across the melting point. Because no information is available with respect to the recent thermal conductivity measurements of Tasman [4, 14], the temperature of the measurement is uncertain. If the thermal diffusivity was assumed to be constant, the thermal conductivity data of Tasman and the heat capacity of Ronchi et al. at 3473 K would give  $8.2 \text{ m}^2 \text{ s}^{-1}$  for the thermal diffusivity of liquid  $\text{UO}_2$ . At the

melting point, this would correspond to a thermal conductivity of  $3.2 \text{ W m}^{-1} \text{ K}^{-1}$ . This is within the range of recommended values.

### **Uncertainty**

The uncertainty in the thermal conductivity and thermal diffusivity of liquid  $\text{UO}_2$  is approximately 40%, the uncertainty given by Tasman et al. [3,4].

### **REFERENCES TO SECTION 6.1.1.6**

- [1] KIM, C.S., HALEY, R.A., FISCHER, J., CHASANOV, M.G. and LEIBOWITZ, L., Measurement of thermal diffusivity of molten  $\text{UO}_2$ , Proc. Seventh Symp. On Thermophysical Properties, A. Cezairliyan, Ed., ASME, New York, p. 338-343 (1977).
- [2] OTTER, C. and DAMIEN, D., Mesure de la diffusivité thermique de  $\text{UO}_2$  fondu, High Temp.-High Pressures 16, 1-6 (1984).
- [3] TASMAN, H.A., PEL, D., RICHTER, J. and SCHMIDT, H.E., Measurement of the thermal conductivity of liquid  $\text{UO}_2$ , High Temp.-High Pressures 15, 419-431 (1983).
- [4] TASMAN, H.A., Thermal conductivity of liquid  $\text{UO}_2$ , Commission of the European Communities Joint Research Centre Annual Report TUAR88, Karlsruhe, Germany (1988); as referenced by C. Ronchi in On the Thermal Conductivity and Diffusivity of Solid and Liquid Uranium Dioxide, J. Phys. Condens. Matter 6, L561-L567 (1994).
- [5] FINK, J.K. and LEIBOWITZ, L., An analysis of measurements of the thermal conductivity of liquid Urania, High Temp.-High Pressures 17, 17-26 (1985).
- [6] RONCHI, C., HIERNAUT, J.P., SELFSLAG, R. and HYLAND, G.J., Laboratory measurement of the heat capacity of Urania up to 8000 K: I. Experiment, Nucl. Sci. Eng 113, 1-19 (1993).
- [7] BOBER, M., SINGER, J. and WAGNER, K., Determination of the optical constants of liquid  $\text{UO}_2$  from reflectivity measurements, Proc. Eighth Symp. On Thermophysical Properties, J. V. Sengers, Ed., ASME, New York, Vol. II, p. 234-244 (1981).
- [8] MILLS, K.C. and WAKEHAM, W.A., Effect of radiation on thermal transport measurements, High Temp.-High Pressures 17, 343-348 (1985).
- [9] FISCHER, S. and OBERMEIER, E., Influence of radiative heat transfer on the effective thermal conductivity of liquids: experimental and theoretical investigation, High Temp.-High Pressures 17, 699-705 (1985).
- [10] OTTER, C. and VANDEVELDE, J., Contribution à l'étude du problème de thermocinétique lié à la mesure de la diffusivité thermique des matériaux liquides à haute température par la méthode du <<flash laser>>, Rev. Int. Hautes Temp. Refract. 19, 41-53 (1982).
- [11] ACKERMANN, R.J., The high temperature, high vacuum vaporization and thermodynamic properties of uranium dioxide, Argonne National Laboratory Report ANL-5482 (1955).
- [12] HUTCHINGS, M.T., High-temperature studies of  $\text{UO}_2$  and  $\text{ThO}_2$  using neutron scattering techniques, J. Chem. Soc., Faraday Trans. II 83, 1083-1103 (1987).
- [13] RONCHI, C. and HYLAND, G.J., Analysis of recent measurements of the heat capacity of uranium dioxide, J. of Alloys and Compounds 213/214 159-168 (1994).
- [14] RONCHI, C., On the thermal conductivity and diffusivity of solid and liquid uranium dioxide, J. Phys. Condens. Matter 6, L561-L567 (1994).
- [15] HARDING, J.H. and MARTIN, D.G., A recommendation for the thermal conductivity of  $\text{UO}_2$ , J. Nucl. Mater. 166, 223-226 (1989).
- [16] HYLAND, G.J., Thermal conductivity of solid  $\text{UO}_2$ : critique and recommendation, J. Nucl. Mater. 113, 125-132 (1983).
- [17] BREITUNG, W. and REIL, K.O., the density and compressibility of liquid (U,Pu)-mixed oxide, Nucl. Sci. Eng. 105, 205-217 (1990).
- [18] DROTNING, W.D., Thermal expansion of molten uranium dioxide, Proceedings of the Eighth Symp. On Thermophysical Properties, Gaithersburg, Maryland, June 15-18, 1981, J. V. Sengers, Ed., ASME, New York, Vol. II, pp 245-249 (1981).
- [19] WEILBACHER, J.C., Measurement of thermal diffusivity of mixed uranium plutonium oxides, CEA Report CEA-R-4572, Centre d'Etudes Nucleaires de Fontenay-aux Roses, France (1974).

- [20] WEILBACHER, J.C., Diffusivité thermique de l'oxyde d'uranium et de l'oxyde de thorium à haute température, High Temp.-High Pressures 4, 431-438 (1972).
- [21] FINK, J.K., Enthalpy and heat capacity of the actinide oxides, In. J. Thermophys. 3(2), 165-200 (1982).
- [22] MARTIN, D.G., The thermal expansion of solid UO<sub>2</sub> and (U,Pu) mixed oxides - A review and recommendations, J. Nucl. Mater. 152 94-101 (1988).
- [23] BROWNING, P., On the relative importance of the electronic and radiative contributions to the thermal conductivity of uranium dioxide, J. Nucl. Mater. 92 33-38 (1982).

#### 6.1.1.7. Thermal conductivity and thermal diffusivity of solid UO<sub>2</sub>

##### **Recommendation**

The recommended equation for the thermal conductivity of 95% dense solid UO<sub>2</sub> consists of a lattice term and a term suggested by Ronchi et al. [1] to represent the small-polaron ambipolar contribution to the thermal conductivity. The lattice term was determined by a least squares fit to the lattice contributions to the thermal conductivity obtained from thermal diffusivity measurements by Ronchi et al. [1], Hobson et al. [2], Bates [3], the Battelle Memorial Institute [4] and Los Alamos Scientific Laboratory [4], and from thermal conductivity measurements by Godfrey et al. [5] and the GE-Nuclear Systems Programs [4]. The recommended equation is

$$\lambda = \frac{100}{7.5408 + 17.692 t + 3.6142 t^2} + \frac{6400}{t^{5/2}} \exp\left(\frac{-16.35}{t}\right) \quad (1)$$

where  $t$  is  $T/1000$ ,  $T$  is in K, and  $\lambda$  is the thermal conductivity for 95% dense UO<sub>2</sub> in  $\text{W} \cdot \text{m}^{-1} \cdot \text{K}^{-1}$ .

Figure 1 compares the recommended values for the thermal conductivity for 95% dense UO<sub>2</sub> with the thermal conductivity data [1–5] used in the determination of the lattice term.

Thermal conductivity values for theoretically dense UO<sub>2</sub> or for a different density may be calculated using the porosity relation derived by Brandt and Neurer [6], which is:

$$\lambda_0 = \frac{\lambda_p}{[1 - \alpha p]}, \quad \alpha = 2.6 - 0.5t \quad (2)$$

where  $t$  is  $T/1000$ ,  $T$  is in K,  $p$  is the porosity fraction,  $\lambda_p$  is the thermal conductivity of UO<sub>2</sub> with porosity  $p$ ,  $\lambda_0$  is the thermal conductivity of fully dense UO<sub>2</sub> (i.e. porosity = 0). Values for the thermal conductivity for 95% dense UO<sub>2</sub> calculated from Eq. (1) and for theoretically dense UO<sub>2</sub> determined from Eqs (1–2) are given in Table 1.

##### **Uncertainty**

Uncertainties were determined from the scatter in the available data and the deviations of the data from the recommended equation. From 298 to 2000 K, the uncertainty is 10%. From 2000 to 3120 K, the uncertainty increased to 20% because of the large discrepancies between measurements by different investigators. Uncertainties are included in Figure 1. Most of the data included in Figure 1 fall within these uncertainty limits. However, some of the low-temperature LASL data [4], which are significantly lower than other data, are below the lower 10% uncertainty. In addition, some of the data of Bates [3], which show considerable scatter, are outside the 10% uncertainty.



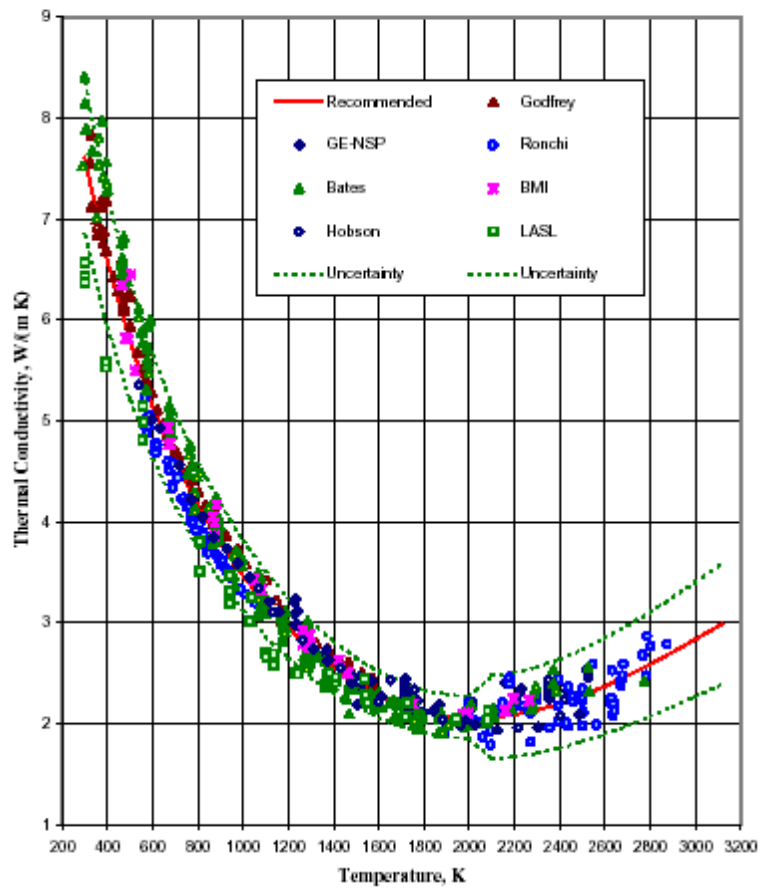


FIG. 1. Thermal conductivity of 95% dense  $\text{UO}_2$

Table 1. Thermal conductivity of UO<sub>2</sub> with 95% and 100% density

TEMPERATURE K	THERMAL CONDUCTIVITY W m <sup>-1</sup> K <sup>-1</sup>	
	95% Dense	100% Dense
298.15	7.61	8.68
300	7.59	8.65
400	6.58	7.48
500	5.78	6.55
600	5.14	5.81
700	4.61	5.19
800	4.17	4.68
900	3.79	4.25
1000	3.47	3.87
1100	3.19	3.55
1200	2.95	3.28
1300	2.74	3.04
1400	2.56	2.83
1500	2.41	2.66
1600	2.29	2.52
1700	2.19	2.40
1800	2.12	2.32
1900	2.08	2.27
2000	2.06	2.24
2100	2.07	2.24
2200	2.09	2.26
2300	2.14	2.30
2400	2.20	2.37
2500	2.28	2.45
2600	2.37	2.54
2700	2.48	2.64
2800	2.59	2.76
2900	2.71	2.88
3000	2.84	3.00
3100	2.97	3.13
3120	2.99	3.16

### Discussion

Data for the thermal diffusivity [1–4, 7–8] and thermal conductivity [4, 5, 9] of solid UO<sub>2</sub> were reassessed for the following reasons:

- (1) The 2000–2900 K thermal diffusivity data of Ronchi et al. [1] indicate that the high-temperature thermal diffusivity values reported by Weilbacher [7,8], which were the main high-temperature data available prior to 1999, are high.
- (2) Advances in understanding the heat transport mechanisms in UO<sub>2</sub> have led to improvements in physically-based thermal conductivity equations [1, 10–11] in which only the coefficients of the lattice contribution are determined from the thermal conductivity data.
- (3) Above 2670 K, heat capacity values [12–14] previously used for conversion of thermal diffusivity data to thermal conductivity are inconsistent with recent high-temperature heat capacity measurements of Ronchi et al. [1]. High-temperature thermal conductivities calculated from thermal diffusivity data using the new heat capacity data have a different temperature dependence than values used in older assessments.

Data included in this reassessment are listed in Table 2, which also gives the percent of theoretical density of the samples, the temperature range of the measurements, and the number of data obtained for each set of measurements. Although Conway and Feith [4] report results of the General Electric (GE) Nuclear Systems Programs (NSP) thermal diffusivity measurements from 600 to 1700 K as well as data from the GE-NSP “round robin” thermal conductivity measurements, only the thermal conductivity data have been included in this assessment because comparison of the thermal diffusivity data with other data show large disagreement above 1200 K. Temperatures for the data of Stora et al. [9] and the data of Godfrey et al. [5] have been converted from the 1948 International Practical Temperature Scale (IPTS) to the 1968 IPTS .

The differences between the thermal diffusivity values of Weilbacher [7] and of Ronchi et al. [1] are clearly shown in Figure 2, which plots the inverse of measured thermal diffusivities [1–4,7] as a function of temperature. The percent of theoretical density of the samples for each set of measurements has been included in the figure legend. From 300 to 2000 K, all the inverse thermal diffusivity data show a linear dependence on temperature. Although the data of Hobson et al. [2] and that of Ronchi et al. [1] continue to increase linearly with temperature to 2400 K, values from the measurements of Weilbacher deviate from the linear dependence above 2000 K. Ronchi et al. [1] attribute the high diffusivity values obtained by Weilbacher to incorrect determinations of the temperature rise of the front of the sample and to errors in the Cowan correction during data reduction. Measurements of Bates [3] on three different samples span almost the entire temperature range but show considerable scatter. At low temperatures, values of the inverse thermal diffusivity from Bates’ measurements are below the values of Ronchi et al. Between 2000 and 2400 K, Bates’ values fall between Weilbacher’s values and those of Ronchi et al. However, the highest temperature datum of Bates is consistent with the data of Ronchi et al.

Table 2. Standard deviations of data from thermal conductivity equations

DATA REFERENCE	PERCENT OF THEORETICAL DENSITY %	TEMPERATURE RANGE K	# OF DATA	STANDARD DEVIATION 5	
				RONCHI Eq. (4)	RECOMMENDED Eq. (1)
<i>Thermal Diffusivity Measurements</i>					
Ronchi et al. 1999 [1]	95	550 – 1100 2000 – 2900	125	8.6	7.2
Hobson et al. 1974 [2]	95	537 – 2488	34	8.0	3.6
Bates (3 samples) 1970 [3]	98.4	289 – 2777	188	8.7	6.0
Battelle Memorial Institute, 1969 [4]	97.4	457 – 2271	27	6.8	4.2
Los Alamos Scientific Lab. 1969 [4]	98	299 – 2083	35	9.7	12.4
Weilbacher (2 runs) 1972 [7,8]	98	773 – 3023	32	7.1	11.4
<i>Thermal Conductivity Measurements</i>					
GE Nuclear Systems Programs, 1969 [4]	98	1229 – 2661	70	5.9	8.0
Godfrey 1964 [5]	93.4	323 – 1573	105	7.5	3.7
Centre d’Etudes Nucleaires (CEN) Grenoble, 1969 [4]	97	373 – 2577	14	8.0	10.6
Stora 1964 [9]	95	473 – 2777	19	8.4	10.9

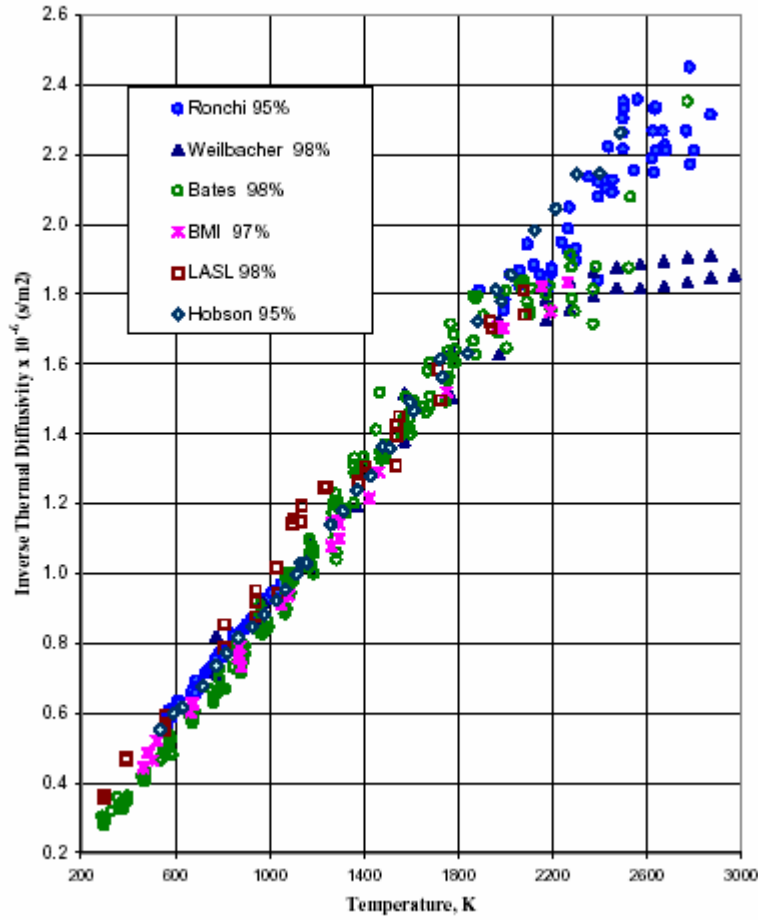


FIG. 2. Inverse thermal diffusivity of  $\text{UO}_2$

Since 1981, theoretical research and new measurements have led to improvements in equations for the thermal conductivity of  $\text{UO}_2$ . The physically-based equation of Hyland [10] included lattice, radiation, and ambipolar contributions. The equation of Hardin and Martin [11], which was recommended in the previous INSC assessment [15], consisted of a lattice term and a small-polaron ambipolar contribution. Since the publication of these equations, Casado, Harding, and Hyland [16] showed that the temperature dependence used by Killeen [17] in analysis of his electrical conductivity data was incorrect. This temperature dependence was incorporated in the small-polaron ambipolar contribution in the thermal conductivity equations of Hyland [10] and of Harding and Martin [11]. Casado et al. [16] report that the correct temperature dependence for the small polaron contribution to the direct current electrical conductivity,  $\sigma(T)$ , is

$$\sigma(T) = \frac{\sigma_1}{T^{3/2}} e^{-\varepsilon/kT} \quad (3)$$

where  $\varepsilon$  is the activation energy in eV of the direct current electrical conductivity,  $\sigma_1$ ,  $k$  is the Boltzmann constant, and  $T$  is the temperature. Ronchi et al. [1] used this temperature dependence to refit the electrical conductivity data of Killeen [17] and determined a new term for the small-polaron ambipolar contribution to the thermal conductivity of  $\text{UO}_2$ . They determined the lattice contribution by fitting the thermal resistivities obtained from their thermal diffusivity measurements from 550 to 1100 K. They concluded that any radiative contribution to the thermal conductivity of solid  $\text{UO}_2$  would be insignificant compared to the lattice and small-polaron ambipolar contributions. The equation given by Ronchi et al. for the thermal conductivity of 95% dense  $\text{UO}_2$  is:

$$\lambda = \frac{100}{6.548 + 23.533t} + \frac{6400}{t^{5/2}} \exp\left(\frac{-16.35}{t}\right) \quad (4)$$

where  $t$  is  $T/1000$ ,  $T$  is in K, and  $\lambda$  is the thermal conductivity for 95% dense  $\text{UO}_2$  in  $\text{W} \cdot \text{m}^{-1} \cdot \text{K}^{-1}$ . The first term of this equation is the lattice contribution; the second term is the small-polaron ambipolar contribution.

Ronchi et al. [1] also fit their data to the polynomial

$$\lambda = +12.57829 - 2.31100 \times 10^2 T + 2.36675 \times 10^5 T^2 - 1.30812 \times 10^8 T^3 + 3.63730 \times 10^{-12} T^4 - 3.90508 \times 10^{-16} T^5 \quad (5)$$

where  $\lambda$  is the thermal conductivity for 95% dense  $\text{UO}_2$  in  $\text{W} \cdot \text{m}^{-1} \cdot \text{K}^{-1}$  and  $T$  is the temperature in K.

In Figure 3, these two equations of Ronchi et al. are compared with the data listed in Table 2 converted to thermal conductivity for 95% dense  $\text{UO}_2$ . Thermal conductivities have been calculated from thermal diffusivity measurements [2–4,7–8] using the relationship

$$\lambda = D \rho C_p \quad (6)$$

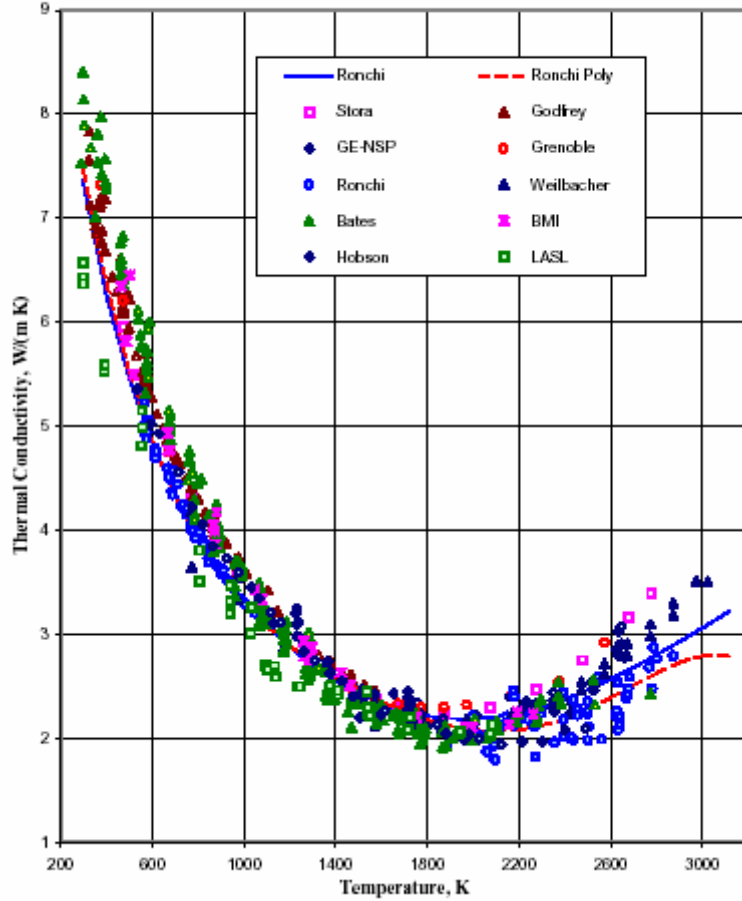


FIG. 3. Equation of Ronchi et al., for the thermal conductivity of 95% dense  $\text{UO}_2$ .

where  $\lambda$  is the thermal conductivity,  $D$  is the measured thermal diffusivity,  $\rho$  is the sample density and  $C_p$  is the heat capacity. The sample density at temperature  $T$ , was calculated using

$$\rho(T) = F \rho(273) \left( \frac{L_{273}}{L_T} \right)^3 \quad (7)$$

where  $F$  is the fraction of theoretical density,  $\rho(273)$  is the theoretical density at 273 K = 10.963 Mg·m<sup>-3</sup>. The ratio  $L_{273}/L_T$  as a function of temperature is given by the equations of Martin [18],

For 273 K ≤  $T$  ≤ 923 K,

$$L_T = L_{273} (9.9734 \times 10^1 + 9.802 \times 10^6 T - 2.705 \times 10^{10} T^2 + 4.391 \times 10^{-13} T^3); \quad (8)$$

For 923 K ≤  $T$  ≤ 3120 K,

$$L_T = L_{273} (9.9672 \times 10^1 + 1.179 \times 10^5 T - 2.429 \times 10^9 T^2 + 1.219 \times 10^{-12} T^3) \quad (9)$$

where  $L_T$  and  $L_{273}$  are the lengths at temperatures  $T$  and 273 K, respectively. The heat capacity,  $C_p$ , was calculated from an equation developed by Fink [19] based on a combined analysis of enthalpy and heat capacity data, which included the new heat capacity data of Ronchi et al. [1].

$$C_p = \frac{C_1 \theta^2 e^{\theta/T}}{T^2 (e^{\theta/T} - 1)^2} + 2 C_2 T + \frac{C_3 E_a e^{-E_a/T}}{T^2} \quad (10)$$

For 298.15 K ≤  $T$  ≤ 3120 K

where  $C_1 = 81.613$ ,  
 $\theta = 548.68$ ,  
 $C_2 = 2.285 \times 10^{-3}$ ,  
 $C_3 = 2.360 \times 10^7$ ,  
 $E_a = 18531.7$ ,

$T$  is the temperature in K, and the heat capacity,  $C_p$ , is in J·mol<sup>-1</sup>·K<sup>-1</sup>. All thermal conductivities were converted to 95% theoretically dense UO<sub>2</sub> using Eq. (2), the equation recommended by Brandt and Neuer [6].

For the thermal diffusivity measurements of Ronchi et al. [1], the values of the thermal conductivities tabulated in their paper have been used in this evaluation because these values obtained from the simultaneous measurements of thermal diffusivity and heat capacity have a higher degree of confidence than values obtained using an equation that fits the heat capacity data but does not exactly reproduce experimental values at any given temperature.

Figure 3 shows that the high-temperature thermal conductivities of Stora [9] and the “round robin” Grenoble data are high compared to the equation suggested by Ronchi et al. These thermal conductivity data were obtained by the radial heat flow method. Ronchi et al. question the reliability of the high-temperature data of Stora [9] because of vaporization of the sample and mechanical deformations above 2500 K. From 2625 to 2657 K, the GE-NSP data show significant scatter. Conway and Feith [4] state that these data should be treated with caution because examination of the GE-NSP samples following high-temperature radial heat flow measurements showed evaporation from the center of the disc and deposition of condensed material along the cooler edges. These questionable data are of the same magnitude or higher than the thermal conductivities obtained from the thermal diffusivity measurements of Weilbacher, which were questioned by Ronchi et al. [1].

Comparison of Eq. (4) with the data, shows that although it appears low relative to the lowest temperature data, it is high relative to the minimum near 2000 K. This might be attributed to the linear temperature dependence of the lattice term, which includes only constant volume three-phonon scattering processes. In their determination of the lattice term from their low temperature data (560–1100 K), Ronchi et al. considered including a quadratic temperature term to account for constant pressure thermal expansion contributions but the additional term was not statistically justified. In an

attempt to improve agreement at low temperatures (below 550 K) and in the region of the thermal conductivity minimum, the lattice contribution has been reexamined.

The lattice term has traditionally been determined by fitting the low-temperature thermal conductivity data because the lattice contribution dominates the thermal conductivity at low temperatures. Figure 4 shows the total thermal conductivity, the lattice contribution, and the ambipolar contribution as a function of temperature that have been calculated from the equation of Ronchi et al., Eq. (4). Below 1300 K, the ambipolar term is insignificant and the total thermal conductivity equals the lattice contribution. Although the ambipolar term begins to have a significant contribution to the total thermal conductivity above 1300 K, it is not larger than the lattice contribution determined by Ronchi et al. until 2800 K. Even at 3120 K, the lattice contribution is still significant. Because Ronchi et al. have developed a theoretically-based term for the ambipolar contribution, which is independent of the thermal conductivity data, it is now possible to determine the lattice contribution for the entire temperature range by subtracting the ambipolar contribution given by Ronchi et al. from the experimentally determined total thermal conductivities. Because the data of Weilbacher, the data of Stora, the Grenoble data and the GE-NSP data above 2600 K are questionable, they have not been included in this analysis.

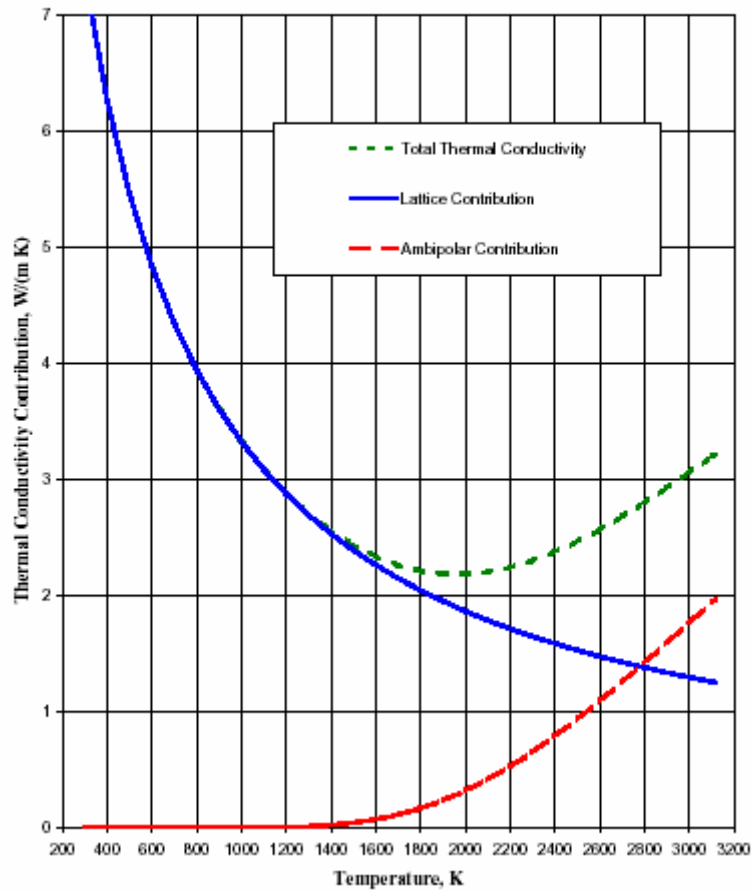


FIG. 4. Thermal conductivity contributions from the equation of Ronchi et al.

The lattice contribution to the thermal conductivity was determined by subtracting the ambipolar contribution calculated from the equation of Ronchi et al., Eq. (4), from the thermal conductivities from the measurements of Ronchi et al. [1], Hobson et al. [2], Bates [3], the Battelle Memorial Institute [4], the Los Alamos Scientific Laboratory [4], Godfrey et al. [5] and the GE-NSP. Only the GE-NSP data below 2600 K have been used. The inverse of the lattice contributions were fit to

equations with both linear and quadratic temperature dependence. Figure 5 shows a comparison of the linear and quadratic fits to the inverse of the lattice contribution to the thermal conductivity. Goodness of fit tests indicated that a quadratic term is justified for this larger set of data, which spans the entire temperature region. In Figure 6, the data for the total thermal conductivity considered in this analysis are compared with (1) an equation consisting of a lattice term that is linear in temperature and the small-polaron ambipolar term given by Ronchi et al. and with (2) an equation consisting of a lattice term with quadratic temperature dependence and the small-polaron ambipolar term given by Ronchi et al. Figures 7 and 8 show the percent deviations of these equations from the data defined as:

$$\% \text{ Deviation} = \frac{(\text{Data} - \text{Equation})}{\text{Data}} \bullet 100\% \quad (11)$$

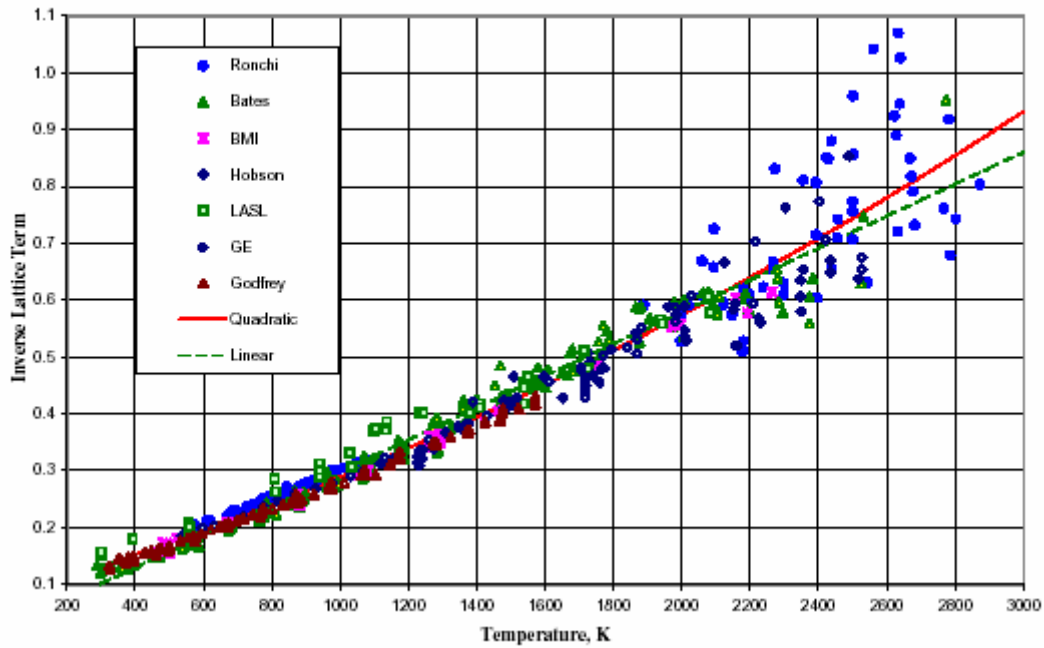


FIG. 5. Linear and quadratic fits to inverse Lattice contributions.

The percent deviations from the equation with the new linear lattice term are skewed with respect to temperature and the deviations are greater than the deviations for the equation with the quadratic lattice term. These deviation plots confirm the statistical analysis that indicates that the quadratic temperature term is justified.

The recommended equation for the thermal conductivity of 95% dense  $\text{UO}_2$ , Eq. (1), includes the quadratic lattice term and the small-polaron ambipolar contribution determined by Ronchi et al. [1]. Figure 9 shows the data fit, the recommended equation, Eq. (1), the equation of Ronchi et al., Eq. (4), and the polynomial fit by Ronchi et al to their data, Eq. (5). The recommended equation fits the data near the thermal conductivity minimum and the low-temperature data of Bates better than Eq. (4). At intermediate and high temperatures, the recommended equation is very close to the polynomial fit to the data of Ronchi et al. Figure 10 shows the percent deviations of the equation of Ronchi et al., Eq. (4), from the data included in the above analysis. The percent deviations are skewed similar to those in Figure 7 for the other equation with a linear lattice term. Comparison of percent deviations in Figure 10 and Figure 8 indicates that, in general, the deviations from Eq.(4) are larger than the deviations from the recommended equation. The recommended equation fits the data of Ronchi et al., Bates, Hobson et al., Godfrey et al., and the ‘round robin’ data from BMI, LASL, and GE-NSP below 2600 K with a percent standard deviation of 6.2%. The standard deviation of these data from the equation given by Ronchi et al., Eq. (4), is 7.9%. Table 2 lists the percent standard deviations from Eq. (1) and from Eq.(4), the equation of Ronchi et al., for each set of data.



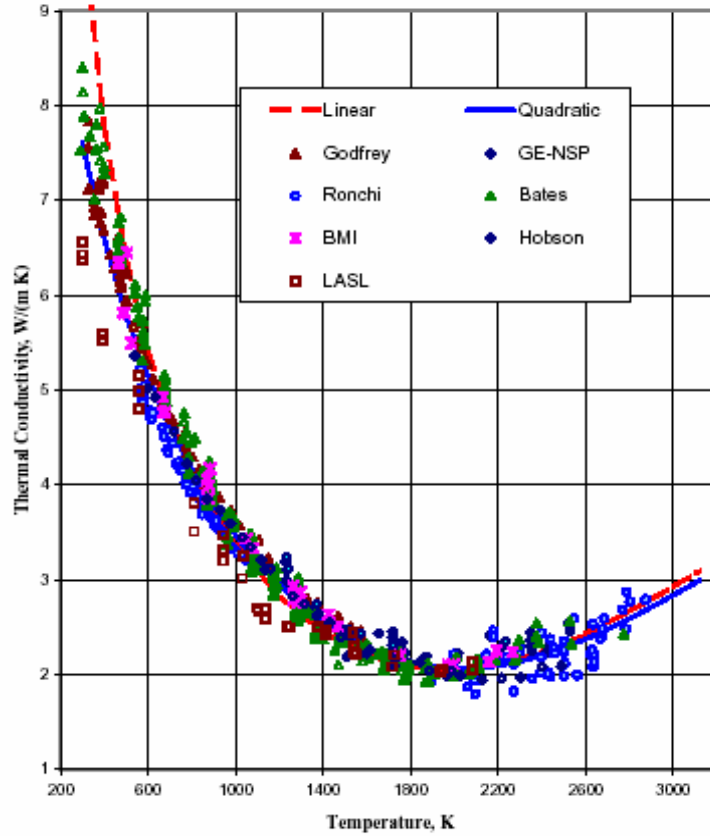


FIG. 6. Comparison of linear and quadratic Lattice term in thermal conductivity equations for 95% dense  $\text{UO}_2$

From their research, Ronchi et al. concluded that the solid thermal conductivity of 95% dense  $\text{UO}_2$  at the melting point,  $T_m$ , should be in the range  $2.4 \leq \lambda(T_m) \leq 3.1 \text{ W} \cdot \text{m}^{-1} \cdot \text{K}^{-1}$ . The thermal conductivity for 95% dense  $\text{UO}_2$  at 3120 K calculated with the recommended equation, Eq. (1), is  $3.0 \text{ W} \cdot \text{m}^{-1} \cdot \text{K}^{-1}$ , which is consistent with the conclusion of Ronchi et al. For theoretically dense  $\text{UO}_2$ , the thermal conductivity at 3120 K calculated from Eq. (1) is  $3.2 \text{ W} \cdot \text{m}^{-1} \cdot \text{K}^{-1}$ . The equation given by Harding and Martin [11], which was previously recommended, in ANL/RE-97/2 [15], gave a melting point thermal conductivity for theoretically dense solid  $\text{UO}_2$  of  $4.0 \text{ W} \cdot \text{m}^{-1} \cdot \text{K}^{-1}$ , which is  $3.8 \text{ W} \cdot \text{m}^{-1} \cdot \text{K}^{-1}$  for 95% dense  $\text{UO}_2$ . In Figure 11, the recommended values for the thermal conductivity of 95% dense  $\text{UO}_2$  are compared with values from the equation of Harding and Martin. The data used in this analysis as well as the excluded data of Stora, Weilbacher, Grenoble, and GE-NSP that had been included in past assessments are shown in Figure 11. The higher melting point thermal conductivity given by the equation of Harding and Martin is consistent with the data of Weilbacher but not with the new measurements of Ronchi et al. Percent deviations of the recommended equation from this larger set of data are shown in Figure 12. Figure 12 shows that most of the percent deviations for this larger set of data fall within the recommended uncertainties (10% below 2000 K; 20% above 2000 K).

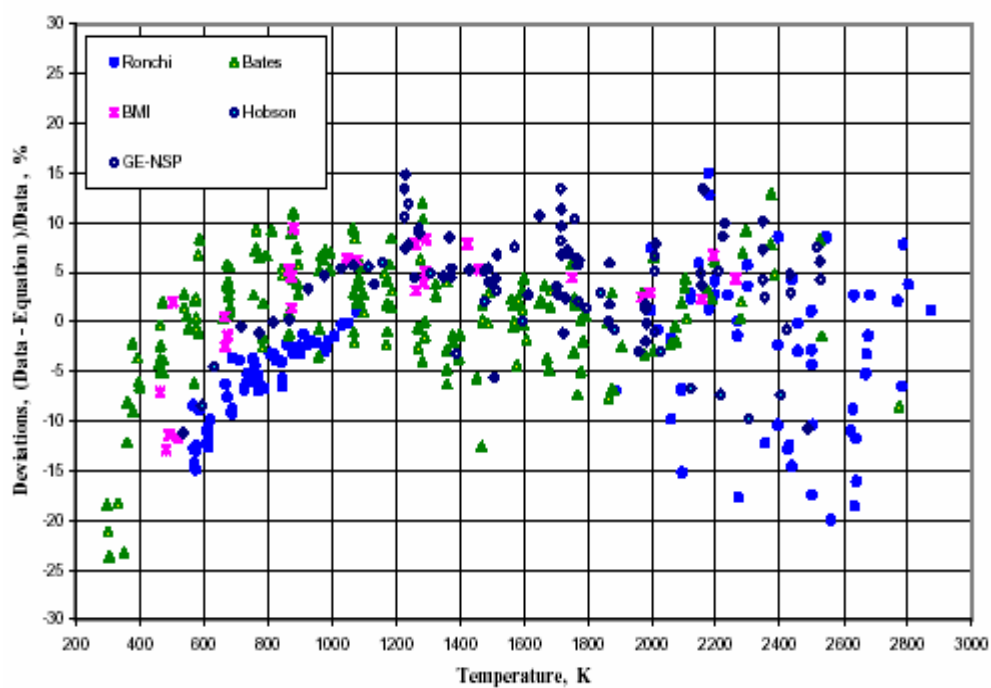


FIG. 7. Percent deviations from equation with new linear Lattice term.

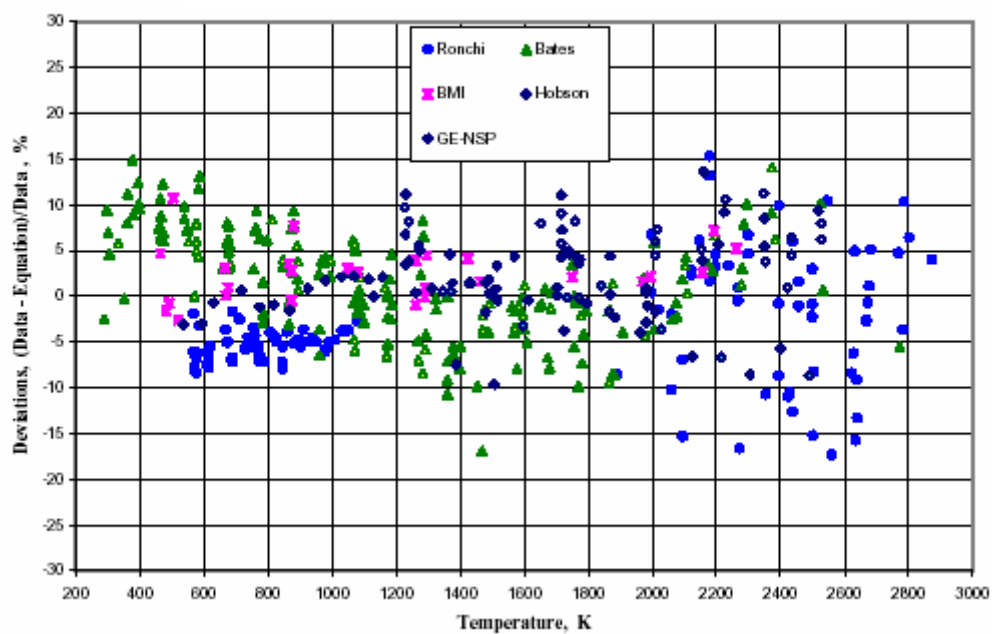


FIG. 8. Percent deviations from equation with quadratic Lattice term.

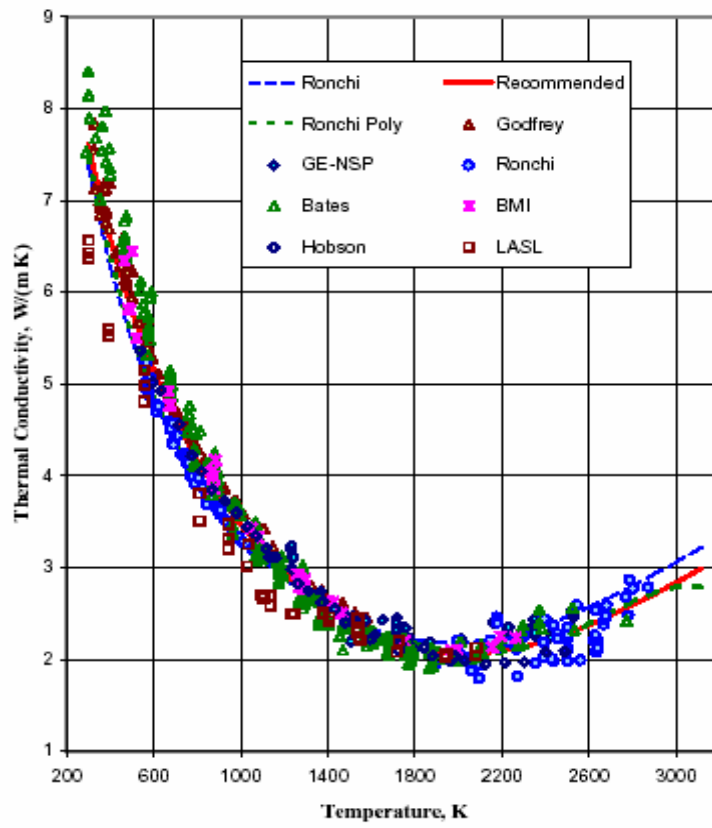


FIG. 9. Thermal conductivity of 95% dense  $UO_2$

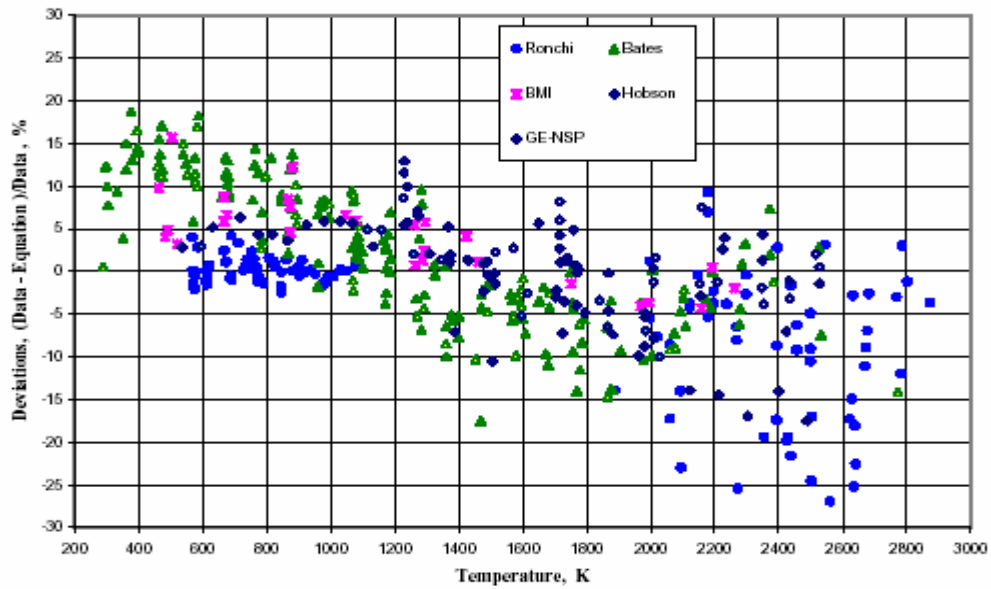


FIG. 10. Present deviations from equation of Ronchi.

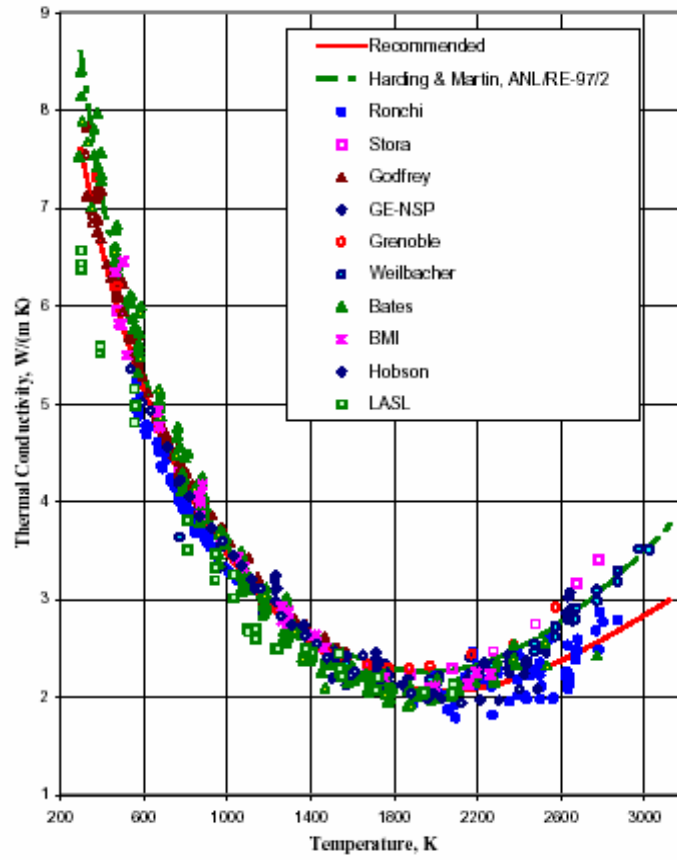


FIG. 11. Comparison of recommended equation with previous recommendation and data for 95% dense  $\text{UO}_2$

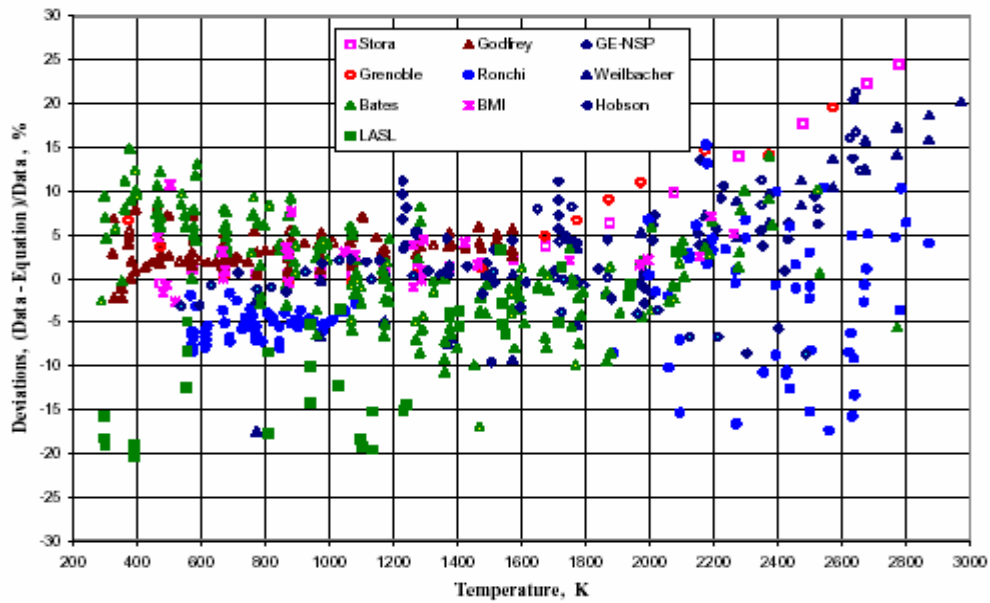


FIG. 12. Percent deviations from recommended equation.

In Figure 13, the recommended values for the thermal conductivity of fully dense  $\text{UO}_2$  are compared with other equations for the thermal conductivity of theoretically dense  $\text{UO}_2$ . Equations included in this comparison are the equation by Ronchi et al. [1], the equation given in the MATPRO database for SCADAP/RELAP5 [14], and the equation of Harding and Martin [15], which had been previously recommended in ANL/RE-97/2. Percent deviations of values calculated with these equations from the recommended values defined as

$$\% \text{ Deviation} = \frac{(\text{Other} - \text{Recommended})}{\text{Recommended}} \bullet 100\% \quad (12)$$

are shown in Figure 14. Most of the deviations are within the uncertainties. However the percent deviations for the equation of Harding and Martin are greater than 20% above 2800 K.

Historically, the paucity of high-temperature thermal conductivity data prompted the practice of comparing thermal conductivity equations to the in-reactor conductivity integral to melt (CIM) defined as:

$$\text{CIM} = \int_{773K}^{T_m} \lambda(T) dT \quad (13)$$

where  $\lambda(T)$  is the thermal conductivity at temperature  $T$  and  $T_m$  is the melting point. This integral represents the reactor linear power at which melting begins on the centerline of a fuel pellet whose outer surface is assumed to be at 773 K. The CIM obtained from the recommended equation, Eq. (1), is  $6.09 \text{ kW} \cdot \text{m}^{-1}$ . The polynomial used by Ronchi et al. to fit their data gives a CIM of  $6.08 \text{ kW} \cdot \text{m}^{-1}$ . Experimental values for CIM range from  $5.5$  to  $7.5 \text{ kW} \cdot \text{m}^{-1}$ . Because in-reactor CIM measurements are subject to systematic errors such as determination of the pellet surface temperature from the cladding temperature and the fuel-cladding gap conductance, and considerable controversy exists in interpretation of the melt boundary from the post-test metallurgical examinations, the CIM value is still uncertain. However, CIM values near  $6.8 \text{ kW} \cdot \text{m}^{-1}$  have been recommended for 95% dense fuel [20]. These values were consistent with equations [10, 11] that gave good agreement with the high-temperature thermal conductivity of Weillbacher. Ronchi et al.[1] state that although the most complete set of measurements at GE-San Jose' gave  $6.3 \pm 0.3 \text{ kW} \cdot \text{m}^{-1}$  for CIM [21], these results were not accepted because they were below values based on laboratory thermal conductivity and thermal diffusivity measurements. The GE values and the previous recommendations should be reconsidered now that more reliable laboratory data are available at high temperatures.

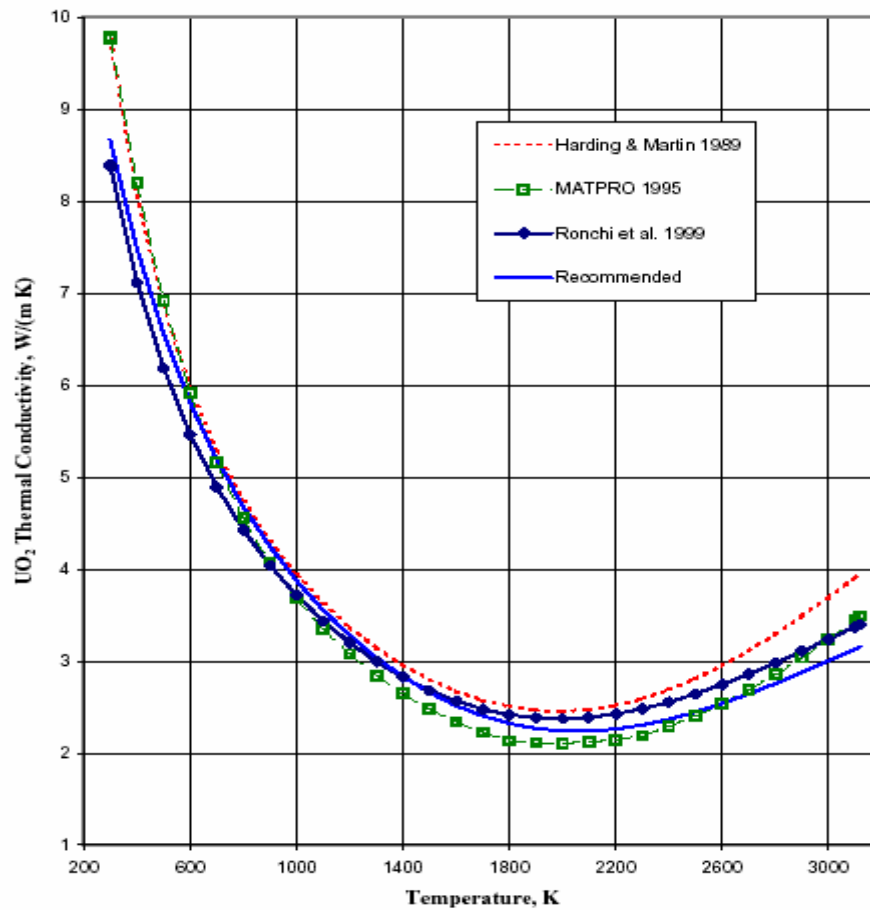


FIG. 13. Comparison of equations for the thermal conductivity of 100% dense  $\text{UO}_2$

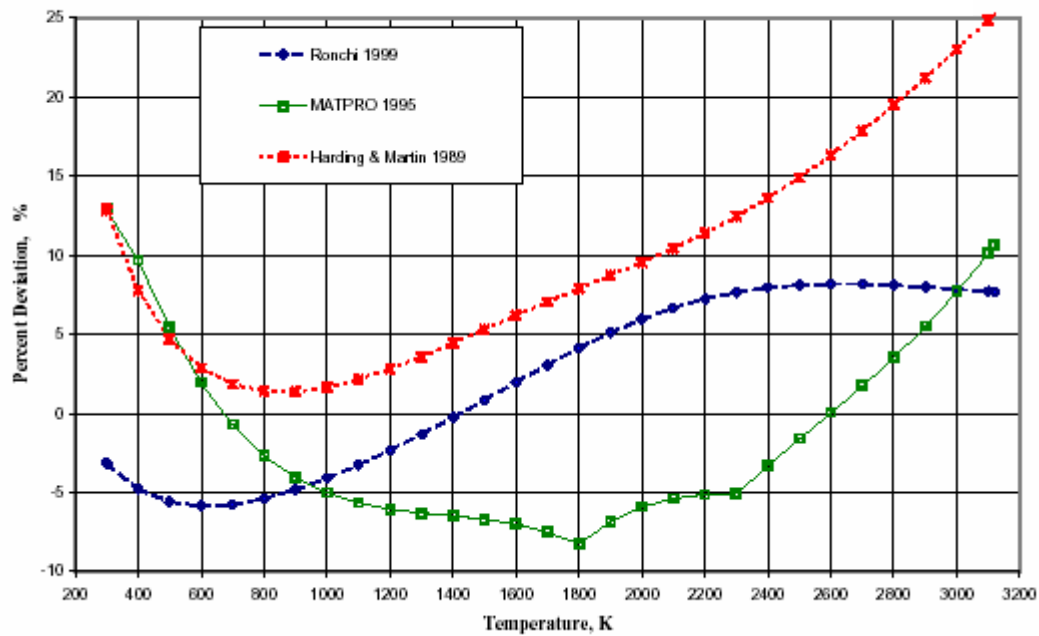


FIG. 14. Percent deviation from recommended  $\text{UO}_2$  thermal conductivities.

## REFERENCES TO SECTION 6.1.1.7

- [1] RONCHI, C., SHEINDLIN, M., MUSELLA, M. and HYLAND, G.J., Thermal conductivity of uranium dioxide up to 2900 K from simultaneous measurement of the heat capacity and thermal diffusivity, *J. Applied Phys.* 85, 776-789 (1999).
- [2] HOBSON, I.C., TAYLOR, R., and AINSCOUGH, J.B., Effect of porosity and stoichiometry on the thermal conductivity of uranium dioxide, *J. of Phys. D: Applied Physics* 7, 1003-1015 (1974).
- [3] LAMBERT BATES, J., High-temperature thermal conductivity of round robin' uranium dioxide, Battelle Memorial Institute Pacific Northwest Laboratories Report BNWL-1431 (1970).
- [4] CONWAY, J.B. and FEITH, A.D., An interim report on a round robin experimental program to measure the thermal conductivity of stoichiometric uranium dioxide, General Electric Report GEMP-715 (1969), also addendum (1970).
- [5] GODFREY, T.G., FULKERSON, W., KOLLIE, T.G., MOORE, J.P. and MCELROY, D.L., The thermal conductivity of uranium dioxide and armco iron by an improved radial heat flow technique, Oak Ridge national Laboratory Report ORNL-3556 (1964).
- [6] BRANDT, R. and NEUER, G., Thermal conductivity and thermal radiation properties of  $\text{UO}_2$ , *J. Non-Equilib. Thermodyn.* 1, 3-23 (1976).
- [7] WEILBACHER, J.C., Measurement of thermal diffusivity of mixed uranium plutonium oxides, Centre d'études nucléaires de Fontenay-aux-Roses, France Report CEA-R-4572 (1974).
- [8] WEILBACHER, J.C., Diffusivité thermique de l'oxyde d'uranium et de l'oxyde de thorium à haute température, *High Temp.-High Pressures* 4, 431-438 (1972).
- [9] STORA, J.C., DE BERNARDY DE SIGOYER, B., DELMAS, R., DESCHAMPS, P., LAVAUD, B. and RINGOT, C., Conductivité thermique de l' $\text{UO}_2$  frite dans les conditions d'utilisation en pile, Centre d'études nucléaires de Saclay France Report CEA-R-2586 (1964).
- [10] HYLAND, G.J., Thermal conductivity of solid  $\text{UO}_2$ : critique and recommendation, *J. Nucl. Mater.* 113, 125-132 (1983).
- [11] HARDING, J.H. and MARTIN, D.J., A recommendation for the thermal conductivity of  $\text{UO}_2$ , *J. Nucl. Mater.* 166, 223-226 (1989).
- [12] FINK, J.K., Enthalpy and heat capacity of the actinide oxides, *Int. J. Thermophys.* 3, 165-200 (1982).
- [13] HARDING, J.H., MARTIN, D.G. and POTTER, P.E., Thermophysical and thermochemical properties of fast reactor materials, Harwell Laboratory UKAEA Report EUR 12402 (1989).
- [14] HAGRMAN, D.T. (Ed.), SCADAP/RELAP5/MOD 3.1 Code Manual Vol. 4: MATPRO - a library of materials properties for light-water-reactor accident analysis, NUREG/CR-6150 (1995).
- [15] FINK, J.K. and PETRI, M.C., Thermophysical properties of uranium dioxide, Argonne National Laboratory Report ANL/RE-97/2 (1997).
- [16] CASADO, J.M., HARDING, J.H. and HYLAND, G.J., Small-polaron hopping in Mott-insulating  $\text{UO}_2$ , *J. Phys.:Condens. Matter* 6, 4685-4698 (1994).
- [17] KILLEEN, J.C., *J. Nucl. Mater.* 92, 136 (1980).
- [18] MARTIN, D.G., The thermal expansion of solid  $\text{UO}_2$  and (U,Pu) mixed oxides - A review and recommendations, *J. Nucl. Mater.* 152, 94-101 (1988).
- [19] See  $\text{UO}_2$  heat capacity in INSC Database Revision 1; also FINK, J.K., Thermophysical properties of uranium dioxide, paper submitted to *J. Nucl. Mater.* (June 1999).
- [20] WASHINGTON, A.B.G., Preferred values for the thermal conductivity of sintered ceramic fuel for fast reactor use, United Kingdom Atomic Energy Authority TRG-Report -2236 (1973).
- [21] LYONS, M.F., COPLIN, D.H., PASHOS, T.J. and WEODEMBAL, B., General Electric Company Report GEAP-44624 (1964), as referenced by Ronchi et al. (Ref. 1).

#### 6.1.1.8. Density of liquid $\text{UO}_2$

##### **Recommended equation**

The recommended equation for the density of liquid uranium dioxide is based on the in-pile effective equation of state measurements of the vapor pressure, density, and isothermal compressibility of liquid (U, Pu) $\text{O}_2$  by Breitung and Reil [1]. Measurements of density as a function of enthalpy and as a function of temperature were obtained from the melting point to 7600 K. The equation of Breitung and Reil for the density of  $\text{UO}_2$  and (U, Pu) $\text{O}_2$  for mole fractions of Pu  $\leq 0.25$  is in good agreement with the equation for the density of  $\text{UO}_2$  from experiments by Drotning [2], which had been recommended in the 1981 assessment by Fink et al. [3, 4].

The recommended equation for the density of  $\text{UO}_2$  as a function of temperature is:

$$\rho = 8.860 - 9.285 \times 10^{-4} (T - 3120) \quad (1)$$

where density ( $\rho$ ) is in  $\text{Mg/m}^3$  and temperature ( $T$ ) is in K. Values for the density and the instantaneous thermal expansion coefficient of  $\text{UO}_2$  are given in Table 1. Figure 1 shows the recommended values for the density of  $\text{UO}_2$ , the uncertainties determined by Breitung and Reil [1], and the  $\text{UO}_2$  density data of Drotning [2] and of Christensen [5].

##### **Uncertainties**

Breitung and Reil determined experimental uncertainties from the uncertainty in the fuel mass ( $\delta m/m = 10\%$ ), the uncertainty in the test volume ( $\delta V/V = 2.5\%$ ), and the uncertainty in the fuel enthalpy ( $\delta h/h = 6\%$ ). From these uncertainties, they obtained upper and lower limiting values in addition to the most probable reference values. Their uncertainty bands correspond to uncertainties in the coefficients in Eq. (1) given by:

$$\rho = 8.860 \pm 0.120 \left[ -9.285 \begin{pmatrix} +0.036 \\ -0.135 \end{pmatrix} \right] \times 10^{-4} (T - 3120) \quad (2)$$

The upper and lower uncertainty limits calculated from Eq.(2) are shown in Figure 1. They correspond to uncertainties of:

- $\pm 1.4\%$  at 3120 K;
- +1.6% and -2% at 3500 K;
- +2.2% and -4% at 4500 K;
- +3% and -6.3% at 5400 K;
- +4.2% and -10% at 6500 K;
- +6% and -15.4% at 7600 K.



Table 1. Density and volumetric thermal expansion coefficient for liquid UO<sub>2</sub>

TEMPERATURE, K	DENSITY, Mg m <sup>-3</sup>	THERMAL EXPANSION, $\alpha_p \times 10^5, K^{-1}$
3120	8.86	10.48
3200	8.79	10.57
3300	8.69	10.68
3400	8.60	10.80
3500	8.51	10.91
3600	8.41	11.03
3700	8.32	11.16
3800	8.23	11.28
3900	8.14	11.41
4000	8.04	11.54
4100	7.95	11.68
4200	7.86	11.82
4300	7.76	11.96
4400	7.67	12.10
4500	7.58	12.25
4600	7.49	12.40
4700	7.39	12.56
4800	7.30	12.72
4900	7.21	12.88
5000	7.11	13.05
5100	7.02	13.22
5200	6.93	13.40
5300	6.84	13.58
5400	6.74	13.77
5500	6.65	13.96
5600	6.56	14.16
5700	6.46	14.36
5800	6.37	14.57
5900	6.28	14.79
6000	6.19	15.01
6100	6.09	15.24
6200	6.00	15.47
6300	5.91	15.72
6400	5.81	15.97
6500	5.72	16.23
6600	5.63	16.50
6700	5.54	16.77
6800	5.44	17.06
6900	5.35	17.35
7000	5.26	17.66
7100	5.16	17.98
7200	5.07	18.31
7300	4.98	18.65
7400	4.89	19.00
7500	4.79	19.37
7600	4.70	19.75

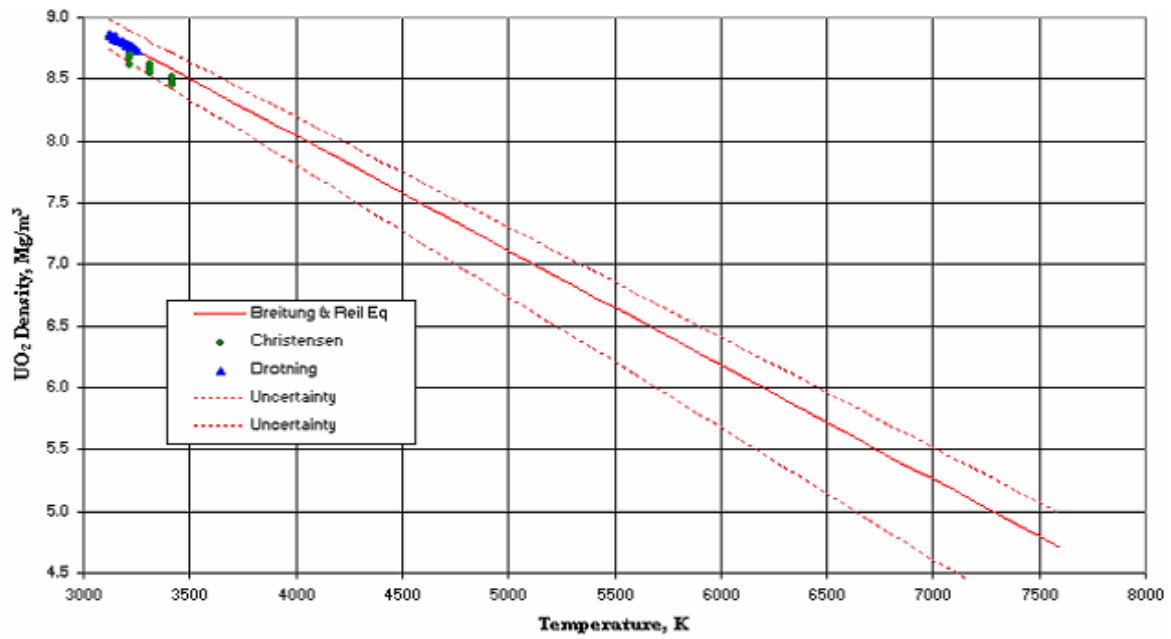


FIG. 1. Liquid density of  $\text{UO}_2$ .

### Discussion of the recommended equation

#### Measurements and assessments

Three experiments have provided data on the density and thermal expansion of liquid  $\text{UO}_2$ . Breitung and Reil [1] determined the density of  $\text{UO}_2$  and  $(\text{U,Pu})\text{O}_2$  from the melting point to 7600 K from measurements of the pressure rise of a sealed capsule during a transient in-pile pulse. Their vapor pressure measurements using ultrapure  $\text{UO}_2$ , reactor grade  $\text{UO}_2$ , and reactor grade  $(\text{U,Pu})\text{O}_2$  showed no significant difference for the vapor pressures of all three fuel types. Drotning [2] determined the density of  $\text{UO}_2$  with O/M ranging from 2.01 to 2.04 as a function of temperature using gamma ray attenuation measurements. Christensen measured the thermal expansion of solid and liquid  $\text{UO}_2$  and the volume change on melting using gamma radiographs to determine the sample dimensions.

$\text{UO}_2$  liquid densities at the melting point measured by Drotning ranged from 8.779 to 8.939  $\text{Mg/m}^3$  with an average of 8.860  $\text{Mg/m}^3$  and a deviation of  $\pm 0.061 \text{ Mg/m}^3$  or 0.7%. His equation for the density of  $\text{UO}_2$  in  $\text{Mg/m}^3$  from 3120 to 3250 K is:

$$\rho = 8.860 \pm 0.06 - (9.16 \pm 0.43) \times 10^{-4} (T - 3120) \quad (3)$$

where temperature is in K. This equation was recommended in the 1981 assessment by Fink et al. [3, 4].

The change of density of  $\text{UO}_2$  at the melting point measured by Christensen was 9.6%. In the liquid range, he measured densities from the melting point (which he measured as 3073 K rather than 3120 K) to 3373 K. At the melting point, he gives solid and liquid densities of  $9.67 \pm 0.13 \text{ Mg/m}^3$  and  $8.74 \pm 0.16 \text{ Mg/m}^3$ , respectively. His equation for the liquid density of  $\text{UO}_2$  adjusted to a melting point of 3120 K is:

$$\rho = 8.74 - 9.18 \times 10^{-4} (T - 3120) \quad (4)$$

where the density is in  $\text{Mg/m}^3$  and temperature is in K.

In their 1989 review of the data on density of liquid  $\text{UO}_2$ , Harding, Martin, and Potter [6] use the solid density at the melting point recommended by Martin [7] ( $9.56 \pm 0.04 \text{ Mg/m}^3$ ) and the change in density at melting determined by Christensen (9.6%) to obtain  $8.64 \pm 0.06 \text{ Mg/m}^3$  for the liquid density at 3120 K. Because of the higher accuracy of Drotning's liquid density measurements compared with the thermal expansion measurements of Christensen, Harding et al. [6] based the slope

of their density equation on the slope given by Drotning corrected to the different density at the melting point, 3120 K. They recommend the equation:

$$\rho = 8.64 \pm 0.06 - (8.93 \pm 0.42) \times 10^{-4} (T - 3120) \quad (5)$$

for the density of  $\text{UO}_2$  in  $\text{Mg/m}^3$ , where temperature is in K. The liquid density at the melting point given by this equation is lower than the lowest density measured by Drotning but is above Christensen's lower uncertainty of  $8.58 \text{ Mg/m}^3$ .

Breitung and Reil set their melting point density of  $\text{UO}_2$  and  $(\text{U,Pu})\text{O}_2$  to  $8.860 \text{ Mg/m}^3$ , the density of  $\text{UO}_2$  at the melting point given by Drotning [2] because of the smaller error in Drotning's measurements ( $\pm 0.7\%$ ) than in Christensen's measurements ( $\pm 2\%$ ). The densities of Christensen and of Drotning agree within their experimental uncertainties. The uncertainty ( $\pm 0.120 \text{ Mg/m}^3$ ) given by Breitung and Reil for this parameter in their density equation is large enough to include the melting point density given by Christensen. The liquid density at the melting point recommended by Fink, Chasanov, and Leibowitz [3,4] was also  $8.860 \text{ Mg/m}^3$ .

#### Equation selection

The equation given by Breitung and Reil, Eq.(1), is recommended because it is based on a careful analysis of the experimental data with experimental uncertainties for the largest temperature range and is consistent with the measurements of Drotning. Figure 2 compares the recommended equation of Breitung and Reil with the equations of Drotning [2], Christensen [5], and Harding et al. [6] and the experimental data of Drotning and of Christensen. In Figure 2, the data of Christensen has been corrected for his temperature offset at the melting point. Figure 2 shows that the slope of the density equation recommended by Breitung and Reil is also consistent with that of Christensen. However, the equation of Harding et al is consistently lower than that of Breitung and Reil in this temperature region due to the melting point density selected by Harding et al. Because the solid density data of Christensen has been shown, by Martin's analysis [7] of the thermal expansion of solid  $\text{UO}_2$ , to be inconsistent with later more accurate measurements of Hutchings [8], there is some question with regard to the reliability of his determination of the change of density on melting. Because the liquid densities at the melting point determined by Drotning and by Christensen are consistent within their error limits and the uncertainties for Drotning's data are less than those for Christensen's, the melting point density of Drotning is preferred to using the density change on melting given by Christensen and the solid density at the melting point given by Martin [7].

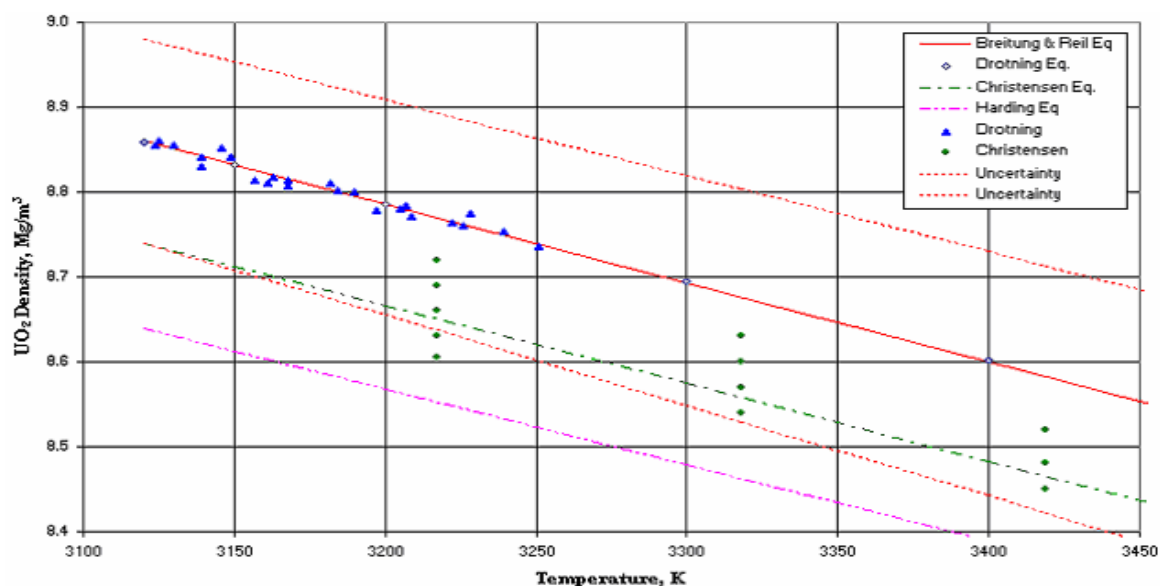


FIG. 2. Liquid density of  $\text{UO}_2$ .

### Deviations from recommended equation

Percent deviations of the densities given by the equations of Drotning, Christensen, and Harding et al. from the recommended values given by the equation of Breitung and Reil are shown in Figure 3. Percent deviations in Figure 3 are defined as:

$$\text{Deviation}(\%) = \frac{\rho(\text{Eq}) - \rho(\text{Breitung})}{\rho(\text{Breitung})} \cdot 100\%$$

The uncertainties given by Breitung and Reil are included in Figure 3, expressed as percents, for comparison with the deviations. Figure 3, shows that all the equations are within the uncertainties of Breitung and Reil except for the equation of Harding et al. for the temperature range 3120 K through 3700 K. Absolute values of the percent deviations for the equation of Harding et al. decrease from a maximum deviation of -2.5% at the melting point to -1.3% at 7600 K. Percent deviations for the density equation of Christensen show little variation with temperature. They range from -1.4% at 3120 K to -1.6% at 7600 K. The smallest deviations occur for Drotning's equation, which gives densities within 1% of those given by Breitung and Reil from the melting point through 7200 K. At 7600 K, the percent deviation for these equations is 1.2%. Thus, for the entire temperature range of interest in severe accidents, the recommended densities of Breitung and Reil are in good agreement with those given by the equation of Drotning which was recommended in the 1981 assessment by Fink et al. [3, 4].

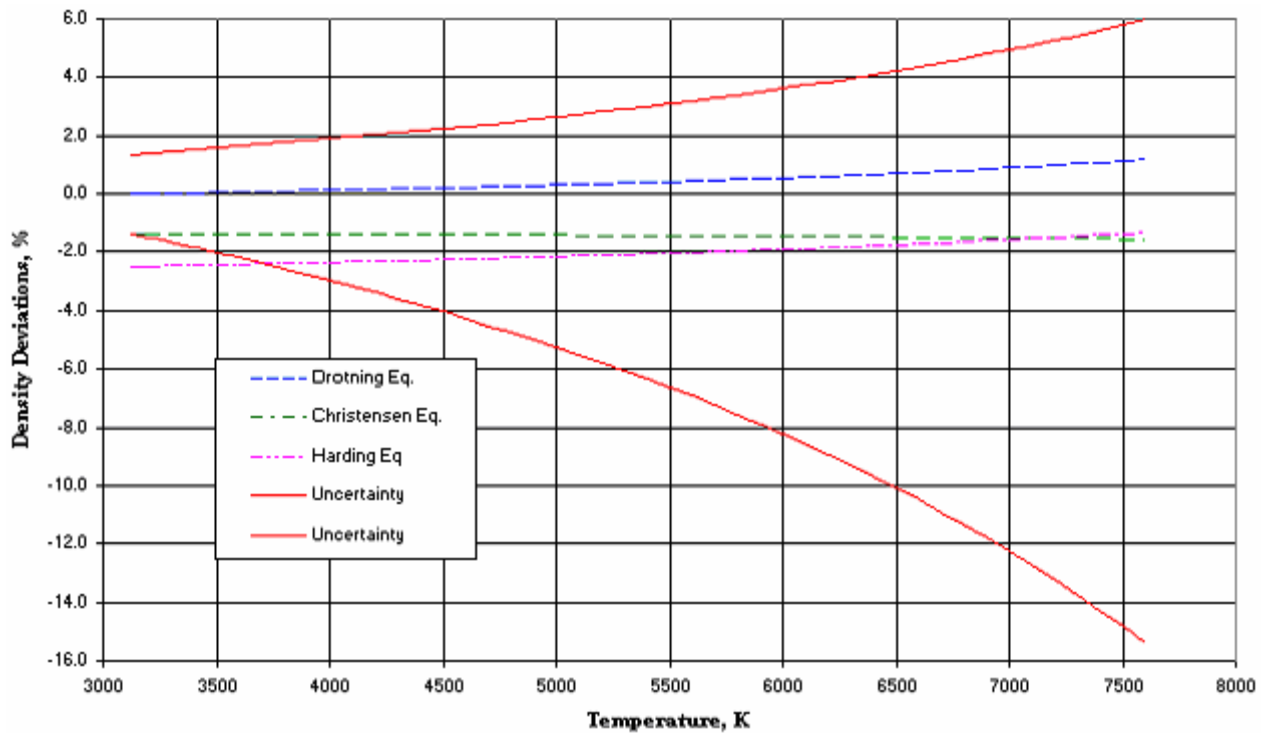


FIG. 3. Deviations from (U,Pu)O<sub>2</sub> liquid density eq. of Breitung & Reil.

### REFERENCES TO SECTION 6.1.1.8

- [1] BREITUNG, W. and REIL, K.O., The density and compressibility of liquid (U,Pu)-mixed oxide, Nuclear Science and Engineering 105, 205-217 (1990).
- [2] DROTNING, W.D., Thermal expansion of molten uranium dioxide, Proceedings of the 8th Symp. On Thermophysical Properties, Gaithersburg, Maryland, June 15-18, 1981, National Bureau of Standard (1981).

- [3] FINK, J.K., CHASANOV, M.G. and LEIBOWITZ, L., Thermophysical properties of uranium dioxide, J. Nucl. Mater. 102 17-25 (1981).
- [4] FINK, J.K., CHASANOV, M.G. and LEIBOWITZ, L., Properties for reactor safety analysis, ANL-CEN-RSD-80-3, Argonne National Laboratory Report (April, 1981).
- [5] CHRISTENSEN, J.A., Thermal expansion and change in volume of uranium dioxide on melting, J. Am. Ceram. Soc. 46, 607-608 (1963).
- [6] HARDING, J.H., MARTIN, D.G. and POTTER, P.E., Thermophysical and thermochemical properties of fast reactor materials, Commission of European Communities Report EUR 12402 (1989).
- [7] MARTIN, D.G., The thermal expansion of solid UO<sub>2</sub> and (U,Pu) mixed oxides - A review and recommendations, J. Nucl. Mater. 152 94-101 (1988).
- [8] HUTCHINGS, M.T., High-temperature studies of UO<sub>2</sub> and ThO<sub>2</sub> using neutron scattering techniques, J. Chem. Soc. Faraday Trans. II 83, 1083-1103 (1987).

#### 6.1.1.9. Thermal expansion coefficient of liquid UO<sub>2</sub>

##### **Recommended equation**

The recommended equation for the thermal expansion coefficient of liquid uranium dioxide is based on the in-pile effective equation of state measurements of the vapor pressure, density, and isothermal compressibility of liquid (U, Pu)O<sub>2</sub> by Breitung and Reil [1]. From these measurements, the density and thermal expansion coefficient as functions of temperature were obtained from the melting point to 7600 K. The equation of Breitung and Reil for the thermal expansion coefficient of UO<sub>2</sub> and (U, Pu)O<sub>2</sub> for mole fractions of Pu ≤ 0.25 is in good agreement with the equation for the thermal expansion coefficient of UO<sub>2</sub> from experiments by Drotning [2], which had been recommended in the 1981 assessment by Fink et al. [3,4].

The recommended equation for the instantaneous volumetric thermal expansion coefficient of UO<sub>2</sub> as a function of temperature is:

$$\alpha_P = \frac{0.9285}{8860 - 0.9285(T - 3120)} \quad (1)$$

where the thermal expansion coefficient ( $\alpha_P$ ) is in K<sup>-1</sup> and temperature ( $T$ ) is in K. Values for the density and the instantaneous volumetric thermal expansion coefficient of UO<sub>2</sub> are given in Table 1. Figure 1 shows the recommended values for the instantaneous volumetric thermal expansion coefficient of UO<sub>2</sub>, the uncertainties determined by Breitung and Reil [1], and the instantaneous volumetric thermal expansion coefficients of UO<sub>2</sub> calculated from equations of Drotning [2], of Christensen [5], and of Harding [6].

##### **Uncertainties**

Breitung and Reil determined experimental uncertainties from the uncertainty in the fuel mass ( $\delta m/m = 10\%$ ), the uncertainty in the test volume ( $\delta V/V = 2.5\%$ ), and the uncertainty in the fuel enthalpy ( $\delta h/h = 6\%$ ). From these uncertainties, they obtained upper and lower limiting cases, which they used to define uncertainties in the parameters in Eq. (1). The liquid density at the melting point, 8860 kg·m<sup>-3</sup>, has an uncertainty of ± 120 kg·m<sup>-3</sup>. The slope of the density,  $(d\rho/dT) = 0.9285$  kg·m<sup>-3</sup>·K<sup>-1</sup>, has uncertainties of + 0.036 kg·m<sup>-3</sup>·K<sup>-1</sup> and - 0.135 kg·m<sup>-3</sup>·K<sup>-1</sup>. The upper and lower uncertainty limits calculated using the uncertainties in these parameters are shown in Figure 1. They correspond to uncertainties of:

- +10% and -12% at 3120 K;
- +10% and -13% at 3500 K;
- +12% and -15% at 4500 K;
- +13% and -17% at 5500 K;
- +15% and -20% at 6500 K;
- +18% and -27% at 7600 K.

Table 1. Density and volumetric thermal expansion coefficient for liquid UO<sub>2</sub>

TEMPERATURE, K	DENSITY, Mg m <sup>-3</sup>	THERMAL EXPANSION, $\alpha_p \times 10^5$ , K <sup>-1</sup>
3120	8.86	10.48
3200	8.79	10.57
3300	8.69	10.68
3400	8.60	10.80
3500	8.51	10.91
3600	8.41	11.03
3700	8.32	11.16
3800	8.23	11.28
3900	8.14	11.41
4000	8.04	11.54
4100	7.95	11.68
4200	7.86	11.82
4300	7.76	11.96
4400	7.67	12.10
4500	7.58	12.25
4600	7.49	12.40
4700	7.39	12.56
4800	7.30	12.72
4900	7.21	12.88
5000	7.11	13.05
5100	7.02	13.22
5200	6.93	13.40
5300	6.84	13.58
5400	6.74	13.77
5500	6.65	13.96
5600	6.56	14.16
5700	6.46	14.36
5800	6.37	14.57
5900	6.28	14.79
6000	6.19	15.01
6100	6.09	15.24
6200	6.00	15.47
6300	5.91	15.72
6400	5.81	15.97
6500	5.72	16.23
6600	5.63	16.50
6700	5.54	16.77
6800	5.44	17.06
6900	5.35	17.35
7000	5.26	17.66
7100	5.16	17.98
7200	5.07	18.31
7300	4.98	18.65
7400	4.89	19.00
7500	4.79	19.37
7600	4.70	19.75

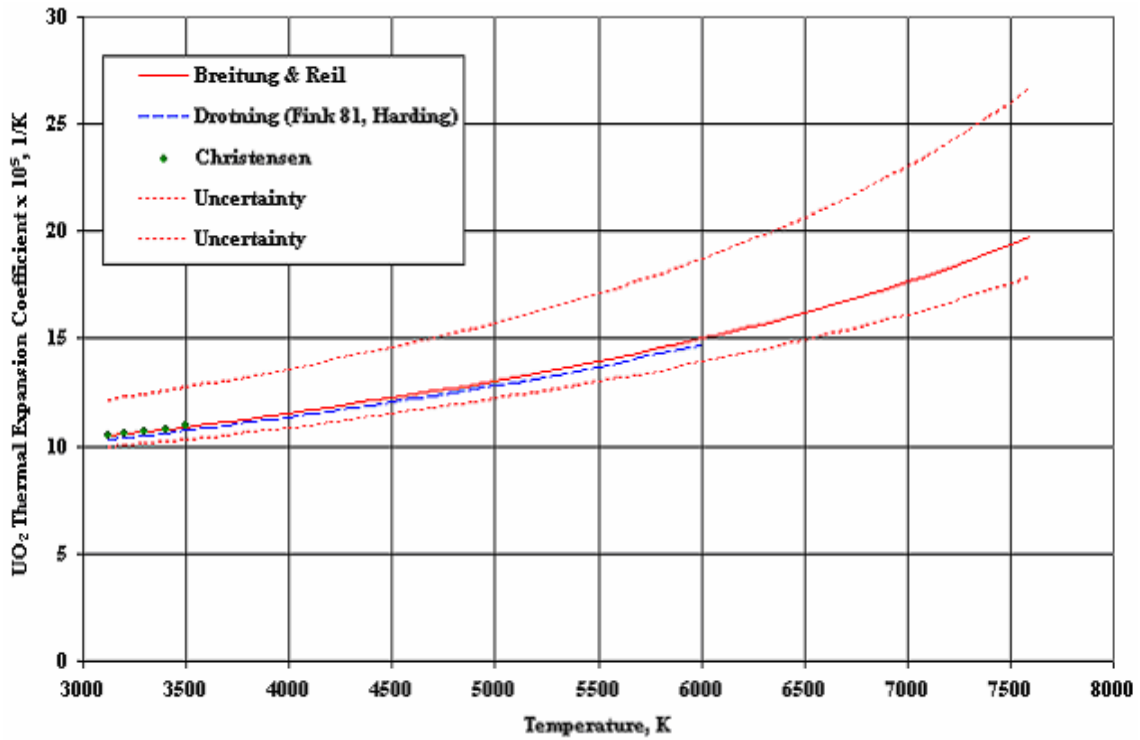


FIG. 1. Coefficient of thermal expansion for liquid  $\text{UO}_2$ .

### Discussion of the recommended equation

#### Thermodynamic relations

The instantaneous volumetric thermal expansion coefficient ( $\alpha_p$ ) is related to the density ( $\rho$ ) by the thermodynamic relation:

$$\alpha_p = -\frac{1}{\rho} \left( \frac{\partial \rho}{\partial T} \right)_\sigma + \beta_T \left( \frac{\partial P}{\partial T} \right)_\sigma \quad (2)$$

where  $\beta_T$  is the isothermal compressibility and  $P$  is the vapor pressure. The subscript  $\sigma$  on the partial derivatives indicates that they are along the saturation curve. Breitung and Reil [1] state that the magnitude of the second term in Eq. (2) is much smaller than the first term and only contributes a few percent at 8000 K. This is because along the saturation curve, the volume change due to the pressure change is much smaller than the corresponding volume change due to thermal expansion. Thus, for  $\text{UO}_2$  and  $(\text{U,Pu})\text{O}_2$ , the thermal expansion coefficient may be evaluated from the density/temperature relation using the first term in Eq. (2).

The linear instantaneous thermal expansion coefficient is one third of the instantaneous volumetric thermal expansion coefficient, given by Eq. (1). Equations relating the instantaneous volumetric thermal expansion coefficient and density to other expansion parameters are given in the appendix, "Density and Thermal Expansion Relations." (Appendix I, Section 6.1.1.3)

#### Comparison with Other Measurements and Assessments

Three experiments have provided data on the density and thermal expansion of liquid  $\text{UO}_2$ . Breitung and Reil [1] determined the density of  $\text{UO}_2$  and  $(\text{U,Pu})\text{O}_2$  from the melting point to 7600 K from measurements of the pressure rise of a sealed capsule during a transient in-pile pulse. Their vapor pressure measurements using ultrapure  $\text{UO}_2$ , reactor grade  $\text{UO}_2$ , and reactor grade  $(\text{U,Pu})\text{O}_2$  showed no significant difference for the vapor pressures of all three fuel types. Drotning [2] determined the density of  $\text{UO}_2$  with O/M ranging from 2.01 to 2.04 as a function of temperature using gamma ray attenuation measurements. Christensen measured the thermal expansion of solid and liquid  $\text{UO}_2$  and the volume change on melting using gamma radiographs to determine the sample dimensions.

The variation of density with temperature from all three measurements is in good agreement. The slope ( $dp/dT$ ) used in the first term of Eq. (2) is:

- 0.9285 kg m<sup>-3</sup> K<sup>-1</sup> (Breitung & Reil)
- 0.916 kg m<sup>-3</sup> K<sup>-1</sup> (Drotning)
- 0.918 kg m<sup>-3</sup> K<sup>-1</sup> (Christensen)

The thermal expansion of Drotning [2] was recommended in the 1981 assessment by Fink et al.[3, 4]. The instantaneous volumetric thermal expansion coefficient calculated from Drotning's density equation using the first term in Eq. (2) is:

$$\alpha_P = \frac{0.916}{8860 - 0.916(T - 3120)} \quad (3)$$

where the thermal expansion coefficient ( $\alpha_P$ ) is in K<sup>-1</sup> and temperature ( $T$ ) is in K. Values of thermal expansion calculated with this equation are shown in Figure 1.

In their 1989 review of the data on density of liquid UO<sub>2</sub>, Harding, Martin, and Potter [6] also recommend the change in density with temperature measured by Drotning. However, they recommended  $8640 \pm 60$  kg·m<sup>-3</sup> for the liquid density at 3120 K. Therefore, the thermal expansion coefficient calculated from the density recommended by Harding et al. using the first term in Eq. (2) is:

$$\alpha_P = \frac{0.893}{8640 - 0.893(T - 3120)} \quad (4)$$

where the volumetric thermal expansion coefficient ( $\alpha_P$ ) is in K<sup>-1</sup> and temperature ( $T$ ) is in K. Because both Eq. (3) and Eq. (4) are based on the variation of density with temperature measured by Drotning, the values of the thermal expansion coefficient calculated using Eq. (4) are almost identical to those calculated using Eq. (3). Differences are 0.03% from the melting point to 4800 K, 0.04% from 4900 to 6600 K, and 0.05% from 6700 to 7600 K.

The instantaneous volumetric thermal expansion coefficient calculated from the liquid density of Christensen and his change of density with temperature is:

$$\alpha_P = \frac{0.918}{8740 - 0.918(T - 3120)} \quad (5)$$

where the thermal expansion coefficient ( $\alpha_P$ ) is in K<sup>-1</sup> and temperature ( $T$ ) is in K. Values of the volumetric thermal expansion coefficient determined from the measurements of Christensen have been included in Figure 1.

Figure 2 shows the deviations of the recommended thermal expansion coefficients of Breitung and Reil from the thermal expansion coefficients determined from measurements of Christensen [5] and of Drotning [2]. Percent deviations in Figure 2 are defined as:

$$Deviation (\%) = \frac{\alpha_P(Eq) - \alpha_P(Breitung)}{\alpha_P(Breitung)} \bullet 100\% \quad (6)$$

Extrapolations of the thermal expansion coefficients from the low temperature measurements of Christensen and of Drotning to 7600 K show good agreement throughout the temperature range. Deviations of recommended values from those determined from measurements by Drotning range from -1.4% at the melting point to -2.5% at 7600 K. Christensen's values deviate from those of Breitung and Reil by 0.2% at the melting temperature and by 0.4% at 7600 K. Figure 2 shows that all deviations are well within the uncertainty limits given by Breitung and Reil.



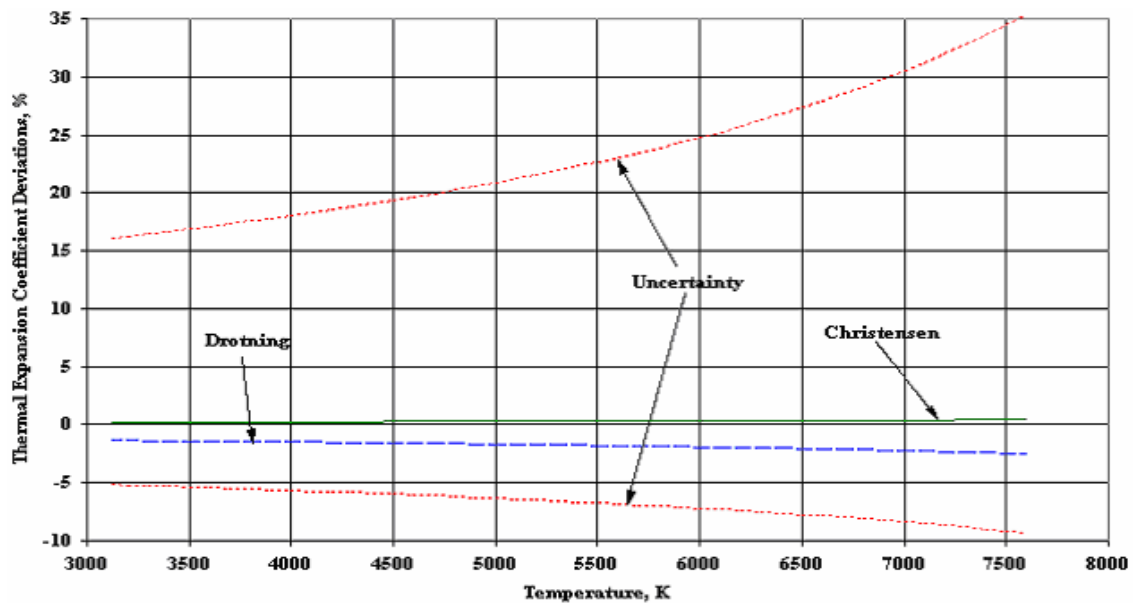


FIG. 2. Deviations from (U,Pu)O<sub>2</sub> liquid thermal expansion eq. of Breitung & Reil.

#### REFERENCES TO SECTION 6.1.1.9

- [1] BREITUNG, W. and REIL, K.O., The density and compressibility of liquid (U,Pu)- mixed oxide, Nuclear Science and Engineering 105, 205-217 (1990).
- [2] DROTNING, W.D., Thermal expansion of molten uranium dioxide, Proceedings of the 8th Symp. On Thermophysical Properties, Gaithersburg, Maryland, June 15-18, 1981, National Bureau of Standard (1981).
- [3] FINK, J.K., CHASANOV, M.G. and LEIBOWITZ, L., Thermophysical properties of uranium dioxide, J. Nucl. Mater. 102 17-25 (1981).
- [4] FINK, J.K., CHASANOV, M.G. and LEIBOWITZ, L., Properties for reactor safety analysis, ANL-CEN-RSD-80-3, Argonne National Laboratory Report (April, 1981).
- [5] CHRISTENSEN, J.A., Thermal expansion and change in volume of uranium dioxide on melting, J. Am. Ceram. Soc. 46, 607-608 (1963).
- [6] HARDING, J.H., MARTIN, D.G. and POTTER, P.E., Thermophysical and thermochemical properties of fast reactor materials, Commission of European Communities Report EUR 12402 (1989).

##### 6.1.1.10. Density of solid UO<sub>2</sub>

##### **Recommended equations**

The recommended equations for the density of solid uranium dioxide are based on the lattice parameter value of 0.54704 nm obtained by Gronvold [1] at 293 K and the 1988 assessment of thermal expansion by D. G. Martin [2]. They are in agreement with the 1989 recommendations of Harding, Martin, and Potter [3]. The lattice parameter of Gronvold is in good agreement with recent measurements by Hutchings [3]. Assuming the molecular weight of UO<sub>2</sub> is 270.0277, this lattice parameter gives a UO<sub>2</sub> density at 293 K of 10.956 Mg·m<sup>-3</sup>. Applying the thermal expansion recommendation of Martin, the density at 273 K is 10.963 Mg · m<sup>-3</sup>.

The density as a function of temperature may be calculated from:

$$\rho(T) = \rho(273) \left( \frac{L(273)}{L(T)} \right)^3 \quad (1)$$

where  $\rho(273)$  is the density at 273 K;  $L(273)$  and  $L(T)$  are the lengths at 273 K and at temperature  $T(K)$ , respectively. The ratio of the length at 273 K to the length at temperature  $T(K)$  may be calculated from Martin's equations for the thermal expansion of solid  $UO_2$ :

for  $273\text{ K} \leq T \leq 923\text{ K}$ ,

$$L(T) = L(273) (9.9734 \times 10^{-1} + 9.802 \times 10^{-6} T - 2.705 \times 10^{-10} T^2 + 4.291 \times 10^{-13} T^3); \quad (2)$$

for  $923\text{ K} \leq T \leq 3120\text{ K}$ ,

$$L(T) = L(273) (9.9672 \times 10^{-1} + 1.179 \times 10^{-5} T - 2.429 \times 10^{-9} T^2 + 1.219 \times 10^{-12} T^3) \quad (3)$$

The densities as a function of temperature of solid  $UO_2$  are given in Table 1.

Table 1. Density of solid uranium dioxide

TEMPERATURE , K	DENSITY, Mg ·m <sup>-3</sup>
273	10.96
298	10.95
300	10.95
400	10.92
500	10.89
600	10.86
700	10.83
800	10.79
900	10.76
1000	10.73
1100	10.69
1200	10.66
1300	10.62
1400	10.58
1500	10.54
1600	10.50
1700	10.46
1800	10.42
1900	10.37
2000	10.32
2100	10.27
2200	10.21
2300	10.16
2400	10.10
2500	10.03
2600	9.96
2700	9.89
2800	9.82
2900	9.74
3000	9.66
3100	9.57
3120	9.56

From assessment of the available data on hyperstoichiometric uranium dioxide ( $\text{UO}_{2+x}$ ), Martin recommends using the same equations for the linear thermal expansion of  $\text{UO}_2$  and of  $\text{UO}_{2+x}$  for  $x$  in the ranges 0 to 0.13 and 0.23 to 0.25. Therefore, equations (1) through (3) are recommended for the density of  $\text{UO}_{2+x}$  for  $x$  in the ranges 0 to 0.13 and 0.23 to 0.25.

No data on the effect of burn-up on density or thermal expansion of  $\text{UO}_2$  are currently available. In the absence of data, equations (1) through (3) are recommended for  $\text{UO}_2$  during irradiation, in accord with the recommendation of Harding, Martin, and Potter [3].

### Uncertainties

The recommended uncertainty in the density of  $\text{UO}_2$  is 1% for the entire temperature range. The uncertainties in the density of  $\text{UO}_2$  calculated from the thermal expansion uncertainties given by Martin [2] are less than 1%. The 1% uncertainty is based on comparison of the recommended density with those of previous recommendations based on different data. Figure 1 shows the recommended density, the 1% uncertainty, and the 1981 recommended values [5] that are based on the thermal expansion values of Olsen [6] and a density at 298.15 K of  $10.97 \text{ Mg} \cdot \text{m}^{-3}$ .

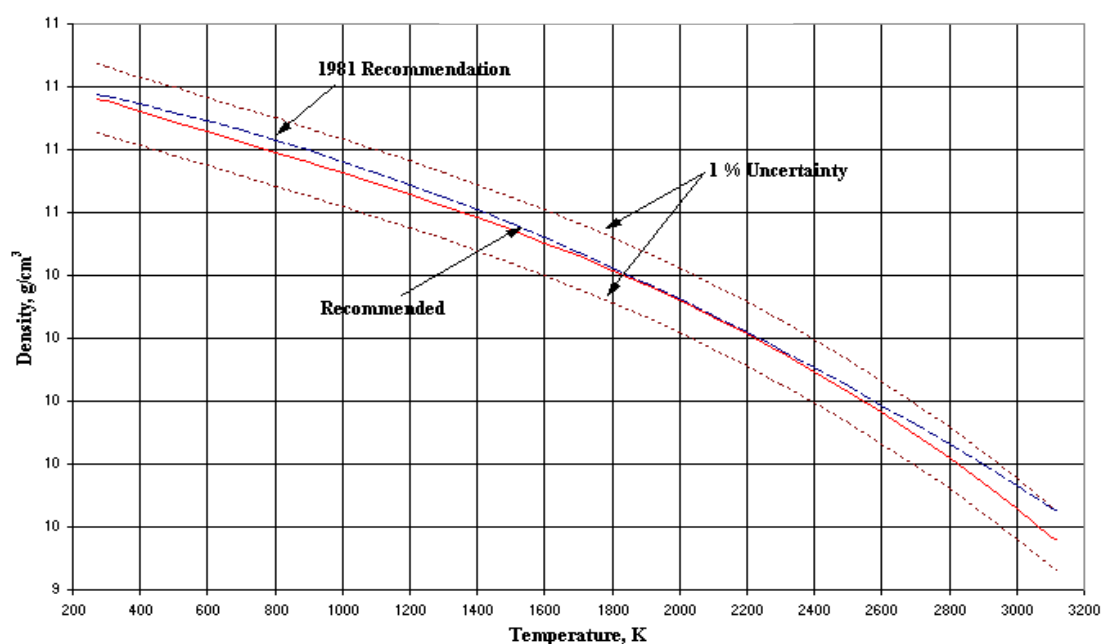


FIG. 1. Density of solid  $\text{UO}_2$ .

### REFERENCES TO SECTION 6.1.1.10

- [1] GRONVOLD, F., J. Inorganic and Nucl. Chem. 1 357, (1955).
- [2] MARTIN, D.G., *The Thermal Expansion of solid  $\text{UO}_2$  and (U,Pu) Mixed Oxides - A Review and Recommendations*, J. Nucl. Mater. 152, 94-101 (1988).
- [3] HARDING, J.H., MARTIN, D.G. and POTTER, P.E., *Thermophysical and Thermochemical Properties of Fast Reactor Materials*, Commission of European Communities Report EUR 12402 (1989).
- [4] HUTCHINGS, M.T., *High-Temperature Studies of  $\text{UO}_2$  and  $\text{ThO}_2$  using Neutron Scattering Techniques*, J. Chem. Soc. Faraday Trans. II 83, 1083-1103 (1987).
- [5] FINK, J.K., CHASANOV, M.G. and LEIBOWITZ, L., *Thermophysical Properties of Uranium Dioxide*, J. Nucl. Mater. 102 17-25 (1981).
- [6] OLSEN, C.S., Fuel thermal expansion (FTHEXP), in *MATPRO- Version 11: A Handbook of Materials Properties for Use in the Analysis of Light Water Reactor Fuel Rod Behavior*, ed. D. R. Hagraman and G. A. Reymann, US Nuclear Regulatory Commission Rep. NUREG/CR-0497 (February 1979); also revision (1981).

#### 6.1.1.11. Surface tension and surface energy of $UO_2$

##### **Summary and recommendation**

###### *Surface tension of liquid $UO_2$*

In 1987, Hall, Mortimer, and Mortimer [1] reported results of a critical review of available data on the surface tension of liquid  $UO_2$  and on the surface energy of solid  $UO_2$ . Because no new data have been reported since this review, the results of this critical review are recommended. The recommended surface tension of liquid  $UO_2$  at the melting point is the average of measurements by Schins [2], Christensen [3], and Bates [4] with a temperature dependence based on an equation derived by Nikopoulos and Schulz [5]:

$$\gamma_{LV} = 0.513 - 0.19 \times 10^{-3} (T - 3120) \quad (1)$$

where the surface tension,  $\gamma_{LV}$ , is in  $J\ m^{-2}$  and temperature,  $T$ , is in K.

###### *Surface energy of solid $UO_2$*

From review of the multi-phase equilibrium measurements of the surface energy of  $UO_2$ , Hall et al. [1] concluded that from 273 to 3120 K the surface energy ( $\gamma_{SV}$ ) in  $J\ m^{-2}$  of solid  $UO_{2.00}$  probably lies between two lines defined as follows:

Line 1

$$\gamma_{SV} = 1.5 - 2.82 \times 10^{-4} (T - 273) \quad (2)$$

and Line 2

$$\gamma_{SV} = 0.20 \quad (3)$$

with the mean line between these given by:

$$\gamma_{SV} = 0.85 - 1.40 \times 10^{-4} (T - 273) \quad (4)$$

where temperature,  $T$ , is in K.

Hall et al. [1] gave the dependence of the solid surface energy on stoichiometry as:

$$(\gamma_{SV})_x - \gamma_{SV} = 6.8x \quad (0 \leq x \leq 0.05; 0 < T < 2170K) \quad (5)$$

where  $(\gamma_{SV})_x$  is the surface energy of  $UO_{2\pm x}$  in  $J\ m^{-2}$ .

Hall et al. [1] concluded that the effective surface energy for pores in  $UO_2$ ,  $\gamma_p$ , is different from  $\gamma_{SV}$ .

It is given by:

$$\gamma_p = 0.41 \gamma_{SV} \quad (6)$$

##### **Uncertainties**

###### *Surface tension of liquid $UO_2$*

The standard error in the average of four measurements [2–4] of the surface tension of liquid  $UO_2$  at the melting point is  $\pm 0.085\ J\ m^{-2}$ , which is an uncertainty of approximately  $\pm 17\%$ .

###### *Surface energy of solid $UO_2$*

Because experimental estimates of the surface energy of solid  $UO_2$  in the temperature range of 1773 to 2173 K from multi-phase equilibration techniques are uncertain up to  $\pm 70\%$  and the sign of the temperature dependence is not unambiguously determined, Hall et al. gave the uncertainty in Eq. (4)

as  $\pm 70\%$ . Although the uncertainty in the dependence on stoichiometry is  $\pm 15\%$ , the  $\text{UO}_{2\pm x}$  surface energy uncertainty is  $> \pm 70\%$  because of the  $\text{UO}_2$  surface energy uncertainty.

## Discussion

### Surface tension of liquid $\text{UO}_2$

The measurements of the surface tension of liquid  $\text{UO}_2$  at the melting point are given in Table 1. The value given by Chasanov has no estimate of uncertainty and has not been included in the assessment by Hall [1]. Therefore, the recommended value for the surface tension at the melting point,  $0.513 \pm 0.085 \text{ J m}^{-2}$ , is the average of the surface tensions given in the first four rows of Table 1. Nikolopoulos and Schulz [5] calculated the surface tension of liquid  $\text{UO}_2$  at three temperatures near the melting point using a theory for ionic liquids developed by Furth [7]. Their calculated values at 3125, 3175 and 3225 K are respectively 0.521, 0.514, and  $0.502 \text{ J m}^{-2}$ . These values are consistent with the average experimental value of the measurements by Schins, Bates, and Christensen. The value obtained by Chasanov [6] is low relative to this calculation. Inclusion of the value,  $0.420 \text{ J m}^{-2}$ , given by Chasanov in the average would give  $0.494 \text{ J m}^{-2}$  for the surface tension at the melting point. This value, recommended by Fink, Leibowitz, and Chasanov [8], is low relative to the calculation of Nikolopoulos and Schulz [5].

Table 1. Measurements of the surface tension of liquid  $\text{UO}_2$  at the melting point

SURFACE TENSION, $\text{J m}^{-2}$	METHOD	EXPERIMENTER	REFERENCE
$0.615 \pm 0.180$	liquid drop measurements	Schins	[2]
$0.441 \pm 0.210$	liquid meniscus shape measurements	Bates	[4]
$0.445 \pm 0.210$	droplet photographs	Christensen	[3]
$0.550 \pm 0.210$	droplet photographs	Christensen	[3]
$0.420^*$	shape of frozen menisci	Chasanov	[6]

\*Not included in the determination of the recommended surface tension.

Nikolopoulos and Schulz [5] used their calculations to estimate the temperature dependence of the surface tension of liquid  $\text{UO}_2$  near the melting point as  $d\gamma_{\text{SV}}/dT = -0.19 \times 10^{-3} \text{ J m}^{-2}$ . Combining this result and the average experimental value at the melting point,  $0.513 \pm 0.085 \text{ J m}^{-2}$ , gives the recommended equation for the surface tension of liquid  $\text{UO}_2$ , Eq. (1). This equation, recommended by Hall et al. [1], is also recommended in the assessment by Harding et al. [9].

### Surface energy of solid $\text{UO}_2$

The experimental data have been most recently reviewed by Hall et al. [1]. The variations between the published data are much larger than the published error bars. The large variations in the data have been attributed to stoichiometry variations and to errors in the measurements of the angles (contact angle, grain boundary groove angle, and dihedral angle) from which the surface energy is calculated. Hall et al. [1] commented that the error in the dihedral angle dominates the uncertainty.

Surface energies obtained from multi-phase equilibration studies have been reported by Hodkin and Nicholas (Cu on  $\text{UO}_2$ ) [10], by Nikolopoulos, Nazare and Thummler (Ni on  $\text{UO}_2$ ) [11], and by Bratton and Beck (Ni on  $\text{UO}_2$ ) [12]. Hodkin and Nicholas [13] used sessile drop measurements of Cu-Th alloys on  $\text{UO}_{2\pm x}$  to study the effect of stoichiometry. Published data from these studies, shown in Figure 1, illustrate the large variation in the available data. Figure 1 includes the two bounding lines and the mean line defined by Hall et al. [1] (Hall line 1, Hall line 2, and Hall Mean), which are given

in Eqs (2–4), as well as estimates at the melting point. Eberhart [14] used the surface tension of liquid  $\text{UO}_2$  to estimate the solid surface energy at the melting point as  $0.56 \pm 0.09 \text{ J m}^{-2}$ . Deshpande, Desai, and Solomon [15] report the surface tension at the melting point as  $0.805 \pm 0.06 \text{ J m}^{-2}$  based on an estimate made by Skapski [16]. Hall et al. commented that both estimation methods are more appropriate for metals than for  $\text{UO}_2$  and, in the absence of a theoretical method, used an average of the two values ( $0.68 \pm 0.06 \text{ J m}^{-2}$ ) in their assessment. Hertzian indentation studies reported by Matzke et al. [17–19] gave surface energies at room temperature as a function of O:M ratio. Their published values are included in Figure 1.

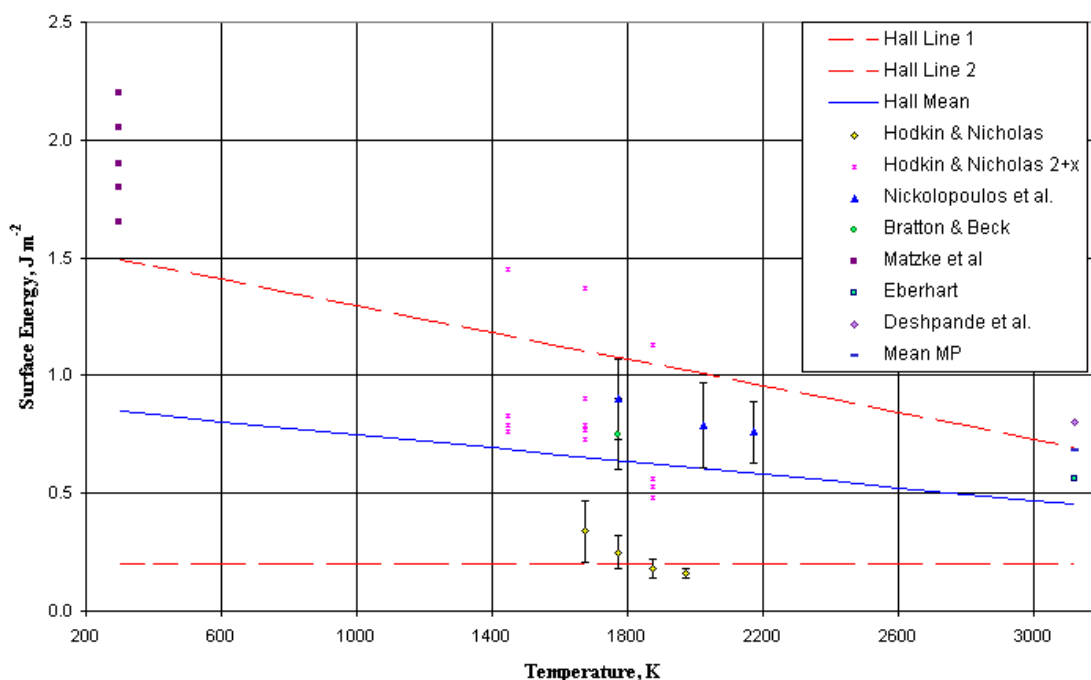


FIG. 1. Comparison of published data on surface energy of solid  $\text{UO}_2$ .

Hall et al. [1] analysed the various individual parameters that go into the calculations for the surface energies and tried to estimate best values of each. This analysis has the effect of smoothing out each parameter. Figure 2 shows the surface energies published by Hodkin and Nicholas, Nikolopoulos et al., Bratton and Beck, and Matzke et al., and the recalculated values obtained by Hall et al. Note that this re-analysis by Hall et al. has reversed the slope of the data of Nikolopoulos et al. and increased the magnitude of the slope of the data by Hodkin and Nicholas. Hall et al. stated that indentation results tend to be high because there is often plastic deformation rather than the elastic behavior assumed in the model. Indentation measurements on  $\text{ThO}_2$  showed that the surface energy was reduced by 35% if the sample had been preheated so that the oxygen becomes mobile [17]. Assuming a similar effect in  $\text{UO}_2$  would reduce the surface energy from  $1.8 \pm 0.3 \text{ J m}^{-2}$  to  $1.2 \pm 0.3 \text{ J m}^{-2}$ , in their re-analysis, Hall et al. applied this correction to the indentation data, as shown in Figure 2.

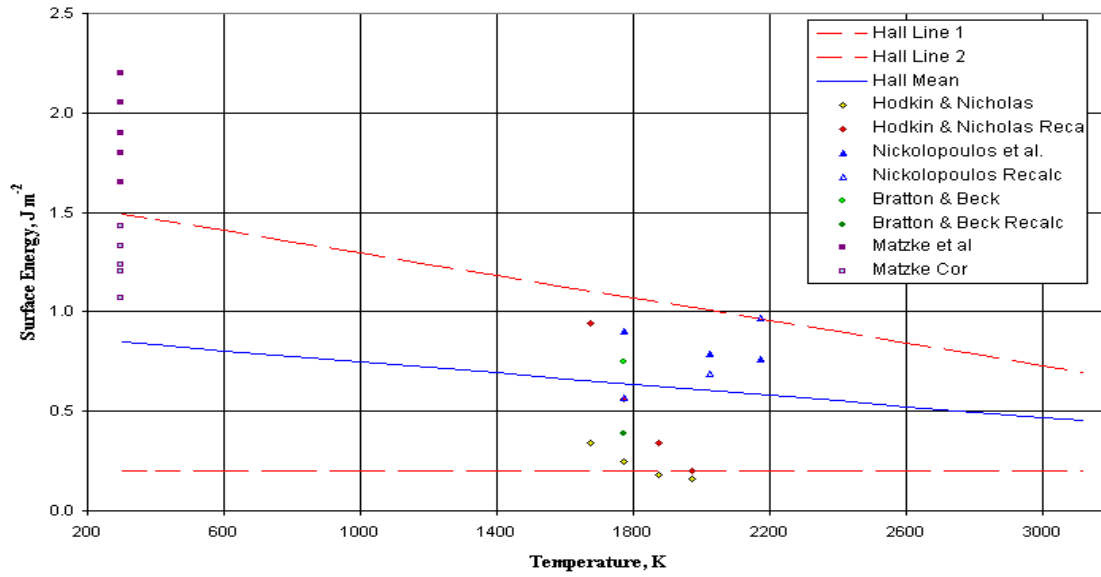


FIG. 2. Corrections by Hall et al. to  $\text{UO}_2$  surface energy data.

The re-analysed data given by Hall et al. with estimated error bars are shown in Figure 3. They commented that the mean value they assumed for the surface energy at the melting point could be in considerable error and the room temperature surface energy for stoichiometric  $\text{UO}_2$  is very dependent on the assumed 35% correction for relaxation. They stated that their analysis supports the conclusion made by Fink et al. [8] that, in view of the scatter in the measurements, there is no clear indication of the temperature dependence within the solid phase. However, their analysis indicates that the surface energy of  $\text{UO}_{2.00}$  is likely to lie in a wedge defined by the two lines given in Eq. (2) and Eq. (3) and shown as dashed lines in Figure 3. Since some of the data, both before and after re-analysis, lie outside this wedge, this recommendation has been made with great reserve. The best values would be expected to lie in the band between these two lines. The mean line in this band is given by Eq. (4) and is shown as a solid line in Figure 3.

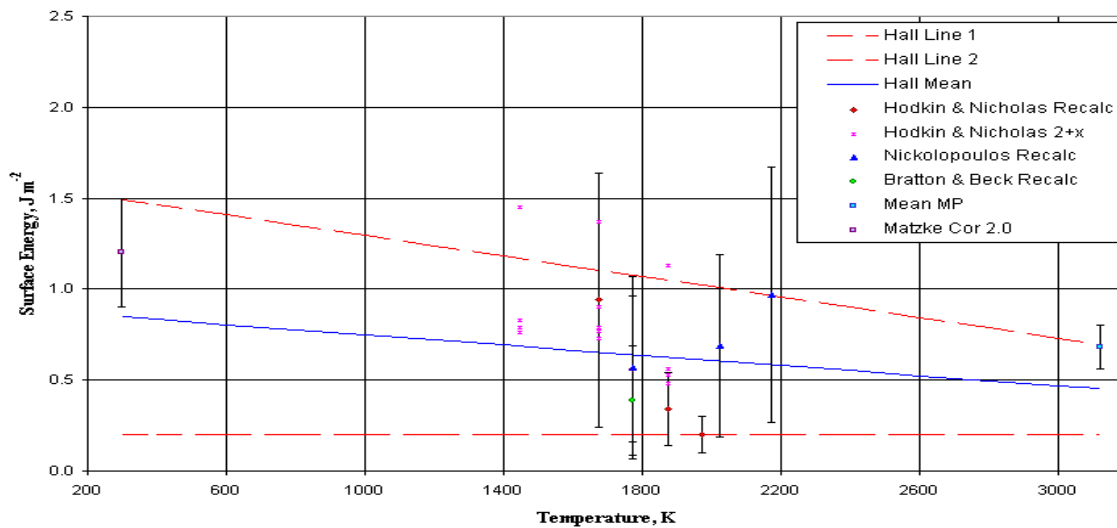


FIG. 3. Surface energy of solid  $\text{UO}_2$  of Hall et al. and corrected data.

Hall et al. also assessed the available data on the variation of surface energy with stoichiometry to obtain Eq. (5). For  $x > 0.05$ , the dependence is more pronounced than given by Eq. (5).

The ratio of the grain boundary energy to surface energy on the free surface is a function of the grain boundary groove angle only and is therefore better known than the grain boundary energy. Hall et al. define this ratio as:

$$\frac{\gamma_{GB}}{\gamma_{SV}} = 0.58 \pm 0.05 \quad (7)$$

where  $\gamma_{GB}$  is the grain boundary energy and  $\gamma_{SV}$  is the surface energy. This relation is assumed by Hall et al. to be correct over the entire temperature range of solid  $UO_2$ . Because the error in the surface energy is so large,  $\pm 70\%$ , the uncertainty in the grain boundary energy calculated from this relation is also large.

Hall et al. discussed pore geometry and defined an empirical surface energy of pores,  $\gamma_P$ , which they related to the grain boundary surface energy  $\gamma_{GB}$  by

$$\frac{\gamma_{GB}}{\gamma_P} = 1.40 \pm 0.02 \quad (8)$$

Substitution of Eq. (7) into Eq. (8) gives the relation of the surface energy of pores and the surface energy of  $UO_2$  given in Eq. (6).

Further experimental measurements are needed to determine more accurate values of these quantities. To reduce the uncertainty in the surface tension of liquid  $UO_2$ , measurements are needed under controlled conditions. To obtain better data for the solid surface energy using the multi-phase equilibration technique, methods must be developed for greater accuracy in the measurements of the angles, which now have errors on the order of  $3^\circ$ . Surface energy values accurate to  $\pm 10\%$  require that the dihedral angle must be reproducible to  $0.05^\circ$ .

#### REFERENCES TO SECTION 6.1.1.11

- [1] HALL, R.O.A., MORTIMER, M.J. and MORTIMER, D.A., Surface Energy Measurements on  $UO_2$ , - A Critical Review, J. Nucl. Mater. 148, 237-256 (1987); see also A. Critical Review of the Surface Energy of  $UO_2$ , J. Less-Common Metals 121, 341-345 (1986); and R. O. A. Hall and M. J. Mortimer, Effect of Changes in Stoichiometry on the Surface Energy of  $UO_2$ , J. Nucl. Mater. 137, 77-85 (1985).
- [2] SCHINS, H., On the Surface Tension of Liquid  $UO_2$ , J. Nucl. Mater. 78, 215-216 (1978).
- [3] CHRISTENSEN, J.A., Battelle-Northwest Laboratory Report, Richland, WA, BNWL-SA-588884-A (1966).
- [4] BATES, J.L., MCNEILLY, C.E. and RASMUSSEN, J.J., Material Science Research 5, 11 (1971); see also Battelle-Northwest Laboratory Report BNWL-SA-3579 (1970).
- [5] NIKOLOPOULOS, O. and SCHULZ, B., Density, Thermal Expansion of Stainless Steel and Interfacial Properties of  $UO_2$  - Stainless Steel Above 1690 K, J. Nucl. Mater. 82, 172-178 (1979).
- [6] CHASANOV, M.G., LEIBOWITZ, L. and GABELNICK, S.D., J. Nucl. Mater. 49, 129 (1974).
- [7] R. FURTH, Proc. Cambr. Phil. Soc. 37, 252 (1941) as referenced by O. Nikolopoulos and B. Schulz, J. Nucl. Mater. 82, 172-178 (1979).
- [8] FINK, J.K., CHASANOV, M.G. and LEIBOWITZ, L., Thermodynamic Properties of Uranium Dioxide, Argonne National Laboratory Report ANL-CEN-RSD-80-3 (1981).
- [9] HARDING, J.H., MARTIN, D.G. and POTTER, P.E., Thermophysical and Thermochemical Properties of Fast Reactor Materials, Commission of the European Communities Report EUR 12402 EN (1989).
- [10] HODKIN, E.N. and NICHOLAS, M.G., The Surface and Interfacial Energies of Stoichiometric Uranium Dioxide, J. Nucl. Mater. 47, 23 (1973).



- [11] NIKOLOPOULOS, P., NAZARE, S. and THUMMLER, F., Surface Grain Boundary and Interfacial Energies in  $\text{UO}_2$  and  $\text{UO}_2\text{-Ni}$ , J. Nucl. Mater. 71, 89-94 (1977); see also Comments on “Surface Grain Boundary and Interfacial Energies in  $\text{UO}_2$  and  $\text{UO}_2\text{-Ni}$ ,” J. Nucl. Mater. 78, 213-214 (1978).
- [12] BRATTON, R.J. and BECK, C.W., Surface Energy of Uranium Dioxide, J. Am. Ceram. Soc. 54, 379-381 (1971).
- [13] HODKIN, E.N. and NICHOLAS, M.G., Surface and Interfacial Properties of Non-Stoichiometric Uranium Dioxide, J. Nucl. Mater. 67, 171-180 (1977); see also Comments on “Surface Grain Boundary and Interfacial Energies in  $\text{UO}_2$  and  $\text{UO}_2\text{-Ni}$ ” by P. Nikolopoulos et al., J. Nucl. Mater. 74, 178 (1978);
- [14] EBERHART, J.G., J. Nucl. Mater. 25, 103 (1968).
- [15] DESHPANDE, M.S., DESAI, P.D. and SOLOMON, A.A., High Temp. Sci. 17 303 (1984).
- [16] SKAPSKI, A.S., Acta Metall. 4 576 (1956), as referenced by R. O. A. Hall, M. J. Mortimer, and D. A. Mortimer, J. Nucl. Mater. 148, 237-256 (1987).
- [17] MATZKE, H., INOUE, T. and WARREN, R., The Surface Energy of  $\text{UO}_2$  as Determined by Hertzian Indentation, J. Nucl. Mater. 91, 205-220 (1980).
- [18] MATZKE, H., J. Mater. Sci. 15, 739 (1980).
- [19] MATZKE, H., The Fracture Surface energy of  $(\text{U}_{0.8}\text{Pu}_{0.2})\text{O}_2$ , J. Nucl. Mater. 113, 273-275 (1983).

#### 6.1.1.12. Melting point of $\text{UO}_2$

##### **Recommendation**

The recommended value for the melting temperature of  $\text{UO}_{2.00}$  is:

$$T_m = 3120 \pm 30 \text{ K (IPITS-68 scale)}$$

This value has been recommended by Rand et al. [1] from their analysis of fourteen experimental studies (over a period of 20 years) of the melting temperature of  $\text{UO}_2$ . This recommendation of Rand et al. was accepted by international agreement and was recommended in our assessment of  $\text{UO}_2$  properties in 1981 [2, 3], and by Harding, Martin, and Potter [4] in their 1989 review of material properties for fast reactor safety.

##### **Discussion of recommendation and effects of burnup**

In their review of experimental measurements on the melting of  $\text{UO}_2$ , Rand et al. noted that the range in the values for the melting temperature decreased with time. Measurements prior to 1965 were reviewed by Hausner [5]. Measurements since 1965 include measurements by Latta and Fryxell [6], Lyon and Bailly [7], and Bates [8]. Measurements have been made using a ‘V’-filament method and by thermal arrest methods. The latter method is more reliable since the sample is encapsulated and vaporization is not a problem. Of the thermal arrest data, those of Latta and Fryxell appear to be the best. Their value,  $3138 \pm 15 \text{ K}$ , agrees within experimental errors with the value reported by Lyon and Bailly,  $3113 \pm 20 \text{ K}$ .

In their 1985 review of experimental data on the melting of irradiated oxide fuels, Adamson et al. [9] comment that the ‘V’-filament method appears to give consistently low melting temperatures when applied to variable-stoichiometry oxides such as  $\text{UO}_{2+x}$  and  $(\text{U,Pu})\text{O}_{2+x}$ . They attribute the low melting (solidus) temperatures obtained with the ‘V’-filament technique, which use small uncontained samples, to pronounced compositional changes that arise from rapid incongruent vaporization and oxygen exchange with the supporting atmosphere (Ar or He) and/or tungsten support. The compositional changes cause changes in the surface emissivity, which lead to measurement errors. Adamson et al. [9] comment that measurements made by Bates [8] and by Christensen [10, 11] on unirradiated samples of stoichiometric  $\text{UO}_2$  gave melting temperatures in the range of 3063-3073 K, which are approximately 50 K lower than its true melting point. The measurements of Bates [8] and Christensen [10, 11] on irradiated  $\text{UO}_2$  gave solidus temperature changes from zero to +130 K for low burnup ( $\leq 1\%$ ) and - 120 K for high burnup (6 to 11%). These data were rejected by Adamson et al. in their assessment because of the unreliability of the ‘V’-filament measurements. Adamson et al. conclude that the effect of burnup on the melting behavior is not large. They developed a model for

mixed oxide fuel that predicts variations in the solidus as a function of burnup. For burnups up to 10%, the solidus of ( $U_{0.75}Pu_{0.25}O_2$ ) is reduced by 22 K [9].

In recent experimental measurements of the heat capacity of liquid  $UO_2$  using laser heating of a 0.5 to 0.8 mm diameter  $UO_2$  sphere, Ronchi et al. [12] made several measurements of the freezing temperature of  $UO_2$  on different samples. For specimens in an inert gas atmosphere with up to 0.1-bar of oxygen, they obtained melting points in the interval  $3070 \pm 20$  K. Higher melting temperatures ( $3140 \pm 20$  K) were obtained for samples in an inert gas atmosphere without oxygen. The variation in melting temperature is in accord with the expected lower oxygen to uranium (O/U) ratio in the latter samples. The O/U ratio of the samples used in these experiments was not determined but the experimenters cannot exclude a slight oxidation up to O/U = 2.03.

The melting point of  $UO_2$  given in MATPRO [13] is 3113.15 K. This temperature is based on measurements by Brassfield et al. [14] and the equations for the solidus and liquidus boundaries of the  $UO_2$ - $PuO_2$  phase diagram given by Lyon and Bailly [7]. Properties in the MATPRO library are used in the SCDAP/RELAP5 code.

### **Uncertainties**

The uncertainty in the recommended temperature of  $UO_2$  is  $\pm 1\%$  ( $1\sigma$ ). The experimental results of Latta and Fryxell [6] and of Lyon and Bailey [7] are well within this uncertainty.

### **REFERENCES TO SECTION 6.1.1.12**

- [1] FINK, J.K., CHASANOV, M.G. and LEIBOWITZ, L., *Properties for Reactor Safety Analysis*, ANL-CEN-RSD-80-3, Argonne National Laboratory Report (1981).
- [2] FINK, J.K., CHASANOV, M.G. and LEIBOWITZ, L., Thermophysical Properties of Uranium Dioxide, *J. Nucl. Mater.* 102 17-25 (1981).
- [3] RAND, M.H., ACKERMANN, R.J., GRONVOLD, F., OETTING, F.L., PATTORET, A., *Rev. Int. Des Hautes Temperatures et des Refractories* 15, 355 (1978).
- [4] HARDING, J.H., MARTIN, D.G. and POTTER, P.E., Thermophysical and Thermochemical Properties of Fast Reactor Materials," Commission of European Communities Report EUR 12402 (1989).
- [5] HAUSNER, A., *J. Nucl. Mater.* 15, 179 (1965).
- [6] LATTA, R.E. and FRYXELL, R.E., *J. Nucl. Mater.* 35, 195 (1970).
- [7] LYON, W.L. and BAILEY, W.E., The Solid-Liquid Phase Diagram for the  $UO_2$ - $PuO_2$  System, *J. Nucl. Mater.* 22, 332 (1967).
- [8] BATES, J.L., *J. Nucl. Mater.* 36, 234 (1970).
- [9] ADAMSON, M.G., AITKEN, E.A. and CAPUTI, R.W., Experimental and Thermodynamic Evaluation of the Melting Behavior of Irradiated Oxide Fuels, *J. Nucl. Mater.* **130**, 349-365 (1985).
- [10] CHRISTENSEN, J.A., ALLIO, R.J. and BIANCHERIA, A., *Trans. American Nuclear Society* 7, 390 (1964); also United States Report WCAP-6065 (1965).
- [11] CHRISTENSEN, J.A., Irradiation Effects on Uranium Dioxide Melting, United States Report HW-69234 (1964).
- [12] RONCHI, C., HIERNAUT, J.P., SELFSLAG, R. and HYLAND, G.J., Laboratory Measurement of the Heat Capacity of Urania up to 8000 K: I. Experiment, *Nuclear Science and Engineering* 113, 1-19 (1993).
- [13] HOHORST, J.K. (Ed.), SCDAP/RELAP5/MOD2 Code Manual, Vol 4: MATPRO- A Library of Materials Properties for Light Water-Reactor Accident Analysis, Section 2.1 Melting Temperature, NUREG/CR-5273 (1990).
- [14] BRASSFIELD, H.C. et al., Recommended Property and Reactor Kinetics Data for Use in Evaluating a Light Water Coolant Reactor Loss-of-Coolant Incident Involving Zircaloy-4 or 304-SS-Clad  $UO_2$ , GEMP-482 (April 1968).

### 6.1.1.13. Viscosity of liquid $UO_2$

#### Summary and recommendation

Viscosities of liquid uranium dioxide were measured in the temperature range of 3143 to 3303 K by Woodley [1], at the melting point (3120 K) by Palinski [2], and from 3083 to 3328 K by Tsai and Olander [3]. The recommended equation is that of Woodley because of the greater precision of his data and the agreement between Woodley and Palinski. The Woodley equation is:

$$\eta = 0.988 \exp\left(\frac{4620}{T}\right) \quad (1)$$

where the kinematic viscosity,  $\eta$ , is in centipoise (mPa.s) and T is in K. Recommended values are given in Table 1 as a function of temperature and graphed in Figure 1. The data of Woodley [1], Palinski [2], and Tsai and Olander [3] as well as estimated uncertainties have been included in Figure 1.

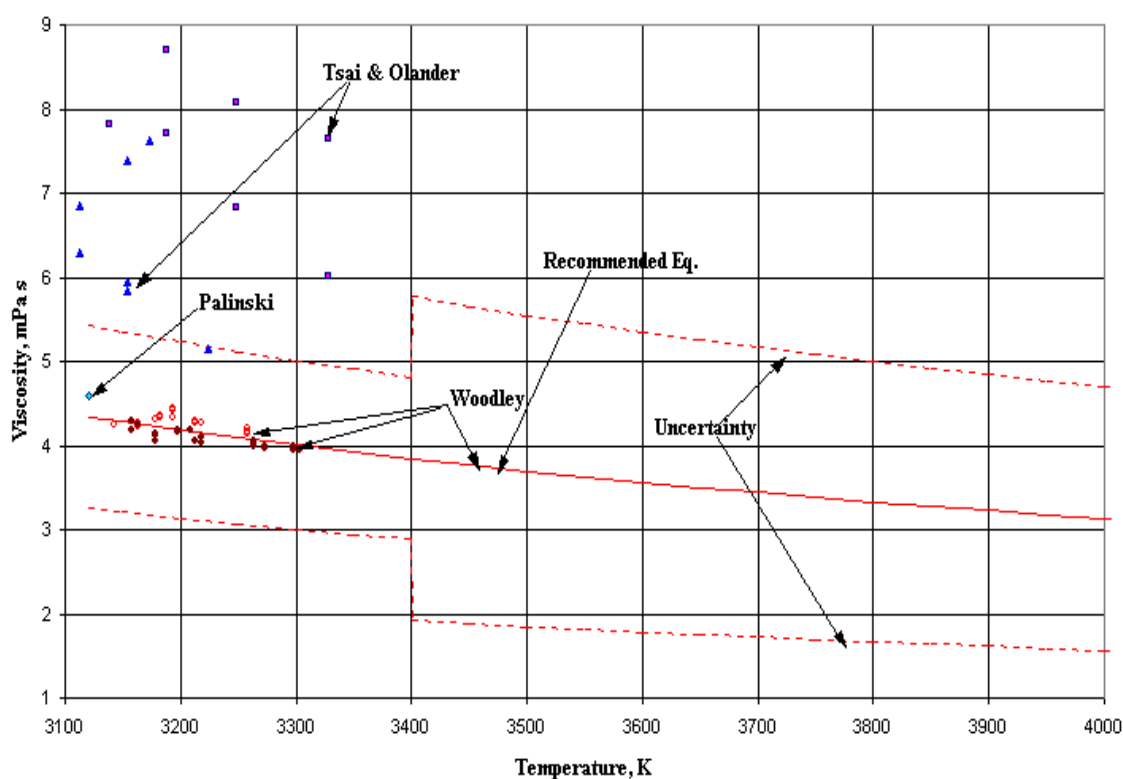


FIG. 1. Viscosity of liquid  $UO_2$ .

#### Uncertainties

The uncertainty in the available data is difficult to estimate because of the lack of high-temperature viscosity standards. For the temperature range of 3120 to 3400 K, the error is estimated as  $\pm 25\%$ . The uncertainty of extrapolated viscosities in the temperature range of 3400 to 4000 K is estimated as  $\pm 50\%$ .

Table 1. Viscosity of liquid uranium dioxide

TEMPERATURE, K	VISCOSITY, mPa.s
3120	4.34
3150	4.28
3200	4.19
3250	4.09
3300	4.01
3350	3.92
3400	3.84
3450	3.77
3500	3.70
3550	3.63
3600	3.57
3650	3.50
3700	3.44
3750	3.39
3800	3.33
3850	3.28
3900	3.23
3950	3.18
4000	3.14

### Discussion

Figure 2 shows the viscosity data of Woodley [1], Tsai and Olander [3], and Palinski [2]. Tsai and Olander made measurements on two different samples. Their viscosities are higher than the values of Woodley and of Palinski and lack the precision of the data of Woodley. In addition, the Tsai and Olander data for the second sample are consistently higher than for the first sample, indicating a possible systematic error. Tsai and Olander gave the melting point of  $\text{UO}_2$  as 3073 K (not 3120 K) so that their lowest temperature datum, 9.2 cP (mPa.s) at 3083 K, is at a temperature that they consider to be completely liquid. They comment that their low melting point may be due to temperature measurement errors, change in stoichiometry of their samples, or contamination of their melt by the tungsten crucible. Figure 1 shows that Woodley's two series of measurements on the same encapsulated sample are in good agreement and in reasonable agreement with the datum of Palinski. The viscosity of  $\text{UO}_{2.003}$  at the melting point measured by Palinski [2] is 4.6 cP (4.6 mPa s) which is within 7% of the value (4.3 cP) obtained with Eq. (1), given by Woodley. Thus, the equation based on the Woodley data is preferred. This equation has also been recommended in the assessment by Harding, Martin, and Potter [4].

The viscosity of  $\text{UO}_2$  was also measured by Nelson et al. [5] at 3028 K and at 3068 K, which they believed was just above the melting point. Their viscosity values at these temperatures are 46 cP and 36 cP, respectively, which are about a factor of 10 above the viscosity at 3120 K calculated with Eq. (1). The temperatures and viscosities obtained by Nelson et al. [4] suggest that these measurements were made below the melting point of  $\text{UO}_2$ . Thus, these data have not been included in this analysis.

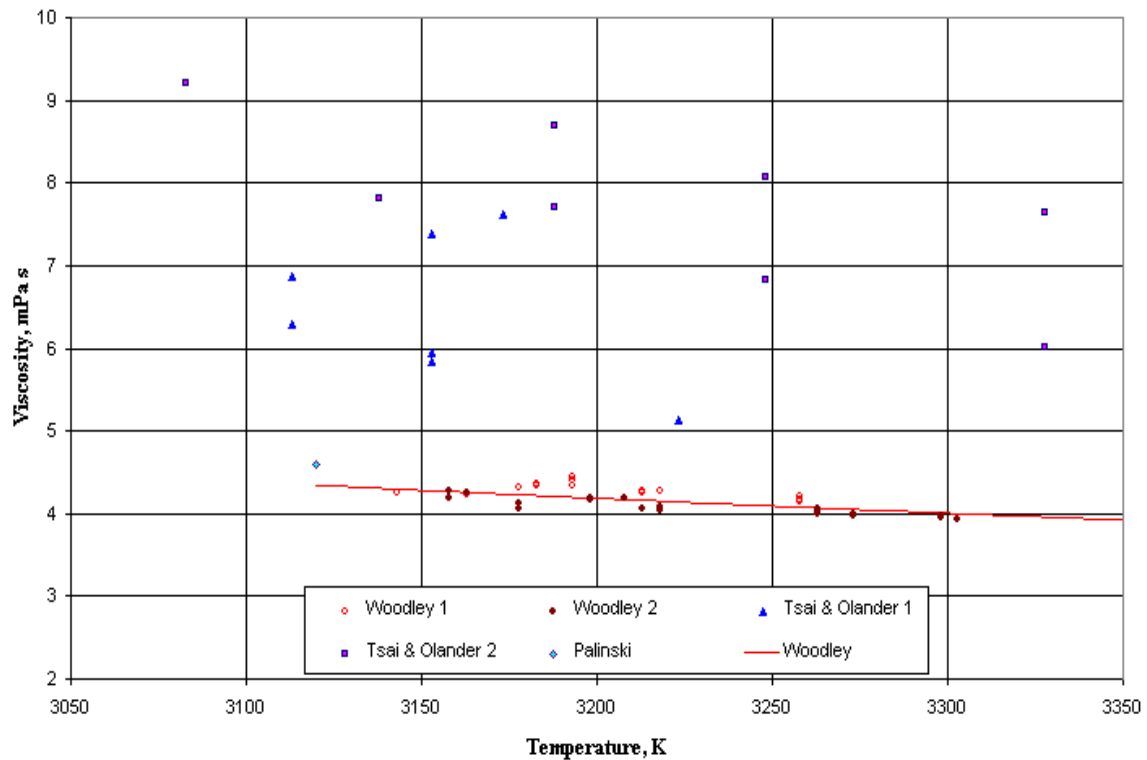


FIG. 2. Viscosity of liquid  $UO_2$ .

#### REFERENCES TO SECTION 6.1.1.13

- [1] WOODLEY, R.E., The Viscosity of Molten Uranium Dioxide, J. Nucl. Mater. 50, 103-106 (1974).
- [2] PALINSKI, R., Core Melts - Measurement of Some Thermophysical Properties of Liquid Reactor Materials at High Temperatures, Commission of European Communities Joint Research Centre, Ispra Establishment, Italy Report EUR 7002 EN (1980).
- [3] TSAI, H.C. and OLANDER, D.R., The Viscosity of Molten Uranium Dioxide, J. Nucl. Mater. 44, 83-86 (1972).
- [4] HARDING, J.H., MARTIN, D.G. and POTTER, P.E., Thermophysical and Thermochemical Properties of Fast Reactor Materials, Commission of the European Communities Report EUR 12402 EN (1989).
- [5] NELSON, R.P., RASMUSSEN, J.J. and SLAGLE, O.D., Properties of Molten Fast-Reactor Oxide Fuels, pp. 2-4 to 2.26 of Battelle-Northwest Laboratory Report BNWL-1279 (February 1970); this study is also briefly described by J.L. Bates, C.E. McNeilly and J.J. Rasmussen, Materials Research 5, 11 (1971).

#### 6.1.1.14. Vapor pressure of $\text{UO}_2$

##### **Summary of recommendations**

###### *Vapor pressure over liquid $\text{UO}_2$*

The recommended equation for the total vapor pressure over liquid  $\text{UO}_2$  from the melting point to 8000 K is the equation derived by Breitung and Reil [1] from their in-pile equation-of-state measurements, and their review of the experimental data. Their equation for the logarithm of the saturated vapor pressure over liquid  $\text{UO}_2$  is:

$$\log_{10} P = 15.961 - \frac{26974}{T} - 2.7600 \log_{10} T \quad (1)$$

where the pressure is in MPa and the temperature is in K. Vapor pressures determined from this equation are given as a function of temperature in Table 1 and shown with estimated uncertainties in Figure 1. This equation gives a boiling point of 3815.1 K.

###### *Vapor pressure over solid $\text{UO}_2$*

The recommended equation for the vapor pressure of  $\text{UO}_2(\text{g})$  over solid  $\text{UO}_2$  is based on measurements by Ackermann, Rauh, and Rand [2] of the pressure of  $\text{UO}_2(\text{g})$  over  $\text{UO}_2$  in the temperature range from 1800 to 2600 K. Their equation for the logarithm of the vapor pressure of  $\text{UO}_2(\text{g})$  is:

$$\log_{10} P = 66.53672 + 4.382 \times 10^{-3} T - 4.411 \times 10^{-7} T^2 - \frac{37090}{T} - 19.070 \log_{10} T \quad (2)$$

where the vapor pressure,  $P$ , is in MPa and the temperature,  $T$ , is in K. Ackermann, Rauh, and Rand stated that in the temperature range of their measurements,  $\text{UO}_2(\text{g})$  comprises approximately 94% of the total vapor pressure over solid  $\text{UO}_2$ . Therefore, below 2600 K, this equation gives a reasonable estimate of the total vapor pressure over solid  $\text{UO}_2$ . Because contributions to the total vapor pressure from other species become significant with increasing temperature [3], this equation does not give a good estimate of the total vapor pressure over solid  $\text{UO}_2$  near the melting point, 3120 K. The equation of Tetenbaum and Hunt [4] is recommended for the total vapor pressure over solid  $\text{UO}_2$  at temperatures above 2600 K. Tetenbaum and Hunt [4] measured the total vapor pressure over uranium dioxide as a function of stoichiometry. Their equation for the total vapor pressure over  $\text{UO}_2(\text{s})$  is:

$$\log_{10} P = -\frac{31284}{T} + 7.616 \quad (3)$$

The vapor pressure of  $\text{UO}_2(\text{g})$  calculated using the equation of Ackermann et al. [2] and the total vapor pressure over  $\text{UO}_2(\text{s})$  calculated using the equation of Tetenbaum and Hunt [4] are tabulated as a function of temperature in Table 2 and shown with estimated uncertainties in Figure 2.

##### **Uncertainties**

The estimated uncertainties in total vapor pressure over liquid  $\text{UO}_2$  calculated from Eq. (1) range from -40%/+60% at 3120 K to -45%/+80% at 6000 K. From 3120 to 6000 K, the negative uncertainties are assumed to decrease linearly:

$$\Delta P/P \text{ (\%)} = -[34.58 + 1.7 \times 10^{-3} T]$$

The positive uncertainties are assumed to increase linearly from +60% at 3120 K to +80% at 4500 K:

$$\Delta P/P \text{ (\%)} = 14.78 + 0.0145 T$$

Above 4500 K, the positive uncertainties are assumed constant (+80%). The uncertainties in the pressure of  $\text{UO}_2(\text{g})$  over solid  $\text{UO}_2$  calculated from Eq. (2) and in the total vapor pressure over solid  $\text{UO}_2$  calculated using Eq. (3) are estimated as -40%/+60% from 1700 to 3120 K.

Table 1. Total vapour pressure over liquid UO<sub>2</sub>

TEMPERATURE, K	PRESSURE, MPa	PRESSURE, atm
3120	0.00469	0.0463
3200	0.00720	0.0711
3300	0.0119	0.118
3400	0.0191	0.188
3500	0.0297	0.293
3600	0.0450	0.444
3700	0.0664	0.656
3800	0.0960	0.948
3900	0.136	1.34
4000	0.189	1.86
4100	0.257	2.54
4200	0.346	3.41
4300	0.457	4.51
4400	0.595	5.87
4500	0.765	7.55
4600	0.972	9.60
4700	1.22	12.1
4800	1.52	15.0
4900	1.87	18.4
5000	2.28	22.5
5100	2.75	27.1
5200	3.29	32.5
5300	3.91	38.6
5400	4.62	45.6
5500	5.41	53.4
5600	6.30	62.2
5700	7.29	71.9
5800	8.38	82.7
5900	9.58	94.6
6000	10.91	107.6

Table 2. Vapor pressures over solid  $\text{UO}_2$  calculated from equations of Ackermann et al. and of Tetenbaum and Hunt

TEMPERATURE, K	$\text{UO}_2$ PRESSURE, MPa (ACKERMANN ET AL.)	TOTAL PRESSURE, MPa (TETENBAUM & HUNT)
1800	$2.05 \times 10^{-10}$	-
1900	$1.67 \times 10^{-09}$	-
2000	$1.10 \times 10^{-08}$	$9.42 \times 10^{-09}$
2100	$5.98 \times 10^{-08}$	$5.23 \times 10^{-08}$
2200	$2.77 \times 10^{-07}$	$2.49 \times 10^{-07}$
2300	$1.12 \times 10^{-06}$	$1.03 \times 10^{-06}$
2400	$3.96 \times 10^{-06}$	$3.81 \times 10^{-06}$
2500	$1.26 \times 10^{-05}$	$1.27 \times 10^{-05}$
2600	$3.62 \times 10^{-05}$	$3.83 \times 10^{-05}$
2700	$9.54 \times 10^{-05}$	$1.07 \times 10^{-04}$
2800	$2.31 \times 10^{-04}$	$2.77 \times 10^{-04}$
2900	$5.22 \times 10^{-04}$	$6.74 \times 10^{-04}$
3000	$1.10 \times 10^{-03}$	$1.54 \times 10^{-03}$
3100	$2.17 \times 10^{-03}$	$3.34 \times 10^{-03}$



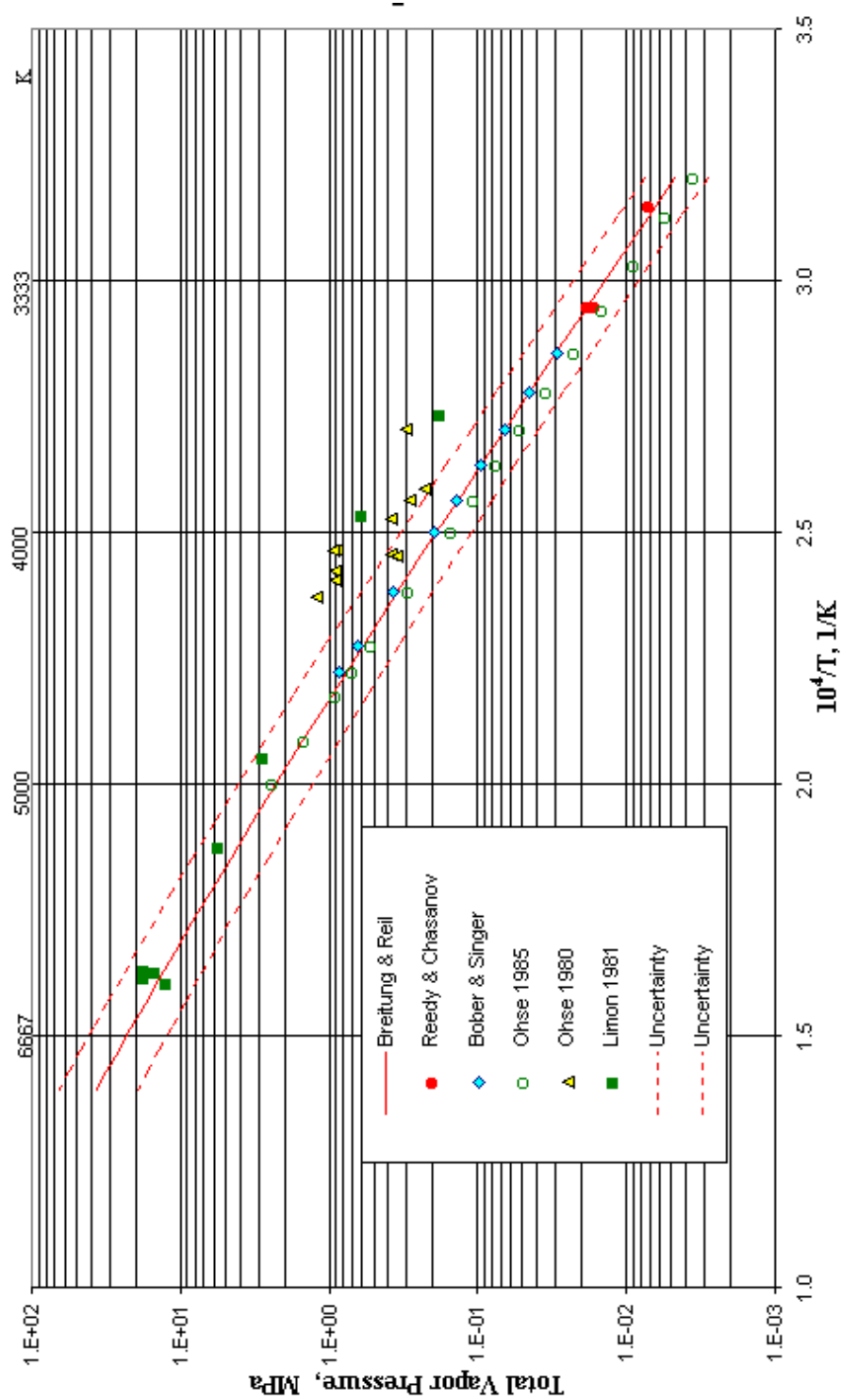


FIG. 1. Total vapor pressure over liquid  $\text{UO}_2$ .

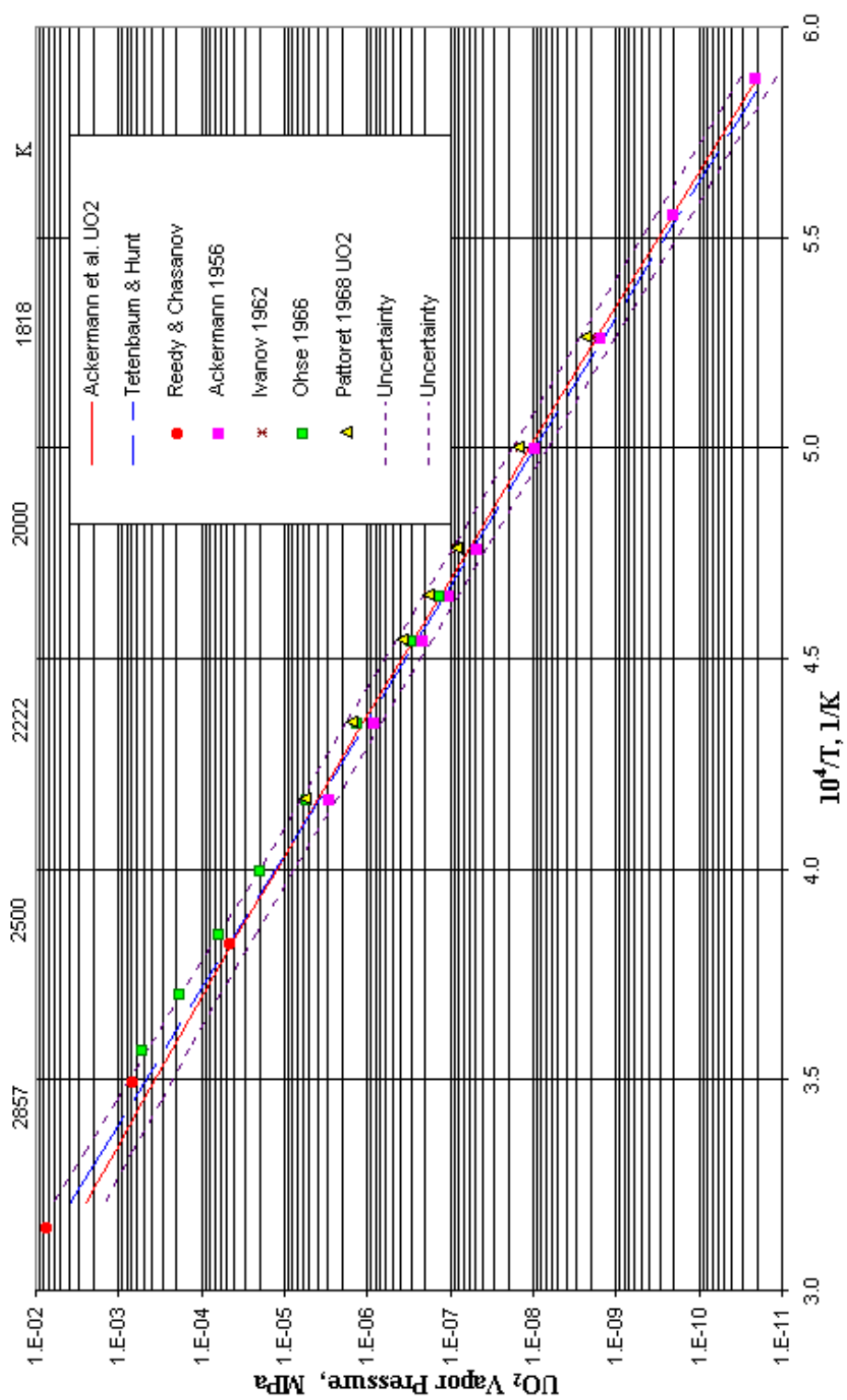


FIG. 2. Vapor pressure over solid  $\text{UO}_2$

## Discussion

### Stoichiometry

Uranium dioxide can exist over a wide range of compositions (hypostoichiometric to hyperstoichiometric with respect to oxygen), which are temperature dependent. The total vapor pressure depends on the oxygen-to-uranium ratio of the condensed phase, so that the total vapor pressure over  $\text{UO}_{2\pm x}$  will depend on the value of  $x$ . The vaporization of  $\text{UO}_2$  is not congruent because the O:U ratio in the gas phase is greater than in the condensed phase. The total vapor pressure above solid and liquid  $\text{UO}_2$  includes contributions from  $\text{UO}_2(\text{g})$ ,  $\text{UO}(\text{g})$ ,  $\text{UO}_3(\text{g})$ ,  $\text{U}(\text{g})$ ,  $\text{O}(\text{g})$ , and  $\text{UO}(\text{g})$ .

### Vapor pressure over liquid $\text{UO}_2$

Breitung and Reil [1] recently reviewed the experimental measurements of the total vapor pressure of liquid  $\text{UO}_2$ . The data used in their assessment are summarized in Table 3. They included both pressure-temperature measurements and pressure-enthalpy measurements in their assessment.

Table 3. Vapor pressure measurements over liquid  $\text{UO}_2$

EXPERIMENTER	METHOD	YEAR	REFERENCE
	OUT-OF-PILE EXPERIMENTS		
Reedy & Chasanov	Transpiration	1972	5
Bober et al.	Laser-heating, expansion into vacuum	1975 1976	6,7
Ohse et al.	Laser-heating, vacuum	1975 1977	8, 9
Tsai et al.	Laser-heating, vacuum	1976	10
Bober, Breitung, & Karow	Laser-heating, vaporization	1978	11
Ohse et al.	Laser-heating, evaporation	1980	12
Ohse et al.	Laser-heating, evaporation	1985	13
Bober & Trapp	Laser-heating in xenon	1984	14
Bober & Singer	Laser-heating in xenon, Boiling point method	1987	15
	IN-PILE EXPERIMENTS		
Reil	Adiabatic enthalpy vs pressure	1977	16
Benson	Isobaric expansion	1977	17
Limon et al.	$\text{UO}_2$ Fission-heated in argon	1981	18
Wright et al.	In-pile fuel disruptive exp'ts	1983	19
Breitung & Reil	Effective equation of state technique	1985- 1989	1

### Pressure-temperature measurements

The transpiration measurements of Reedy and Chasanov [5] were weighted high in the assessment of Breitung and Reil [1] for the following reasons: (1) they are the only measurements on both solid and liquid  $\text{UO}_2$ , (2) the technique produces true equilibrium data, and (3) the experimental uncertainties are very small ( $\pm 10\%$  in pressure;  $\pm 1\%$  in temperature). In these experiments, the  $\text{UO}_2$  was contained

in tungsten, which limited the temperature range (2615 - 3390 K). At 2615 and 2860 K, the O:U ratio of the condensed phase was 1.98. At 3390 K, the O:U ratio of the liquid was 1.94.

The laser-heated vapor pressure measurements listed in Table 3 may be divided into two groups: (1) measurements performed far from thermodynamic equilibrium [6–13] and (2) measurements close to thermodynamic equilibrium [14, 15]. Measurements far from thermodynamic equilibrium consist of experiments in which the fuel vapor expands into a vacuum or a rare gas environment. Such experiments require a theoretical model to convert properties of the expanding nonequilibrium plasma into saturation vapor pressures. The large scatter in the data from different experiments of this type is indicative of the difficulty of obtaining saturation vapor pressure data from these nonequilibrium measurements. Measurements close to equilibrium use a boiling point technique that determines the temperature at which a laser-generated  $\text{UO}_2$  vapor cloud begins to expand against a xenon cover gas of a given pressure. At this temperature, the  $\text{UO}_2$  vapor pressure is assumed to be equal to the gas pressure. The xenon gas atoms initially confine the laser-generated vapor cloud so that evaporation proceeds close to thermodynamic equilibrium. The recent boiling-point experiments by Bober and Singer [15] included corrections for optical absorption (by the vapor cloud) of thermal radiation emitted from the liquid surface. Breitung and Reil concluded that the recent measurements by Bober and Singer are the most reliable saturation vapor pressure data for liquid  $\text{UO}_2$  from the laser experiments.

#### *In-reactor experiments*

The first in-reactor measurements of vapor pressure as a function of adiabatic fuel enthalpy by Reil [16] determined upper and lower bounds for the vapor pressure. Later calculations showed that these values were overly conservative [1]. Benson [17] measured the isobaric expansion of a 25- $\mu\text{m}$ -thick layer of  $\text{UO}_2$  powder confined by two movable pistons as it was heated to a certain internal energy in one microsecond. Results of this experiment were inconsistent with the expansion of a single-component liquid-vapor system. An unknown source of pressure, such as water vapor, adsorbed by the fine  $\text{UO}_2$  powder is believed to have contributed to the measured pressure. Fission heating was used in the eight Commissariat à l'Energie Atomique (CEA) experiments by Limon et al. [18] to heat a thin solid  $\text{UO}_2$  disk to boiling under constant argon pressure. The boiling point was determined by the sudden increase in pressure. The average energy deposited in the  $\text{UO}_2$  was assumed to be equal to the fuel enthalpy in the boiling zone. This assumption led to deviations of only a few percent in six high-enthalpy tests but the actual enthalpy in the boiling zone may have been on the order of 10% higher for the two low-enthalpy tests [1].

Breitung and Reil [1] measured the saturation vapor pressure of pure  $\text{UO}_{2.01}$ , reactor grade  $\text{UO}_{2.08}$ , and reactor grade ( $\text{U}_{0.77}\text{Pu}_{0.23}$ ) $\text{O}_{2.09}$  as a function of enthalpy for enthalpies from 2000 to 3700  $\text{kJ kg}^{-1}$ . Their six effective equation-of-state experiments at the annular core research reactor at Sandia National Laboratories determined the saturation vapor pressure as a function of enthalpy at conditions that are very close to those of the disassembly phase of a core disruptive accident. These experiments gave very reproducible results. They found that under these conditions

- (1) the fuel saturation vapor pressure for fuel containing uranium-plutonium mixed oxide was essentially identical to that of pure  $\text{UO}_2$ ;
- (2) the fuel impurities from fabrication did not noticeably contribute to the pressure;
- (3) the stoichiometry variations have no strong influence on the saturation vapor pressure for  $\text{UO}_{2.01}$ , and  $\text{UO}_{2.08}$ ; and
- (4) the replacement of uranium by plutonium in concentrations equivalent to mixed oxide fuel, e.g., ( $\text{U}_{0.77}\text{Pu}_{0.23}$ ) $\text{O}_{2.09}$ , does not significantly affect the measured vapor pressure.

From the data obtained in these six experiments, Breitung and Reil developed an equation for the vapor pressure for all three fuels:

$$\log_{10} P(z) = -9.7652 + 8.0934 \times 10^{-3} z - 2.0515 \times 10^{-6} z^2 + 1.9013 \times 10^{-10} z^3 \quad (4)$$

where  $z = h - h_{298}$  is the enthalpy increment in  $\text{kJ kg}^{-1}$  and  $P$  is the saturation pressure in MPa. This equation fits their data for all three fuel types within their experimental uncertainties of  $\pm 0.5$  MPa in

pressure and  $\pm 3\%$  in enthalpy. Breitung and Reil [1] converted their pressure-enthalpy equation to a pressure-temperature equation, Eq. (1), using Fischer's [20] theoretical prediction for the saturation pressure as a function of internal energy of liquid  $\text{UO}_2$  and the melting point enthalpy given by Fink et al. [21] (1398.6 kJ/kg). Their equation for pressure as a function of temperature, Eq. (1), is slightly different from an earlier equation given by Breitung and Reil [22, 23] (which was recommended by Harding et al. [24]) because different equations were used to convert from pressure-enthalpy to pressure-temperature. Breitung and Reil [1] stated that the main uncertainty in the conversion is the choice of equation for the heat capacity. The large variations in the available equations for the heat capacity of liquid  $\text{UO}_2$  are shown in Figure 3. The data in Figure 3 are those determined by Ronchi et al. [25] from their cooling curve experiments. In the analysis of these experiments, Ronchi et al. assumed a constant thermal conductivity of  $2.5 \text{ W m}^{-1} \text{ K}^{-1}$ . The solid line is the fit by Ronchi et al. [25] to their data. The dashed line labeled "H+Cp Fit Fink" is a combined fit to the enthalpy data [26, 27] and the heat capacity data of Ronchi et al. [25] from 3100 to 4500 K. The line labeled "Rand et al." is the constant heat capacity obtained from the linear fit by Rand et al. [28] to the enthalpy data [26, 27]. The heat capacities of Fischer [20] were preferred by Breitung and Reil to the equation they used previously (labeled "Breitung and Reil KfK 3939") because the model used by Fischer was anchored at experimental results for the vapor pressure and density of liquid  $\text{UO}_2$ . Figure 3 shows that values from both equations used by Breitung and Reil are high relative to the values given by Ronchi et al. [25]. Harding et al. [24] have pointed out that the heat capacity may be varied without significant effect on the vapor pressure at a given temperature. They stated that a 20% variation in heat capacity at 6000 K gives a 30% change in the vapor pressure.

#### *Comparison of recommended equation with data*

In Figure 4, the recommended equation of Breitung and Reil for the total vapor pressure over liquid  $\text{UO}_2$  is compared with the most recent and reliable vapor pressure data from each experimental method, with the equation formulated by the 1978 IAEA International Working Group on Fast Reactors (IWGFR) [29], and with vapor pressures calculated by Green and Leibowitz [3]. The IWGFR equation was based on a review of the data available in 1978 and was recommended for use up to 5000 K. The vapor pressures and vapor compositions above uranium dioxide calculated by Green and Leibowitz [3] are based on a statistical-mechanical calculation of the thermodynamic functions of the individual vapor species using molecular energy levels from spectroscopic data and an oxygen potential model. Experimental data included in Figure 4 are: transpiration data of Reedy and Chasanov [5], the boiling-point data of Bober and Singer [15], data from the most recent laser-heating vaporization experiments of Ohse et al. [12, 13], and data from the in-pile experiments of Limon et al. [18]. The equation recommended by Limon et al. to best describe their data has also been included. Breitung and Reil's earlier vapor pressure equation that was obtained by using a different heat capacity [22, 23] to convert their data has been included in Figure 4 to show the effect of differences in choice of heat capacity on the final vapor pressure equation. It is labeled "Breitung KfK3939." Figure 4 shows that at high temperatures, it gives lower pressures than the recommended equation of Breitung and Reil. Therefore, the recommended equation is in better agreement with the high-temperature data of Limon et al.

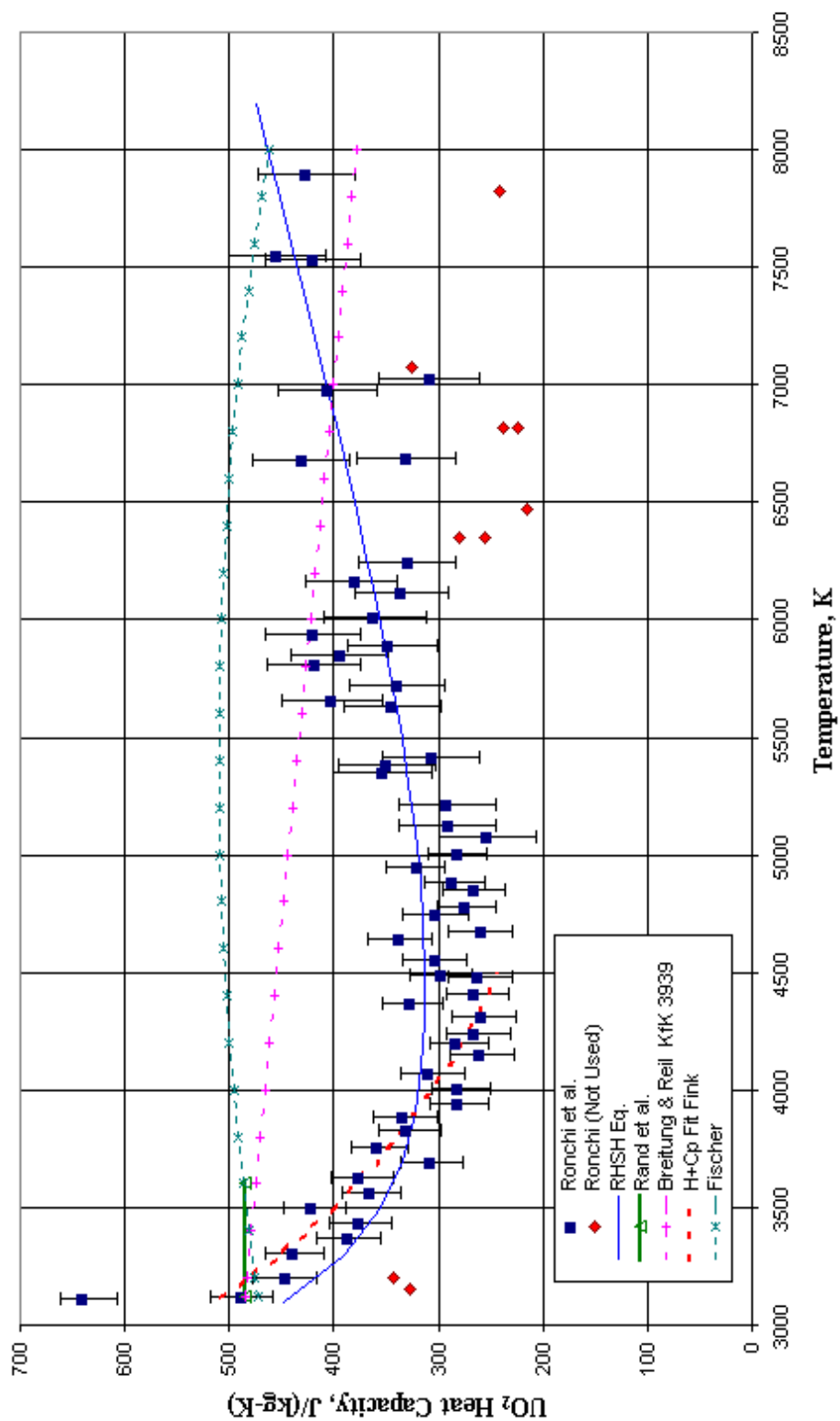


FIG. 3. Comparison of liquid UO<sub>2</sub> heat capacity data and equations.

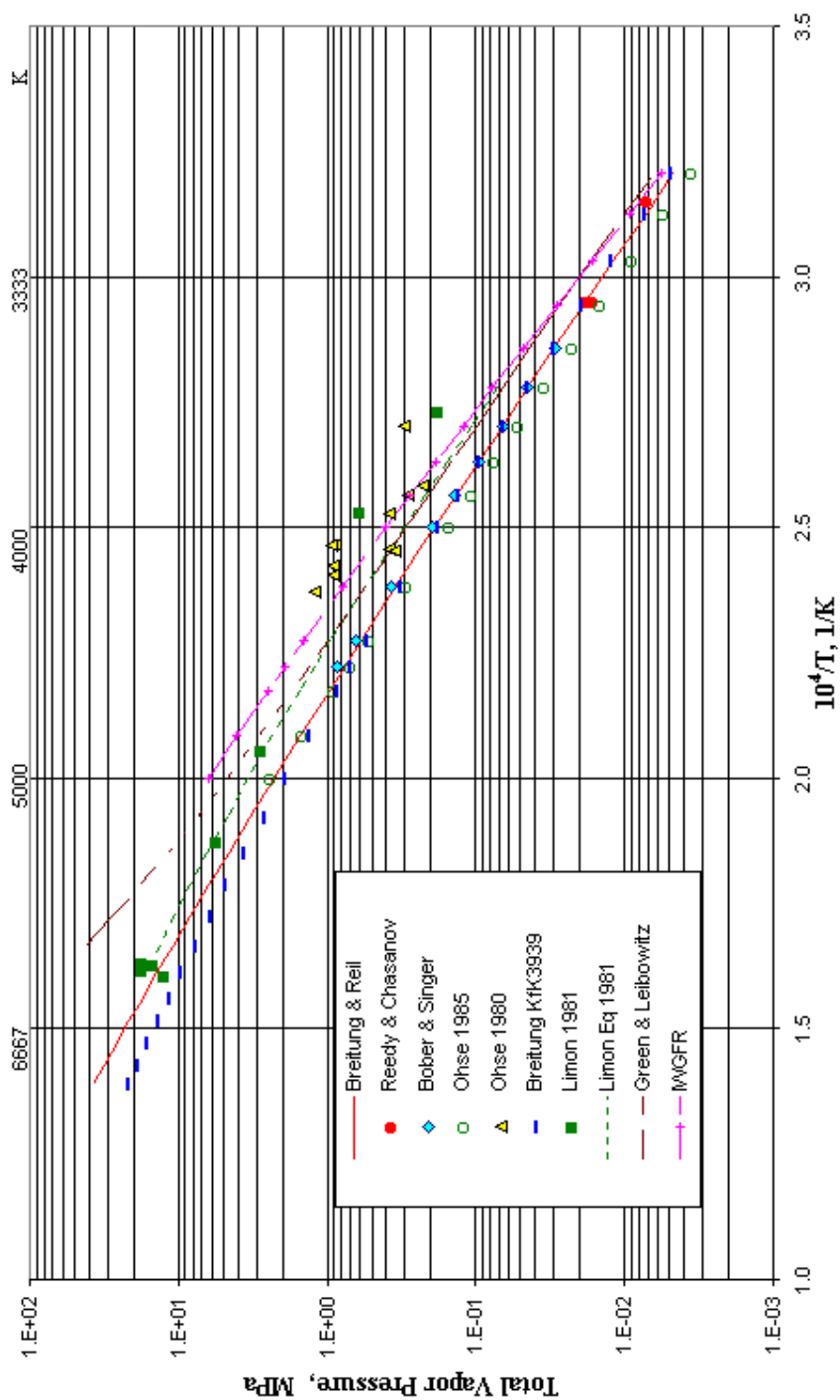


FIG. 4. Total vapor pressure over liquid  $UO_2$ .

The IWGFR equation is consistent with the total pressures calculated by Green and Leibowitz [3] and with the early laser-vaporization data, which were higher than the 1980 data of Ohse et al. [12]. The data at 4220 K from the 1980 measurements of Ohse et al. [12] is a factor of 3.3 higher than the vapor pressure at 4220 K calculated using the recommended equation of Breitung and Reil [1]. At 4000 K, vapor pressures obtained from the IWGFR equation and calculations by Green and Leibowitz [3] are, respectively, factors of 2.1 and 1.6 higher than the vapor pressure calculated with the equation of Breitung and Reil [1]. The recommended equation of Breitung and Reil is in good agreement with the vapor pressures determined from laser-vaporization experiments in 1985 by Ohse et al. [13], with the low-temperature data of Reedy and Chasanov [5], with the high-temperature data of Limon et al. [18], and with the data of Bober and Singer [15]. It is a good representation of all equilibrium in-pile and out-of-pile data.

Breitung and Reil [1] noted that if the two low-temperature CEA data points of Limon et al. [18] are disregarded, all in-pile results are located close to an almost linear extension of the transpiration data of Reedy and Chasanov [5] and the laser boiling point data of Bober and Singer [15]. All these methods provide conditions very close to equilibrium vaporization so that the slope of the line connecting these data should give the heat of vaporization. They attributed the steeper slopes obtained from the earlier laser-vaporization experiments (as characterized by the 1980 data of Ohse et al.) to the use of nonequilibrium pressure models to reduce the data and/or to the neglect of optical absorption of thermal surface radiation in the vapor cloud. Application of the Clausius -Clapeyron equation to their vapor pressure equation gives an effective heat of vaporization:

$$\Delta H_{vap} = 516382 - 22.946 T \quad (5)$$

where  $\Delta H_{vap}$  is in  $\text{J mol}^{-1}$  and  $T$  in K ranges from 3120 to 8000 K. The heat of vaporization at the normal boiling point (3815.1 K) is  $413.5 \text{ kJ mol}^{-1}$ .

#### *Vapor pressure over solid $\text{UO}_2$*

Although the total vapor pressure above solid  $\text{UO}_2$  includes contributions from  $\text{UO}_2(\text{g})$ ,  $\text{UO}(\text{g})$ ,  $\text{UO}_3(\text{g})$ ,  $\text{U}(\text{g})$ ,  $\text{O}(\text{g})$ , and  $\text{UO}(\text{g})$ , the greatest contribution is from  $\text{UO}_2(\text{g})$ . Ackermann et al. [2] measured the vapor pressure of  $\text{UO}_2(\text{g})$  above solid  $\text{UO}_2$  from 1800 to 2600 K and commented that  $\text{UO}_2(\text{g})$  comprises 94% of the total pressure at 2150 K. Tetenbaum and Hunt [4] determined the total vapor pressure above  $\text{UO}_{2-x}$  in the temperature range 2080 to 2705 K. Green and Leibowitz [3] used models for the partial Gibbs free energy of oxygen above  $\text{UO}_2$  to determine the contributions of the various vapor species above hypostoichiometric uranium dioxide for  $\text{UO}_{2.00}$  through  $\text{UO}_{1.90}$ .

Measurements of the total vapor pressure above solid  $\text{UO}_2$  by Knudson effusion [30–33], Langmuir surface evaporation [35], and transpiration [4, 36] methods and have been reviewed by Ackermann et al. [2] and compared with measurements of the vapor pressure due to  $\text{UO}_2(\text{g})$  determined from mass-spectrometric measurements by Pattoret et al. [37] and by Ackermann et al. [2]. They found reasonable agreement between the different measurements. Table 4 shows the vapor pressures at 2150 K, determined from the experiments included in the assessment by Ackermann et al. [2]. Ackermann et al. corrected the data of Alexander et al. [36] for a systematic error. Consequently, the vapor pressure attributed to Alexander et al. in Table 4 (which is from the table of Ackermann et al. [2]) differs from the value given in the original paper by Alexander et al. [36]. The average of the values, excluding the value from the 1979 mass spectroscopy measurements by Ackermann et al. [2], is  $1.38 \times 10^{-7} \text{ MPa}$ . This is in good agreement with the vapor pressure of  $\text{UO}_2(\text{g})$  ( $1.32 \times 10^{-7} \text{ MPa}$ ) determined by Ackermann et al. in 1979.



Table 4. Measurements of the vapor pressure of  $\text{UO}_2$  at 2150 K

VAPOR PRESSURE AT 2150 K, $10^7\text{MPa}$	EXPERIMENTER	YEAR	METHOD	TEMPERATURE RANGE, K
1.23	Ackermann et al. [30]	1956	mass effusion	1758 - 2378
1.94	Ivanov et al. [31]	1962	mass effusion	1930 - 2160
0.58	Voronov et al. [35]	1962	Langmuir	1723 - 2573
1.34	Ohse [32]	1966	mass effusion	2200 - 2800
0.93	Alexander et al. [36]	1967	transpiration	2090 - 2900
2.00	Gorban et al. [33]	1967	mass effusion	1873 - 2573
1.83	Pattoret et al. [37]	1968	mass spectroscopy	1890 - 2420
1.18	Tetenbaum & Hunt [4]	1970	transpiration	2080 - 2705
1.32	Ackermann et al. [2]	1979	mass spectroscopy	1813 - 2463

The recommended equation for the vapor pressure of  $\text{UO}_2(\text{g})$  over  $\text{UO}_2$ , Eq. (2), is from the 1979 measurements and assessment of Ackermann et al. [2]. It is in reasonable agreement with other data and was derived with considerations for consistency with the thermodynamic functions for solid  $\text{UO}_2$  and the enthalpy of sublimation from the solid. It is consistent with a heat capacity that has a phase transition at 2670 K. In Figure 5, this recommended equation of Ackermann et al. [2] for the vapor pressure of  $\text{UO}_2(\text{g})$  over solid  $\text{UO}_2$  is compared with vapor pressure equations and data from earlier measurements and with the vapor pressure of  $\text{UO}_2(\text{g})$  and the total vapor pressure over  $\text{UO}_{2.00}$  calculated by Green and Leibowitz [3]. In the legend for Figure 5, the notation  $\text{UO}_2$  has been included to distinguish measurements or calculations of the pressure due to the vapor species  $\text{UO}_2(\text{g})$  from the total vapor pressure over  $\text{UO}_2$ . Below 2450 K, the 1956 low-temperature data of Ackermann et al. [30] and the equation of Tetenbaum and Hunt [4] are in excellent agreement with the recommended equation of Ackermann et al. [2]. Above 2615 K, the equation of Tetenbaum and Hunt for the total vapor pressure over  $\text{UO}_2$  gives higher vapor pressures than the equation of Ackermann et al. for the vapor pressure of  $\text{UO}_2(\text{g})$ . Two data from transpiration measurements of the total vapor pressure over  $\text{UO}_{1.98}$  by Reedy and Chasanov [5] have been included in Figure 5. These are the only vapor pressure measurements over uranium dioxide in both the liquid and solid phases. The Reedy and Chasanov data at 2615 K is in good agreement with the equation of Ackermann et al. but their datum at 2860 K is higher than values from both the equation of Ackermann et al. and the equation of Tetenbaum and Hunt. Total vapor pressures over  $\text{UO}_2$  measured by Ohse et al. [32] are in good agreement with the equation of Ackermann et al. at low temperatures but are higher at high temperatures. Above 2500 K, the data of Ohse et al. approach total pressures calculated by Green and Leibowitz. The contribution to the total vapor pressure from  $\text{UO}_2(\text{g})$  calculated by Green and Leibowitz is in good agreement with the equation of Ackermann et al. [2] above 2600 K. However, the total vapor pressure over  $\text{UO}_2$  calculated by Green and Leibowitz is consistently higher than the  $\text{UO}_2(\text{g})$  pressure given by the equation of Ackermann et al. The difference between these values increases with temperature. The contribution to the total vapor pressure from  $\text{UO}_2(\text{g})$  calculated by Green and Leibowitz decreases with increasing temperature. It is 70% at 2100 K, 54% at 2500 K, and only 37% at 3100 K. These comparisons indicate that the equation for the vapor pressure of  $\text{UO}_2(\text{g})$  over solid  $\text{UO}_2$  is a reasonable approximation of the total vapor pressure over solid  $\text{UO}_2$  up to 2600 K but not at higher temperatures. At higher temperatures, extrapolation of the equation of Tetenbaum and Hunt [Eq. (3)] is a better approximation to the total vapor pressure over solid  $\text{UO}_2$ .

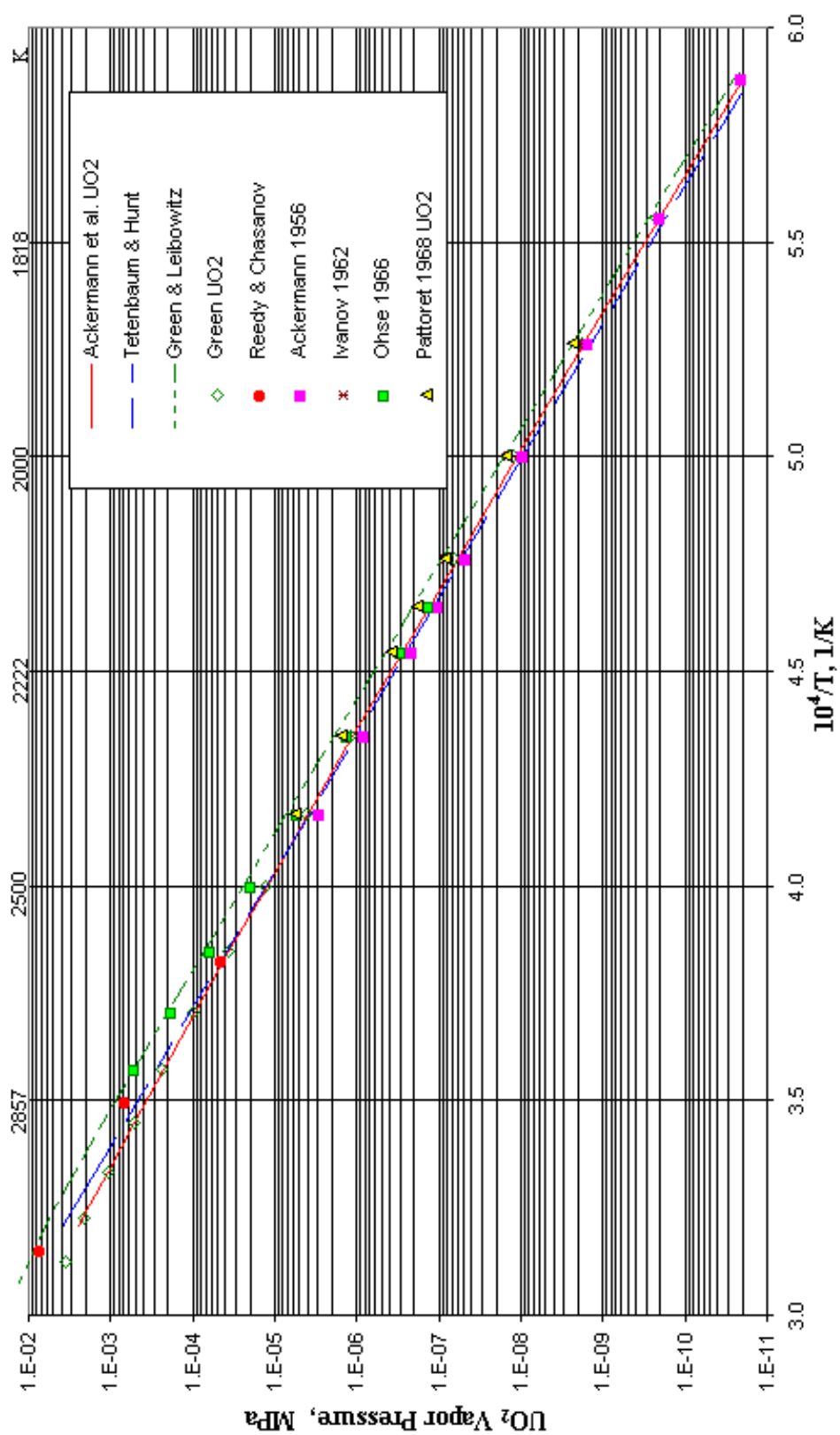


FIG. 5. Vapor pressure over solid UO<sub>2</sub>.

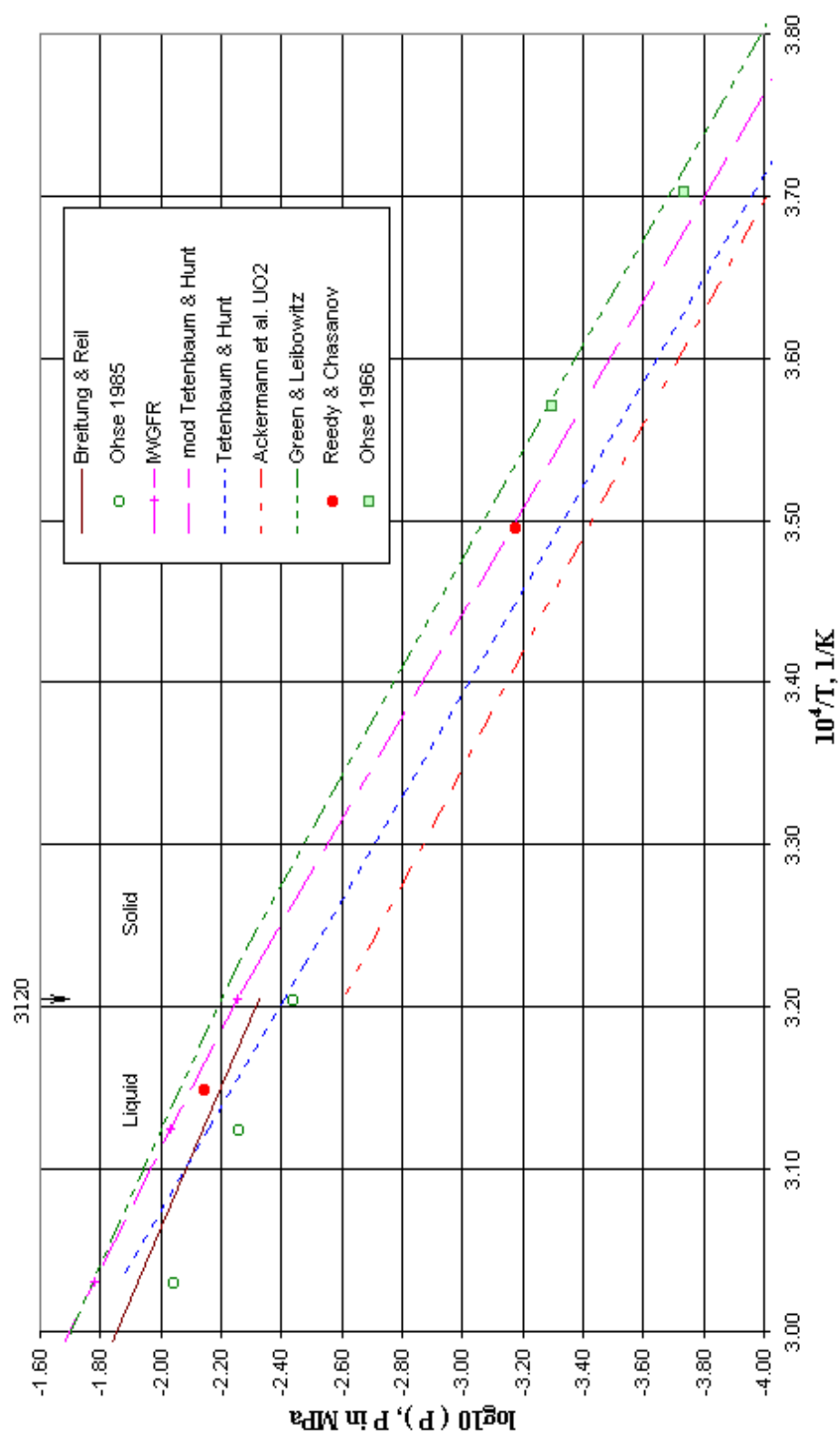


FIG. 6. Vapor pressure over  $UO_2$  at solid/liquid interface.

The logarithm to the base 10 of the vapor pressures determined from a number of vapor pressure equations near the solid/liquid phase boundary are compared in Figure 6. Equations included in Figure 6 are: the 1978 IWGFR equation [29] for the vapor pressure over liquid  $\text{UO}_2$ , the equation of Breitung and Reil [2] for the vapor pressure over liquid  $\text{UO}_2$ , the equation of Ackermann et al. for the vapor pressure of  $\text{UO}_2(\text{g})$  over solid  $\text{UO}_2$ , the equation of Tetenbaum and Hunt [4] for the total vapor pressure over solid  $\text{UO}_2$ , and a modified equation of Tetenbaum and Hunt [21]. The equation of Tetenbaum and Hunt was modified by Fink, Leibowitz, and Chasanov [21] for continuity at the solid/liquid interface with the IWGFR equation [29] for the vapor pressure over liquid uranium. The logarithms of the total vapor pressures over  $\text{UO}_2$  calculated by Green and Leibowitz [3] are also shown in Figure 6. The total vapor pressure data of Reedy and Chasanov [5] that spans this temperature range and the 1985 liquid vapor pressure data of Ohse et al. [13] have also been included in the figure. Harding et al. [24] have recommended the equation of Ackermann et al. [2] as an approximation to the total vapor pressure over solid  $\text{UO}_2$  up to the melting point. However, Figure 6 shows that extrapolation of the equation of Ackermann et al. to the melting point gives vapor pressures that are lower than the experimental data and 47% lower than the liquid vapor pressures at the melting point calculated from the equation of Breitung and Reil. Extrapolation of the equation of Tetenbaum and Hunt [4] into the liquid region gives vapor pressures that are consistent with the vapor pressures over the liquid determined in 1985 by Ohse et al. [13] but the vapor pressure at the melting point calculated with this extrapolated equation is 17% lower than that calculated using the equation of Breitung and Reil. The modified equation of Tetenbaum and Hunt [21] is consistent with the IWGFR equation and with the data of Reedy and Chasanov but the vapor pressure at the melting point calculated with this modified equation is 19% higher than the vapor pressure calculated with the equation of Breitung and Reil. Thus, the deviations from the equation of Breitung and Reil by the original equation of Tetenbaum and Hunt [4] and the modified equation of Tetenbaum and Hunt [21] are similar in magnitude but opposite in sign. The original equation of Tetenbaum and Hunt [4] is preferred to the modified equation of Tetenbaum and Hunt [21] because the original equation of Tetenbaum and Hunt was based on experimental data and it agrees better with the low-temperature vapor pressure data over solid  $\text{UO}_2$  and with the equation of Ackermann et al. below 2450 K.

#### REFERENCES TO SECTION 6.1.1.14

- [1] BREITUNG, W. and REIL, K.O., Vapor Pressure Measurements on Liquid Uranium Oxide and (U,Pu) Mixed Oxide, Nucl. Sci. Eng. 101, 26-40 (1989).
- [2] ACKERMANN, R.J., RAUH, E.G. and RAND, M.H., A Re-Determination and Re-Assessment of the Thermodynamics of Sublimation of Uranium Dioxide, Symp. on Thermodynamics of Nuclear Materials Julich 1979, Vol.1, IAEA, pp.11-27, Vienna (1980).
- [3] GREEN, D.W. and LEIBOWITZ, L., Vapor Pressures and Vapor Compositions in Equilibrium with Hypostoichiometric Uranium Dioxide at High Temperatures, Argonne National Laboratory Report AN-CEN-RSD-81-1 (June 1981); also J. Nucl. Mater. 105, 94 (1982).
- [4] TETENBAUM, M. and HUNT, P.D., Total Pressure of Uranium-Bearing Species over Oxygen-Deficient Urania, J. Nucl. Mater. 34, 86-91 (1970).
- [5] REEDY, G.T. and CHASANOV, M.G., Total Pressure of Uranium-Bearing Species over Molten Urania, J. Nucl. Mater. 42 341-344 (1972).
- [6] BOBER, M., KAROW, H.U. and SCHRETZMANN, K., Evaporation Experiments to Determine the Vapor Pressure of  $\text{UO}_2$  Fuel (3000 -5000 K), IAEA Symp. on Thermodynamics of Nuclear Materials, Vol. 1, 295 (1975); Nucl. Technol. 26, 237 (1975).
- [7] BOBER, M., BREITUNG, W., KAROW, H.U. and SCHRETZMANN, K., Evaporation Studies of Liquid Oxide Fuel at Very High Temperatures Using Laser Beam Heating, KFK-2366, Kernforschungszentrum Karlsruhe (1976).
- [8] OHSE, R.W., BERRIE, P.G., BOGENBERGER, H.G. and FISCHER, E.A., Thermodyn. Nucl. Mater. 1, 307 (1975).
- [9] BABELOT, J.F., BRUMME, G.D., KINSMAN, P.R. and OHSE, R.W., Atomwirtsch. Atomtech., 12, 387 (1977), as referenced by W. Breitung, and K. O. Reil, Nucl. Sci. Eng. 101, 26-40 (1989).

- [10] TSAI, H.C., CONVINGTON, A. and OLANDER, D.R., Laser Vaporization of  $\text{UO}_2$ , in Materials and Molecular Research Division Annual Report LBL-6016, Lawrence Berkeley Laboratory, University of California, Berkeley (1976).
- [11] BOBER, M., BREITUNG, W. and KAROW, H.U., Thermodynamic Calculation and Experimental Determination of the Equation of State of Oxide Fuels up to 5000 K, KfK-2689, Kernforschungszentrum Karlsruhe (1978).
- [12] OHSE, R.W., BABELOT, J.F., FREZZOTTI, A., LONG, K.A. and MAGILL, J., Equation of State of Uranium Oxide: Mach-disk Investigation of Transient Laser-induced Vaporization of  $\text{UO}_2$  up to 5000 K, High Temp.-High Pressures 12, 537 (1980).
- [13] OHSE, R.W., BABELOT, J.F., CERCIGNANI, C., HIERNAUT, J.P., HOCH, M., HYLAND, G.J. and MAGILL, J., J. Nucl. Mater. 130, 165 (1985).
- [14] BOBER, M. and TRAPP, M., Bestimmung des Dampfdrucks von flüssigem Uranoxid mittels Laseraufheizung, Kernforschungszentrum Karlsruhe (unpublished), as referenced by W. Breitung, and K. O. Reil, Nucl. Sci. Eng. 101, 26-40 (1989).
- [15] BOBER, M. and SINGER, J., Nucl. Vapor Pressure Determination of Liquid  $\text{UO}_2$ , Using a Boiling Point Technique, Nucl. Sci. Eng. 97, 344-352 (1987).
- [16] REIL, K.O., Effective Equation of State Measurements on Uranium Dioxide, Dissertation, University of New Mexico (May 1977), as referenced by W. Breitung, and K. O. Reil, Nucl. Sci. Eng. 101, 26-40 (1989).
- [17] BENSON, D.A., Application of Pulsed Electron Beam, Vaporization to Studies of  $\text{UO}_2$ , SAND77-0429, Sandia National Laboratories (1977).
- [18] LIMON, R., SUTREN, G., COMBETTER, P. and BARBRY, F., Equation of State of Non-Irradiated  $\text{UO}_2$ , Proc. ENA/ANS Topical Meeting on Reactor Safety Aspects of Fuel Behavior, Sun Valley, Idaho, August 2-6, 1981, Vol. 2, pp. 2-576 to 2-583, CEA-CONF-5816, American Nuclear Society (1981).
- [19] WRIGHT, S.A., WORLEDGE, D.H., CANO, G.L., MAST, P.K. and BRISCOE, F., Fuel-Disruption Experiments Under High-Ramp-Rate Heating Conditions, SAND81-0413, Sandia National Laboratories (Oct. 1983).
- [20] FISCHER, E.A., Evaluation of the Urania Equation of State Based on Recent Vapour Pressure Measurements, KfK- 4084 Kernforschungszentrum Karlsruhe (Sept. 1987).
- [21] FINK, J.K., CHASANOV, M.G. and LEIBOWITZ, L., Thermodynamic Properties of Uranium Dioxide, J. Nucl. Mater. 102, 17-25 (1981); see also Thermophysical Properties of Uranium Dioxide, ANL-CEN-RSD-80-3, Argonne National Laboratory (April 1981).
- [22] BREITUNG, W. and REIL, K.O., In-Pile Vapor Pressure Measurements on  $\text{UO}_2$  and  $(\text{U,Pu})\text{O}_2$  from 5000 to 8000 K, Proc. of Conf. on Science and Technology of Fast Reactor Safety, Guernsey, U. K., May 12-16, 1986, p. 501.
- [23] BREITUNG, W. and REIL, K.O., In-Pile Vapor Pressure Measurements on  $\text{UO}_2$  and  $(\text{U,Pu})\text{O}_2$ , KfK-3939 Kernforschungszentrum Karlsruhe (Aug. 1985).
- [24] HARDING, J.H., MARTIN, D.G. and POTTER, P.E., Thermophysical and Thermochemical Properties of Fast Reactor Materials, Commission of the European Communities Report EUR 12402 EN (1989).
- [25] RONCHI, C., HIERNAUT, J.P., SELFSLAG, R. and HYLAND, G.J., Laboratory Measurement of the Heat Capacity of Urania up to 8000 K: I. Experiment, Nucl. Sci. Eng. 113, 1-19 (1993).
- [26] LEIBOWITZ, L., CHASANOV, M.G., MISHLER, L.W. and FISCHER, D.F., Enthalpy of Liquid Uranium Dioxide to 3500 K, J. Nucl. Mater. 39 115-116 (1971).
- [27] HEIN, R.A. and FLAGELLA, P.N., Enthalpy Measurements of  $\text{UO}_2$  and Tungsten to 3260 K, General Electric Report GEMP-578 (February 16, 1968).
- [28] RAND, M.H., ACKERMANN, R.J., GRONVOLD, F., OETTING, F.L. and PATTORET, A., The Thermodynamic Properties of the Urania Phase, Rev. Int. Hautes Temp. Refract. 15, 355-365 (1978).
- [29] INTERNATIONAL ATOMIC ENERGY AGENCY/INTERNATIONAL WORKING GROUP ON FAST REACTORS, Specialists' Meeting on Equations of State of Materials of Relevance to the Analysis of Hypothetical Fast Breeder Reactor Accidents, Harwell, U. K., June 19-23, 1978, IWGFR/26, IAEA (1978).
- [30] ACKERMANN, R.J., GILES, P.W., THORN, R.H., J. Chem. Phys. 25, 1089 (1956).

- [31] IVANOV, V.E., KRUGLYKH, A.A., PAVLOV, V.S., KOVTIN, G.P. and MONENKO, V.M., Proc. Symp. On Thermodynamics of Nuclear Materials, Vienna 1962, IAEA, p. 735, Vienna (1962).
- [32] OHSE, R.W., J. Chem. Phys. 44, 1375 (1966).
- [33] GORBAN, Y.A., PAVLINOV, L.V. and VYKOV, V.N., At. Ehnerg. 22, 465 (1955), as referenced by R. J. Ackermann, E. G. Rauh, and M. H. Rand, A Re-Determination and Re-Assessment of the Thermodynamics of Sublimation of Uranium Dioxide, Proc. Symp. on Thermodynamics of Nuclear Materials, Julich, 1979 Vol.1, IAEA, pp.11-27, Vienna (1980).
- [34] ACKERMANN, R.J., RAUH, E.G. and CHANDRASEKHARIAH, M.S., J. Phys. Chem. 73, 762 (1969).
- [35] VORONOV, N.M., DANILIN, A.S., KOVALEV, I.T., Symp. on Thermodynamics of Nuclear Materials Vienna 1962, IAEA, p. 789, Vienna (1962).
- [36] ALEXANDER, C.A., OGDEN, J.S. and CUNNINGHAM, G.C., Battelle Memorial Institute Report BMI-1789 (Jan. 1967), as referenced by R. J. Ackermann, E. G. Rauh, and M. H. Rand, A Re-Determination and Re-Assessment of the Thermodynamics of Sublimation of Uranium Dioxide, Proc. Symp. on Thermodynamics of Nuclear Materials, Julich, 1979 Vol.1, IAEA, pp.11-27, Vienna (1980).
- [37] PATTORET, A., DROWART, J. and SMOES, J., Proc. Symp. Thermodynamics of Nuclear Materials, Vienna 1967, IAEA, p. 613, Vienna (1968).

### 6.1.2. Thermal conductivity of irradiated $UO_2$

As described in Section 6.1.1.7 the thermal conductivity of unirradiated solid  $UO_2$  was reassessed and the following equation was recommended by Fink [1] for the thermal conductivity of 95% dense  $UO_2$  which includes the new phonon lattice term and small polaron ambipolar contribution determined by Ronchi et al. [2]

$$\lambda_0 = \frac{100}{7.5408 + 17.692t + 3.6142t^2} + \frac{6400}{t^{5/2}} \exp\left(\frac{-16.35}{t}\right)$$

where  $t = T(K)/1000$  and  $\lambda$  is in  $Wm^{-1}K^{-1}$ .

In this assessment, the above equation for unirradiated  $UO_2$  is shown as a reference to the data available in the literature for irradiated  $UO_2$ . Several models are available in the literature for the thermal conductivity of irradiated  $UO_2$  which are reviewed below:

#### *Lucuta Model [3]*

Based on the measured values of SIMFUEL and the modeling, Lucuta et al. proposed the parametric dependence of irradiated  $UO_2$  thermal conductivity,  $\lambda$ , in a form of contributing factors for each individual effect:

$$\lambda = k_{1d} k_{1p} k_{2p} k_{3x} k_{4x} \lambda_0$$

where  $k_1$  is the burn-up dependence factor,  $k_2$  is the porosity/bubbles contribution,  $k_3$  describes the effect of O/M ratio,  $k_4$  refers to the radiation damage and  $\lambda_0$  is an analytical expression for the thermal conductivity of unirradiated  $UO_2$ .

The analytical expression that is slightly different from the MATPRO [5] suggestion in the exponential term was chosen for  $\lambda_0$  in his model:

$$\lambda_0 = \frac{1}{0.0375 + 2.165 \times 10^{-4} T} + \frac{4.715 \times 10^9}{T^2} \exp\left(-\frac{16361}{T}\right)$$

Lucuta et. al. claimed that the solid fission products formed during irradiation (dissolved and precipitated) affect the fuel thermal conductivity in two ways, agitation of phonon heat current  $k_{1d}$  and dispersion of the precipitated fission products  $k_{1p}$ .

They suggested the following expressions for the two factors:

$$k_{1d}(\beta) = \left( \frac{1.09}{\beta^{3.265}} + \frac{0.0643}{\sqrt{\beta}} \sqrt{T} \right) \arctan\left( \frac{1}{1.09 / \beta^{3.265} + (0.0643 / \sqrt{\beta}) \sqrt{T}} \right)$$

$$k_{1p}(\beta) = 1 + \frac{0.019\beta}{(3 - 0.019\beta)} \frac{1}{1 + \exp(-(T - 1200)/100)}$$

In the above expression:  $T$  represents the temperature in Kelvin and  $\beta$  is the burn-up in *at. %*.

#### *Halden Model [4]*

Since many processes change the temperature distribution of the fuel during irradiation, attention was particularly focused on  $\text{UO}_2$  conductivity degradation with increasing burn-up. The quantification of this effect with in-pile data has therefore been a major task of the experimental program that had been carried out in the Halden Project.

Halden model basically took the parameter  $a$  and  $b$  for the impurities and lattice faults term and for the phonon-phonon collisions term, respectively, from the MATPRO formulation for 95% T.D. fuel [5] and modified the expression to the following burn-up dependent form:

$$\lambda = \frac{1}{0.1148 + 0.0035 \cdot B + 2.475 \cdot 10^{-4} \cdot (1 - 0.00333 \cdot B) \cdot T} + 0.0132 \cdot \exp^{0.00188T}$$

with temperature  $T$  in  $^{\circ}\text{C}$ , burn-up  $B$  in  $\text{MWd/kgUO}_2$ , and conductivity  $\lambda$  in  $\text{W/mK}$  for 95% T.D. fuel. This equation is valid up to a burn-up of  $75 \text{ MWd/kgUO}_2$ .

As in the MATPRO formulation, this model assumed that the conductivity enhances with the increasing electron conduction at high temperature.

#### *Carbajo Model [6]*

Carbajo et al. reviewed all the available thermo-physical properties of MOX and  $\text{UO}_2$  fuel and recommend the Lucuta et al.'s model with the replacement of  $\lambda_0$  with Fink's expression [1].

#### *Minato Model [7]*

Minato and his colleagues measured the thermal diffusivities of irradiated  $\text{UO}_2$  and  $\text{UO}_2\text{-10wt\%Gd}_2\text{O}_3$  with the laser flash method using disk samples.

Their measurement data on the irradiated  $\text{UO}_2$  fuel at 4% FIMA are as follows:

TEMPERATURE	0 MWd/MtU	17,480 MWd/MtU	
		1 Run	2 Run
382	-	4.31	6.06
400	7.94	-	-
473	-	4.19	5.94
482	7.50	-	-

TEMPERATURE	0 MWd/MtU	17,480 MWd/MtU	
		1 Run	2 Run
573	-	3.88	5.31
600	6.50	-	-
673	-	3.50	4.63
682	5.69	-	-
782	4.88	3.13	4.00
873	-	3.00	3.63
882	4.38	-	-
973	-	2.88	3.31
982	3.88	-	-
1073	-	2.69	-
1173	-	2.63	2.94
1082	3.63	-	-
1182	3.38	-	-
1273	-	2.50	-
1282	3.13	-	-
1373	-	2.44	2.56
1382	3.00	-	-
1473	-	2.31	-
1482	2.88	-	-
1573	-	2.30	2.31
1582	2.75	-	-
1673	-	-	2.31
1682	2.63	-	-
1773	-	2.19	2.20
1782	2.50	-	-

#### *Amaya Model [8]*

Thermal diffusivities of  $\text{UO}_2$  and  $(\text{U,Gd})\text{O}_2$  pellets irradiated in a commercial reactor were measured up to about 2000 K using the laser flash method by Amaya and co-workers. The diffusivities after recovery were close to those of simulated soluble fission products doped  $\text{UO}_2$  and  $(\text{U,Gd})\text{O}_2$  pellets.

Their measurement data on the irradiated  $\text{UO}_2$  fuel at 60 GWd/MtU are as follows:

TEMPERATURE	39,300 MWd/MtU			60,000 MWd/MtU		
	1 Run	2 Run	3 Run	1 Run	2 Run	3 Run
302	2.96	-	-	-	-	-
465	3.1	3.65	5.05	-	-	-
495	-	-	-	2.72	3.22	-
516	-	-	-	-	-	3.76
564	3.04	-	-	2.47	-	-
671	2.81	3.15	3.79	-	-	-



TEMPERATURE	39,300 MWd/MtU			60,000 MWd/MtU		
	1 Run	2 Run	3 Run	1 Run	2 Run	3 Run
685	-	-	-	2.44	2.69	3.26
770	2.71	-	-	-	-	-
783	-	-	-	2.32	-	-
832	-	-	-	-	-	2.85
841	-	-	-	-	2.57	-
854	-	-	-	2.38	-	-
875	2.62	2.84	3.21	-	-	-
979	2.59	-	-	2.38	-	-
1061	-	-	-	-	-	2.64
1083	-	2.59	-	-	-	-
1176	2.48	-	-	2.11	-	-
1275	-	2.40	-	-	-	-
1285	-	-	-	-	2.27	-
1383	-	2.44	-	-	-	-
1401	-	-	-	-	2.26	-
1488	-	-	2.42	-	-	-
1498	-	-	-	-	2.13	-
1575	-	-	2.25	-	-	-
1605	-	-	-	-	-	2.17
1682	-	-	2.19	-	-	-
1709	-	-	-	-	-	2.05
1783	-	-	2.23	-	-	-
1816	-	-	-	-	-	1.98
1879	-	-	2.22	-	-	-
1895	-	-	-	-	-	1.77

#### *Ronchi Model [9]*

The thermal diffusivity and specific heat capacity of reactor-irradiated UO<sub>2</sub> fuel have been measured by Ronchi and his colleagues and an accurate but complicated formula for the in-pile thermal conductivity of irradiated UO<sub>2</sub> was proposed. In the final recommendation, Ronchi et al included the data available from other sources for a burn-up 100 GWd/MtU. The Ronchi et al formulation accounts for not only the effects such as non-volatile soluble fission products, fission gas, Cs and its state, and irradiation defects but also the effects due to thermal recovery, such as precipitation of the fission gas-in-solid and annihilation of the irradiation defects.

From the phonon transport mechanism Ronchi et al formulated the following equation:

$$\lambda = \frac{1}{A(T_{irr}, T_{ann}, bu) + B(T_{irr}, T_{ann}, bu)T}$$

where  $A(T_{irr}, T_{ann}, bu) = 0.046 + \Gamma(bu, GIS) + \delta A$  in  $mKW^{-1}$ ,

$$B(T_{irr}, T_{ann}, bu) = B_0 + (B_1 - B_0)(1 - \delta B / 6.5 \times 10^{-5}) \text{ in } mW^{-1},$$

$T_{irr}$  is irradiation temperature, and  $T_{ann}$  is maximum annealing temperature.

Here total phonon scattering coefficient  $\Gamma(bu, GIS)$  is given by

$$\Gamma(bu, GIS) = 9.02 \times 10^{-4} \cdot bu \cdot GIS + 1.74 \times 10^{-3} \cdot bu + 7.51 \times 10^{-3}$$

where  $bu$  is in the unit of GWd/MtU and gas-in-solid  $GIS$  is

$$GIS(bu, T_{irr}, T_{ann}) = \frac{1 - 0.9 \left[ 1 + \exp\left(\frac{T_{irr} - 950}{30}\right) \right]^{-1} \left[ 1 + \exp\left(\frac{73 - bu}{2}\right) \right]^{-1}}{\left[ 1 + \exp\left(\frac{T_{irr} - 1350}{200}\right) \right] \left[ 1 + \exp\left(\frac{T_{ann} - 1350}{200}\right) \right]}.$$

Effect of the irradiation defects  $\delta A$  consists of two terms, out-of-pile self-irradiation effects  $\delta A_{self}$  and in-pile damage effect  $\delta A_{EOL}$ :

$$\delta A = \delta A_{self}(T_m, bu) + \delta A_{EOL}(T_m, bu)$$

where  $T_m$  is defined as a function of  $\max(T_{irr}, T_{ann})$ ,

$$\delta A_{self}(T_{ann}, bu) = \begin{bmatrix} 0.02F(bu) & \text{if } T_{ann} \leq 900 \\ 0.02F(bu) \frac{1450 - T_{ann}}{1450 - 900} & \text{if } 900K < T_{ann} < 1450K \\ 0 & \text{if } T_{ann} \geq 1450K \end{bmatrix},$$

$$\delta A_{EOL}(T_m, bu) = \frac{bu}{850} \left[ \left\{ 1 + \exp\left(\frac{T_m - 950}{25}\right) \right\}^{-1} + \left\{ 1 + \exp\left(\frac{T_m - 1300}{35}\right) \right\}^{-1} - 0.0525 \right], \text{ and}$$

$$F(bu) = \left[ \left\{ 1 + \exp\left(\frac{20 - bu}{6}\right) \right\}^{-1} - 0.015267 \right].$$

For the variation of  $B(T_{irr}, T_{ann}, bu)$ ,

$$B_0 = -1.65 \times 10^{-6} bu + 2.55 \times 10^{-4} - 3.6 \times 10^{-5} \left\{ 1 + \exp\left(\frac{T_{irr} - 950}{30}\right) \right\}^{-1} \left\{ 1 + \exp\left(\frac{73 - bu}{2}\right) \right\}^{-1}$$

$$B_1 = 4.2 \times 10^{-7} bu + 2.75 \times 10^{-4}, \quad \delta B = F(bu) \delta B_{EOL}(T_m, bu), \text{ and}$$

$$\delta B_{EOL}(T_m, bu) = \frac{bu}{34} \left[ 4.0 \times 10^{-5} \left\{ 1 + \exp\left(\frac{T_m - 950}{25}\right) \right\}^{-1} + 2.5 \times 10^{-5} \left\{ 1 + \exp\left(\frac{T_m - 1300}{35}\right) \right\}^{-1} \right]$$

In Figure 1 a comparison of the assessment results from various models for zero burn-up with the recommendation by Fink for unirradiated fuel is shown. In Figures 2-4 the thermal conductivity degradation with increasing burn-up are shown, where the Fink model is again shown for reference.

### **Recommendation**

The Halden model equation is recommended for the thermal conductivity of 95% dense irradiated solid  $UO_2$  since their data covers a wide range of temperature and burn-up, and lie within the experimental scatter of the measurements reported in the literature.

$$\lambda = \frac{1}{0.1148 + 0.0035 \cdot B + 2.475 \cdot 10^{-4} \cdot (1 - 0.00333 \cdot B) \cdot T} + 0.0132 \cdot \exp^{0.00188T}$$

with temperature  $T$  in  $^{\circ}C$ , burn-up  $B$  in  $MWd/kgUO_2$ , and thermal conductivity  $\lambda$  in  $W/mK$  for 95% T.D. fuel.

### **Uncertainty**

Uncertainties were determined from the scatter in the available data and the deviations of the data from the recommended equation. From room temperature to 2000 K the uncertainty remains within 20%. For temperatures greater than 2000K, the uncertainty was not determined, since only the Halden data were available.

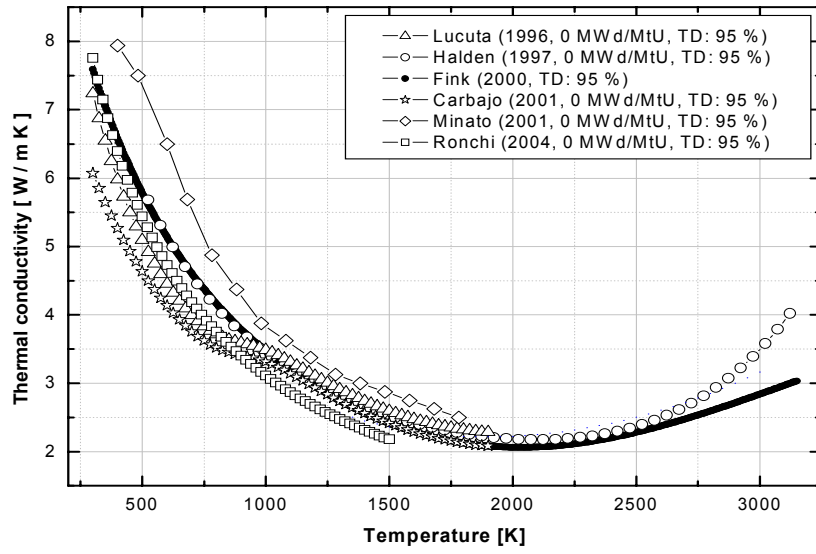


FIG. 1. Thermal conductivity of irradiated  $UO_2$  at zero burn-up.

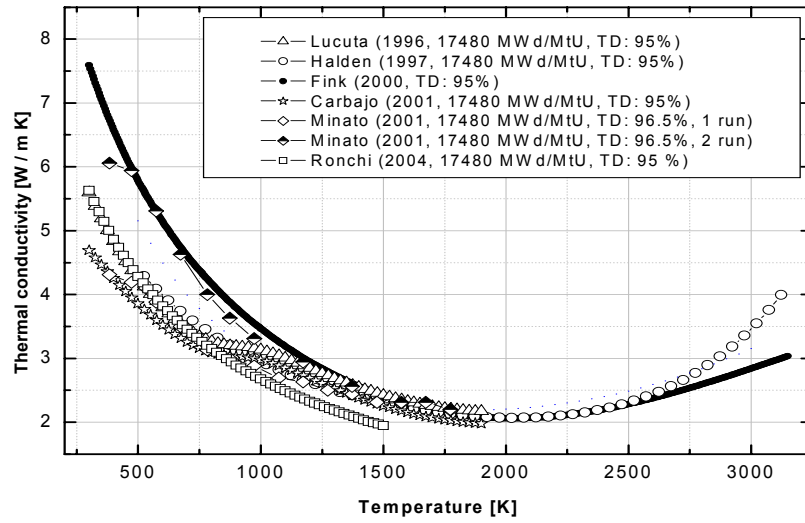


FIG. 2. Thermal conductivity of irradiated  $UO_2$  at 17,480 MWd/MtU burn-up.

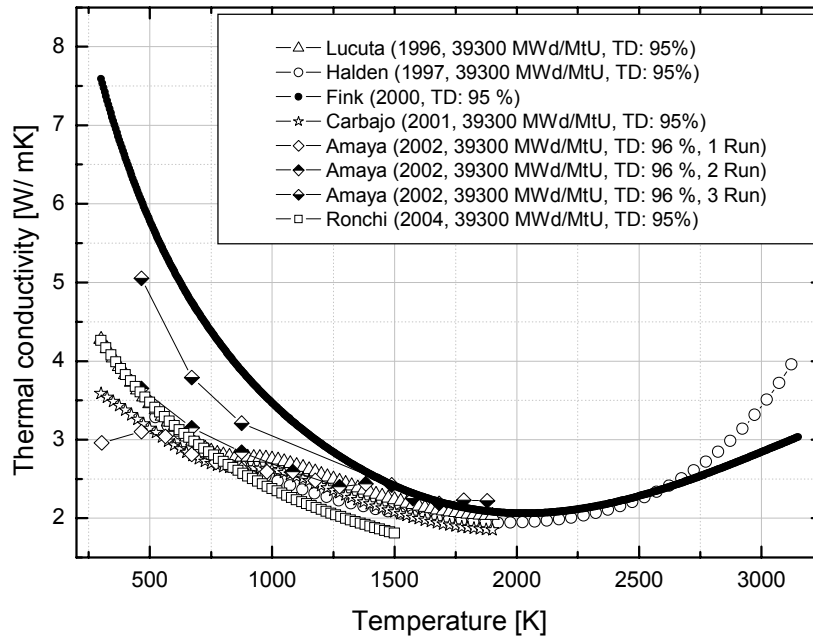


FIG. 3. Thermal conductivity of irradiated  $UO_2$  at 39,300 MWd/MtU burn-up.

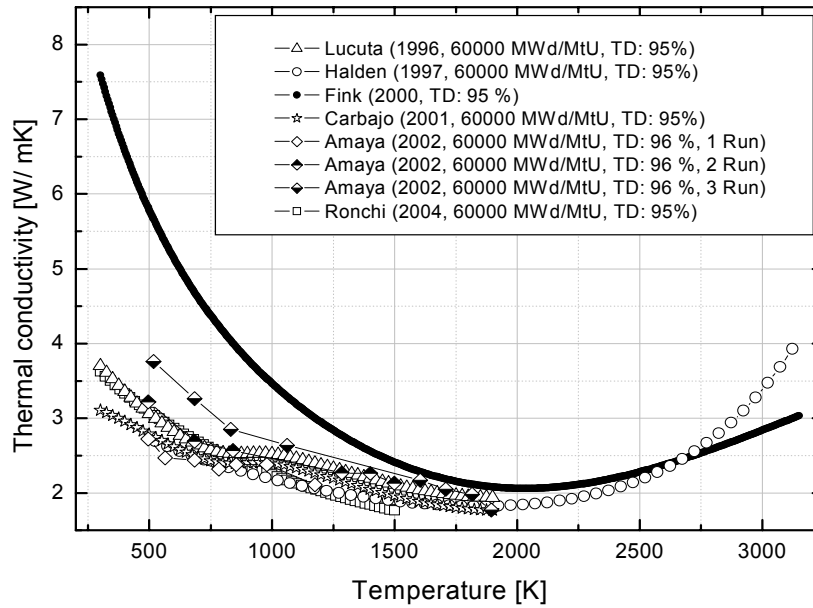


FIG. 4. Thermal conductivity of irradiated  $UO_2$  at 60,000 MWd/MtU burn-up.

## REFERENCES TO SECTION 6.1.2

- [1] FINK, J.K. Review: Thermo-physical properties of uranium dioxide, J. Nucl. Mater. 279 (2000) 1.
- [2] RONCHI, C., SHEINDLIN, M., MUSELLA, M., HYLAND, G.J., J. Appl. Phys. 85 (1999) 776.
- [3] LUCUTA, P.G., MATZKE, HJ., HASTINGS, I.J., A Pragmatic approach to modeling thermal conductivity of irradiated UO<sub>2</sub> fuel: review and recommendations, J. Nucl. Mater. 232 (1996) 166.
- [4] WIESENACK, W. Assessment of UO<sub>2</sub> conductivity degradation based on in-pile temperature data, Proc. International Topical Meeting on Light Water Reactor Fuel Performance, Portland, Oregon, March 2-6, 1997 (1997).
- [5] HAGRMAN, D.L. and REYMANN, G.A. (eds.): MATPRO version 11-A, Handbook of Materials Properties for Use in the Analysis of Light Water Reactor Fuel Rod Behavior, TREE-NUREC-1280 (1979).
- [6] CARBAJO, J.J., YODER, G.L., POPOV, S.G., IVANOV, V.K. A Review of thermophysical properties of MOX and UO<sub>2</sub> fuel, J. Nucl. Mater. 299 (2001) 181.
- [7] MINATO, K., et al, Thermal conductivities of irradiated UO<sub>2</sub> and (U, Gd)O<sub>2</sub>, J. Nucl. Mater. 288 (2001) 57.
- [8] M. AMAYA, et al, Thermal conductivities of irradiated UO<sub>2</sub> and (U, Gd)O<sub>2</sub> pellets, J. Nucl. Mater. 300 (2002) 57.
- [9] RONCHI, C., SHEINDLIN, M., STAICU, D., KINOSHITA, M. Effect of burn-up on the thermal conductivity of uranium dioxide up to 100.000 MWd/MTU, J. Nucl. Mater. 327 (2004) 58.

### 6.1.3 Thermal properties of (U, Gd)O<sub>2</sub>

#### 6.1.3.1. Heat capacity of solid (U,Gd)O<sub>2</sub>

##### Summary and recommended equations

No heat capacity data for solid (U,Gd)O<sub>2</sub> above 2000K have been published in the open literature so far. The following expressions (2) to (9) are recommended for the heat capacity of solid (U,Gd)O<sub>2</sub> from 300 to 2000K. Equation 1 is the enthalpy of (U,Gd)O<sub>2</sub> relative to the enthalpy at 298.15K:

$$H_T - H_{298.15} = a(T - 298.15) + \frac{b}{2}(T^2 - 298.15^2) + \frac{c}{T} - \frac{c}{298.15} + \sqrt{2}\Delta H \exp\left(\frac{\Delta S}{2R}\right) \left[ \exp\left(\frac{-\Delta H}{2RT}\right) - \exp\left(\frac{-\Delta H}{596.3R}\right) \right] \quad (1)$$

$$C_p = C_{p_0} + \Delta C_p \quad (2)$$

$$C_{p_0} = a + bT - \frac{c}{T^2} \quad (3)$$

$$\Delta C_p = \frac{(\Delta H)}{\sqrt{2}RT^2} \exp\left(\frac{\Delta S}{2R}\right) \exp\left(\frac{-\Delta H}{2RT}\right) \quad (4)$$

$$a = 79.8 \text{ J.mol}^{-1}.\text{K}^{-1} \quad (5)$$

$$b = 0.1263y^2 - 0.0073y + 0.0061 \text{ J.mol}^{-1}.\text{K}^{-2} \quad (6)$$

$$c = (1.68 - 1.48y).10^6 \text{ J.mol}^{-1}.\text{K}^{-3} \quad (7)$$

$$\Delta H = (-73880y^3 + 10190y^2 - 612.13y + 310).10^3 \text{ J.mol}^{-1} \quad (8)$$

$$\Delta S = 61.969 - 45.564y \text{ J.mol}^{-1} \quad (9)$$

Where  $\Delta H$  (J.mol<sup>-1</sup>) is the enthalpy of activation and  $\Delta S$  (J.mol<sup>-1</sup>) is the entropy of activation of the Frenkel defect formation.  $C_p$  is the heat capacity of (U,Gd)O<sub>2</sub>,  $\Delta C_p$  is the anomalous increase of heat capacity of (U,Gd)O<sub>2</sub>,  $y$  is gadolinium content of (U<sub>1-y</sub>,Gd<sub>y</sub>)O<sub>2</sub>,  $T$  is in K.

Data used for the assessment of the heat capacity of (U,Gd)O<sub>2</sub> and UO<sub>2</sub> are shown in Table 1. Values for heat capacity in J.mol<sup>-1</sup>.K<sup>-1</sup> were calculated using the above equations, which are tabulated as a function of temperature in Table 2. Equation 3 for  $C_{p_0}$  is obtained by fitting the data of Indaba [1] and the Eq. 4 for  $\Delta C_{p_0}$  is obtained by fitting the data of Jiang [2]. Their data are in good agreement with most of the available data in the literature. Comparisons of heat capacity for solid (U,Gd)O<sub>2</sub>, calculated from the above equations, with the experimental data [1–6] are shown in Fig. 4. The recommended values for the heat capacity with uncertainties are shown in Fig. 5.

##### Uncertainties

The uncertainty for the heat capacity of solid (U,Gd)O<sub>2</sub> for the range of gadolinium content between 0 and 14.2 mol% is 3% in the temperature range 298.15K to 2000K.

Table 1. Collected data in the assessment of heat capacity of (U,Gd)O<sub>2</sub> and UO<sub>2</sub>

Author	Temperature range (K)	Content of Gd (%mol)	Accuracy(%)
Inaba[1]	310-1500	0, 4.4, 10.1, 14.2	1.5
Jiang[2]	400-2100	0, 4.4, 10.1, 14.2	3.0
Bruct[3]	500-1000	8.06	No detailed
Inaba[4]	310-1500	7.3	1.5
Mills[5]	298-1800	4.4, 7.3	3.0
Hyland[6]	400-1100	7.3, 8.7, 10.0, 14.2,	1.5
Fink[7]	298-2100	0	2.0

Table 2. Recommended values for heat capacity of (U,Gd)O<sub>2</sub> in J.mol<sup>-1</sup>.K<sup>-1</sup>

Tem(K)	Content of gadolinium , mol			
	0	0.044	0.101	0.142
300	63.0	63.7	64.8	65.8
400	71.7	72.1	72.9	73.7
500	76.1	76.4	77.0	77.7
600	78.8	78.9	79.5	80.3
700	80.6	80.7	81.3	82.1
800	82.1	82.1	82.7	83.6
900	83.2	83.2	83.9	84.9
1000	84.2	84.2	84.9	86.2
1100	85.1	85.1	85.9	87.6
1200	86.0	86.0	86.9	89.4
1300	86.9	86.9	87.9	91.7
1400	87.8	87.8	89.1	94.9
1500	88.8	89.0	90.5	98.9
1600	90.1	90.4	92.3	104.0
1700	91.6	92.1	94.6	110.3
1800	93.6	94.4	97.5	117.8
1900	96.1	97.2	101.1	126.3
2000	99.2	100.7	105.4	136.0



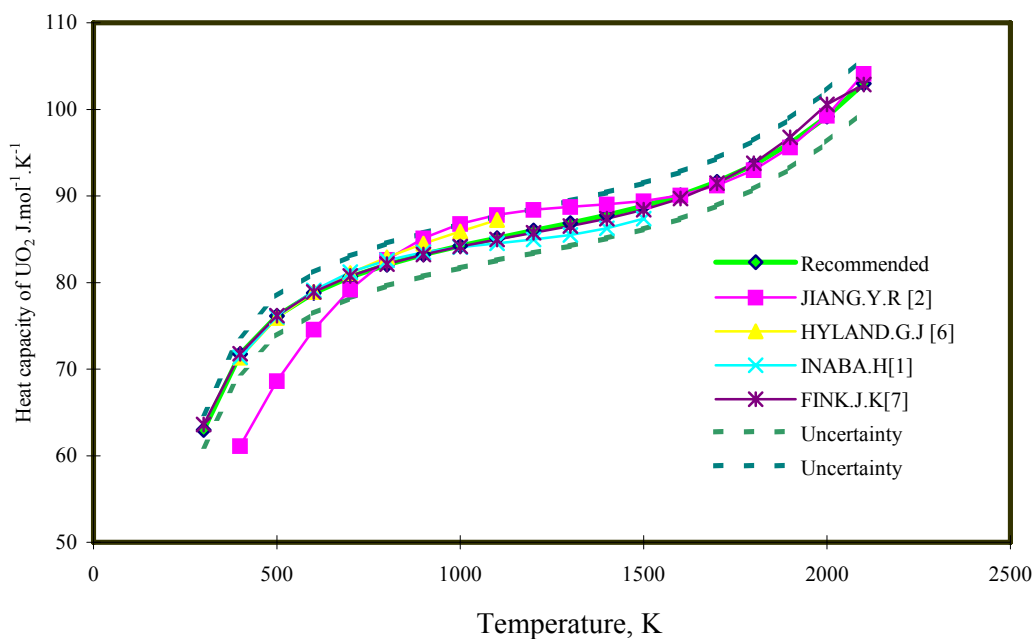


FIG. 1. Recommended values of heat capacity of  $\text{UO}_2$  with experimental data.

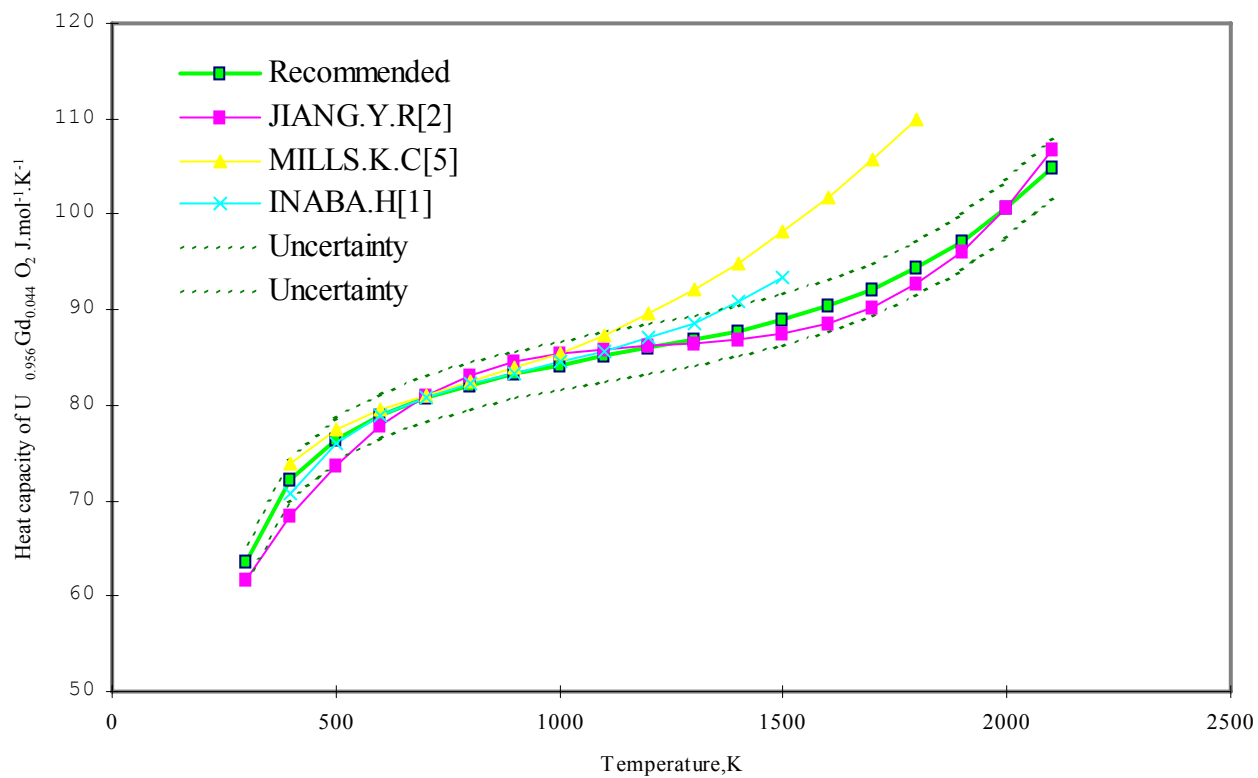


FIG. 2. Recommended values of heat capacity of  $\text{U}_{0.956}\text{Gd}_{0.044}$  with experimental data.

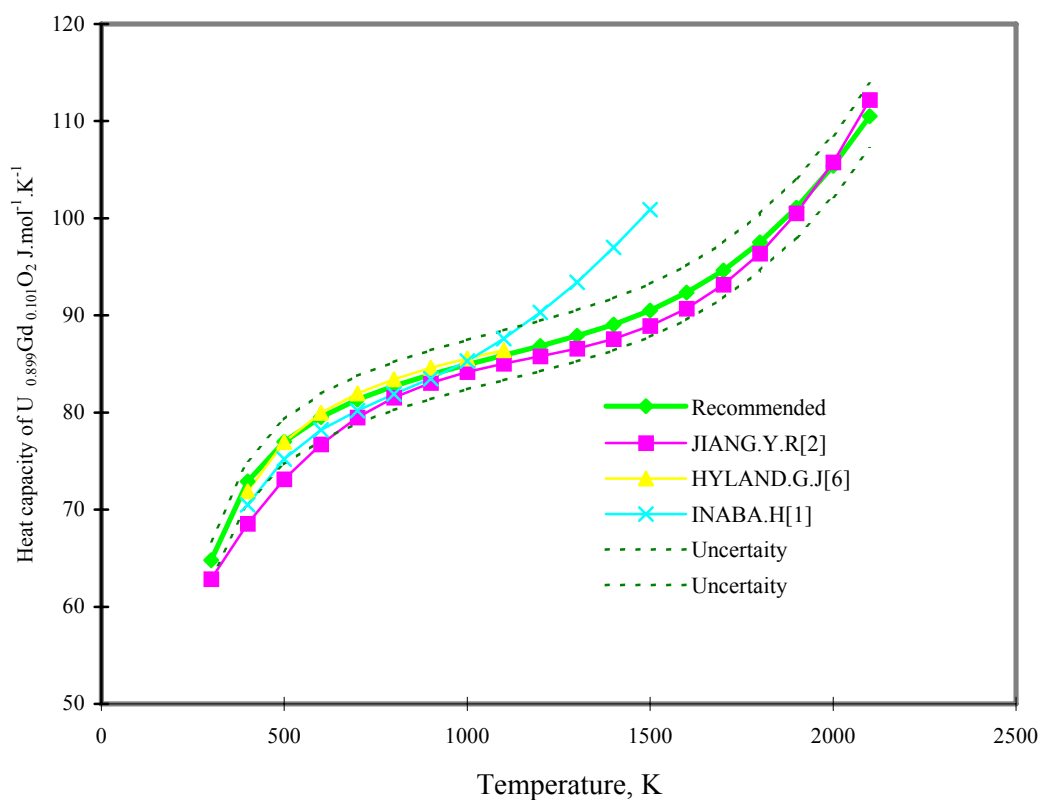


FIG. 3. Recommended values of heat capacity of  $U_{0.899}Gd_{0.101}O_2$  with experimental data.

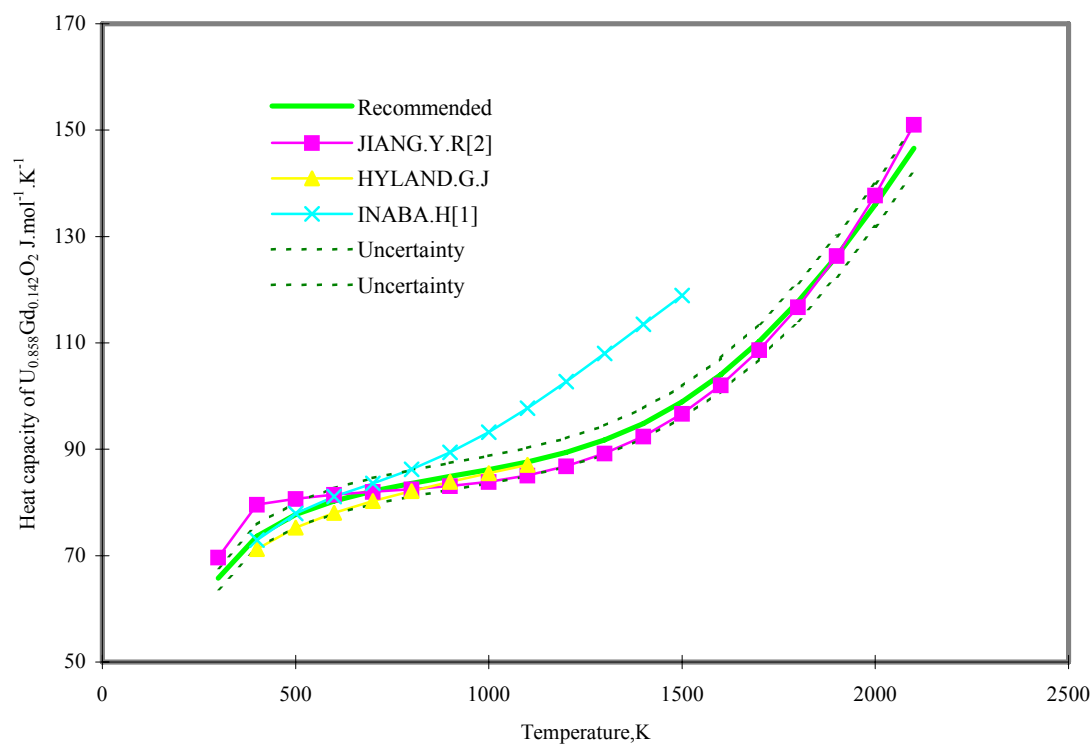


FIG. 4. Recommended heatcCapacity of  $U_{0.858}Gd_{0.142}O_2$  with experimental data.

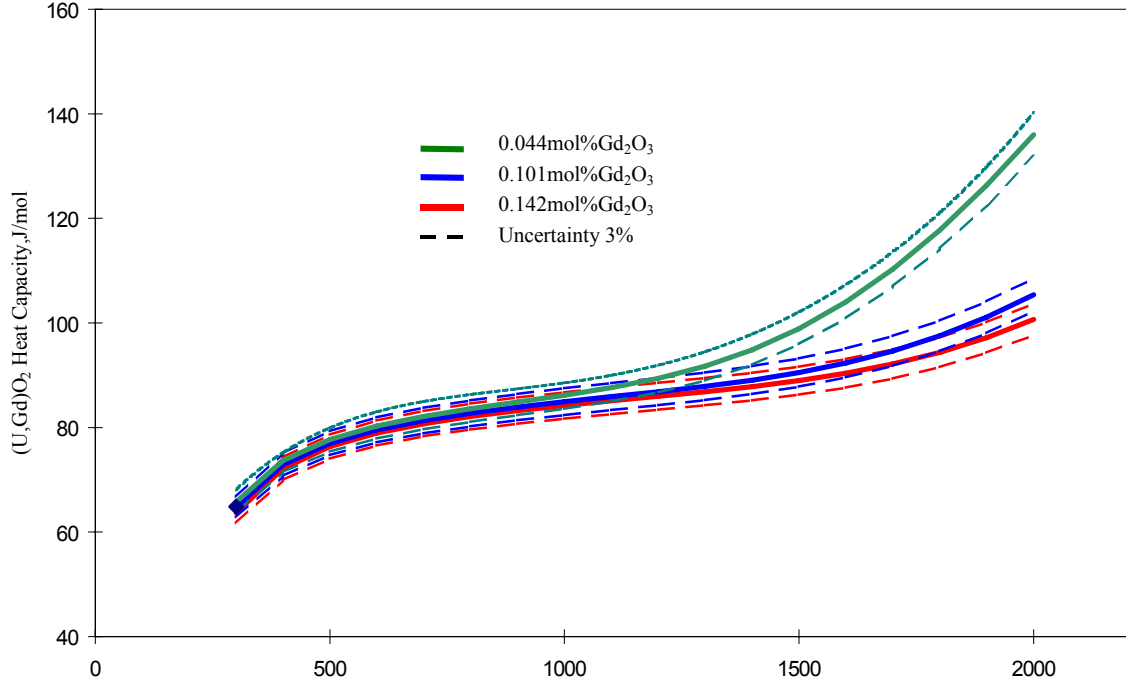


FIG. 5. Recommended heat capacity of solid  $(U,Gd)O_2$  with uncertainties.

### Discussion

The recommendations are based on the current theoretical understanding and comparisons with available data. The recommended equations for the heat capacity of  $(U,Gd)O_2$  are based on the data on the heat capacity of  $(U,Gd)O_2$  [1, 2]. Data from experiments on the heat capacity of  $(U_{1-y},Gd_y)O_2$  show an increase with Gd-content. Experimental data were excluded from the analysis if the value of heat capacity of  $(U_{1-y},Gd_y)O_2$  is lower than that of  $UO_2$  recommended by Fink [7] at the same reference temperature, because the theory of heat capacity of  $(U_{1-y},Gd_y)O_2$  may be interpreted similar to the heat capacity of  $UO_2$  [8, 9].

Naito [10] observed an onset of anomalous increase in the heat capacity curve at lower temperatures compared with undoped  $UO_2$ , the onset temperature ( $T_r$ ) of the increase in the heat capacity curve decreased with increasing Gd content. But Hyland [6] found no appreciable anomaly in the heat capacity curves of any of the  $(U_{1-y},Gd_y)O_2$  samples up to 1500K. This observation [1, 4] claimed a considerable increase in the heat capacity curve above 800K, and at 1500K, their heat capacity value is about 1.4 times greater than that of Naito [10] and that of  $UO_2$ . Most heat capacity data of  $(U,Gd)O_2$  in the open literature imply no anomalous increase from room temperature to 1500K.

The experimental studies on thermal diffusivity and conductivity of  $(U,Gd)O_2$  [11–13] showed that at around 1500K the values of thermal diffusivity and conductivity are almost the same as that of  $UO_2$ , regardless of the Gd content. Taking into account the well-known relation  $\lambda = \alpha C_p \rho$ , where  $\lambda$  is the thermal conductivity,  $\alpha$  the thermal diffusivity and  $\rho$  the density, the values of  $\lambda$  of  $(U,Gd)O_2$  are seen to be proportional to the values of  $C_p$ . Inaba's data [1, 4] are not consistent with the thermal diffusivity data available in the literature. The increase of heat capacity of  $(U,Gd)O_2$  is almost equivalent to the decrease in density, of which only 5 percent at 1500K is due to increase of Gd content from 0 to 0.142mol [14].

Ronchi and Hyland [15] discussed in detail the dominant contributors to the heat capacity in each of the four temperature intervals for  $UO_2$ : From room temperature to 1000K, the increase in heat capacity is governed by the harmonic lattice vibrations, which may be approximated by Debye model. By 1000K, this contribution becomes constant. From 1000 to 1500K, the heat capacity increases due to

increases in the anharmonicity of the lattice vibrations as evidenced in thermal expansion. From 1500 to 2670K, the increase in heat capacity is due to the formation of lattice and electronic defects. The peak in the heat capacity at 2670K was attributed to Frenkel defects, both from theoretical considerations [15] and neutron scattering measurements of the oxygen defect concentration as a function of temperature [16]. It is reasonable to suggest that the increase in heat capacity of  $\text{UO}_2$  below the phase transition is due to coupling between electronic disorder and Frenkel disorder. Ronchi et al. [15] point out that the increase in the electronic conductivity in that temperature interval indicates a contribution from electronic defects, but the small polaron contribution from electron-hole interactions is minor compared to the contributions due to Frenkel defects.

The excess heat capacity of  $(\text{U,Gd})\text{O}_2$  in the temperature region below 2000K is expressed as follows:

$$\Delta C = C_p - C_h - C_d - C_{ah} \quad (10)$$

Where  $C_h$  is the harmonic lattice contribution,  $C_{ah}$  the anharmonic lattice contribution,  $C_d$  the dilation contribution,  $\Delta C$  The excess heat capacity, and  $C_p$  the heat capacity. Szwarc [8] first interpreted the excess heat capacity of  $\text{UO}_2$  at high temperatures as due to the formation of Frenkel pairs of oxygen. The excess heat capacity  $\Delta C$  is thus expressed as:

$$\Delta C = \frac{(\Delta H_f)^2}{\sqrt{2RT^2}} \exp\left(\frac{\Delta S_f}{2R}\right) \exp\left(\frac{-\Delta H_f}{2RT}\right) \quad (11)$$

where  $\Delta S_f$  and  $\Delta H_f$  are the entropy and enthalpy of formation per Frenkel pair. Several investigators [12, 17, 18], however, claimed that the energy for the formation of the Frenkel pairs of oxygen obtained was rather large (i.e. 5eV) and insisted on the electronic excitation for the large excess heat capacity on the basis that the calculated energy for the electronic excitation was around 2eV [12, 17, 18]. The enthalpies of activation of  $\text{UO}_2$ ,  $\Delta H_f$ , obtained from the excess heat capacity of Szwarc [8], Kerrik and Browning [9] and Clifton [19] are between 3.1 and 3.5eV, while the calculated values, based on the mechanism of electron-hole disorder, by Catlow [12], Hyland and Ralph [20] and Harding et al. [17] are higher than 4.6eV.

Since the experimentally obtained  $\Delta H_f$  are between those of the two mechanisms, i.e. the formation of electron-hole pairs, there still remain two possibilities of the mechanism for the excess capacity of  $(\text{U,Gd})\text{O}_2$ . By the introduction of  $\text{Gd}^{3+}$  in  $\text{UO}_2$ , oxygen sub-lattice around the  $\text{Gd}^{3+}$  tends to form an oxygen vacancy, which produce an oxygen interstitial in the neighborhood to keep nearly stoichiometric composition  $(\text{U,Gd})\text{O}_2$  [5]. Gadolinia additions apparently decreased the enthalpy of formation of these Frenkel defects to a value below that derived for  $\text{UO}_{2.00}$ .

The onset temperature ( $T_r$ ) and the entropy and enthalpy of formation per Frenkel pair for doped  $\text{UO}_2$  decreases with the Gd content, the extrapolation of data to zero Gd content yields the estimated values for undoped  $\text{UO}_2$ :  $\Delta H_f = 3.0\text{eV}$  and  $\Delta S_f = 62\text{J.mol}^{-1}.\text{K}^{-1}$ , which are in good agreement with the experimental values of the undoped  $\text{UO}_2$  reported so far. The excess heat capacity of doped  $\text{UO}_2$  is due to the formation of the defects because the defect concentration increases in proportion to the Gd content.

The enthalpy of activation obtained for  $(\text{U,Gd})\text{O}_2$  is considerably smaller than that reported for  $\text{UO}_2$ , 1.55eV by Szwarc [8], 1.64eV by Kerrisk and Clifton [19], and 1.71eV by Browning. Among these the first two authors interpreted this enthalpy term as due to the formation of Frenkel pairs of oxygen. Therefore, the importance of electronic excitation (1.64–1.7eV) obtained by Harding et al. [17] is nearly the same as the observed one [8, 9, 19]. The smaller enthalpy of activation obtained for  $(\text{U,Gd})\text{O}_2$  may be ascribed to the doping effect of  $\text{Gd}^{3+}$  on the process of the electronic excitation. It would be expected on the basis of the Law of Mass Action that the interstitial oxygen atoms present in the ternary compound would reduce the number of interstitial oxygen formed by Frenkel defects. It is possible that differences in the stoichiometry of the  $(\text{U,Gd})\text{O}_2$  samples could have a significant effect on the  $C_p$ - $T$  relationships, particularly at high temperature. In the previous study [19], the sample was stoichiometric ( $y \approx 2.00$ ) and consequently must contain a significant concentration of  $\text{U}^{5+}$  ions. In contrast to this, the sub-stoichiometric sample ( $y = 1.96\text{--}1.88$ ) would contain no  $\text{U}^{5+}$  ions, which could

have a significant effect on the formation of Frenkel effects and consequently on the heat capacity at high temperature.

Comparison with recommendation

The deviation from 298.15 to 2000K is defined by:

$$Deviation(\%) = \frac{C_p(Data) - C_p(Recommended)}{C_p(Recommended)} \times 100\% \quad (12)$$

Percent deviations of the data from this equation are shown in Fig. 6. Data from measurements by Jiang [2] are 2 to 7% at temperatures less than 600K, while data from measurements by Inaba and Mills [1, 5] are high by 2 to 11%. Above 1500K, deviations for other data are mainly  $\pm 3\%$  or less.

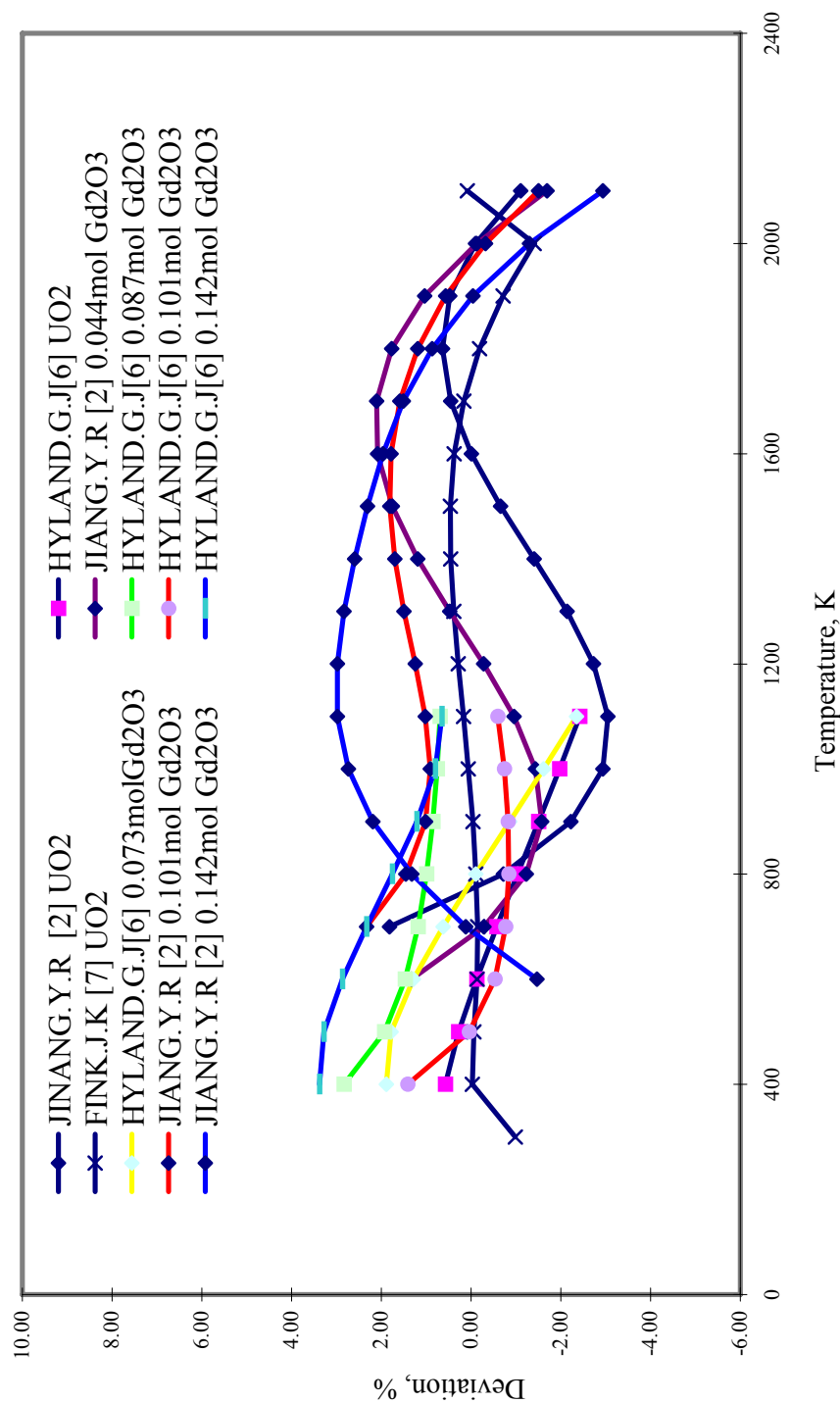


FIG. 6. Deviation of (U,Gd)O<sub>2</sub> heat capacity from the recommended equation of JIANG, Y.R.

## REFERENCES TO SECTION 6.1.3.1

- [1] INABA, H., J.Nucl.Mater.149, 341-348 (1987).
- [2] JIANG, Y., the first meeting of the Co-ordination Research program on “Establishment of a Thermophysical Properties Database for Light Water Reactors and Heavy Water Reactors”, Vienna (1999).
- [3] BRUET, M., ENC 86 Trans., Geneva. June 1-69; Vol.4 ENC-4, Topic VI, 269-278 (1986).
- [4] INABA, H., J.Nucl.Mater.137, 176-178 (1986).
- [5] MILLS, K.C., Thermochim.Acta 139, 107-120 (1989).
- [6] HYLAND, G.J., High Temp-High Press. 19, 343 (1987).
- [7] FINK, J.K., J.Nucl.Mater.279, 1 (2001).
- [8] SZWARC, R., J.Phys.Chem.Solids 30, 705 (1969).
- [9] BROWNING, P., J.Nucl.Mater.98, 345 (1981).
- [10] NAITO, K., J.Nucl.Mater.167, 30 (1989).
- [11] JACKSON, R.A., et.al., J.Chem.Soc.Farad.Trans.2,83, 1171 (1987).
- [12] CATLOW, C.R.A., Proc.R.Soc.London A353, 533 (1977).
- [13] THORN, R.J., et.al., J.Nucl.Mater.87, 416 (1979).
- [14] UNE, K., J.Nucl.Sci.Technol.23, 1020-1022, (1986).
- [15] RONCHI, C. and HYLAND, G.J., Analysis of Recent Measurements of the Heat Capacity of Uranium Dioxide, J.of Alloys and Compounds 213/214 159-168 (1994).
- [16] HUTCHINGS, T., High-Temperature Studies of UO<sub>2</sub> and ThO<sub>2</sub> Using Neutron Scattering Techniques, J.Chem.Soc.Faraday Trans II 83, 1083-1103 (1987).
- [17] HARDING, H., et.al., J.Nucl.Mater.92, 73 (1980).
- [18] YOUNG, R.A., J.Nucl.Mater.87, 283 (1979).
- [19] KETTISK, J.F., and CLIFTON, D.G., Nucl.Technol.16, 531 (1972).
- [20] HYLAND, G.J. and RALPH, J., High Temp-High Press. 15, 179 (1983).
- [21] CLAUSEN, K., et.al., Phys.Rev.Lett.52, 1238 (1984).
- [22] BROWNING, P., et.al., High Temp-High Press. 15, 169 (1983).

### *1.1.1.1. 6.1.3.2. Thermal conductivity of solid (U,Gd)O<sub>2</sub>*

#### **Summary and recommended equations**

The recommended equation for the thermal conductivity of solid (U,Gd)O<sub>2</sub> is from Ishimoto [1]. Ishimoto carefully considered the theoretical aspects related to the thermal conductivity of (U,Gd)O<sub>2</sub>, when phonon-phonon scattering and phonon-point defect scattering occur simultaneously and obtained a physically based equation for the temperature rang of 300K to 2000K. This equation is recommended because it is in good agreement with earlier equations, which are based on statistical fits to experimental data. The thermal conductivity was expressed as a function of Gd<sub>2</sub>O<sub>3</sub> atomic fraction and temperature within a fitting error of 6%. The recommended equation of Ishimoto [1] for the thermal conductivity, K, in W.m<sup>-1</sup>.K<sup>-1</sup> is:

$$K_{95} = \frac{K_0}{x} \arctan(x) + 3.94 \times 10^{-11} T^3 \quad (1)$$

$$K_0 = \frac{1}{2.45 \times 10^{-2} + 2.56 \times 10^{-4} T} \quad (2)$$

$$x = 3.31 \exp(-7.61 \times 10^{-4} T) \sqrt{y K_0} \quad (3)$$

y: Gd<sub>2</sub>O<sub>3</sub> Content,

where the temperature, T is in K. K<sub>0</sub> is the thermal conductivity for point defect free UO<sub>2</sub>, x is the phonon scattering parameter by the impurity, The first term in this Eq. 1 represents the contribution

from phonons. The second term represents the electron contribution. Data used for the assessment of thermal conductivity of (U,Gd)O<sub>2</sub> and UO<sub>2</sub> are shown in Table 1. Calculated values of the thermal conductivity for solid (U,Gd)O<sub>2</sub> from Eq. 1 are tabulated as a function of temperature in Table 2 and are shown in Fig. 1, which includes uncertainty bands. Comparisons of thermal conductivity of solid (U,Gd)O<sub>2</sub> from these equations with the experimental data [3, 5–11] are shown in Fig. 2–6.

### Uncertainties

Ishimoto [1] estimated the uncertainties in thermal conductivities calculated with their equation as 6% from 400K to 2000K.

### Discussion

The theory of thermal conductivity of (U,Gd)O<sub>2</sub> may be interpreted as similar to the case for UO<sub>2</sub>. The total thermal conductivity results from the phonon contribution and electron contributions.

$$K = K_p + K_e + K_r \quad (4)$$

$$K_p = \frac{1}{A + BT} \quad (5)$$

$$K_e = DT \exp\left(-\frac{E_a}{kT}\right) \left[ 1 + H\left(\frac{E_a}{kT} + 2\right)^2 \right] \quad (6)$$

$$K_r = kT^3 \quad (7)$$

K<sub>p</sub>: thermal conductivities due to the phonon contribution, K<sub>e</sub>: thermal transport by electronic charge carriers with both electrons and holes contributing to the conduction, K<sub>r</sub> thermal conductivity due to heat radiation. E<sub>a</sub> is activation energy of electron or void, k is the Boltzmann constant, A,B,D,H are constants.

The Gd<sub>2</sub>O<sub>3</sub> natural structure is built on a cubic body-centered lattice with a mesh parameter equal to 10.818Å (with 16 molecules by unit cell) against 5.4682 Å for the UO<sub>2</sub> cubic face-centered lattice (with 4 molecules by unit cell) [12]. Even if Gadolinium is homogeneously mixed with Uranium, the Gd<sub>2</sub>O<sub>3</sub> motifs are much more complex than that of UO<sub>2</sub>. The presence of Gadolinium means a strong distortion the UO<sub>2</sub> lattice in its surrounding and results in an increase of the defects population. It can be assumed that the number of defects increase faster and faster as gadolinium content increases; so the thermal conductivities decrease gradually with increase in gadolinium content. But their decreasing rates become smaller at higher temperatures. The additional thermal resistivity caused by phonon-lattice defect interactions can be reasonably explained by the lattice defect model for dielectric solids considering U<sup>4+</sup>, U<sup>5+</sup> and Gd<sup>3+</sup> ions in the lattice as phonon scattering centers. The lattice strain caused by the dissolution of gadolinium contributes predominantly to the lattice defect thermal resistivity compared to the mass difference. On the other hand, the Gadolinium modifies also phonon-phonon scattering because of its different mass (157g against 238g for Uranium).

Fukushima [2] gives the following equation of the thermal conductivities due to the phonon contribution based on theoretical consideration and experimental data

$$K = \frac{1}{A + BT} \quad (8)$$

The temperature dependence of the thermal conductivities up to around 1600K satisfies the phonon conduction equation (Eq. 8), when the values of A increase gradually with gadolinium content, while those of B decrease slightly [2, 13]. The data of Fukushima [2] are about 10~30% lower than that of most authors for Gd content from 0 to 14.2% mol. His calculated data are lower than his experimental data up to 10% mol Gd at high temperature.



Massih [5] described the overall thermal conductivity correlation used for (U,Gd)O<sub>2</sub> by the extension of Reymann's correlation [14] to urania-gadolinia fuel:

$$K = p \left[ \frac{1}{A + a_0 x + BT} + C \exp(dT) \right] \quad (9)$$

Where p is the porosity correction factor:

$$p = \frac{1 - \beta(1 - \rho_{TD})}{1 - \beta(1 - 0.95)} \quad (10)$$

$\beta = 2.58 - 0.58T$ , T the temperature in degrees Celsius,  $\rho_{TD}$  the fraction of theoretical density and  $A = 0.1149$ ,  $a_0 = 1.1599$ ,  $B = 2.48 \times 10^{-4}$ ,  $C = 0.01216$ ,  $d = 0.001867$ . The thermal conductivity calculated from Eq. 9 is lower than found in most experiments.

The thermal conductivity is described by a continuous decreasing function of temperature. However, it can be observed that at high temperatures (2000°C) the fuel thermal conductivity increases. This behaviour is representative of an improvement of the energy transportation by free electrons at high temperatures. Free electrons population increases faster and faster when temperature increases. This often leads to describe this term as proportional to the temperature at the third power.

$$K_e = CT^3 \quad (11)$$

Finally the thermal conductivity can be empirically simulated by a formula of the following type:

$$K = \left( \frac{1}{A + BT} + CT^3 \right) D(T) \quad (\text{W/m/K}) \quad (12)$$

$$A = A_0 + A_1 X + A_2 y + A_3 y^2 \quad (13)$$

$$B = B_0 + B_1 y + B_2 y^2 \quad (14)$$

Where  $A_0 = 0.0524$        $A_1 = 4.0$        $A_2 = 0.3079$        $A_3 = 12.2031$

$B_0 = 2.553 \times 10^{-4}$        $B_1 = 8.606 \times 10^{-6}$        $B_2 = -0.0154$

X: absolute value of (2-O/MO)

T: local temperature (°C),

y: gadolinium content

Porosity correction (LOEB and ROESS law [15])

$$D(T) = \frac{1 - \rho \alpha(T)}{1 - 0.05 \alpha(T)} \quad (15)$$

$$\alpha(T) = 2.7384 - 0.58 \times 10^{-3} T \quad T < 1273.15 \text{ } ^\circ\text{C} \quad (16)$$

$$\alpha(T) = 2 \quad T > 1273.15 \text{ } ^\circ\text{C} \quad (17)$$

Baron [7] considered in detail the effect of stoichiometry, Porosity(p) and the Gd content on thermal conductivity of (U,Gd)O<sub>2</sub>. But thermal conductivity given by equations of Baron [7] are higher than most experimental data.

Klemens [16, 17] proposed a thermal conductivity model based on relaxation-time theory when phonon-phonon scattering and phonon-point defect scattering occur simultaneously. The phonon scattering parameter, X, is nearly proportional to the square root of the concentrations of Gd<sup>3+</sup> from the thermal conductivity analyses of Gd<sub>2</sub>O<sub>3</sub> [6, 18] and UO<sub>2-x</sub>. Hirai [6], Amaya [8], Ishimoto [1] proposed

the equations of the lattice thermal conductivity in the same form. Ishimoto[1] corrected the parameters in the Eq. 1 and developed the Eq. 1–3. A large effect from phonon-phonon scattering occurs in  $\text{UO}_2$  at low  $\text{Gd}_2\text{O}_3$  content solid solutions, while the phonon-point defect scattering dominates the thermal transfer process in the high  $\text{Gd}_2\text{O}_3$  content doped  $\text{UO}_2$  solid solutions.

### ***Comparison with recommendation***

The recommended equation of Ishimoto [1] is compared in Figure 6 with curves from the available data [3, 5–11]. The recommended equation is close to the equation of Hirai [6], which is lower relative to the equation [1] on higher content of Gd. The equations of Baron [7] are higher than the recommended data [1] from 373 to 2000K; the experimental data of Fukushima [2] are lower than the recommended data by Ishimoto [1] from 688K to 1688K.

The deviation from 300 to 2000K is defined by:

$$\text{Deviation}(\%) = \frac{K(\text{Data}) - K(\text{Recommended})}{K(\text{Recommended})} \times 100\% \quad (18)$$

Percent deviations of the data from this equation are shown in Fig.7.

Effect of Porosity:

Thermal conductivity was normalized to 95% of the theoretical density using the modified Loeb equation by Hirai [6]:

$$K_m = K_{th} (1 - \beta\rho) \quad (19)$$

Where  $K_{th}$  is the thermal conductivity of sample with a density of 100%TD.  $\rho$  the porosity and  $\beta$  the experimental parameter. Goldsmith and Douglas [20] found that the constant  $\beta$  was very sensitive to the stoichiometry of sample, and reported  $\beta$  values varying between 2.8 and 1.5 for samples oxygen-uranium ratios of 2.00 and 2.015 respectively, but Moor and McElroy reported a much lower values of 1.2, Breandt & Neuer[19] reported that is:  $\beta = 2.6 - 5 \times 10^{-4} (T - 273.15)$ , where T is the temperature in K. Thermal conductivity normalized to 95%TD,  $K_{95}$  could be expressed by:

$$K_{95} = K_m \frac{1 - 0.05\beta}{1 - \beta\rho} \quad (20)$$

Where subscript M and 95 denote the measured value and the value corresponding to 95% of theoretical density, respectively,  $\rho$  is the fraction of the porosity.

Table 1. Assessed data of thermal conductivity of (U,Gd)O<sub>2</sub> and UO<sub>2</sub>

Author	Year	Temperature range (K)	Content of Gd (mol%)	Accuracy(%)
Fukushima[2]	1982	688-1688	1.5, 3.0, 6.0, 9.0, 12.0, 15.0	10
Jl[3]	1983	573.15-1873.15	7.27	5
Preston[4]	1989	293-1630	4.4, 7.3	5
Massih[5]	1990	500-1900	14.2	
Hirai[6]	1991	400-2023	4.4,7.3,10.1,14.2	6
Ishimoto[1]	1994	298-1800	4.4,7.3,10.1,14.2	
Baron[7]	1995	250-1800	0~16.9	
Amaya[8]	1996	293-1400	14.2	
Amaya[9]	1997	300-1400	14.2	
Jiang[10]	1999	400-2100	4.4,10.1,14.2	5
Fink[11]	2001	298-2670	0	7

Table 2. Recommended values for thermal conductivity of (U,Gd)O<sub>2</sub> in W.m<sup>-1</sup>.K<sup>-1</sup>

Temp (K)	Content of Gd <sub>2</sub> O <sub>3</sub> , mol%				
	0	4.4	7.3	10.1	14.2
300	7.35	5.96	5.08	4.53	3.99
400	6.27	5.28	4.58	4.13	3.67
500	5.46	4.77	4.2	3.83	3.43
600	4.84	4.35	3.9	3.59	3.25
700	4.34	4.01	3.65	3.39	3.1
800	3.94	3.71	3.43	3.21	2.96
900	3.61	3.46	3.23	3.05	2.85
1000	3.32	3.24	3.06	2.91	2.74
1100	3.08	3.05	2.9	2.79	2.64
1200	2.88	2.88	2.76	2.67	2.55
1300	2.70	2.73	2.64	2.56	2.47
1400	2.56	2.6	2.53	2.47	2.39
1500	2.43	2.49	2.44	2.39	2.32
1600	2.33	2.39	2.35	2.31	2.26
1700	2.26	2.31	2.28	2.25	2.21
1800	2.21	2.25	2.22	2.2	2.16
1900	2.19	2.19	2.17	2.15	2.13
2000	2.18	2.15	2.14	2.12	2.1
2100	2.20	2.12	2.11	2.1	2.08

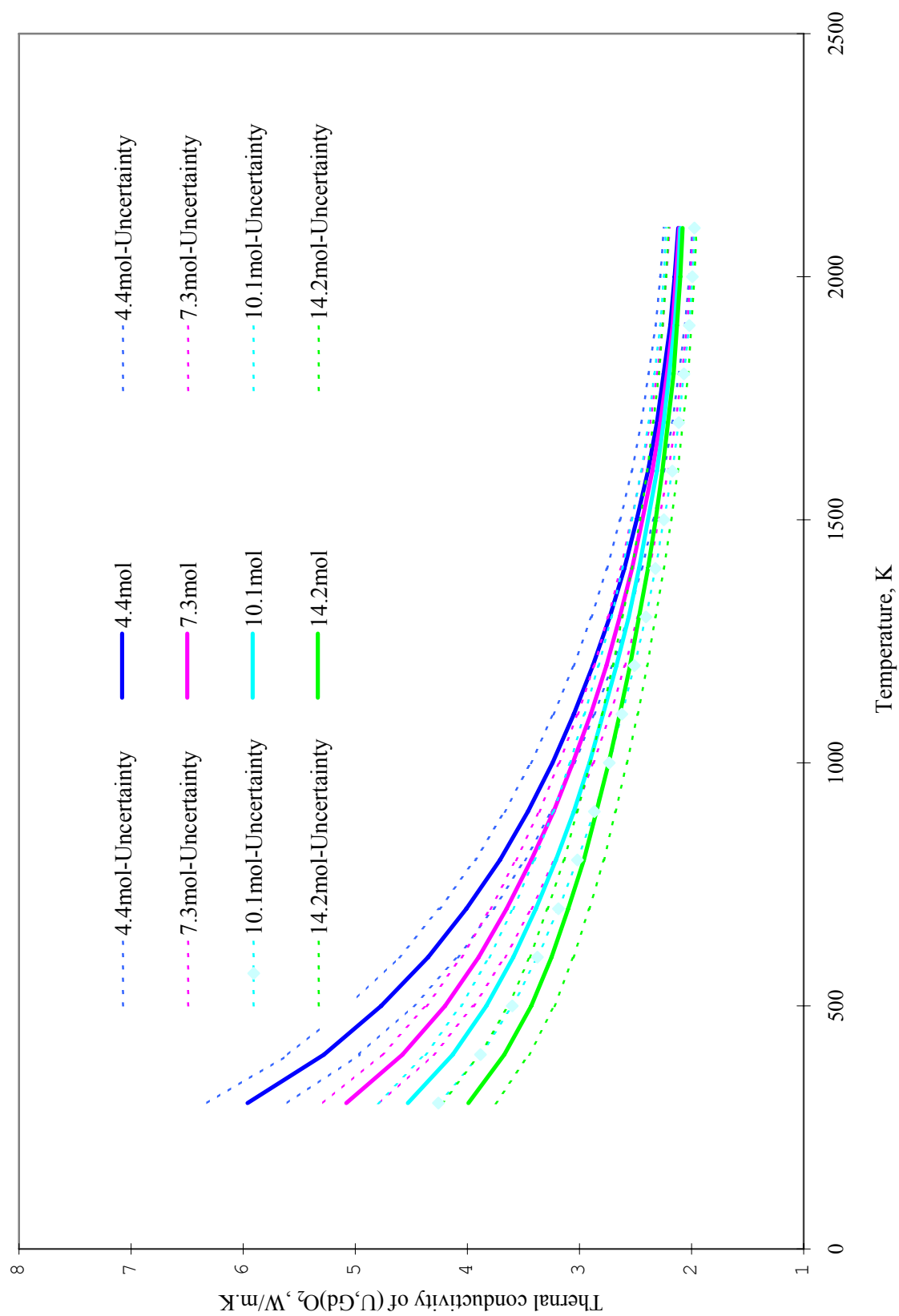


FIG. 1. Recommended values of thermal conductivity of (U,Gd) O<sub>2</sub>..

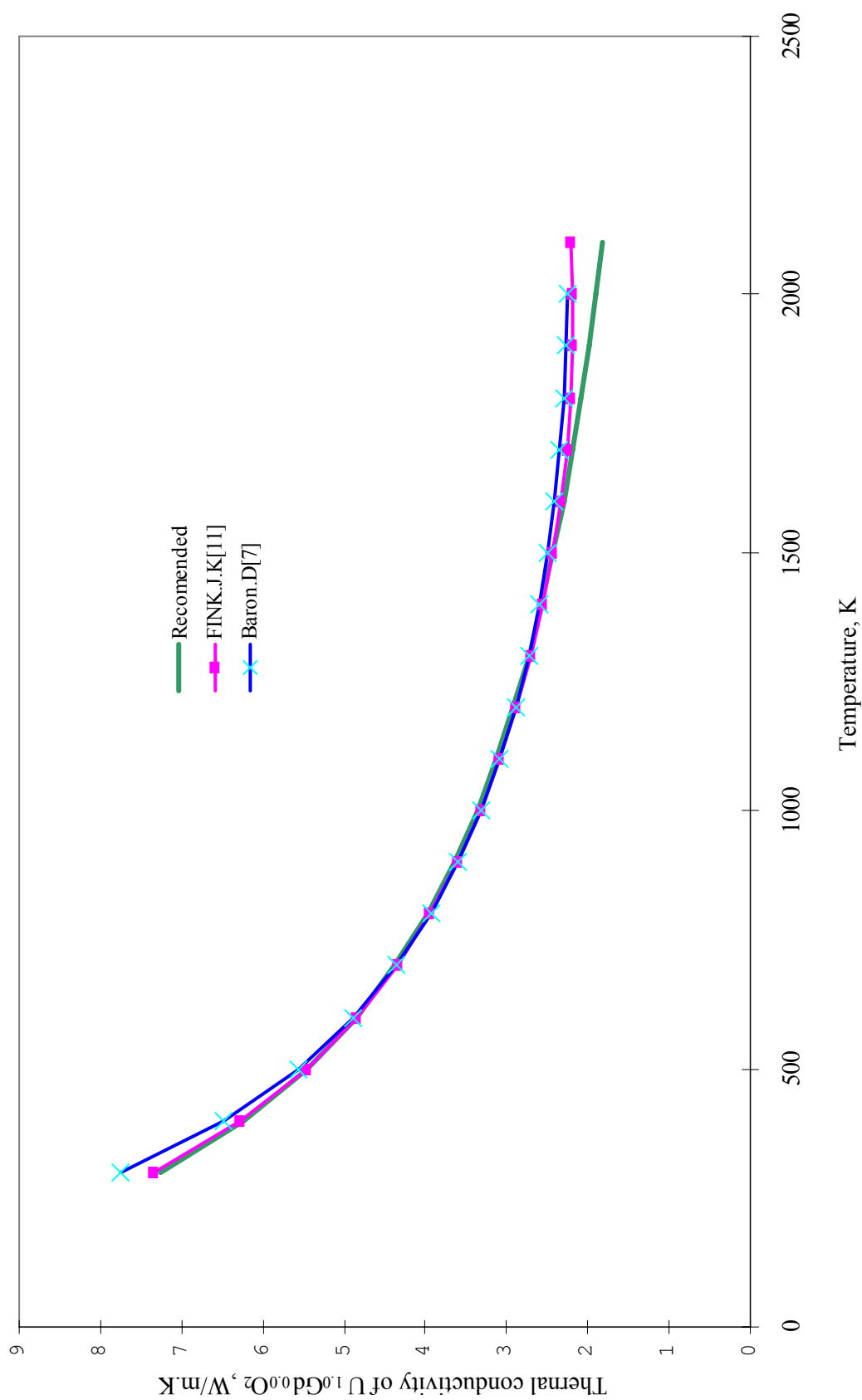


FIG. 2. Recommended values of thermal conductivity of  $U_{1.0}Gd_{0.0}O_2$  with Fink fit to  $UO_2$  Data.

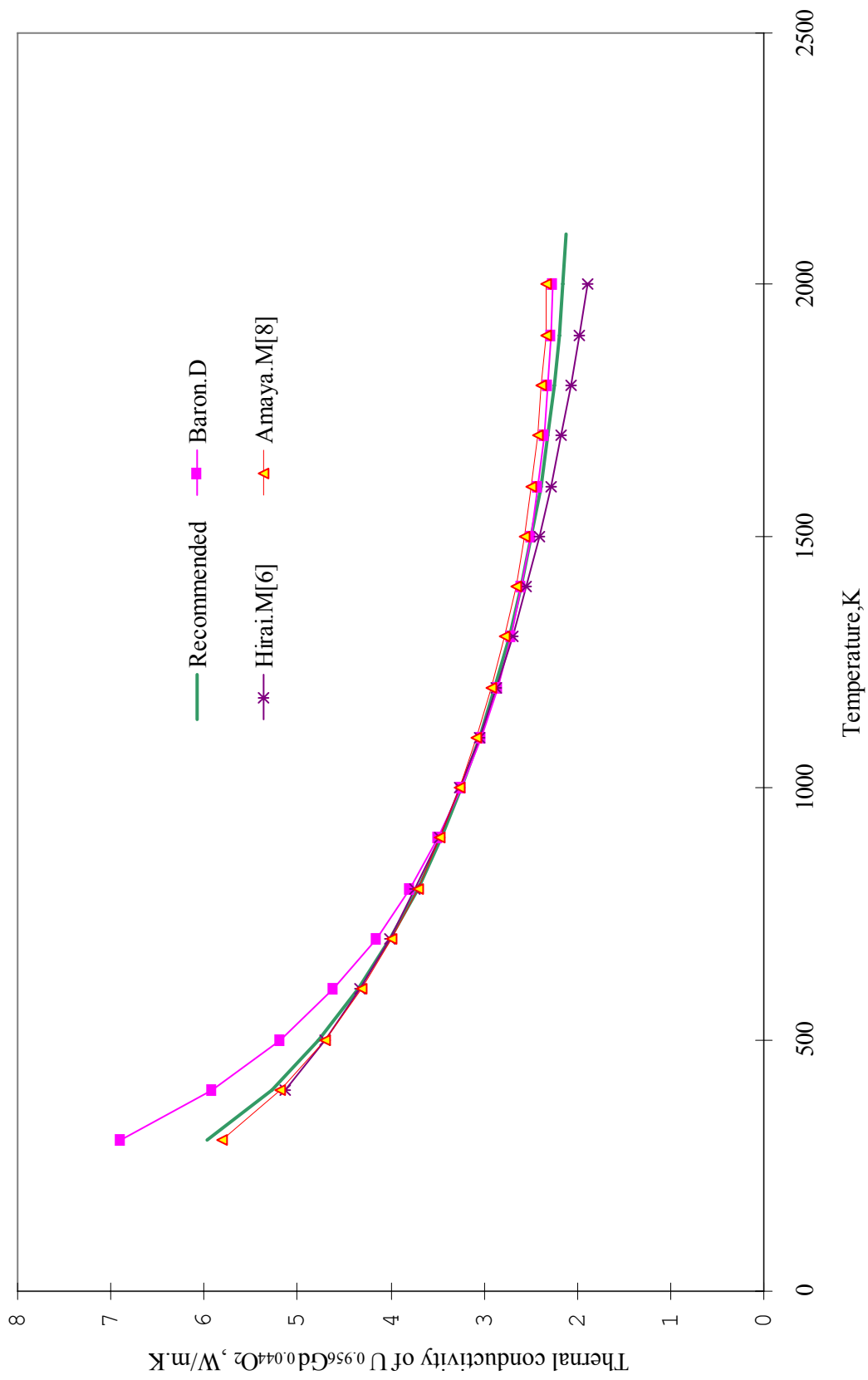


FIG. 3. Recommended values of thermal conductivity of  $U_{0.956}Gd_{0.044}O_2$  with experimental data.

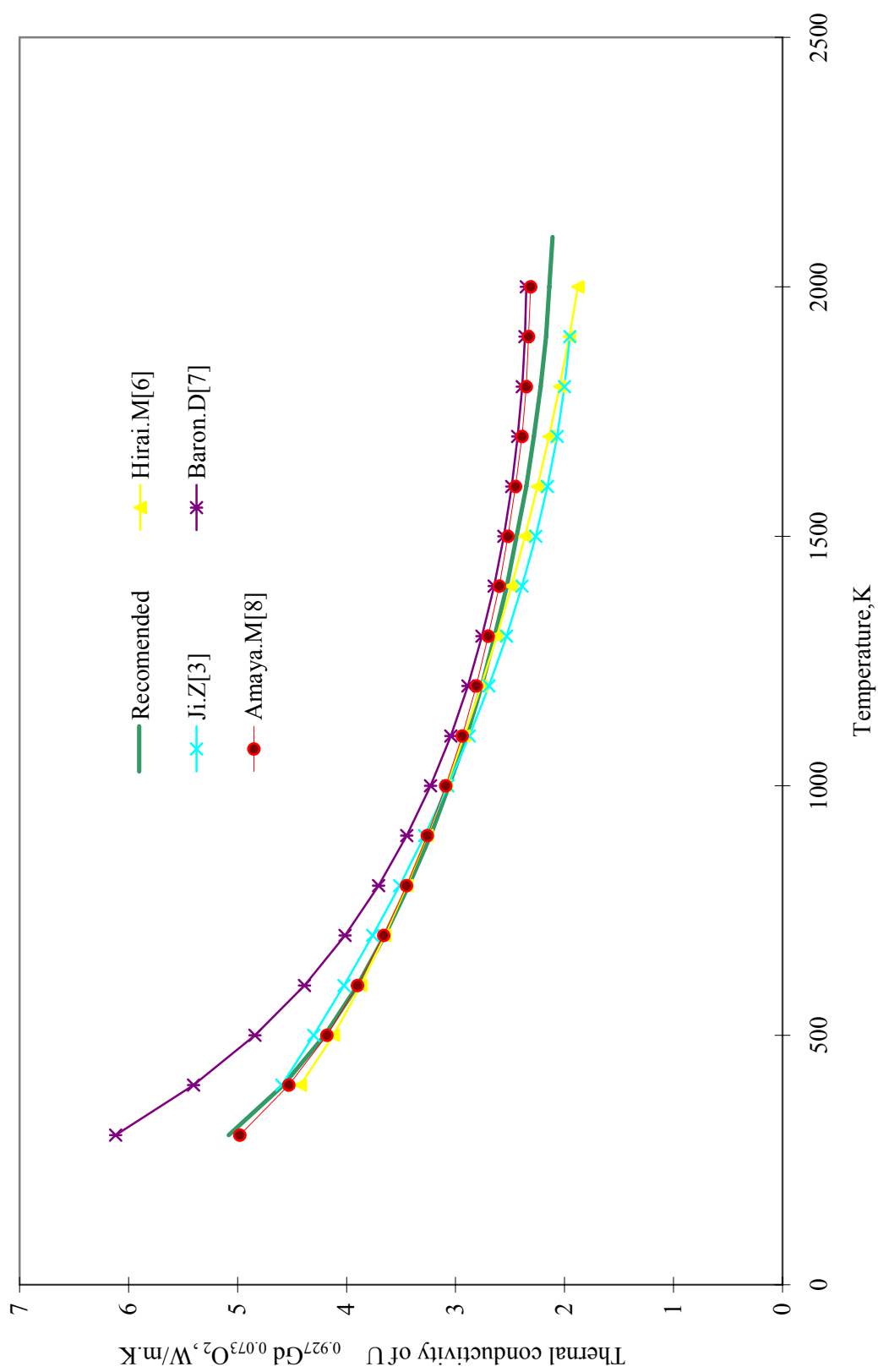


FIG. 4. Recommended values of thermal conductivity of  $U_{0.927}Gd_{0.073}O_2$  with experimental data.

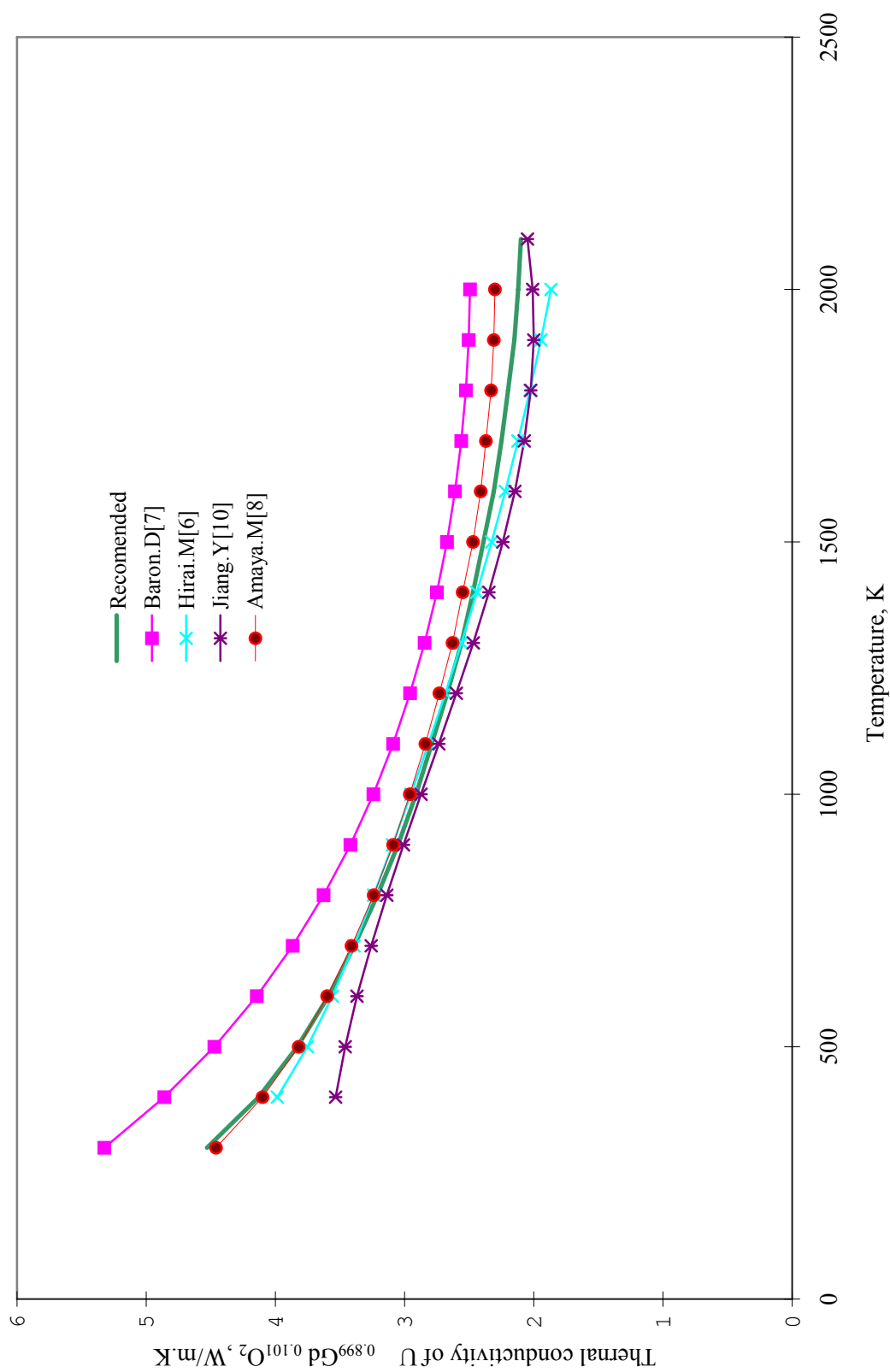


FIG. 5. Recommended values of thermal conductivity of  $U_{0.899}Gd_{0.101}O_2$  with experimental data.



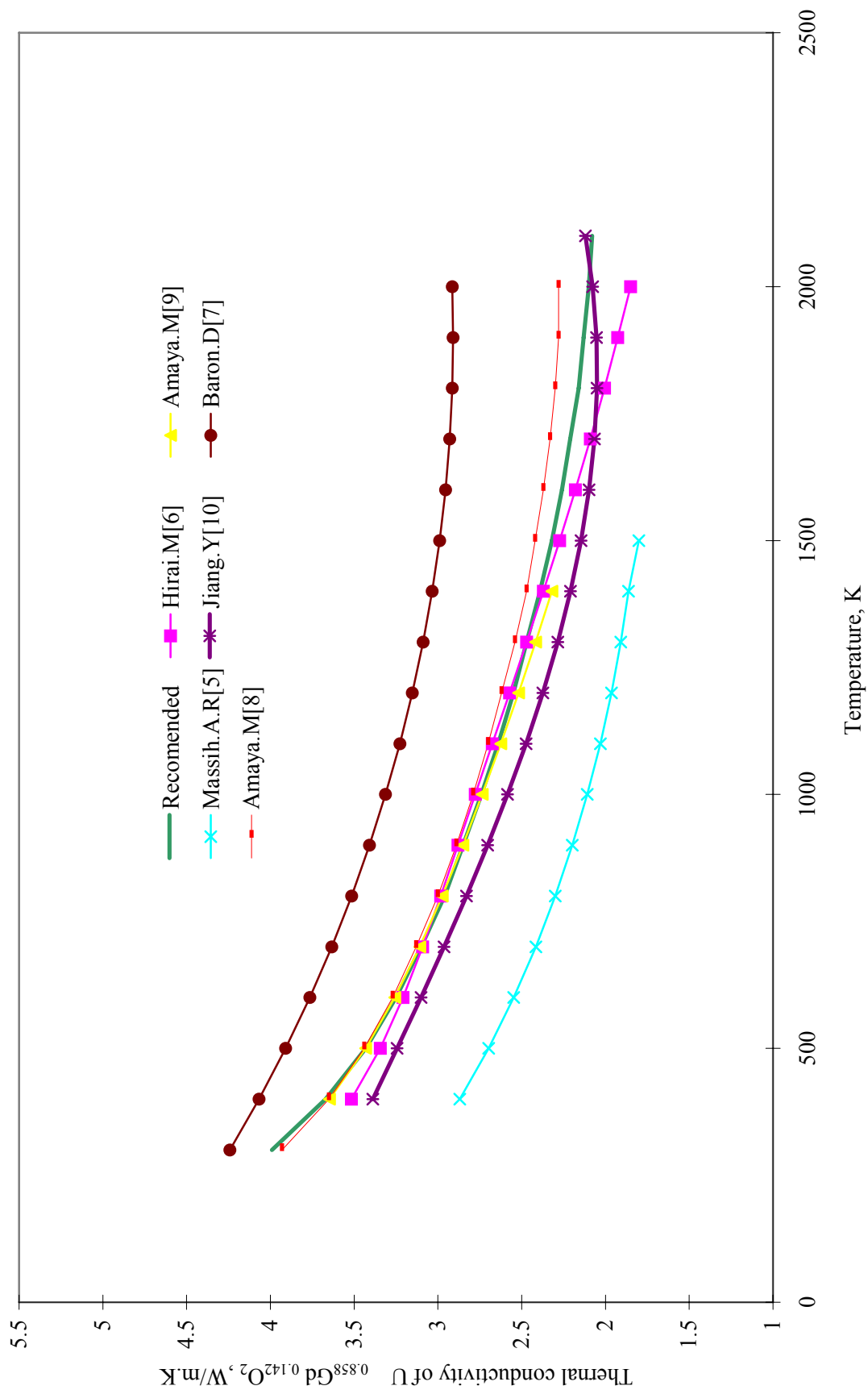


FIG. 6. Recommended values of thermal conductivity of  $U_{0.858}Gd_{0.142}O_2$  with experimental data.

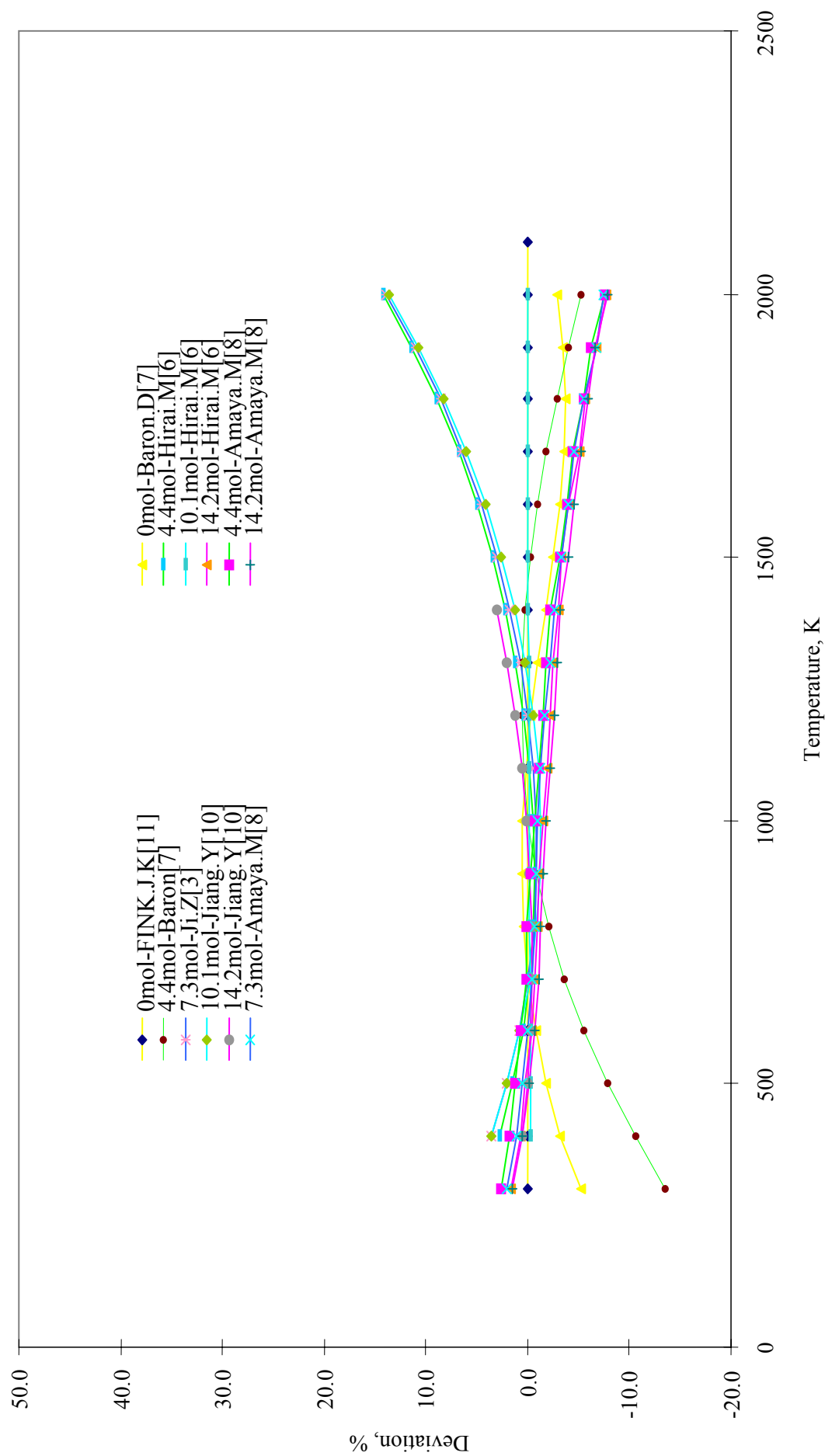


FIG. 7. Deviation of  $(U,Gd)O_2$  thermal conductivity from the recommended equation of Ishimoto [1].

## REFERENCES TO SECTION 6.1.3.2

- [1] ISHIMOTO, S., J.Nucl.Sci.Technol.31, 796 (1994).
- [2] FUKUSHIMA, S., J.Nucl.Mater.105, 201 (1982).
- [3] JI, Z., YING, S., Conference on Nuclear Materials of China , Chengdu. (1983).
- [4] PRESTON, S.D., High Tem-High Press 21, 287-295 (1989).
- [5] MASSIH, A.R., J.Nucl.Mater.173, 247 (1990).
- [6] HIRAI, M., J.Nucl.Sci.Technol.28, 995-1000 (1991).
- [7] BARON, D., COUTY, J.C., A proposal for a unified fuel thermal conductivity model available for UO<sub>2</sub>, (U-Pu)O<sub>2</sub> and UO<sub>2</sub>-Gd<sub>2</sub>O<sub>3</sub> PWR fuel. IAEA-TECDOC-957, p229 (1995).
- [8] AMAYA, M., J.Nucl.Mater.231, 29 (1996).
- [9] AMAYA, M., J.Nucl.Mater.246, 158 (1997).
- [10] JIANG, Y., the first meeting of the Co-ordination Research Program on “Establishment of a Thermophysical Properties Database for Light Water Reactors and Heavy Water Reactors”, Vienna, (1999).
- [11] FINK, J.K., J.Nucl.Mater.279, 1 (2001).
- [12] TAYLOR, A., KAGLE, B.J., Crystallographic data on metal and alloy structures, Westinghouse Research Laboratories, S1013-Dover Publications New York, (1962).
- [13] YING, S. and JI, Z., Thermal Diffusivity and Thermal Conductivity of Sintered UO<sub>2</sub> and UO<sub>2</sub>-Gd<sub>2</sub>O<sub>3</sub>, Proceedings of the 1<sup>st</sup> Asian Thermophysical properties Conference, Beijing, ISTIC-TR-C-000241, (1986).
- [14] REYAMANN, G.A., in: MATPRO version II: A Handbook of Materials Properties for Use in the Analysis of Light Water Reactor Fuel Behavior, eds. D.L.Hagrman and G.A. Reymann, EG and G.Idaho Report NUREG-CR-0497 (1979).
- [15] LORB, A.L., Journal of American Ceramic Society, 37:96, (1954).
- [16] KLEMENTS, P.G., Proc.Phys.Soc.A68, 1113 (1955).
- [17] Idem:Phys. Rev., 119:507 (1960).
- [18] AMAYA, M., HIRAI, M., KUBO, T., J.Nucl.Mater.231, 29 (1996).
- [19] BRANDT, R., et al., J. Non-Equilib. Thermodyn, 1:3 (1976)
- [20] GOLDSMITH, L.A., DOUGLAS, J.A.M., J.Nucl.Mater.47, 31 (1973).

### *1.1.1.2. 6.1.3.3. Thermal expansion of solid (U,Gd)O<sub>2</sub>*

#### **Summary and recommended equations**

Based on the thermal expansion data of (U,Gd)O<sub>2</sub> measured by Une [1], Jiang deduced the recommended equations, for the temperature range from 300 to 2000 K as a function of the Gd<sub>2</sub>O<sub>3</sub> content. No data on the linear thermal expansion for (U,Gd)O<sub>2</sub> above 2200K have been published in open literature. The recommended equations can be extended to 2200 K with 4% uncertainty.

The recommended equations for the linear thermal expansion of (U,Gd)O<sub>2</sub> by Jiang are:

$$L = L_{273}(a + bT + cT^2) \quad (1)$$

$$a = 9.9866 \times 10^{-1} \quad b = 7.2512 \times 10^{-6}$$

$$c = 2.0463 \times 10^{-13} g^2 + 3.4846 \times 10^{-11} g + 2.0653 \times 10^{-9}$$

g: Gd<sub>2</sub>O<sub>3</sub> weight percent

where L and L<sub>273</sub> are the lengths at temperature T(K) and 273 K, respectively. Data used in the assessment of the linear thermal expansion of (U,Gd)O<sub>2</sub> and UO<sub>2</sub> are shown in Table 1. The fractional change in the linear thermal expansion of (U,Gd)O<sub>2</sub>,  $\Delta L/L_{273}$ , expressed as a percent is shown in Fig. 1 with the uncertainties recommended by JIANG given as dotted lines. Recommended values are tabulated in Table 2. Comparison of the linear thermal expansion of (U,Gd)O<sub>2</sub>, calculated with these equations and the data of Une [1], FINK [2], Newman [3], Jiang [4], Qu [5] are shown in Figs 2–4.

Values for the fractional change in the volumetric thermal expansion of (U,Gd)O<sub>2</sub>,  $\Delta V/V_{273}$ , are given in Table 3.

The recommended equations for the instantaneous linear thermal expansion coefficients,  $\alpha$ , are linear

approximations to the exact partial differentials  $\left(\frac{1}{L} \cdot \frac{\partial L}{\partial T}\right)_p$  of eq.(1). The deviation of the instantaneous linear thermal expansion coefficients is not more than 3%. JIANG recommends:

$$\alpha = (b + 2cT) \quad (2)$$

Where  $\alpha$  is the linear thermal expansion coefficient in 1/K. Recommended values of the instantaneous linear thermal expansion coefficient of (U,Gd)O<sub>2</sub> are shown in Table2. Values for the instantaneous volumetric thermal expansion coefficient,  $\alpha$ , are given in Table 3

### Uncertainties

Une gave 3% accuracy for his data. Deviations from Une's data and the recommended data are 8% at 300K, 3.4% at 400K and less than 1% from 500 to 2000K respectively (Fig. 5). So the uncertainties are 85% at 300K, 6.5% at 400K and 4% from 500 to 2000K respectively.

### Discussion

Wada et al [6] measured the average thermal expansion coefficient for solid (U,Gd)O<sub>2</sub> in the composition range of 0~30 wt% Gd<sub>2</sub>O<sub>3</sub> up to a temperature of 1233 K, using a dilatometer. They found that additions of Gd<sub>2</sub>O<sub>3</sub> up to 12 wt% in UO<sub>2</sub> had little effect on the average thermal expansion coefficient which was  $10.5 \times 10^{-6} \text{ K}^{-1}$ . Beyond 12 wt%, the expansion coefficient increased slightly with Gd<sub>2</sub>O<sub>3</sub> content and was  $11.7 \times 10^{-6} \text{ K}^{-1}$  at 30% Gd<sub>2</sub>O<sub>3</sub>. Monin and Mathews [7] measured the linear thermal expansion of UO<sub>2</sub> and UO<sub>2</sub>-1.5 wt% Gd<sub>2</sub>O<sub>3</sub> in the temperature range of 298~1700 K, using high temperature X-ray diffractometry. They obtained an average thermal expansion coefficient ( $9.38 \times 10^{-6} \text{ K}^{-1}$ ) for UO<sub>2</sub>-1.5 wt% Gd<sub>2</sub>O<sub>3</sub> which was slightly smaller than that ( $10.07 \times 10^{-6} \text{ K}^{-1}$ ) for UO<sub>2</sub>. Their results are inconsistent with those by Wada et al [6].

Une [1] found that the linear thermal expansion of UO<sub>2</sub>-Gd<sub>2</sub>O<sub>3</sub> pellets increased with increasing Gd<sub>2</sub>O<sub>3</sub> content. The linear thermal expansions can be expressed by the following least square fitted equation for the temperature range from 298 to 1973K:

$$\Delta L/L_0 = A + BT + CT^2$$

Une [1] gave the following regression constants A, B and C, for the UO<sub>2</sub>-Gd<sub>2</sub>O<sub>3</sub> pellets (Table 4). The residual standard deviations range from  $5.2 \times 10^{-6}$  to  $9.4 \times 10^{-6}$ .

Jiang excluded data, which did not agree with the common consensus. In his assessment Jiang excluded the data of the linear thermal expansion of UO<sub>2</sub>-5.66%Gd<sub>2</sub>O<sub>3</sub> and UO<sub>2</sub>-8.5%Gd<sub>2</sub>O<sub>3</sub> from Newman [3] and of UO<sub>2</sub>-7%Gd<sub>2</sub>O<sub>3</sub> from Jiang [4] because their data are very close to that of UO<sub>2</sub>. The data for UO<sub>2</sub>-1.5%Gd<sub>2</sub>O<sub>3</sub> from Momin [7] were also discarded because his data are lower than that of UO<sub>2</sub>. Table 1 shows the thermal expansion data assessed by Jiang.

Percent deviations of the data from the recommended equations of Jiang are shown in Fig. 6. The percent deviations are defined as:

$$Deviation(\%) = \frac{\frac{\Delta L(Data)}{L} - \frac{\Delta L(Jiang)}{L}}{\frac{\Delta L(Jiang)}{L}} \cdot 100\% \quad (3)$$

The uncertainties are included in Fig. 6 which are expressed as a percentage.

Martin [8] examined the linear thermal expansion of UO<sub>2+x</sub>, and concluded that the thermal expansion of UO<sub>2+x</sub> is the same as that of UO<sub>2</sub> for x values from 0 to 0.13 and from 0.235 to 0.25 up to 1520K.

Because no data are available for the linear thermal expansion of (U,Gd)O<sub>2+x</sub>, Jiang assumes that the recommended equations here can be used to calculate the linear thermal expansion of (U,Gd)O<sub>2+x</sub> for x values of from 0 to 0.13.

Table 1. Data used for the assessment of the linear thermal expansion of (U,Gd)O<sub>2</sub> and UO<sub>2</sub>

AUTHOR	TEMPERATURE RANGE (K)	CONTENT OF GD <sub>2</sub> O <sub>3</sub> (Wt)	ACCURACY (%)
FINK.[2]	298-2000	0	3.0
Une [1]	298-1973	0,5,8,10	3.0
Newman [3]	298-1800	0,2.98,5.66,	No detailed
Jiang[4]	298-2000	0,3,7,10	2.0
Qu [5]	287-1800	5,8.5	2.0

Table 2. Recommended data for linear thermal expansion of (U,Gd)O<sub>2</sub>

T (K)	0		5		8		10	
	$\Delta L/L$ %	$\alpha \times 10^6 K^{-1}$	$\Delta L/L$ %	$\alpha \times 10^6 K^{-1}$	$\Delta L/L$ %	$\alpha \times 10^6 K^{-1}$	$\Delta L/L$ %	$\alpha \times 10^6 K^{-1}$
273	0.000	8.38	0.000	8.47	0.000	8.52	0.000	8.56
300	0.006	8.49	0.008	8.59	0.008	8.65	0.009	8.69
400	0.093	8.90	0.096	9.04	0.097	9.12	0.098	9.17
500	0.184	9.32	0.188	9.49	0.191	9.58	0.192	9.64
600	0.279	9.73	0.285	9.93	0.289	10.05	0.291	10.12
700	0.379	10.14	0.387	10.38	0.392	10.51	0.395	10.60
800	0.482	10.56	0.493	10.83	0.499	10.98	0.503	11.08
900	0.590	10.97	0.603	11.27	0.611	11.45	0.616	11.56
1000	0.702	11.38	0.718	11.72	0.728	11.91	0.734	12.04
1100	0.817	11.79	0.838	12.17	0.850	12.38	0.857	12.52
1200	0.937	12.21	0.962	12.61	0.976	12.85	0.985	13.00
1300	1.061	12.62	1.090	13.06	1.106	13.31	1.117	13.47
1400	1.190	13.03	1.223	13.51	1.242	13.78	1.254	13.95
1500	1.322	13.45	1.360	13.95	1.382	14.24	1.396	14.43
1600	1.459	13.86	1.502	14.40	1.527	14.71	1.543	14.91
1700	1.599	14.27	1.648	14.85	1.676	15.18	1.694	15.39
1800	1.744	14.69	1.799	15.30	1.830	15.64	1.850	15.87
1900	1.893	15.10	1.954	15.74	1.989	16.11	2.011	16.35
2000	2.046	15.51	2.114	16.19	2.152	16.58	2.177	16.82

Table 3. Recommended data for volumetric thermal expansion of (U,Gd)O<sub>2</sub>

T(K)	0		5		8		10	
	$\Delta V/V$ %	$\alpha \times 10^6 K^{-1}$	$\Delta V/V$ %	$\alpha \times 10^6 K^{-1}$	$\Delta V/LV\%$	$\alpha \times 10^6 K^{-1}$	$\Delta V/V$ %	$\alpha \times 10^6 K^{-1}$
273	0	25.14	0	25.41	0	25.56	0	25.68
300	0.018	25.47	0.024	25.77	0.024	25.95	0.027	26.07
400	0.279	26.7	0.288	27.12	0.291	27.36	0.294	27.51
500	0.552	27.96	0.564	28.47	0.573	28.74	0.576	28.92
600	0.837	29.19	0.855	29.79	0.867	30.15	0.873	30.36
700	1.137	30.42	1.161	31.14	1.176	31.53	1.185	31.8
800	1.446	31.68	1.479	32.49	1.497	32.94	1.509	33.24
900	1.77	32.91	1.809	33.81	1.833	34.35	1.848	34.68
1000	2.106	34.14	2.154	35.16	2.184	35.73	2.202	36.12
1100	2.451	35.37	2.514	36.51	2.55	37.14	2.571	37.56
1200	2.811	36.63	2.886	37.83	2.928	38.55	2.955	39
1300	3.183	37.86	3.27	39.18	3.318	39.93	3.351	40.41
1400	3.57	39.09	3.669	40.53	3.726	41.34	3.762	41.85
1500	3.966	40.35	4.08	41.85	4.146	42.72	4.188	43.29
1600	4.377	41.58	4.506	43.2	4.581	44.13	4.629	44.73
1700	4.797	42.81	4.944	44.55	5.028	45.54	5.082	46.17
1800	5.232	44.07	5.397	45.9	5.49	46.92	5.55	47.61
1900	5.679	45.3	5.862	47.22	5.967	48.33	6.033	49.05
2000	6.138	46.53	6.342	48.57	6.456	49.74	6.531	50.46

Table 4. Regression constants for equation of linear thermal expansion of UO<sub>2</sub>-Gd<sub>2</sub>O<sub>3</sub>

Gd <sub>2</sub> O <sub>3</sub> CONTENT(%)	A( $\times 10^{-3}$ )	B( $\times 10^{-6}$ )	C( $\times 10^{-9}$ )	STANDARD DEVIATION ( $\times 10^{-6}$ )	STANDARD DEVIATION FITTED TO Eq.(1) ( $\times 10^{-6}$ )
0	-2.238	7.165	2.095	5.2	1.69
5	-2.314	7.358	2.156	7.1	6.42
8	-2.391	7.433	2.278	9.4	6.53
10	-2.284	7.162	2.43	7.4	2.70

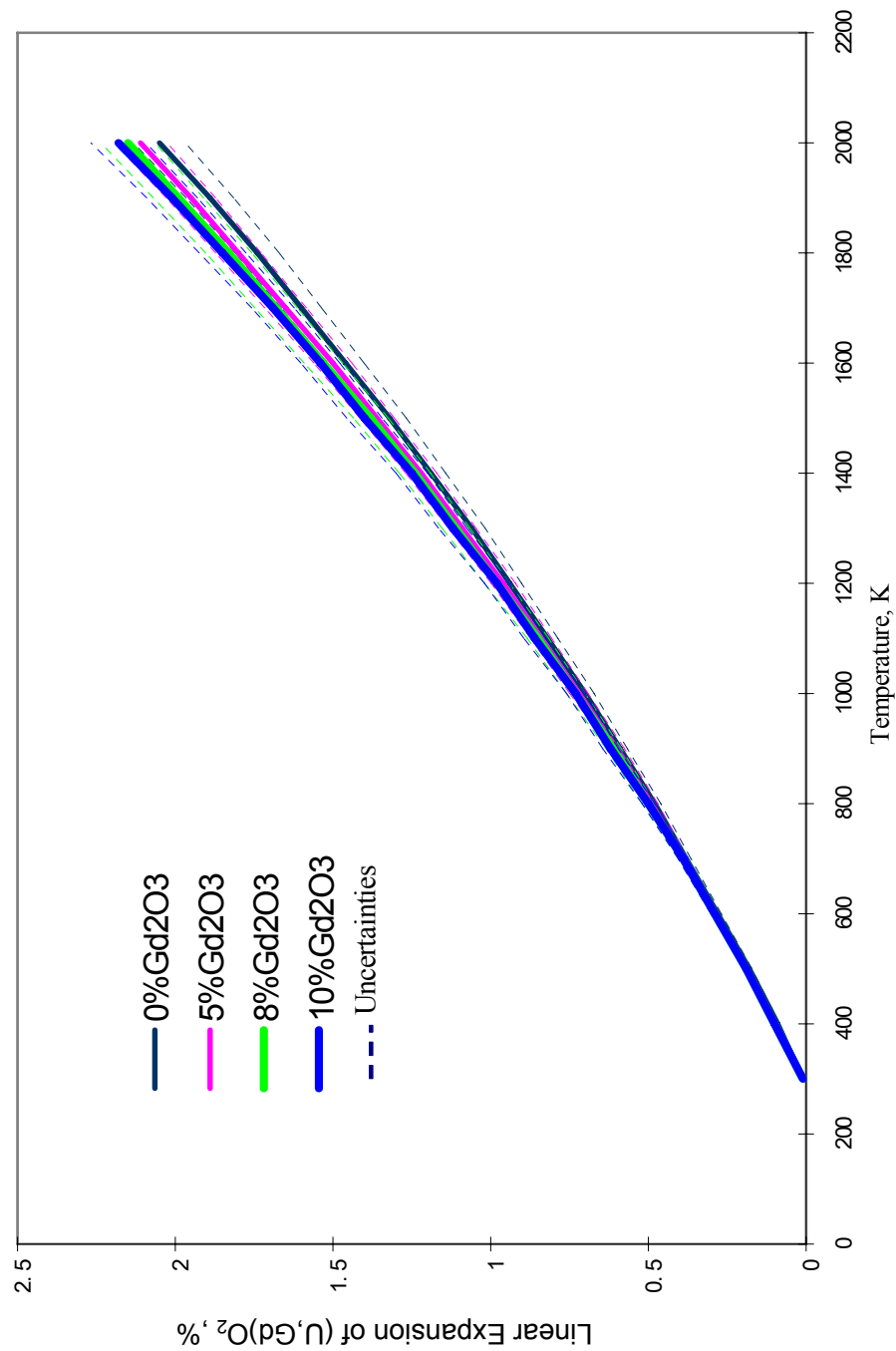


FIG. 1. Recommended linear expansion of (U,Gd)O<sub>2</sub>.

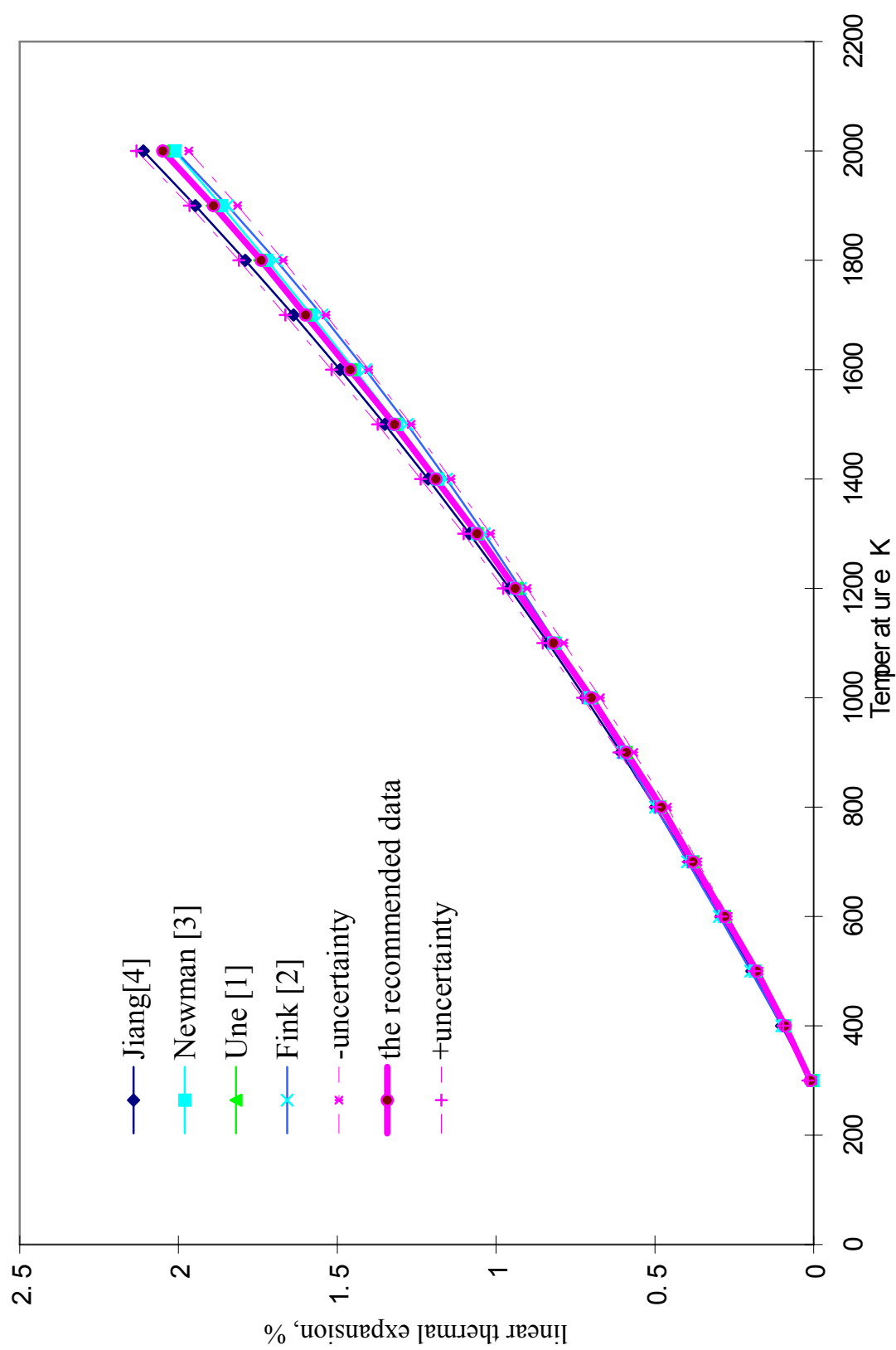


FIG. 2. Recommended  $UO_2-0\%Gd_2O_3$  linear thermal expansion with data published.



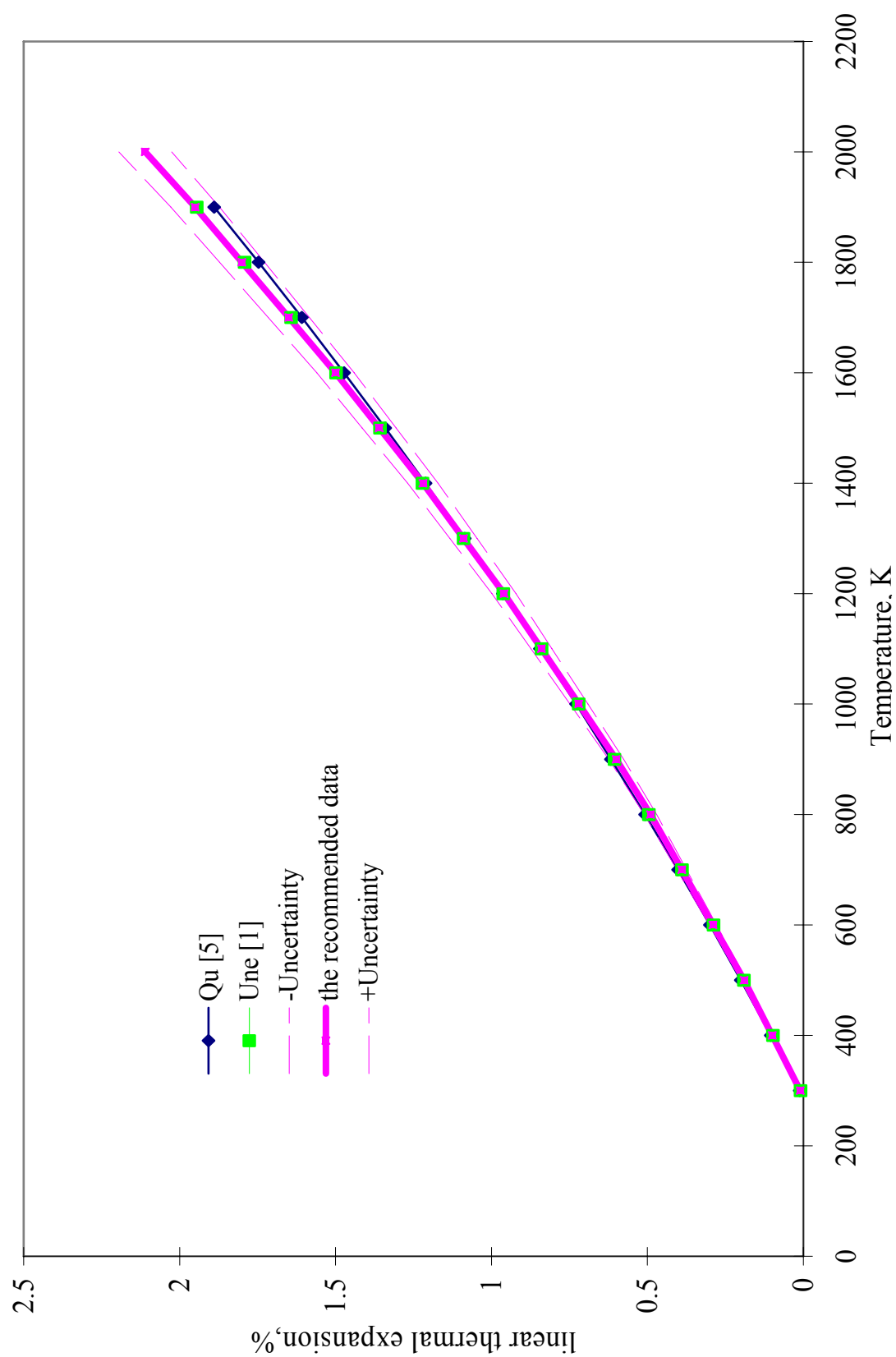


FIG. 3. Recommended  $\text{UO}_2\text{-5\%Gd}_2\text{O}_3$  linear thermal expansion with data published.

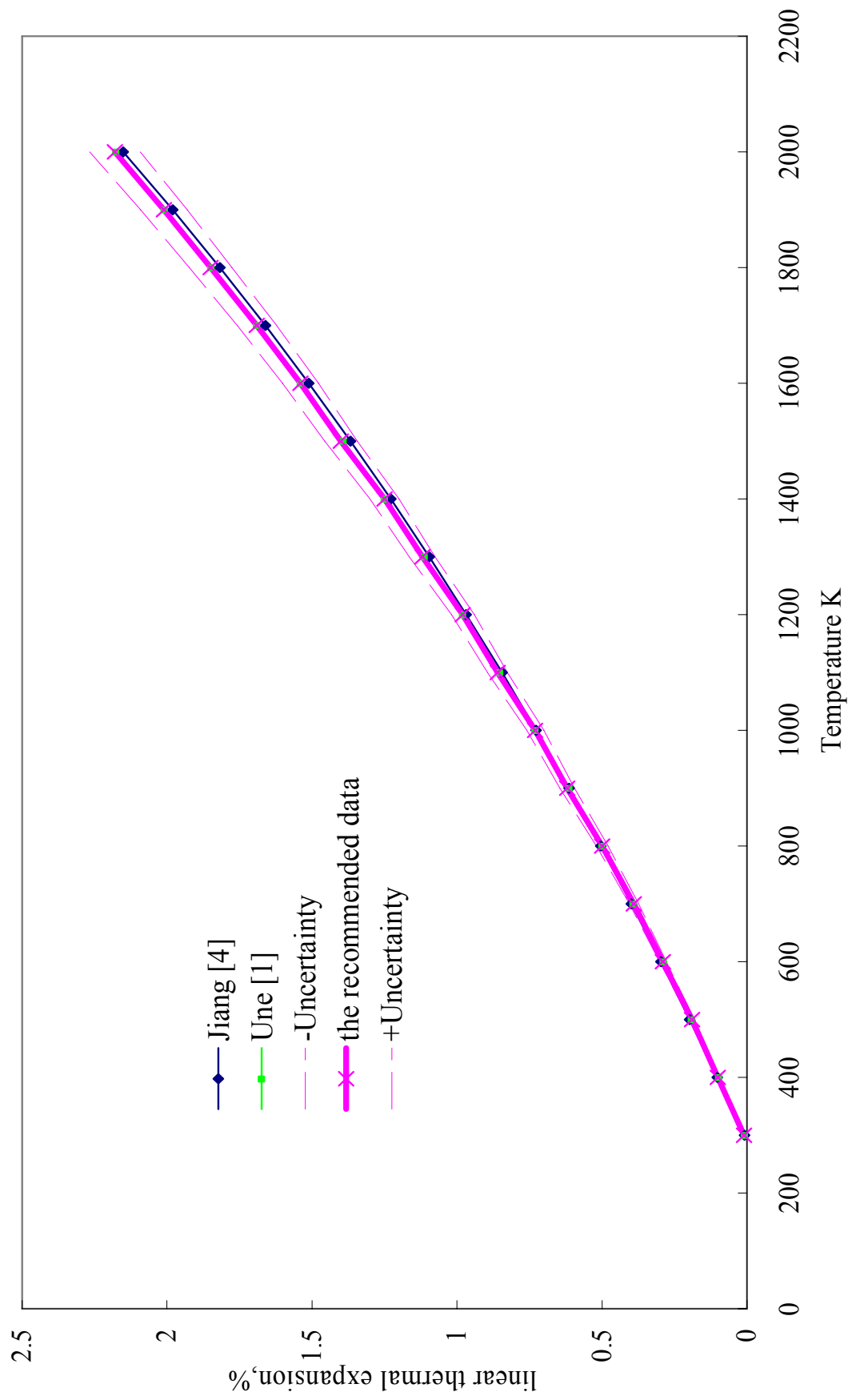


FIG. 4. Recommended  $\text{UO}_2\text{-10\%Gd}_2\text{O}_3$  linear thermal expansion with data published.

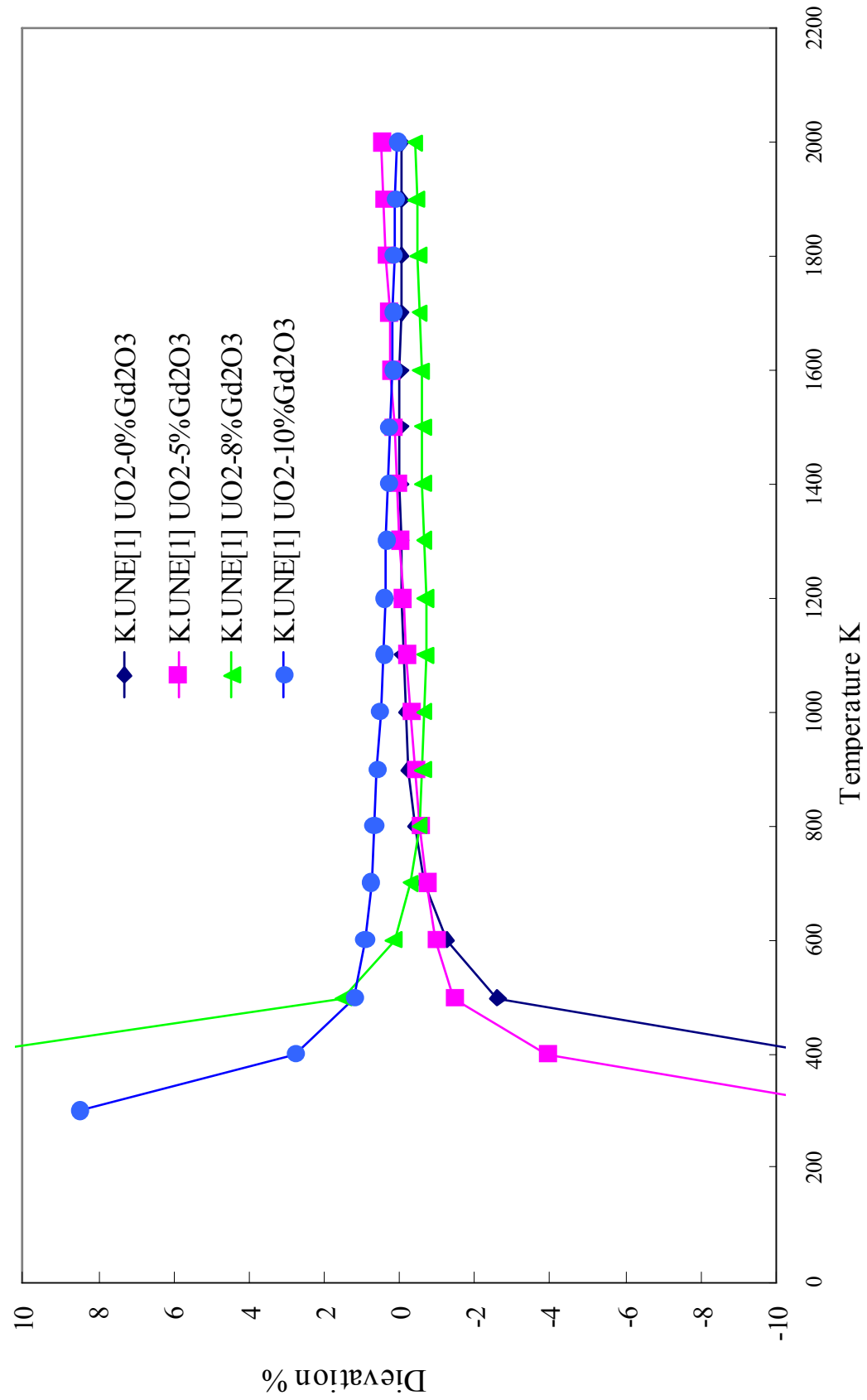


FIG. 5. Deviation between Une' and recommended data.

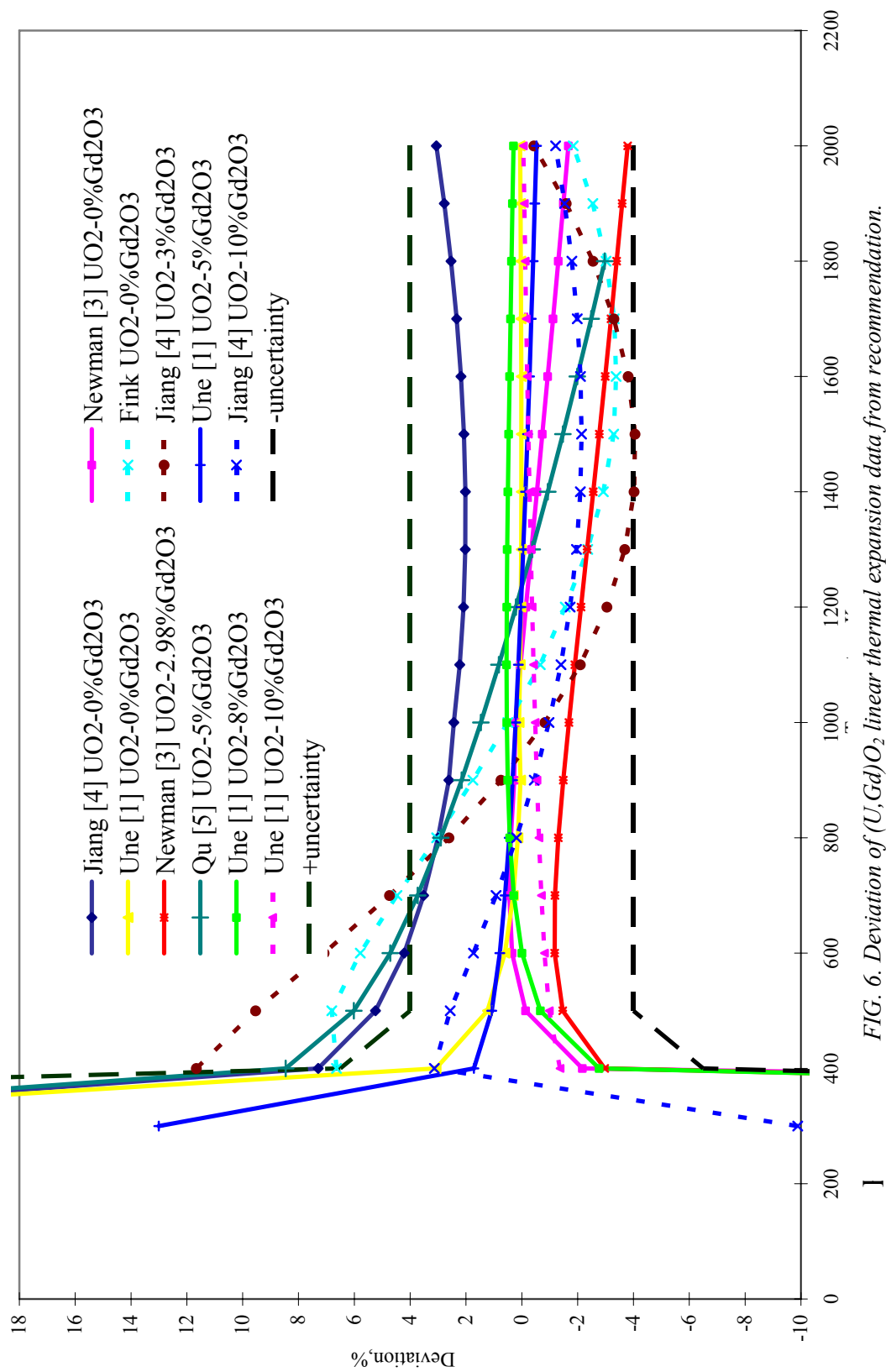


FIG. 6. Deviation of  $(U,Gd)O_2$  linear thermal expansion data from recommendation.

### REFERENCES TO SECTION 6.1.3.3

- [1] UNE, K., J.Nucl.Sci.Technol.23, 1020-1022 (1986).
- [2] FINK, J.K., J.Nucl.Mater.279, 1(2001).
- [3] NEWMAN, L., Thermal and Physical Properties of  $\text{UO}_2\text{-Gd}_2\text{O}_3$ . Babcock and Wilcox Utility Power Generation. Rep RAW-1759.86p, (1984).
- [4] JIANG, Y.R., the first meeting of the Co-ordination research program on “Establishment of a Thermophysical Properties Database for Light Water Reactors and Heavy Water Reactors”, Vienna,. (1999).
- [5] QU, F.Y., SUN, L.C., Conference of Nuclear materials (in Chinese), (1983).
- [6] WADA, T., NORO, K., TSUKUI, K., Prec.Int.Conf.of Nuclear Fuel Performance, London, p63, (1973).
- [7] MOMIN, A.C., MATHEWS, M.D, Indian J Chem. 15a, 1096 (1977).
- [8] MARTIN, D.G., J.Nucl.mater.152, 94 (1988).

#### 6.1.4 $\text{ThO}_2$ , $(\text{Th}_{1-y}\text{U}_y)\text{O}_2$ and $(\text{Th}_{1-y}\text{Pu}_y)\text{O}_2$ properties

##### *Introduction*

Thorium based fuels containing Uranium ( $\text{U}^{233}$ ) or Plutonium as the fissile content could be used in LWRs and PHWRs to breed  $\text{U}^{233}$ . In the process, the fertile element Thoria gets converted to fissile  $\text{U}^{233}$  increasing the fissile content in the fuel further.

Thorium utilization in Indian Nuclear Power programme to produce fissile  $\text{U}^{233}$  has of late become important because of its limited Uranium; but vast Thorium reserves. India has a very ambitious power programme to utilize its Thorium reserves in the Advanced Heavy Water Reactor (AHWR). The driver fuel will be in the form of  $\text{ThO}_2\text{-2\%U}^{233}\text{O}_2$  and  $\text{ThO}_2\text{-4\%PuO}_2$ . The advantages of Thoria based fuels are that the fissile  $\text{U}^{233}$  produced is burnt in the same reactor thereby reducing the problems related to handling, transportation and safeguard. Moreover, the transuranium wastes like ‘Pu’, ‘Np’ and ‘Am’ which are high level and long lived isotopes are reduced causing less problems in waste management.

To predict the performance of thorium based fuel or to generate a computer code for predicting in-pile fuel behavior under normal and accidental conditions, knowledge of thermophysical properties data base is of utmost importance. In this context, some of the important properties of  $(\text{Th}_y\text{U}_{1-y})\text{O}_2$  and  $(\text{Th}_y\text{Pu}_{1-y})\text{O}_2$  fuels systems have been measured as a function of composition (‘U’ and ‘Pu’ content) and temperature. The data generated or assessed on density, melting point, heat capacity/specific heat, thermal diffusivity/conductivity and thermal expansion have been reported in the following sections. These studies and the data reported form a part of an IAEA Co-ordinated Research Programme (IAEA CRP) on “Establishment of a thermophysical properties data base for LWRs and HWRs” under contract no 10683.

##### 6.1.4.1. *Melting point of $\text{ThO}_2$*

The assessments of the Melting point of  $\text{ThO}_2$  were provided by the Radiometallurgy Division, Bhabha Atomic Research Center, Mumbai, India.

##### *Recommendation*

The melting temperature of  $\text{ThO}_2$  recommended from the assessment here is 3651 K, which is the most recent and experimental data [8], and is in fairly good agreement with majority of the previous studies.

### **Uncertainties**

The uncertainty in the temperature measurement is  $\pm 17$  K.

### **Discussion**

The melting point of ThO<sub>2</sub> was experimentally measured or estimated by several authors [1–8]. Their results are summarized in Table 1. The reported values vary from 3323 to 3808 K. Peterson and Curtis [9], in their compilation of data on thorium based ceramics, arrived at two different values e.g. 3573 $\pm$ 100K from the work of Lambertson et.al. [4] on ThO<sub>2</sub>–UO<sub>2</sub> system and 3663 K from the work of Benz [5] on Th–ThO<sub>2</sub> system. Lambertson et. al. [4] first estimated the melting point of ThO<sub>2</sub> to be between 3558 K to 3828 K and subsequently arrived at an intermediate value of 3623 K by extrapolating the melting point data of (Th,U)O<sub>2</sub> compositions corresponding to zero UO<sub>2</sub> content. They further refined their data by introducing some corrections for the liquidus/ solidus curve to effect a curvature correction for the pure ThO<sub>2</sub> end to that of pure UO<sub>2</sub> end of the temperature composition diagram. Their final recommended data was 3575 K, which is in good agreement with the data 3543 K recommended by Christensen [6] from his experimentally measured melting point data on ThO<sub>2</sub>–UO<sub>2</sub> system and subsequent extrapolation to zero UO<sub>2</sub> content. Rand [10] however in his assessment of the data on thermo chemical properties, disagree with the curvature corrections made by others on the thorium or urania rich side of the temperature composition curve. He justified that the curvature need not be same at both the terminal compositions and the difference could be due to loss of ‘O’ from UO<sub>2</sub> in Urania rich side, which is different for Thoria rich side. He recommended a value of 3643 $\pm$  30 K, which is the average of the higher value of Lambertson et. al.[4] of 3613 K and that reported by Benz [5] for congruent melting temperature of 3663 K. Belle and Berman [11] used 3640 K as the melting point of ThO<sub>2</sub>, recommended by Rand [10] in his work on ThO<sub>2</sub>.

Ronchi and Hiernaut [8] had recently measured the melting temperature of ThO<sub>2</sub> (both stoichiometric and hypostoichiometric) material experimentally by heating a spherical sample by four symmetrically spaced pulsed Nd YAG laser and observing the cooling/heating curve with time. For stoichiometric ThO<sub>2</sub>, the measured melting point was found to be 3651 $\pm$ 17 K. This recent data of Ronchi and Hiernaut [8] reasonably agrees with the data generated by Benz [5] (3660 $\pm$ 100 K) and is also close to that recommended by Rand [10] (3643 $\pm$ 30 K). All these values are markedly different from those of Lambertson et.al. [4] It is also well understood that the curvature difference at the Uranium and Thorium rich side of the Temperature vs. composition diagram is quite justifiable and was attributed to the loss of ‘O’. Hence, the recommended melting temperature of ThO<sub>2</sub> should be taken as 3651 $\pm$ 17 K, which is the most recent and experimental data, and is in fairly good agreement with majority of the previous studies.

#### **6.1.4.2. Density of ThO<sub>2</sub> and (Th,U)O<sub>2</sub>**

The assessments of the Density of ThO<sub>2</sub> and (Th,U)O<sub>2</sub> solid solution were provided by the Radiometallurgy Division, Bhabha Atomic Research Center, Mumbai, India.

### **Recommendation**

The recommended equation for the theoretical density of ThO<sub>2</sub> –UO<sub>2</sub> as a function of the UO<sub>2</sub> content x and temperature (298–1600 K) is represented by

$$D = 10.087 - 2.891 \times 10^{-4} \cdot T - 6.354 \times 10^{-7} (x) \cdot T + 9.279 \times 10^{-3} (x) + 5.111 \times 10^{-6} (x)^2$$

### **Uncertainties**

The uncertainty of the above equation for estimation of theoretical density is  $\pm 0.28\%$ .

### **Discussion**

Theoretical density (D) of ThO<sub>2</sub> or (Th,U)O<sub>2</sub> solid solution can be estimated from the equation

$$D = 6.6423 \times 10^{-3} M/a^3 \quad (1)$$

where ‘M’ is the molecular weight, ‘a’ is the lattice parameter. Belle and Berman [11] calculated the theoretical density of ThO<sub>2</sub> – UO<sub>2</sub> solid solution for different UO<sub>2</sub> content (x) from the lattice

parameter data of Cohen & Berman [12]. The following equation shows the relationship between the theoretical density and the lattice constants.

$$D = 9.9981 + 0.0094 \cdot x - 8.7463 \cdot 10^{-6} \cdot x^2 + 1.1192 \cdot 10^{-7} \cdot x^3 \quad (2)$$

Density of (Th,U)O<sub>2</sub> system has also been calculated as a function of temperature by Momin & Venketeswarulu [13], Momin & Karkhanwala [14], Kempter and Elliott [15] and Springer et al. [16] from the lattice and bulk expansion data.

Their data are shown in Fig.1 and also presented in Table 2. Since the lattice expansion data is lower than that of bulk expansion, this results in lower bulk density than X-ray density. For example, at 298K the bulk density of ThO<sub>2</sub> is 9.49 Kg/m<sup>3</sup>, while the density measured from lattice parameter (X-ray) is 9.99 Kg/m<sup>3</sup>. Christensen [17] and Slage [18] determined the density of solid and liquid for UO<sub>2</sub> in the temperature range [273–3400 K] and [298–3100 K] respectively. Their data are also shown in Fig.1.

The density of (Th,U)O<sub>2</sub> system as a function of temperature and UO<sub>2</sub> content has been estimated in the following way. First, a linear relationship of lattice parameters of (Th,U)O<sub>2</sub> as a function of UO<sub>2</sub> was obtained from the literature data of lattice parameters [11, 12, 15, 19–28] at 298K (Fig. 2 ).

$$a_{298} = 0.55972 - 1.27819 \cdot 10^{-4} [\% \text{UO}_2] \quad (3)$$

$$\text{with } [R^2 = 0.99471, \text{SD} = 4.79 \times 10^{-4}]$$

A relationship for the average coefficient of linear thermal expansion in the temperature range (298–1600K) as a function of UO<sub>2</sub> content was obtained from the literature using the high temperature lattice parameter measurements by X-ray method [11, 15, 26–30] [Fig. 3].

Theoretical density was calculated as a function of UO<sub>2</sub> content using Eq. (1). Subsequently, the theoretical density was derived as a function of temperature and UO<sub>2</sub> content from the basic mass balance equation i.e.,

$$\rho_T \cdot V_T = \rho_o \cdot V_o \quad (4)$$

where  $\rho_T$ ,  $\rho_o$ ,  $V_T$ ,  $V_o$  are the densities and volumes at temperatures T and T<sub>o</sub> respectively.

With the coefficient of thermal expansion, the following equation was derived for the theoretical density:

$$D = 10.087 - 2.891 \cdot 10^{-4} \cdot T - 6.354 \cdot 10^{-7} (x) \cdot T + 9.279 \cdot 10^{-3} (x) + 5.111 \cdot 10^{-6} (x)^2 \quad (5)$$

The results are given in Table 3 along with the literature data and presented graphically in Fig.4.

It is observed that the variation in density obtained from equation (5) and that from literature is within  $\pm 0.28\%$ . Hence, the recommended density of ThO<sub>2</sub> as a function of UO<sub>2</sub> (w/o) and temperature (298–1600 K) can be represented by equation (5).

Table 1. Melting point of ThO<sub>2</sub>

T(K)	AUTHORS	YEAR
3323	Ruff et al. [1]	1929
3803	Wartenberg and Reusch [2]	1932
3323 $\pm$ 25	Geach and Harper[3]	1953
3573 $\pm$ 100	Lambertson et al.[4]	1953
3663 $\pm$ 100	Benz et al. [5]	1969
3543	Christensen, J.A. [6]	1970
3573	Chikalle et al. [7]	1972
3651 $\pm$ 17	Ronchi and Hiernaut[8]	1996

Table 2. Specific density of pure ThO<sub>2</sub>, UO<sub>2</sub> and ThO<sub>2</sub>-UO<sub>2</sub> solid solutions

Temp. (K)	SPECIFIC DENSITY $\rho$ (Kg.m <sup>-3</sup> )*10 <sup>-3</sup>						
	BULK DENSITY			X-RAY DENSITY			
	ThO <sub>2</sub> Ref.[16]	ThO <sub>2</sub> - 10w/oUO <sub>2</sub> Ref.[16]	ThO <sub>2</sub> - 20w/oUO <sub>2</sub> Ref.[16]	ThO <sub>2</sub> Ref.[14]	ThO <sub>2</sub> - 50w/oUO <sub>2</sub> Ref.[15]	UO <sub>2</sub> Ref.[14]	UO <sub>2</sub> Ref.[18]
298	9.49	9.52	9.61	9.99	10.46	10.96	10.97
473	9.46	9.47	9.56	9.95	10.41	10.92	10.93
673	9.41	9.42	9.51	9.91	10.35	10.86	10.87
873	9.36	9.36	9.45	9.85	10.29	10.79	10.80
1073	9.30	9.30	9.39	9.79	10.22	10.72	10.73
1273	9.24	9.24	9.33	9.74	10.16	10.65	10.66
1473	9.18	9.18	9.27	9.68		10.57	10.57
1673	9.11	9.12	9.20	9.61		10.48	10.48
1873	9.05	9.06	9.13	9.55		10.39	10.39
2073	8.99	9.00	9.06	9.49		10.29	10.29
2273	8.93	8.93	8.99	9.42		10.19	10.18
2473							10.06
2673							9.94
2873							9.81
3073							9.68

Table 3. Theoretical density of ThO<sub>2</sub>,ThO<sub>2</sub>+50.5 m/o UO<sub>2</sub>, and UO<sub>2</sub>.

Temp. (K)	ThO <sub>2</sub> [14]	ThO <sub>2</sub>	ThO <sub>2</sub> + 50.5 m/o UO <sub>2</sub> [15]	ThO <sub>2</sub> + 50.5m/oUO <sub>2</sub>	UO <sub>2</sub> [14]	UO <sub>2</sub>
298	9.99	10.00	10.46	10.478	10.96	10.96
473	9.95	9.95	10.41	10.422	10.92	10.90
673	9.91	9.89	10.35	10.358	10.86	10.83
873	9.85	9.83	10.29	10.293	10.79	10.76
1073	9.79	9.78	10.22	10.229	10.72	10.69
1273	9.74	9.72	10.16	10.165	10.65	10.62
1473	9.68	9.66			10.57	10.55
1673	9.61	9.60			10.48	10.48



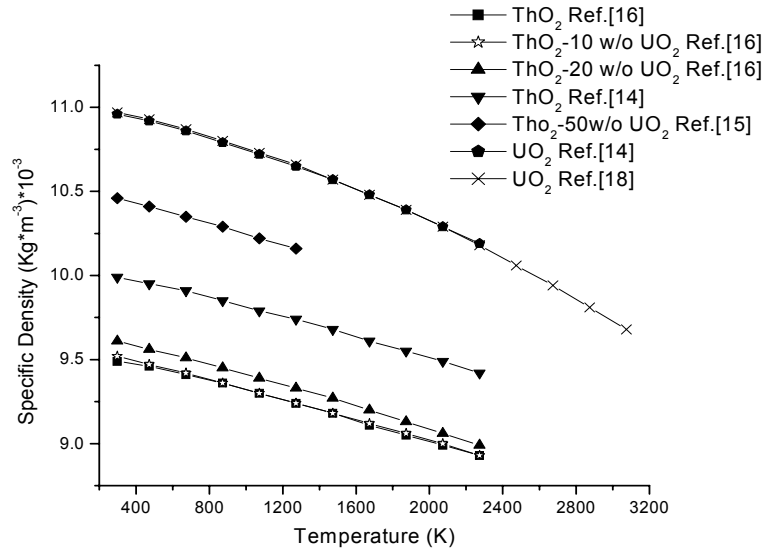


FIG.1. Variation of specific density with temperature for pure  $\text{UO}_2$ ,  $\text{ThO}_2$  and mixed  $(\text{Th},\text{U})\text{O}_2$ .

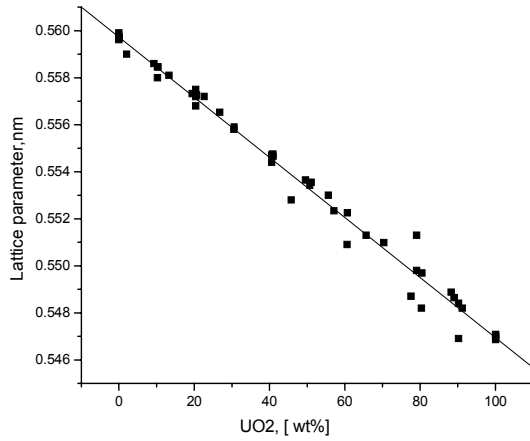


FIG. 2. Variation of Lattice parameter of  $(\text{Th},\text{U})\text{O}_2$  with  $\text{UO}_2$  content.

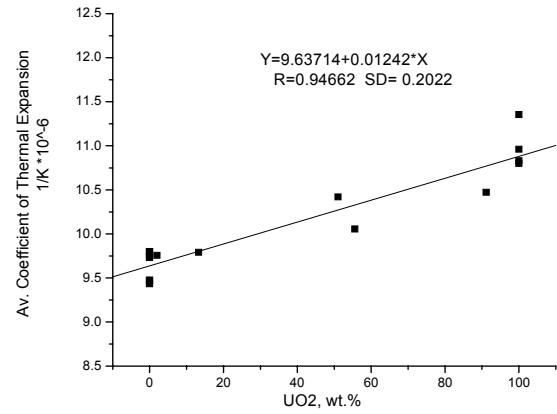


FIG.3. Average co-efficient of thermal expansion as a function of  $\text{UO}_2$  content.

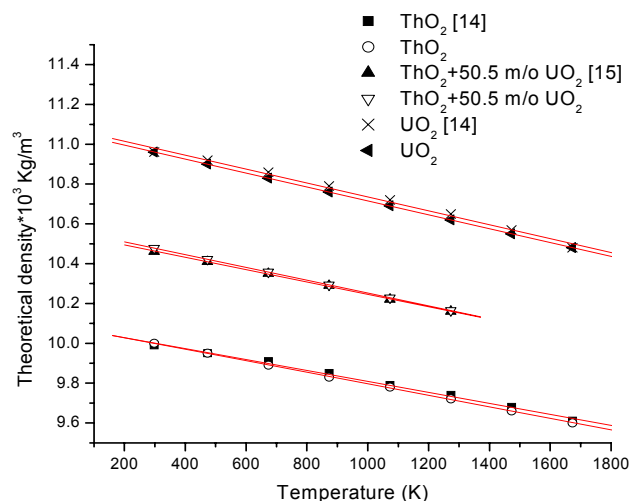


FIG. 4. Variation of theoretical density with temperature.

#### REFERENCES TO SECTIONS 6.1.4.1 and 6.1.4.2

- [1] RUFF, O., EBERT F. and. WOITINEK: H. Z. Anorg. Allgem. Chem. 180 (1929) 252,
- [2] WARTENBERG H. and RAUSCH H. J: Z. Anorg. Allgem. Chem. 208 (1932) 369,
- [3] Geach G. A and Harper, M.E.: Metallurgia 47 (1953) 269,
- [4] LAMBERTSON, W. A, MUELLER M.H and GUNZEL F.H. J. Am. Ceram. Soc. 36 (1953) 397,
- [5] BENZ, R. J. Nucl. Mater. 29 (1969) 43,
- [6] CHRISTENSEN, J.A. "UO<sub>2</sub>-ThO<sub>2</sub> Phase Studies" HN-76559 (1963) 11.5,
- [7] CHIKALLE, T. D. MCNEILLY, C.E., BATES J. L and RASMUSSEN, J.J. Colloq. Int.Centre Nat. Rech. Sci. N 205 (1972) 351,
- [8] RONCHI C and HIERNAUT J. P.: J. alloys Comp. 240 (1996) 179,
- [9] PETERSON, S. AND CURTIS, C.E. Thorium Ceramics Data Manual, VOL.1, Oxides, ORNL-4503 (1970),
- [10] RAND, M.H.: "Part 1. Thermochemical Properties" in Thorium. physico-chemical properties of its compounds and Alloys, O Kubaschewski (editor) Atomic Energy Review, special issue no 5, IAEA, Vienna, 1975, pp 33-41,
- [11] BELLE J. and BERMAN, R.M. 'Thorium Dioxide: properties and Nuclear application' DOE/NE/0060 (1984),
- [12] COHEN, I. and BERMAN, R.M.: J. Nucl. Mater. 18(1966), 77-107,
- [13] MOMIN, A.C. and VENKATESWARLU, K.S.: BARC report, BARC-1171 (1982),
- [14] MOMIN, A.C. and KARKHANVALA: High Temp. Sci., 10 (1978) 45,
- [15] KEMPTER, C.P. and ELLIOTT, R.O.: J. Chem. Phys., 30 (1959) 1524,
- [16] SPRINGER, J.R., ELDRIDGE, E.A., GOODYEAR, M.U., WRIGHT, T.R. and LAGEDRAST, J.F. Report No. BMI-X-10210 (1968),
- [17] CHRISTENSEN, J.A.: J. Am. Ceram. Soc., 46 (1963) 607,
- [18] SLAGE, O.D.: J. Nucl. Mater., 102 (1981) 19,
- [19] KINO, M. et. al. : J. Nucl. Sci. Technol. 19 (1982) 956,
- [20] HOLZER, J. and MCCARTHY G.: JCPDS-File card No 42-1462,
- [21] SLOWINSKI, E. and ELLIOTT, N.: Acta Crystallgr. 5(1952) 768,
- [22] LAMBERTSON W.A and MUELLER M.H.: J. Am. Ceram. Soc. 36 (1953) 397,
- [23] TRZEBIATOWSKI W.: J. Am. Chem. Soc. 72 (1950) 4504,
- [24] COHEN I. and SCHANER B.E.: J. of Nucl. Mater. 9 (1963) 18,

- [25] CORDFUNKE E.H.P. and KONIGS R.J.M. 'Thermo physical data of reactor materials and fission products' (Elsevier AMSTERDAM, 1990).
- [26] TYAGI A.K. and MATHEWS M.D.: J. of Nucl. Mater. 278 (2000) 123-125,
- [27] ANTONYSAMY, G. PANIRSELVAM G. and VASUDEVA RAO: P.R. Proc. Of the 12<sup>th</sup> National symposium on Thermal Analysis THERMANS 2000, Gorakhpur, March 26-27, 2000, 29
- [28] MOMIN: J. of Nucl. Mater. 185,(1991) 308-310.
- [29] TOULOUKIAN, Y.S.KIRBY, R.K TAYLOR R.E.and LEE T.Y.R. ' Thermal Expansion: Nonmetallic SOLIDS (IFI/ PLENUM, NEW YORK, 1970),
- [30] PANIRSELVAM G. NUCAR 99 PP 183-184.

#### 6.1.4.3 Enthalpy increments and heat capacities of $\text{ThO}_2$ and $(\text{Th}_y\text{U}_{1-y})\text{O}_2$

This work was carried out by the Fuel Chemistry Division, Bhabha Atomic Research Centre, Mumbai India. The research did not recommend final values for enthalpy increments and heat capacities for  $\text{ThO}_2$  and  $(\text{Th}_y\text{U}_{1-y})\text{O}_2$ , but made a good comparison with those in the literature. Their contribution is appended here for completeness.

#### **Introduction**

The available literature data on enthalpy increment and heat capacity of the compounds,  $\text{ThO}_2$ ,  $\text{UO}_2$  and  $(\text{Th,U})\text{O}_2$  were critically analysed. A high temperature Calvet calorimeter was used for determining the enthalpy increment values of  $\text{ThO}_2$ , and various compositions of  $(\text{Th,U})\text{O}_2$ . The values were optimised together with literature data. Estimated heat capacity values of the mixed oxide,  $(\text{Th,U})\text{O}_2$ , using Neumann-Kopp's additivity rule were compared with the heat capacity values calculated from the polynomial fits obtained from experimental enthalpy increment data.

#### **Experimental details**

The enthalpy increment measurements of  $\text{ThO}_2$ ,  $(\text{Th}_{0.9804}\text{U}_{0.0196})\text{O}_2$ ,  $(\text{Th}_{0.961}\text{U}_{0.039})\text{O}_2$ ,  $(\text{Th}_{0.941}\text{U}_{0.059})\text{O}_2$  and  $(\text{Th}_{0.902}\text{U}_{0.098})\text{O}_2$  compounds, were carried out using high temperature Calvet calorimeter in the temperature range 375 to 991 K. The thoria and urania samples were prepared by an oxalate route. To obtain high density pellets at low sintering temperature, the oxides were mixed with approximately 500 ppm of MgO in the solution state, before precipitation. For making  $(\text{Th,U})\text{O}_2$  of different compositions, the  $\text{ThO}_2$  (total impurity < 1000 ppm) and  $\text{UO}_2$  (total impurity < 400 ppm) were mixed in required molar ratios and co-milled. Progressive milling technique was used for better homogeneity. The milled powders were compacted at 300 MPa, using a hydraulic press. The green pellets were sintered at 1923 K for 4 hrs in a molybdenum resistance furnace, in a  $\text{N}_2+8\%\text{H}_2$  atmosphere.

The details of the instrument used for determining enthalpy increment of the samples are given elsewhere [1]. For reference, a brief description of the instrument is given here. The high temperature Calvet calorimeter used for the present experiments, is an identical twin calorimeter with two identical alumina tubes. Two identical sets of Pt/Pt-Rh thermopiles are used for measuring heat flux from these alumina tubes during the experiment. The whole set up is surrounded by a massive block of alumina bricks to minimize thermal fluctuations. Through a vacuum tight assembly, a sample introducer is attached to the alumina tubes. The samples were loaded in the sample introducer and maintained at the ambient temperature. The heat change in the crucible when the sample was dropped from the ambient temperature (298.15 K) to the experimental temperature was measured by heat flux principle. All the present enthalpy increment measurements were carried out in isothermal condition. To carry out the present measurements, 7 cm long quartz tubes were placed in the above mentioned alumina tubes. The whole set up was evacuated and flushed with argon two to three times while heating it to the test temperature. The experiments were carried out under a steady argon atmosphere (purity 99.999%) at 1 atm pressure. When equilibrium was attained at the test temperature, the thermopile output remained constant. At the equilibrium test temperature, the calorimeter was calibrated using NBS standard synthetic sapphire (SRM 620). A weighed amount of the reference material was dropped from the ambient temperature (298.15 K) into the calorimeter at the temperature. After four-five such drops,

weighed amounts of the sample material were dropped at the same experimental temperature. The measurements were repeated three to four times at the same temperature to confirm reproducibility of the measurements. Values showed good reproducibility with a standard deviation less than 1.0. For calibration, the enthalpy increment values of synthetic sapphire were used [2]. Enthalpy increment values,  $\Delta H_{298.15\text{ K}}^T$  of  $\text{ThO}_2$ ,  $(\text{Th}_{0.9804}\text{U}_{0.0196})\text{O}_2$ ,  $(\text{Th}_{0.961}\text{U}_{0.039})\text{O}_2$ ,  $(\text{Th}_{0.941}\text{U}_{0.059})\text{O}_2$  and  $(\text{Th}_{0.902}\text{U}_{0.098})\text{O}_2$  were determined at various temperatures.

### Test results

The experimentally determined enthalpy increment data acquired by above technique are listed in Tables 1 to 3. Enthalpy increment data of each selected compound was least square fitted into a polynomial equation, with a constraint,  $\Delta H_{298.15\text{ K}}^T = 0$  at  $T = 298.15\text{ K}$ , using the Origin software. The following set of polynomial equations were obtained:

$$\Delta H_{298.15\text{ K}}^T (\text{J/mol}) \text{ThO}_2 = -25479.4 + 71.6726 T + 4.1266 \times 10^{-3} T^2 + 1116094/T \quad (1)$$

(298.15 - 940 K)

$$\Delta H_{298.15\text{ K}}^T (\text{J/mol}) (\text{Th}_{0.9804}\text{U}_{0.0196})\text{O}_2 = -29409.5 + 76.8601 T + 1.7974 \times 10^{-3} T^2 + 1888448/T \quad (2)$$

(298.15 - 981 K)

$$\Delta H_{298.15\text{ K}}^T (\text{J/mol}) (\text{Th}_{0.961}\text{U}_{0.039})\text{O}_2 = -22908.8 + 67.8243 T + 4.399 \times 10^{-3} T^2 + 684523/T \quad (3)$$

(298.15 - 914 K)

$$\Delta H_{298.15\text{ K}}^T (\text{J/mol}) (\text{Th}_{0.941}\text{U}_{0.059})\text{O}_2 = -29836.2 + 78.8135 T - 3.042 \times 10^{-4} T^2 + 1897724/T \quad (4)$$

(298.15 - 991 K)

$$\Delta H_{298.15\text{ K}}^T (\text{J/mol}) (\text{Th}_{0.902}\text{U}_{0.098})\text{O}_2 = -29336.0 + 78.3578 T + 2.328 \times 10^{-4} T^2 + 1774856/T \quad (5)$$

(298.15 - 991 K)

Recently Bakker et al. [3] have evaluated thermal properties of  $\text{ThO}_2$ . After a critical review of the enthalpy increment and heat capacity data available in the literature, Bakker et al. [3] have derived an enthalpy increment equation based on the recommended data of Southard [4], Hoch and Johnston [5] and Fischer et al. [6]. The authors ignored the data of Victor and Douglas [7], Jaeger and Veenstra [8] and Springer et al. [9, 10] as they found that their values were not reliable in low temperature region. Fink [11] recently published an excellent review on the thermophysical properties of  $\text{UO}_2$ , where, the author gave equations for heat capacity and enthalpy increment of  $\text{UO}_2$ , obtained by a combined fit of some recommended enthalpy increment and heat capacity data [12–20], while ignoring some other publications [21–24] due to their disagreement with the recommended data. The equations for  $\text{ThO}_2$  given by Bakker et al. and  $\text{UO}_2$  given by Fink are as follows:

$$\Delta H_{298.15\text{ K}}^T (\text{J/mol}) \text{ThO}_2 = -20581.7 + 55.9620 T + 25.62895 \times 10^{-3} T^2 - 12.2674 \times 10^{-6} T^3 + 2.30613 \times 10^{-9} T^4 + 5.740310 \times 10^5/T \quad (6)$$

$$\Delta H_{298.15\text{ K}}^T (\text{J/mol}) \text{UO}_2 = -21176.2 + 52.1743 T + 43.9735 \times 10^{-3} T^2 - 28.0804 \times 10^{-6} T^3 + 7.88552 \times 10^{-9} T^4 - 0.52668 \times 10^{-12} T^5 + 7.1391 \times 10^5/T \quad (7)$$

Fink gave also another expression for the enthalpy increment of  $\text{UO}_2$ , a conventional form consisting of lattice, electronic contributions etc. Normally this fits the enthalpy increment data better than the polynomial fit. Based on Browning et al. [25] comments that the constants determined by these fitting procedures need not necessarily have much relevance to the physical parameters that contribute to the heat capacity, Fink recommended that the above polynomial and the following expression are equally good.

$$\Delta H_{298.15\text{ K}}^T (\text{J/mol}) \text{UO}_2 = 44779.42 \left[ \left( e^{548.68/T} - 1 \right)^{-1} - \left( e^{548.68/298.15} - 1 \right)^{-1} \right] + 2.285 \times 10^{-3} [T^2 - (298.15)^2] + 2.360 \times 10^7 e^{-18531.7/T} \quad (8)$$

In Figure 1, the present experimentally determined enthalpy increment values of pure thorium oxide and (Th,U)O<sub>2</sub> mixed oxides are compared with polynomial fits of thorium oxide given by Bakker et al. [3] and uranium oxide given by Fink [11].

The following heat capacity equations of ThO<sub>2</sub> and mixed oxides were obtained by differentiating enthalpy increment expressions in equations (1-5), with respect to temperature.

$$c_p \text{ (J/mol)} \text{ ThO}_2 = 71.6726 + 8.2532 \times 10^{-3} T - 1116094/T^2 \quad (9)$$

$$c_p \text{ (J/mol)} \text{ (Th}_{0.9804}\text{U}_{0.0196}\text{)O}_2 = 76.8601 + 3.598 \times 10^{-3} T - 1888448/T^2 \quad (10)$$

$$c_p \text{ (J/mol)} \text{ (Th}_{0.961}\text{U}_{0.039}\text{)O}_2 = 67.8243 + 8.798 \times 10^{-3} T - 684523/T^2 \quad (11)$$

$$c_p \text{ (J/mol)} \text{ (Th}_{0.941}\text{U}_{0.059}\text{)O}_2 = 78.8135 - 6.083 \times 10^{-4} T - 1897724/T^2 \quad (12)$$

$$c_p \text{ (J/mol)} \text{ (Th}_{0.902}\text{U}_{0.098}\text{)O}_2 = 78.3578 + 4.657 \times 10^{-4} T - 1774856/T^2 \quad (13)$$

On differentiating the enthalpy increment equation (6) for ThO<sub>2</sub>, given by Bakker et al. [3] and equation (7) and (8) for UO<sub>2</sub>, given by Fink [11], the following expressions for heat capacity were obtained.

$$c_p \text{ (J/mol.K)} \text{ ThO}_2 = 55.9620 + 0.05126 T - 3.6802 \times 10^{-5} T^2 + 9.2245 \times 10^{-9} T^3 - 5.7403 \times 10^5/T^2 \quad (14)$$

$$c_p \text{ (J/mol.K)} \text{ UO}_2 = 52.1743 + 0.08795 T - 8.4241 \times 10^{-5} T^2 + 3.1542 \times 10^{-8} T^3 - 2.6334 \times 10^{-12} T^4 - 7.1391 \times 10^5/T^2 \quad (15)$$

$$c_p \text{ (J/mol.K)} \text{ UO}_2 = \frac{2.45696 \times 10^7 e^{(548.68/T)}}{T^2 (e^{(548.68/T)} - 1)^2} + 4.57 \times 10^{-3} T + \frac{4.37348 \times 10^{11} e^{-18531.7/T}}{T^2} \quad (16)$$

Based on the heat capacity equations, (14) and (15) for pure ThO<sub>2</sub> and UO<sub>2</sub>, respectively, the following equation was obtained for the heat capacity of mixed oxide (Th<sub>y</sub>U<sub>(1-y)</sub>)O<sub>2</sub>, estimated using Neumann Kopp's method.

$$c_p \text{ (J/mol.K)} \text{ (Th}_y\text{U}_{(1-y)})\text{O}_2 = y(55.9620 + 0.05126 T - 3.6802 \times 10^{-5} T^2 + 9.2245 \times 10^{-9} T^3 - 5.7403 \times 10^5/T^2) + (1-y)(52.1743 + 0.08795 T - 8.4241 \times 10^{-5} T^2 + 3.1542 \times 10^{-8} T^3 - 2.6334 \times 10^{-12} T^4 - 7.1391 \times 10^5/T^2) \quad (17)$$

## Discussion

The mixed oxides, (Th<sub>y</sub>U<sub>(1-y)</sub>)O<sub>2</sub> taken for the present experimental work contained ≤ 10 at% UO<sub>2</sub>. Whereas, Fischer et al. [26] measured the enthalpy increment of (Th<sub>0.70</sub>U<sub>0.30</sub>)O<sub>2</sub>, (Th<sub>0.85</sub>U<sub>0.15</sub>)O<sub>2</sub> and (Th<sub>0.92</sub>U<sub>0.08</sub>)O<sub>2</sub> in the temperature range 2300 to 3400 K, using inverse drop calorimeter, where the samples were heated to required experimental temperature and dropped into an adiabatic calorimeter. The investigated samples were prepared from enriched UO<sub>2</sub> with 93% <sup>235</sup>U isotope. They marked a discontinuity in the enthalpy increment data of these mixed oxides, though the transitions were less pronounced than in ThO<sub>2</sub>. They reported the transition temperatures as 2900 K, 2950 K and 2850 K for (Th<sub>0.70</sub>U<sub>0.30</sub>)O<sub>2</sub>, (Th<sub>0.85</sub>U<sub>0.15</sub>)O<sub>2</sub> and (Th<sub>0.92</sub>U<sub>0.08</sub>)O<sub>2</sub>, respectively. In their previous work Fischer et al. [6] reported a transition temperature of 2950 K for ThO<sub>2</sub>. It is interesting to observe the change in the transition temperature with change in UO<sub>2</sub> content. When UO<sub>2</sub> is added to ThO<sub>2</sub>, a sudden decrease in the transition temperature from 2950 K (for ThO<sub>2</sub>) to 2850 K (for (Th<sub>0.92</sub>U<sub>0.08</sub>)O<sub>2</sub>) is reported. On further addition of UO<sub>2</sub>, the transition temperature increases back to 2950 K for (Th<sub>0.85</sub>U<sub>0.15</sub>)O<sub>2</sub> but then starts decreasing slowly with increasing UO<sub>2</sub> content. This trend is similar to the observation made for heat capacity variation of the mixed oxides with change in composition. The heat capacity of pure UO<sub>2</sub> is higher than that of ThO<sub>2</sub>, but in mixed oxides it was observed that with increase in UO<sub>2</sub> content, the heat capacity decreases until the U/(Th+U) fraction is approximately 0.04. Then, the heat capacity values of the mixed oxide start increasing with further additions of UO<sub>2</sub>. As seen from Figure 2, the heat capacity values of (Th<sub>0.8</sub>U<sub>0.2</sub>)O<sub>2</sub> calculated from the enthalpy increment fit equation given by Springer et al. [9] are very similar to those of ThO<sub>2</sub>. Springer et al. reported enthalpy increment values of ThO<sub>2</sub>, (Th<sub>0.902</sub>U<sub>0.098</sub>)O<sub>2</sub> and (Th<sub>0.804</sub>U<sub>0.196</sub>)O<sub>2</sub>, in the temperature range 273–2270 K. They also give least square fit expression for the enthalpy increment data of the above mentioned compounds. As the data given by Springer et al. were for the enthalpy increments from

273 K to the experimental temperature, the values were corrected for enthalpy increments from 273 K to 298 K by subtracting the  $\Delta H_{273\text{ K}}^{298\text{ K}}$  values calculated from the polynomial enthalpy increment expressions given by them. These correction factors were 1474, 1425 and 1442 J/mol.K for  $\text{ThO}_2$ ,  $(\text{Th}_{0.902}\text{U}_{0.098})\text{O}_2$  and  $(\text{Th}_{0.804}\text{U}_{0.196})\text{O}_2$ , respectively. For consistency, polynomial fits given by Springer et al. were also converted from cal/g.K to J/mol.K unit and are as follows:

$$\Delta H_{298.15\text{ K}}^T (\text{J/mol}) \text{ThO}_2 = -21856.8 + 66.6205 T + 5.043 \times 10^{-3} T^2 + 460828/T \quad (18)$$

$$\Delta H_{298.15\text{ K}}^T (\text{J/mol}) (\text{Th}_{0.902}\text{U}_{0.098})\text{O}_2 = -23526.1 + 70.0038 T + 3.595 \times 10^{-3} T^2 + 696160/T \quad (19)$$

$$\Delta H_{298.15\text{ K}}^T (\text{J/mol}) (\text{Th}_{0.804}\text{U}_{0.196})\text{O}_2 = -24569.4 + 71.7804 T + 3.479 \times 10^{-3} T^2 + 852371/T \quad (20)$$

$$c_p (\text{J/mol.K}) (\text{Th}_{0.902}\text{U}_{0.098})\text{O}_2 = 70.0038 + 7.19 \times 10^{-3} T - 696160/T^2 \quad (21)$$

$$c_p (\text{J/mol.K}) (\text{Th}_{0.804}\text{U}_{0.196})\text{O}_2 = 71.7804 + 6.958 \times 10^{-3} T - 852371/T^2 \quad (22)$$

Other than the enthalpy increment data of  $(\text{Th}_{0.902}\text{U}_{0.098})\text{O}_2$  by Springer et al. in the temperature range 273 to 2270 K and that of  $(\text{Th}_{0.92}\text{U}_{0.08})\text{O}_2$  by Fischer et al. [26] in the temperature range 2303 to 3302 K, all other mixed oxides investigated previously contained much higher U/(Th+U) compared to the present study. As the composition and temperature range of enthalpy increment data reported by Springer et al. [9] overlapped with the present work, the data was used along with the present enthalpy increment data for  $(\text{Th}_{0.902}\text{U}_{0.098})\text{O}_2$  to obtain a polynomial fit. The polynomial fit obtained from the combined enthalpy increment data of Springer et al. and the present work for  $(\text{Th}_{0.902}\text{U}_{0.098})\text{O}_2$  is given below along with heat capacity expression obtained by differentiating the enthalpy increment equation with temperature.

$$\Delta H_{298.15\text{ K}}^T (\text{J/mol}) (\text{Th}_{0.902}\text{U}_{0.098})\text{O}_2 = -24843.6 + 71.62 T + 3.07 \times 10^{-3} T^2 + 959490/T \quad (23)$$

$$c_p (\text{J/mol.K}) (\text{Th}_{0.902}\text{U}_{0.098})\text{O}_2 = 71.62 + 6.14 \times 10^{-3} T - 959490/T^2 \quad (24)$$

Another least square polynomial fit was calculated using the Origin software based on the enthalpy increment values of the present experiments and that reported by Springer for  $(\text{Th}_{0.902}\text{U}_{0.098})\text{O}_2$  along with the data of Fischer et al. [26] for  $(\text{Th}_{0.92}\text{U}_{0.08})\text{O}_2$  in the temperature range 2303 K to 2800 K. Though Fischer et al. have reported enthalpy increment data of this composition in the temperature range 2303 K to 3302 K, the values at temperatures  $\geq 2850$  K were not considered as Fischer et al. have reported a discontinuity in enthalpy increment for  $(\text{Th}_{0.92}\text{U}_{0.08})\text{O}_2$  at 2850 K. The best fitting polynomial expression (minimum chi-square value) obtained for this combined set of data is as follows:

$$\Delta H_{298.15\text{ K}}^T (\text{J/mol}) (\text{Th}_{0.9}\text{U}_{0.1})\text{O}_2 = -31835.8 + 85.1418 T - 6.698 \times 10^{-3} T^2 + 2.274 \times 10^{-6} T^3 + 2082847/T \quad (25)$$

$$c_p (\text{J/mol.K}) (\text{Th}_{0.9}\text{U}_{0.1})\text{O}_2 = 85.1418 - 1.3396 \times 10^{-2} T + 6.822 \times 10^{-6} T^2 - 2082847/T^2 \quad (26)$$

The heat capacity values calculated from equations (13, 17, 21, 24, 26) are compared in table 3. It can be seen that the heat capacity values obtained from Neumann-Kopp's additivity rule are higher than the heat capacity values calculated from the present enthalpy increment data and this difference increases with increase in temperature and is maximum at the highest measurement temperature of the present studies. i.e., 991 K. Though Springer et al. [9] have measured enthalpy increment in the wide temperature range, 273–2270 K, but heat capacity calculated from their data also showed a maximum deviation from Neumann-Kopp's estimated heat capacity values in the same temperature zone. This can be explained from the observation that the heat capacity of thorium shows a flatter temperature dependence in the approximate temperature range 1000 to 1400 K. Whereas, heat capacity calculated from the present enthalpy increment data or the one calculated from the data of Springer et al. showed

a change in slope at much lower temperature,  $\sim 650$  K. Therefore, up to this temperature the heat capacity values calculated from the present enthalpy increment data are in very good agreement with those of Neumann-Kopp's. The heat capacity values calculated from the data of Springer et al. [9] showed only a slight decrease in slope at this temperature, whereas, the heat capacity of  $\text{ThO}_2$  is almost independent of temperature in the above mentioned temperature range. The heat capacity values calculated from equation (26) follow the generic trend followed by heat capacities of  $\text{ThO}_2$  and  $\text{UO}_2$  compounds. All the three show a steep heat capacity increase with increase in temperature, near room temperature, followed by a temperature region where the heat capacity variation with temperature is much flatter. After that heat capacity again increases steeply with increase in temperature. The heat capacity values calculated from equation (21), based on the enthalpy increment data given by Springer et al. and the heat capacity values calculated from equation (24), based on the present enthalpy increment data combined with that of Springer et al., are in good agreement with each other. They both show a steep increase in heat capacity with increase in temperature at lower temperatures but at temperatures greater than approximately 600 K, this effect decreases a little. They do not show a plateau region as observed in case of heat capacities of  $\text{ThO}_2$  and  $\text{UO}_2$ . It was observed that in the temperature range of the present experiments, compared to the heat capacity values calculated from the enthalpy increment data of Springer et al., the heat capacity values obtained from the present enthalpy increment data were in better agreement with the ones calculated from equation (26).

The present heat capacity equation (13) gives reasonably reliable heat capacity values when extrapolated by 200–300 K beyond experimental temperature range but after this the values are not reliable. Heat capacity values calculated from the enthalpy increment equation given by Fischer et al. for  $(\text{Th}_{0.92}\text{U}_{0.08})\text{O}_2$  are very low compared to others. They have reported enthalpy increment measurements in temperature range 2303–2850 K, however, gave a temperature range 298.15–2850 K, for the polynomial equation obtained by fitting their enthalpy increment data. The disagreement between the heat capacity values obtained from other fits and those of Fischer et al. indicates that the temperature range of validity of their equation should be same as the temperature range of their measurements i.e., 2303–2850 K. The heat capacity equation (26) for  $(\text{Th}_{0.9}\text{U}_{0.1})\text{O}_2$ , calculated from a combined fit of the enthalpy increment data in the temperature ranges 340 to 2271 K by Springer et al., 2303 to 2800 K by Fischer et al. [26] and 298.15 to 991 K of the present investigations, should be more reliable in the wide temperature range 298.15 to 2800 K. As seen in figure 2, the heat capacity values obtained from equation (26) are most reasonable over this wide temperature range as they do not deviate much from the heat capacity values of pure  $\text{ThO}_2$  or heat capacity values of  $(\text{Th}_{0.9}\text{U}_{0.1})\text{O}_2$  estimated using Neumann-Kopp's rule and has similar contours.

One important use of the heat capacity data is to calculate thermal conductivity of the material from the measured thermal diffusivity data. In the absence of any experimental heat capacity data, estimated heat capacity values, generally from Neumann-Kopp's method are used for the calculation of thermal conductivity. In the light of the present heat capacity values of the mixed oxide, it was considered important to understand the effect of this difference in estimated heat capacity values and the ones calculated from enthalpy increment data, on the thermal conductivity values. Sengupta et al. [27] have measured thermal diffusivity of  $(\text{Th}_y\text{U}_{(1-y)})\text{O}_2$  for  $y = 1.0, 0.9804, 0.961, 0.941, 0.902$  and  $0.804$  in the temperature range 973–1973 K. They have also reported thermal conductivity values calculated from their experimental data of thermal diffusivity and density and using Neumann-Kopp's heat capacity values, equation (14) for heat capacity of  $\text{ThO}_2$  and equation (16) for heat capacity of  $\text{UO}_2$ . The temperature range of their thermal diffusivity measurements were such that the heat capacity values obtained from the present enthalpy increment data could not be used reliably over the whole temperature range. The thermal conductivity values of  $(\text{Th}_{0.804}\text{U}_{0.196})\text{O}_2$  and  $(\text{Th}_{0.902}\text{U}_{0.098})\text{O}_2$  were recalculated using the thermal diffusivity and density data given by them and the heat capacity values given by Springer et al. [9], i.e., equation (22) for  $(\text{Th}_{0.804}\text{U}_{0.196})\text{O}_2$  and the heat capacity values obtained from the combined enthalpy increment data, equation (26) for  $(\text{Th}_{0.902}\text{U}_{0.098})\text{O}_2$ . The thermal conductivity values of  $(\text{Th}_{0.804}\text{U}_{0.196})\text{O}_2$  and  $(\text{Th}_{0.902}\text{U}_{0.098})\text{O}_2$  thus calculated were compared with the values obtained using Neumann-Kopp's estimated heat capacity. These values are given in table 4 and compared in figure 3. For the compositions,  $y = 0.9804, 0.961$  and  $0.941$ , the thermal conductivity was recalculated using extrapolation of heat capacity equations obtained from the present enthalpy increment data to 1200 K. These values were also compared with thermal conductivity calculated

using Neumann-Kopp's heat capacity data. All the thermal conductivity values were normalized to 95% TD before comparison. These values are given in table 5 and plotted in figure 3. As seen from the table, the maximum difference between the values calculated using estimated and experimental heat capacity values was not more than  $\pm 5$  %. As expected, maximum deviation between the two sets of thermal conductivity data was observed for  $(\text{Th}_{0.961}\text{U}_{0.039})\text{O}_2$ . This means that in the absence of experimental heat capacity values, Neumann-Kopp's estimated heat capacity values can also be used to get reasonably reliable thermal conductivity values for  $(\text{Th}_y\text{U}_{(1-y)})\text{O}_2$ . The thermal conductivity of  $(\text{Th}_{0.9804}\text{U}_{0.0196})\text{O}_2$  in this temperature range is almost equal to that of pure  $\text{ThO}_2$ , therefore, the crossover of the curves seen in the figure is representative of scatter in the data. The effect of  $\text{UO}_2$  addition on thermal conductivity in  $(\text{Th}_y\text{U}_{(1-y)})\text{O}_2$  decreases with increase in temperature. A clear trend of decrease in thermal conductivity with increase in  $\text{UO}_2$  content for  $y \geq 0.9$  was observed for temperatures up to 1000 K [28,29]. However, as the temperature increases, thermal conductivity of the solid-solution decreases and so does the difference between the values of different U/M. Springer et al. [30] have reported that the thermal conductivity values were consistently lower for  $(\text{Th}_y\text{U}_{(1-y)})\text{O}_2$  with  $y = 0.9695$  and  $0.925$ , particularly at low temperatures. Ferro et al. have also reported thermal diffusivity of  $(\text{Th}_y\text{U}_{(1-y)})\text{O}_2$  for  $y = 0.99, 0.9, 0.96$  [31] and  $y = 1.0, 0.94$  [32]. In their earlier publication they have given density of the samples along with thermal diffusivity values, therefore, it was possible to calculate thermal conductivity using their data and heat capacity values calculated by Neumann-Kopp's estimation. But these values showed too big a scatter to understand any trend, therefore, they were not used for the present comparison. In the later publication, they have given only relative densities and not actual densities. Therefore, thermal conductivity values were calculated by back calculating the densities. These calculated values of thermal conductivity for  $y = 0.94$  and  $1.0$  are shown in the figure 3. Pillai and Raj [33] have also reported thermal conductivity of  $\text{ThO}_2$  and  $(\text{Th}_{98}\text{U}_{0.02})\text{O}_2$ . Instead of actual experimental values, they have given coefficients of the thermal conductivity fit,  $1/(A+BT)$ . For the purpose of comparison, thermal conductivity values of the two compounds were calculated using these coefficients, as shown in figure 3.



Table 1. A comparison of experimental enthalpy increment values ( $\Delta_1 H_{298.15\text{ K}}^T$ ) of  $\text{ThO}_2$  and  $(\text{Th}_{0.9804}\text{U}_{0.0196})\text{O}_2$  with enthalpy increment values calculated ( $\Delta_2 H_{298.15\text{ K}}^T$ ) using equations (1) and (2), respectively, and a comparison of their heat capacity values with Bakker et al. (eq. 14) and equation (17), respectively

ThO <sub>2</sub>							(Th <sub>0.9804</sub> U <sub>0.0196</sub> )O <sub>2</sub>				
T(K)	Δ <sub>1</sub> H <sup>T</sup> <sub>298.15 K</sub> (J/mol)	Δ <sub>2</sub> H <sup>T</sup> <sub>298.15 K</sub> (J/mol)	$\frac{100 \times \Delta_1 H^T - \Delta_2 H^T}{\Delta_1 H^T}$	c <sub>p</sub> (eq. 9) (J/mol.K)	c <sub>p</sub> (eq 14) (J/mol.K)	T(K)	Δ <sub>1</sub> H <sup>T</sup> <sub>298.15 K</sub> (J/mol)	Δ <sub>2</sub> H <sup>T</sup> <sub>298.15 K</sub> (J/mol)	$\frac{100 \times \Delta_1 H^T - \Delta_2 H^T}{\Delta_1 H^T}$	c <sub>p</sub> (eq 10) (J/mol.K)	c <sub>p</sub> (eq 17) (J/mol.K)
376	4719	5021	-6.40	66.88	66.46	376	4780	4766	0.28	64.85	66.53
406	6839	7049	-3.07	68.25	67.84	406	6753	6743	0.14	66.86	67.92
406	7099	7049	0.71	68.25	67.84	427	8178	8160	0.22	68.04	68.79
437	9150	9184	-0.37	69.43	69.10	458	10253	10293	-0.39	69.50	69.95
458	10642	10649	-0.07	70.13	69.87	478	11740	11691	0.42	70.31	70.64
478	12288	12058	1.87	70.73	70.55	509	14024	13888	0.97	71.40	71.61
509	14568	14264	2.09	71.57	71.52	540	16184	16116	0.42	72.33	72.49
540	16496	16494	0.01	72.30	72.39	570	18381	18298	0.45	73.10	73.26
581	19320	19476	-0.81	73.16	73.43	601	20540	20575	-0.17	73.79	73.99
611	21490	21680	-0.88	73.73	74.11	632	22689	22872	-0.81	74.40	74.65
642	24433	23974	1.88	74.26	74.75	663	24955	25187	-0.93	74.95	75.26
673	25948	26284	-1.29	74.76	75.34	704	28189	28273	-0.30	75.58	75.97
714	30160	29362	2.65	75.38	76.03	734	30289	30547	-0.85	75.99	76.45
745	31152	31705	-1.78	75.81	76.50	765	32886	32909	-0.07	76.38	76.89
786	34990	34825	0.47	76.35	77.07	796	35562	35282	0.79	76.74	77.30
817	36764	37198	-1.18	76.74	77.45	817	37120	36896	0.60	76.97	77.55
847	38937	39505	-1.46	77.11	77.78	837	38690	38438	0.65	77.17	77.78
878	42019	41901	0.28	77.47	78.10	878	41664	41610	0.13	77.57	78.20
909	44944	44309	1.41	77.82	78.38	899	43163	43241	-0.18	77.76	78.39
940	46534	46726	-0.41	78.17	78.64	919	44687	44798	-0.25	77.93	78.57
						950	47033	47218	-0.39	78.18	78.82
						981	49672	49645	0.05	78.42	79.04

Table 2. A comparison of experimental enthalpy increment values ( $\Delta_1 H_{298.15\text{ K}}^T$ ) of  $(\text{Th}_{0.961}\text{U}_{0.039})\text{O}_2$  and  $(\text{Th}_{0.941}\text{U}_{0.059})\text{O}_2$  with enthalpy increment values calculated ( $\Delta_2 H_{298.15\text{ K}}^T$ ) from equations (3) and (4), respectively. A comparison of heat capacity values calculated from equations (11) and (12) with estimated heat capacity values calculated from equation (17).

T(K)	$(\text{Th}_{0.961}\text{U}_{0.039})\text{O}_2$						$(\text{Th}_{0.941}\text{U}_{0.059})\text{O}_2$				
	$\Delta_1 H_{298.15\text{ K}}^T$ (J/mol)	$\Delta_2 H_{298.15\text{ K}}^T$ (J/mol)	$\frac{100 \times \Delta_1 H - \Delta_2 H}{\Delta_1 H}$	$c_p$ (eq 11) (J/mol.K)	$c_p$ (eq 17) J/mol.K	T(K)	$\Delta_1 H_{298.15\text{ K}}^T$ (J/mol)	$\Delta_2 H_{298.15\text{ K}}^T$ (J/mol)	$\frac{100 \times \Delta_1 H - \Delta_2 H}{\Delta_1 H}$	$c_p$ (eq 12) (J/mol.K)	$c_p$ (eq 17) J/mol.K
376	4952	5036	-1.69	66.29	66.60	376	4806	4802	0.09	65.16	66.60
427	8314	8457	-1.72	67.83	68.87	401	6467	6452	0.24	66.77	68.87
453	10140	10229	-0.88	68.47	69.86	427	8203	8206	-0.04	68.15	69.86
478	12000	11948	0.43	69.03	70.73	427	8304	8206	1.18	68.15	70.73
504	13734	13750	-0.12	69.56	71.56	453	9947	9993	-0.46	69.29	71.56
529	15618	15495	0.79	70.03	72.29	478	11739	11737	0.01	70.22	72.29
581	19202	19160	0.22	70.91	73.63	504	13531	13574	-0.32	71.04	73.63
632	23000	22796	0.89	71.67	74.76	529	15391	15358	0.21	71.71	74.76
683	26605	26470	0.51	72.37	75.72	555	17230	17231	-0.01	72.31	75.72
734	30273	30177	0.32	73.01	76.55	555	17190	17231	-0.24	72.31	76.55
760	31824	32079	-0.80	73.33	76.93	581	19064	19118	-0.28	72.84	76.93
786	33764	33990	-0.67	73.63	77.27	581	19054	19118	-0.34	72.84	77.27
811	35360	35834	-1.34	73.92	77.58	581	19078	19118	-0.21	72.84	77.58
837	38276	37760	1.35	74.21	77.88	606	20966	20945	0.10	73.28	77.88
863	39833	39693	0.35	74.50	78.15	632	22912	22855	0.25	73.68	78.15
888	41326	41559	-0.56	74.77	78.39	683	26686	26630	0.21	74.33	78.39
914	43668	43506	0.37	75.05	78.63	734	30413	30434	-0.07	74.84	78.63
						786	34409	34338	0.21	75.26	77.39
						837	38259	38185	0.19	75.60	77.99
						888	42046	42047	0.00	75.87	78.50
						914	43903	44021	-0.27	75.99	78.73
						940	45955	45999	-0.09	76.09	78.95
						965	47958	47902	0.12	76.19	79.13
						991	49870	49884	-0.03	76.28	79.31

Table 3. A comparison of experimental enthalpy increment values ( $\Delta_1 H_{298.15\text{ K}}^\circ$ ) of  $(\text{Th}_{0.902}\text{U}_{0.098})\text{O}_2$  with enthalpy increment values calculated from equation (5) ( $\Delta_2 H_{298.15\text{ K}}^\circ$ ). A comparison of heat capacity values calculated from equation (13) with estimated heat capacity values calculated from equation (17) and others

T(K)	$(\text{Th}_{0.902}\text{U}_{0.098})\text{O}_2$							
	$\Delta_1 H_{298.15\text{ K}}^\circ$ (J/mol)	$\Delta_2 H_{298.15\text{ K}}^\circ$ (J/mol)	$\frac{100 \times \Delta_1 H - \Delta_2 H}{\Delta_1 H}$	$c_p$ (eq 13) (J/mol.K)	$c_p$ (eq 17) J/mol.K	$c_p$ (eq 21) J/mol.K	$c_p$ (eq 24) J/mol.K	$c_p$ (eq 26) J/mol.K
376	4864	4880	-0.32	65.98	66.80	67.73	67.14	66.34
401	6498	6549	-0.78	67.51	68.00	68.51	68.12	67.91
427	8366	8322	0.53	68.82	69.11	69.21	68.98	69.24
453	10092	10126	-0.34	69.92	70.12	69.82	69.73	70.32
478	11930	11885	0.37	70.81	71.00	70.34	70.36	71.18
504	13651	13737	-0.63	71.61	71.84	70.84	70.94	71.92
529	15650	15536	0.73	72.26	72.58	71.27	71.44	72.52
555	17482	17422	0.34	72.85	73.28	71.68	71.91	73.05
581	19289	19323	-0.18	73.37	73.94	72.07	72.34	73.49
606	21215	21163	0.24	73.81	74.51	72.41	72.73	73.86
632	23017	23087	-0.31	74.21	75.07	72.75	73.10	74.19
683	26979	26890	0.33	74.87	76.04	73.37	73.76	74.71
734	29866	30722	-2.87	75.41	76.87	73.94	74.35	75.12
786	35718	34655	2.98	75.85	77.59	74.47	74.89	75.46
837	38655	38533	0.32	76.21	78.19	74.97	75.39	75.74
888	42430	42428	0.00	76.52	78.70	75.45	75.86	75.98
914	44053	44419	-0.83	76.66	78.93	75.69	76.08	76.1
940	46000	46414	-0.90	76.79	79.14	75.92	76.31	76.22
965	48387	48335	0.11	76.90	79.32	76.14	76.51	76.33
991	50629	50336	0.58	77.01	79.50	76.36	76.73	76.44

Table 4. A comparison of thermal conductivity values of (Th<sub>0.902</sub>U<sub>0.098</sub>)O<sub>2</sub> and (Th<sub>0.804</sub>U<sub>0.196</sub>)O<sub>2</sub>, calculated using Neumann-Kopp's heat capacity values with the ones calculated using heat capacity equations (26) and (22), respectively

T (K)	Thermal Conductivity (W/mK) of (Th <sub>0.902</sub> U <sub>0.098</sub> )O <sub>2</sub>				T (K)	Thermal Conductivity (W/mK) of (Th <sub>0.804</sub> U <sub>0.196</sub> )O <sub>2</sub>			
	Measured <sup>(1)</sup>	Corrected <sup>(1)</sup> (95% TD)	Measured <sup>(2)</sup>	Corrected <sup>(2)</sup> (95% TD)		Measured <sup>(1)</sup>	Corrected <sup>(1)</sup> (95% TD)	Measured <sup>(3)</sup>	Corrected <sup>(3)</sup> (95% TD)
873	5.3454	5.5917	5.167	5.4051	873	4.5826	5.02585	4.4469	4.877
973	4.8729	5.0974	4.6875	4.9035	973	4.4335	4.86224	4.3063	4.7228
1043	4.482	4.6885	4.3042	4.5026	1043	3.9893	4.37507	3.882	4.2574
1123	3.9742	4.1572	3.8152	3.9909	1123	3.5113	3.85085	3.4271	3.7585
1213	3.6537	3.822	3.5123	3.6741	1213	3.1928	3.50153	3.1289	3.4315
1313	3.3018	3.454	3.1844	3.3312	1313	2.9813	3.26959	2.9359	3.2199
1313	3.3018	3.454	3.1844	3.3312	1313	2.9815	3.26978	2.9361	3.2201
1413	3.0869	3.2291	2.9907	3.1284	1413	2.7688	3.03657	2.7392	3.0041
1513	2.6217	2.7425	2.5532	2.6708	1513	2.1678	2.3774	2.1523	2.3603
1613	2.2732	2.3779	2.225	2.3275	1613	2.0119	2.20636	2.0009	2.1943
1613	2.2087	2.3104	2.1618	2.2614	1613	2.0119	2.20636	2.0009	2.1943
1713	2.0541	2.1487	2.0191	2.1121	1713	1.9713	2.16194	1.9588	2.1482
1813	2.0464	2.1407	2.0171	2.11	1813	1.7085	1.8736	1.6904	1.8538
		<b>2.</b>			1873	1.6943	1.85807	1.6689	1.8303

(1) Using estimated Neumann-Kopp's heat capacity values.

(2) Using heat capacity values calculated from equation (26).

(3) Using heat capacity values calculated from equation (22).

Table 5. A comparison of thermal conductivity values of  $(Th_{0.9804}U_{0.0196})O_2$ ,  $(Th_{0.961}U_{0.039})O_2$  and  $(Th_{0.941}U_{0.059})O_2$ , calculated using Neumann-Kopp's heat capacity values with the ones calculated using heat capacity equations (10), (11) and (12), respectively

T (K)	Thermal Conductivity (W/mK) of $(Th_{0.9804}U_{0.0196})O_2$				Thermal Conductivity (W/mK) of $(Th_{0.961}U_{0.039})O_2$				Thermal Conductivity (W/mK) of $(Th_{0.941}U_{0.059})O_2$			
	Measured <sup>(1)</sup>	Corrected <sup>(1)</sup> (95% TD)	Measured <sup>(2)</sup>	Corrected <sup>(2)</sup> (95% TD)	Measured <sup>(1)</sup>	Corrected <sup>(1)</sup> (95% TD)	measured <sup>(3)</sup>	Corrected <sup>(3)</sup> (95% TD)	Measured <sup>(1)</sup>	Corrected <sup>(1)</sup> (95% TD)	measured <sup>(4)</sup>	Corrected <sup>(4)</sup> (95% TD)
873	7.0526	6.9699	6.9959	6.9139	6.0127	6.0451	5.7333	5.7642	5.8903	5.9807	5.6993	5.7867
973	6.3455	6.2711	6.2957	6.2218	6.0061	6.0385	5.7460	5.7770	5.3312	5.413	5.1318	5.2105
1043	5.6587	5.5923	5.6195	5.5535	5.1841	5.2121	4.9779	5.0048	4.7143	4.7868	4.5252	4.5947
1123	5.0763	5.0168	5.0498	4.9906	4.6912	4.7165	4.5283	4.5527	4.3672	4.4343	4.1811	4.2453
1213	4.6007	4.5468	4.5880	4.5342	4.1632	4.1857	4.0459	4.0678	3.9588	4.0196	3.7810	3.8391

<sup>(1)</sup>Using estimated Neumann-Kopp's heat capacity values.

<sup>(2)</sup>Using heat capacity values calculated from equation (10).

<sup>(3)</sup>Using heat capacity values calculated from equation (11).

<sup>(4)</sup>Using heat capacity values calculated from equation (12).

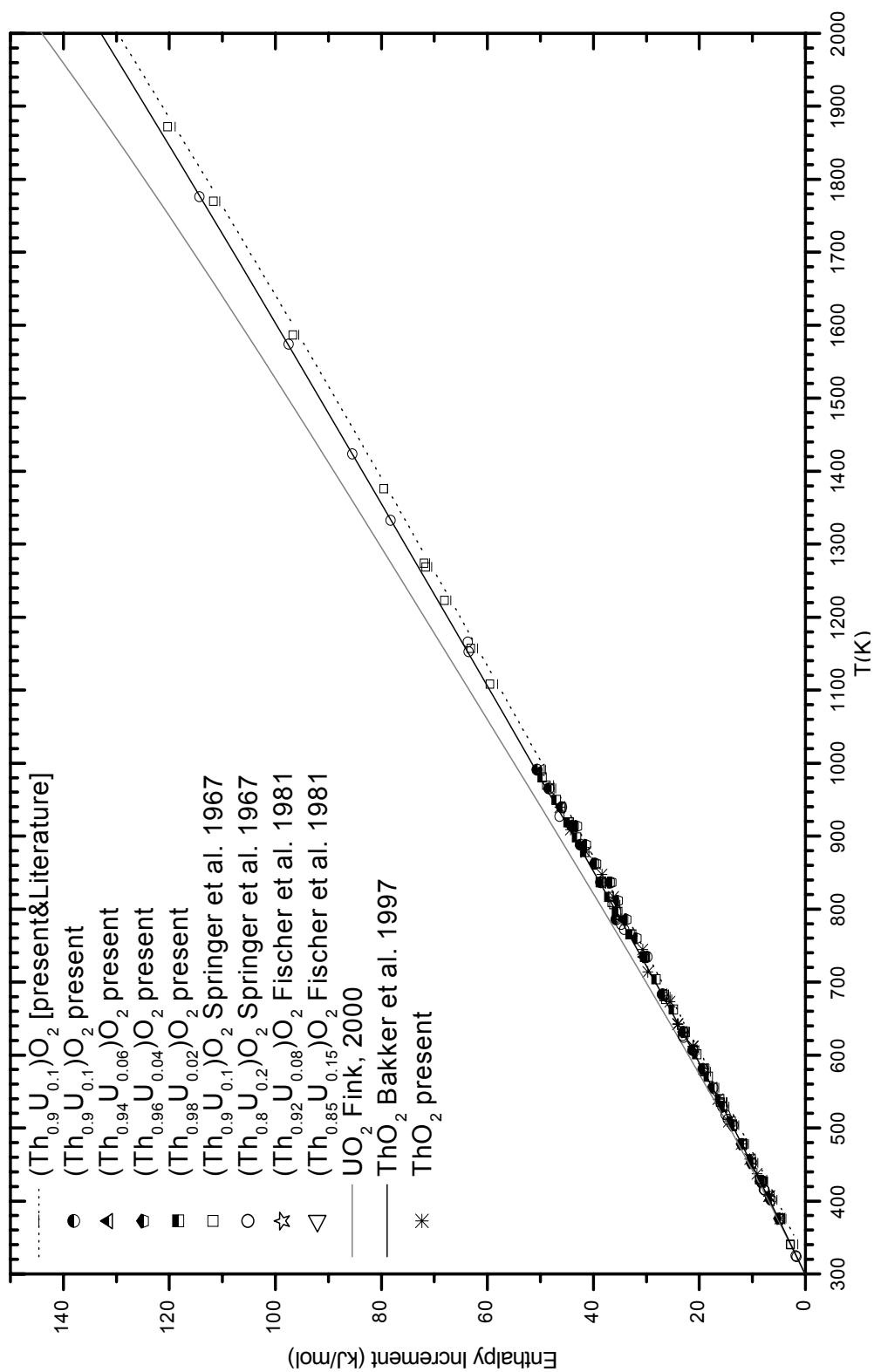


FIG. 1. Present enthalpy increment data of  $(\text{Th}, \text{U})\text{O}_2$  and simfuel compared with literature data. are data.

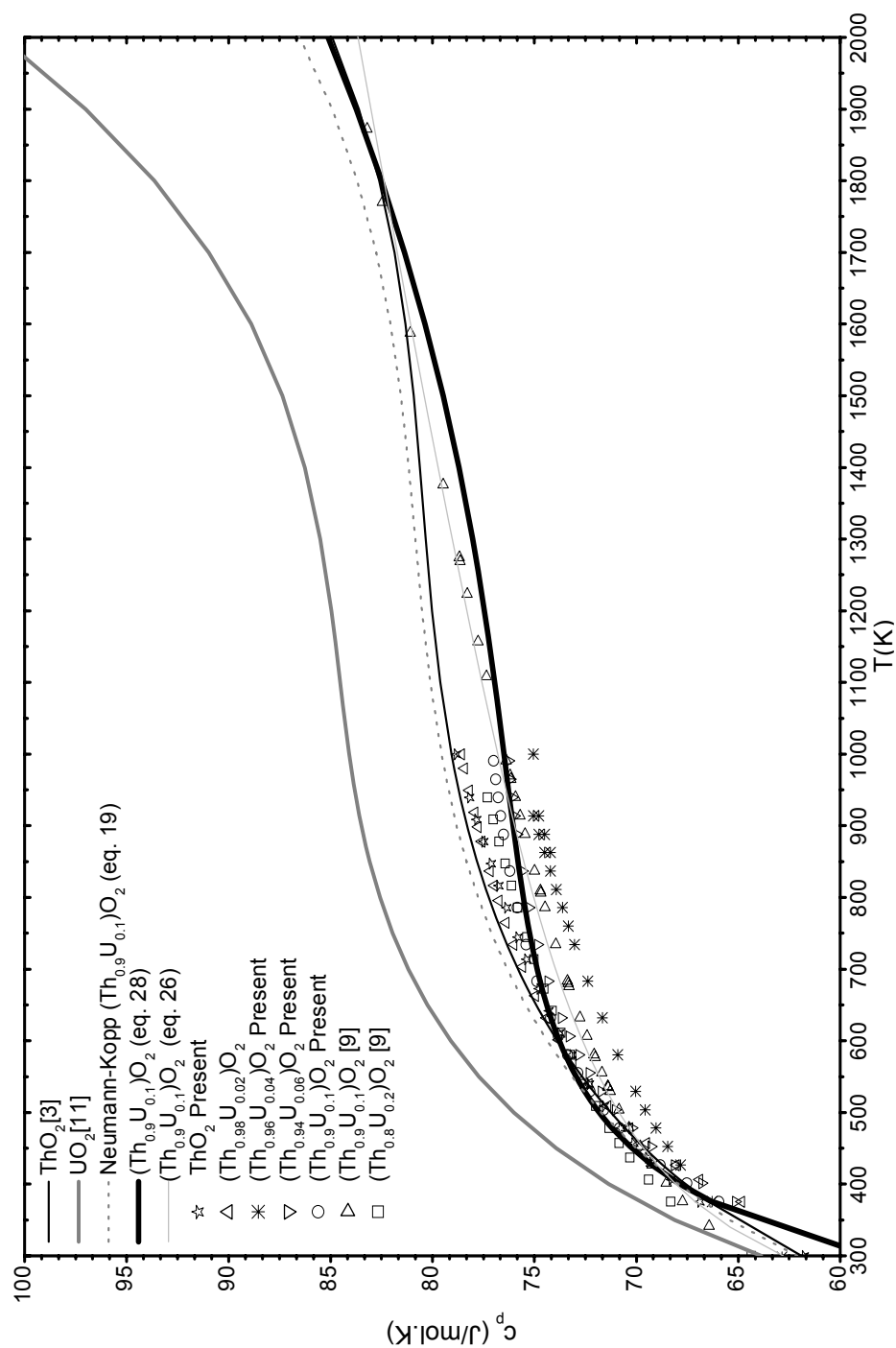


FIG. 2. A comparison of heat capacity data calculated from present enthalpy increment data with those calculated from enthalpy increment data reported in literature.

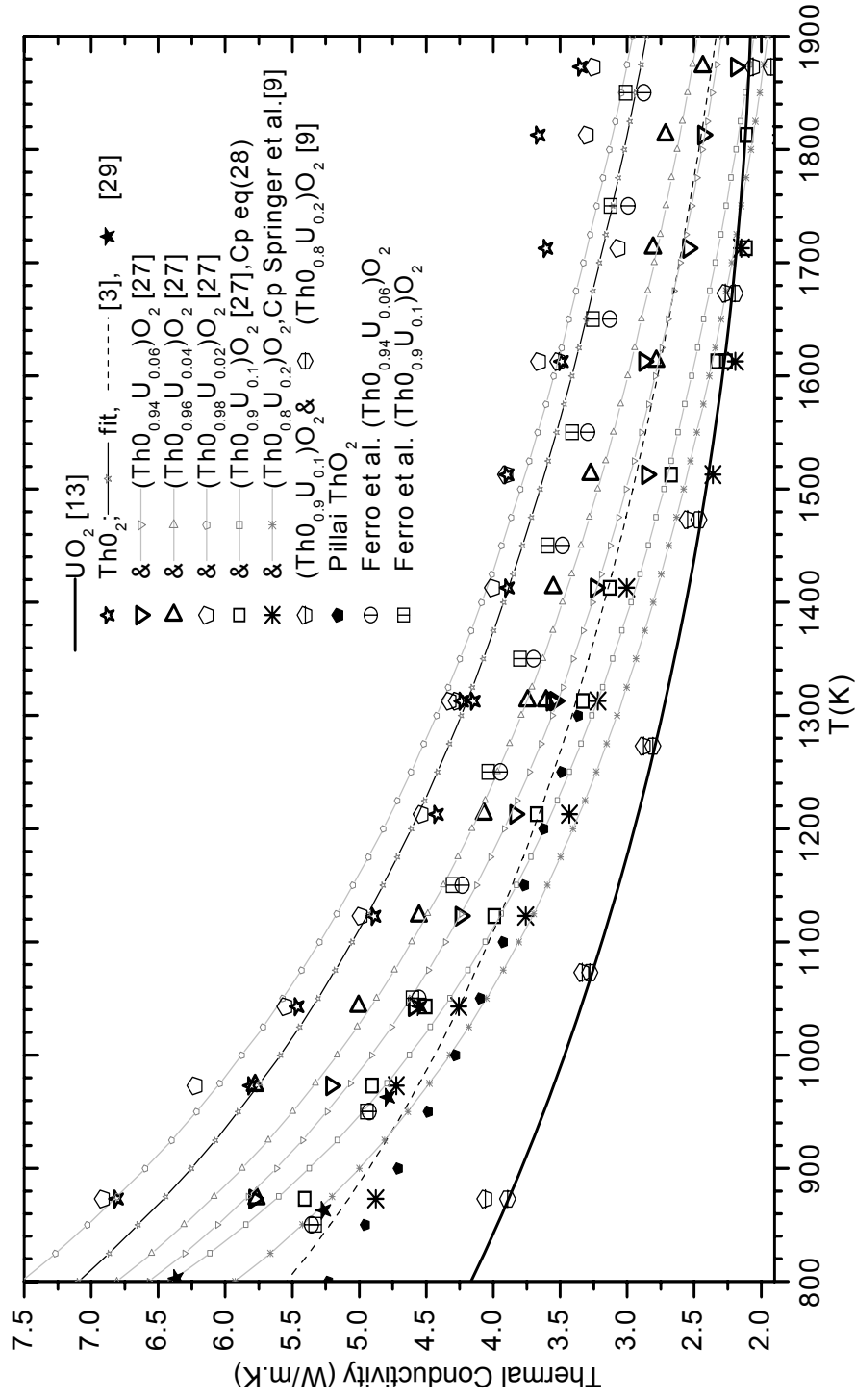


FIG. 3. Comparison of thermal conductivity values calculated from thermal diffusivity values given by Sen et al. with literature data.



### REFERENCES TO SECTION 6.1.4.3

- [1] RENU AGARWAL, K.N. ROY, V., VENUGOPAL, R. PRASAD, D.D. SOOD, M.L. JAYANTKUMAR and M.R. PONKSHE, 1987, BARC/I-875.
- [2] N.B.S. Certified Standard Reference Material 720 Synthetic Sapphire (Al<sub>2</sub>O<sub>3</sub>). U.S. Department of Commerce, (1982).
- [3] BAKKER, K., CORFUNKE, E.H.P., KONINGS, R.J.M. and SCHARM, R.P.C. J. Nucl. Mat., 250 (1997) 1-12.
- [4] SOUTHARD, J.C. J. Am. Chem. Soc., 63 (1941) 3142.
- [5] HOCH, M. and JOHNSTON, H.G. J. Phys. Chemistry, 65 (1961) 1184.
- [6] FISCHER, D.F., FINK, J.K. and LEIBOWITZ, L. J. Nucl. Mater. 102 (1981) 220.
- [7] VICTOR, A.C. and DOUGLAS, T.B. J. Res. Nat. Bur. Stand, A65 (1961) 105.
- [8] JAEGER, F.M. and VEENSTRA, W.A. Proc. Acad. Sci. Amst., 37 (1934) 327.
- [9] SPRINGER, J.R., ELDRIDGE, E.A., GOODYEAR, N.U., WRIGHT, T.R. and LAGEDROX, J.F. BMI-X-10210 (1967).
- [10] SPRINGER, J.R., LANGEDROST, J.F. Battelle Memorial Institute Report BMI-X-10231 (1968).
- [11] FINK, J.K. J. Nucl. Mater., 279 (2000) 1-18.
- [12] RONCHI, C., SHEINDLIN, M., MUSELLA, M., HYLAND, G.J. J. Appl. Phys. 85 (1999) 776.
- [13] OGARD, A.E., LEARY, J.A. Thermodynamics of Nuclear Materials 1967, IAEA, Vienna (1969), p651.
- [14] MOORE, G.E., KELLY, K.K. J. Am. Chem. Soc., 69 (1947) 2105.
- [15] FRERICKSON, D.R., CHASANOV, M.G. J. Chem. Thermo., 2 (1970) 263.
- [16] HEIN, R.A., SJODAHL, L.A., SZWARC, R. J. Nucl. Mater., 25 (1968) 99.
- [17] HEIN, R.A. and FLAGELLA, P.N. Enthalpy Increment measurements of UO<sub>2</sub> and Tungsten to 3260 K, General Electric Report GEMP-578 (1968).
- [18] LEIBOWITZ, L., MISHLER, L.W., CHASANOV, M.G. J. Nucl. Mater., 29 (1969) 356.
- [19] J.J. Hunzicker, E.F. Westrum, J. Chem. Thermo., 3 (1971) 61.
- [20] GRONVOLD, F., KVESETH, N.J., SVEEN, A., TICHY, J. J. Chem. Thermo. 2 (1970) 665.
- [21] C. Affortit, High Temp. – High Press., 1 (1969) 27.
- [22] C. Affortit, J. Marcon, Rev. Int. Hautes Temp. Refract., 7 (1970) 236.
- [23] POPOV, M.M., GALCHENKO, G.L., SENIV, M.D., ZH. NEORG. KIM. 3 (1958) 1734 [English translation: J. Inorganic Chem., 3 (1958) 18].
- [24] ENGEL, T.K. J. Nucl. Mater., 31 (1969) 211.
- [25] BROWNING, P., HYLAND, G.J., RALPH, J. High Temp. – High Press. 15 (1983) 169.
- [26] FISCHER, D.F., FINK, J.K., LEIBOWITZ, L. and BELLE, J. J. Nucl. Mater, 118 (1983) 342-348.
- [27] SENGUPTA, A.K., JARVIS, T., NAIR, M.R., RAMACHANDRAN, R., MUJUMDAR, S. and PURUSHOTHAM, D.S.C. Bhabha Atomic Research Centre, Mumbai, India, BARC/200/E/015 (2000).
- [28] MURABAYASHI, M. J. Nuclear Science and Tech, 7 (11) (1970) 559-563.
- [29] MURABAYASHI, M., NAMBA, S., TAKAHASHI, Y. and MUKAIBO, T. J. Nucl. Sc. Tech., 6(3) (1969) 128-131.
- [30] SPRINGER, J.R., LANGEDROST, J.F. Battelle Memorial Institute Report BMI-X-10231 (1968).
- [31] FERRO, C., MORETTI, S. and PATIMO, C. Eighth Conference on Thermal Conductivity, Plenum Press, C.Y. Ho and R.R. Taylor Editors, (1969) pp 815-822.
- [32] FERRO, C., PATIMO, C. and PICONI, C. J. Nucl. Mat., 43 (1972) 273-276.
- [33] PiLLAI, C.G.S. and RAJ, P. J. Nucl. Mat., 277 (2000) 116-119.

#### 6.1.4.4. Thermal conductivity of $(Th_{1-y}U_y)O_2$ fuels

This experimental measurements and assessments of the thermal conductivity of  $ThO_2$  and  $(Th,U)O_2$  solid solutions were provided by the Radiometallurgy Division, Bhabha Atomic Research Center, Mumbai, India.

##### Introduction

In the present study, thermal conductivity ( $k$ ) of  $ThO_2$  and  $(Th_{1-y}U_y)O_2$  solid solution containing 4, 6, 10 and 20w/o  $UO_2$  have been calculated from the experimentally measured thermal diffusivity data ( $\alpha$ ,  $cm^2/s$ ) by laser flash method, temperature corrected measured density ( $\rho$ , g/cc) and literature values of specific heat ( $C_p$ , J/gK) using the following relation.

$$k = C_p \cdot \alpha \cdot \rho \quad (W/mK) \quad (1)$$

Density of the sample is corrected at each temperature using the co-efficient of thermal expansion of  $(Th,U)O_2$ . The specific heat of mixed  $(Th_{1-y}U_y)O_2$  solid solutions at any temperature were calculated from the literature values of specific heats for pure  $ThO_2$  [1] and  $UO_2$  [2] using Vegard's law. The following relations were used to calculate  $C_p$  of  $(Th_{1-y}U_y)O_2$

$$C_p(Th_{1-y}U_y)O_2 = (1-y) \cdot C_p(ThO_2) + y \cdot C_p(UO_2) \quad (2)$$

where 'y' is the weight fraction of  $UO_2$ ;  $C_p(UO_2)$  and  $C_p(ThO_2)$  are obtained from literature [1, 2] and given by the following equations.

$$C_p(ThO_2) = 55.9620 + 51.2579 \cdot 10^{-3} \cdot T - 36.8022 \cdot 10^{-6} \cdot T^2 + 9.22452 \cdot 10^{-9} \cdot T^3 - 5.7403 \cdot 10^{-5} \cdot T^{-2} \quad (J \cdot mol^{-1} \cdot K^{-1}) \quad (3)$$

where  $T$  is the temperature.

$$C_p(UO_2) = \frac{C_1 \theta^2 e^{\theta/T}}{T^2 (e^{\theta/T} - 1)^2} + 2C_2 T + \frac{C_3 E_a e^{-E_a/T}}{T^2} \quad (4)$$

where  $C_1 = 81.613$ ,  $C_2 = 2.285 \times 10^{-3}$ ,  $C_3 = 2.360 \times 10^7$ ,  $\theta = 548.68$  and  $E_a = 18531.7$ .

The thermal conductivity data was normalized corresponding to a density of 95% T.D. using the following relation [3].

$$f = (1-p)^{1.5} \quad (5)$$

where "f" is the fractional thermal conductivity and "p" the porosity. This equation describes the influence of randomly oriented, spherical porosity on the thermal conductivity. The thermal conductivity data thus obtained could be expressed in the following standard form applicable for insulators and dielectric solids.

$$k = \frac{1}{A + B \cdot T} \quad (6)$$

where 'A' and 'B' are constants. The parameter 'A' represents the influence of phonon scattering by lattice imperfections and 'B' describes the influence of phonon-phonon scattering. The parameter 'A' depends on the difference in mass and radius between the substituted atom and the host atom, while 'B' remains constant theoretically. The details of the factor affecting 'A' and 'B' could be obtained elsewhere [4].

## **Experimental**

### **Material**

ThO<sub>2</sub> is a highly stable stoichiometric compound with very high melting point. Hence, to obtain high-density pellet at relatively lower sintering temperature, it is necessary to dope thorium powder with about 500 ppm MgO. For better homogeneity, the dopant was added in the solution stage before precipitation of oxalate. The characteristics of thorium and uranium powders used in this study are given in Table 1.

ThO<sub>2</sub> powder was pre-milled and co-milled with UO<sub>2</sub> powder in a high energy planetary ball mill for two hours. Progressive milling technique was used for obtaining good homogeneity. The milled powders were double precompacted at 105 MPa and 150MPa and granulated. These granules were compacted in a double acting hydraulic press at 300 MPa using a 12 mm die, lubricated with 1% steric acid.

Sintering of these compacts was carried out in a Molybdenum resistance batch- furnace at 1923 K for 4 hrs. in Nitrogen+8%Hydrogen atmosphere. Addition of UO<sub>2</sub> to ThO<sub>2</sub> brings down the sintered density progressively with increase in UO<sub>2</sub> content. Average green and sintered density as well as chemical analysis results for Thorium & Uranium and the contents in the sintered pellets of different lots are given in Table 2 and Table 3 respectively. The details of the fabrication procedure along with the flow sheet are given elsewhere [5]. The circular cross sections of sintered pellet samples were coated with a thin spray of graphite to ensure complete and uniform absorption of the laser energy during the measurement.

### **Measurement procedure**

Thermal diffusivity was measured by the transient Laser flash method. The details of the experimental setup have been given in reference [6]. The method consists of irradiating one surface of the sample, maintained under adiabatic condition with a pulsed laser. As the heat pulse travels through the specimen, the temperature rise of the other surface is monitored as a function of time using an InSb base IR detector. The time-temperature history of the back surface is directly related to the thermal diffusivity of the specimen.

Measurements were carried out in vacuum ( $6.65 \cdot 10^{-3}$  Pa) from 873 K to 1873 K in a Tungsten-mesh high temperature resistance furnace. At each temperature, the sample equilibrated to the measurement temperature by was soaking for about 5 minutes before the laser irradiation. Few measurements were also performed during cooling cycle of the sample in order to ascertain that the characteristic of the sample has not changed. The time taken for the rear surface of the sample to reach 20, 30, 40, 50, 60, 70 and 80% of the maximum temperature rise was recorded and thermal diffusivity was calculated using Clark and Taylor [7] method of radiation heat loss correction.

The accuracy and reproducibility of the equipment was estimated by measuring thermal diffusivity of fine-grained isotropic graphite standards (NBS SRM 8425) in the same temperature range. The uncertainty based on these measurements is estimated to be  $\pm 2\%$  as shown in Table 4.

### **Results and discussion**

Table 5 shows an overview of the thermal conductivity data of the (Th<sub>1-y</sub>U<sub>y</sub>)O<sub>2</sub> system published by several authors. This indicates that most of the measurements were carried out in the 80's. The data on pure ThO<sub>2</sub> and UO<sub>2</sub> are well established [1,2]. Amongst the different measuring techniques, Laser flash method was used by Springer et al.[8], Murabayashi [9], Ferro et al. [10], Berman et al.[11], and Belle et al.[12] while Kingery [13] and many others have made use of the steady state method and the measurements were carried out in air. Bakker et al [1] has reviewed the thermal conductivity data of (Th<sub>1-y</sub>U<sub>y</sub>)O<sub>2</sub>, in recent time.

Figure 1 shows the thermal conductivity data of ThO<sub>2</sub> and (Th<sub>1-y</sub>U<sub>y</sub>)O<sub>2</sub> as a function of temperature for various UO<sub>2</sub> content and temperature range as published by several authors. The data obtained in the present study are also shown in this figure. All the data were converted to 95% T.D using the relation (5) to enable us to compare the data of different authors. Figure 1 indicates that the compositions (ThO<sub>2</sub>-UO<sub>2</sub>) and temperature range are different for different investigators, like Murabayashi's [9]

data is limited from ambient to 500 C, whereas Springer, Berman, and Belle [8, 11, 12] have reported data from ambient to 1900C. In order to assess the data and come out with recommendations, the data of this study along with those in literatures for the same composition range. These are presented in figures 2, 3, 4, 5, & 6.

Table 6 shows the calculated thermal conductivity data of this study for pure ThO<sub>2</sub> and thorium containing 4, 6, 10, and 20w% of UO<sub>2</sub> as a function of temperature.

### Recommendation

Figure 2 and 4 shows the thermal conductivity data of ThO<sub>2</sub> and (Th<sub>0.94</sub>U<sub>0.06</sub>)O<sub>2</sub> respectively as function of temperature obtained in the present study along with that of Berman et. al. [11]. It is evident that the thermal conductivity data for both the compositions are in close agreement. Similarly Figure 3 shows thermal conductivity data of (Th<sub>0.96</sub>U<sub>0.04</sub>)O<sub>2</sub> along with that of Ferro et al.[10] and Berman et al. [11]. Many authors have presented thermal conductivity data for (Th<sub>0.90</sub>U<sub>0.10</sub>)O<sub>2</sub> and (Th<sub>0.80</sub>U<sub>0.20</sub>)O<sub>2</sub> solid solution as shown in the figures 5 and 6 respectively. While generating these recommended equations for higher UO<sub>2</sub> content of 10 and 20 % the data points of Springer[8] were also included, as they closely matched with the present set of data generated.

The following are the recommended equations for the thermal conductivity (*k*) as a function of temperature (T/K) which is valid from 873 to 1873K, for 0, 4, 6, 10, and 20% of UO<sub>2</sub>.

$$k[\text{ThO}_2] = 1/(-0.03198 + 2.3559 \cdot 10^{-4} \cdot T) \quad (7)$$

$$k[\text{Th}_{0.96}\text{U}_{0.04}\text{O}_2] = 1/(-0.04505 + 2.6241 \cdot 10^{-4} \cdot T) \quad (8)$$

$$k[\text{Th}_{0.94}\text{U}_{0.06}\text{O}_2] = 1/(-0.02884 + 2.6034 \cdot 10^{-4} \cdot T) \quad (9)$$

$$k[\text{Th}_{0.90}\text{U}_{0.10}\text{O}_2] = 1/(-0.1751 + 2.5827 \cdot 10^{-4} \cdot T) \quad (10)$$

$$k[\text{Th}_{0.80}\text{U}_{0.20}\text{O}_2] = 1/(0.02771 + 2.4695 \cdot 10^{-4} \cdot T) \quad (11)$$

Subsequently best fit equation for thermal conductivity of (Th<sub>1-y</sub>U<sub>y</sub>)O<sub>2</sub> of 95% theoretical Density as a function of composition (y/ wt<sub>0</sub>) and temperature (T/K) has been derived, which is valid through 873 to 1873K.

$$k_{(y,T)} = 1/[-0.0464 + 0.0034 \cdot y + (2.5185 \cdot 10^{-4} + 1.0733 \cdot 10^{-7} \cdot y)T] \quad (12)$$

Table 1. Powder characteristics

CHARACTERIZATION	ThO <sub>2</sub>	UO <sub>2</sub>
Powder Preparation	Ex-Oxalate	Ex-ADU
BET Surface area (m <sup>2</sup> /g)	3.716	3.062
Apparent Density (g/cm <sup>3</sup> )	1.230	1.732
Tap density (g/cm <sup>3</sup> )	2.280	2.474
Total Impurity (ppm)	<1000	<400
O/U ratio	-	2.08

Table 2. Density of ThO<sub>2</sub> and ThO<sub>2</sub>-UO<sub>2</sub> pellets

Sr. No.	COMPOSITION	AVERAGE GREEN DENSITY (%TD)	AVERAGE SINTERED DENSITY (%TD)
1.	ThO <sub>2</sub>	66.48	96.43
2.	ThO <sub>2</sub> + 4%UO <sub>2</sub>	65.33	94.66
3.	ThO <sub>2</sub> + 6%UO <sub>2</sub>	65.42	94.04
4.	ThO <sub>2</sub> + 10%UO <sub>2</sub>	64.72	92.19
5.	ThO <sub>2</sub> + 20%UO <sub>2</sub>	63.89	89.33

Table 3. Chemical analysis results for Th & U Content in ThO<sub>2</sub>-UO<sub>2</sub> pellets

SR.NO.	COMPOSITION	Th CONTENT (w%)	U CONTENT (w%)
1.	ThO <sub>2</sub>	86.65 ± 0.43	--
2.	ThO <sub>2</sub> + 4%UO <sub>2</sub>	83.70 ± 0.42	3.490 ± 0.017
3.	ThO <sub>2</sub> + 6%UO <sub>2</sub>	82.60 ± 0.41	5.232 ± 0.026
4.	ThO <sub>2</sub> + 10%UO <sub>2</sub>	78.94 ± 0.39	8.756 ± 0.044
5.	ThO <sub>2</sub> + 20%UO <sub>2</sub>	69.98 ± 0.35	17.453 ± 0.087

Table 4. Thermal diffusivity of graphite (NBS SRM 8425)

TEMP. (K)	RECOMMENDED (cm <sup>2</sup> /s)	EXPERIMENTAL (cm <sup>2</sup> /s)
1000	0.1862	0.1888
1100	0.1691	0.1728
1200	0.1548	0.1588
1300	0.1435	0.1466
1400	0.1329	0.1373
1500	0.1236	0.1284
1600	0.1173	0.1209
1800	0.1111	0.1131

Table 5. Overview of thermal conductivity measurements

YEAR	AUTHORS	T (K)	% ThO <sub>2</sub>
1959	Kingery [6]	373-1070	0,10,26,31,100
1966	Harbinsom and Walker [7]	1073-2073	10,100
1967	Belle et al. [8]	393	0,10,20,30,50,90,100
1968	Springer et al. [9]	573-2173	3,5,7,10,13,20,25,30,100
1968	Ferro C.,Moretti S. et al. [15]	873-1673	1,4,10
1969	MacEwan and Stoute [10]	333	0,1.3
1970	Murabayashi [11]	293-1073	1,3,5,10
1972	R.M. Berman et al.[12]	573-2273	0,2,5,10,20
1972	Ferro.et al. [13]	923-2973	6,10
1981	Rodriguez et al. [14]	773-1773	0,20,100
1997	K.Bakker et al. [1]		Review

Table 6. Calculated thermal conductivity data of (Th<sub>1-y</sub>U<sub>y</sub>)O<sub>2</sub> from the measured thermal diffusivity data (this study)

TEMPERATURE (K)	ThO <sub>2</sub> (W/mK)	ThO <sub>2</sub> +4% UO <sub>2</sub> (W/mK)	ThO <sub>2</sub> +6% UO <sub>2</sub> (W/mK)	ThO <sub>2</sub> +10% UO <sub>2</sub> (W/mK)	ThO <sub>2</sub> +10% UO <sub>2</sub> (W/mK)
873	-	5.25915	4.7255	4.8796	4.4002
973	-	-	4.5794	4.4650	4.2365
1043	4.6306	4.5344	4.0631	4.0926	3.8264
1123	4.3014	4.1033	3.9256	3.6384	3.3656
1213	3.9658	3.6414	3.6443	3.3454	3.0550
1313	3.6361	3.2002	3.2799	3.0060	2.8604
1413	3.3517	3.1297	3.0202	2.8094	2.6565
1513	3.1127	2.8615	2.4818	-	2.4990
1613	2.7708	-	2.5155	2.4936	2.3263
1713	2.6679	2.4406	2.5022	-	2.2570
1813	2.6279	2.3378	-	-	-
1873	2.7068	-	-	-	-

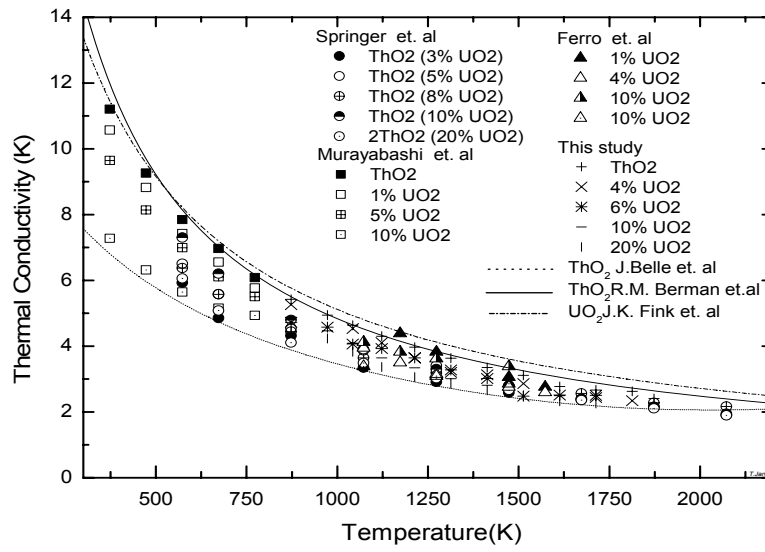


FIG. 1. Thermal conductivity of  $(Th_{1-y}U_y)O_2$  as a function of temperature as reported by various authors.

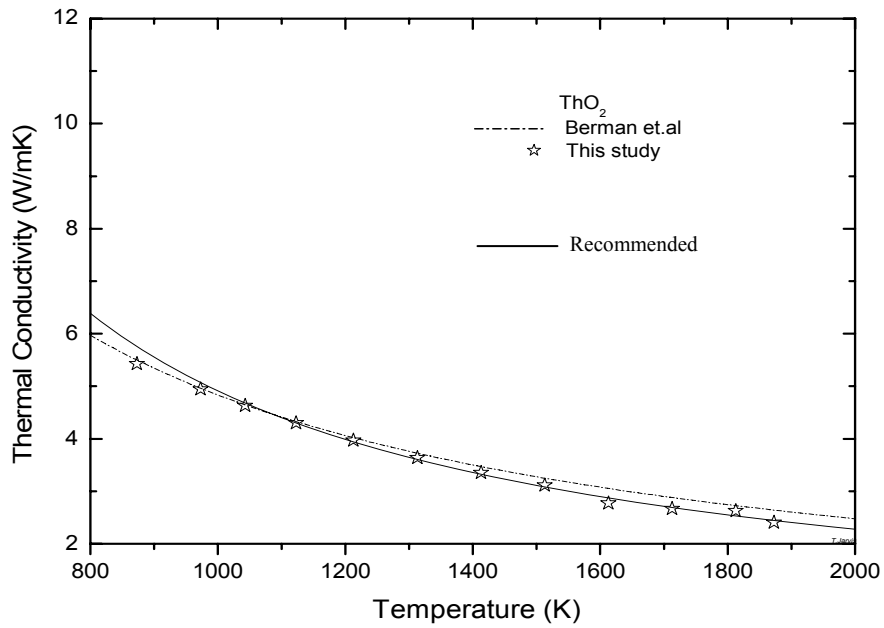


FIG. 2. Thermal conductivity of pure  $ThO_2$  (95% T.D.).

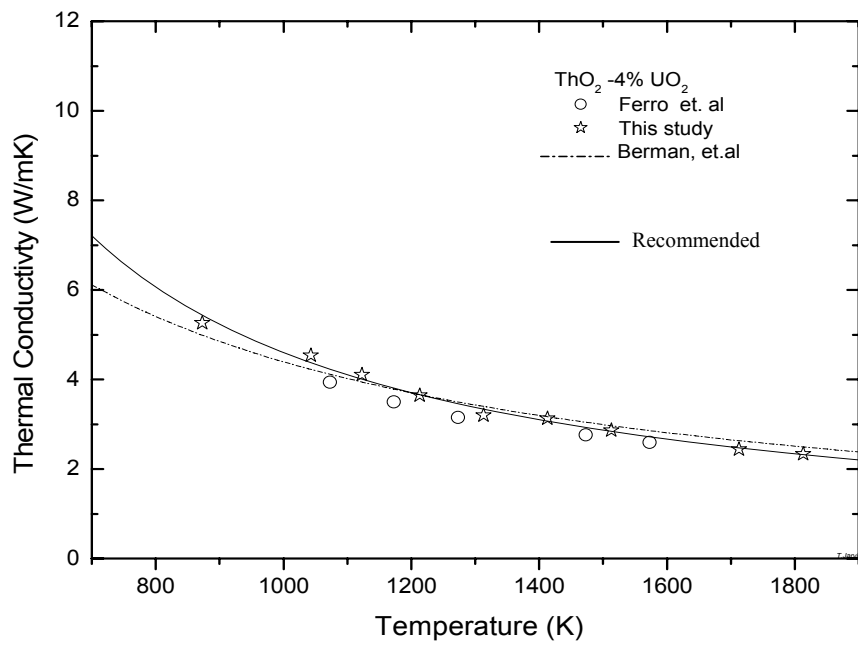


FIG. 3. Thermal conductivity of  $(Th_{0.96}U_{0.04})O_2$  (95% T D) as a function of temperature.

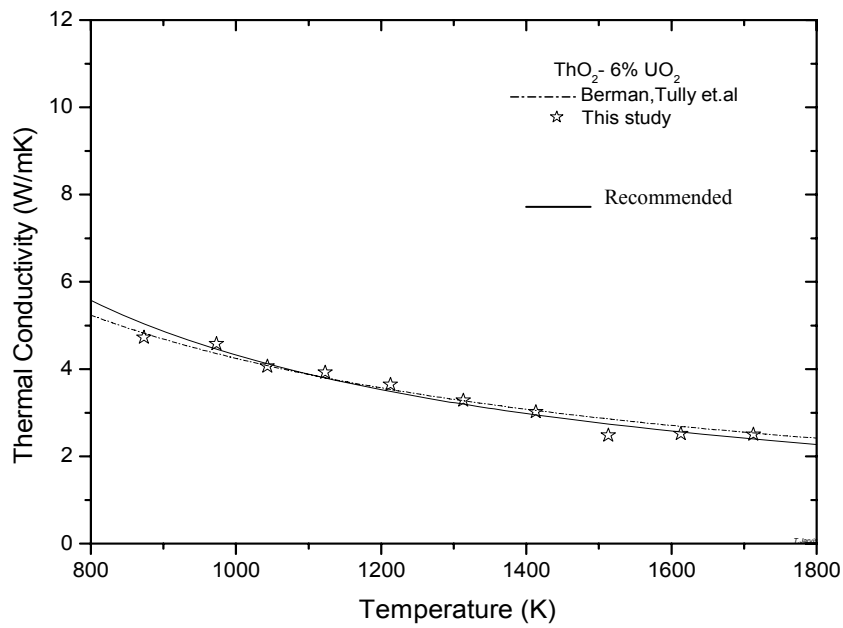


FIG. 4. Thermal conductivity of  $(Th_{0.94}U_{0.06})O_2$  (95% T D) as a function of temperature.

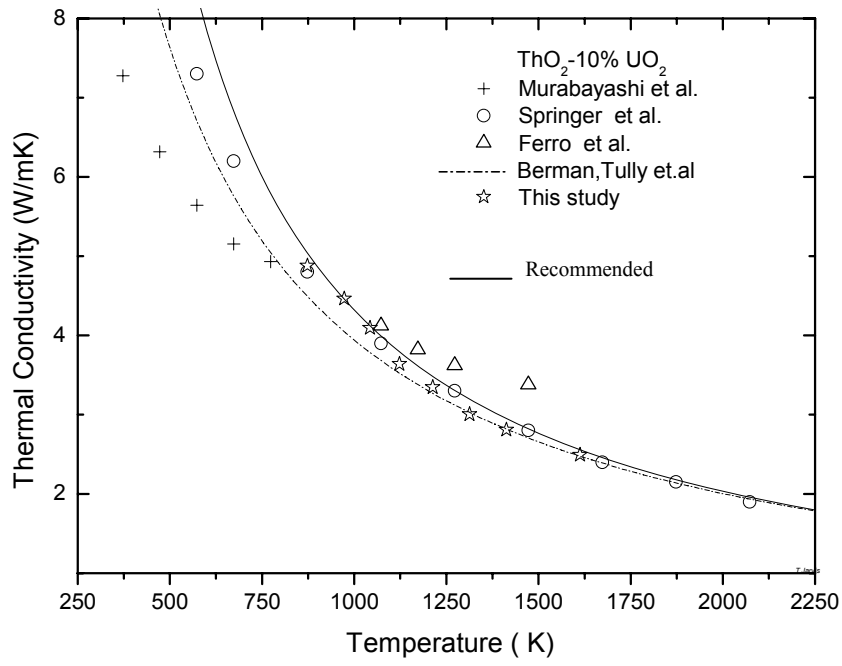


FIG. 5. Thermal conductivity of  $(\text{Th}_{0.90}\text{U}_{0.10})\text{O}_2$  (95%TD) as a function of temperature.

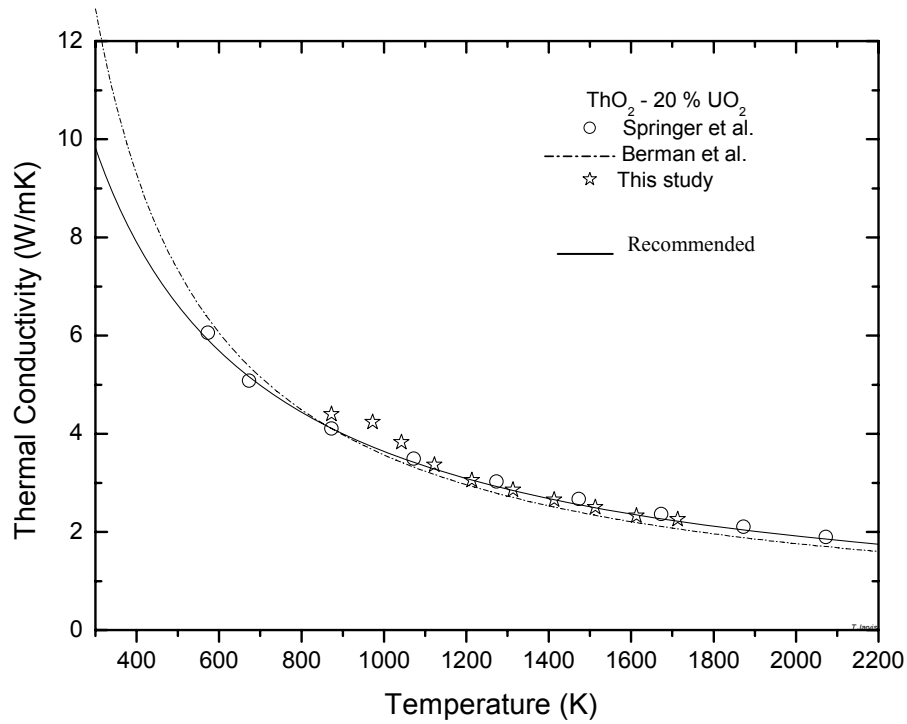


FIG. 6. Thermal conductivity of  $(\text{Th}_{0.80}\text{U}_{0.20})\text{O}_2$  (95%TD) as a function of temperature.



## REFERENCES TO SECTION 6.1.4.4

- [1] BAKKER.K, CORDFUNKE E.H.P.,et al. "Critical evaluation of the thermal propertie of ThO<sub>2</sub> and Th<sub>1-y</sub> U<sub>y</sub>O<sub>2</sub> and a survey of the literature data on (Th<sub>1-y</sub> Pu<sub>y</sub>)O<sub>2</sub>" Journal of Nuclear Materials, 250(1997) 1-12.
- [2] FINK, J.K. "Thermophysical properties of uranium dioxide" Journal of Nuclear Materials 279 (2000) 1-18.
- [3] SCHULZ, B. High Temp.-High Press. 13 (1981) 649.
- [4] TAKAHASHI, Y., MURABAYASHI, M, "Measurement of Thermal Properties of Nuclear Materials by Laser Flash Method", J. Nucl. Sci. Technol., 12 (3), 133 (1975)
- [5] NAIR, M.R., BASAK, U., RAMACHANDRAN, R. and MAJUMDAR, S. Proceeding of the International Symposium and Annual Technical meeting of Powder Metallurgy Association of India (PMAI), Hyderabad, March 23-25(1999).
- [6] SENGUPTA, A.K., GANGULY, C., MAJUMDAR, S. and ROY, P.R. "Proceedings of the 5<sup>th</sup> National symposium on thermal analysis" IIT Kharagpur, India. Dec 20-22 (1985).
- [7] CLARK, L.M., and TAYLOR, R.E. Journal of Applied Physics. 46(2), 714-719(1975).
- [8] SPRINGER, J.R., ELDRIDGE, E.A., GOODYEAR, M.U., WRIGHT, T.R. and LANGEDROST, J.F. Battelle Memorial Institute BMI-X-10210 (1967).
- [9] MURABAYASHI, M. "Thermal Conductivity of Ceramic solid solutions", Journal of Nuclear Science and Technology 7[11], 559, (1970).
- [10] FERRO C., MORETTI.S and PATIMO C. "Proceedings of the eighth conference on thermal conductivity." Purdue University, West Indiana, Oct.7-10, Plenum Press, New York, 815-822, (1968).
- [11] BERMAN, R.M., TULLY, T.S., BELLE, J.and GOLDBERG, I. " The thermal conductivity of polycrystalline thoria and thoria-urania solid solution.(LMWR Development Program WAPD.TM.908).
- [12] BELLE, J. and BERMAN, R.M. "Thorium Dioxide: Properties and nuclear applications." DOE/NE-0060.
- [13] KINGERY. W.D. "Thermal Conductivity: XIV, Conductivity of multi-component Systems." Journal of The American Ceramic Soc. 42, 617, (1959).
- [14] HARBINSON, R.J.WALKER, Trans. American Nuclear Society. 9 (1966) 26.
- [15] MACEWAN J.R. and STOUTE R.L. "Annealing of irradiation-induced thermal conductivity changes in ThO<sub>2</sub>-1.3 w% UO<sub>2</sub>". Journal of the American Ceramic Society Vol. 52 No.3 page 160 (1969).
- [16] RODRIGUEZ, P.C., SUNDARAM, V. Journal of Nuclear Materials. 100 (1981) 227.

### 6.1.4.5. Thermal conductivity of (Th<sub>1-y</sub>Pu<sub>y</sub>)O<sub>2</sub>

The assessment of the thermal conductivity of (Th<sub>1-y</sub>Pu<sub>y</sub>)O<sub>2</sub> was provided by the Radiometallurgy Division, Bhabha Atomic Research Center, Mumbai, India.

#### **Recommendation**

The best-fit equation for the thermal conductivity, k [W/m.K], of (Th<sub>1-y</sub>Pu<sub>y</sub>)O<sub>2</sub> as a function of composition, y [wt%], and temperature, T [K], was derived for the temperature range from 873 to 1873K.

$$k_{(y,T)} = 1/[-0.08388 + 1.7378 \cdot y + (2.62524 \cdot 10^{-4} + 1.7405 \cdot 10^{-4} \cdot y)T]$$

$$(R^2 = 0.965 ; S.D = 0.2117)$$

## Discussion

(Th<sub>1-y</sub>Pu<sub>y</sub>)O<sub>2</sub> is considered as a potential fuel for the heavy water reactor and is a candidate fuel for the forthcoming Indian Advanced Heavy Water Reactor (AHWR), which is a part of Thorium utilisation program. Thermal conductivity is one of the most important thermo-physical properties to predict the fuel performance and is an important parameter for the fuel designer. Thermal conductivity data of this relatively new fuel are not available in literature and an attempt has been made to establish a data bank of thermal conductivity as a function of temperature and plutonium content.

Thermal conductivity ( $k$ ) of ThO<sub>2</sub> and (Th<sub>1-y</sub>Pu<sub>y</sub>)O<sub>2</sub> solid solution with PuO<sub>2</sub> containing 2, 4, 6 and 10 wt% has been calculated from the experimentally measured thermal diffusivity data,  $\alpha$  (cm<sup>2</sup>/s), by laser flash method, its density,  $\rho$  (g/cc), corrected for temperature using the measured expansion values and literature values of specific heat,  $C_p$  (J/gK). The following equation was used to calculate the thermal conductivity.

$$k = C_p \cdot \alpha \cdot \rho \quad (\text{W/mK}) \quad (1)$$

The specific heat of mixed (Th<sub>1-y</sub>Pu<sub>y</sub>)O<sub>2</sub> solid solutions was calculated from the literature values of specific heats of pure ThO<sub>2</sub> [1] and PuO<sub>2</sub>[2] and subsequently using Vegard's law (assuming an ideal solid solution behaviour). The following equations were used to calculate  $C_p$  [J mol<sup>-1</sup>K<sup>-1</sup>] of (Th<sub>1-y</sub>U<sub>y</sub>)O<sub>2</sub>

$$C_{p(\text{Th}_{1-y}\text{Pu}_y)\text{O}_2} = (1-y) \cdot C_{p(\text{ThO}_2)} + y \cdot C_{p(\text{PuO}_2)} \quad (2)$$

where 'y' is the weight fraction of PuO<sub>2</sub>.

$C_{p(\text{PuO}_2)}$  and  $C_{p(\text{ThO}_2)}$  are given by the following equations:

$$C_{p(\text{ThO}_2)} = 55.9620 + 51.2579 \cdot 10^{-3} \cdot T - 36.8022 \cdot 10^{-6} \cdot T^2 + 9.22452 \cdot 10^{-9} \cdot T^3 - 5.7403 \cdot 10^5 \cdot T^{-2} \quad (3)$$

and

$$C_{p(\text{PuO}_2)} = \frac{347.4 \cdot 571^2 e^{\frac{572}{T}}}{T^2 \left[ e^{\left(\frac{571}{T}\right)} - 1 \right]^2} + 3.95 \cdot 10^{-4} \cdot T + \frac{3.860 \cdot 10^7 \cdot 1.967 \cdot 10^5}{RT^2} \cdot e^{\left(\frac{-1.965 \cdot 10^5}{RT}\right)} \quad (4)$$

where T is the Temperature in K and R is the universal gas constant.

The thermal conductivity data was normalized corresponding to a density of 95% theoretical density using the following equation [3]:

$$f = (1-p)^{1.5} \quad (5)$$

where 'f' is the fraction thermal conductivity and 'p' the porosity. This equation describes the influence of randomly oriented, spherical porosity on the thermal conductivity.

## Experimental measurements

### Material preparation

(Th<sub>1-y</sub>Pu<sub>y</sub>)O<sub>2</sub> pellets of compositions 0, 2, 4, 6 and 10% PuO<sub>2</sub> were fabricated by powder pellet route, involving mechanical mixing, cold compaction and high temperature sintering. The characteristics of the starting powders are summarized in Table 1. ThO<sub>2</sub> powder used for this work was doped with 500 ppm MgO as sintering aid.

The fabrication procedure followed for ThO<sub>2</sub> and (Th<sub>1-y</sub>Pu<sub>y</sub>)O<sub>2</sub> pellets were similar. To improve the sinterability of the ThO<sub>2</sub> powder, it was milled for 4 hrs in a planetary ball mill before mixing with PuO<sub>2</sub>. The PuO<sub>2</sub> and ThO<sub>2</sub> powders in required proportions were co-milled for 2 hrs. Progressive mixing technique was adopted for getting good micro-homogeneity. The mixture was double

precompacted at 105 and 150 MPa and granulated. Final compaction of the granules was done at 300 MPa in a die of 12 mm diameter. The green pellets were sintered at 1650<sup>0</sup> C for 4 hrs in N<sub>2</sub> + 8% H<sub>2</sub> atmosphere. The densities and the O/M ratios of the sintered pellets were measured and given in Table 2. The details of the fabrication procedure along with the flow sheet are given elsewhere [4]. These sintered cylindrical pellet samples were sliced to around 2 mm thickness and coated with a thin spray of graphite to ensure complete and uniform absorption of the laser energy during the measurement.

### **Measurement procedure**

The thermal diffusivity was measured by the transient Laser flash method. The details of the experimental set up have been given in reference [5]. The method consists of placing a thin disk-shaped specimen in an isothermal zone of a furnace adiabatically and irradiating one face with a pulsed laser. As the heat pulse travels through the specimen, the temperature rise of the other face is monitored as a function of time using an InSb base IR detector. The time-temperature history of the back surface is directly related to the thermal diffusivity of the specimen. The time taken for the rear surface of the sample to reach 20, 30, 40, 50, 60, 70 and 80% of the maximum temperature rise was recorded and the thermal diffusivity thus obtained was corrected for radiation heat loss, as proposed by Clark and Taylor [6].

Measurements were carried out in vacuum ( $6.65 \times 10^{-3}$  Pa) from 873 K to 1873 K at 100K intervals in a Tungsten-mesh high temperature resistance furnace. At each temperature, the sample was soaked for about 5 minutes before irradiating with the laser pulse. Few measurements were also performed during cooling cycle of the sample in order to ensure that there is no stoichiometric or any other characteristic changes in the sample during the experiment.

### **Results and discussion**

The thermal conductivity of pure ThO<sub>2</sub> is well established [1]. It is predicted that the thermal conductivity of (Th,Pu)O<sub>2</sub> decreases with the addition of PuO<sub>2</sub>. However there is not sufficient reported data to substantiate the claim. Since CeO<sub>2</sub> and PuO<sub>2</sub> have similar thermodynamic and crystallographic properties [7, 8], Murabayashi [9] tried to simulate the thermal conductivity as a function of temperature and CeO<sub>2</sub> up to 10 wt%, using Laser flash method. Jeffs [10] determined the Integral thermal conductivity of irradiated (Th<sub>1-y</sub> Pu<sub>y</sub>)O<sub>2</sub> containing 1.10, 1.75, 2.72 wt% of PuO<sub>2</sub> using a steady state method. Bakkar et al. [1] conducted a survey of the literature data on (Th<sub>1-y</sub> Pu<sub>y</sub>)O<sub>2</sub>.

Figure 1 shows the thermal conductivity  $\lambda$ , of (Th<sub>1-y</sub>U<sub>y</sub>)O<sub>2</sub> as a function of temperature and PuO<sub>2</sub> content as obtained in this study, fitted to equation (6), after correcting to 95% theoretical density. Being a dielectric material, the temperature dependence of the thermal resistivity ( $R$ ), which is the reciprocal of the thermal conductivity, ( $\lambda$ ), is described by the equation:

$$R = \frac{1}{\lambda} = A + B.T \quad (6)$$

where ' $\lambda$ ' is in (W/mK). The constant 'A' corresponds to the defect thermal resistivity caused by phonon interactions with lattice imperfections, impurities etc. The lattice strain caused by the dissolution of PuO<sub>2</sub> contributes largely to the lattice defect thermal resistivity; hence 'A' generally increases with the PuO<sub>2</sub> content. The term ' $B.T$ ' corresponds to the intrinsic thermal resistivity, which is caused by phonon-phonon interactions (Umklapp process).

Figure 1 shows a systematic decrease of thermal conductivity with increasing PuO<sub>2</sub> content and temperature. The data are comparable with those obtained by Murabayashi [9] on simulated fuel samples of the composition ranging from 0 to 10 w% CeO<sub>2</sub>. Jeffs [10] derived the thermal conductivity of ThO<sub>2</sub> with 1.10, 1.75 and 2.72 wt% from the values of linear heat rating obtained during the irradiation condition in the reactor. The derived thermal conductivity data are much lower than that obtained in this present study, convincingly due to irradiation damage of the sample. At lower temperature, the decrease in thermal conductivity with increase in PuO<sub>2</sub> is more prominent than that at high temperature.

The thermal conductivity data obtained in this study are presented in Table 3. The values of constants ‘A’ and ‘B’ of the fitted equations for each composition are given in Table 4. The best-fit equation for the thermal conductivity of  $(\text{Th}_{1-y}\text{Pu}_y)\text{O}_2$  as a function of composition, y [wt% ], and temperature, T [K], was derived for the temperature range from 873 to 1873K.

$$k_{(y,T)} = 1/[-0.08388 + 1.7378 \cdot y + (2.62524 \cdot 10^{-4} + 1.7405 \cdot 10^{-4} \cdot y)T] \quad (7)$$

$$(R^2 = 0.965 ; \text{S.D} = 0.2117)$$

### Conclusions

The thermal diffusivity of  $(\text{Th}_{1-y}\text{Pu}_y)\text{O}_2$  solid solutions containing 0, 2, 4, 6 and 10, wt%  $\text{PuO}_2$  were measured in vacuum from 873K to 1873K by Laser flash method. From those data, the thermal conductivity of the compositions was calculated using literature values of specific heat and measured density. Thermal conductivity data were normalized to 95% of theoretical density and equations were generated as a function of compositions and temperature. The data show that thermal conductivity decreases with increase in temperature and  $\text{PuO}_2$  content. The decrease in the conductivity of  $(\text{Th}_{1-y}\text{Pu}_y)\text{O}_2$  solid solution due to  $\text{PuO}_2$  addition was attributed to the additional thermal resistivity caused by lattice strain caused by the dissolution of  $\text{PuO}_2$ . The decrease in thermal conductivity with increase in temperature is attributed to the influence of phonon-phonon scattering.

Table 1. Powder characteristics

BASIS OF CHARACTERIZATION	$\text{PuO}_2$	$\text{ThO}_2$
Powder Preparation	Ex-Oxalate	Ex-Oxalate
BET Surface area ( $\text{m}^2/\text{g}$ )	5.938	3.716
Apparent Density ( $\text{g}/\text{cm}^3$ )	2.097	1.230
Tap density ( $\text{g}/\text{cm}^3$ )	2.696	2.280
Total Impurity (ppm)	<2000	<1500
Metal Content (wt %)	85.23	86.35

Table 2. Density of  $\text{ThO}_2$  and  $(\text{Th}_{1-y}\text{Pu}_y)\text{O}_2$  pellets

SR. NO.	COMPOSITION	AVERAGE GREEN DENSITY (%TD)	AVERAGE SINTERED DENSITY (%TD)	O/M
1.	$\text{ThO}_2$	61.05	91.80	2.000
2.	$\text{ThO}_2 + 2\%\text{PuO}_2$	63.44	94.16	1.978
3.	$\text{ThO}_2 + 4\%\text{PuO}_2$	65.00	92.78	1.972
4.	$\text{ThO}_2 + 6\%\text{PuO}_2$	63.78	93.18	1.978
5.	$\text{ThO}_2 + 10\%\text{PuO}_2$	63.90	91.42	1.973

Table 3. Calculated thermal conductivity data of  $(\text{Th}_{1-y}\text{Pu}_y)\text{O}_2$  from the measured thermal diffusivity data

TEMPERATURE (K)	$\text{ThO}_2$	$\text{ThO}_2\text{-2\%PuO}_2$	$\text{ThO}_2\text{-4\%PuO}_2$	$\text{ThO}_2\text{-6\%PuO}_2$	$\text{ThO}_2\text{-10\%PuO}_2$
873	5.85717	5.26669	4.52924	—	3.3781
973	4.94972	4.65943	3.89819	3.65713	3.11763
1040	4.524	4.22765	3.70189	3.47754	2.97146
1123	4.32014	4.03734	3.49861	3.33162	2.8879
1213	3.96416	3.62552	3.18849	2.94253	2.7417
1313	3.68172	3.27935	2.91752	2.68068	2.59559
1413	3.37919	3.02083	2.65776	2.5161	2.39614
1513	3.11333	2.72782	—	2.41708	2.28786
1613	2.88816	2.58238	2.35462	2.25912	—
1713	2.70118	—	—	—	2.0411
1813	2.48857	2.29628	2.12028	—	—

Table 4. Values of the constants  $A$ ,  $B$  of thermal conductivity  $(k) = (A+BT)^{-1}$

CONSTANTS	$\text{ThO}_2$	$\text{ThO}_2\text{-2\%PuO}_2$	$\text{ThO}_2\text{-4\%PuO}_2$	$\text{ThO}_2\text{-6\%PuO}_2$	$\text{ThO}_2\text{-10\%PuO}_2$
$A$ ( $\text{m}^{-1}\text{K}^{-1}\text{W}^{-1}$ )	-0.03093	-0.04501	-0.0091	0.00424	0.09665
$B$ ( $\text{mW}^{-1}$ )	$2.346 \times 10^{-4}$	$2.66927 \times 10^{-4}$	$2.67642 \times 10^{-4}$	$2.73889 \times 10^{-4}$	$2.25893 \times 10^{-4}$
$R^2$	0.998	0.999	0.999	0.994	0.997

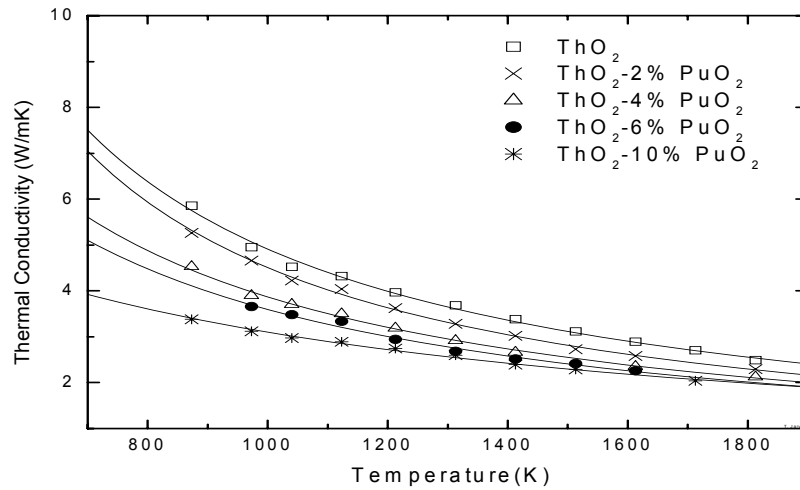


FIG. 1. Thermal conductivity of  $(\text{Th}_{1-y}\text{Pu}_y)\text{O}_2$  as a function of temperature.

## REFERENCES TO SECTION 6.1.4.5

- [1] BAKKER.K, CORDFUNKE, E.H.P., et al., Critical evaluation of the thermal properties of  $\text{ThO}_2$  and  $\text{Th}_{1-y}\text{U}_y\text{O}_2$  and a survey of the literature data on  $(\text{Th}_{1-y}\text{Pu}_y)\text{O}_2$ , Journal of Nuclear Materials, 250 (1997) 1-12.
- [2] INTERNATIONAL ATOMIC ENERGY AGENCY, Thermophysical properties of materials for watercooled reactors, IAEA-TECDOC-949 p. 51 (1997).
- [3] SCHULZ, B., High Temp.-High Press. 13 (1981) 649.
- [4] NAIR, M.R., BASAK, U., RAMACHANDRAN, R. and MAJUMDAR, S., Proceeding of the International Symposium and Annual Technical meeting of Powder Metallurgy Association of India (PMAI), Hyderabad, March 23-25(1999).
- [5] TAYLOR, R.E., Heat pulse thermal diffusivity measurements, High Temperature-High pressure, Vol II, 43-58 (1979).
- [6] CLARK, L.M. and TAYLOR, R.E., Journal of Applied Physics. 46(2), 714-719(1975).
- [7] YUKSEL ALTAS, et al., Structural and thermal investigations on cerium oxalate and derived oxide powders for the preparation of  $(\text{Th,Ce})\text{O}_2$  pellets, Journal of nuclear materials, 298 (2001)316-320.
- [8] JEFFS, A.T., BOUCHER, R.R. and NORLOCK, L.R., Fabrication of  $\text{UO}_2$ - $\text{PuO}_2$  and  $\text{ThO}_2$ - $\text{PuO}_2$  experimental fuel” IAEA , STI/PUB/153, Vienna (1967).
- [9] MURABAYASHI, M., Thermal conductivity of ceramic solid solutions, Journal of Nuclear Science and Technology 7[11], 559 (1970).
- [10] JEFFS, A.T., Thermal conductivity of  $\text{ThO}_2$ - $\text{PuO}_2$  under irradiation, AECL-3294.

### 6.1.4.6. Thermal expansion of $\text{ThO}_2$ - $\text{UO}_2$ and $\text{ThO}_2$ - $\text{PuO}_2$ system in the temperature range 300K-1773K

The measurement and assessment of the thermal expansion of  $(\text{Th}_{1-y}\text{U}_y)\text{O}_{2a}$  and  $(\text{Th}_{1-y}\text{Pu}_y)\text{O}_{2a}$  were provided by the Radiometallurgy Division , Bhabha Atomic research Center, Mumbai, India.

#### **Introduction**

In the present investigation thermal expansion data of  $(\text{Th}_{1-y}\text{U}_y)\text{O}_2$  solid solutions with  $\text{UO}_2$  content varying from 2 to 20 wt% and  $(\text{Th}_{1-y}\text{Pu}_y)\text{O}_2$  solid solutions with  $\text{PuO}_2$  content varying from 2 to 10 wt% have been generated experimentally using a high temperature dilatometer. Finally an assessment of these properties data has been made taking into account the literature data available and recommendations made.

#### **Experimental**

##### *Material*

Sintered fuel pellets of dimensions: 6 mm in diameter and 8 mm long have been prepared by conventional powder metallurgy technique. The compositions chosen for measurement of thermal expansion are pure  $\text{ThO}_2$  and  $\text{ThO}_2$  containing 2,4,6,10 and 20 wt%  $\text{UO}_2$  for thoria-urania system and  $\text{ThO}_2$  containing 2,4,6 and 10 wt%  $\text{PuO}_2$  for the thoria-plutonia system. The details of the pellet fabrication procedure and the characteristics of the sintered pellets are given in details in the previous paper on thermal conductivity of thoria-urania and thoria-plutonia system.

##### *Procedure*

Thermal expansion was measured in a high temperature horizontal dilatometer (Model: 402 E/7; Make: M/s Netzsch Germany) in the temperature range 300K–1773K. During the measurement, the samples were heated continuously from room temperature to 1773 K in a graphite sample holder and push rod assembly at a heating rate of 6 K/min in argon atmosphere with a flow rate of 200cc/min. A small force of 0.2 N was applied to the sample through the push rod. The length change of the sample was measured continuously by an LVDT maintained at constant temperature by means of water circulation from a constant temperature bath. The dilatometer is capable of measuring a length change of  $\pm 0.1\mu\text{m}$ . The experimental data for each sample was later corrected for the expansion of the push

rod and sample holder assembly by taking a standard sample (POCO graphite, NIST) run under identical experimental condition. The experimentally measured data for Tungsten (NBS SRM 737), after graphite correction, were plotted against the recommended data of NBS and is shown in Figure 1. It is observed from the figure that the experimental data and NBS recommended values are in close agreement.

### Results

The experimental data was expressed as percentage linear thermal expansion and were fitted to a third degree polynomial for each composition and can be expressed as a function of temperature (K) in the form given below:

$$[(\Delta L)/L_0]_T \cdot 100 = A + B.T + C.T^2 + D.T^3 \quad (1)$$

where  $\Delta L$  is the change in length at temperature  $T$  (K),  $L_0$  is the original length and A,B,C,D are constants. The value of the constants for each composition of  $\text{ThO}_2\text{-UO}_2$  and  $\text{ThO}_2\text{-PuO}_2$  solid solutions are given in Table 1 and Table 2 respectively. Figure 2 shows the plot of thermal expansion data against temperature for thorium-uranium solid solutions while Figure 3 shows the same for thorium-plutonium system.

The uncertainty in the values of  $\Delta L/L_0$  (equation no 1) may arise from three factors, namely accuracy in temperature measurement (i.e. the accuracy of the thermocouple), accuracy in LVDT and the accuracy in the digital micrometer for the measurement of the initial length of the sample ( $L_0$ ). The thermocouple used in the present study was W-3% Re & W-25% Re. having an accuracy of  $\pm 13$  K in the temperature range of 300K–699 K and  $\pm 1\%$  in the temperature range of 700 K–2023 K. The LVDT of the dilatometer is capable of measuring a length change of  $\pm 0.1 \mu\text{m}$ . The digital micrometer used for initial length measurement has an accuracy of  $\pm 1 \mu\text{m}$ . The uncertainty (maximum) in the above values of  $\Delta L/L_0$  estimated by taking into account all the three above mentioned possible errors was found to be  $\pm 5\%$ , in the temperature range from 573 K–1773 K for both  $\text{ThO}_2\text{-UO}_2$  and  $\text{ThO}_2\text{-PuO}_2$  solid solutions.

### Assessment of data and recommendations

#### $(\text{Th}_{1-y}\text{U}_y)\text{O}_2$ system

Literature survey reveals that a number of measurements have been carried out by different authors in different laboratories. A list of the authors and the year of publications are given in Table 3. It appears from the table that most of these measurements were carried out in late 50's and 60's and the most recent experimental data would be the one presented here.

Touloukian et al [1] recommended the equation for percentage linear thermal expansion  $[(\Delta L/L_0) \times 100]$  of pure  $\text{ThO}_2$  in the temperature range 150 K to 2000 K and has been widely accepted. Similarly, Martin [2] had reviewed thermal expansion data for  $\text{UO}_2$  and has been accepted as the most authenticated data set. Bakker et al [3] has recommended the percentage linear thermal expansion data of  $(\text{Th}_{1-y}\text{U}_y)\text{O}_2$  ( $0 < y < 1$ ) by obtaining the linear interpolation of the values of Touloukian [1] and Martin [2] and obtained two different relations in two different set of temperature ranges:

$$(\Delta L/L_0) \times 100 = -0.179 - y * 0.087 + (5.097 \times 10^{-4} + y * 4.705 \times 10^{-4}).T + (3.732 \times 10^{-7} - y * 4.002 \times 10^{-7}).T^2 - (7.594 \times 10^{-11} - y * 11.98 \times 10^{-11}).T^3 \quad (2)$$

(for 273 K < T < 923 K)

$$(\Delta L/L_0) \times 100 = -0.179 - y * 0.149 + (5.097 \times 10^{-4} + y * 6.693 \times 10^{-4}).T + (3.732 \times 10^{-7} - y * 6.161 \times 10^{-7}).T^2 - (7.594 \times 10^{-11} - y * 19.784 \times 10^{-11}).T^3 \quad (3)$$

(for 923 K < T < 2000 K)

Momin et al [4] measured lattice thermal expansion of  $(\text{Th,U})\text{O}_2$  system by X-ray diffraction method. He obtained coefficient of expansion data for pure  $\text{ThO}_2$  and  $(\text{Th}_{0.8}\text{U}_{0.2})\text{O}_2$  to be  $9.5 \times 10^{-6} \text{ K}^{-1}$  and  $7.1 \times 10^{-6} \text{ K}^{-1}$  respectively in the temperature range 298-1600 K. It was observed that the coefficient of thermal expansion of  $(\text{Th}_{0.8}\text{U}_{0.2})\text{O}_2$  is lower than either of  $\text{ThO}_2$  and  $\text{UO}_2$ , which is quite unreasonable, and hence in the absence of any explanation this data has not been considered. In the present investigation, the mean linear thermal expansion coefficient (1/K) in the same temperature range (298-1600K) for these compositions is calculated from the experimentally measured data of

percentage linear thermal expansion and were found to be  $11.0659 \times 10^{-6} \text{ K}^{-1}$  and  $11.0505 \times 10^{-6} \text{ K}^{-1}$  respectively. The coefficient of expansion data of Momin et al [4], Springer et al [5], Turner and Smith [6], Kempter & Elliot [7] and Lynch and Beals [8] shows a wide scatter of data points when plotted against composition (mol%  $\text{ThO}_2$ ). Rodriguez and Sundaram [9] in their review article reported an average linear thermal expansion coefficient of  $9.67 \times 10^{-6} \text{ K}^{-1}$  for  $\text{ThO}_2$  (293–2273 K) and  $12.5 \times 10^{-6} \text{ K}^{-1}$  for  $(\text{Th}_{0.8}\text{U}_{0.2})\text{O}_2$  (1100–2400K). Powers and Shapiro [10] mentioned same average linear thermal expansion coefficient value of  $9 \times 10^{-6} \text{ K}^{-1}$  for both pure  $\text{UO}_2$  and  $(\text{U}_{0.064}\text{Th}_{0.936})\text{O}_2$  (up to 1073 K). He obtained lower coefficient value ( $8 \times 10^{-6} \text{ K}^{-1}$  up to 1073 K) for  $(\text{Th}_{0.8}\text{U}_{0.2})\text{O}_2$ . However, no explanation was given for this unusual behaviour. Figure 4 shows the experimental percentage thermal expansion data of  $\text{ThO}_2$ - $\text{UO}_2$  and the data recommended by other authors.

The present experimental thermal expansion data of  $\text{ThO}_2$  containing 4 and 10 wt.%  $\text{UO}_2$  were only considered as for other compositions thermal expansion data were more than that of  $\text{ThO}_2$  suggested by Touloukian. The experimental data for these two compositions are fitted to a third degree polynomial equation (equation 1) and are given below:

Percentage linear thermal expansion for  $\text{ThO}_2$  containing 4%  $\text{UO}_2$  ( $300 \leq T \leq 1473 \text{ K}$ ) :-

$$(\Delta L/L_0) \times 100 = -0.272 + 8.152 \times 10^{-4} \cdot T + 2.220 \times 10^{-7} \cdot T^2 - 8.734 \times 10^{-11} \cdot T^3 \quad (4)$$

( $R^2$  : 0.99969; SD: 0.00772)

Percentage linear thermal expansion for  $\text{ThO}_2$  containing 10%  $\text{UO}_2$  ( $300 \leq T \leq 1473 \text{ K}$ ):-

$$(\Delta L/L_0) \times 100 = -0.2448 + 6.831 \times 10^{-4} \cdot T + 4.436 \times 10^{-7} \cdot T^2 - 16.537 \times 10^{-11} \cdot T^3 \quad (5)$$

( $R^2$  : 0.99978; SD: 0.00688)

The data obtained by taking average between the present experimental data and the data recommended by Bakker (equation no 2 and 3) for the two compositions:  $\text{ThO}_2$  containing 4%  $\text{UO}_2$  and  $\text{ThO}_2$  containing 10%  $\text{UO}_2$  were fitted into a third degree polynomial (equation 1) and is recommended (given below). Figure 5 shows the plot of these recommended percentage thermal expansion for the compositions:  $\text{ThO}_2$  containing 4%  $\text{UO}_2$  and  $\text{ThO}_2$  containing 10%  $\text{UO}_2$  against temperature (K) along with the recommended data for  $\text{ThO}_2$  by Touloukian and for  $\text{UO}_2$  by Martin. For pure  $\text{ThO}_2$  and pure  $\text{UO}_2$ , the data of Touloukian and the data of Martin for  $\text{UO}_2$  are recommended and are also given below.

Recommended percentage linear thermal expansion for  $\text{ThO}_2$  containing 4%  $\text{UO}_2$  ( $300 \leq T \leq 1773 \text{ K}$ ) :-

$$(\Delta L/L_0) \times 100 = -0.246 + 7.762 \times 10^{-4} \cdot T + 1.206 \times 10^{-7} \cdot T^2 - 4.735 \times 10^{-12} \cdot T^3 \quad (6)$$

( $R^2$  : 0.99971; SD: 0.00841)

Recommended percentage linear thermal expansion for  $\text{ThO}_2$  containing 10%  $\text{UO}_2$  ( $300 \leq T \leq 1773 \text{ K}$ ):-

$$(\Delta L/L_0) \times 100 = -0.229 + 7.013 \times 10^{-4} \cdot T + 2.433 \times 10^{-7} \cdot T^2 - 5.174 \times 10^{-11} \cdot T^3 \quad (7)$$

( $R^2$  : 0.99916; SD: 0.01452)

Recommended percentage linear thermal expansion for  $\text{ThO}_2$  ( $150 \leq T \leq 2000 \text{ K}$ ) by Touloukian[1] :-

$$(\Delta L/L_0) \times 100 = -0.179 + 5.097 \times 10^{-4} \cdot T + 3.732 \times 10^{-7} \cdot T^2 - 7.594 \times 10^{-11} \cdot T^3 \quad (8)$$

Recommended percentage linear thermal expansion for  $\text{UO}_2$  by Martin [2] :-

$$(\Delta L/L_0) \times 100 = -0.266 + 9.802 \times 10^{-4} \cdot T - 2.705 \times 10^{-8} \cdot T^2 + 4.391 \times 10^{-11} \cdot T^3 \quad (9)$$

(273 K < T < 923 K)

$$(\Delta L/L_0) \times 100 = -0.328 + 1.179 \times 10^{-3} \cdot T - 2.429 \times 10^{-7} \cdot T^2 + 1.219 \times 10^{-10} \cdot T^3 \quad (10)$$

(923 K < T < 2000 K)

$\text{ThO}_2$  and  $\text{UO}_2$  form an ideal solid solution and the lattice parameter changes linearly at room temperature in the whole composition range. The vapour pressure measurements [11] also indicate ideal solution behaviour at high temperature. From this observation Bakker et al. [3] concluded that thermal expansion of the solid solutions  $(\text{Th}_{1-y}\text{U}_y)\text{O}_2$  could be reasonably approximated at various temperatures by taking linear interpolated expansion data of  $\text{ThO}_2$  and  $\text{UO}_2$  as per their weight fraction. In the absence of experimental data for compositions other than  $\text{ThO}_2$  containing 4%  $\text{UO}_2$  and  $\text{ThO}_2$  containing 10%  $\text{UO}_2$ , the percentage linear thermal expansion can be reasonably



approximated by taking linear interpolated expansion data of ThO<sub>2</sub> and UO<sub>2</sub> as per their weight fraction (equation no 2 and 3).

*(Th<sub>1-y</sub>Pu<sub>y</sub>)O<sub>2</sub> system*

Mathews et al. [12] has recently measured bulk thermal expansion of (Th,Ce)O<sub>2</sub> system using CeO<sub>2</sub> as a surrogate material in place of PuO<sub>2</sub>. The data recommended by Mathews for (Th<sub>0.9</sub>Ce<sub>0.1</sub>)O<sub>2</sub> [equivalent to ThO<sub>2</sub> containing 10.23wt% PuO<sub>2</sub>] and by Touloukian for ThO<sub>2</sub> along with the present experimental data for ThO<sub>2</sub>-PuO<sub>2</sub> are shown in Figure 6. The simulated data generated by linear interpolation method (described later, equation (17)) for compositions: ThO<sub>2</sub> containing 2, 4, 6 and 10% PuO<sub>2</sub> are also shown in the same figure. It can be seen that the present experimental data for ThO<sub>2</sub> is falling below the recommended data by Touloukian. Hence those experimental data for ThO<sub>2</sub> are not further considered. In the absence of available literature data for thorium-plutonium system, the present experimental data for compositions: ThO<sub>2</sub> containing 2, 4, 6 and 10% PuO<sub>2</sub> are recommended. The experimental data are fitted into a third degree polynomial equation (equation (1)) and the recommended percentage linear thermal expansion for the four compositions is given below.

Recommended percentage linear thermal expansion for ThO<sub>2</sub> containing 2% PuO<sub>2</sub> (300≤T≤1773):-

$$(\Delta L/L_0) \times 100 = -0.35225 + 9.31439 \times 10^{-4} \cdot T + 2.91932 \times 10^{-7} \cdot T^2 - 8.45619 \times 10^{-11} \cdot T^3 \quad (11)$$

(R<sup>2</sup> : 0.99986; SD: 0.00641)

Recommended percentage linear thermal expansion for ThO<sub>2</sub> containing 4% PuO<sub>2</sub> (300≤T≤1773):-

$$(\Delta L/L_0) \times 100 = -0.37948 + 11.4 \times 10^{-4} \cdot T + 1.87253 \times 10^{-8} \cdot T^2 + 5.16207 \times 10^{-12} \cdot T^3 \quad (12)$$

(R<sup>2</sup> : 0.9999; SD: 0.00537)

Recommended percentage linear thermal expansion for ThO<sub>2</sub> containing 6% PuO<sub>2</sub> (300≤T≤1773):-

$$(\Delta L/L_0) \times 100 = -0.37166 + 10.5 \times 10^{-4} \cdot T + 2.36946 \times 10^{-7} \cdot T^2 - 9.09797 \times 10^{-11} \cdot T^3 \quad (13)$$

(R<sup>2</sup>: 0.99939; SD: 0.01312)

Recommended percentage linear thermal expansion for ThO<sub>2</sub> containing 10% PuO<sub>2</sub> (300≤T≤1773):-

$$(\Delta L/L_0) \times 100 = -0.44122 + 13.5 \times 10^{-4} \cdot T - 1.55649 \times 10^{-7} \cdot T^2 + 5.66701 \times 10^{-11} \cdot T^3 \quad (14)$$

(R<sup>2</sup> : 0.9999; SD: 0.00542)

ThO<sub>2</sub> and PuO<sub>2</sub> form an ideal solid solution in the whole compositional range [13]. The lattice parameter of (Th<sub>1-y</sub>Pu<sub>y</sub>)O<sub>2</sub> decreases linearly from pure ThO<sub>2</sub> to pure PuO<sub>2</sub> [14]. Assuming ideal solid solution behaviour at high temperatures for ThO<sub>2</sub> and PuO<sub>2</sub>, it would be expected that this linear decrease in lattice parameter would also happen at elevated temperatures. So thermal expansion of the solid solutions (Th<sub>1-y</sub>Pu<sub>y</sub>)O<sub>2</sub> could be reasonably approximated at various temperatures by taking linear interpolated expansion data of ThO<sub>2</sub> and PuO<sub>2</sub> as per their weight fraction. For the generation of equations by the “interpolation method”, the recommended equation by Touloukian [1] for ThO<sub>2</sub> and the following equation for pure PuO<sub>2</sub> as recommended by MATPRO in Ref. [15] were taken for calculations.

$$\epsilon = K_1 \cdot T - K_2 + K_3 \exp(-E_D/k_B T) \quad (15)$$

where  $\epsilon$  is the linear strain (equal to zero at 300 K, m/m), T is the temperature (K),  $k_B$  is Boltzman's constant ( $1.38 \times 10^{-23}$  J/K), and  $E_D$ ,  $K_1$ ,  $K_2$ ,  $K_3$  are constants having values  $7 \times 10^{-20}$  (J),  $9 \times 10^{-6}$  (K<sup>-1</sup>),  $2.7 \times 10^{-3}$  (unit less) and  $7 \times 10^{-2}$  (unit less) respectively. Data generated from Equation (15) were fitted in a third degree polynomial equation, which is given below:

PuO<sub>2</sub>:

$$(\Delta L/L_0) \times 100 = -0.22812 + 7.3476 \times 10^{-4} \cdot T + 1.2262 \times 10^{-7} \cdot T^2 + 4.85977 \times 10^{-11} \cdot T^3 \quad (16)$$

Percentage linear thermal expansion for (Th<sub>1-y</sub>Pu<sub>y</sub>)O<sub>2</sub> (0<y<1) obtained by linear interpolation of the data of ThO<sub>2</sub> (Eq. 2) and data for PuO<sub>2</sub> (Eq. 19) and can be expressed as (in the temperature range of 300K-1773K):

(Th<sub>1-y</sub>Pu<sub>y</sub>)O<sub>2</sub> where 0<y<1 :-

$$(\Delta L/L_0) \times 100 = -0.179 - 0.049 \cdot y + (5.079 \times 10^{-4} + 2.251 \times 10^{-4} \cdot y) \cdot T + (3.732 \times 10^{-7} - 2.506 \times 10^{-7} \cdot y) \cdot T^2 + (-7.594 \times 10^{-11} + 12.454 \times 10^{-11} \cdot y) \cdot T^3 \quad (17)$$

In the absence of available literature data for the compositions other than ThO<sub>2</sub> containing 2, 4, 6 and 10% PuO<sub>2</sub> (recommended equations are given in equations (11) to (14)), the percentage linear thermal expansion data for the solid solutions (Th<sub>1-y</sub>Pu<sub>y</sub>)O<sub>2</sub> could be reasonably approximated at various temperatures by taking linear interpolated expansion data of ThO<sub>2</sub> and PuO<sub>2</sub> as per their weight fraction as given in equation (17).

Table 1. Experimental values of polynomial constants for ThO<sub>2</sub>-UO<sub>2</sub> solid solutions

	ThO <sub>2</sub>	ThO <sub>2</sub> + 2% UO <sub>2</sub>	ThO <sub>2</sub> + 4% UO <sub>2</sub>	ThO <sub>2</sub> + 6% UO <sub>2</sub>	ThO <sub>2</sub> + 10% UO <sub>2</sub>	ThO <sub>2</sub> + 20% UO <sub>2</sub>
A	-2.2153E-01	-2.7410E-01	-2.9339E-01	-1.9517E-01	-2.1185E-01	-3.0895E-01
B	4.3281E-04	6.8563E-04	9.1239E-04	3.7726E-04	5.2536E-04	9.2751E-04
C	8.7599E-07	6.1777E-07	1.0431E-07	8.4561E-07	6.6001E-07	2.7319E-07
D	-3.1072E-10	-2.0041E-10	-5.3996E-11	-2.8244E-10	-2.5302E-10	-1.0636E-10

Table 2. Experimental values of polynomial constants for ThO<sub>2</sub>-PuO<sub>2</sub> solid solutions

	ThO <sub>2</sub>	ThO <sub>2</sub> + 2% PuO <sub>2</sub>	ThO <sub>2</sub> + 4% PuO <sub>2</sub>	ThO <sub>2</sub> + 6% PuO <sub>2</sub>	ThO <sub>2</sub> + 10% PuO <sub>2</sub>
A	-0.22153	-0.35225	-0.37948	-0.37166	-0.44122
B	4.32806×10 <sup>-4</sup>	9.31439×10 <sup>-4</sup>	11.4×10 <sup>-4</sup>	10.5×10 <sup>-4</sup>	13.5×10 <sup>-4</sup>
C	8.75991×10 <sup>-7</sup>	2.91932×10 <sup>-7</sup>	1.87253×10 <sup>-8</sup>	2.36946×10 <sup>-7</sup>	-1.55649×10 <sup>-7</sup>
D	-3.10723×10 <sup>-10</sup>	-8.45619×10 <sup>-11</sup>	5.16207×10 <sup>-12</sup>	-9.09797×10 <sup>-11</sup>	5.66701×10 <sup>-11</sup>

Table 3. List of the authors and year of publications

AUTHORS	YEAR	REMARK
Bakker et al. [3]	1997	Review Paper
Momin et al [4]	1991	Measurement by XRD, (298-1600K )
D.G.Martin [2]	1988	Review Paper
Rodriguez & Sundaram [9]	1981	Review Paper
Touloukian et al [1]	1970	Review Paper
Springer et al [5]	1967	Measurement (293K-2273K)
Turner & Smith [6]	1967	Measurement
Lynch & Beals [8]	1962	Measurement (up to 1173)
Kemper & Elliot [7]	1959	Measurement (293 K- 1173 K)
Powers & Shapiro [10]	1959	Measurement, (up to 1073 K)

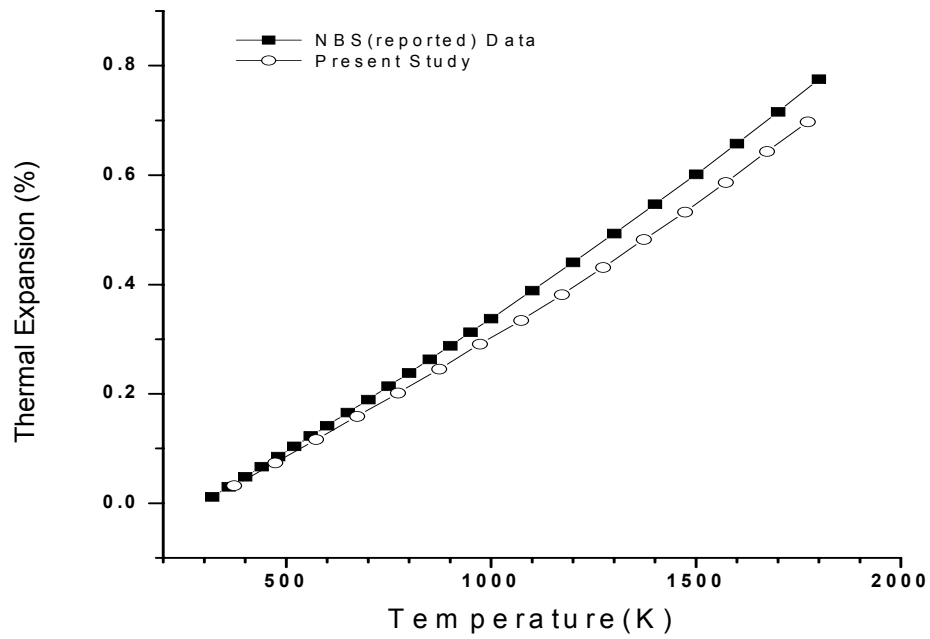


FIG. 1. Recommended and experimental data of thermal expansion for Tungsten (NBS SRM 737) as a function of temperature.

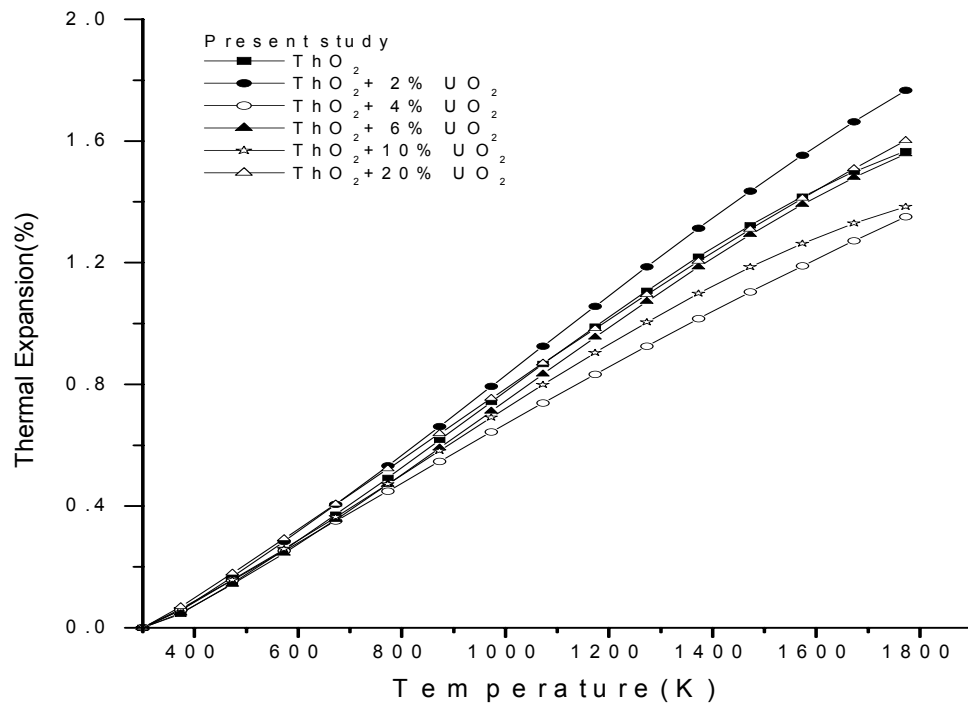


FIG. 2. Polynomial fitted curves of thermal expansion (%) for ThO<sub>2</sub>-UO<sub>2</sub> solid solutions as a function of temperature.

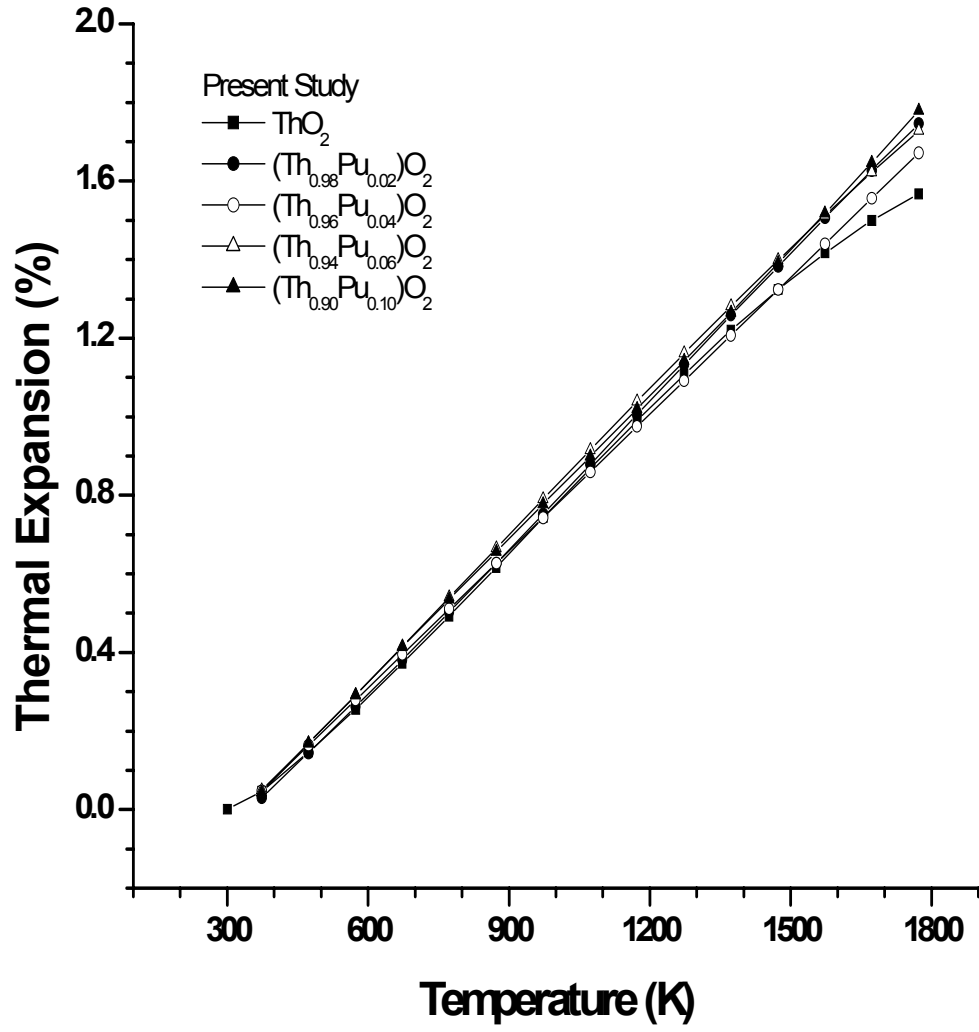


FIG. 3. Polynomial fitted curves of experimental data of percentage linear thermal expansion (%) for ThO<sub>2</sub>-PuO<sub>2</sub> solid solutions as a function of temperature.

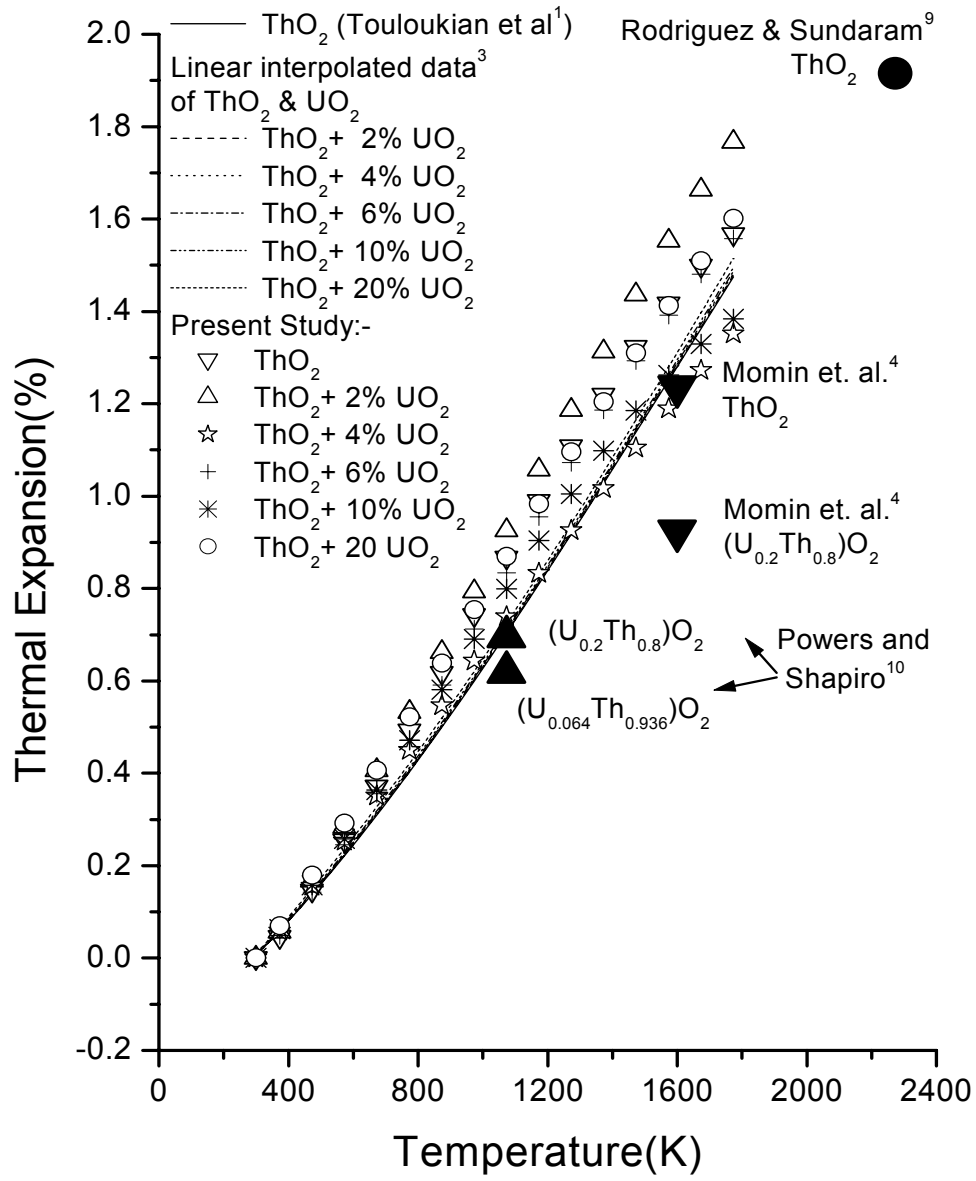


FIG. 4. Experimental thermal expansion (%) data of  $\text{ThO}_2\text{-UO}_2$  solid solutions along with available literature data.

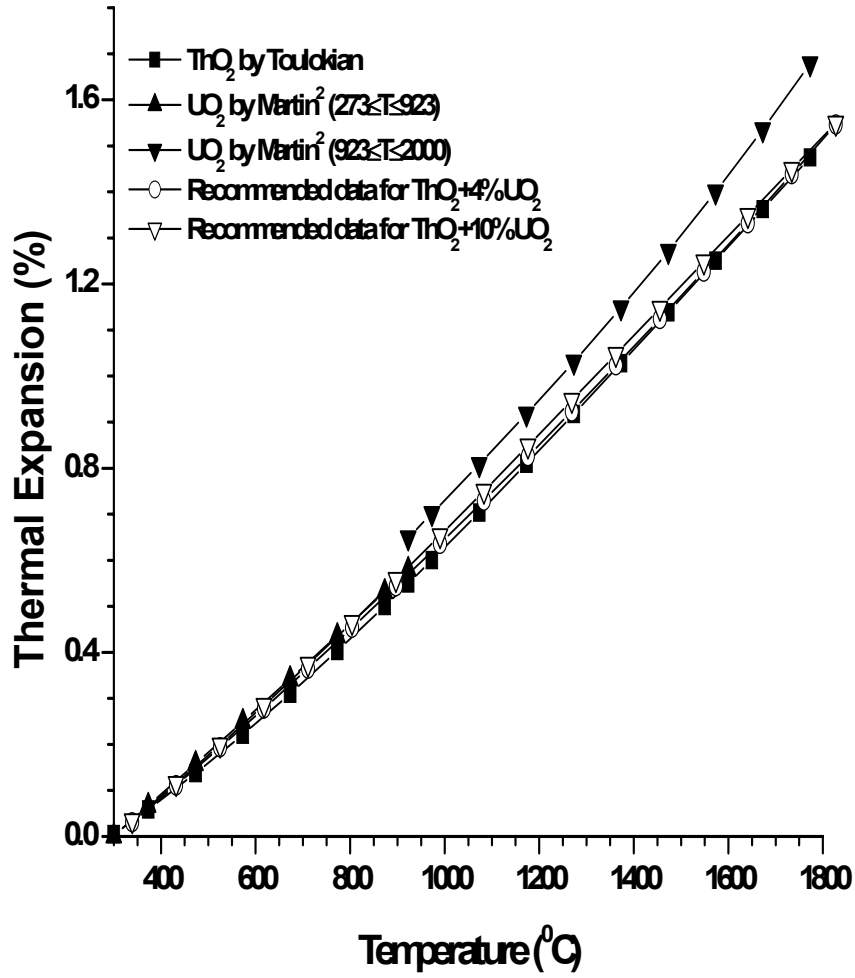


FIG. 5. Recommended linear percentage thermal expansion data for ThO<sub>2</sub> containing 4 and 10% UO<sub>2</sub> as a function of temperature along with the literature data for ThO<sub>2</sub> by Touloukian and UO<sub>2</sub> by Martin.

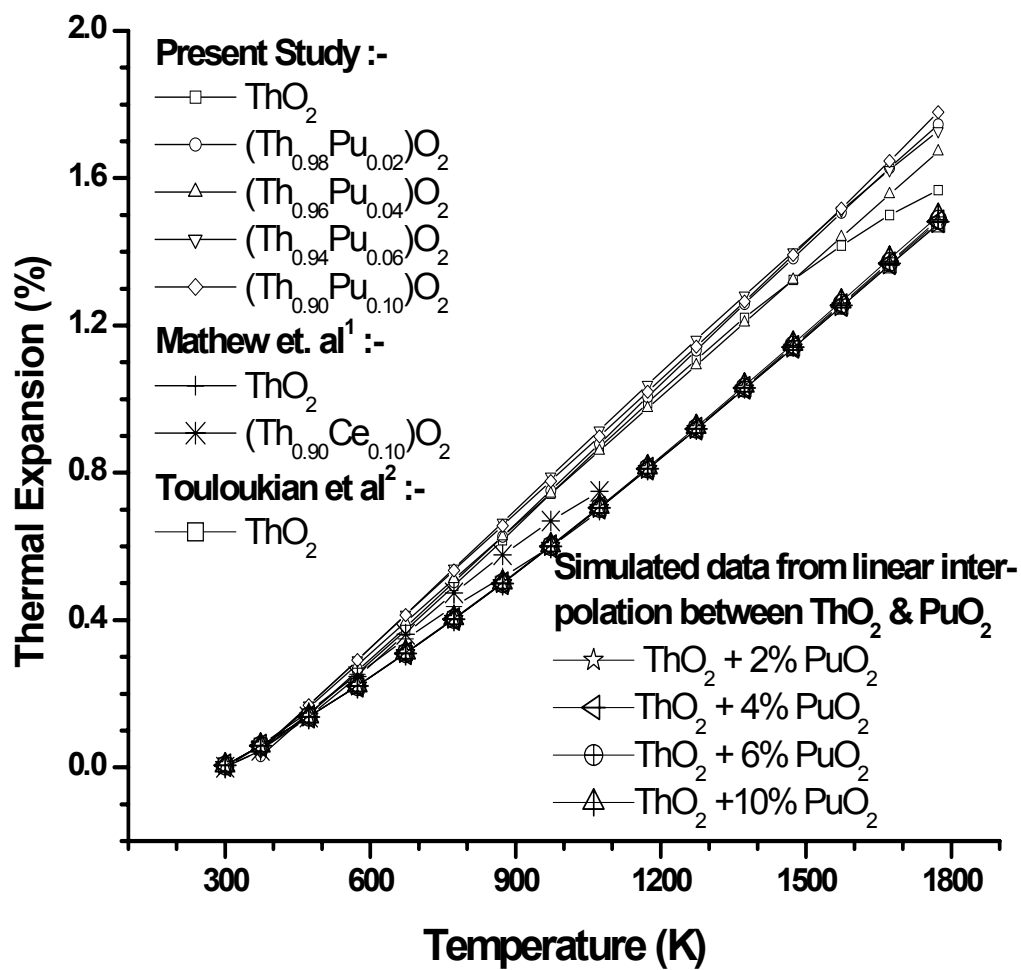


FIG. 6. Percentage linear thermal expansion (%) for  $(\text{Th}_{1-y}\text{Pu}_y)\text{O}_2$  as a function of temperature showing both experimental data and simulated data by linear interpolation method.

## REFERENCES TO SECTION 6.1.4.6

- [1] TOULOUKIAN, Y.S., KIRBY, R.K., TAYLOR, R.E., LEE, T.Y.R. Thermal Expansion. Nonmetallic Solids (IFI/Plenum, New York, 1970).
- [2] MARTIN, D.G., J. Nucl. Mater, 152 (1988) 94.
- [3] BAKKER, K., CORDFUNKE, E.H.P., KONINGS, R.J.M., SCHRAM, R.P.C. J. Nucl. Mater, 250 (1997) 1.
- [4] MOMIN, A.C., MIRZA, E.B., MATHEWS, M.D. J. Nucl. Mater., 185(1991)308.
- [5] J.R.Springer, E.A Eldrige, M.U.Goodyear, T.R.Wright, J.F.Langedrost, Battelle Memorial Institute Report BMI-X-10210,1967.
- [6] TURNER, D.N., SMITH, P.D., Australian Atomic Energy Commission report AAEC E183, 1967.
- [7] KEMPER, C.P., ELLIOT, R.O. J.Chem. Phys., 30 (1959) 1524.
- [8] LYNCH, E.D., BEALS, R.J. Argonne National Laboratory Annual report for 1962. ANL- 6677, 1962, p.101.
- [9] RODRIGUEZ, P., SUNDARAM, C.V. J. Nucl. Mater. 100 (1981) 227.
- [10] POWERS, R.M., SHAPIRO, H. Quarterly Technical Progress Report, Sylvania Corning Nuclear Corp. SCNC-301. 1959.
- [11] ALEXANDER, C.A., OGDEN, J.S., CUNNINGHAM, G.W. Battelle Memorial Institute Report BMI- 1789,1967.
- [12] MATHEWS, M.D., AMBEKAR, B.R., TYAGI, A.K. J. Nucl. Mater, 288 (2001) 83-85.
- [13] FRESHLEY, M.D., MATTYS, H.M., General Electric Report HW-76559. 1962. p 11.6.
- [14] BAKKER, K. E.H.P. Cordfunke, R.J.M. Konings, R.P.C. Schram, J. Nucl. Mater, 250 (1997) 1.
- [15] IAEA TECDOC 949, June 1997, p.53-54.

## 6.2. Cladding and pressure tube materials

### 6.2.1. Zircaloy

#### 6.2.1.1. Heat capacity

##### *Recommendations*

The recommended equations for the heat capacity of Zircaloy in the  $\alpha$ -,  $\beta$ -, and combined ( $\alpha + \beta$ )-phases are based on least square fits to the available data on the heat capacity of Zircaloy-2 [1–9], which are listed in Table 1. No measurements of the heat capacity of Zircaloy-4 have been found in the open literature.

The recommended equation for the heat capacity of Zircaloy-2 in the  $\alpha$  - phase is:

For 273 K < T < 1100 K,

$$C_P = 255.66 + 0.1024 T \quad (1)$$

where temperature is in K and heat capacity is in J kg<sup>-1</sup> K<sup>-1</sup>.

The recommended equation for the heat capacity of Zircaloy-2 in the  $\beta$  - phase is the quadratic equation obtained by Righini et al.[6] from fitting their  $\beta$  - phase data.

For 1320 K < T < 2000 K

$$C_P = 597.1 - 0.4088 T + 1.565 \times 10^{-4} T^2 \quad (2)$$

where temperature is in K and heat capacity is in J kg<sup>-1</sup> K<sup>-1</sup>.



The Zircaloy-2 heat capacity data in the  $(\alpha + \beta)$ -phase-transition region of Righini et al.[8] have been fit by a Gaussian function plus the equations for the dominant  $\alpha$ - or  $\beta$ -phase. This Gaussian function is

$$f(T) = 1058.4 \exp\left[\frac{(T - 1213.8)^2}{719.61}\right] \quad (3)$$

where temperature is in K and heat capacity is in  $\text{J kg}^{-1} \text{K}^{-1}$ . From 1100 K through 1214 K, the recommended values for the heat capacity of Zircaloy-2 are obtained from the sum of Eq.(1) + Eq.(3). From 1214 to 1320 K, the recommended values for the heat capacity of Zircaloy-2 are obtained from the sum of Eq. (2) + Eq. (3). Recommended values for the heat capacity of Zircaloy-2 are tabulated in Table 2, and shown in Figure 1.

### Uncertainty

The two-standard deviation uncertainty for the recommended Zircaloy-2  $\alpha$ -phase heat capacities is 2–3%. The errors in the regression coefficients for 95% confidence, which is an uncertainty of two standard deviations, are:

$$C_P = (255.66 \pm 3.75) + (0.10240 \pm 0.00537) T \quad (4)$$

The uncertainties for the  $\alpha$ -phase heat capacities calculated from Eq.(4) are shown as dotted lines in Figure 2, which shows the recommended values (solid line) and the experimental data. These uncertainties for the  $\alpha$ -phase heat capacities are consistent with an uncertainty of  $\pm 10 \text{ J kg}^{-1} \text{K}^{-1}$  (3%) given in MATPRO [10].

The estimated uncertainty in the recommended values for Zircaloy-2 heat capacity in the  $\beta$ -phase is 10% ( $\sim \pm 30 \text{ J kg}^{-1} \text{K}^{-1}$ ) from 1300 K to 1600 K and increases linearly to 20% ( $\sim \pm 70 \text{ J kg}^{-1} \text{K}^{-1}$ ) at 1700 K and higher temperatures. These uncertainties are greater than the root mean square of the sum of the squares of the errors given by Righini et al. [6] for the imprecision in the fit (1.2%) and inaccuracy (4%) in the heat capacity measurements but they are much less than the  $\pm 100 \text{ J kg}^{-1} \text{K}^{-1}$  uncertainty given by MATPRO [10] for the constant heat capacity recommended by MATPRO for this phase. In Figure 3, the recommended values and uncertainties are compared with the data of Righini et al. [6], of Maglic et al. [9] and the constant  $\beta$ -phase heat capacity given in MATPRO [10]. The larger uncertainty than the 4% obtained from statistical analysis of the known analytical and experimental errors of Righini et al. [6] is warranted because the data of Deem and Eldridge [1] deviates by 10% from that of Righini et al. [6] and above 1600 K, the data of Maglic et al. [9] deviates by more than 10% from that of Righini et al. [6].

The uncertainty in recommended values for the  $(\alpha + \beta)$ -transition phase is estimated as 10%, which is larger than the uncertainty of  $\pm 25 \text{ J kg}^{-1} \text{K}^{-1}$  given in MATPRO. This larger uncertainty reflects the disagreements in the heat capacity phase transition data of three different investigators [1, 8, 9] and the sensitivity of the phase transition temperature and the heat capacity in the two-phase region to the temperature history of the samples (such as annealing) that was found by Righini et al. [8]. It is consistent with the 10% variation in the total energy absorbed during the phase transition that was found by Righini et al. for samples with different thermal histories that were heated using different heating rates. The phase transition temperature and the heat capacity in the two-phase region are also very sensitive to oxygen content. Thus, even larger uncertainties may be appropriate if oxygen dissolution in the Zircaloy is suspected and the amount of oxygen in the Zircaloy is not known.

Uncertainties for application of the Zircaloy-2 heat capacity equations to Zircaloy-4 are 20% for the  $\alpha$ -phase and 30% for the  $(\alpha + \beta)$ -transition phase and the  $\beta$ -phase. These uncertainties are based on the absence of data for Zircaloy-4 and the differences between measured Zircaloy-2 heat capacities and Zircaloy-4 heat capacity values calculated from measurements of thermal diffusivity, thermal conductivity, and thermal expansion.

## Discussion

### Phases

Unlike zirconium, which has a sharp  $\alpha \rightarrow \beta$  transition at 1139 K, Zircaloy has no sharp change from the  $\alpha$ -phase to the  $\beta$ -phase but has a two-phase ( $\alpha + \beta$ ) region. For Zircaloy-2, the temperature range for this transition given by Bunnell et al. [11] is 1083 to 1223 K. However, Righini et al. [8] found that the coexistence region ranges from 1050 K to 1400 K and the exact temperature range depends on the sample's thermal history and heating rate. The phase boundaries are also a function of dissolved oxygen in the sample. The effect of dissolved oxygen on the  $\alpha$ - and  $\beta$ -phase boundaries of the ( $\alpha + \beta$ ) two-phase region in Zircaloy-4 has been studied by Chung et al. [12, 13]. The effect of dissolved oxygen in Zircaloy-2 on these phase boundaries has been studied by Rubenstein et al. [14], Mallet et al. [15], Ostberg [16] and Chung et al. [12, 13]. Dissolved oxygen stabilizes the  $\alpha$ -phase to higher temperatures and produces a broader two-phase ( $\alpha + \beta$ ) region.

### $\alpha$ -phase heat capacity

Table 1 lists the available data for the heat capacity of Zircaloy-2. Most of the available data are for the  $\alpha$ -phase. In Figure 4, the Zircaloy-2 heat capacity data for the  $\alpha$ -phase are compared with the MATPRO [10] recommended values, which are based on the 1966 measurements of Brooks and Stansbury [2]. Since the MATPRO assessment, new heat capacity measurements have been made by six experimental groups and their data are not consistent with the MATPRO recommendation. Therefore, the  $\alpha$ -phase Zircaloy-2 heat capacity data have been reanalysed. Righini et al. [8] studied the effect of annealing and heating rate on the heat capacity in the  $\alpha$ -phase. Their results for as received samples (s1 and s2) showed no significant difference from their sample s3, which was annealed at 1300 K in a high vacuum for one hour. Heat capacities obtained from experiments with slow and fast heating rates on two annealed samples showed variations of  $\pm 0.1\%$  to  $\pm 1.1\%$  with no systematic trends. Thus, Righini et al. [8] concluded that the heat capacity of Zircaloy-2 in the  $\alpha$ -phase does not depend on either the heating rate or the thermal history of the sample. Consequently, all the  $\alpha$ -phase data from the measurements shown in Table 1 have been analysed together.

A least squares fit of these data showed that they are well represented by a linear equation. Equation (1) fits the 247 heat capacity data in the  $\alpha$ -phase with a multiple correlation coefficient,  $R$ , of 0.92. This recommended equation is compared with the MATPRO recommended values and the available  $\alpha$ -phase data in Figure 5. Percent deviations of the data from this equation defined by

$$\text{Deviation}(\%) = \frac{[C_p(\text{Data}) - C_p(\text{Recommended})]100\%}{C_p(\text{Recommended})} \quad (5)$$

are shown in Figure 6. Data from measurements by Murabayashi et al. [3] are 4 to 7% higher than the recommended values while data from measurements by Gilchrist [5] are low by 2 to 11%. Deviations for other data are mainly  $\pm 4\%$  or less. Data of Casey and Yates [4], of Righini et al. [8] and of Deem and Eldridge [1] are all within  $\pm 2\%$  of the recommended equation. Except for the data of Casey and Yates [4], of Righini et al. [8] and of Deem and Eldridge [1], the data by each experimenter is consistently high or low, indicating the deviations are systematic.

### $\beta$ -phase heat capacity

Only the data of Deem and Eldridge [1], of Righini et al. [6, 8] and of Maglic et al. [9] extend beyond the  $\alpha$ -phase and through the phase transition region. The Deem and Eldridge data do not extend far enough into the  $\beta$ -phase to provide information on the temperature dependence in this phase. The  $\beta$ -phase data of Maglic et al. [9] and that of Righini et al. [6] have significantly different temperature behavior. Consequently, a combined fit of these data is not recommended. Measurements by Righini et al. [6] were on as received samples, which had no annealing, and were well characterized with respect to composition and density. The data reported by Righini et al. [6] are the averages of seven measurements on specimen-1, four experiments for specimen-2, and five experiments for specimen-3. Three different heating rates were used for each specimen to determine if heating rate affected the

measured property. No dependence on heating rate was observed for the heat capacity in the  $\beta$ -phase. Measurements by Maglic et al. [9] were on samples annealed in a vacuum at 823 K. Maglic et al. [9] reported considerable difficulty with measurements at high temperatures using both Type-S and W/Re thermocouples. Of thirty-three experiments, only fourteen were considered reliable and only one of these reached the maximum temperature reported. Thus, the data of Maglic et al. [9] in the  $\beta$ -phase are not considered to be as reliable as the data of Righini et al. [6]. Therefore, the quadratic equation obtained by Righini et al. from their least squares fit to their data is recommended. The relative standard deviation of an individual data point from their recommended equation, Eq. (2), is 1.2%. This equation is shown with uncertainties in Figure 3 along with the MATPRO [10] constant heat capacity, the data of Righini et al. [6] and the data of Maglic et al. [9].

#### *Heat capacity in the phase transition region*

The effects of previous thermal history and heating rate on the temperature limits of the phase transition and on the heat capacity in the phase transition region have been extensively studied by Righini et al. [8, 17] for Zircaloy-2 and by Peletsky et al. [18, 19] for Zr-1%Nb. Righini et al. [8] found that both the heat capacity and the temperature limits of the phase transition have a strong dependence on the thermal history of the sample and a weak dependence on heating rate. Differences in the phase-transition region heat capacities for as received and annealed samples of Zircaloy-2 obtained by Righini et al. [8] during their first heating cycle are shown in Figure 7. Table 3 gives the thermal history of each sample referred to in Figure 7. Heat capacities for the two as received samples (s1a, s2a) are similar with a narrow peak just above 1210 K. The annealed samples show greater variation with wider lower peaks at temperatures that are higher by 20 to 25 K. Righini et al. [8] observed consistent differences between the first heating cycle and subsequent cycles. In general, the presence of the  $\beta$ -phase (either from annealing or from previous measurements) in the sample creates a wider temperature range for the phase transformation with respect to as-received samples. Measurements after the first heating cycle tended to be reproducible. In their study of the kinetics of the phase transformation in Zircaloy-2, Corchia and Righini [17] found that the kinetics are a function of the microstructure of the sample, which is dependent on the thermal and metallurgical history. Experiments after the first cycle tend to be reproducible because the pulse heating through the phase transition changes the microstructure of the sample,

In their study of effects of heating rate, Righini et al. [8] showed that the shape of the heat capacity curve is maintained in slow and fast experiments but the phase-transition peak in slow experiments tends to be lower by 10 to 20 K. Figure 7 shows that the heat capacity data of Deem and Eldridge [1] that was obtained by isothermal calorimetry have a wide peak that is shifted toward lower temperatures with a shape similar to the curves obtained by Righini et al. [8] after the first heating cycle. Righini et al. [8] commented that this shift to low temperatures is consistent with the very low heating rate for equilibrium calorimetry. This shift of the phase-transition peak in zirconium alloys to low temperatures during slow heating was confirmed by Lusternik et al. [18], who measured the heat capacities of Zr-1%Nb in the phase-transition region using both a subsecond pulse heating method (heating rate of  $2000 \text{ K s}^{-1}$ ) and by adiabatic calorimetry (heating rate of  $0.02 \text{ K s}^{-1}$ ). Figure 7 shows that the peak of the heat capacity data of Maglic et al. is shifted to higher temperatures. This is consistent with the observation of Righini et al. [8] that annealing and/or repeated cycling through the  $\beta$ -phase shifts the heat capacity peak to higher temperatures (see sample s3n2). The shape of the peak of the data of Maglic et al. is similar to the peak obtained by Deem and Eldridge.

For ten measurements on samples with different thermal histories and different heating rates, Righini et al. [8] integrated the heat capacities in the phase transition region (from 1050 K through 1390 K) to determine the total absorbed energy of the transition for each sample. The total absorbed energy ranged from 188.5 to 207.8  $\text{J g}^{-1}$  with no discernable trend. Thus, although the location of the phase transition peak and the shape of the peak differ in accord with the thermal history of the sample, the absorbed energy difference is within 10%. So, the use of Zircaloy-2 heat capacity values in this transition region from a sample with a different thermal history than that of the material in a nuclear reactor would give an uncertainty of about 10% in the total heat needed to heat Zircaloy-2 from the  $\alpha$ -phase to the  $\beta$ -phase during a reactor accident. For the nonequilibrium conditions of a nuclear

reactor accident, Righini et al.[8] recommend using their heat capacities for the as received samples during their first cycle of heating (s1a, s2a).

To obtain equations for the heat capacities in the two-phase region that are consistent with recommended equations for the  $\alpha$  - and  $\beta$  - phases, a non-linear least-squares minimization was used to determine a Gaussian function to represent the increase in heat capacity peak given by the heat capacity data of samples s1a and s2a (as received - first heating cycle) of Righini et al. [8] The phase transition data from 1133 to 1353 K of Maglic et al. and that of Deem and Eldridge above 1083 K were not included in this analysis because they are not consistent with heat capacity measurements on a first cycle of as received samples at a heating rate consistent with a reactor accident conditions. In this least squares minimization, the  $\alpha$ -phase (273–1100 K) was represented by the linear equation Eq. (1), the  $\beta$ -phase (1320–2000 K) was represented by the quadratic equation Eq. (2), and the combined phase was represented by a Gaussian function plus Eq. (1) up to the phase transition peak and a Gaussian function plus Eq. (2) from the phase-transition peak to the end of the transition region. The parameters for the Gaussian function (including the temperature for the peak and the width of the Gaussian) and the temperature ranges for the linear and quadratic equations in the two-phase region were free to vary in this non-linear least squares minimization. The best fit was obtained with the Gaussian function given in Eq. (3) for the temperature range from 1100 to 1320 K, the linear equation [Eq. (1)] from 273 to 1213.8 K, and the quadratic equation [Eq. (2)] from 1213.8 to 2000 K. Thus, the Zircaloy-2 heat capacities in the transition region are represented by the sum of Eq. (1) + Eq.(3) from 1100 K to 1214 K and by the sum of Eq. (2) + Eq. (3) from 1214 K to 1320 K. The recommended equations from 273 to 2000 K are shown in Figure 8 with the data and the MATPRO recommendation for comparison.

#### *Zircaloy-4*

No measurements of the heat capacity of Zircaloy-4 have been found in the open literature. However, Bunnell et al. [11] have calculated the heat capacity of Zircaloy-4 from their measurements of the Zircaloy-4 thermal expansion, thermal conductivity, and thermal diffusivity because they found that the constant heat capacity recommended by MATPRO [10] for the  $\beta$  - phase was inconsistent with their thermal conductivity and thermal diffusivity measurements. Their calculated heat capacities for Zircaloy-4 are shown in Figure 9 and compared with the Zircaloy-2 data and the recommended equations for the heat capacity of Zircaloy-2. The temperature dependence of their calculated Zircaloy-4 heat capacities is similar to that of the Zircaloy-2 data but the magnitude of the Zircaloy-4 heat capacities is higher. It is not clear if the higher values are real or due to the calculation. Until measurements of the heat capacity of Zircaloy-4 are available, the Zircaloy-2 equations are recommended with the caution that the actual heat capacities for Zircaloy-4 may be higher by 10 to 20% in the  $\alpha$  - phase and by 30% in the  $\beta$  - phase. Thus the uncertainties for application of the Zircaloy-2 heat capacity equations to Zircaloy-4 should be significantly higher. The estimated uncertainties are 20% for the  $\alpha$  - phase and 30% for the combined phase and the  $\beta$  - phase.

Table 1. Zircaloy-2 heat capacity data

EXPERIMENTER	REF	YEAR	TEMPERATURE (K)	NO. OF POINTS	METHOD	COMMENTS
Deem & Eldridge	1	1963	273-1323	23	Calorimetry	
Brooks & Stansbury	2	1966	323-973	91	Dynamic Adiabatic Calorimetry	97.1% Zr 1.29% Sn 0.012% O <sub>2</sub>
Casey & Yates	3	1974	300 - 570	38	Adiabatic Calorimetry	
Murabayashi et al.	4	1975	300-850	21	Laser Flash	98.2% Zr 1.49% Sn
Gilchrist	5	1976	298-1010	18	Differential Scanning Calorimetry	98.2% Zr 1.53% Sn
Righini et al.	6	1977	1320 - 2000	54	Pulse heating	98.08% Zr 1.42% Sn 0.154% Fe 0.125% Cr 0.052% Ni as received
Price	7	1980	340 - 675	36		Annealed & Cold-worked
Righini et al.	8	1981	800 - 1100 1040 - 1380	37 132	Pulse heating, slow & fast rates	as received samples & samples annealed at 1300 K
Maglic et al.	9	1994	298-1773	40	Millisecond- resolution direct electrical pulse heating	Annealed at 823 K in vacuum

Table 2. Recommended values for the heat capacity of zircaloy-2

TEMPERATURE, K	HEAT CAPACITY, J/(kg K)
273	283.6
300	286.4
400	296.6
500	306.9
600	317.1
700	327.3
800	337.6
900	347.8
1000	358.1
1100	368.3
1120	370.4
1140	372.9
1160	393.3
1180	592.3
1200	1190.0
1210	1416.6
1214	1438.3
1220	1335.1
1240	739.3
1260	385.2
1280	332.7
1300	330.2
1400	331.5
1500	336.0
1600	343.7
1700	354.4
1800	368.3
1900	385.3
2000	405.5

Table 3. Thermal history of heat capacity samples in Figure 7

SAMPLE	CONDITION	HEATING RATE
Righini s1a	as received	fast
Righini s2a	as received	fast
Righini s3n	annealed at 1300 K for 1 hr	fast
Righini s3n2	annealed at 1300 K for 1 hr; second annealing at 1300 K for 10 hrs	fast
Righini s4n	annealed at 1300 K for 10 hrs	slow
Deem & Eldridge	(repeated cycling ?)	slow (equilibrium)
Maglic et al.	annealed at 923 K, repeated cycling above 1300 K	fast

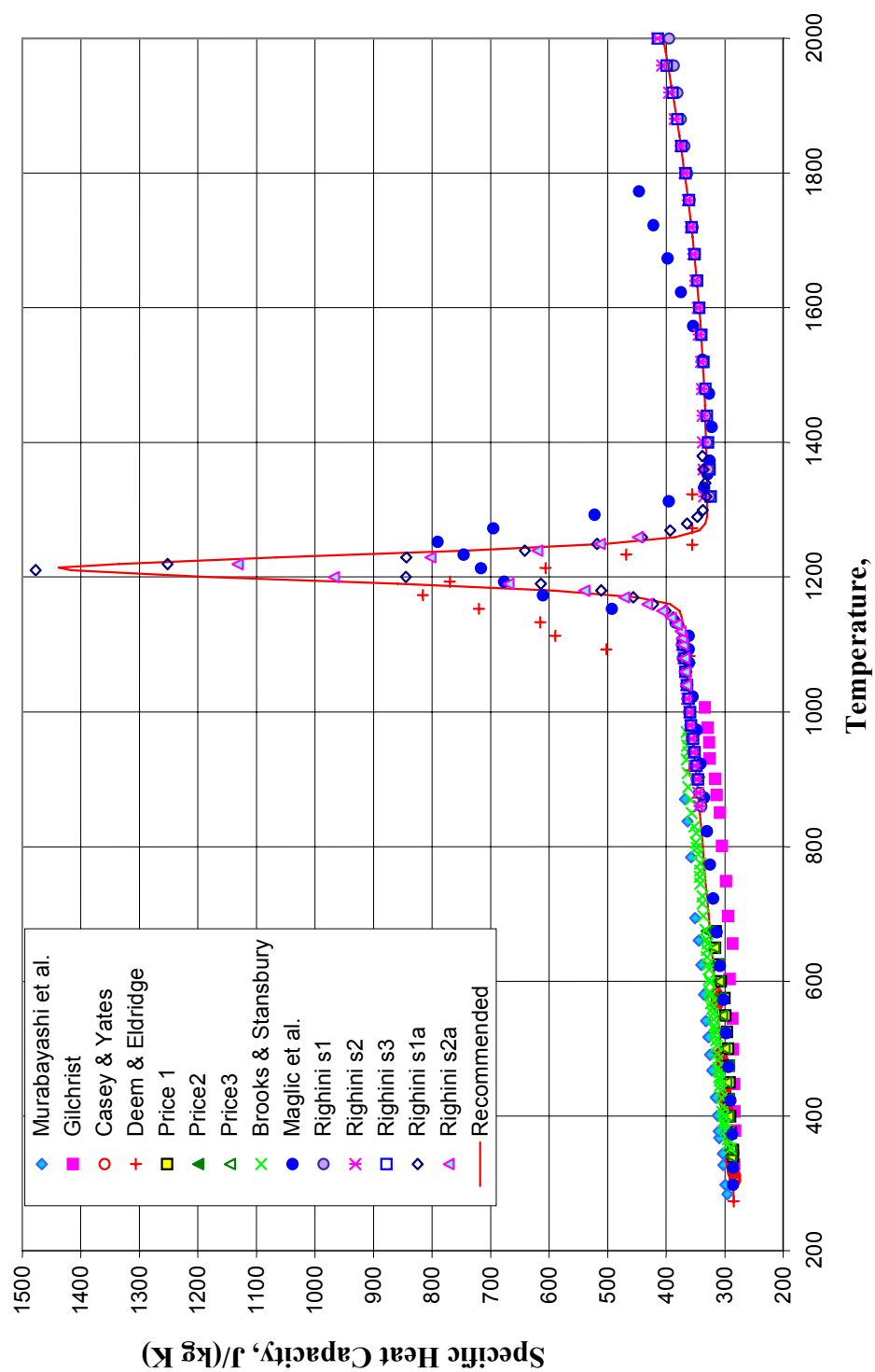


FIG. 1. Recommended fit to zircaloy-2 heat capacity data.

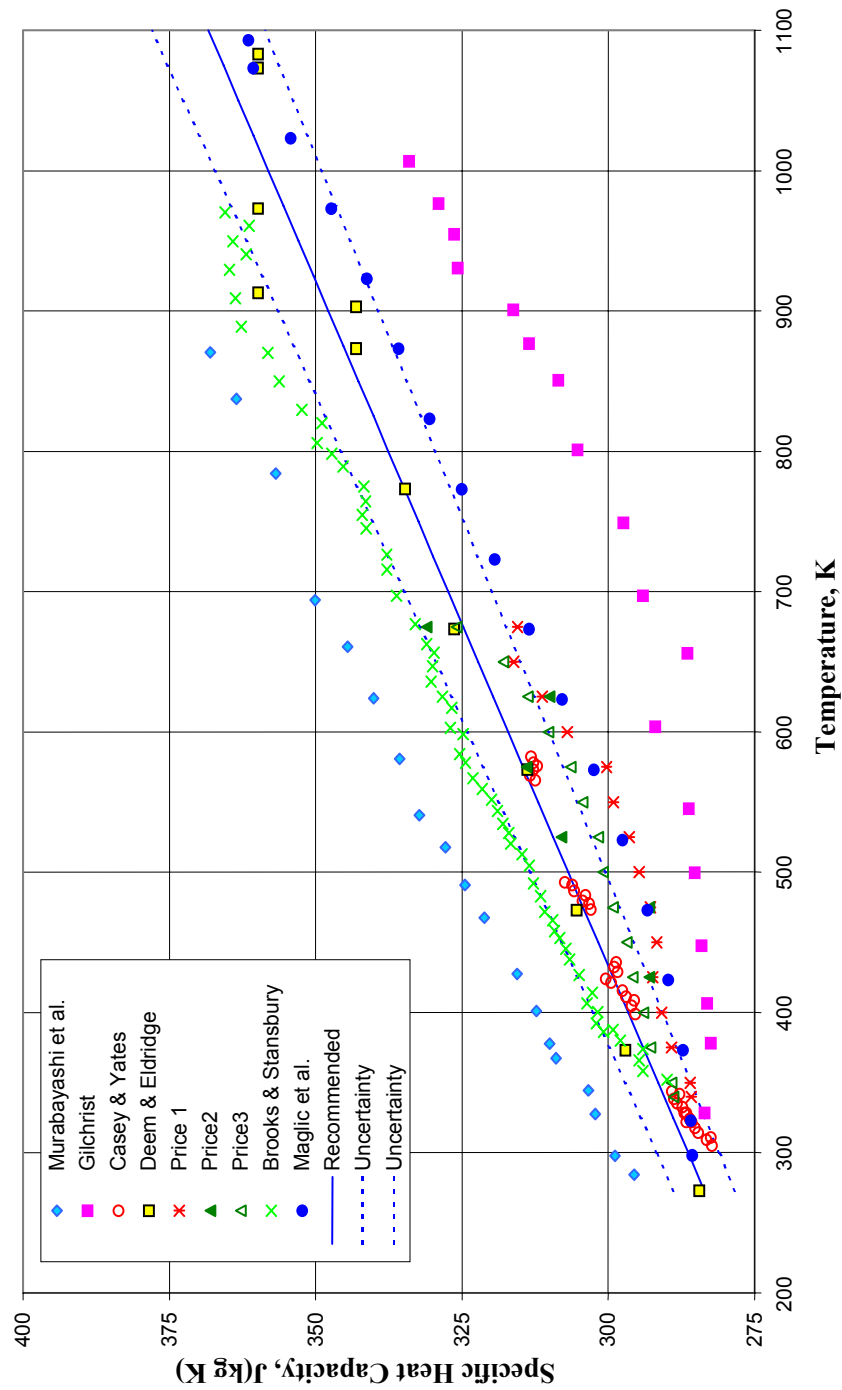


FIG. 2. Recommended equation for the  $\alpha$ -phase heat capacity of Zircaloy-2.



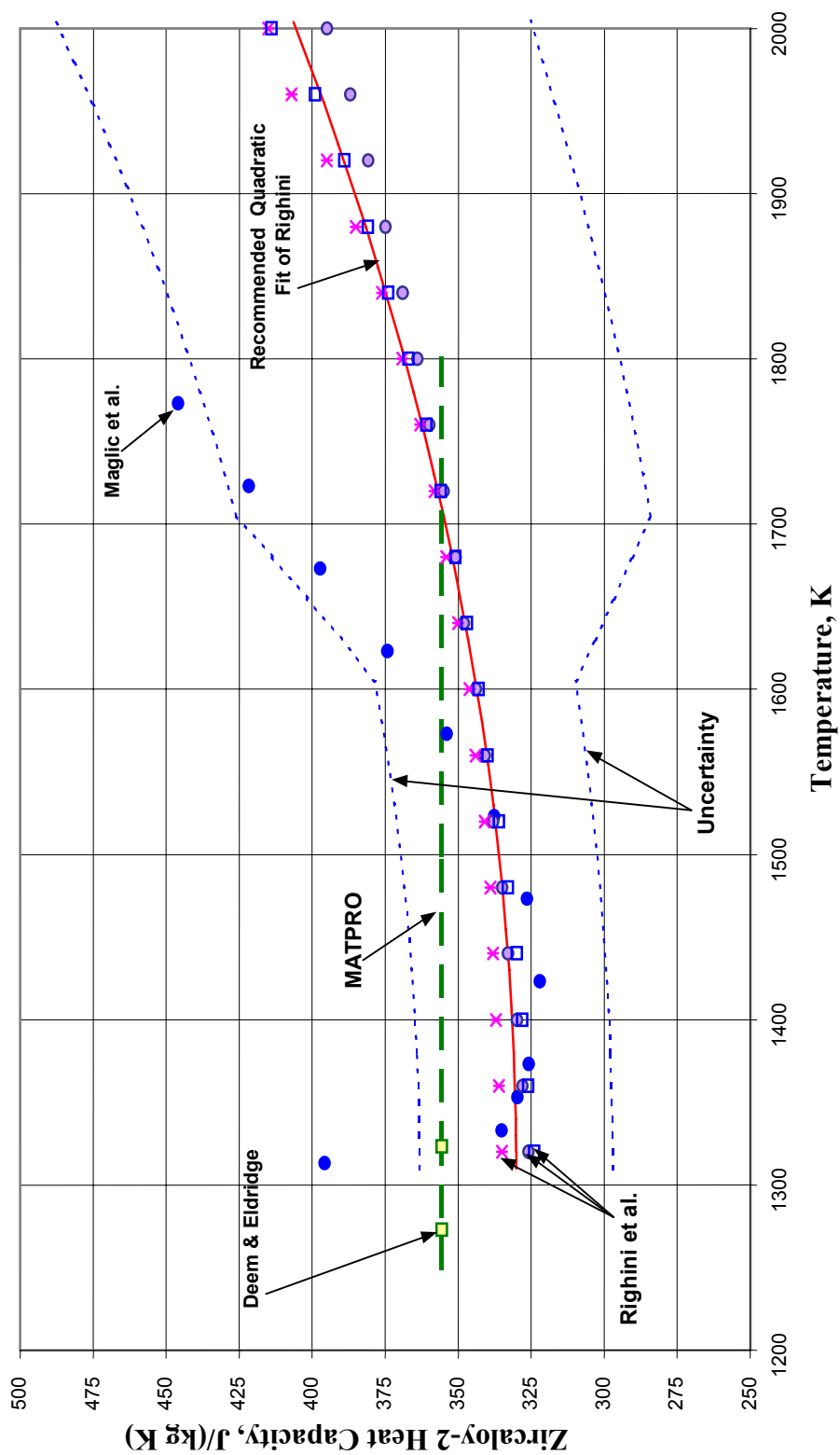


FIG. 3. Recommended equation for the  $\beta$ -phase heat capacity of Zircaloy-2.

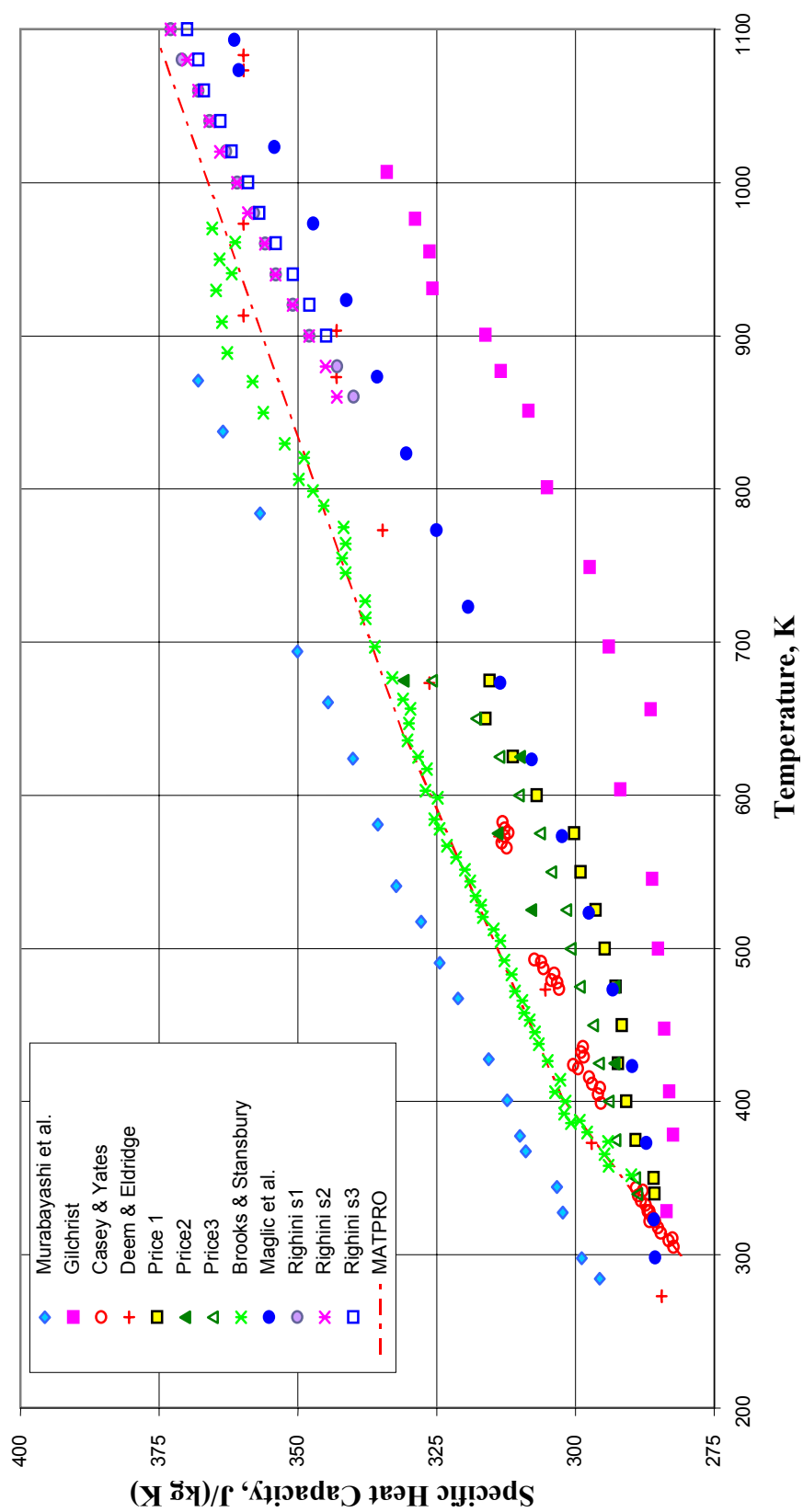


FIG. 4. Comparison of MATPRO values with Zircaloy-2  $\alpha$ -phase heat capacity data.

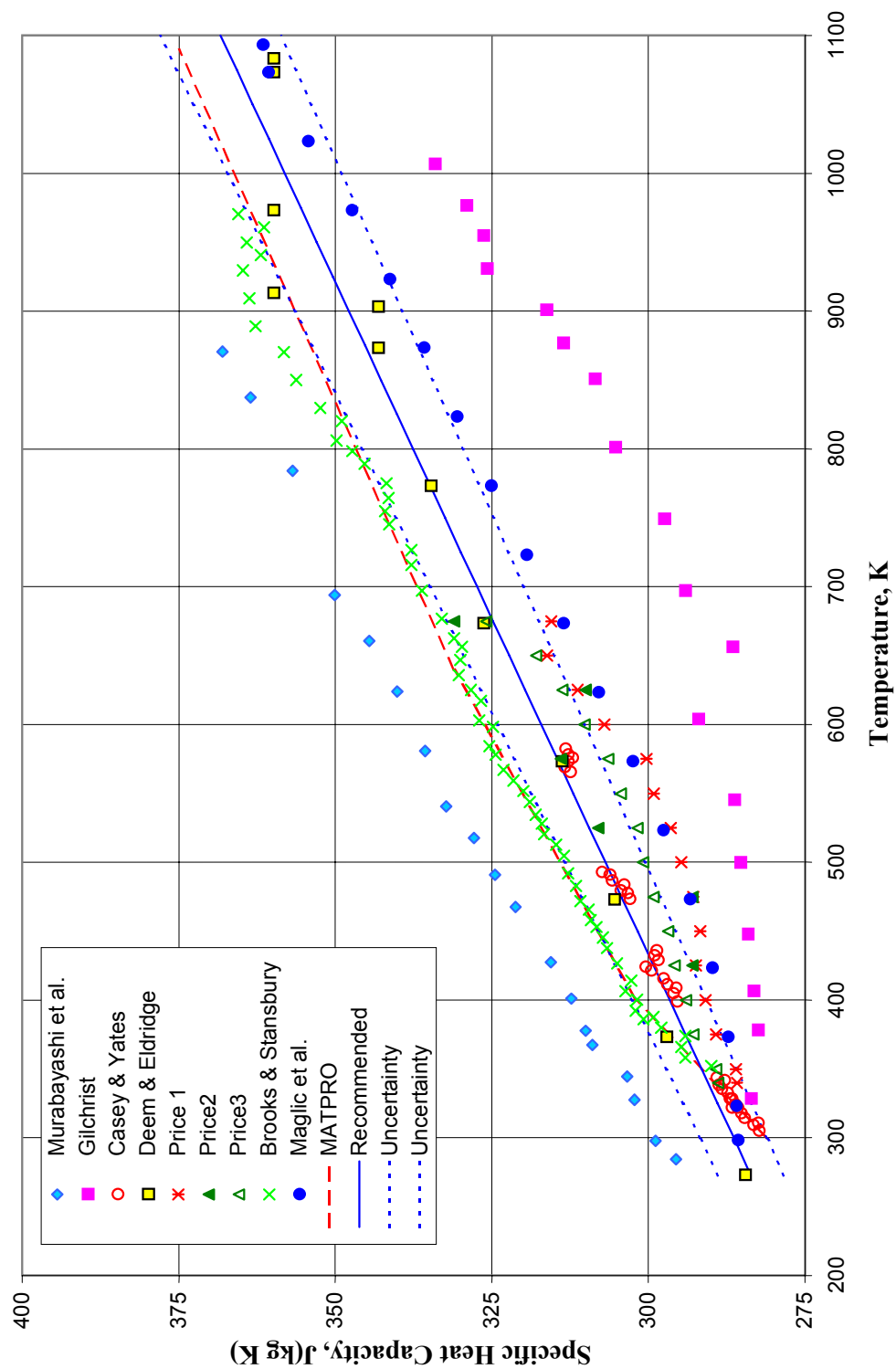


FIG. 5. Recommended linear fit to the  $\alpha$ -phase heat capacity of Zircaloy-2.

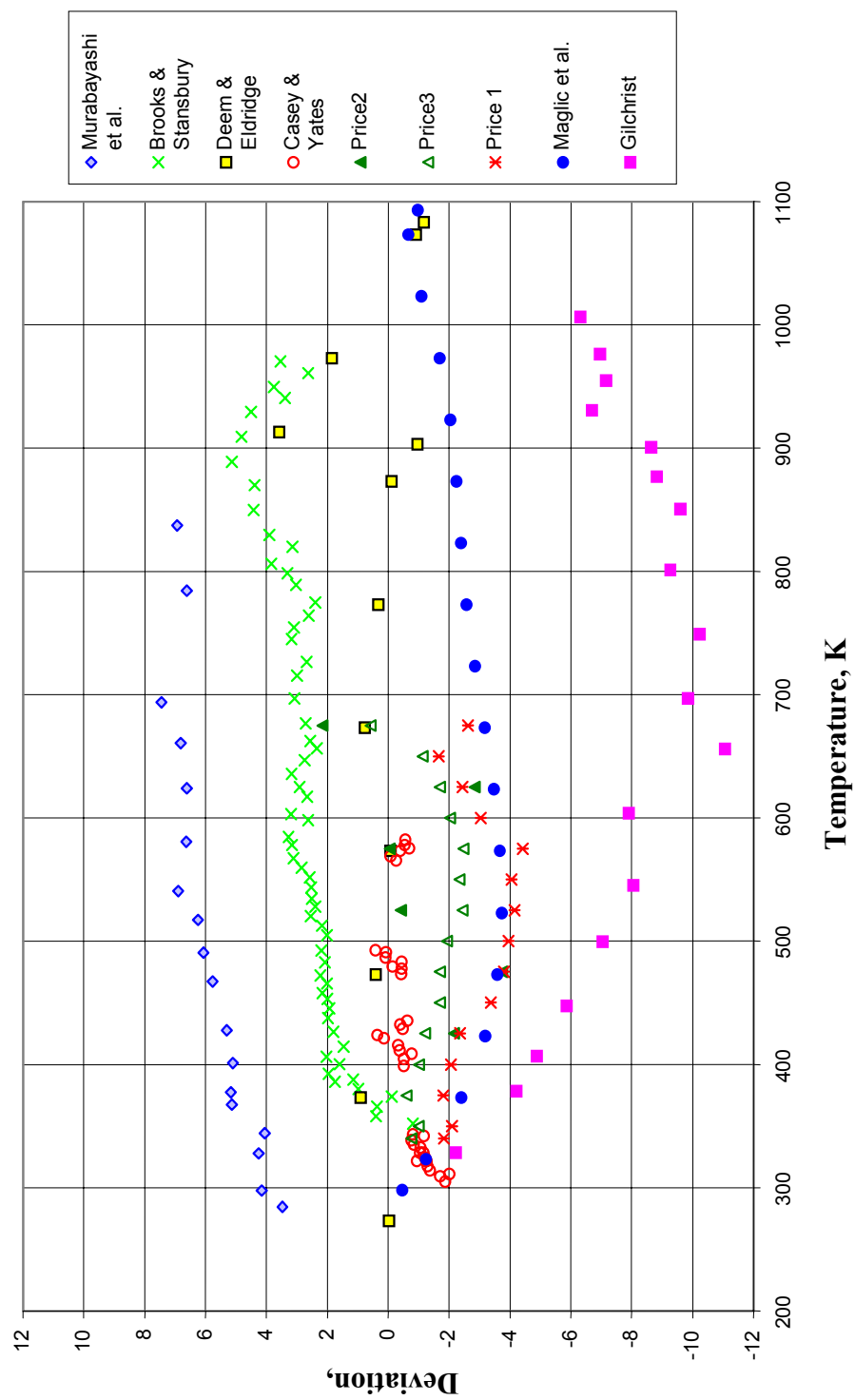


FIG. 6. Deviation of Zircaloy-2 heat capacity data from linear equation.

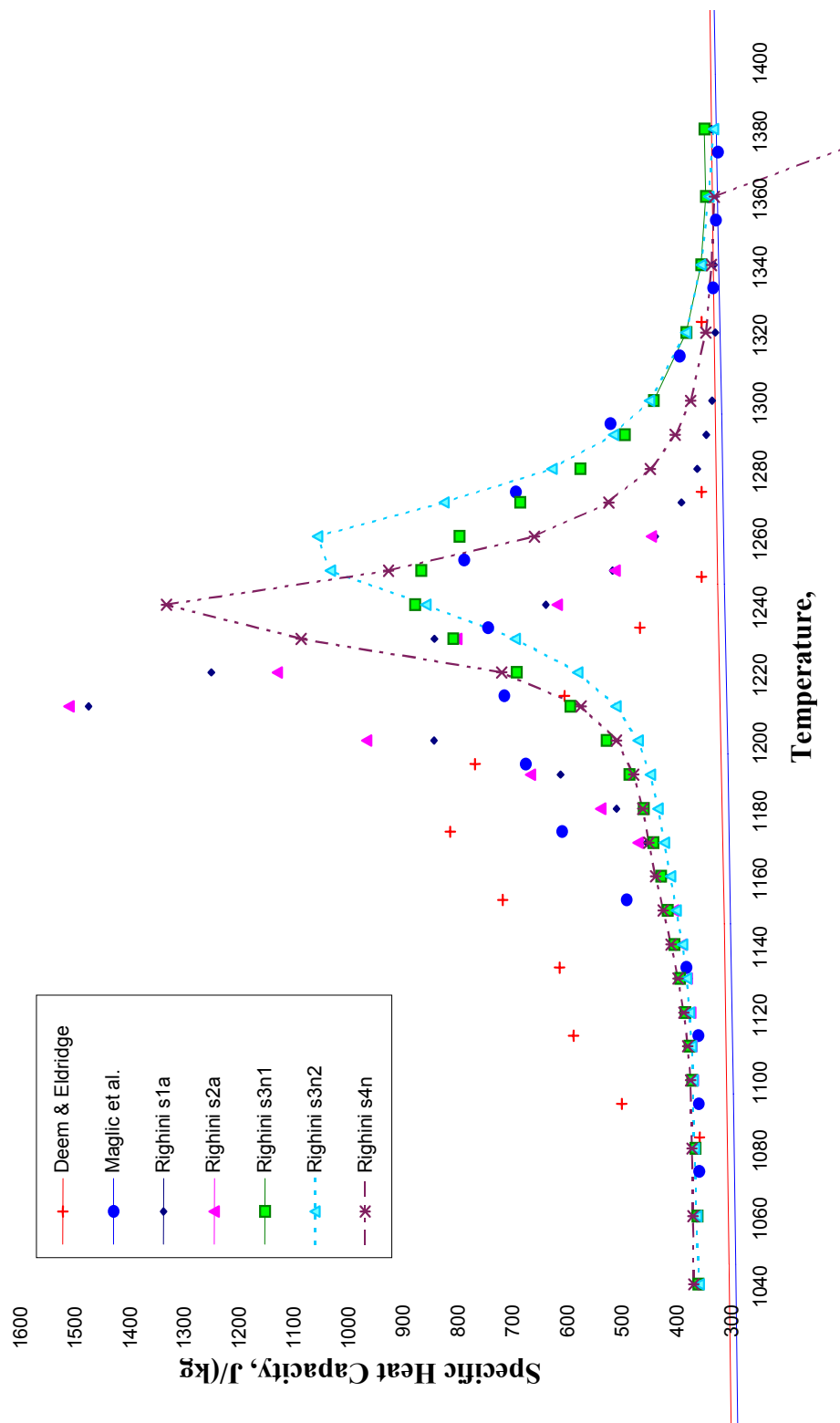


FIG. 7. Comparison of heat capacity data in the phase transition region.

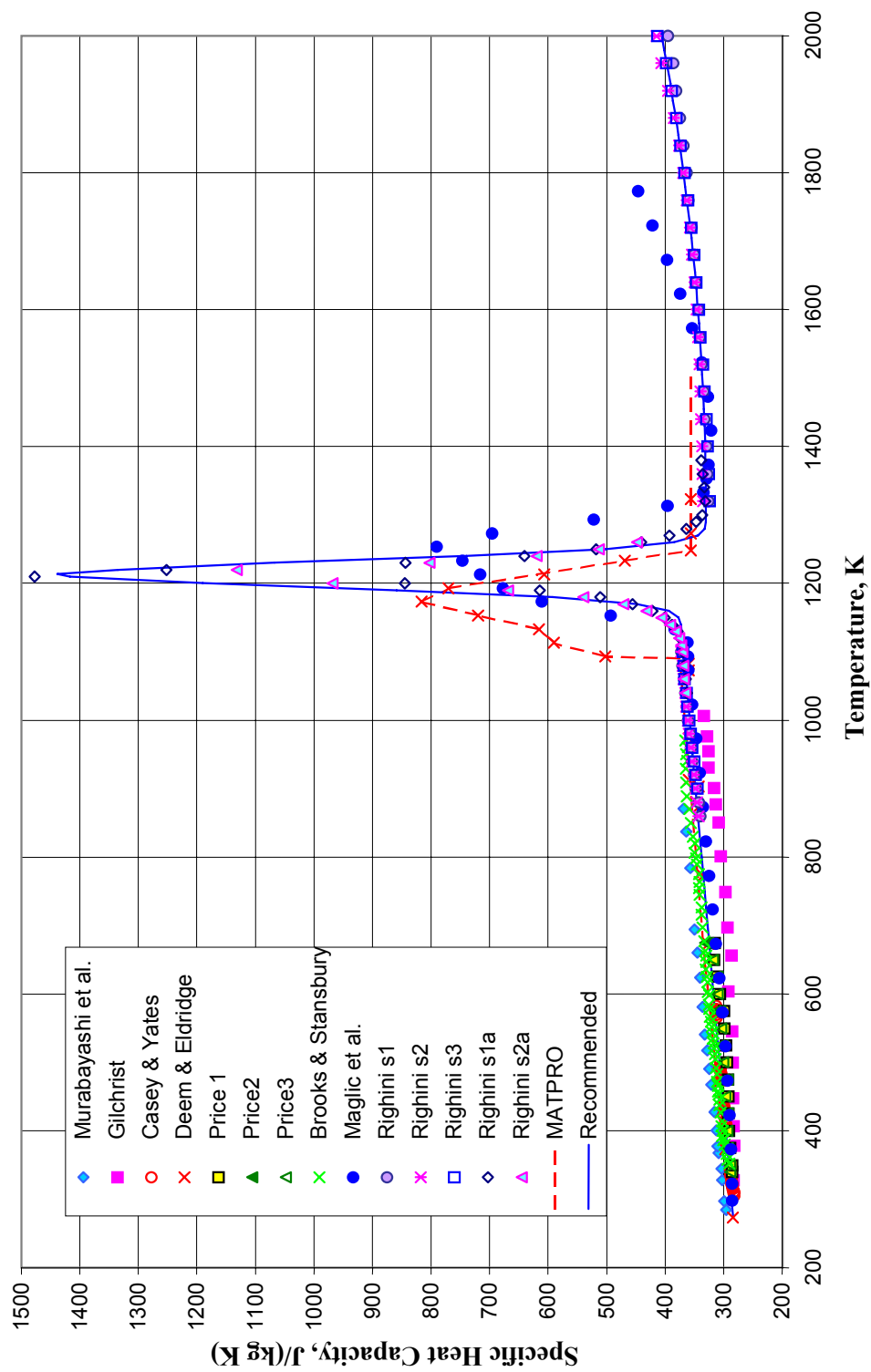


FIG. 8. Comparison of MATPRO & recommended fit to Zircaloy-2 heat capacity data.

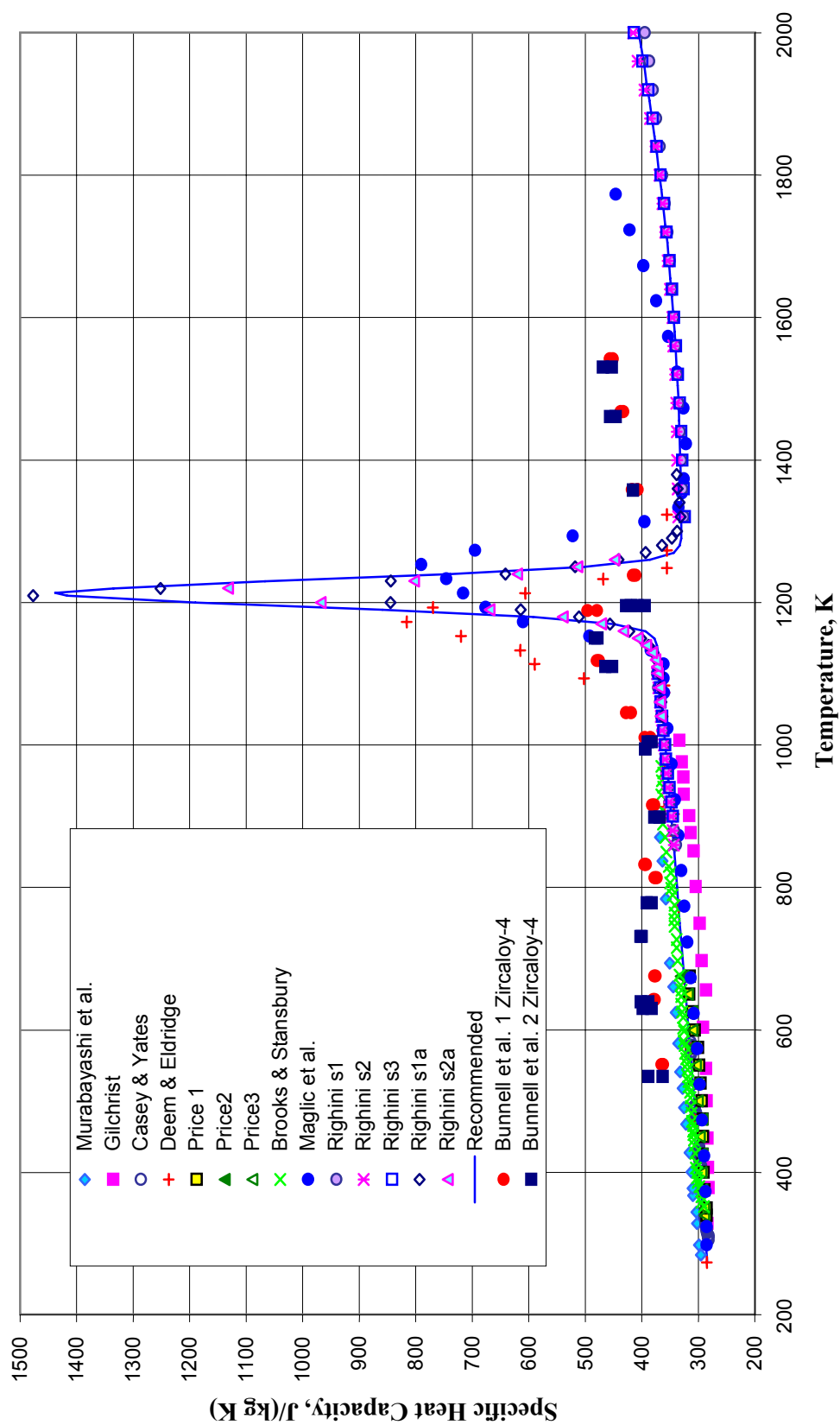


FIG. 9. Comparison Zircaloy-2 and Zircaloy-4 heat capacities.

## REFERENCES TO SECTION 6.2.1.1

- [1] DEEM, H.W. and ELDRIDGE, E.A., USAEC Report BMI-1644 (1963), as tabulated and referenced by Y. S. Touloukian et al., Thermophysical properties of matter volume 4: specific heat metallic elements and alloys, p. 502-503, Plenum, New York (1970). See also H. W. Deem and E. A. Eldridge, Specific heats and heat of transformation of zircaloy-2 and low nickel zircaloy-2, USAEC Report BMI-1803 (1967).
- [2] BROOKS, C.R. and STANSBURY, E.E., The Specific heat of zircaloy-2 from 50 to 700 °C, J. Nucl. Mater. 18, 233-234 (1966).
- [3] MURABAYASHI, M., TANAKA, S. and TAKAHASHI, Y., Thermal conductivity and heat capacity of zircaloy-2, -4, and Unalloyed Zirconium, J. Nucl. Sci. Technol. 12, 661-662 (1975).
- [4] CASEY, D.N. and YATES, B., The specific heat capacities of boron-containing alloys and cermets of zircaloy-2, and related thermodynamic properties of zirconium, High Temp. -High Press. 6, 33-46 (1974).
- [5] GILCHRIST, K.E., Thermal property measurements on zircaloy-2 and associated oxide layers up to 1200 °C, J. Nucl. Mater. 62, 257-264 (1976).
- [6] RIGHINI, F., ROSSO, A. and COSLOVI, L., Measurement of thermophysical properties by a pulse-heating method: zircaloy-2, 1320 to 2000 K, Proceedings of the Seventh Symposium on Thermophysical Properties, Gaithersburg, Maryland, May 10-12, 1977, A. Cezairliyan ed, pp. 358-368, ASME (1977).
- [7] PRICE, E.G., Thermal conductivity, electrical resistivity, and specific heat of CANDU constructional alloys and AISI type 403 end fitting, TDVI-368 (1980), as tabulated and referenced by J. Cleveland, editor, Thermophysical Properties of Materials for Water-Cooled Reactors, IAEA TECDOC-949 (1997).
- [8] RIGHINI, F., COSLOVI, L. and ROSSO, A., Measurement of thermophysical properties by a pulse-heating method: the phase transformation of zircaloy-2, (800 -1400 K), Proceedings of the Eighth Symposium on Thermophysical Properties, Gaithersburg, Maryland, June 15-18, 1981, J. V. Sengers, ed., Vol.II, pp. 51-61, ASME (1982).
- [9] MAGLIC, K.D., PEROVIC, N.L.J. and STANIMIROVIC, M., Calorimetric and transport properties of zircaloy 2, zircaloy 4, and Inconel 625, Int. J. of Thermophysics 15, 741-755 (1994).
- [10] HAGRMAN, D.T. et al., SCDAP/RELAP5/MOD 3.1 Code Manual MATPRO - A library of materials properties for light-water-reactor accident analysis, USNRC Report NUREG/CR-6150, EGG-2720 Vol. 4 (1995).
- [11] BUNNELL, L.R., BATES, J.L. and MELLINGER, G.B., Some high-temperature properties of zircaloy-oxygen alloys, J. Nucl. Mater. 116, 219-232 (1983).
- [12] CHUNG, H.M. and KASSNER, T.F., Pseudobinary zircaloy-oxygen phase diagram, J. Nucl. Mater. 84, 327-339 (1979).
- [13] CHUNG, H.M., GARDE, A.M. and KASSNER, T.F., in Light-water-reactor safety research program: Quarterly Progress Report, April-June 1975, Argonne National Laboratory Report ANL-75-58, pp. 63-74 (1975).
- [14] RUBENSTEIN, L.S., GOODWIN, J.G. and SHUBERT, F.L., Effect of oxygen on the properties of zircaloy-2, Transactions of the ASM 54, 20-30 (1961).
- [15] MALLET, M.W., ALBRECHT, W.M. and WILSON, P.R., J. Electrochem. Soc. 106, 181 (1959).
- [16] OSTERBERG, G., Metallographic study of isothermal transformation of beta phase in zircaloy-2, Jernkontoets Ann. 145 119 (1963).
- [17] CORCHIA, M. and RIGHINI, F., Kinetic aspects of the phase transformation in zircaloy-2, J. Nucl. Mater. 97, 137-148 (1981).
- [18] LUSTERNICK, V.E., PELETISKY, V.E. and PETROVA, I.I., High temperature calorimetric measurements of Zr-0.01Nb alloy at various rates of heating, High Temp.-High Press. 25, 539-543 (1993).
- [19] PELETISKY, V.E. and PETROVA, I.I., Investigation of the thermophysical properties of the alloy Zr-0.01Nb by a subsecond pulse-heating technique, High Temp.-High Press. 29, 373-378 (1997).



### 6.2.1.2. Viscosity

The recommendation for the viscosity of molten Zircaloy is

$$15_{-7}^{+2} \text{ mPa. s}$$

This value was obtained from measurements on Zircaloy-2 from 2075 to 2175 K by Bunnell and Prater [1]. They found that, in this temperature range, the viscosity of Zircaloy-2 is a constant.

#### **Uncertainty**

The large negative uncertainty arises from differences between the viscosity of Zircaloy-2 measured by Bunnell and Prater and the viscosity of molten zirconium at similar temperatures that was determined by Yelvutin et al.[2]. From measurements using a graphite crucible, Yelvutin et al. [2] determined the viscosity of molten zirconium to be 8 mPa.s. Iida and Guthrie [3] report that differences between viscosities of dilute alloys and pure metals is small (1-5%). Thus, the viscosity of Zircaloy-2 (98 wt% Zr, 1.2-1.7 wt% Sn, 0.18-0.38 wt% Fe+Cr+Ni) is expected to be similar to that of zirconium. The positive uncertainty indicates the expected experimental error of 10-15%.

#### **Discussion**

The viscosity of Zircaloy-2 was measured by Bunnell and Prater [2] as a function of temperature from 2075 to 2175 K. They found that, in this temperature range, the viscosity of Zircaloy-2 is a constant equal to 15 mPa.s. Bunnell and Prater comment that the different viscosities obtained for zirconium and Zircaloy-2 may be due either to differences in viscosity of Zircaloy-2 and zirconium or to impurity effects introduced by the crucible used in the measurements. Yelvutin et al. used a graphite crucible whereas Bunnell and Prater used a less reactive thoria crucible. At high temperatures, zirconium reacts with graphite to form ZrC. No data are available on the post-test analysis of the solidified liquid from the viscosity measurements of Yelvutin et al. Thus, it is possible that their reported viscosity is that of a liquid mixture of ZrC + Zr or of zirconium with carbon in solution, and not that of pure zirconium.

In order to rule out contamination of their sample from interaction with the thoria crucible, Bunnell and Prater [1] repeated their measurements after holding the sample at temperature for 2 hrs. They obtained the same viscosities. Metallographic examination of the sample after these 2 hr experiments showed metallic thorium precipitates. X-ray fluorescence measurements indicated 2 mol% thorium in the Zircaloy. Bunnell and Prater also measured the viscosity of Zr-UO<sub>2</sub> mixtures containing 70 to 94.9 mol% zirconium. Analysis of the samples of these mixtures after the viscosity measurements showed that thorium contamination was less than 1 mol%. These measurements indicate that the mixture viscosity increases with increasing zirconium content from 10 mPa.s for 70 mol% Zr to 17 mPa.s for 94.9 mol% zirconium. These results are consistent with the viscosity obtained for Zircaloy-2 and with other viscosity measurements on UO<sub>2</sub>-Zr mixtures.

Although Bunnell and Prater report an abrupt change in viscosity when the sample became molten, it is possible that their measurements were made just as the sample began to flow when a solid phase was still present and the Zircaloy was between the solidus and liquidus. The liquidus temperatures of Zircaloy are a function of the amount of oxygen in the Zircaloy and range from 2136 to 2243 K for oxygen atom fractions of 0.007 to 0.19 [4]. The measurement by Yelvutin et al. was most likely made on a completely liquid sample since, unlike the alloy, the pure metal has a sharp melting point.

Based on the above data and considerations, it is clear that additional measurements of the viscosity of Zircaloy and zirconium are needed under well-controlled atmospheres without contamination from containers. Until such data are available, a viscosity of 15 mPa.s is recommended for modeling the beginning of melting of Zircaloy with an oxide coating when the material begins to flow down the wall of the cladding.

## REFERENCES TO SECTION 6.2.1.2

- [1] BUNNELL, L.R. and PRATER, J.T., Viscosity of zirconium-uranium oxide (Zr-UO<sub>2</sub>) mixtures at 1800 to 2100°C, U.S. Nuclear Regulatory Commission Report NUREG/CR-4495 (September 1986); Viscosity of Zirconium Uranium Oxide (Zr-UO<sub>2</sub>) Mixtures at 2075 to 2375 K, Pacific Northwest Laboratory Report PNL-SA-15644 (1988).
- [2] YELVUTIN, V.P., et al., Chernage Met 7 (128) (1965); as referenced by Bunnell and Prater (Reference 1).
- [3] IIDA, T. and GUTHRIE, R.I.L., The physical properties of liquid metals, Clarendon Press, Oxford (1993).
- [4] HAGRMAN, D.T. (ed.), SCADAP/RELAP5/MOD3.1 Code manual MATPRO - a library of materials properties for light-water-reactor accident analysis, NUREG/CR-6150, EGG-2720 Vol. 4 (1995), p 4-1 to 4-5.

### 6.2.1.3. Zircaloy-4 (O) solidus temperatures

#### **Recommendation**

The recommended equations for the solidus of Zircaloy-4 (O) are based on the recent measurements by Hayward and George [1]. The curve given by Hayward and George to represent their data was read from their graph and fit by the following equations in which X stands for the oxygen content in atom percent.

For  $0 \leq X \leq 11.01 \text{ at\%}$ ,

$$T_s(K) = 2025.33 + 15.1043X + 0.0930X^2; \quad (1)$$

For  $11.01 \text{ at\%} \leq X \leq 15.5 \text{ at\%}$ ,

$$T_s(K) = 2203; \quad (2)$$

For  $15.5 \text{ at\%} \leq X \leq 21.3 \text{ at\%}$ ,

$$T_s(K) = 175.48 + 207.987X - 4.979X^2; \quad (3)$$

For  $21.3 \text{ at\%} \leq X \leq 22.5 \text{ at\%}$ ,

$$T_s(K) = 2348; \quad (4)$$

For  $22.5 \text{ at\%} \leq X \leq 29 \text{ at\%}$ ,

$$T_s(K) = 2222.248 + 13.506X - 0.35188X^2; \quad (5)$$

For  $X > 29 \text{ at\%}$ ,

$$T_s(K) = 2318; \quad (6)$$

The large number of significant figures in equations (1), (3), and (5) arise from the constraint of continuity at the endpoints. The data obtained by Hayward and George [1] and the curve produced by the above equations, which reproduces the curve presented by Hayward and George [1] are shown in Figure 1. Tabulated values of the solidus temperature for Zircaloy-4 (O) as a function of oxygen are given in Table 1 and compared with the data of Hayward and George. Hayward and George give an uncertainty of  $\pm 20 \text{ K}$  for their data, which has been included as error bars in Figure 1.

### Uncertainty

The estimated uncertainty in the recommended values is that given by Hayward and George for their data,  $\pm 20$  K, which is about 1%. Except for the 2301 K datum at an oxygen level of 17.1 at%, the uncertainty in reproducing the curve and fitting the data is much smaller than the quoted uncertainty in the data. The uncertainty for this datum is 1.01%.

### Discussion

Hayward and George compared their data with Zr-O solidus data of Ackermann et al. [2] and with values from MATPRO [3]. This comparison is shown in Figure 2. The MATPRO equations for the Zircaloy-O solidus temperature,  $T_{sol}$ , in K as a function of atom fraction of oxygen,  $y$ , are:

For  $y \leq 0.1$

$$T_{sol} = 2098 + 1150y; \quad (7)$$

For  $0.1 < y \leq 0.18$

$$T_{sol} = 2213; \quad (8)$$

For  $0.18 < y \leq 0.29$

$$T_{sol} = 13389.5317 + 7640.0748y - 17029.172y^2; \quad (9)$$

For  $0.29 < y \leq 0.63$

$$T_{sol} = 2173; \quad (10)$$

For  $0.63 < y \leq 0.667$

$$T_{sol} = -11573.454 + 21818.181y; \quad (11)$$

For  $y > 0.667$

$$T_{sol} = -11572.454 + y(1.334 - y)21818.181; \quad (12)$$

Hayward and George found reasonable agreement between their Zircaloy-O and the Zr-O composition ranges of Ackermann et al.[2] for the various types of reactions (i.e. peritectic, eutectic, congruent melting). They attributed the lower solidus temperatures at low oxygen content for Zircaloy-O compared to Zr-O to either influences of the Zircaloy alloy elements such as Sn or to possible pre-oxidation of Zr samples of Ackermann et al. during heating in high density ZrO<sub>2</sub>. From comparison of their data at high oxygen content with the solidus temperatures for O-saturated Zircaloy given in MATPRO, they concluded that the values quoted in MATPRO are probably low by 145-185 K and recommended a value of  $2318 \pm 20$  K be used for the solidus temperature of O-saturated cladding in future model revisions.

The recommended equations were obtained by least squares fits of the curve given by Hayward and George constrained for continuity at the endpoints of each equation. In Table 1, values calculated with the recommended equations are compared with the data tabulated by Hayward and George. These equations fit the data of Hayward and George with an error of less than 1% except for the datum 2301 K at 17.1 at% O, which is fit within 1.01%, or 24 K. Hayward and George estimate the experimental uncertainty of their data as  $\pm 20$ K. Thus except for this one datum, which is higher than the recommended equation by 24K, all the values given by the recommended equations are within the experimental uncertainty given by Hayward and George.

Figure 3 shows the data of Hayward and George, the fit to the recommended equations, Eq. (1)-Eq.(6), the data of Ackermann et al., and the equations given in MATPRO. The MATPRO equations are about 4% higher than the data of Hayward and George at low oxygen levels (less than 10 at%) and are within 1% of the data at oxygen levels from 10 to 15 atm%. Above 15 at% oxygen, the MATPRO equations are low relative to the data of Hayward and George by 4% to 6% with the deviation increasing as the oxygen level approaches saturation. Hayward and George state that at saturation, the

MATPRO recommendation is low by 145 K to 185 K or by 6 to 8%. Therefore the equations based on the curve of Hayward and George are recommended in place of the equations given in MATPRO.

Table 1. Comparison of recommended equations with data of Hayward & George

OXYGEN, atm%	SOLIDUS TEMPERATURE, K	
	DATA	RECOMMENDED
0.74	2037	2037
2.3	2070	2061
3.7	2072	2082
5.5	2112	2111
8.3	2153	2157
8.7	2169	2164
9.1	2151	2170
9.9	2188	2184
10.2	2207	2189
10.4	2195	2192
11.2	2188	2203
15.5	2207	2203
17.1	2301	2277
21.0	2327	2347
21.3	2358	2348
25.7	2328	2337
26.9	2337	2331
29.2	2321	2318
32.5	2318	2318
34.4	2318	2318

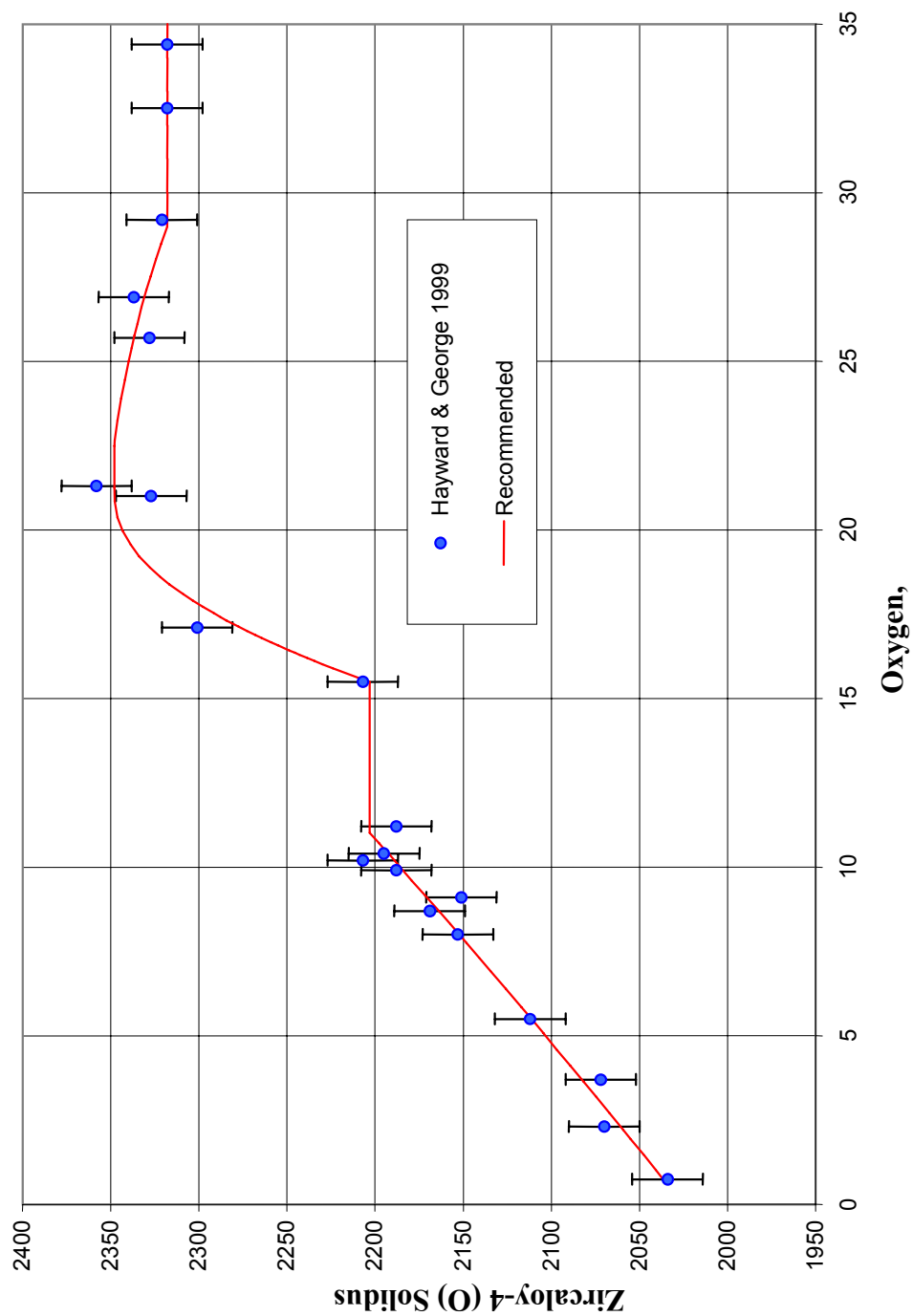


FIG. 1 Recommended equations for Zircaloy-4(O) Solidus temperature.

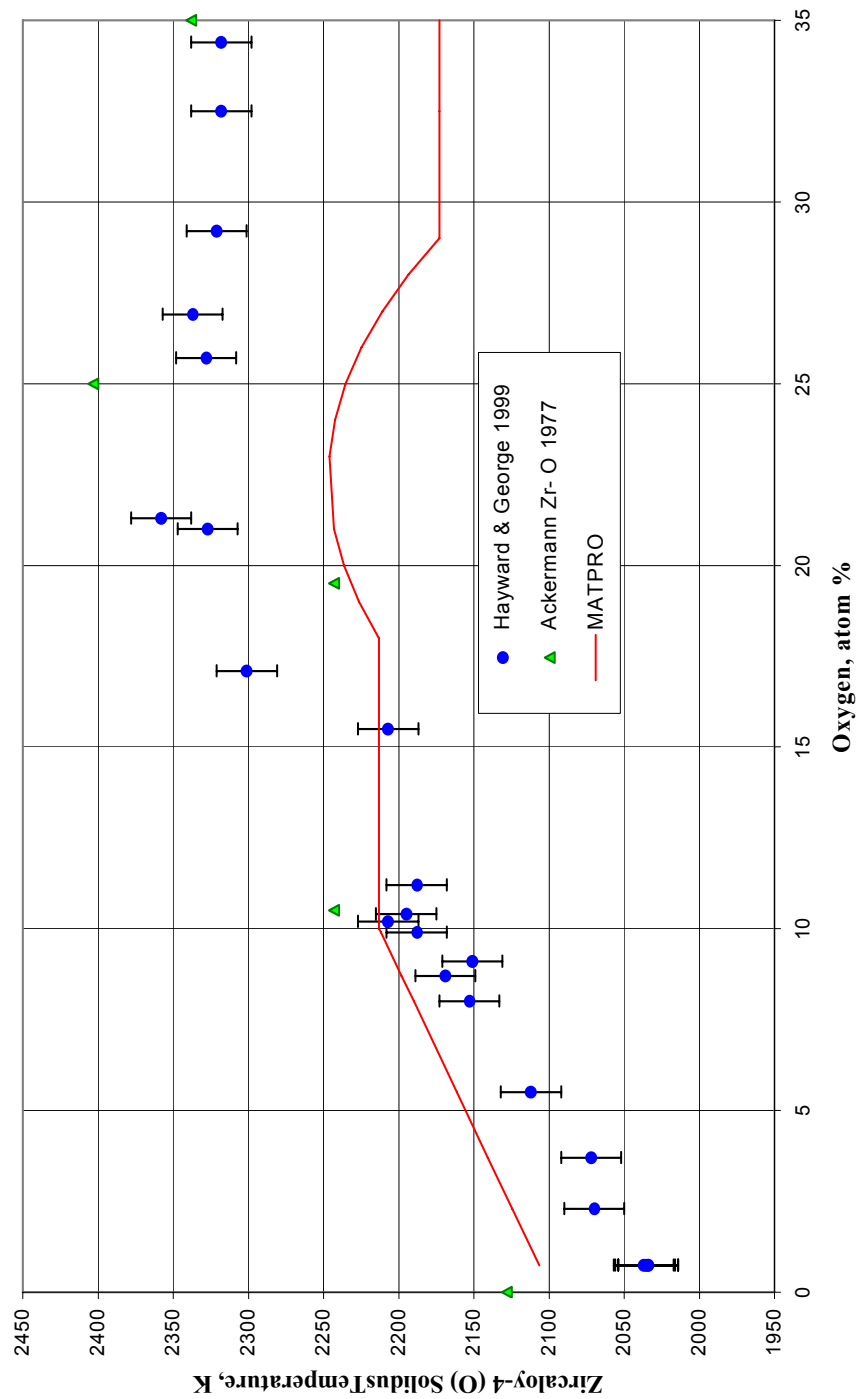


FIG. 2. Comparison of Zircaloy-4 (O) Solidus temperature data with MATPRO.

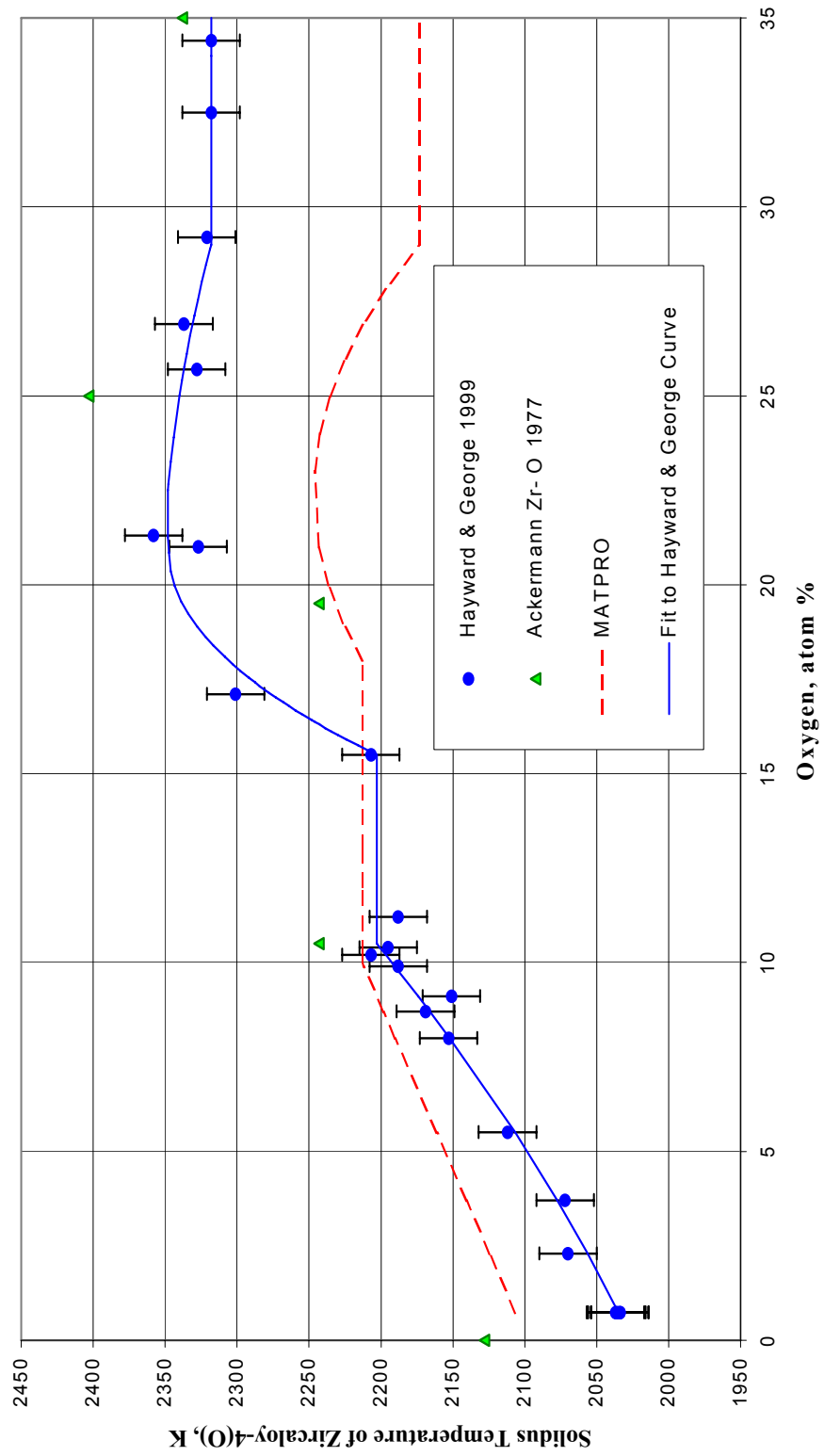


FIG. 3. Comparison of recommended equation with MATPRO and data.

## REFERENCES TO SECTION 6.2.1.3

- [1] HAYWARD, P.J. and GEORGE, I.M., Determination of the solidus temperatures of Zircaloy-4/oxygen alloys, J. Nucl. Mat. 273, 294-301 (1999).
- [2] ACKERMANN, R.J., GARG, S.P. and RAUH, E.G., J. Am. Ceram. Soc. 60, 341 (1977).
- [3] HAGRMAN, D.T. (ed), SCDAP/RELAP5/MOD 3.1 Code manual: MATPRO – a library of materials properties for light-water-reactor accident analysis, NUREG/CR-6150, EGG-2720 Vol.4 (1995).

### 2.1.1.1. 6.2.1.4. *Thermal conductivity*

#### **Recommendation**

The equation recommended for the thermal conductivity of Zircaloy is

$$\lambda = 12.767 - 5.4348 \times 10^{-4} T + 8.9818 \times 10^{-6} T^2 \quad (1)$$

where  $\lambda$  is the thermal conductivity in  $\text{W m}^{-1} \text{K}^{-1}$  and  $T$  is the temperature in K. This equation was obtained from a least squares analysis of the available thermal conductivity data from direct measurements and derived from thermal diffusivity data on Zircaloy-2 and Zircaloy-4. Figure 1 compares the values of the thermal conductivity obtained from this equation with the Zircaloy-2 and Zircaloy-4 data included in the analysis. One standard deviation uncertainty bands have been included in the figure. This equation is valid for the temperature range 300 to 1800 K. Extrapolation to higher temperatures, where no data are available, is not recommended because it is a polynomial fit to the data and not a physically-based equation. Tabulated values of the thermal conductivity calculated from Eq.(1) are given in Table 1.

#### **Uncertainty**

Figure 1 shows the one standard deviation uncertainties for the recommended equation. They increase with temperature from 4% at 300 K to 5% at 500 K, 6% at 800 K and 7% at 1200 K. Average uncertainties from 1200 to 1800 K are 7%.

#### **Discussion**

##### *Review of thermal conductivity data*

Table 2 lists the measurements of the thermal conductivity of Zircaloy-2 and Zircaloy-4 in chronological order and gives the year of measurement, the temperature range, and number of data. Data from 1958 through 1966, which includes the data of Lucks and Deem [1], Chirigos et al.[2], Powers [3], Anderson et al. [4], Scott [5], and Feith [6] were used in the development of the MATPRO equation [10] for the thermal conductivity of Zircaloy. The MATPRO equation for the thermal conductivity of Zircaloy is

$$\lambda = 7.51 + 2.09 \times 10^{-2} T - 1.45 \times 10^{-5} T^2 + 7.67 \times 10^{-9} T^3 \quad (2)$$

where  $\lambda$  is the thermal conductivity in  $\text{W m}^{-1} \text{K}^{-1}$  and  $T$  is the temperature in K. In Figure 2, the MATPRO equation is shown with these data that were included in its derivation. In addition to the data listed in Table 2, the MATPRO manual [10] lists Zircaloy-2 data given by Chirigos et al. [2] and an additional set of data for Zircaloy-2 data reported by Powers [3]. Examination of these data [2,3] showed that both sets of data are from measurements at the Battelle Memorial Institute and are identical to the data reported by Lucks and Deem [1]. Inclusion of these duplicate sets of data in the derivation of the MATPRO equation had the effect of weighting the data of Lucks and Deem by a factor of three. More recent data tabulated in the 1997 IAEA technical document “Thermophysical Properties of Materials for Water Cooled Reactors” [7] are the Atomic Energy of Canada Limited (AECL) data reported by Price [8] and Mills et al. [9] and new measurements by the Institute of Atomic Energy of China. Figure 3, which compares these new data with the MATPRO equation and the older data fit by the MATPRO equation, indicates that some of the AECL data [7-9] are high relative to the MATPRO equation. However, some of the data fit by the MATPRO equation are also high relative to the MATPRO equation.



### *Review of thermal diffusivity data*

No thermal diffusivity data were considered in the formulation of the MATPRO equation. In 1970, Wheeler [11] reported anomalous results of thermal diffusivity measurements on Zircaloy-2 using a modulated electron beam technique. These measurements gave thermal diffusivities that were constant in the temperature range from 550 to 925 K but varied with the thickness of the sample. Walter et al. [12] studied effects of sample orientation and thickness on thermal diffusivity of Zircaloy-2 plate. Although no difference in the thermal diffusivity was observed for specimens from different directions, thickness effects were detected in measurements made at Harwell [12] using thermocouples but not in measurements at Manchester [12] that used infrared detectors. These results are shown in Figure 4, where H indicates Harwell measurements using thermocouples and M denotes the Manchester measurements using an infrared detector. Sample thickness has been included in the legend. Based on results of these measurements, the Wheeler data [11] and the Harwell data on small samples reported by Walter et al. [12] have not been included in this analysis. The Manchester data and the data from Harwell on 2 mm samples are consistent with later measurements on Zircaloy-2 and Zircaloy-4 by Murabayashi et al. [13], by Taylor [14], and by Maglic [15].

Thermal diffusivity data for unoxidized Zircaloy-2 and Zircaloy-4 are listed in chronological order in Table 3 and shown in Figure 5. Figure 5 shows that although the data of Gilchrist et al. [16] are consistent with the AECL data [7–9] for the thermal diffusivity of an annealed rod in the axial direction, these data are higher than other diffusivity data.

Data on the effects of oxidation on the thermal diffusivity of Zircaloy-2 and Zircaloy-4 [16–20] are not being included in this analysis, which is to determine the thermal conductivity of unoxidized Zircaloy. In their oxidation studies, Gilchrist [16, 17], Peggs et al. [18] and Bunnell et al. [19, 20] also report results of thermal diffusivity measurements on samples that were not oxidized in steam. Peggs et al. report no measurement data but show curves for the thermal diffusivities of a Zircaloy-2 tube in the radial direction, a Zircaloy-2 calandria tube, and a Zircaloy-4 fuel sheath. In Figure 6, the curves reported by Peggs et al. are compared with the low-temperature thermal diffusivity data listed in Table 3. It shows that the results reported by Peggs et al. are consistently higher than other data and appear to have a different slope indicating either a systematic error or differences due to the condition of the surface. Thus, these results reported by Peggs et al. have not been included in this analysis. In Figure 7, the data of Bunnell et al. [19, 20] for as received samples of Zircaloy-4 tube, Zircaloy-4 bar, and Zircaloy-2 and the fits to these data by Bunnell et al. [19, 20] are compared with the thermal diffusivity data listed in Table 3. Although some of the data of Bunnell et al. are in the same range as other data, the recommended curves of Bunnell et al. are consistently low compared to other data. Thus, the data and equations of Bunnell et al. have not been included in this analysis.

### *Data analysis*

The temperatures for all data obtained prior to 1968 were converted from the 1948 International Practical Temperature Scale (IPTS) to the 1968 IPTS. Thermal diffusivity data have been converted to thermal conductivity using the equation

$$\lambda = D C_p \rho \quad (3)$$

where  $\lambda$  is the thermal conductivity,  $D$  is the thermal diffusivity,  $C_p$  is the heat capacity, and  $\rho$  is the density. The heat capacity was calculated from equations for the heat capacity of Zircaloy-2. For the  $\alpha$ -phase, from 273 K <  $T$  < 1100 K,

$$C_p = 255.66 + 0.1024 T \quad (4)$$

where temperature is in K and the heat capacity is in J kg<sup>-1</sup> K<sup>-1</sup>. For the  $\beta$ -phase from 1320 K <  $T$  < 2000 K

$$C_p = 597.1 - 0.4088 T + 1.565 \times 10^{-4} T^2 \quad (5)$$

where temperature is in K and heat capacity is in J kg<sup>-1</sup> K<sup>-1</sup>. From 1100 K through 1214 K, in the (  $\alpha + \beta$  )- phase-transition region, the heat capacity of Zircaloy-2 has been calculated from the sum of Eq. (4) and a Gaussian function that represents the peak of the transition. This Gaussian function is:

$$f ( T ) = 1058.4 \exp \left[ \frac{(T - 1213.8)^2}{719.61} \right] \quad (6)$$

where temperature is in K and  $f ( T )$  is in J kg<sup>-1</sup> K<sup>-1</sup>. From 1214 to 1320 K, the heat capacity of Zircaloy-2 is calculated from the sum of Eq. (5) + Eq. (6).

The Zircaloy density as a function of temperature has been calculated from the room temperature density, 6501 kg m<sup>-3</sup>, and the change in volume obtained from the linear thermal expansion in three orthogonal directions. For the  $\alpha$ -phase (T < 1083 K), the calculated densities are well represented by the linear equation

$$\rho = 6595.2 - 0.1477 T \quad (7)$$

where  $\rho$  is the density in kg m<sup>-3</sup> and T is the temperature in K. The change in density through the (  $\alpha + \beta$  )- phase-transition region was set equal to 0.67%, the value recommended for zirconium by Guillermet [21]. In the  $\beta$ -phase (1144–1800 K), the density has been calculated from the linear equation

$$\rho = 6690.0 - 0.1855 T \quad (8)$$

where  $\rho$  is the density in kg m<sup>-3</sup> and T is the temperature in K.

Figure 8 shows both the thermal conductivity and thermal diffusivity data expressed as thermal conductivity. Some of the low-temperature AECL data and the data of Scott and of Gilchrist appear high relative to other data in the same temperature range. In Figure 9, the MATPRO equation is compared with the data fit by the MATPRO equation, the more recent thermal conductivity data, and the thermal conductivities obtained from the thermal diffusivity measurements. It shows that from 400 to 1200 K, the MATPRO equation is high relative to data from thermal diffusivity measurements.

Because much new data have been obtained since the derivation of the MATPRO equation and the MATPRO equation is not a good representation of all these data, a new analysis has been completed to determine a new equation for the thermal conductivity of Zircaloy. The thermal conductivity and thermal diffusivity data listed in Tables 2 and 3 have been considered in this analysis. To determine if some of the sets of data listed in Tables 2 and 3 and shown in Figure 8 do not belong to the same statistical set and should not be included in the final analysis, all the data shown in Figure 8 were fit to a quadratic function by a least squares analysis. This quadratic equation

$$\lambda = 13.09 - 7.920 \times 10^{-4} T + 9.043 \times 10^{-6} T^2 \quad (9)$$

represents the common consensus of all the data. The data, quadratic fit, and error bands at two standard deviations from the quadratic fit are shown in Figure 10. Sets of data that have points outside these error bands have been identified in the legend and are shown as filled symbols in the graph. The high datum in Figure 10 at 925 K is from measurements by Feith [6]. The two unusually low data at approximately 1140K are from measurements by Maglic et al. [15]. These data, which are obviously bad points, have not been included in the final analysis.

To determine how well each set of data are represented by the MATPRO equation and by the quadratic fit, modified variances relative to the MATPRO equation and the quadratic fit were calculated for each set of data. These modified variances,  $\sigma^2$ , are defined as

$$\sigma^2 = \frac{1}{N} \sum [\lambda_{Eq}(T_i) - \lambda(T_i)]^2 \quad (10)$$

where N is the number of points in the data set,  $\lambda_{Eq}(T_i)$  is the thermal conductivity at temperature  $T_i$  determined by the MATPRO equation or the quadratic fit, and  $\lambda(T_i)$  is a data point in the data set. These modified variances are given in Tables 2 and 3 for each set of data. Sets of data for which the

majority of points fell outside two standard deviations and/or for which the modified variance of the quadratic equation, Eq. (9), is greater than 2.5 have been excluded from the final analysis. Data excluded from the analysis are shown in Figure 11. Thermal conductivity measurements not included are data sets AECL4 Zircaloy-2 cold-worked tube, AECL5 Zircaloy-2 annealed strip in the transverse direction, AECL6 Zircaloy-2 stress-relieved thin-wall tube in the circumferential direction, and AECL7 Zircaloy-2 annealed rod. Thermal diffusivity data excluded from this analysis are the AECL3 Zircaloy-2 annealed rod in the axial direction and the 1976 Zircaloy-2 measurements of Gilchrist. Although only one datum of Gilchrist falls outside the two standard deviations, these data clearly have a different temperature behavior than the data included in the final analysis. For example, the data of Gilchrist [16] show a distinct discontinuity at the phase transition that is not evident in thermal conductivities obtained from other measurements. The low-temperature data of Gilchrist are high with a different slope from the common consensus. These deviations of the Gilchrist data from the common consensus are illustrated by modified variances of 2.5 and 2.7, respectively relative to the MATPRO equation and the quadratic fit.

The final analysis included 321 data-points from the datasets listed in Table 4. Because the number of data obtained by the measurements by Maglic et al. are considerably higher than that of any other investigator, these data were reduced to 53 data-points by averaging the temperatures and thermal conductivities of data that were obtained at nearly the same temperature. This prevented excessive weighting of the measurements by Maglic et al. in the final analysis.

The data listed in Table 4 were fit using multiple regression analysis to three functional forms: quadratic, cubic, and quadratic + 1/T. The quadratic + 1/T functional form was included because Fink and Leibowitz [22] found that it provided the best fit to the thermal conductivity of zirconium. The goodness of fit for each functional form is shown in Table 5, which gives  $\chi^2$  (the sum of the squares of the deviation of the data from the fit), the variance ( $\chi^2$  / [N-free parameters], where N = the number of points), and the standard deviation. For completeness, these statistics for the MATPRO equation have also been included in Table 5. All the new equations fit the data considerably better than the MATPRO equation. Because the statistics given in Table 5 indicate that the quadratic + 1/T form does not fit the data any better than the quadratic equation, this functional form has been excluded from further consideration. The quadratic equation referred to in Table 4 and 5 is Eq. (1). The cubic equation is:

$$\lambda = 11.498 + 4.6765 \times 10^{-3} T + 2.761 \times 10^{-6} T^2 + 2.2147 \times 10^{-9} T^3 \quad (11)$$

where  $\lambda$  is the thermal conductivity in  $\text{W m}^{-1} \text{K}^{-1}$  and  $T$  is the temperature in K. The MATPRO equation is Eq. (2).

The data included in this analysis are compared with the cubic [Eq. (11)], quadratic [Eq. (1)], and MATPRO [Eq. (2)] equations in Figure 12. Figure 13 shows the deviations of the data from the cubic and quadratic equations. Examination of Figures 12 and 13 shows that the cubic equation improvement is mainly from better fitting of the high-temperature points. In fact, some low-temperature data are better fit using the quadratic form. Table 4 gives the modified variances defined according to Eq. (10) for each set of data relative to the MATPRO equation and the quadratic and cubic equations. It shows that the cubic equation provides better fits than the quadratic equation for the data of Lucks and Deem, Anderson, Scott, Feith, and Taylor and the AECL thermal conductivity data. Although the cubic equation provides slightly better fits to some sets of data and to the highest temperature points, an F test comparing the quadratic and cubic fits of these data shows that the additional term in the cubic equation is not statistically justified. Therefore, the quadratic equation, Eq. (1) that fits the combined thermal conductivity and thermal diffusivity data has been recommended.

Table 1. Thermal conductivity of Zircaloy

TEMPERATURE K	THERMAL CONDUCTIVITY $\text{W m}^{-1} \text{K}^{-1}$
300	13.41
400	13.99
500	14.74
600	15.67
700	16.79
800	18.08
900	19.55
1000	21.21
1100	23.04
1200	25.05
1300	27.24
1400	29.61
1500	32.16
1600	34.89
1700	37.80
1800	40.89

Table 2. Thermal conductivity measurements

EXPERIMENTER	YEAR	TEMPERATUREK	NO. OF POINTS	VARIANCE		MATERIAL, COMMENTS Zr-2 =Zircaloy-2; Zr-4=Zircaloy-4)
				MAT-PRO	QUAD-RATIC	
C. F. Lucks & H. W. Deem [1]	1958	293-1100	9	0.11	0.32	Zr-2, used in obtaining MATPRO eq.
J. N. Chirigos et al. [2]	1961	373 -1100	9	2.18	2.13	Zr-4, used in obtaining MATPRO eq.
A. E. Powers [3]	1961	293-1100	8	1.83	1.03	Zr-2, used in obtaining MATPRO eq.
			8	0.70	0.54	Zr-4, used in obtaining MATPRO eq.
W. K. Anderson et al. [4]	1962	380-900	6	0.10	0.21	Zr-2, used in obtaining MATPRO eq.
P. B. Scott [5]	1965	350-1100	18	1.46	2.10	Zr-4, used in obtaining MATPRO eq.
A. D. Feith [6]	1966	600 -1800	53	0.96	1.33	Zr-4, used in obtaining MATPRO eq.
E. G. Price, R. W. Mills et al. (AECL data) [7-9]	1980 1997	300-700	5	0.30	0.49	AECL1 Zr-2 cold-worked tube, axial
			5	0.64	1.31	AECL2 Zr-2 annealed strip, rolling
			5	0.13	0.55	AECL3 Zr-2 thin-wall tube, axial
			5	8.95	8.66	AECL4 Zr-2 cold-worked tube
			5	2.03	2.83	AECL5 Zr-2 annealed strip, transverse
			5	2.31	3.15	AECL6 Zr-2 stress-rel.thin-wall tube, circ.
			5	4.26	5.91	AECL7 Zr-2 annealed rod
China: Institute of Atomic Energy [7]	1997	293-1400	23	1.86	0.93	Zr-2 tube 0.65 mm thick, 10 mm d, radial
			23	0.70	0.40	Zr-4 rod, axial

Table 3. Thermal diffusivity measurements included in analysis

EXPERIMENTER	YEAR	TEMPERATURE K	NO. OF POINTS	VARIANCE		Material, Comments, Sample thickness (Zr-2 =Zircaloy-2; Zr-4=Zircaloy-4)
				MAT- PRO	QUAD- RATIC	
A. J. Walter et al. [12]	1972	300-800	6	0.87	0.16	Zr-2, transverse 2.05 mm, Harwell, infrared detector
			6	1.78	0.62	Zr-2, normal, 2.05 mm, Harwell, infrared detector
			6	1.20	0.34	Zr-2, rolling, 2.0 mm, Harwell, infrared detector
			6	1.32	0.27	Zr-2, 2.06 mm, Manchester, infrared detector
			6	0.81	0.09	Zr-2, 1.04 mm, Manchester, infrared detector
			6	1.07	0.22	Zr-2, 0.63 mm, Manchester, infrared detector
M. Murabayashi et al. [13]	1975	300-900	14	0.59	0.04	Zr-2, 2mm
			10	1.99	0.91	Zr-2, 0.6 mm
			19	1.24	0.53	Zr-4, 2 mm
K. E. Gilchrist [16]	1976	298-1500	18	2.47	2.67	Zr-2, 2.5 mm, 1.97 mm
E. G. Price, R. W. Mills et al. (AECL data) [7-9]	1980	290-673	5	0.53	0.02	AECLd1 Zr-2, cold-worked tube, radial
	1997		5	1.20	0.55	AECLd2 Zr-2, annealed strip, through thickness
			5	4.01	5.49	AECLd3 Zr-2, annealed rod, axial,
R. E. Taylor [14]	1991	300-1500	10	1.11	1.32	Zr-4
K. D. Maglic et al. [15]	1994	298-1373	84	0.89	0.65	Zr-2, annealed sheet
			154			Zr-4, 1.7 mm thick, annealed sheet

Table 4. Thermal conductivity and diffusivity data included in the final analysis

EXPERIMENTER	YEAR	TEMPERATURE K	NO. OF POINTS	VARIANCE			PROPERTY, MATERIAL, COMMENTS ( $\lambda$ =conductivity; D=diffusivity; Zr-2 =Zircaloy-2; Zr-4=Zircaloy-4)
				MAT- PRO	QUAD- RATIC	CUBIC	
Lucks & Deem [1]	1958	293-1100	9	0.11	0.33	0.29	$\lambda$ , Zr-2, included in MATPRO analysis
Chirigos et al. [2]	1961	373 -1125	9	2.18	2.32	2.47	$\lambda$ , Zr-4, included in MATPRO analysis
Powers [3]	1961	293-1100	8	1.83	0.83	0.82	$\lambda$ Zr-2, included in MATPRO analysis
			8	0.70	0.58	0.61	$\lambda$ Zr-4, included in MATPRO analysis
Anderson et al. [4]	1962	380-900	6	0.10	0.27	0.22	$\lambda$ Zr-2, included in MATPRO analysis
Scott [5]	1965	350-1100	18	1.46	2.47	2.31	$\lambda$ Zr-4, included in MATPRO analysis
Feith [6]	1966	600 -1800	52	0.96	1.21	1.09	$\lambda$ Zr-4, included in MATPRO analysis, bad datum at 925K not included
Walter et al. [12]	1972	300-800	6	0.87	0.07	0.12	D, Zr-2, transverse 2.05 mm,
			6	1.78	0.40	0.52	D, Zr-2, normal, 2.05 mm,
			6	1.20	0.19	0.26	D, Zr-2, rolling, 2.0 mm,
			6	1.32	0.13	0.19	D, Zr-2, 2.06 mm,
			6	0.81	0.03	0.05	D, Zr-2, 1.04 mm,
			6	1.07	0.10	0.15	D, Zr-2, 0.63 mm,
Murabayashi et al. [13]	1975	300-900	14	0.59	0.04	0.08	D, Zr-2, 2 mm
			10	1.99	0.59	0.68	D, Zr-2, 0.6 mm
			19	1.24	0.28	0.31	D, Zr-4, 2 mm
Price [7, 8] Mills et al. [7, 9]; (AECL data)	1980 1997	300-700	5	0.30	0.77	0.71	$\lambda$ , AECL1, Zr-2 cold-worked tube, axial
			5	0.64	1.68	1.54	$\lambda$ , AECL2, Zr-2 annealed strip, rolling
			5	0.13	0.75	0.65	$\lambda$ , AECL3, Zr-2 stress-relieved tube, axial
Price [7, 8] Mills et al. [7, 9]; (AECL data)	1980 1997	290-673	5	0.53	0.06	0.10	D, AECLd1 Zr-2 cold-work tube, radial
			5	1.20	0.29	0.34	D, AECLd2 Zr-2; annealed strip, through thickness
Taylor [14]	1991	300-1500	10	1.11	1.17	1.10	D, Zr-4
Maglic et al. [15]	1994	298-1373	53	0.89	0.37	0.38	D, Zr-2 & Zr-4; reduced to 53 points by averaging data at same temperature
China: Institute of Atomic Energy [7]	1997	293-1400	23	1.86	0.70	0.78	$\lambda$ , Zr-2 tube, radial
			23	0.70	0.26	0.23	$\lambda$ , Zr-4 rod, axial

Table 5. Regression statistics for fits to Zircaloy thermal conductivity

STATISTIC/FUNCTIONAL FORM	CUBIC	QUADRATIC	QUADRATIC + 1/T	MATPRO
$\chi^2$	230	234	233	322
Free parameters	4	3	4	4
Variance	0.725	0.736	0.736	1.017
Standard Deviation	0.851	0.858	0.858	1.008



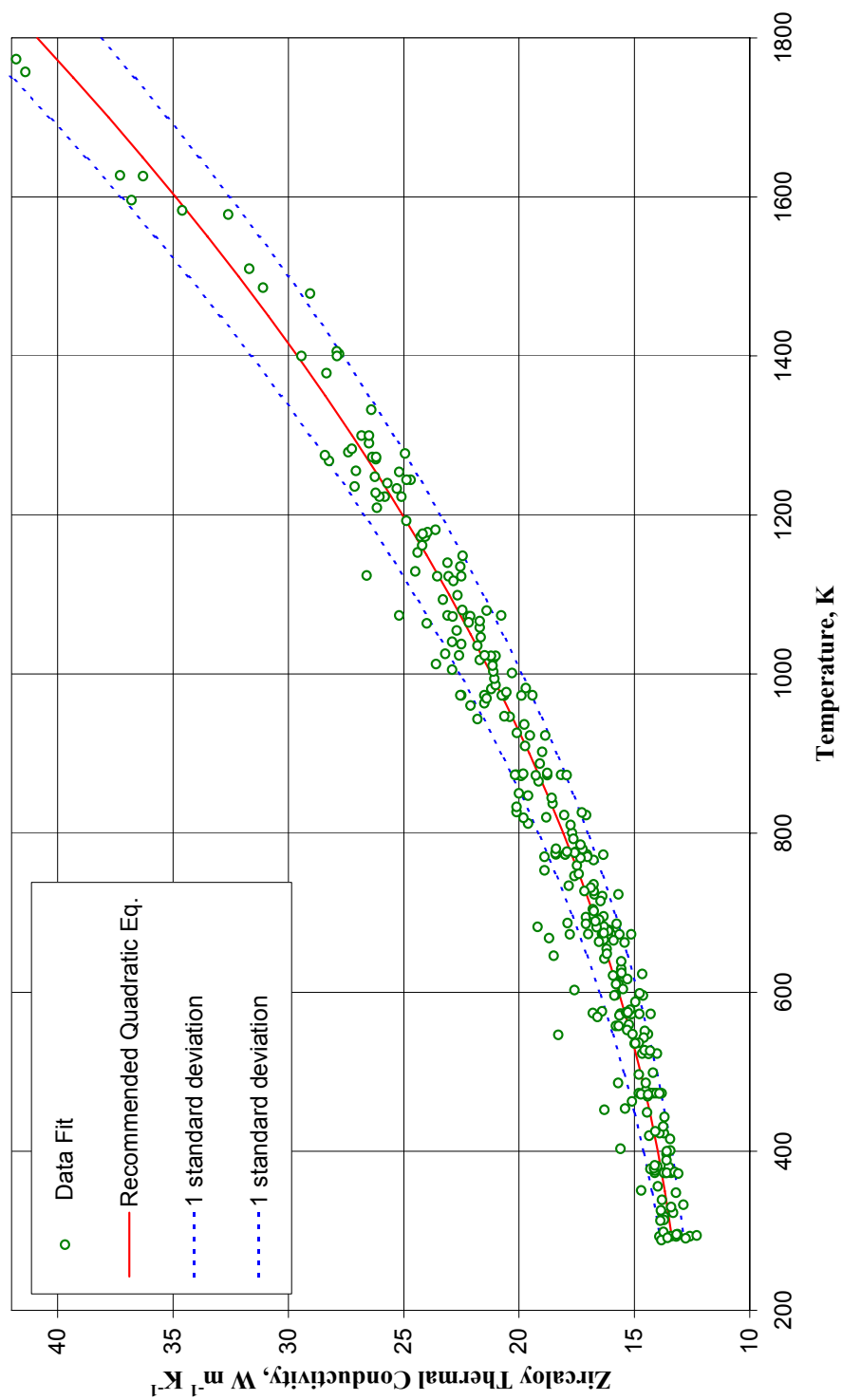


FIG 1. Recommended equation for Zircaloy thermal conductivity.

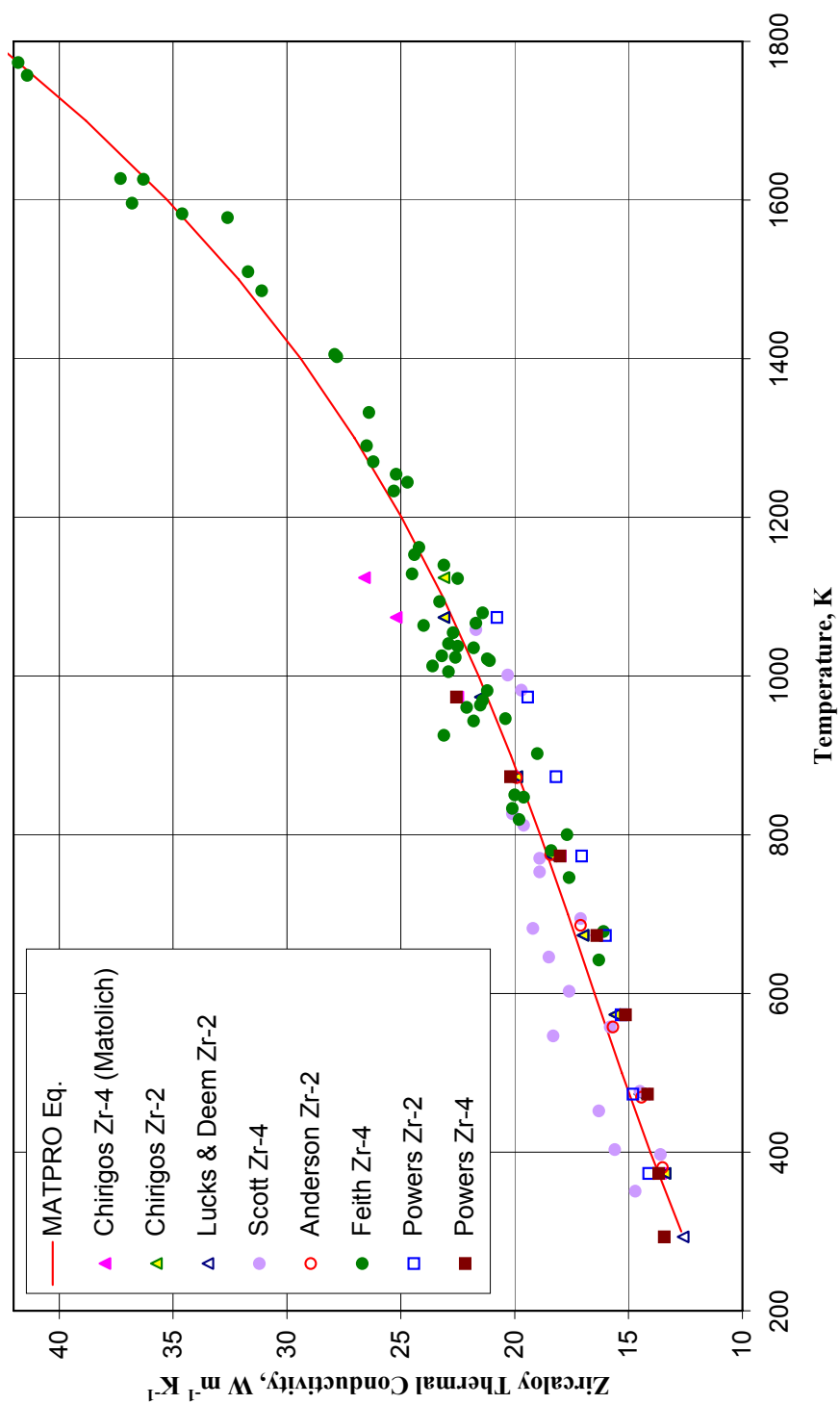


FIG. 2. Comparison of MATPRO equation with data analysed in MATPRO.

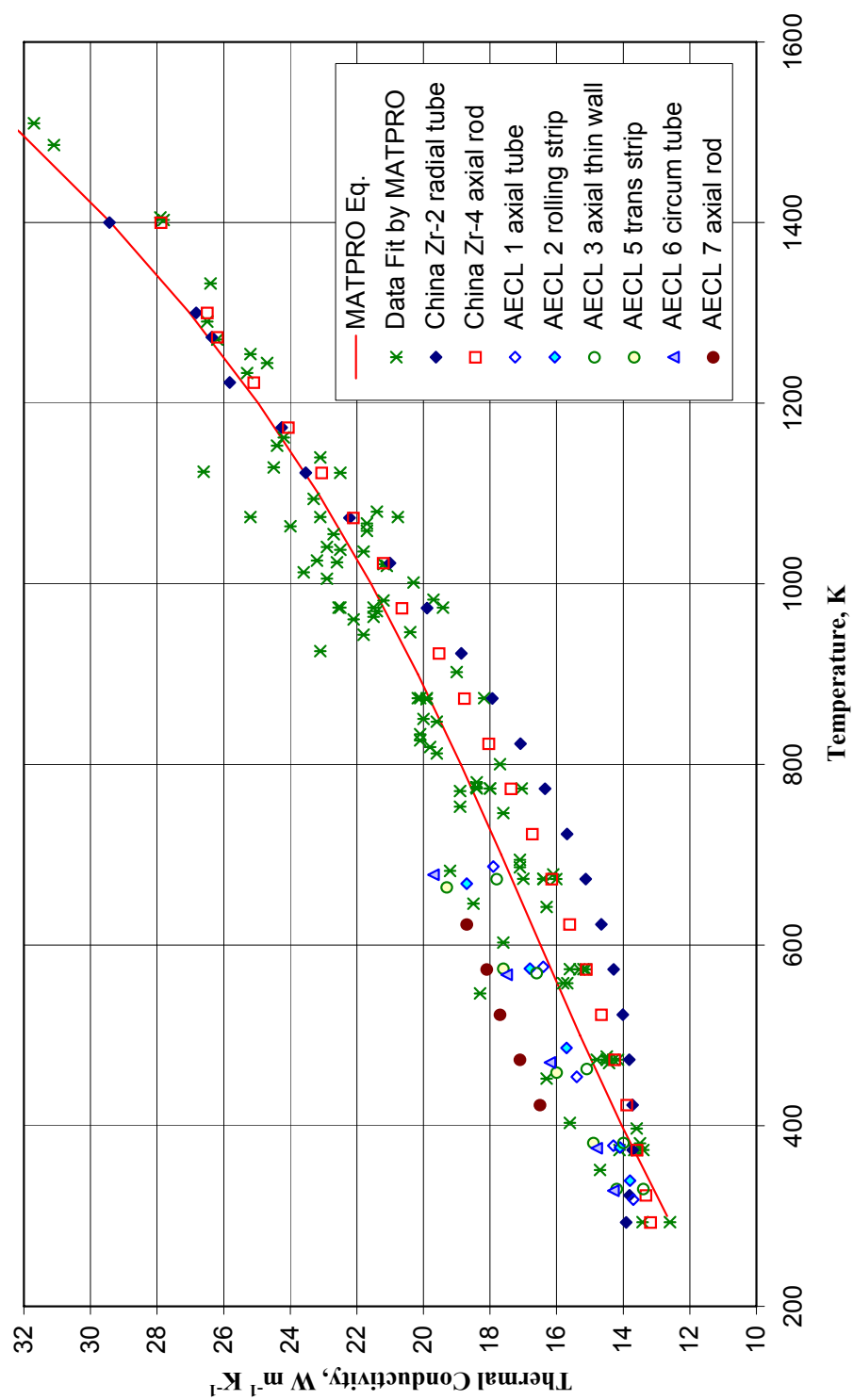


FIG. 3. Comparison of Zircaloy thermal conductivity data with MATPRO Eq.

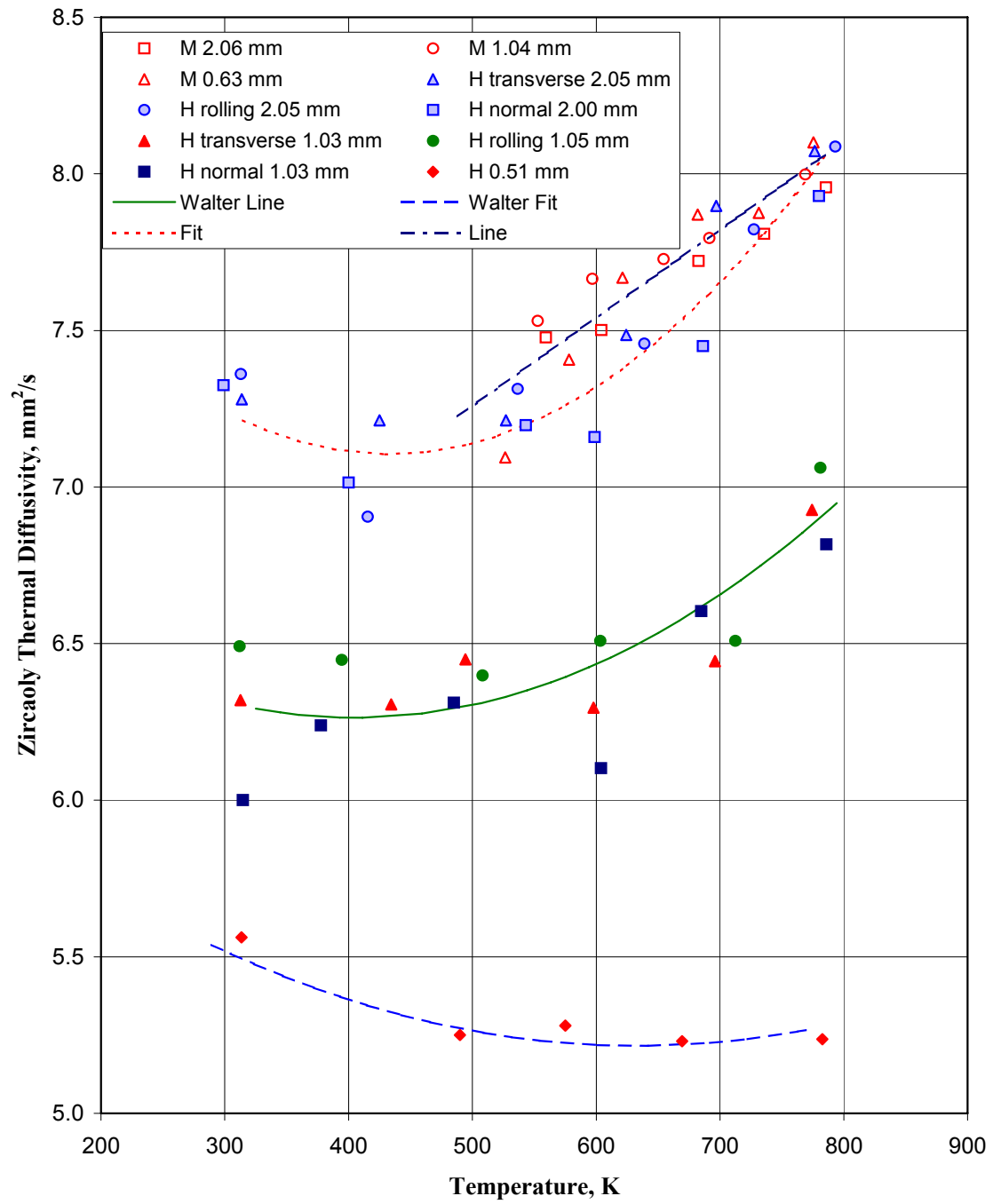


FIG. 4. Study of effects of thickness and direction of Zircaloy thermal diffusivity by Walter et al. [12].

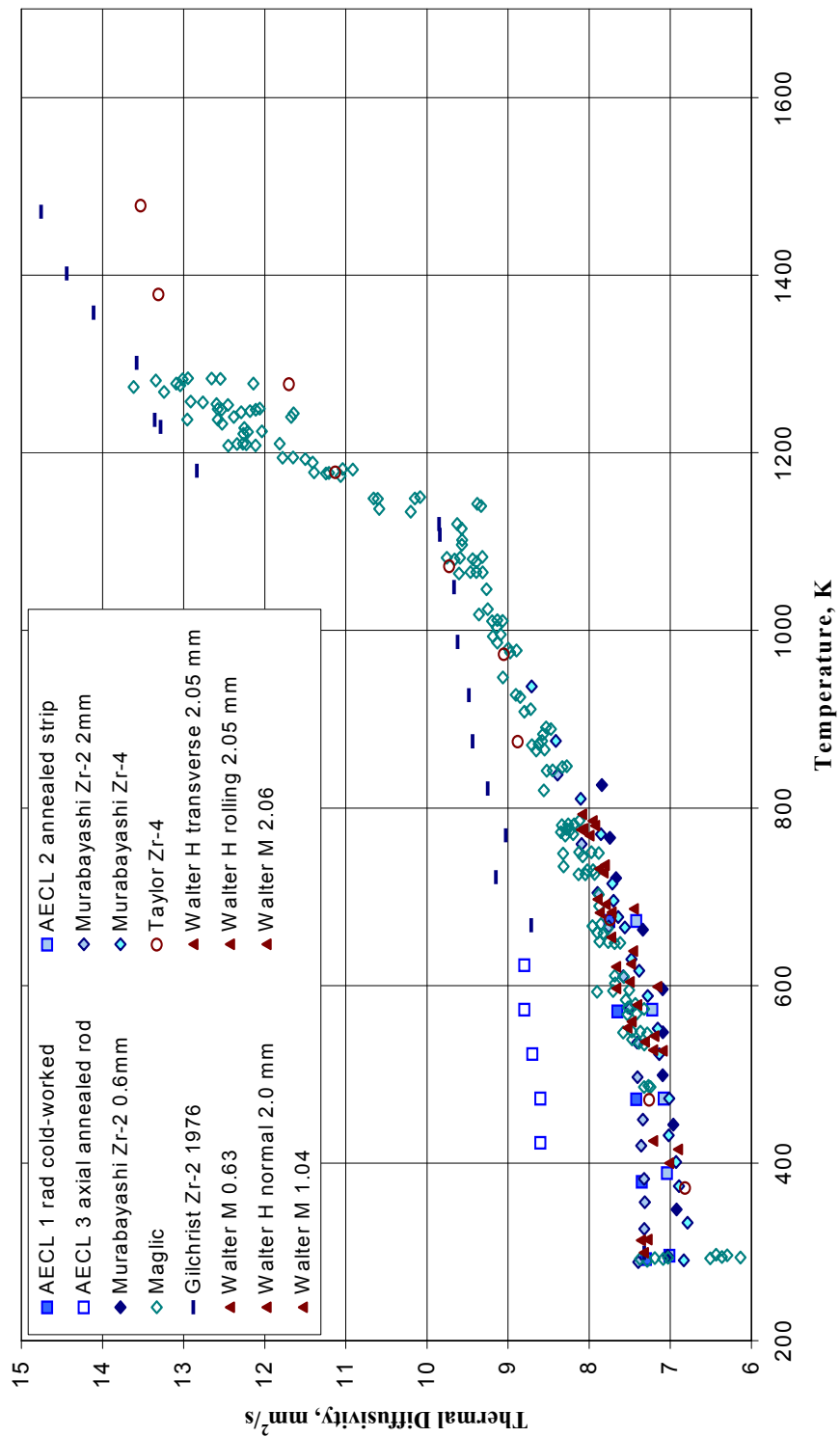


FIG. 5. Zircaloy thermal diffusivity data considered in this analysis.

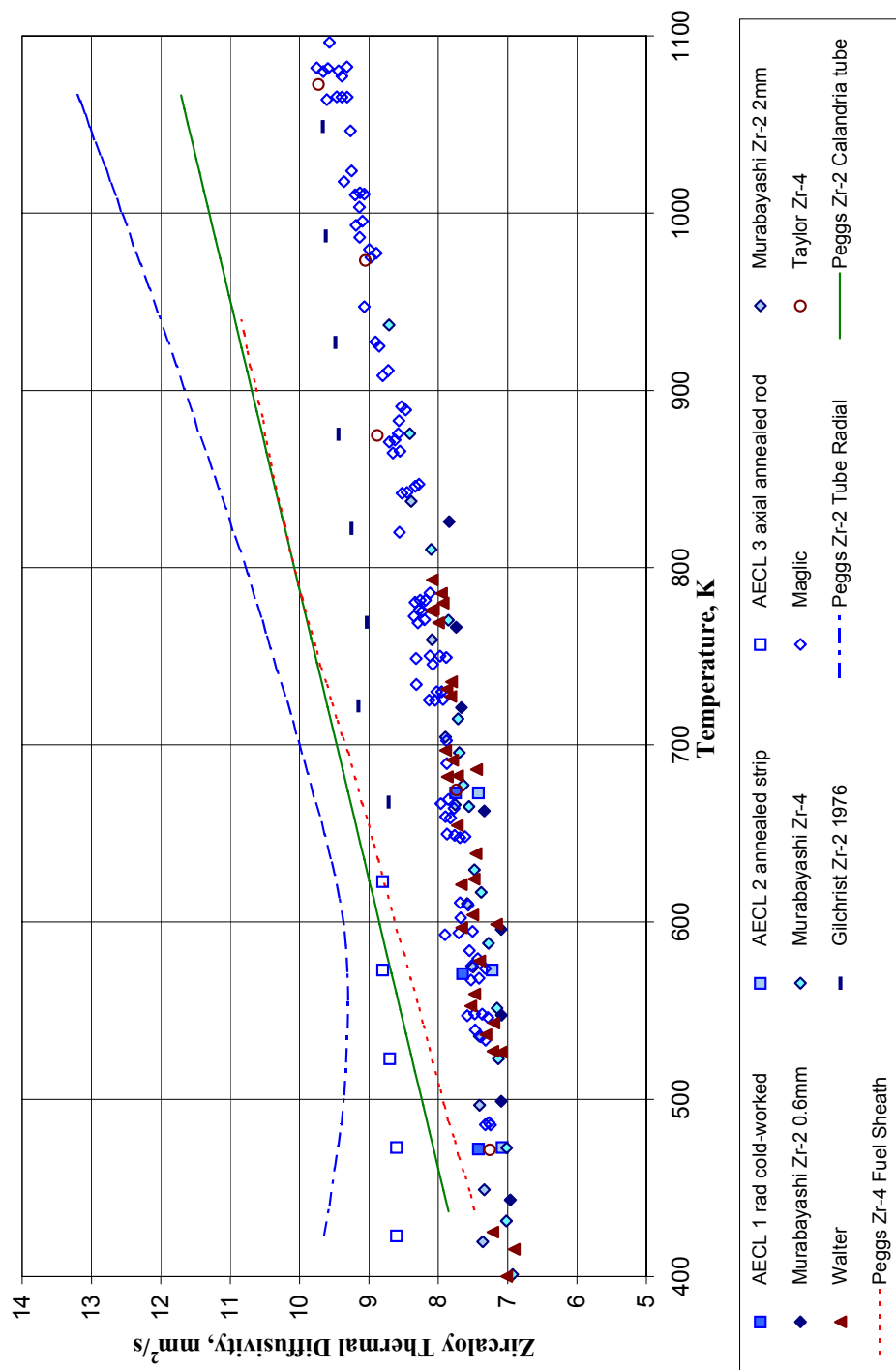


FIG. 6. Comparison of low temperature Zircaloy thermal diffusivity data.

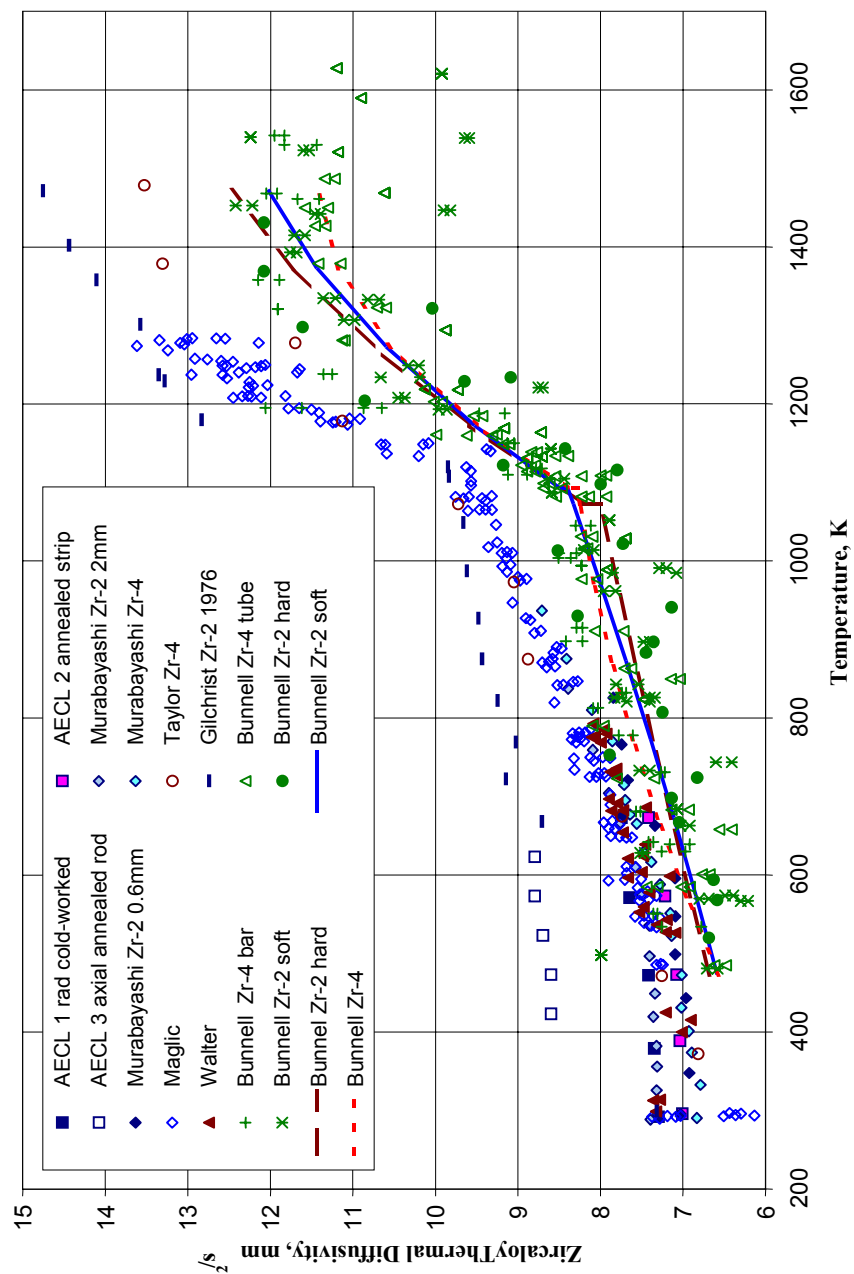


FIG. 7. Comparison of thermal diffusivity results of Bunnell et al. with other data.

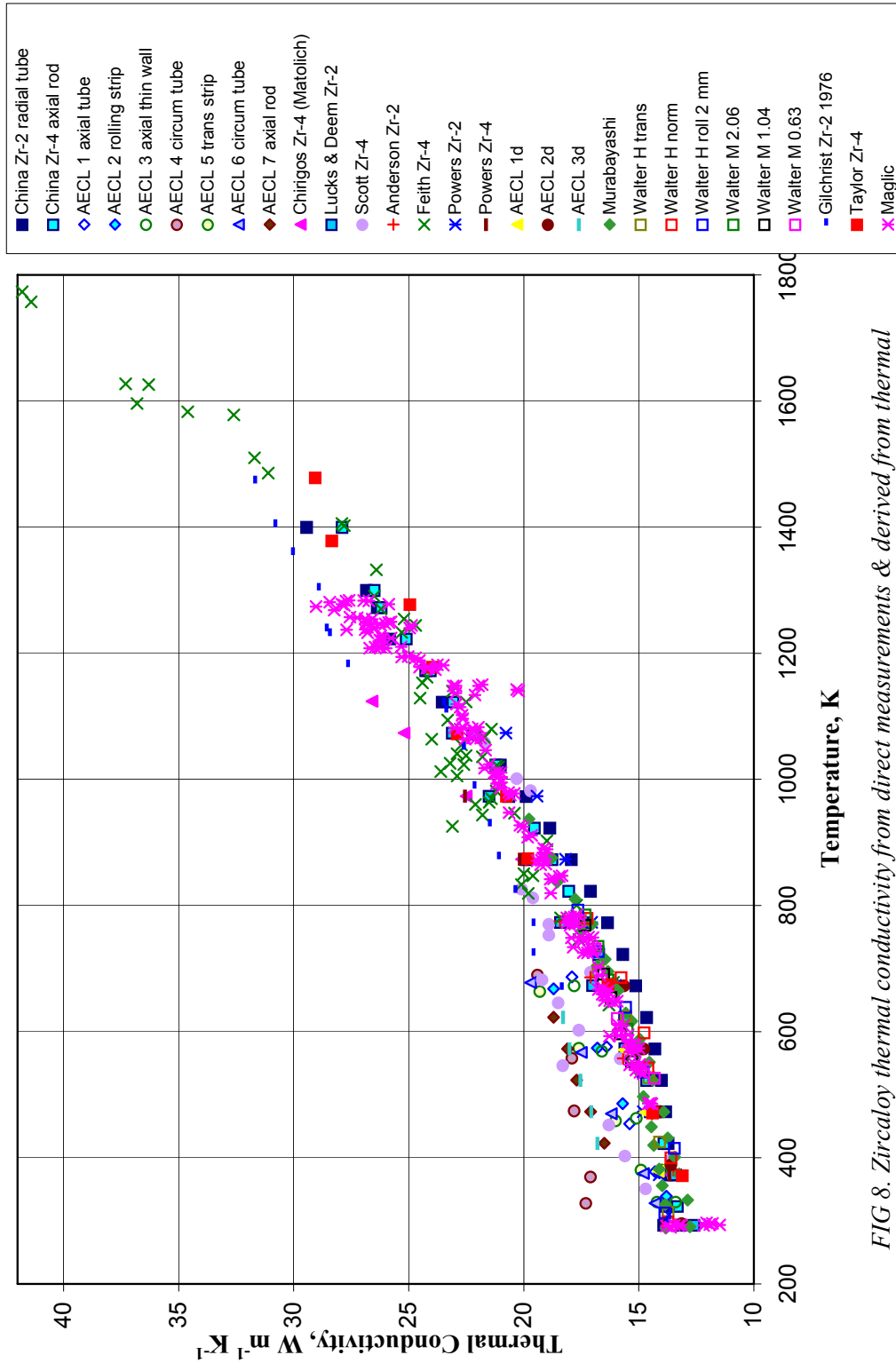


FIG 8. Zircaloy thermal conductivity from direct measurements & derived from thermal diffusivity data.



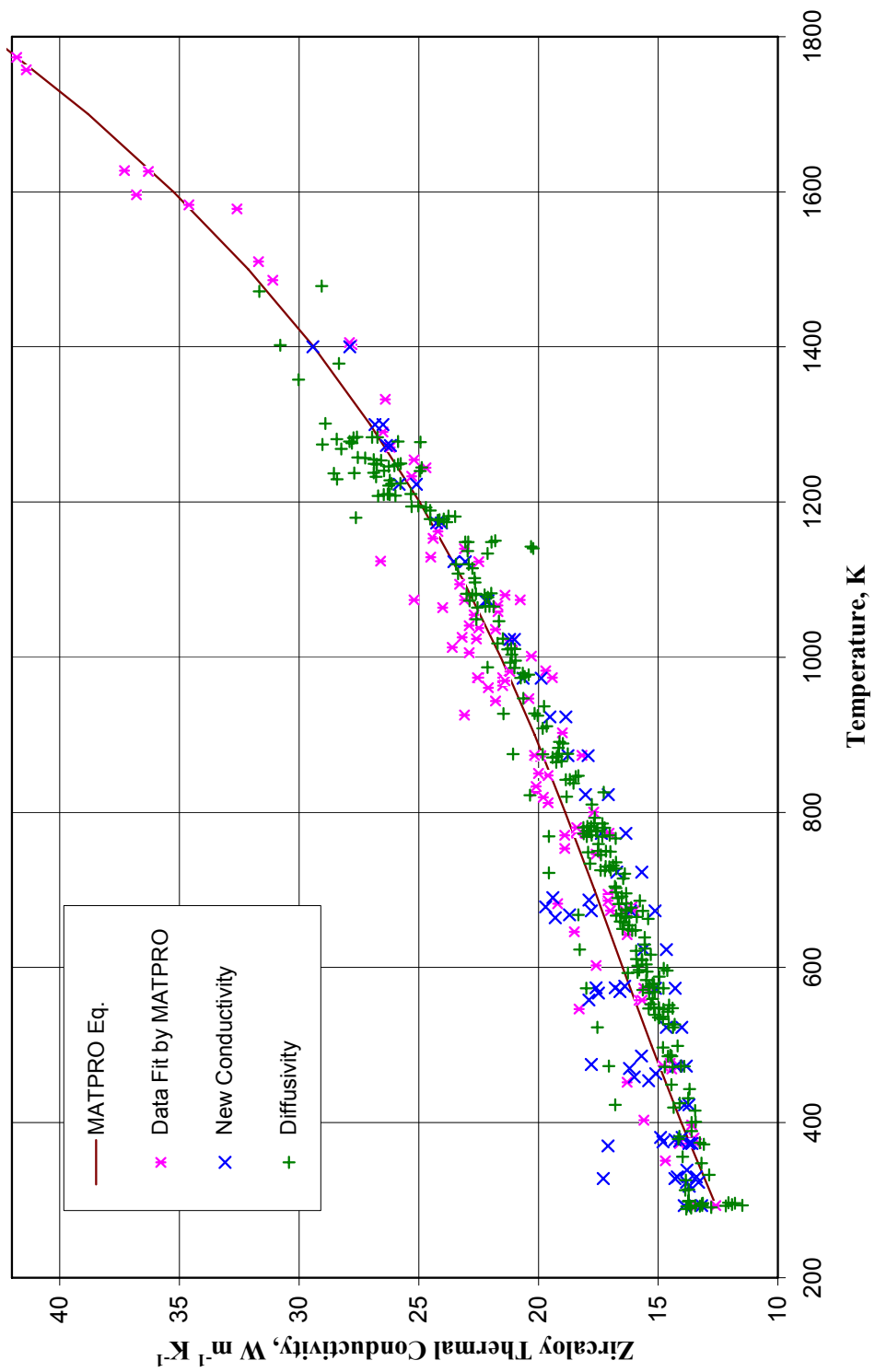


FIG. 9. MATPRO Eq. compared with thermal conductivity from direct measurements & derived from thermal diffusivity data.

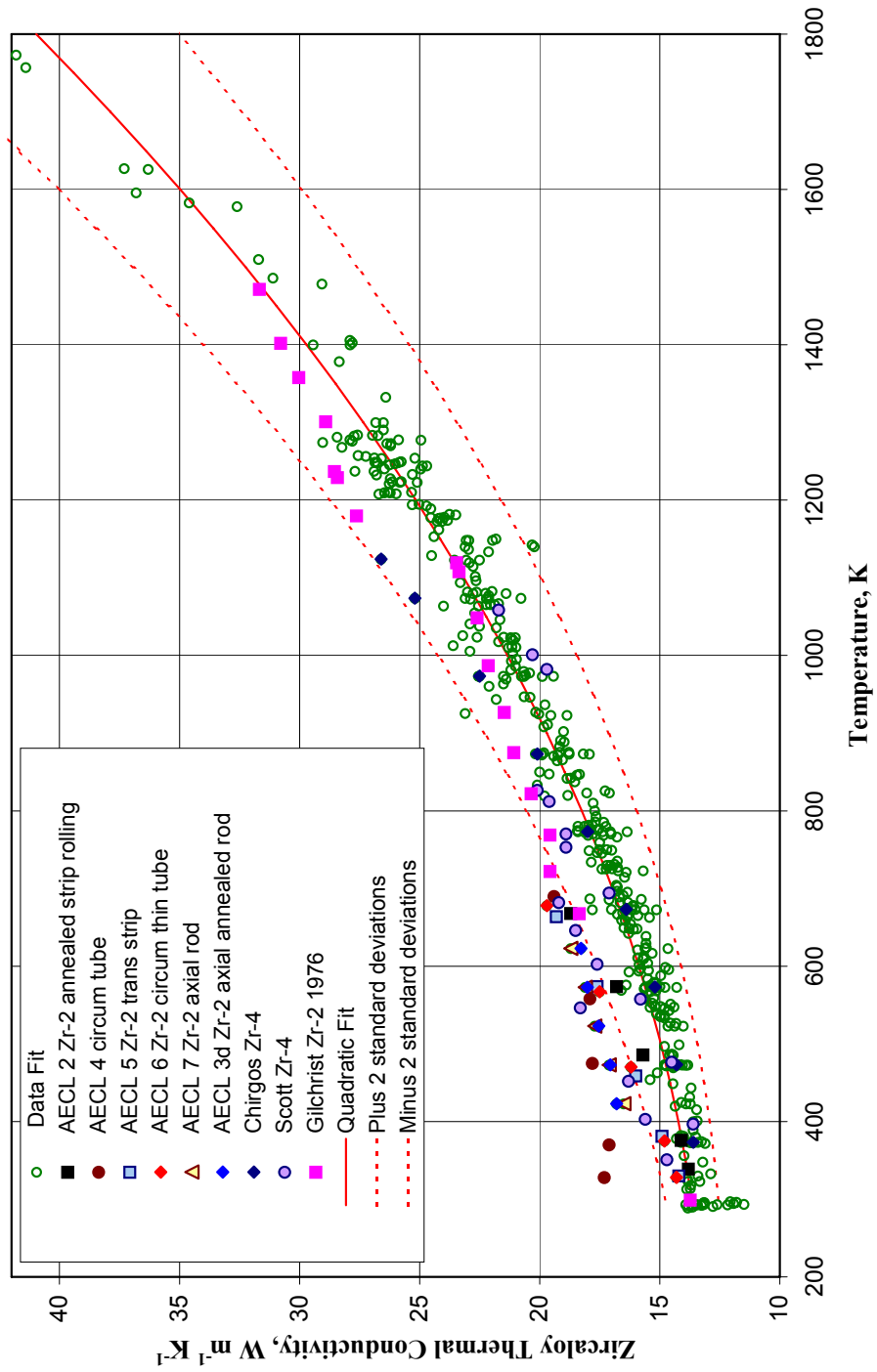


FIG. 10. Comparison of data with quadratic fit and 2 standard deviations.

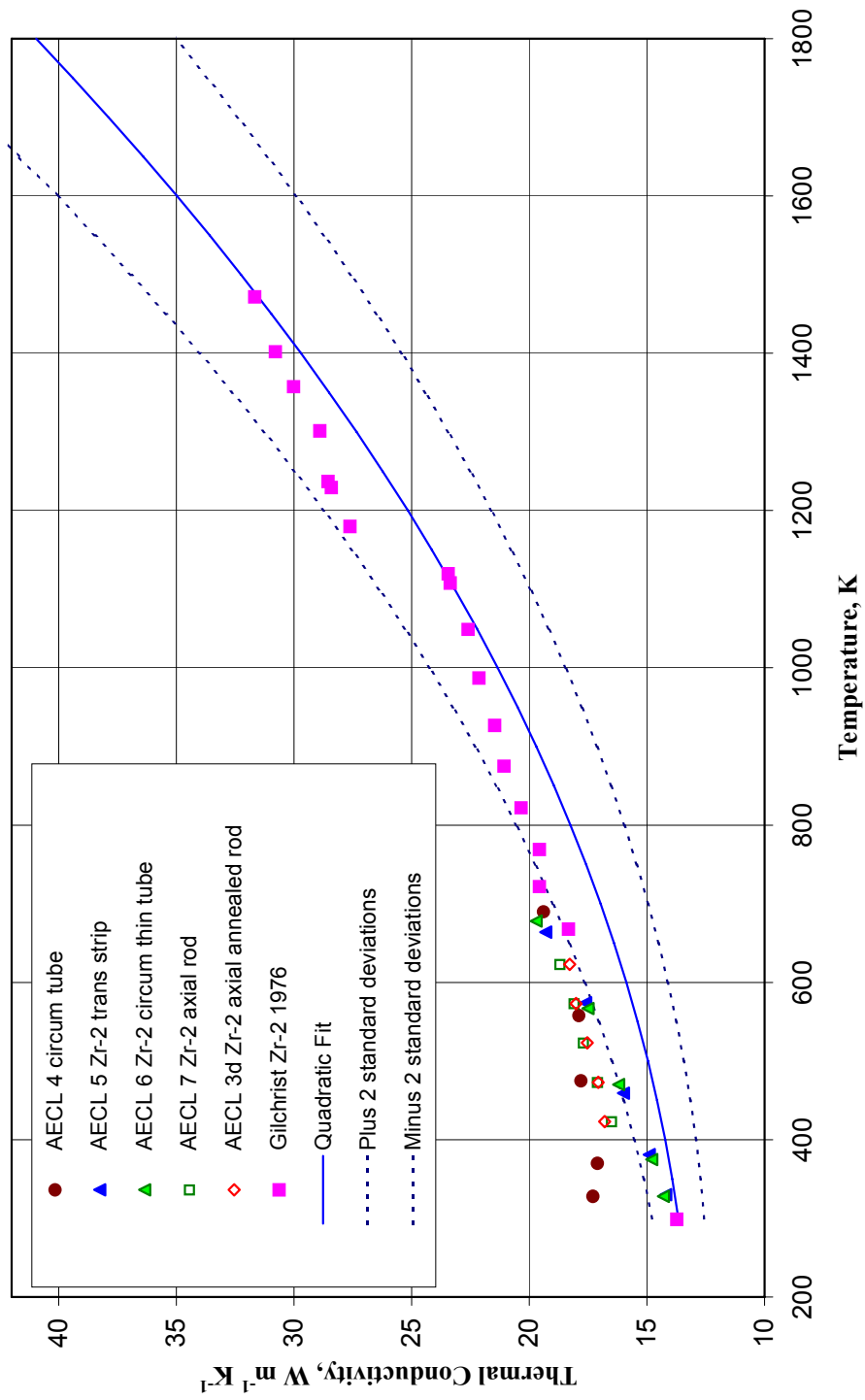


FIG. 11. Comparison of Zircaloy thermal conductivity data not included in final analysis with quadratic line through all the data.

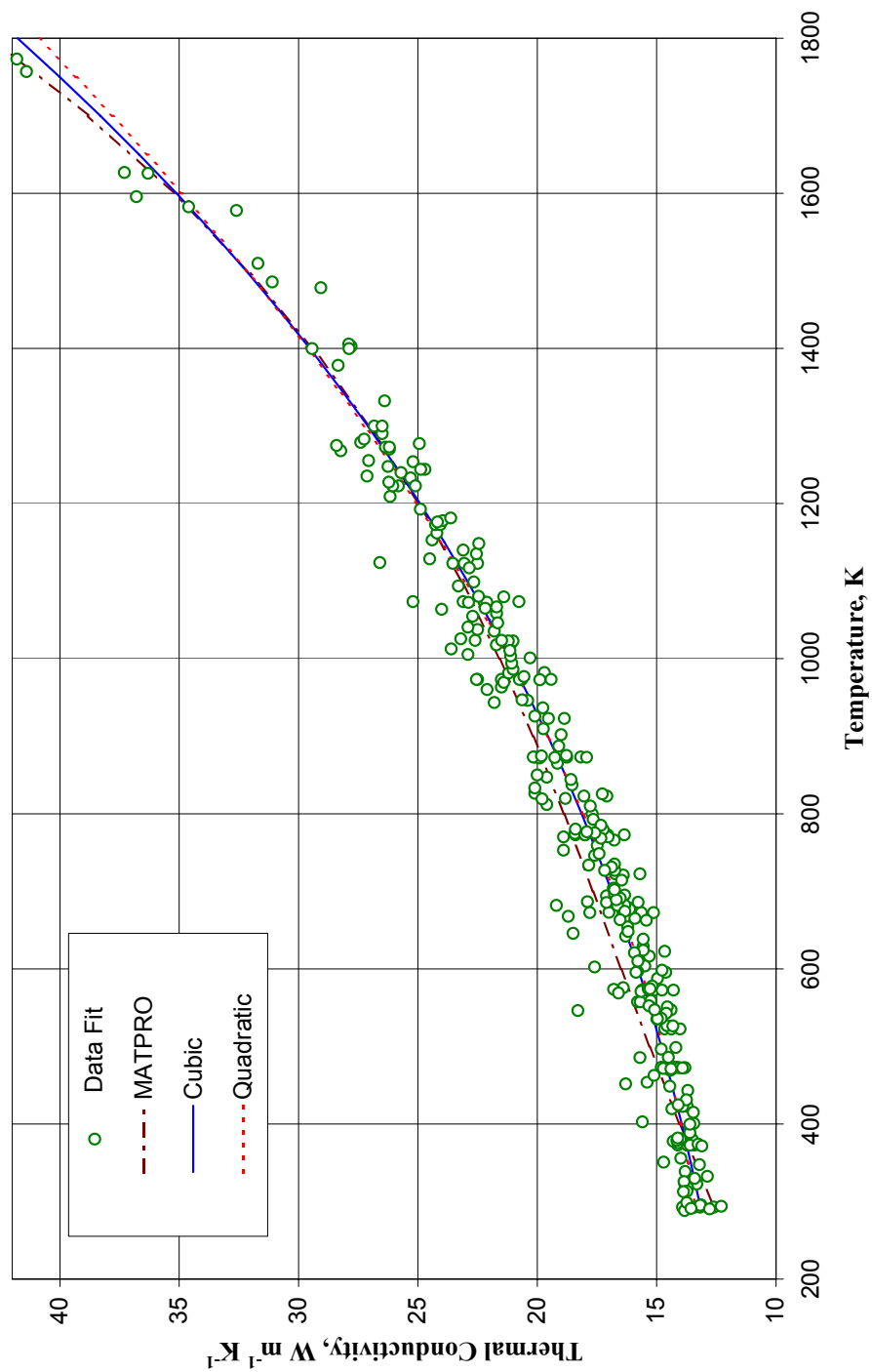


FIG. 12. Comparison of Zircaloy data with equations.

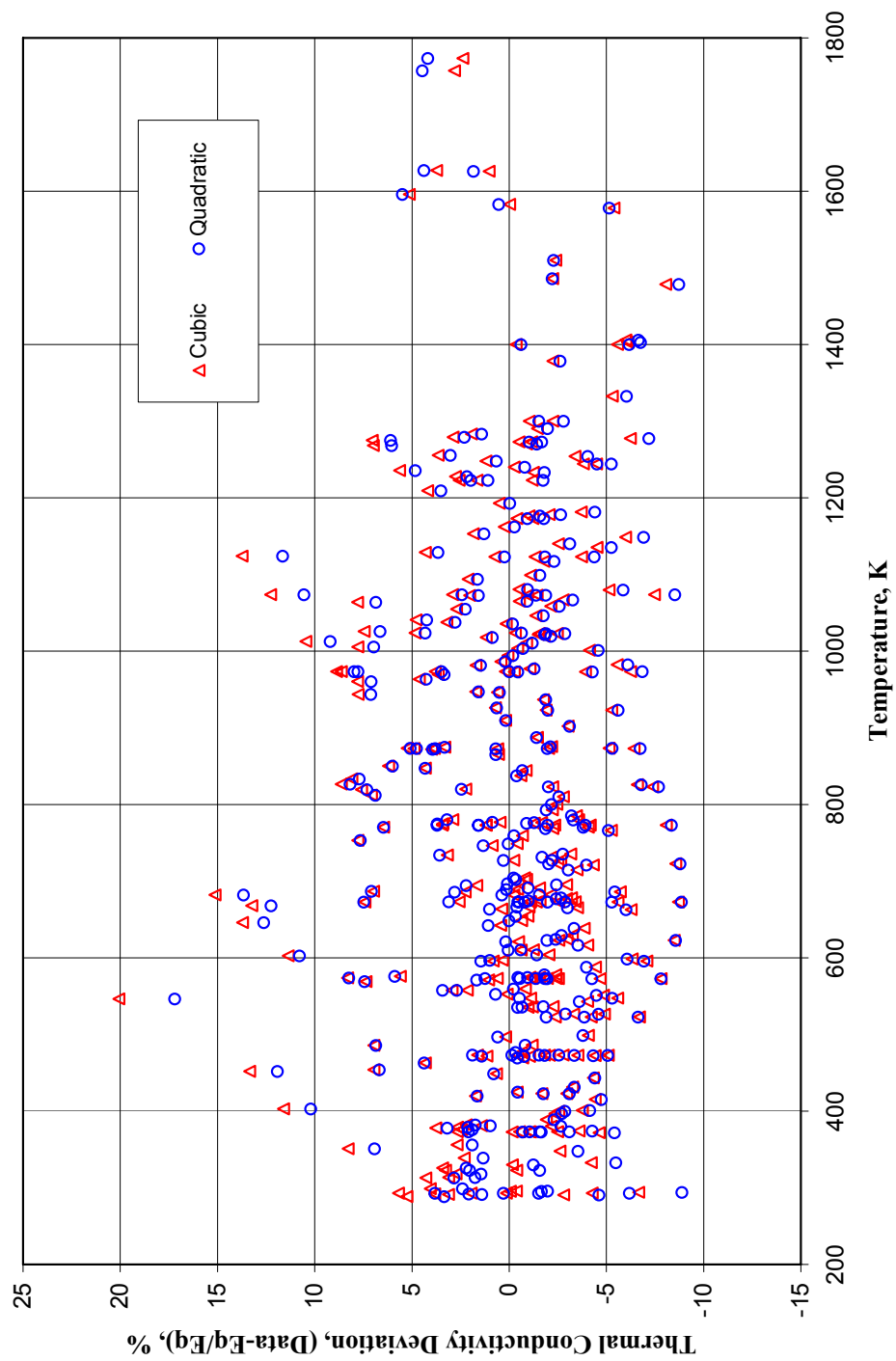


FIG. 13. Deviation of Zircaloy data from cubic and quadratic equations.

## REFERENCES TO SECTION 6.2.1.4

- [1] LUCKS, C.F. and DEEM, H.W., Progress relating to civilian applications during June 1958: thermal conductivity of uranium and  $\text{UO}_2$ , [ ] USAEC Report BMI-1273, 1-62 (1958).
- [2] CHIRIGOS, J.N., KASS, S., KIRK, W.W. and SALVAGGIO, G.J., Development of Zircaloy-4, in fuel element fabrication with special emphasis on cladding materials, Proceedings of a Symposium held in Vienna, May 10-13, 1960, Vol. 1, pp. 19-56, Academic Press, London for the International Atomic Energy Agency (1961).
- [3] POWERS, A.E., Application of the Ewing equation for calculating thermal conductivity from electrical conductivity, Knolls Atomic Power Laboratory of General Electric Report KAPL-2146, (1961).
- [4] ANDERSON, W.K., BECK, C.J., KEPHART, A.R. and THEILACKER, J.S., Zirconium alloys, [ ] reactor structural materials: engineering properties as affected by nuclear reactor service, ASTM-STP-314 (1962), pp. 62-93; as referenced in ASCDAP/RELAP5/MOD 3.1 Code Manual: MATPRO - A Library of Materials Properties for Light-Water-Reactor Accident Analysis, NUREG/CR-6150, EGG-2720 Vol. 4 (1995).
- [5] SCOTT, D.B., Physical and mechanical properties of Zircaloy 2 and 4", USAEC Report WCAP-3269-41, 1-68 (1965).
- [6] FEITH, A.D., High-temperature materials program: property measurements, USAEC Report GEMP-61, 153-155 (1966), C. G. Collins, pp 157-169.
- [7] INTERNATIONAL ATOMIC ENERGY AGENCY, Thermophysical Properties of Materials for Water Cooled Reactors, IAEA-TECDOC-949, pp. 77 (1997).
- [8] PRICE, E.G., Thermal conductivity, electrical resistivity, and specific heat of CANDU construction alloys and AISI Type 403 end fitting, [ ] AECL Report TDVI-3680 (1980), as tabulated in Thermophysical Properties of Materials for Water Cooled Reactors, IAEA-TECDOC-949, p. 78 (1997).
- [9] MILLS, R.W., SCHANKULA, M.H., LANGE, B.A., The thermal conductivity of zirconium, Zircaloy-2, and zirconium-2.5 wt% niobium and some of their hydrides from 150°C to 350°C, AECL Internal Document, as tabulated in A Thermophysical Properties of Materials for Water Cooled Reactors, J. Cleveland (ed.), International Atomic Energy Agency Report IAEA-TECDOC-949, p. 78 (1997).
- [10] HAGRMAN, T. (ed.), SCDAP/RELAP5/MOD 3.1 Code manual: MATPRO - a library of materials properties for light-water-reactor accident analysis, NUREG/CR-6150, EGG-2720 Vol. 4 (1995).
- [11] WHEELER, M.J., Some anomalous thermal diffusivity results on hafnium, niobium and Zircaloy 2, Rev. Int. Hautes Temper. et Refract. 7, 335-340 (1970).
- [12] WALTER, A.J., DELL, R.M., GILCHRIST, K.E. and TAYLOR, R., A comparative study of the thermal diffusivities of stainless steel, hafnium, and Zircaloy, High Temp.-High Press. 4, 439-446 (1972).
- [13] MURABAYASHI, M., TANAKA, S. and TAKAHASHI, Y., Thermal conductivity and heat capacity of Zircaloy-2, -4, and unalloyed Zirconium, J. Nucl. Sci. And Tech. 12, 661-662 (1975).
- [14] TAYLOR, R.E., private communication to K. D. Maglic, reported in K. D. Maglic, N. Lj. Perovic, and A. M. Stanimirovic, Calorimetric and transport properties of Zircaloy 2, Zircaloy 4, and Inconel 625, Int. J. of Thermophys. 15, 741-755 (1994).
- [15] MAGLIC, K.d., perovic, n.lj. and stanimirovic, a.m., calorimetric and transport properties of Zircaloy 2, Zircaloy 4, and Inconel 625, Int. J. of Thermophys. 15, 741-755 (1994).
- [16] GILCHRIST, K.E., Thermal property measurements on Zircaloy-2 and associated oxide layers up to 1200°C, J. Nucl. Mater. 62, 257-264 (1976).
- [17] GILCHRIST, K.E., Thermal conductivity of oxide deposited on Zircaloy fuel tube material - a continuation of previous work, J. Nucl. Mater. 82, 193-194 (1979).
- [18] PEGGS, D., STADNYK, A.M. and GODIN, D.P., Thermophysical properties of Zirconium-alloy fuel-channel components, High Temp.-High Pressures 8, 441-450 (1976).
- [19] BUNNELL, L.R., BATES, J.L. and MELLINGER, G.B., Some high-temperature properties of Zircaloy-oxygen alloys, J. Nucl. Mater. 116, 219-232 (1983);

- [20] BUNNELL, L.R., BATES, J.L. and MELLINGER, G.B., High-temperature properties of Zircaloy-oxygen alloys, EPRI NP-524, Research Project 251-1 (1977).  
 [21] GUILLERMET, A.F., Critical evaluation of the thermodynamic properties of zirconium, High Temp. - High Press. 19, 119-160 (1987).  
 [22] FINK, K. and LEIBOWITZ, L., Thermal conductivity of zirconium, J. Nucl. Mater. 226, 44-50 (1995).

#### 6.2.1.5. Thermal expansion

##### **Recommendation**

##### *$\alpha$ - Phase for $300\text{ K} < T < 1083\text{ K}$ Single Crystal*

The preliminary recommendation for the thermal expansion of Zircaloy-2 and Zircaloy-4 in the  $\alpha$ -phase are equations given in MATPRO [1] that were determined by fitting the data from measurements of Bunnell et al. [2] converted to the orientation of the single crystals. Because Zircaloy is anisotropic, thermal expansions in three orthogonal directions are required. In development of the thermal expansion model, basal plane symmetry was assumed for the single crystal so that the thermal expansions along two of the crystal axis are equal ( $\epsilon_{11} = \epsilon_{22}$ ). The MATPRO equations for Zircaloy single crystal thermal expansion are:

$$\epsilon_{11} = 4.95 \times 10^{-6} T - 1.485 \times 10^{-3} \quad (1)$$

$$\epsilon_{33} = 1.26 \times 10^{-5} T - 3.78 \times 10^{-3} \quad (2)$$

where  $\epsilon_{11} = (\Delta L/L)_{11}$  is the circumferential single crystal thermal expansion in m/m,

$\epsilon_{22} = (\Delta L/L)_{22}$  is the radial single crystal thermal expansion in m/m =  $\epsilon_{11}$ ,

$\epsilon_{33} = (\Delta L/L)_{33}$  is the axial single crystal thermal expansion in m/m, and

T is the temperature in K.

To calculate the cladding thermal expansion from these single crystal thermal expansions, the orientation of the crystal structure of the cladding is required so that a volume weighted average over the cladding can be done. This averaging requires a pole figure. The thermal expansion of the cladding in the laboratory system (Lab) is calculated from the thermal expansions for single crystals from the relations:

$$\begin{aligned} \epsilon_{11}(\text{Lab}) &= \epsilon_{11}(\sin^2 \phi) + \epsilon_{22}(\cos^2 \theta \cos^2 \phi) + \epsilon_{33}(\sin^2 \theta \cos^2 \phi) \\ \epsilon_{22}(\text{Lab}) &= \epsilon_{11}(\cos^2 \phi) + \epsilon_{22}(\cos^2 \theta \sin^2 \phi) + \epsilon_{33}(\sin^2 \theta \sin^2 \phi) \\ \epsilon_{33}(\text{Lab}) &= \epsilon_{22}(\sin^2 \theta) + \epsilon_{33}(\cos^2 \theta) \end{aligned} \quad (3)$$

where (Lab) designates the cladding or laboratory system,

$\phi$  is the angle between the circumferential direction of the cladding and the projection of the c-axis of the single crystal onto the circumferential-axial plane of the cladding, and

$\theta$  is the angle between the radial direction of the cladding and the c-axis of the single crystals.

In the MATPRO manual,  $\epsilon_{11}(\text{Lab})$  is defined as thermal expansion of the cladding in the circumferential direction,  $\epsilon_{22}(\text{Lab})$  as the thermal expansion of the cladding in the axial direction, and  $\epsilon_{33}(\text{Lab})$  as the thermal expansion of the cladding in the radial direction.

##### *$\alpha$ - Phase for $300\text{ K} < T < 1083\text{ K}$ (Cladding when orientation not known)*

Very often, the orientation of the crystalline c-axis in the cladding is not known. In this case, the equations reported in the MATPRO manual [1] for the data of Bunnell et al. [2, 3] are recommended because these equations provide reasonable agreement with other cladding thermal expansions in the

same directions. However, the directions for  $\varepsilon_{11}$  (Lab) and  $\varepsilon_{33}$  (Lab) given in the MATPRO manual are not consistent with the cladding direction labels reported by Bunnell et al. [2, 3]. In fact, the Bunnell et al. [2] “diametral” data are tabulated in the MATPRO manual as “circumferential” thermal expansions. Bunnell et al. [2, 3] report no thermal expansion data for the circumferential direction. The direction labels given below are the directions for the experimental data reported by Bunnell et al. [2,3] and are consistent with other experimental data. The recommended equations for the thermal expansion of Zircaloy cladding are:

$$\left(\frac{\Delta L}{L}\right)_{Diam} = \varepsilon_{11}(Lab) = -2.128 \times 10^{-3} + 7.092 \times 10^{-6} T \quad (4)$$

$$\left(\frac{\Delta L}{L}\right)_{Circum} = \varepsilon_{33}(Lab) = -2.998 \times 10^{-3} + 9.999 \times 10^{-6} T \quad (5)$$

$$\left(\frac{\Delta L}{L}\right)_{Axial} = \varepsilon_{22}(Lab) = -1.623 \times 10^{-3} + 5.458 \times 10^{-6} T \quad (6)$$

Figure 1 shows the Zircaloy-4 diametral thermal expansion data of Bunnell et al. adjusted to give zero at 300 K and Eq. (4), which is the MATPRO equation for  $\varepsilon_{11}$  (Lab) for the data of Bunnell et al. {labeled “MATPRO 11 Lab B” in Figure 1}. The  $\alpha$ -phase Zircaloy-4 axial thermal expansion data of Bunnell et al. adjusted to zero at 300 K and the MATPRO equation for the axial thermal expansion for cladding with the orientation of Bunnell’s data, Eq. (5), are shown in Figure 2.

*Transition region between the  $\alpha$ - and  $\beta$ -phases,  $1035K < T < 1144 K$*

The recommended equation for Zircaloy-4 thermal expansion in the axial direction is:

$$\left(\frac{\Delta L}{L}\right)_{Axial} = -6.528 \times 10^{-3} + 9.796 \times 10^{-6} T + 6.187 \times 10^{-4} e^{\frac{(T-1063)^2}{2130}} \quad (7)$$

Insufficient data are available to recommend an equation in the transition region for other directions of the cladding in the laboratory (cladding) frame or for the single crystals.

*$\beta$ -phase,  $T > 1144 K$*

The recommended equation for Zircaloy-4 cladding thermal expansion in the axial direction in the  $\beta$ -phase is

$$\left(\frac{\Delta L}{L}\right)_{Axial} = -6.394 \times 10^{-3} + 9.7 \times 10^{-6} T \quad (8)$$

Although insufficient data are available to recommend equations for the  $\beta$ -phase for the other two orthogonal directions, the temperature behavior, ie. the slope, may be assumed to be the same as for the axial direction. This slope,  $9.7 \times 10^{-6}$ , is the slope for the average thermal expansion of zirconium in the  $\beta$ -phase. It is also the recommended slope for the thermal expansion of Zircaloy-4 single crystals in the  $\beta$ -phase.

Recommended values, calculated with the recommended equations, Eq. (4) through Eq. (8) are given in Table 1. Figure 3 shows the recommended values for the linear thermal expansion of Zircaloy-4 in the axial direction for the  $\alpha$ -phase, transition region and  $\beta$ -phase. Uncertainties have been included in the figure.

### **Uncertainty**

The uncertainties given in the MATPRO manual for the Zircaloy-4 single-crystal thermal expansion in the  $\alpha$ -phase are respectively, 8% for the axial direction,  $\varepsilon_{33}$ , and 12% for the circumferential direction,  $\varepsilon_{11}$ . The uncertainty for the diametral thermal expansion of Zircaloy-4 cladding in the  $\alpha$ -phase, as



defined in Eq. (4), is 15%. The uncertainty for the axial thermal expansion of Zircaloy cladding in the  $\alpha$ -phase, as given in Eq. (5), is 12%. These uncertainties are based on the scatter in the available  $\alpha$ -phase data. The  $\beta$ -phase uncertainty is 20%. This uncertainty has been chosen large enough so that the uncertainty bands include the  $\beta$ -phase data for soft Zircaloy-2 and the data for zirconium. In the transition region, the uncertainty is assumed to increase linearly from 12% to 20%.

## Discussion

### $\alpha$ - Phase, $300\text{ K} < T < 1083\text{ K}$

The equations for the single crystal linear thermal expansion of Zircaloy-4 in the  $\alpha$ -phase are from a model developed for the MATPRO database of RELAP [1]. The model was developed using the Zircaloy-4 thermal expansion data and equations obtained by Bunnell et al. [2, 3]. Because the data and fitting equations of Bunnell et al. did not give zero expansion at 300 K, they were first adjusted to give zero at 300 K. The data were fit and the equations converted from the laboratory frame of the cladding to the single crystal frame using Eq. (3) and the orientation of the single crystals in the cladding. The angles  $\theta$  and  $\phi$  that define this orientation for the data of Bunnell et al. [2,3] are:  $\theta = 35.67^\circ$  and  $\phi = 25.10^\circ$ . The resulting equations that relate the laboratory frame thermal expansion data of Bunnell et al. to the single crystal thermal expansions  $\epsilon_{11}$  and  $\epsilon_{33}$  are:

$$\left(\frac{\Delta L}{L}\right)_{Diam} = \epsilon_{11}(Lab) = 0.72 \epsilon_{11} + 0.28 \epsilon_{33} \quad (9)$$

$$\left(\frac{\Delta L}{L}\right)_{Axial} = \epsilon_{22}(Lab) = 0.94 \epsilon_{11} + 0.06 \epsilon_{33} \quad (10)$$

$$\left(\frac{\Delta L}{L}\right)_{Circum} = \epsilon_{33}(Lab) = 0.34 \epsilon_{11} + 0.66 \epsilon_{33} \quad (11)$$

where the single crystal expansions in the radial and circumferential directions are equal, ie.,  $\epsilon_{11} = \epsilon_{22}$ , and  $\epsilon_{33}$  is the single crystal expansion in the axial direction. Substituting the MATPRO single crystal thermal expansions for  $\epsilon_{11}$  and  $\epsilon_{33}$  from Eq. (1–2) in Eq. (9–10) gives Eqs (4–6). In Eqs (4–6) and Eqs (9–10), the labels, *Diam*, *Axial*, *Circum*, refer to the diametral, axial, and circumferential thermal expansions for the cladding and are consistent with the directions reported by Bunnell et al. [2, 3]. In MATPRO,  $\epsilon_{11}(Lab)$  is termed the “circumferential” expansion in the laboratory frame. However, Figure 4, which shows the MATPRO values for  $\epsilon_{11}(Lab)$ ,  $\epsilon_{22}(Lab)$ , and  $\epsilon_{33}(Lab)$  for cladding with Bunnell’s orientation and the axial and diametral Zircaloy-4 data of Bunnell et al. adjusted to zero at 300K, indicates that  $\epsilon_{11}(Lab)$  as defined in Eq. (9) and Eq. (4) is consistent with the diametral thermal expansion values of Bunnell et al. In addition, Figure 4 shows that  $\epsilon_{33}(Lab)$  is not consistent with either the diametral or axial data and  $\epsilon_{22}$ .

As a check on the reliability of the single crystal equations, Eq. (1) and Eq. (2), developed from the data of Bunnell et al. [2, 3], these equations were compared with old data of Douglas [4], Scott [5], and Kearns [6]. The MATPRO manual reports that the data in the axial direction gave agreement within 10% and that most of the data in the circumferential direction agreed within 20%. Comparisons were also made with plate thermal expansions in the longitudinal and transverse directions obtained by Mehan and Wiesinger [7]. The percent difference between the MATPRO model slope and that of the data of Mehan and Wiesinger in the longitudinal direction is 15%. The percent difference for the transverse direction is 7%. Thus, the MATPRO single-crystal equations may be used to provide a reasonable representation of Zircaloy thermal expansion when the angle of orientation of the single crystals in the cladding are known.

If the orientation is not known, equations (4) through (6), which were derived to represent the data of Bunnell et al., are recommended. Although the MATPRO manual gives different equations for a “typical” LWR cladding tube of Zircaloy-4, the equations based on Bunnell’s data are preferred because they give better agreement with other available data. For example, Figure 5 shows that the

axial thermal expansion data of Bunnell et al. [2, 3] for soft and hard samples of Zircaloy-2 cladding agree better with Eq. (5) than with the MATPRO equation for axial thermal expansion for a “typical” LWR Zircaloy-4 cladding tube. However, care must be taken in the use of Eqs. (4) through (6) when nothing is known with respect to the orientation, oxygen content, and heat treatment. In Figure 6, the Zircaloy-2 and Zircaloy-4 axial thermal expansion data of Bunnell et al. and the MATPRO axial equation that fits the Zircaloy-4 axial expansion data of Bunnell et al. are compared with the axial thermal expansion data of Peggs et al. [8] for a Zircaloy-2 pressure tube, a Zircaloy-4 fuel sheath, and a Zircaloy-2 calandria tube. Although the axial thermal expansion data for the Zircaloy-2 pressure tube is within the scatter of the data of Bunnell et al. for Zircaloy-4, the axial thermal expansion data of Peggs et al. for a Zircaloy-2 pressure tube and a Zircaloy-4 fuel sheath have a different slope and deviate from a linear dependence at around 800 K. Bunnell et al. [2, 3] showed that the oxygen content has a significant effect on the thermal expansion and developed equations for the axial and diametral thermal expansion of Zircaloy-4 for oxygen content from 0.7 at% to 22.4 at% and of Zircaloy-2 for oxygen contents of 0.7 at% and 5.2 at%.

#### *$\beta$ -phase and transition region between the $\alpha$ - and $\beta$ -phases*

The MATPRO single crystal thermal expansion equations for the  $\beta$ -phase have been based on the thermal expansion of zirconium in the  $\beta$ -phase obtained by Skinner and Johnston [9] because there was insufficient data on Zircaloy thermal expansion in the  $\beta$ -phase to construct a detailed model. The MATPRO equations for single crystal thermal expansion are

For  $T > 1244$  K,

$$\varepsilon_{33} = 9.7 \times 10^{-6} T - 4.4 \times 10^{-3} \quad (12)$$

$$\varepsilon_{11} = 9.7 \times 10^{-6} T - 1.04 \times 10^{-2} \quad (13)$$

where  $\varepsilon_{11}$  is the single crystal circumferential thermal expansion in m/m,

$\varepsilon_{33}$  is the single crystal axial thermal expansion in m/m,

$\varepsilon_{22} = \varepsilon_{11}$ , and

$T$  is the temperature in K.

The slope of these equations,  $9.7 \times 10^{-6}$ , is the slope of the linear equation that fits the linear thermal expansion data of Skinner and Johnston.

The MATPRO equations for the single crystal thermal expansion in the transition region are correlations developed using the constraint that at 1035 K, the thermal expansion must be equal to the thermal expansion in the  $\alpha$ -phase at 1035K and at 1144 K, the thermal expansion must be equal to the thermal expansion in the  $\beta$ -phase. These two values are linked by a cosine function to give the expected curvature from the  $\alpha$ -phase to the  $\beta$ -phase. The MATPRO single crystal equations for the circumferential thermal expansion,  $\varepsilon_{11}$ , and the axial thermal expansion,  $\varepsilon_{33}$ , in the transition region are

For  $1083 \text{ K} \leq T \leq 1244 \text{ K}$ ,

$$\varepsilon_{11} = \left[ 2.77763 = 1.09822 \cos\left(\frac{T - 1083}{161} \pi\right) \right] \times 10^{-3} \quad (14)$$

$$\varepsilon_{33} = \left[ 8.76758 = 1.09822 \cos\left(\frac{T - 1083}{161} \pi\right) \right] \times 10^{-3} \quad (15)$$

where the arguments for the cosines are in radians. The large number of significant figures in these equations are to prevent discontinuities. Figure 7 shows the MATPRO single crystal thermal expansion equations for the  $\beta$ -phase and the phase transition region, Eqs (12–15), the data of Skinner and Johnston for the average linear thermal expansion of zirconium in the  $\beta$ -phase, transition region, and upper temperature region of the  $\alpha$ -phase, and the linear fit to the  $\beta$ -phase thermal expansion data of Skinner and Johnston.

Although Bunnell et al. [2, 3] do not report thermal expansion for the circumferential or diametral directions in the  $\beta$ -phase, they report axial thermal expansions at temperatures in the transition region and the  $\beta$ -phase for Zircaloy-4 and hard and soft Zircaloy-2. In order to assess the reliability of the single crystal Zircaloy thermal expansion equations for the  $\beta$ -phase and transition region, Eq. (10) was used to calculate the axial thermal expansion for the cladding from the single crystal values for  $\epsilon_{11}$ , and  $\epsilon_{33}$  given in Eqs (12–15). In Figure 8, the cladding axial thermal expansion calculated from the MATPRO single-crystal equations for the orientation of the Zircaloy-4 cladding of Bunnell et al. (labeled “MATPRO 22 Lab B”) are compared with the Zircaloy-4 and Zircaloy-2 axial thermal expansion data of Bunnell et al. for the  $\alpha$ -phase,  $\beta$ -phase, and transition region. Although there is excellent agreement for the  $\alpha$ -phase, the MATPRO values for the transition region and  $\beta$ -phase do not agree with the data. Because the axial thermal expansion values for the  $\beta$ -phase, and transition region obtained from the MATPRO single crystal equations using the orientation for the Zircaloy-4 sample of Bunnell et al. do not agree with the available data of Bunnell et al., the MATPRO single crystal equations for the  $\beta$ -phase and transition region are not recommended.

Figure 9 shows the three orthogonal thermal expansions for the  $\alpha$ - and  $\beta$ -phases and transition region for Zircaloy-4, which were calculated from the MATPRO single crystal thermal expansions using Eqs (9–11). The curves for the single crystal thermal expansions in each region have been included in Figure 9. The available Zircaloy thermal expansion data in the diametral direction and axial direction from the measurements by Bunnell et al. [2, 3] have been included in Figure 9 for comparison with the laboratory thermal expansion equations determined from the MATPRO relations. For completeness, Figure 9 also shows the data of Skinner and Johnston for the average linear thermal expansion of zirconium and the equation, which fits their data in the  $\beta$ -phase. This equation for the average thermal expansion of zirconium in the  $\beta$ -phase is

$$\left( \frac{\Delta L}{L} \right)_{Axial} = -7.200 \times 10^{-3} + 9.7 \times 10^{-6} T \quad (16)$$

Figure 9 shows that the thermal expansions for the Zircaloy cladding in the  $\beta$ -phase have a slope that is similar to that of the zirconium data. Note that the transition from the  $\alpha$ -phase to the  $\beta$ -phase for the available Zircaloy axial thermal expansion data does not have the large decrease predicted by the MATPRO model. In fact, even the zirconium data for the transition from the  $\alpha$ -phase to the  $\beta$ -phase do not show the same curvature that exists for the MATPTRO single crystals because the data of Skinner and Johnston for the average linear thermal expansion of zirconium in the  $\alpha$ -phase show reasonable agreement with the data of Bunnell et al. for the  $\alpha$ -phase thermal expansion of Zircaloy-4 in the diametral direction. The data for the  $\beta$ -phase axial thermal expansions of Zircaloy-4 and hard Zircaloy-2 are closer to the MATPRO Zircaloy laboratory-frame curve labeled “MATPRO 11 Lab B” than for the curve “MATPRO 22 Lab B” that gives the expansion in the axial direction in the laboratory frame for the orientation of the cladding of Bunnell et al. The data for the thermal expansion of soft Zircaloy-2 in the axial direction in the  $\beta$ -phase are closer to the zirconium data than the other axial Zircaloy data and indicates the effects of sample variation on the magnitude of the change in thermal expansion at the phase transition.

Figure 10 shows a linear regression fit to the Zircaloy-4 and hard Zircaloy-2 axial thermal expansion data of Bunnell et al. in the  $\beta$ -phase. These data are fit by the equation

$$\left( \frac{\Delta L}{L} \right)_{Axial} = -5.674 \times 10^{-3} + 9.2 \times 10^{-6} T \quad (17)$$

Equation (8), which has the same slope as that of the fit to the zirconium data of Skinner and Johnston [9], has also been included in Figure 10. The root mean square standard deviation of the data from Eq. (17) is 0.091, whereas the root mean square standard deviation of the data from Eq. (8) is 0.095. Equation (8) has been recommended for the axial thermal expansion of Zircaloy cladding in the

$\beta$ -phase because all the available data for Zircaloy and zirconium in the  $\beta$ -phase are consistent with the slope of the zirconium data and the difference in the standard deviations from the two equations is small.

Examination of the axial data for Zircaloy-4 and hard Zircaloy-2 in the transition region between the  $\alpha$ - and  $\beta$ -phases showed that these data are not consistent with the cosine function suggested in the MATPRO manual. A sine function also does not provide an adequate representation of these data. A nonlinear least squares technique was used to fit these data to Eq. (7), which has a linear and Gaussian temperature dependence. This equation was constrained to give the  $\alpha$ - and  $\beta$ -phase values at the end points of the transition region. Figure 11 shows the recommended equations for the axial thermal expansion for Zircaloy-4 for the  $\alpha$ -phase, transition region, and  $\beta$ -phase and the uncertainties for each phase. The uncertainty chosen for the  $\beta$ -phase, 20%, has been selected so that it is large enough to include the data for the axial thermal expansion of soft Zircaloy-2 in the  $\beta$ -phase. Included in Figure 11 are the axial linear expansion data for soft Zircaloy-2, which agree with the other data in the  $\alpha$ -phase but are lower in the  $\beta$ -phase.

Table 1. Recommended values for the linear thermal expansion of Zircaloy

TEMPERATURE (K)	LINEAR THERMAL EXPANSION	
	$\Delta L/L \times 10^3$ (m/m)	
	AXIAL	DIAMETRICAL
300	0.00	0.00
350	0.29	0.35
400	0.56	0.71
450	0.83	1.06
500	1.11	1.42
550	1.38	1.77
600	1.65	2.13
650	1.92	2.48
700	2.20	2.84
750	2.47	3.19
800	2.74	3.55
850	3.02	3.90
900	3.29	4.25
950	3.56	4.61
1000	3.84	4.96
1050	4.33	5.32
1100	4.57	
1150	4.76	
1200	5.25	
1250	5.73	
1300	6.22	
1350	6.70	
1400	7.19	
1450	7.67	
1500	8.16	

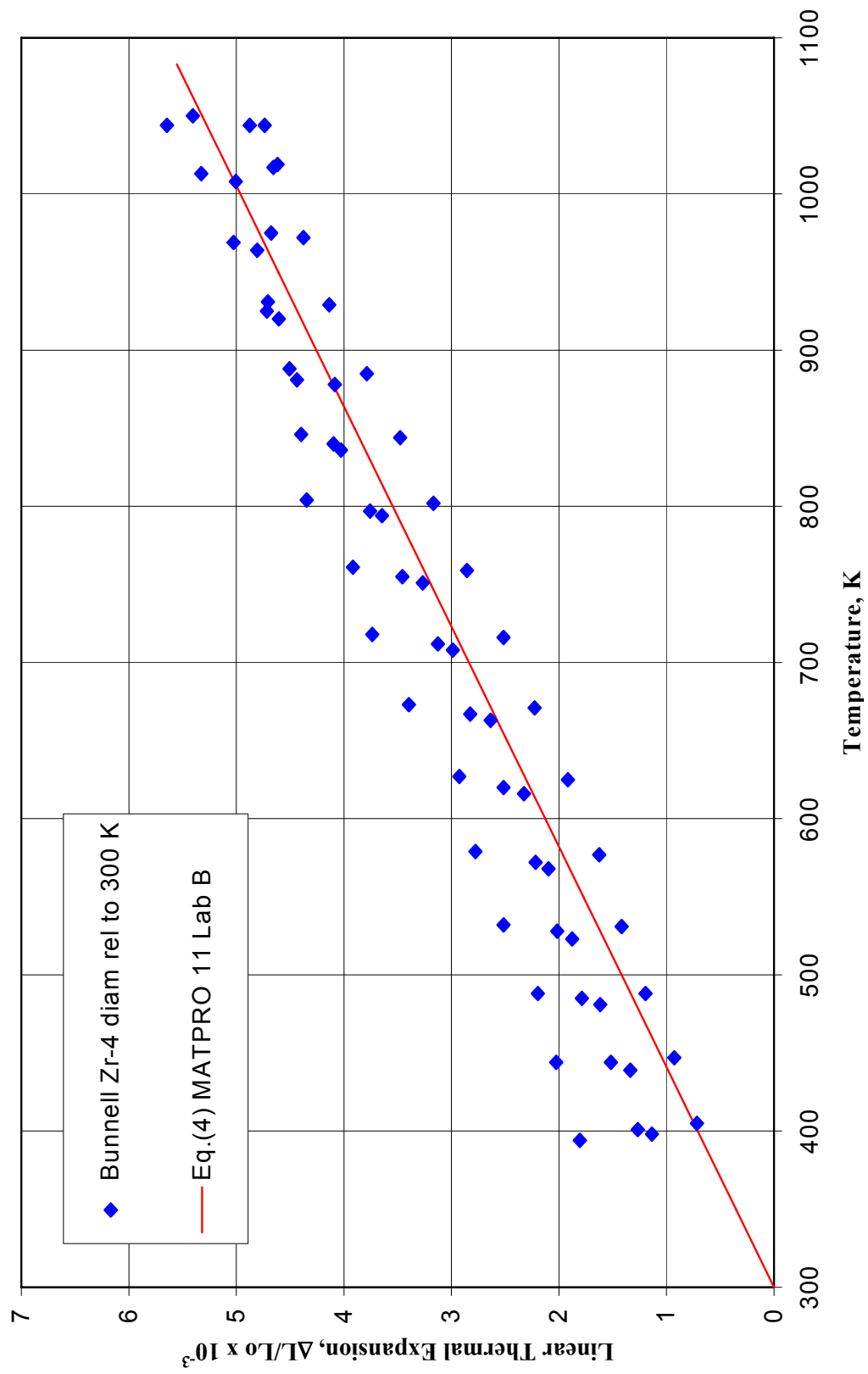


FIG. 1. MATPRO fit to Bunnell Zircaloy-4 diametral linear thermal expansion.

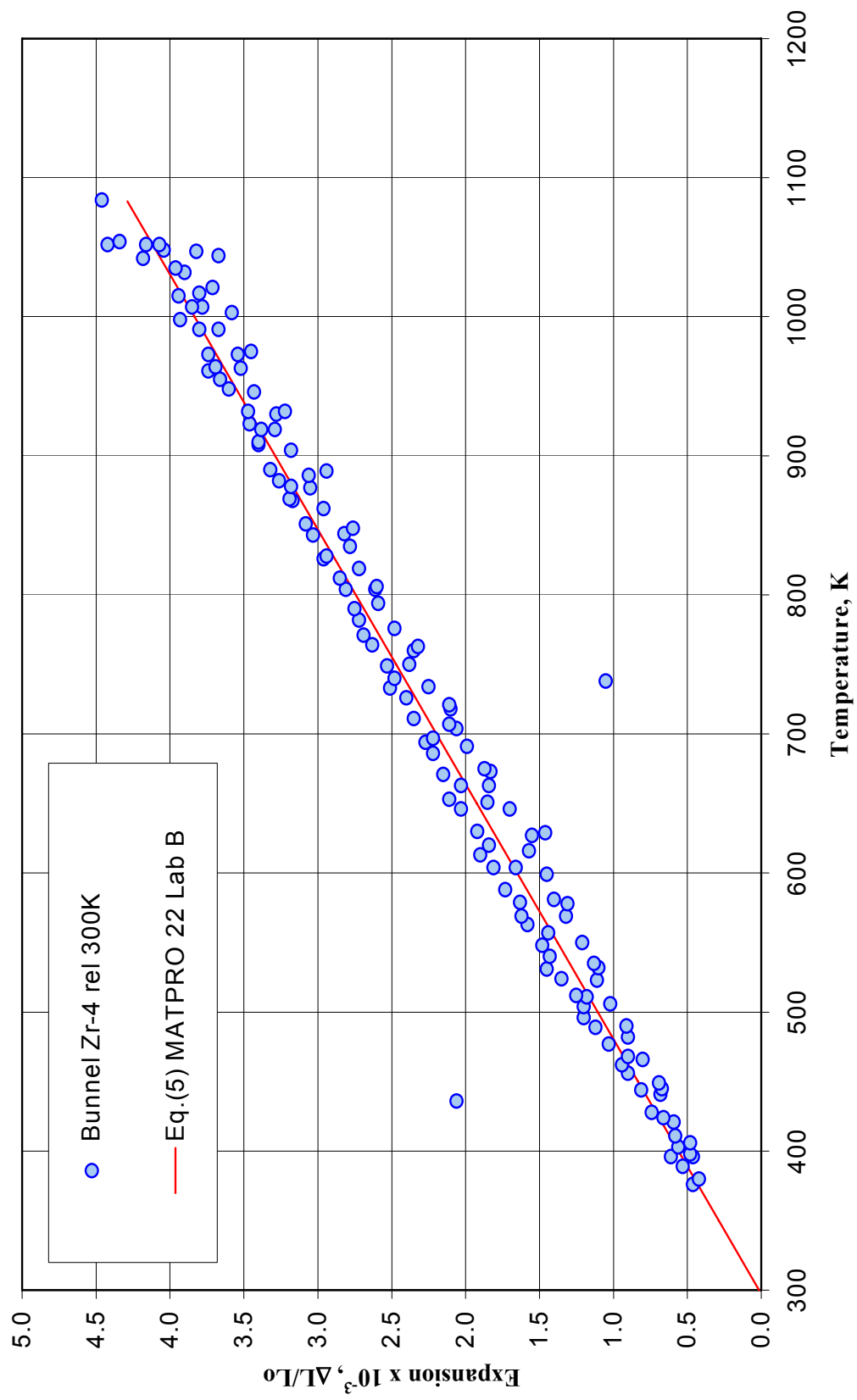


FIG. 2. MATPRO fit to Bunnell's Zircaloy-4 axial linear thermal expansion.

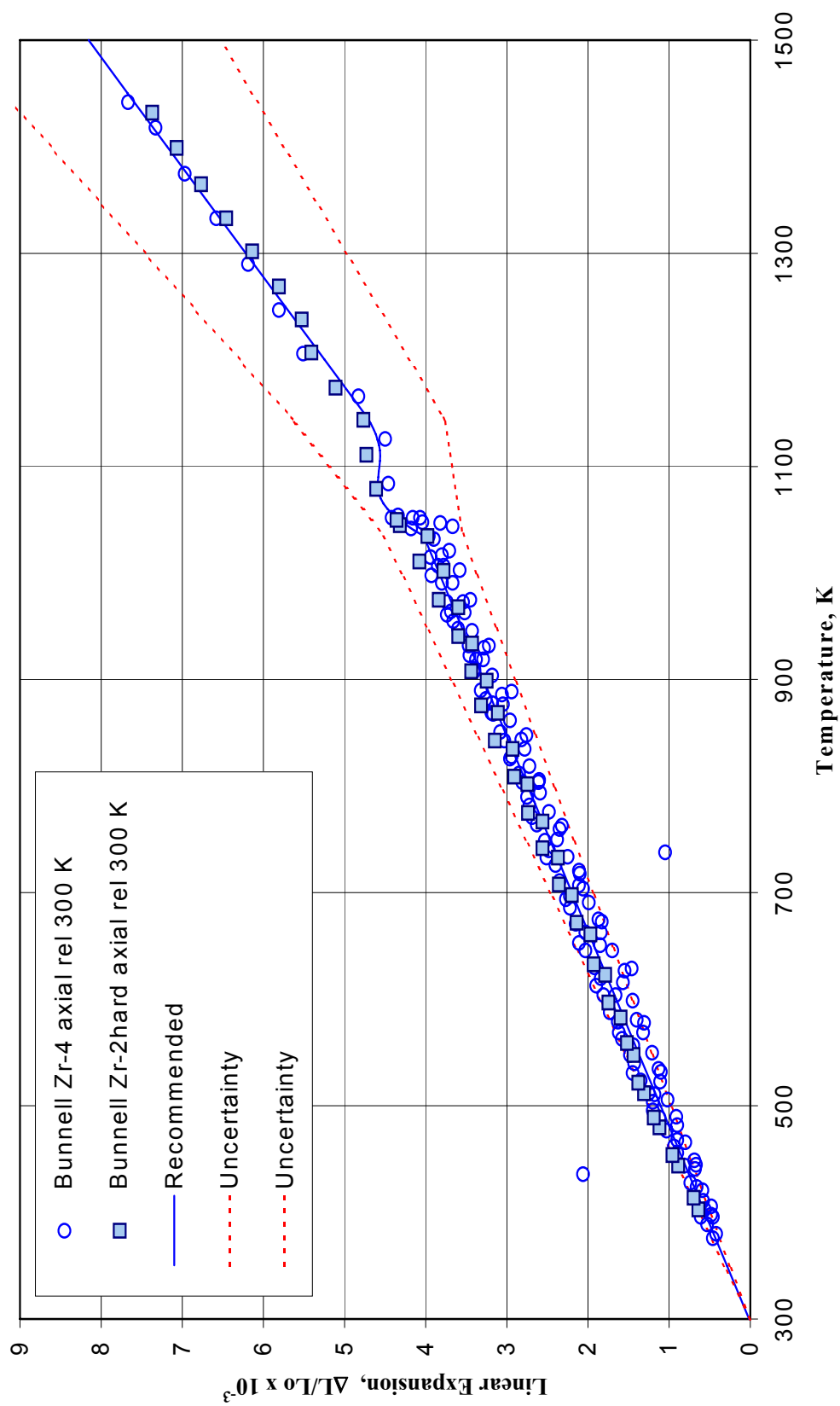


FIG. 3. Zircalov axial linear thermal expansion in  $\alpha$ . transition and  $\beta$  phases.

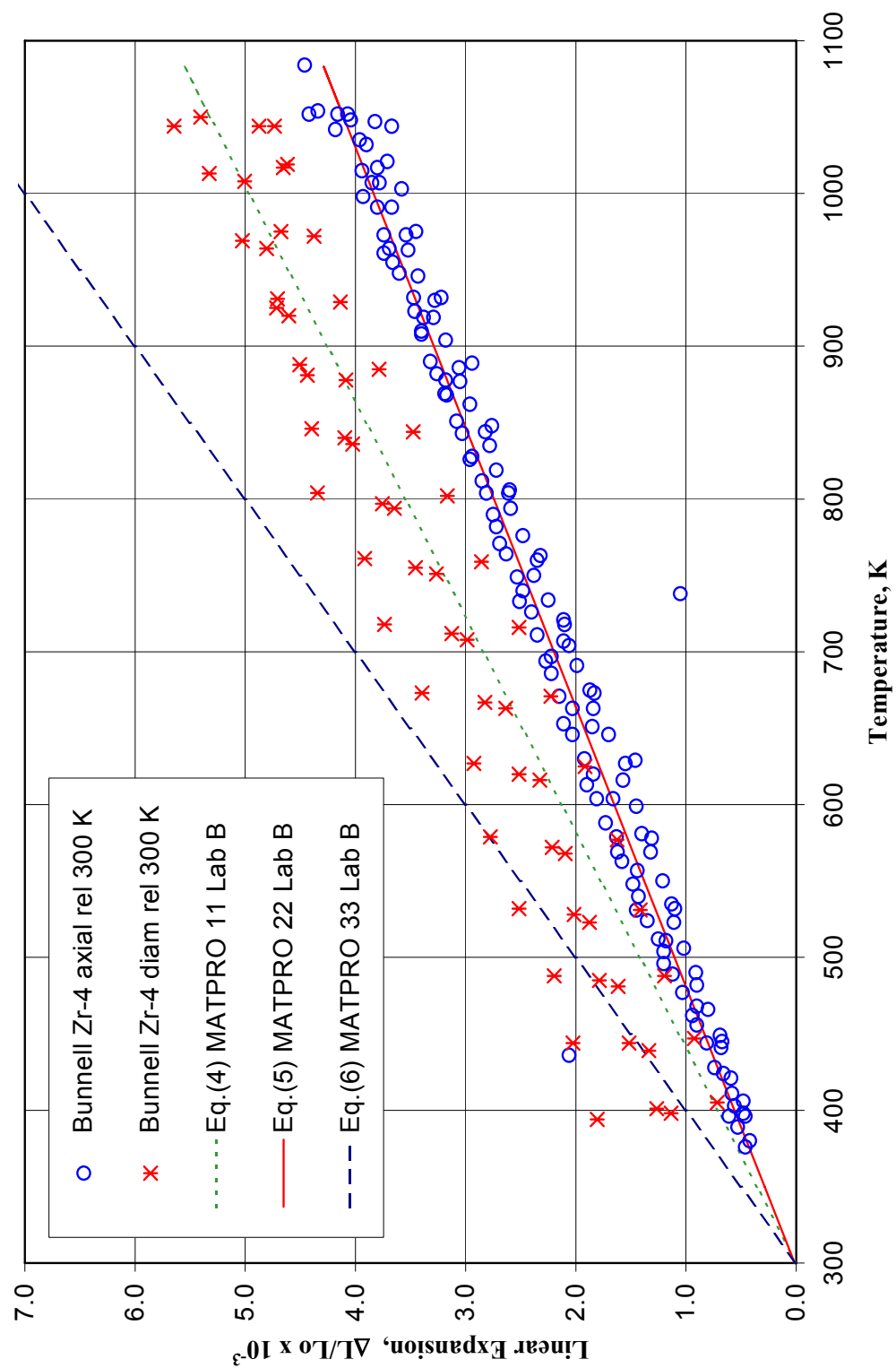


FIG. 4. Comparison of MATPRO values with Zircaloy-4 data of Bunnell et al.



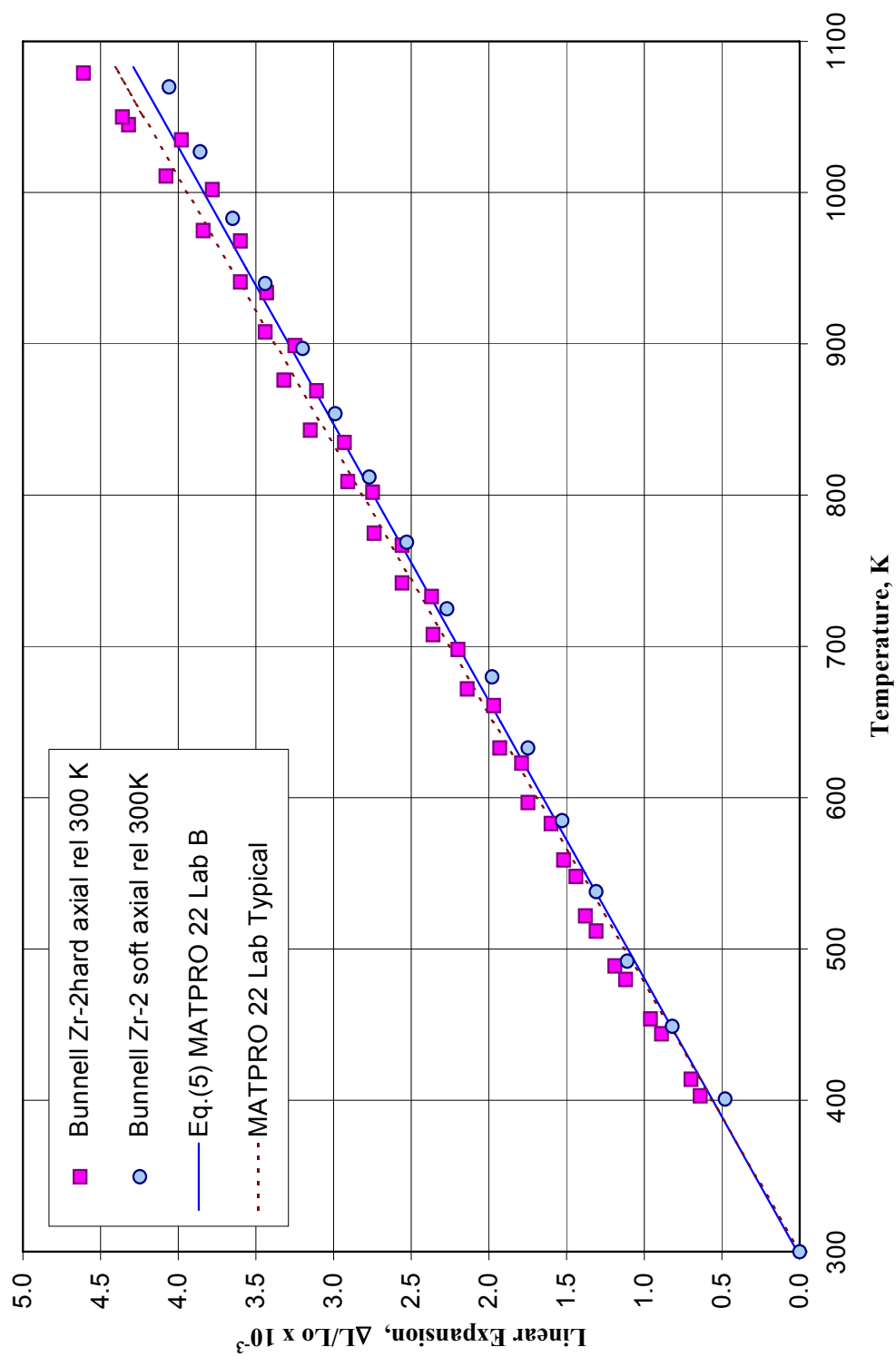


FIG. 5. Zircaloy-2 cladding axial linear thermal expansion.

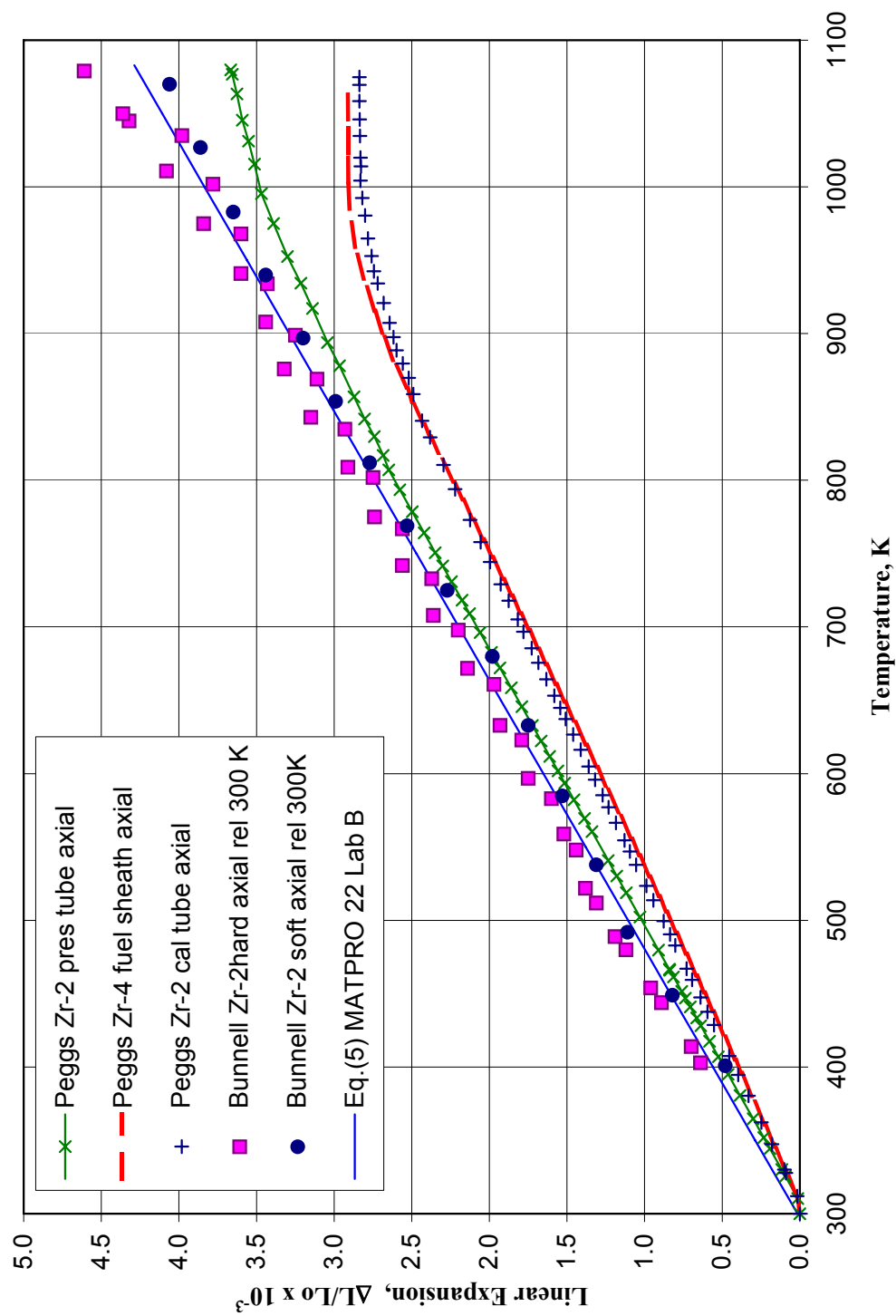


FIG. 6. Zircaloy-2 and Zircaloy-4 axial linear thermal expansion.

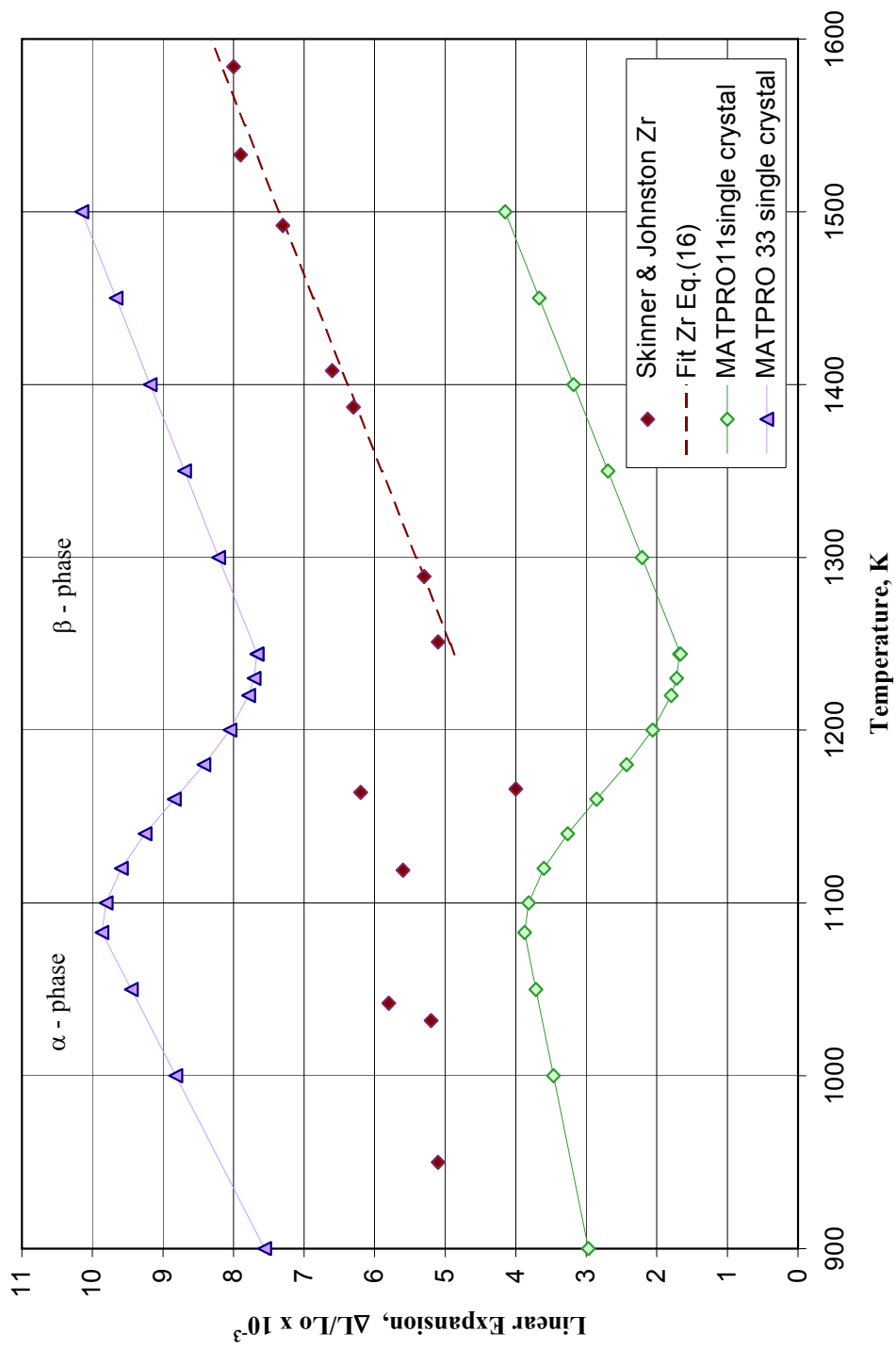


FIG. 7. Zircaloy single crystal linear thermal expansion.

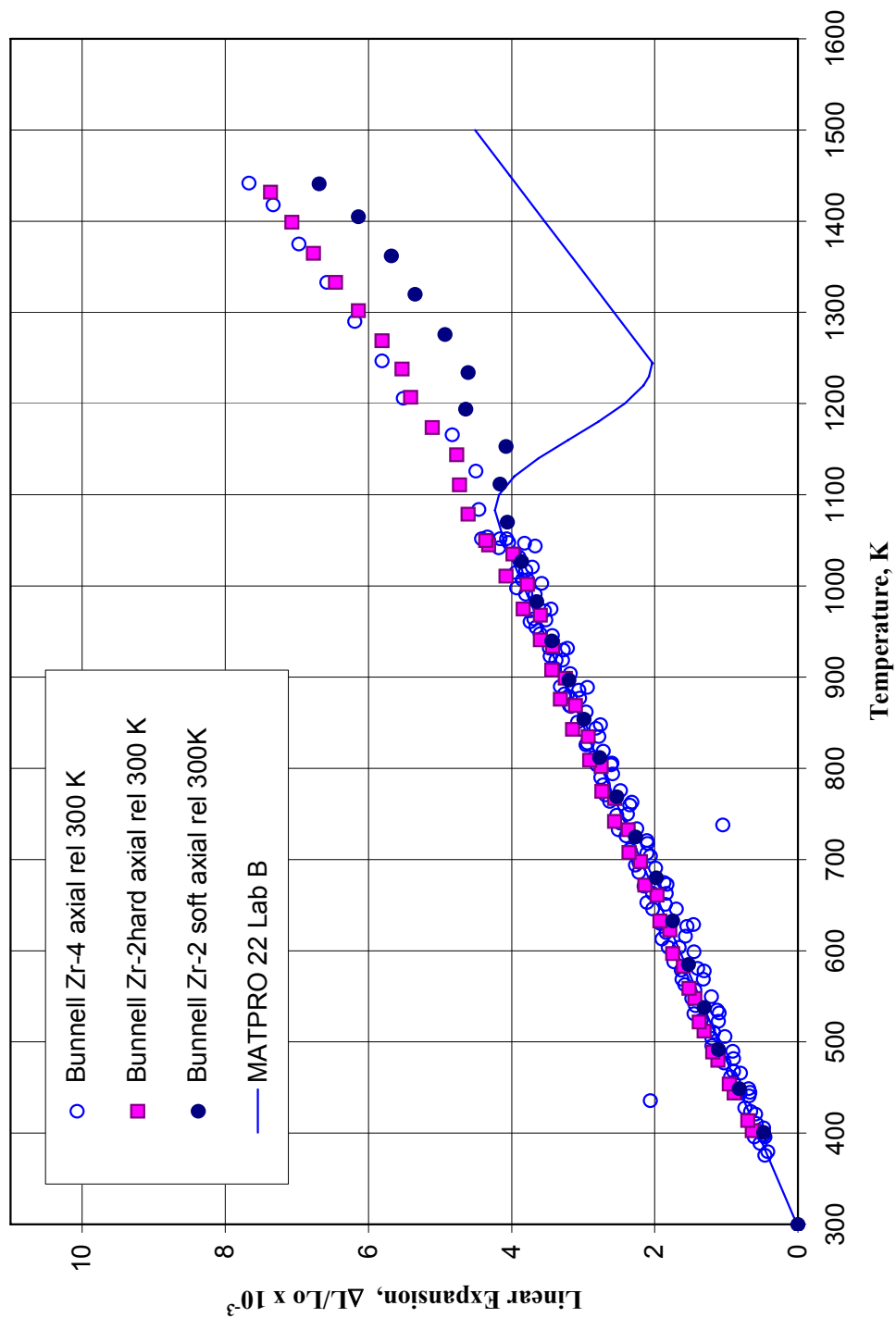


FIG. 8. Zircaloy axial linear thermal expansion.

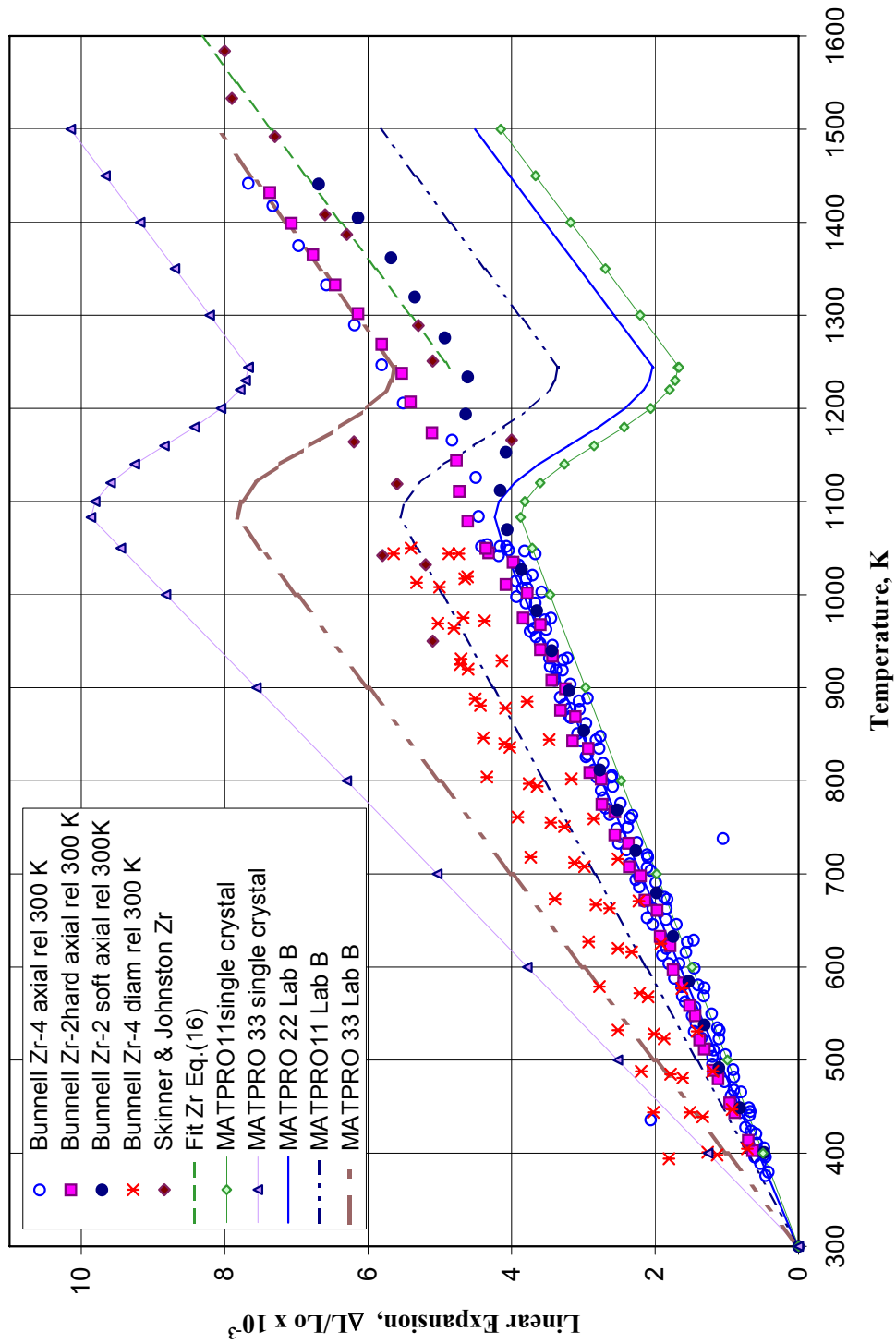


FIG. 9. Zircaloy axial linear thermal expansion.

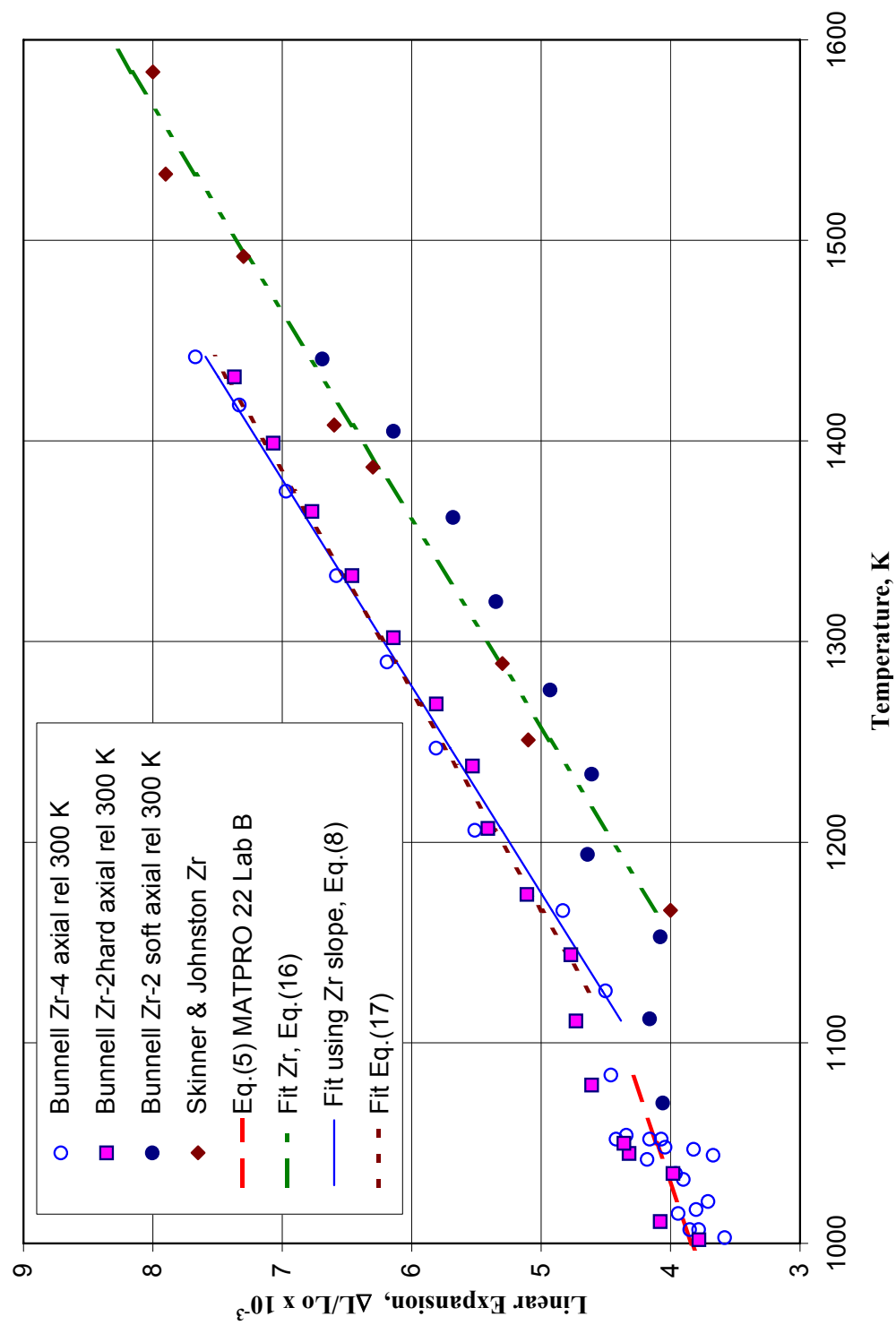


FIG. 10. Zircaloy axial linear thermal expansion in Beta phase.

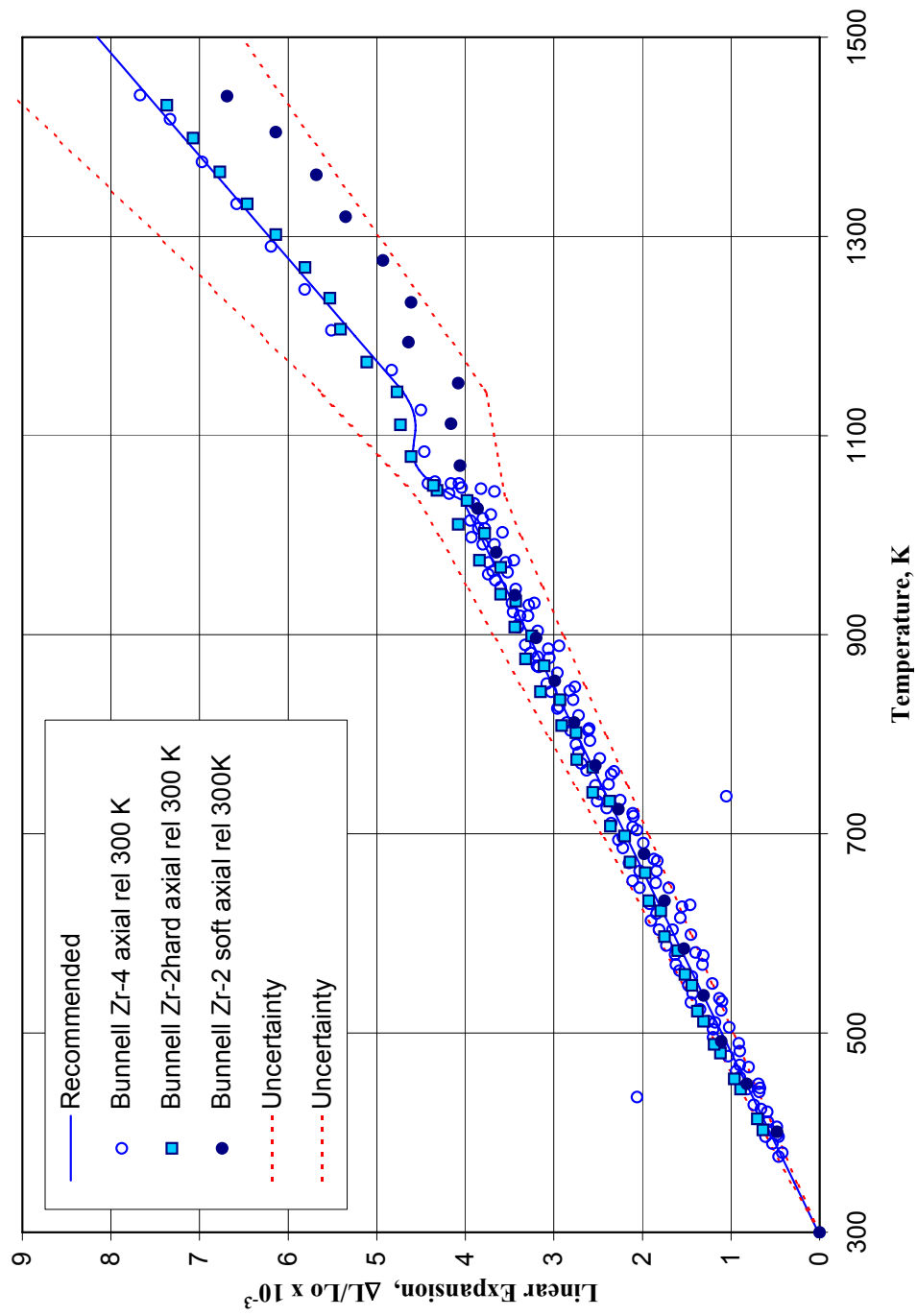


FIG. 11. Zircaloy linear thermal expansion in  $\alpha$  , transition and  $\beta$  phases.

## REFERENCES TO SECTION 6.2.1.5

- [1] HAGRMAN, D.T. (ed.), [SCDAP/RELAP5/MOD 3.1 Code manual: MATPRO - a library of materials properties for light-water-reactor accident analysis, NUREG/CR-6150, EGG-2720 Vol. 4 (1995).
- [2] BUNNELL, L.R., MELLINGER, G.B., BATES, J.L. and HANN, C.R., High-temperature properties of zircaloy-oxygen alloys, Electric Power Research Institute Report EPRI NP-524 (March 1977).
- [3] BUNNELL, L.R., BATES, J.L. and MELLINGER, G.B., Some high-temperature properties of zircaloy-oxygen alloys, J. Nucl. Mater. 116, 219-232 (1983).
- [4] DOUGLASS, D.L., The physical metallurgy of zirconium, Atomic Energy Review 1, (4), 73-74, (1962).
- [5] SCOTT, P.B., Physical and mechanical properties of Zircaloy-2 and -4, WCAP-3269-41 (1965), as referenced by D. T. Hagrman in the MATPRO Manual (ref. 1).
- [6] KEARNS, J.J., Thermal expansion and preferred orientation in Zircaloy, WAPD-TM-472, (1965), pp. 17-18, as referenced by D. T. Hagrman in the MATPRO Manual (ref. 1).
- [7] MEHAN, R.L. and WIESINGER, F.W., Mechanical properties of Zircaloy-2, General Electric, Knolls Atomic Power Laboratory Report KAPL-2110, pp. 8-11 (1961).
- [8] PEGGS, I.D., STADNYK, A.M. and GODIN, D.P., Thermophysical properties of zirconium-alloy fuel-channel components, High Temp.-High Pressures 8, 441-450 (1976).
- [9] SKINNER, G.B. and JOHNSTON, H.L., Thermal expansion of zirconium between 298 K and 1600 K, J. Chemical Physics 21 (8), 1383-1384 (1953).

### 6.2.2. Thermal conductivity of Zr-1%Nb

#### *Preliminary recommendation*

The preliminary recommendation for the thermal conductivity of Zr-1%Nb are the equations obtained by Peletskii et al. [1] from measurements on Zr-1%Nb rods along the length of the rod. No data are available comparing thermal conductivity in different directions.

For the  $\alpha$ -phase and  $\beta$ -phase from 300–1150 K,

$$\lambda \text{ (W} \cdot \text{m}^{-1} \cdot \text{K}^{-1}\text{)} = 23.48 - 1.92 \times 10^{-2} T + 1.68 \times 10^{-5} T^2 \quad (1)$$

for the  $\beta$ -phase from 1150–1600 K,

$$\lambda \text{ (W} \cdot \text{m}^{-1} \cdot \text{K}^{-1}\text{)} = 1.51 + 0.020 T \quad (2)$$

The experimental data and the recommended equations are shown in Figure 1. Tabulated values for thermal conductivity of Zr-1% Nb are given in Table I.

#### *Uncertainty*

The root-mean square deviation of the data from Eq. (1) is  $0.32 \text{ W m}^{-1} \text{ K}^{-1}$ . The root-mean square deviation for Eq. (2) is  $0.73 \text{ W m}^{-1} \text{ K}^{-1}$ . Figure 2 shows the percent deviations of the data from the recommended equations. All data are within 6% of the recommended equations. Because no other data are available for comparison, a 10% uncertainty appears to be reasonable.

#### *Discussion*

Peletskii et al. [1] measured the thermal conductivity of Zr-1%Nb rods using a stationary heat flux method. This method is used to determine the thermal conductivity along the length of the rod. For Zr-1%Nb, no data were found comparing thermal conductivity in different directions. However, in the Russian International Nuclear Safety Center review [2] of the recommended equations given by the Nuclear Safety Institute of the Russian Academy of Sciences (IBRAE) [3], Efanov et al. [2] noted that



thermal conductivity measurements on Zr-1%Nb by the Institute of Physics and Power Engineering (IPPE) give higher values for the  $\alpha$ -phase thermal conductivity and these data have a different temperature dependence than the data of Peletskii et al. Unfortunately, no information is available regarding the IPPE measurements and the IPPE data have not been made available. It is possible that Efanov et al. [2] were referring to the measurements by Mikryukov [3] on Zr-1.5%Nb, which are high relative to the data of Peletskii et al. [1] for Zr-1%Nb and also high relative to Canadian and Chinese data for Zr-2.5%Nb. It is also possible that the source of the discrepancy between the IPPE data and the data of Peletskii et al. is that the measurements were done in different directions. However, insufficient information is available on the IPPE measurements to confirm this hypotheses.

Table 1. Thermal conductivity of Zr-1% Nb

TEMPERATURE K	THERMAL CONDUCTIVITY $\text{W m}^{-1} \text{K}^{-1}$
300	19.2
400	18.5
500	18.1
600	18.0
700	18.3
800	18.9
900	19.8
1000	21.1
1100	22.7
1200	25.5
1300	27.5
1400	29.5
1500	31.5
1600	33.5

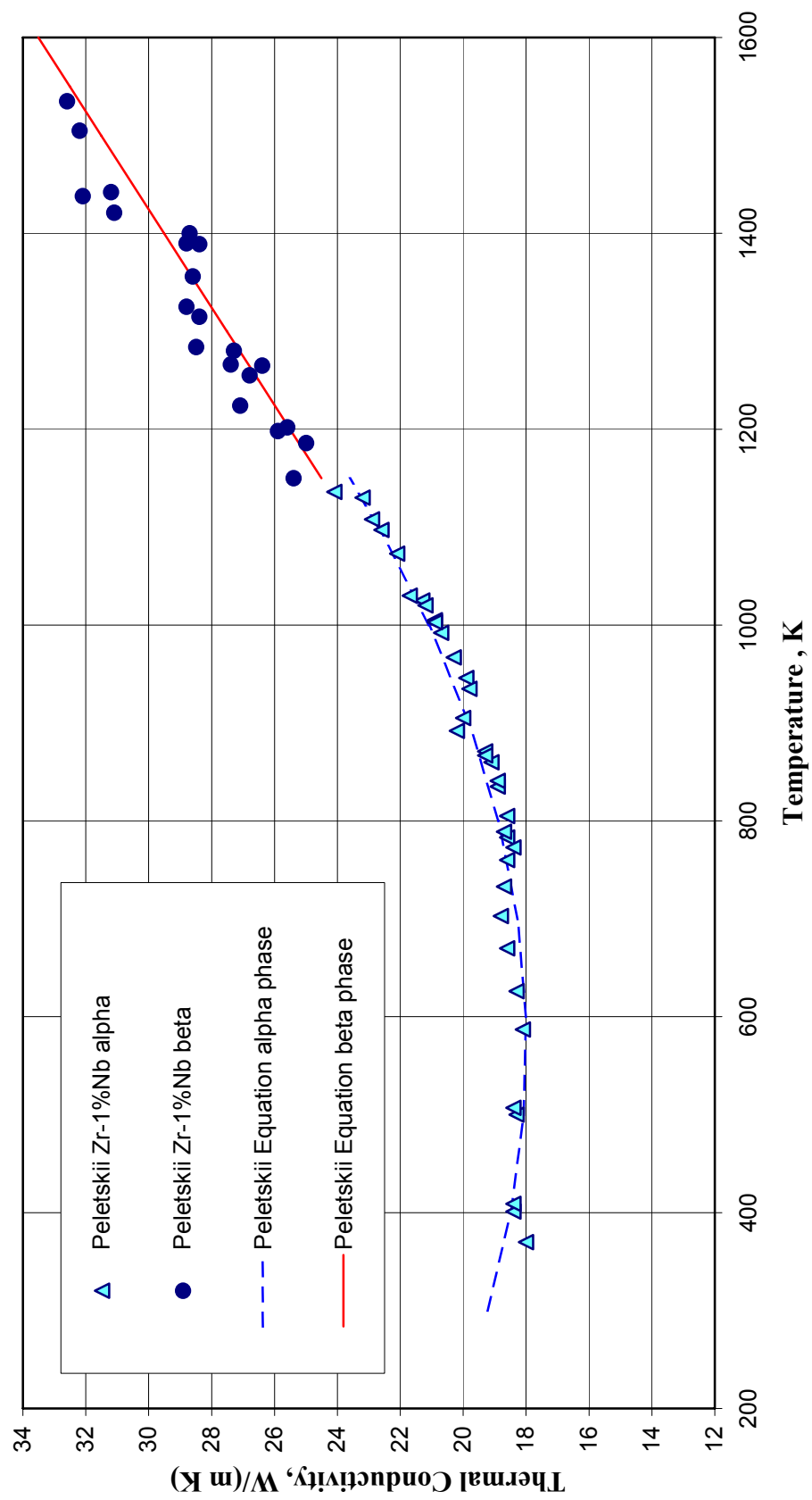


FIG. 1. Thermal conductivity of Zr-1%Nb.

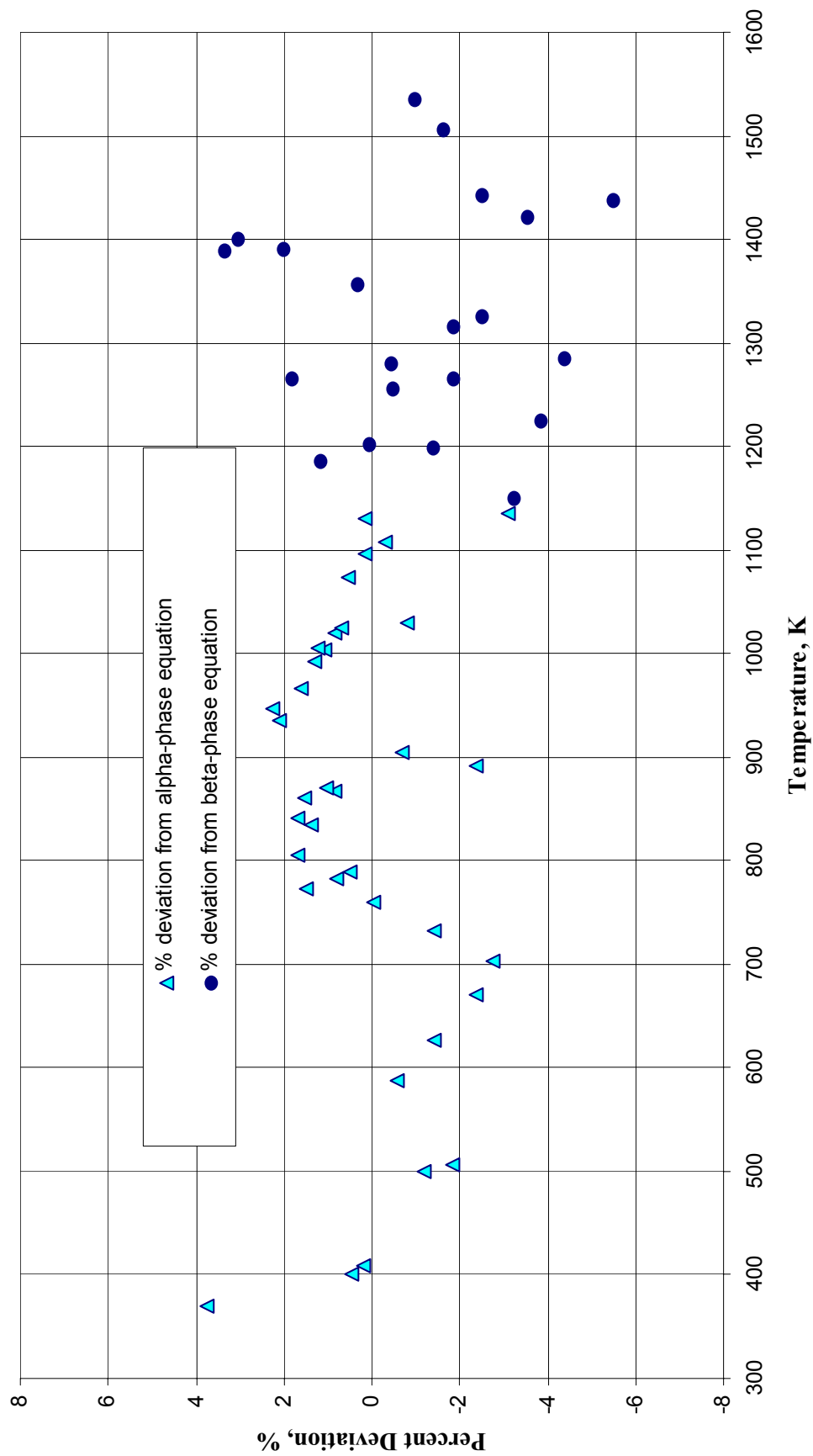


FIG. 2. Deviation of Zr-1%Nb thermal conductivity data from equations.

## REFERENCES TO SECTION 6.2.2

- [1] PELETSKII, V.E., GRISHCHUCK, A.P. and MUSAEVA, Z.A., The kinetic properties of E-11 reactor alloy in the high temperature range, *Teplofiz. Vys. Temp.* 32, No. 6, 820-824 (1994) [in Russian], *High Temperature* 32, 766-770 (1994) [English Translation].
- [2] EFANOV, A.D., SMOGALEV, I.P., BOBKOV, V.P., VINOGRADOV, V.N. and ROUMYANTSEV, V.N., Critical review of data and recommendations on zirconium niobium alloys given in the IBRAE report NSI-SARR-34-96, RINSC Report (1997).
- [3] OZRIN, V.T., ZITCERMAN, V.YU, GEFTER, V.M. and BAJBUIZ, V.F., Material properties for international nuclear safety database, IBRAE Report NSI-SARR-34-96 (1996).

### 6.2.3. Thermal conductivity of Zr-2.5%Nb

The assessment in this section was performed by IPPE. A comparison was made with data available from CIAE, AECL and IHED and a statistical assessment was performed. The current analysis does not provide a firm recommendation, since additional information on the experimental techniques and information are needed.

#### *Analysis of currently available data*

In reference [1], the available data on thermal conductivity of Zr-2.5%Nb alloy from CIAE (China) and AECL (Canada) were presented. Later in 2003, new experimental data were made available to IAEA by IHED, Moscow, Russia [2]. Data from the three sources were analysed and are presented here as an interim assessment.

The measurement uncertainty for the new data of IHED is estimated to be in the range 5%–6%. They used standard industrial rod specimens of 12 mm in diameter and 60 mm in length. Chromel-Alumel thermocouples were used up to 1600 K and an optical pyrometer was used for higher temperatures. Figure 1 shows the data from CIAE, AECL and IHED.

The data of IHED (solid curve in Figure 1) show the complex temperature trend in the whole region. The major points are the minimum at  $T \approx 600$  K and the bend point close to the temperature above which only  $\beta$ -phase exists ( $\sim 1200$  K). After Dr. V.Peletsky [3], 870 K is the temperature of the ( $\alpha$ + $\beta$ ) mixed phase start up and 1170 K is the temperature above which only  $\beta$ -phase exists.

Figure 1 shows, that qualitatively only the data of CIAE for specimen #1 show similar trend with IHED data. The material used for the investigations by CIAE and IHED differed: IHED used a rod specimen and CIAE used pressure tube material. A statistical analysis to determine the significance of the observed trend in the IHED data, optimal fits of the IHED data were carried out by two methods: (a) the Pade approximation method [3] and (b) the standard regression procedure using the least squares method. The data were taken from the plot.

The Pade approximaton gives:

$$\lambda_{\text{Pade}} = 27.3952 + (9687.14 \cdot T - 0.126187 \cdot 10^8) / [(T - 1067.64)^2 + 0.397548 \cdot 10^6] \quad (1)$$

where  $\lambda$  is the thermal conductivity in W/m.K and T is the temperature in K. The mean square error is 3.3% and, the maximum error is about 5 %.

The least square regression gives:

$$\lambda_{\text{lin}} = 3.1721373 + 14.7577453 \cdot (0.001 \cdot T)^2 - 2.4350669 \cdot (0.001 \cdot T)^3 + 4.831339 / (0.001 \cdot T),$$

where  $\lambda$  is the thermal conductivity in W/m.K and T is the temperature in K. The mean square error is 4.1% and, the maximum error is about 8%.

These Pade analysis results are compared with Dr. V.Peletsky's regression data in Figure 2. It can be seen from the results that the mentioned trend of a minimum and a bend point is statistically significant. Both the minimum and the bend point of the data are correctly replicated in the final curve. Such a trend was observed qualitatively only for one CIAE data set, as shown in Fig. 3.

To draw any final conclusions and recommendations from the available data, it is necessary to obtain additional information on the experimental methods data analysis used by the researchers.

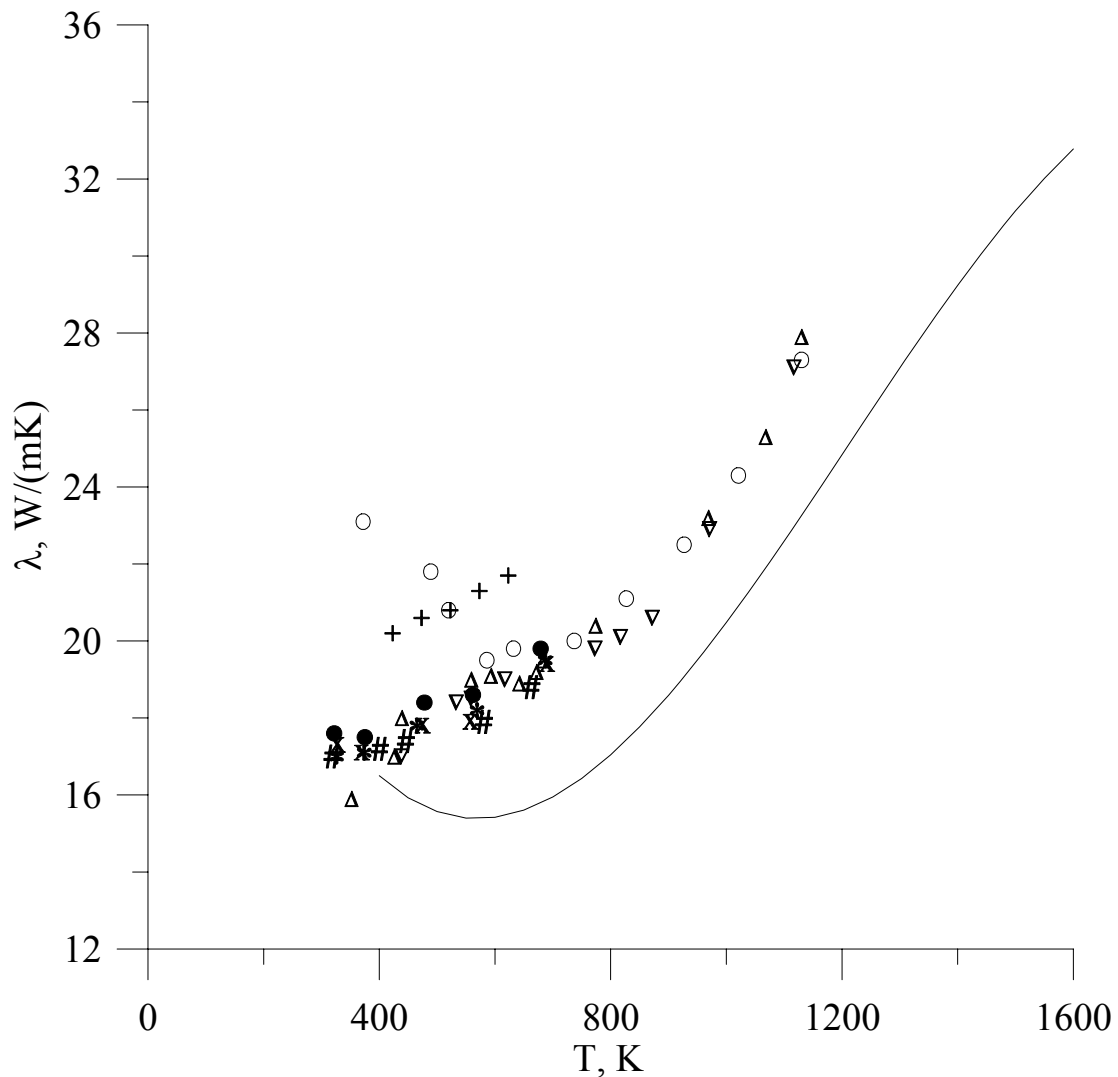


FIG. 1. The data of CIAE, China (3 specimens), and AECL, Canada (5 specimens) compared with data from Dr. V. Peletsky's regression (solid curve).

The legend for the data of CIAE, China:

- specimen #1 ('o') – pressure tube (axial) annealed at 673 K;
- specimen #2 ('Δ') – pressure tube (axial) annealed at 1073 K;
- specimen #3 ('∇') – pressure tube (axial) annealed at 1123 K;

The legend for the data of AECL, Canada:

- specimen #1 ('•') – cold worked pressure tube (axial);
- specimen #2 ('+') – cold worked rod (longitudinal);
- specimen #3 ('\*') – heat treated pressure tube (axial);
- specimen #4 ('x') – cold worked pressure tube (circumferential)
- specimen #5 ('#') – heat treated pressure tube (circumferential)

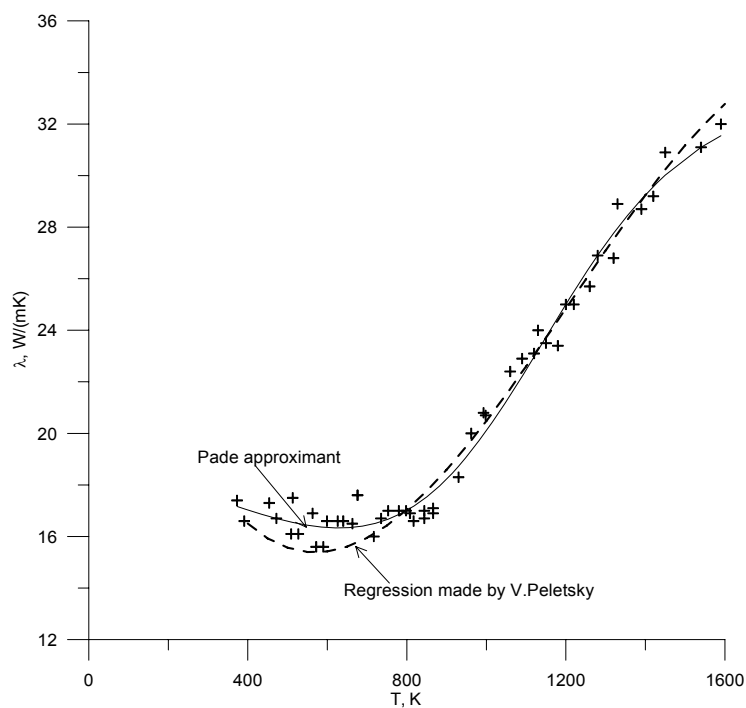


FIG. 2. IHED data and the results of statistical analysis.

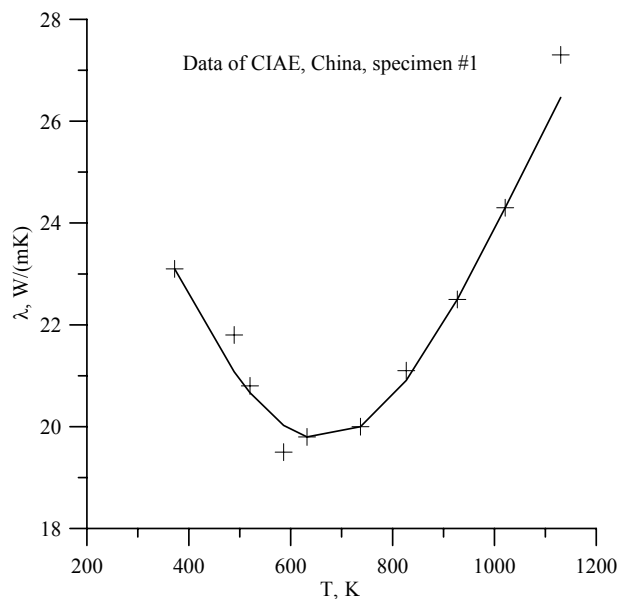


FIG. 3. Pade approximation (solid curve) against the data of CIAE, for specimen #1.

### REFERENCES TO SECTION 6.2.3

- [1] INTERNATIONAL ATOMIC ENERGY AGENCY. Thermophysical properties of materials for watercooled reactors, IAEA-TECDOC-949, IAEA, Vienna (1997).
- [2] FORTOV, V., et al., Thermophysical properties of Zr-2,5%Nb alloy, hafnium dioxide, liquid zirconium and hafnium, Report presented on 3<sup>rd</sup> RCM, CRP "Establishment of a Thermophysical Properties Data Base for Materials of LWRs and HWR", IAEA, Vienna (2003).
- [3] VINOGRADOV, V.N., GAY, E.V., RABOTNOV, N.S., Analytical approximation of data in nuclear and neutron physics, Moscow, Energoatomizdat (1987).

### 6.3. Absorber materials and their oxides

Some of the thermo-physical properties of Hafnium were provided by IHED, which are included in Section 6.3.1. The Hafnium oxide properties were provided by CEA, which are included in Section 6.3.2.

#### 6.3.1. Hafnium

Hafnium is an absorber material. The Hf absorber rod can be used without cladding. It is more long-living than B<sub>4</sub>C rod and is cheaper than alloy Ag-In-Cd rod.

From studies of various properties, it is known, that hafnium undergoes a polymorphous transformation in solid in the temperature range 1970–2270 K. Wide scatter of data is observed in that temperature range. Hafnium is a strong oxygen-getter and at high temperatures it absorbs oxygen and nitrogen even in a vacuum of  $10^{-5}$ – $10^{-6}$  mm Hg, which is the vacuum generally used in the investigation of materials thermal properties. Oxygen and nitrogen, dissolved in hafnium, stabilize  $\alpha$ -phase and increase the phase transition temperature  $T_{ph}$ . Therefore, most reliable results are obtained from experiments conducted on massive samples, with fine vacuum and short experiment duration.

The most reasonable value of  $T_{ph}$  is 2015 K; the same was given in [1]. The literature data on thermal expansion, enthalpy, heat capacity and emissivity of hafnium are considered and recommended values are proposed below.

##### 6.3.1.1. Thermal expansion

A summary of the results of various investigations of thermal expansion of hafnium is given in Table 1, which shows the test conditions, sample sizes, the test methods and the impurities present in the sample.

Investigations at high temperatures were conducted using the X-ray method [2–4]. The X-ray method is not very accurate for thermal expansion measurements. The scatter in the data is about 30%. Hafnium is unisotropic in the  $\alpha$ -phase; the expansion along the  $c$  axis is almost twice the expansion along  $a$  axis.

Figure 1 shows the results of poly-crystal samples investigations. The  $\alpha$ -phase X-ray thermal expansion was calculated for a poly-crystal using the formula  $\alpha = (2\alpha_{\perp c} + \alpha_{\parallel c})/3$ . The results for the  $\beta$ -phase were obtained only by two investigators using the X-ray method. Rosse and Hume Rothery [2] reported decrease of hafnium volume at phase transition, and Romans et al [4] reported a volume increase.

To arrive at a recommendation for the thermal expansion of the data on  $\beta$ -phase above 2000 K were discarded. All the data were then co-processed by the least square method. To assign a weighting to various data, the following criteria were adopted.

1. Method used for thermal expansion measurement;
2. Quality of Method used;
3. Purity of specimen investigated, and possibility of their contamination during the study;
4. Precision estimation given by the authors of the work;
5. Character and quality of results representation;
6. The author's results quality on thermal expansion of other materials.

The statistical weights used in the analysis are shown in Table 2. For the mean thermal expansion coefficient  $\alpha_m = (L(T) - L_{293})/(L_{293}(T - 293))$  the following equation is obtained:

$$\alpha_m \times 10^6 = 6.578 - 3.337 \times 10^{-4}(T - 293) + 5.754 \times 10^{-7}(T - 293)^2, \text{ K}^{-1} \quad (1)$$

where  $\alpha^m$  is the mean thermal expansion coefficient in  $10^{-6} [\text{K}^{-1}]$  and  $T$  is the temperature in K. The recommended curve for the mean coefficient of thermal expansion is shown on Fig. 1 and the data are reproduced in Table 3. The 95% confidence bands are presented on Fig. 2.

### 6.3.1.2. Enthalpy and heat capacity

The experimental investigations of enthalpy and heat capacity of hafnium are presented in Table 4, which shows the test method and the test conditions for the various investigations, such as the test temperature range, atmosphere, impurity, size of sample and test time, when available. The maximum temperature (2350 K) was achieved by Cats [11] in his investigations; but the recommendation here is limited to the phase transition temperature up to 2000 K.

In the  $\beta$ -phase, insufficient data are available to recommend a temperature dependence of hafnium heat capacity. All available data are presented in Fig. 3. Golutvin [5], Hawkins [10] and Kats [11] measured the enthalpy of hafnium  $H_T - H_{298}$ . Here their results are presented as a mean heat capacity of the form  $c_p^m = (H_T - H_{298})/(T-298)$ . Arutyunov [9] and Peletsky [12] presented their data as heat capacity  $C_p$ .

The data on mean specific heat capacity and the heat capacity of hafnium were co-processed by the least square method to obtain consistent recommended values using a unified linear (relative to the coefficients) equation. In this calculation procedure, a minimization procedure was used to minimize the sum of the squares of deviations of the measured values of the true and mean heat capacities from their regressions.

The temperature dependence of heat capacity can be described with the equation

$$c_p = a_1 + a_2T + a_3T^2 \quad (2)$$

where  $a_j$ , denotes the coefficients of the equation to be calculated;

The temperature dependency of enthalpy can be described by the equation

$$H_T - H_{T_0} = a_1(T - T_0) + a_2(T^2 - T_0^2)/2 + a_3(T^3 - T_0^3)/3, \quad (3)$$

Where,  $T_0 = 298.15$  K. The temperature dependency of the mean heat capacity can be described by the equation

$$c_p^m = a_1 + a_2(T^2 - T_0^2)/(2(T - T_0)) + a_3(T^3 - T_0^3)/(3(T - T_0)). \quad (4)$$

Assuming the statistical weight of point  $i$  to be  $w_i$ , the sum of squares of deviations can be represented as:

$$R = \sum_{i=1}^N w_i \varepsilon_i^2 = \sum_{i=1}^N w_i [C_i - \alpha c_i - (1 - \alpha)c_i^m]^2 \quad (5)$$

Here,  $\alpha = 1$ , if  $C_i$  is the measured value of heat capacity and  $\alpha = 0$  if  $C_i$  is the measured value of mean heat capacity.  $c_i$ , and  $c_i^m$  are the investigated regressions of respective heat capacities;  $\varepsilon_i$  is the deviation of the measured value from the value of its regression at point  $i$ ; and  $N$  is the total number of points processed.

The sum of squares of deviations was minimized relative to the coefficients of the selected model for Eqs (3) and (4) to derive a system of equations

$$\partial R / \partial a_j = \sum 2w_i [C_i - \alpha c_i - (1 - \alpha)c_i^m] \partial \{ \sum [C_i - \alpha c_i - (1 - \alpha)c_i^m] \} / \partial a_j = 0 \quad (6)$$

which enables us to determine the coefficients of the sought equations and obtain the information for analysing the selected model.

A weighting was assigned for the statistical analysis with the help of expert estimations. To arrive at the weighting, the same criteria as used for thermal expansion, were applied. Statistical weights are presented in Table 5.

From the analyses, the following equations were obtained for the heat capacity, mean heat capacity and enthalpy:



$$c_p = 23.1945 + 7.917 \times 10^{-3} T - 7.596 \times 10^{-8} T^2, (\text{Jmole}^{-1} \text{K}^{-1}) \quad (7)$$

$$c_p^m = 23.1945 + 7.917 \times 10^{-3} (T + T_0)/2 - 7.596 \times 10^{-8} (T^3 - T_0^3)/(3(T - T_0)), (\text{Jmole}^{-1} \text{K}^{-1}) \quad (8)$$

$$H_T - H_{298} = 23.1945(T - T_0) + 7.917 \times 10^{-3} (T^2 - T_0^2)/2 - 7.596 \times 10^{-8} (T^3 - T_0^3)/3 (\text{Jmole}^{-1}) \quad (9)$$

The calculated heat capacity and mean heat capacity recommended values are shown as solid lines in Fig.3 and presented in Table 6. The relative deviations of the heat capacity experimental points, the mean heat capacity data and the 95% confidence limits of recommended values are shown on Fig. 4.

#### 6.3.1.3. Emissivity

##### **Total hemispherical emissivity of hafnium**

Among metals the radiation characteristics of hafnium are the least studied. The test conditions, sample characteristics etc. used in the experimental investigations to measure the total hemispherical emissivity ( $\varepsilon_{ht}$ ) of hafnium are presented in Table 7. In all measurements a calorimetric technique, in which the radiant flux emitted by the sample surface was measured and the emissivity was obtained from the ratio of the measured radiant heat flux to the calculated radiant heat flux from a black-body surface under the same temperature.

In the data analysis, special attention was paid to the description of the surface condition and factors, such as mechanical treatment of the sample surface, its roughness, chemical composition of the sample before and after the experiment, preliminary annealing of the sample (vacuum, temperature, duration), and test conditions (vacuum, temperature).

It is known that hafnium possesses high affinity to oxygen that leads to oxygen adsorption, oxygen diffusion into the sample and oxide film formation on the sample surface. The oxide film formation and changes in the film during the experiment can significantly affect the emissivity. The investigations in Table 7 do not provide information on the oxygen uptake during the experiment.

The data from all the investigations were co-processed with the least square method using polynomials of the first and second order. A weighting procedure was used in the statistical analysis with the help of expert estimations. For the weighting estimations the same criteria, as was used in the case of thermal expansion, were adopted. The statistical weighting values are represented in the Tab. 8 and the results of the investigations are given on Fig. 5.

The calculations revealed that a polynomial of first power as given in Eq. (10) is most appropriate:

$$\varepsilon_{ht} = 2.178 \times 10^{-1} + 5.47 \times 10^{-5} T. \quad (10)$$

The recommended straight line for the total hemispherical emissivity of hafnium calculated with the equation (10) is shown on Fig. 5 as a bold line and values are tabulated in Tab. 9. The 95% confidence bands are included in Fig. 5.

##### **Total normal spectral emissivity of hafnium**

Most of the data available on the normal spectral emissivity of hafnium are at 0.65  $\mu\text{m}$ . The results of the investigations of  $\varepsilon_{\lambda n}$  at 0.65  $\mu\text{m}$  and the authors of the works are presented in Fig. 6.

Peletsky [12] measured  $\varepsilon_{\lambda n}$  of hafnium at 1700–1900 K and the value of 0.406 was obtained. Arutyunov et al [9] found that  $\varepsilon_{\lambda n}$  at 1200–1400 K decreased from 0.52 to 0.44 and it was nearly constant at 1400–2000 K. Tingwaldt [16] calculated the normal spectral emissivity of hafnium at 1510 K and at 1735 K on the basis of the optical properties of hafnium (index of refraction  $n$  and index of absorption  $k$ ) measured in this work.

Shaw [17] measured the normal spectral emissivity of hafnium in the temperature range 1630–1790 K with an optical pyrometer. The hafnium sample was a square piece of cold-rolled ribbon with dimensions 1.016  $\times$  1.016  $\times$  0.152 mm. and was spot-welded to the center of a tungsten filament. In the experiment the brightness of this hafnium-loaded filament and another tungsten filament with the same dimensions was compared with the pyrometer. The filaments were heated by direct current in

vacuum  $(1.3\text{--}2.6)\cdot 10^{-4}$  Pa. The brightness of hafnium appeared to be the same as that of tungsten filament. Therefore it was concluded that the spectral normal emissivity of hafnium at  $0.65\text{ }\mu\text{m}$  was equal to that of tungsten and was  $0.45 \pm 2\%$  in the temperature range  $1630 < T < 1790\text{ K}$ .

Figure 6 shows that the average value remains at  $\sim 0.44$ . Therefore the average of these results has been taken as the recommended value of  $\varepsilon_{\lambda n}$  of hafnium. The value for the normal spectral emissivity of hafnium at  $0.65\text{ }\mu\text{m}$  is  $0.44 \pm 0.02$ .

### ***The normal total emissivity of hafnium***

Only Blickensderfer et al [18] determined the normal total emissivity of hafnium at  $400\text{--}850\text{ K}$  with the help of a special constructed emissometer. A disc specimen with  $32\text{ mm}$  in diameter and  $5\text{ mm}$  thick, polished metallographically on the test surface with a roughness of  $0.17 \pm 0.02\text{ }\mu\text{m}$ , was used in the measurements. The emissometer was calibrated with a black body cavity with an emissivity of  $0.98$ . Temperatures were measured with a chromel-alumel thermocouple. The operating pressure was less than  $6.7 \cdot 10^{-3}$  Pa. The values obtained were corrected on internal reflections in the emissometer and was estimated to be accurate within  $\pm 5\%$ . The data are presented in Tab. 10.

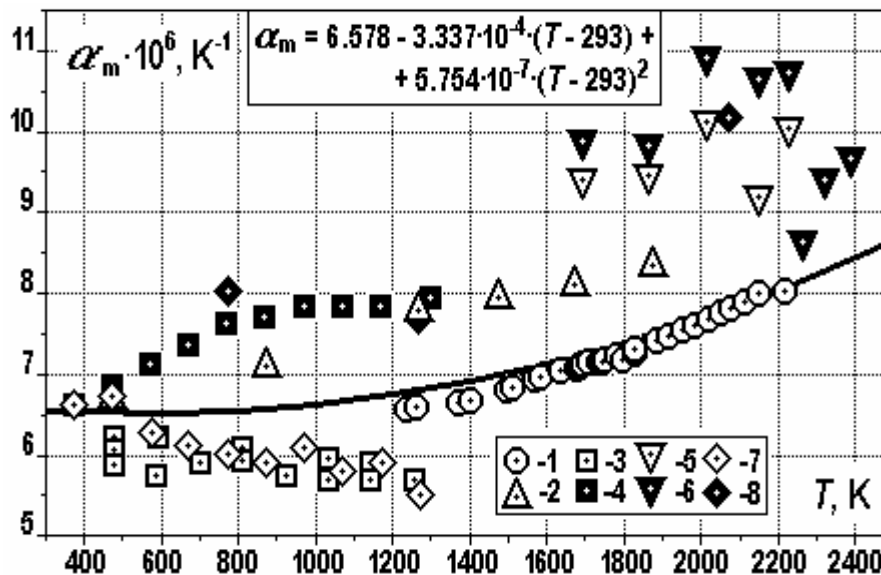


FIG. 1. Mean coefficient of thermal expansion of hafnium:

1 – Petukhov [8]; 2 – Krug [3]; 3 – Andestedt [6], 4 – Golutvin [5]; 5, 6 – Ross [2]; 7 – Baldwin [7]; 8 – Romans [4].

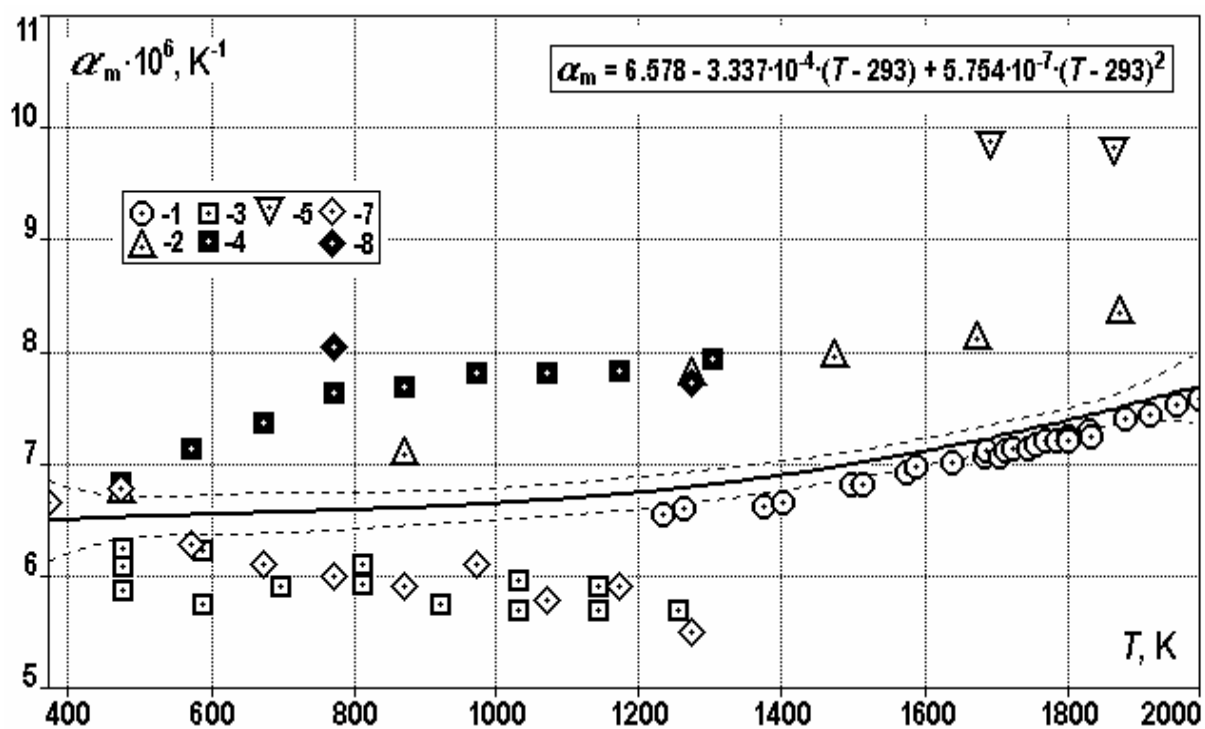


FIG. 2. Recommended values of mean coefficient of thermal expansion of hafnium and confidence limits. The symbols are the same as on Fig. 1.

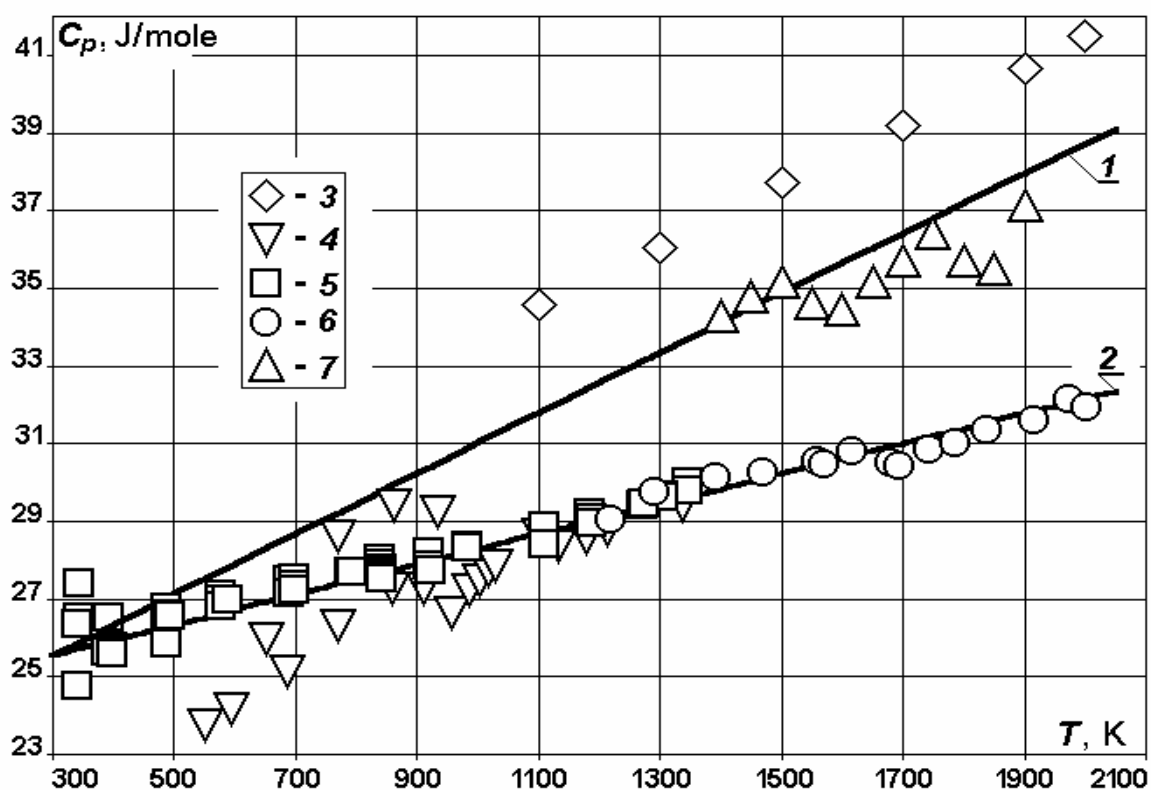


FIG. 3. Heat Capacity and Mean Heat Capacity of Hafnium:

1 – heat capacity  $c_p$ ; 2 – mean heat capacity  $c_p^m$ ; 3 – Arutyunov [9]; 4 – Golutvin [5]; 5 – Hawkins [10]; 6 – Kats [11]; 7 – Peletsky [12].

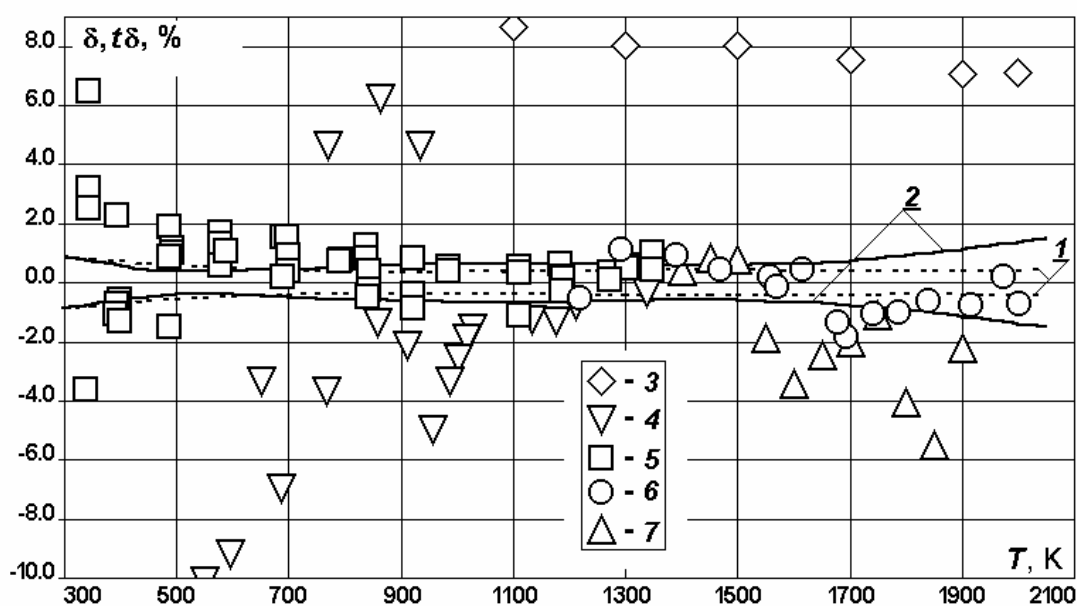


FIG. 4. Relative deviation of data on enthalpy and heat capacity of hafnium:

1 – confidence limits of mean heat capacity data; 2 – confidence limits of heat capacity data;  
3 – Arutyunov [9]; 4 – Golutvin [5]; 5 – Hawkins [10]; 6 – Kats [11]; 7 – Peletsky [12].

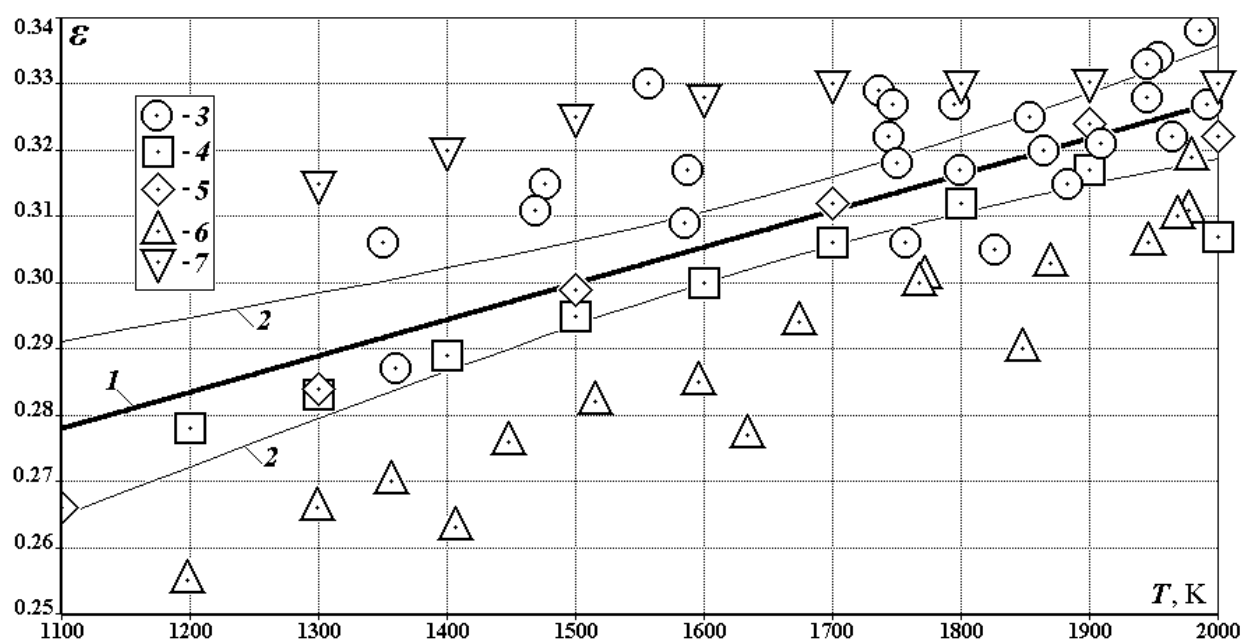


FIG. 5. The total hemispherical emittance of hafnium:

1 – the recommended values (equation (2.1)); 2 – the confidence bounds of the regression at 0.95 confidence probability; 3 – Timrot [14], 4 – Peletsky [12], 5 – Arutyunov [9],  
6 – Bedford [13], 7 – Zhorov [15].

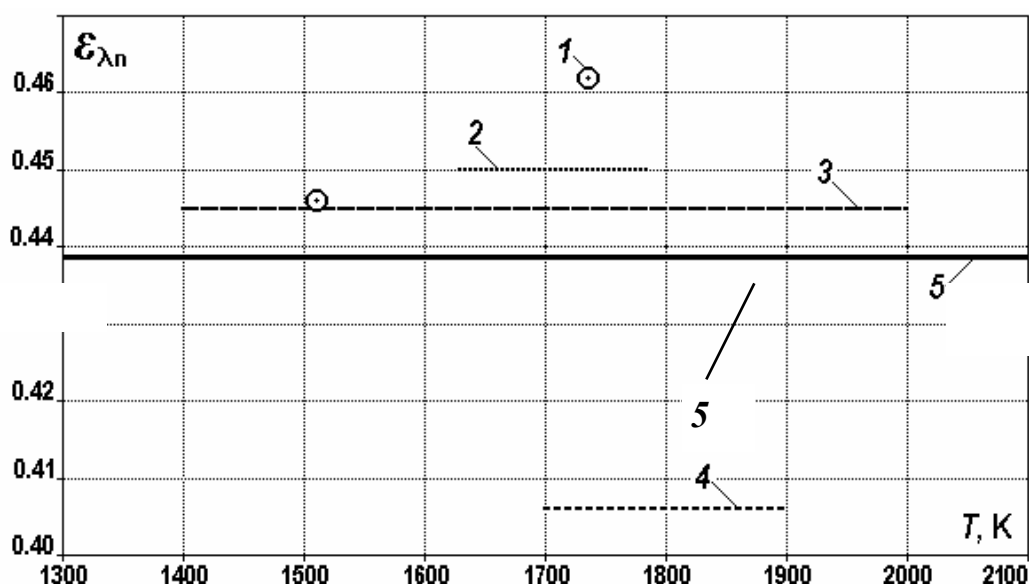


FIG. 6. The spectral normal emissivity of hafnium at 0,65  $\mu\text{m}$ :

1 –Tingwaldt [16]; 2- Shaw [17]; 3 – Arutyunov [9]; 4 – Peletsky [12]; 5 – Recommended values.

Table 1. Test and sample conditions for the investigation of thermal expansion of hafnium

AUTHOR	METHOD	$T$ , K	ATMOSPHERE	IMPURITIES, wt. %	SAMPLE	REMARKS
Ross and Hume-Rothery, 1963, [2]	X-ray	1693-2388	Vacuum $10^{-5}$ mm Hg or inert gas	1.6 Zr, <0.001 other metals	Wire $\varnothing 0.5$ mm	
Krug and Davis, 1970, [3]	X-ray	296-1873	Vacuum $5 \cdot 10^{-9}$ mm Hg before the heating	2.1 Zr, 0.0125 O <sub>2</sub> , 0.0035 other	Square, 10 mm across and 1-2 mm thick	The samples were etched
Romans et al, 1965, [4]	X-ray	298-2073	Vacuum $1 \cdot 10^{-6}$ mm Hg, ion getter pump	1.5 Zr, 0.01 O <sub>2</sub> , 0.021 other	Disk $\varnothing 6$ mm, 0.13 mm thick	5 min experiment
Golutvin et al, 1970, [5]	<b>PRD</b>	298-1302	Helium flow	0.79 Zr, 0.16 other	Rod $\varnothing 6$ mm	
Adenstedt, 1952, [6]		300-1335	Vacuum	99 Hf		Slow heating ~20h
Baldwin, 1954, [7]	<b>PRD</b>	293-1258	-	-	-	Annealed at 1023K
Petukhov, 2001, [8]	<b>TM</b>	960-1948	Vacuum $1 \cdot 10^{-6}$ mm Hg	99 Hf, 0.66 Zr	Bar $\varnothing 10$ mm, $l = 60$ mm	3 h experiment

**PRD** - Push-rod dilatometer; **TM** – Telemicroscope

Table 2. Statistic weight variable for estimation of mean coefficient of thermal expansion of hafnium

AUTHOR	WEIGHT VARIABLE
Petukhov, [8]	0.6
Golutvin, [5]	0.4
Adenstedt, [6]	0.3
Krug, [3]	0.4
Ross, [2]	0.2
Baldwin, [7]	0.3
Romans, [4]	0.2

Table 3. Recommended values of thermal expansion of hafnium

$T, K$	$\Delta L/L_{293},$ %	$\alpha_m 10^6,$ $K^{-1}$	$T,$ $K$	$\Delta L/L_{293},$ %	$\alpha_m 10^6,$ $K^{-1}$
293	0.000	6.58	1150	0.575	6.71
300	0.005	6.58	1200	0.612	6.75
350	0.037	6.56	1250	0.649	6.79
400	0.070	6.55	1300	0.687	6.83
450	0.103	6.54	1350	0.726	6.87
500	0.135	6.53	1400	0.765	6.91
550	0.168	6.53	1450	0.806	6.96
600	0.200	6.53	1500	0.847	7.01
650	0.233	6.53	1550	0.888	7.07
700	0.266	6.54	1600	0.931	7.12
750	0.299	6.55	1650	0.975	7.18
800	0.332	6.56	1700	1.020	7.25
850	0.366	6.57	1750	1.066	7.31
900	0.400	6.59	1800	1.112	7.38
950	0.434	6.61	1850	1.160	7.45
1000	0.469	6.63	1900	1.210	7.53
1050	0.504	6.66	1950	1.260	7.60
1100	0.539	6.68	2000	1.312	7.69

Table 4. Investigation of enthalpy and heat capacity of hafnium

AUTHOR	METHOD, MEASURED VALUE	$T$ , K	$T_{ph}$ , K	$\Delta H_{ph}$ , kJ/mole	ATMOS- PHERE	IMPURITIES, wt. %	SAMPLE	REMARKS
Golutvin, 1970, [5]	<b>DC</b>	298- 1400	-	-	He	99.8Hf+ 0.79Zr	Rod	Error not presented
Arutyunov, 1972, [9]	<b>RTV</b>	1100- 2050	1990	-	V <sub>1</sub>	99,3Hf+ 0.65Zr	d = 10 mm, l = 98 mm	Error 5%
Hawkins, 1963, [10]	<b>DC</b>	338- 1346	-	-	Ar	97.14Hf+ 2.8Zr+ 0.055other	-	0.26% sample weight increasing after the experiment
Katz, 1985, [11]	<b>DC</b>	1220- 2350	2001- 2127	7.543	Ar	99.8Hf+ 0.78Zr	-	<0.01% sample weight increasing after the experiment. Error: $\delta H$ <~1%, $\delta C_p$ = 1-3%
Peletski and Druzhinin, 1971, [12]	<b>RR</b>	1400- 2150	1970±5	-	V <sub>2</sub>	99Hf+ 0.66Zr	d = 8 mm, l = 18 mm	Error 7-8%

$T_{ph}$  - Temperature of phase transition;  $\Delta H_{ph}$  - Heat of phase transition; **DC** - Drop calorimeter ( $H_T-H_{T_0}$ ); **RTV** - Radial thermal values ( $C_p$ ); **RR** - Regular regime ( $C_p$ ); Ar – Argon; He - Helium flow; V<sub>1</sub> - Vacuum ( $10^{-6}$  mm Hg); V<sub>2</sub> - Vacuum ( $10^{-5}$ - $10^{-6}$  mm Hg)

Table 5. Statistical weight variable for estimation of heat capacity and enthalpy of hafnium

AUTHOR	STATISTICAL WEIGHT VARIABLE
Arutyunov, [9]	0.2
Havkins, [10]	0.5
Katz, [11]	0.6
Peletsky, [12]	0.3
Golutvin, [5]	0.4

Table 6. Recommended values of enthalpy and heat capacity of hafnium

$T$ , K	$H_T-H_{T_0}$ , J/mole3	$c_p^m$ , J/(mole K)	$c_p$ , J/(mole K)	$T$ , K	$H_T-H_{T_0}$ , J/mole	$c_p^m$ , J/(mole K)	$c_p$ , J/(mole K)
298.15	0,000	25,55	25,55	1150	29525	28,88	32,20
300	51,67	25,56	25,56	1200	31615	29,08	32,59
350	1469	25,75	25,96	1250	33744	29,27	32,97
400	2925	25,95	26,35	1300	35913	29,47	33,36
450	4422	26,15	26,74	1400	40370	29,85	34,13
500	5957	26,34	27,13	1450	42658	30,05	34,51
550	7533	26,54	27,53	1500	44986	30,24	34,90
600	9148	26,73	27,92	1550	47353	30,44	35,28
650	10802	26,93	28,31	1600	49760	30,63	35,67
700	12496	27,13	28,70	1650	52206	30,82	36,05
750	14230	27,32	29,09	1700	54692	31,02	36,43
800	16003	27,52	29,48	1750	57217	31,21	36,82
850	17816	27,71	29,87	1800	59782	31,40	37,20
900	19669	27,91	30,26	1850	62387	31,60	37,58
950	21561	28,10	30,65	1900	65031	31,79	37,96
1000	23492	28,30	31,04	1950	67714	31,98	38,34
1050	25464	28,49	31,42	2000	70438	32,17	38,72
1100	27474	28,69	31,81				

Table 7. The investigations of the total hemispherical emissivity of hafnium

AUTHOR	METHOD	$T$ , K	PRESSURE, Pa	IMPURITIES, wt. %	SAMPLE	REMARKS
Bedford, 1965, [13]	<b>CDECH</b>	1200-2250	$6.7 \cdot 10^{-5}$	$\approx 97.57$ Hf, 2.4 Zr	Strip: 115×2.5×0.25 mm	Error not presented
Timrot, 1966, [14]	<b>CEBH</b>	1300-2000	$6.7 \cdot 10^{-3}$	Not presented	Rod: d = 12 mm, l = 65 mm.	Error - 7 %, iodide hafnium
Zhorov, 1970, [15]	<b>CDECH</b>	1300-2000	$6.7 \cdot 10^{-3}$	$\approx 98.92$ Hf 0.96 Zr	Rod: d = 12 mm, l = 340 mm	Error 7 % iodide hafnium
Peletsky, 1971, [12]	<b>CEBH</b>	1200-2200	$1.3 \cdot 10^{-3}$ - $1.3 \cdot 10^{-4}$	$\approx 99$ % Hf, 0.66 % Zr	Rod: d = 8 mm, l = 18 mm	Error 5 % iodide hafnium
Arutyunov, 1972, [9]	<b>CIH</b>	1100-2150	$1.3 \cdot 10^{-4}$	$\approx 99,3$ % Hf, 0.65 % Zr,	Rod: d = 10 mm, l = 98 mm	Error 5% iodide hafnium

Notes: **CDECH** - Calorimetric, Direct electrical current. Heating; **CEBH** - Calorimetric, Electron bombardment heating; **CIH** - Calorimetric, Inductive heating.



Table 8. Statistical weight variables for assessment of the total hemispherical emissivity of hafnium

AUTHOR	STATISTICAL WEIGHT
Bedford, [13]	0.3
Timrot, [14]	0.6
Zhorov, [15]	0.5
Peletsky, [12]	0.7
Arutyunov, [9]	0.7

Table 9. Recommended values of the total hemispherical emissivity of hafnium

№	$T$ , K	$\varepsilon_{ht}$	№	$T$ , K	$\varepsilon_{ht}$
1	1100	0.278	11	1600	0.305
2	1150	0.281	12	1650	0.308
3	1200	0.284	13	1700	0.311
4	1250	0.286	14	1750	0.314
5	1300	0.289	15	1800	0.316
6	1350	0.292	16	1850	0.319
7	1400	0.294	17	1900	0.322
8	1450	0.297	18	1950	0.325
9	1500	0.300	19	2000	0.327
10	1550	0.303			

Table 10. The normal total emissivity of hafnium

$T$ , K	400	450	500	550	600	650	700	750	800	850
$\varepsilon_{nt}$	0.088	0.100	0.115	0.131	0.149	0.167	0.186	0.206	0.227	0.248

### REFERENCES TO SECTION 6.3.1

- [1] TOULOUKIAN, Y.S., et al., Thermal Expansion. Metallic Elements and Alloys. Vol. 12 of Thermo-physical Properties of Matter - The TPRC Data Series, IFI/Plenum, New York - Washington (1975), 1348 pp.
- [2] ROSS, R.G., HUME-ROTHERY, W., High Temperature X-Ray Metallography. J. Less-Common Metals, (1963), 5, N3, 258
- [3] KRUG, M.P., DAVIS, B.E., The anisotropic thermal expansion of the crystal lattice of  $\alpha$  hafnium. J. Less-Common Metals, (1970), 22, N3, 363
- [4] ROMANS, P.A., PAASCHE, O.G., KATO, H., The transition temperature of hafnium. J. Less-Common Metals, 8 (1965), p. 213-215.
- [5] GOLUTVIN, YU.M., MASLENNIKOVA, E.G., About enthalpy of metallic hafnium. Izvestiya AN SSSR. Metally, N5, p.174-183 (1970) (in Russian).
- [6] ADENSTEDT, H.K., Physical, Thermal, and Electrical Properties of Hafnium and High Purity Zirconium. Trans. Am. Soc. Metals. V.44, p.p.949-973 (1949).

- [7] BALDWIN, E.E., The Thermal Expansion and Elevated Temperature Mechanical Strength of Hafnium. Report N1.USAEC Rept. KAPL-M-EEB-7, 14 h.h., 1954 (In Touloukian Y.S., et al. Thermal Expansion. Metallic Elements and Alloys. Vol.12: of Thermo-physical Properties of Matter - The TPRC Data Series, IFI/Plenum, New York - Washington (1975).
- [8] PETUKHOV, V.A., Thermo-physical properties of hafnium. In the report on CRP on "Establishment of a Thermo-physical Properties Data Base for Materials of LWRs and HWRs" (2001).
- [9] ARUTYUNOV, A.B., BANCHILA, S.N., FILIPPOV, L.P., Thermal, electrical and radiating properties of hafnium in high temperature region. Teplof. Vysok. Temp. V.10, N2 (1972), p.425-428. (in Russian)
- [10] HAWKINS, D.T., ONILLON, M. and ORR, R.L., High-temperature heat content of hafnium, J. of Chem. and Engineering Data, V. 8 No, 4 (1963), p. 628-629.
- [11] KATS, S.A., CHEKHOVSKOI, V.YA., KOVALENKO, M.D., Thermo-physical properties of zirconium and hafnium at high temperatures, Teplofizika Vysokikh Temperatur, N2 (1985), p.395. (in Russian).
- [12] PELETSKY, V.E., DRUZHININ, V.P., Experimental investigation of some physical properties of hafnium at high temperatures, Teplofizika Vysokikh Temperatur, V.9, N3 (1971), p.539-545. (in Russian).
- [13] BEDFORD, R.G., High-temperature electrical resistivity and allotropic transformation temperature of hafnium, J. Appl. Phys., V. 36, N 1 (1965), p.113-117.
- [14] TIMROT, D.L., PELETSKY, V.E., VOSKRESENSKY, V.YU., Thermal conductivity and emittance of hafnium, Teplofizika Vysokikh Temperatur, V.4, N 6 (1966), p. 874-875. (in Russian).
- [15] ZHOROV, G.A., The emittance of metals of IV b sub-group at high temperatures. Teplofizika Vysokikh Temperatur, V 8, N 3 (1970), p. 532-536. (in Russian).
- [16] TINGWALDT, C., et al., The optical constants of tungsten and hafnium at high temperatures. Optik, Bd 22, Heft 1, 1965, S. 48-59 (in German).
- [17] SHAW, M.L., Spectral emittance of hafnium at 0.65  $\mu$ . J. Appl. Phys., V.37, No 2 (1966), p. 919-920.
- [18] BLICKENSDECKER, R., et al., Normal total emittance at 400-850 K and normal spectral reflectance at room temperature of Be, Hf, Nb, Ta, Ti, V and Zr. J. Less-Comm. Metals, 51 (1977), p. 13-23.

### 6.3.2. *Hafnium dioxide*

#### *Assessment of enthalpy and heat capacity*

Hafnium dioxide is reported to be a stable stoichiometric compound with three solid-state phases. Curtis et al. [[1]] reported a transition from monoclinic to tetragonal at about 1973 K, using high temperature XRD. Based on their linear thermal expansion work, Ohnysty and Rose [[2]] reported an inversion in the temperature range 1866-2089 K. On the basis of data reported by other authors, it can be deduced that it should be due to monoclinic  $\leftrightarrow$  tetragonal transition. Ruh et al. [[3]] have reported monoclinic  $\leftrightarrow$  tetragonal transition by high temperature XRD as, 1893-1923 K (heating) and 1893-1793 K (cooling). Using DTA technique they measured this for various compositions of  $\text{ZrO}_2\text{-HfO}_2$  system. These values when extrapolated to pure  $\text{HfO}_2$ , give inversion temperatures, 2023-2056 K (heating) and 1973-1923 K (cooling). All these transitions show considerable hysteresis while cooling as well as heating. Using XRD technique, Boganov et al. [[4]] reported a tetragonal  $\leftrightarrow$  cubic transition similar to  $\text{ZrO}_2$  at 2973 K. Bocquillon et al. [[5]] reported an orthorhombic at 1273 K and 200 kbar.

Monoclinic:  $a=5.11$ ,  $b=5.14$ ,  $c=5.28$ ,  $\beta=99^\circ 44'$  at 298.15 K;  $a=5.128$ ,  $b=5.167$ ,  $c=5.294$ ,  $\beta=99^\circ 18'$  at 1273 K;  $a=5.21$ ,  $b=5.15$ ,  $c=5.43$ ,  $\beta=98^\circ 48'$  at 1920 K, density = temperature range: 298.15 to 1973 K, theoretical density: 9.68  $\text{gm/cm}^3$ , Coefficient of linear thermal expansion:  $5.8 \times 10^{-6}$  inches/K (523-1573 K)

Tetragonal:  $a=5.14$ ,  $c=5.25$ , temperature range: 1973 to 2973 K, theoretical density: 10.01  $\text{g/cm}^3$

Face Centered Cubic: temperature range: 2973 to 3173 K

Melting temperature: 3173 K

Enthalpy of formation of hafnium dioxide is reported by many authors. Roth and Becker [6], Humphery [7] and Paputskij et al. [8] determined enthalpy of formation of  $\text{HfO}_2$  at 298.15 K by oxygen-bomb combustion calorimetry and reported values of  $-271.5$  (at 298 K),  $-266.1 \pm 0.3$  and  $-271.0 \pm 1.5$ , respectively. Huber and Holley [9], and Kornilov and Ushakova [10], had reported values of  $-273.6 \pm 0.3$  and  $-267.1 \pm 0.6$  kcal/mol, respectively. Later these two groups made a joint attempt to understand the discrepancy in their results and re-determined the enthalpy of formation value of  $\text{HfO}_2$  [11]. The analysis of their samples showed the presence of  $\text{ZrO}_2$ , which was not uniformly distributed. After correcting the enthalpy of combustion values for these impurities, mainly zirconium, they found a good match in their enthalpy of formation values and reported a final value of  $-267.1 \pm 0.3$  kcal/mol at 298.15 K. which has been accepted by us as the most reliable value for enthalpy of formation of  $\text{HfO}_2$ .

Low temperature heat capacity values of hafnium dioxide, in the temperature range 51–298 K, are reported by Todd [12]. He calculated entropy of  $\text{HfO}_2$  at 298.15 K by integrating heat capacity values against  $\log T$  over the temperature range 51–298 K, using Simpson-rule and extrapolated value for the range 0–51 K by means of Debye-Einstein empirical function. The value thus calculated is given as  $14.18 \pm 0.10$  cal/K.mol, which is in reasonably good agreement with  $12.12 \pm 0.08$  cal/K.mol, reported by Kelley [13]. Others [14], [15] have measured enthalpy increment of the compound, at temperatures higher than room temperature, by drop calorimetry. In the present work these enthalpy increment values are fitted in polynomial equations by least square method using Origin computer software. The first derivative of these equations with respect to temperature was used to derive heat capacity equations of different hafnium dioxide phases.

The least square fit of the low temperature heat capacity values reported by Todd [12] into a polynomial, gave the following equation:

$$C_p (\text{J/mol.K}) = -9.7516 + 0.3779 T - 0.00048 T^2 + 1421.87 / T^2 \quad (1)$$

The reported literature values and the fit values are compared in table 1 and are plotted in fig. 1. Using Shomate method [16], a combined fit of the enthalpy increment values reported by Orr [15] in the temperature range, 382.7–1803.6 K and those of Fortov et al. [14] in the temperature range, 1187–2039 K, into a polynomial equation was carried out. The constraint used for this fit were,  $\Delta H_{298.15\text{K}}^T = 0$  and  $C_p = 60.25$  J/mol.K at  $T = 298.15$  K. The following enthalpy increment equation was thus obtained:

$$\Delta H_{298.15\text{K}}^T (\text{J/mol}) = -28327.3 + 77.3007 T + 0.00079 T^2 + 1556018.75 / T \quad (298.15\text{--}2040 \text{ K}) \quad (2)$$

The following heat capacity equation derived by temperature differential of the above enthalpy increment polynomial, on extrapolation to 298.15 K, gave an excellent fit with the low temperature heat capacity data of Todd [12].

$$C_p (\text{J/mol.K}) = 77.3007 + 0.00158 T - 1556018.75 / T^2 \quad (3)$$

The reported enthalpy increment values and calculated enthalpy increment and heat capacity values, using above polynomial fits, for corresponding temperatures are compared in tables 2 and 3. As mentioned in most of the literature work on  $\text{HfO}_2$ , the compound undergoes transition over a range of temperature. The plot of enthalpy increment vs. temperature, shown in fig. 2, clearly indicates that the enthalpy increment values in the temperature range 2039 K to 2134 K correspond to this transition. Therefore, the enthalpy increment values of Fortov et al. [14], for temperatures  $\geq 2134$  K were used to get the following, temperature dependent, polynomial fit for tetragonal phase of  $\text{HfO}_2$ :

$$\Delta H_{298.15\text{K}}^T (\text{J/mol}) = 48227.1499 + 19.89111 T + 0.01309 T^2 \quad (4)$$

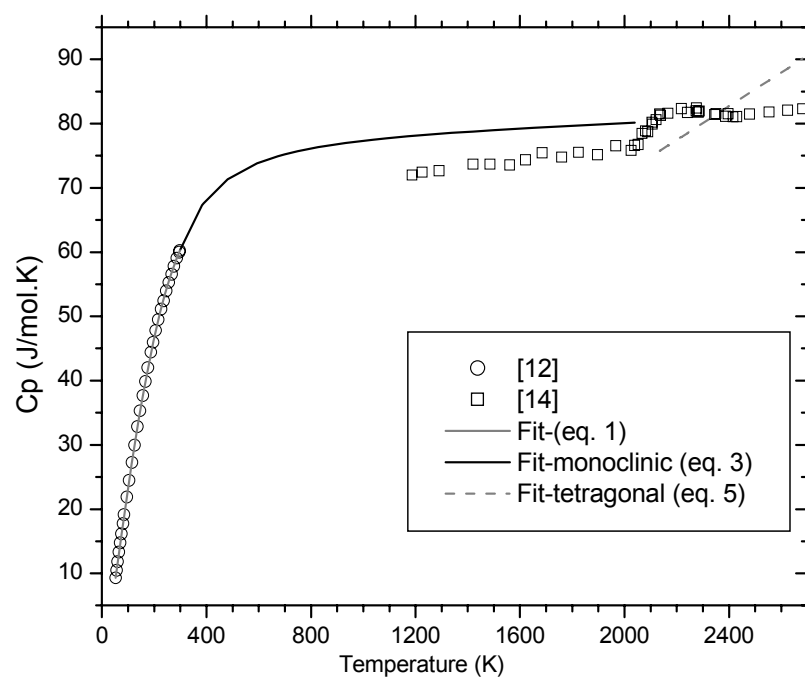


FIG. 1. A comparison of reported heat capacity data with present calculations.

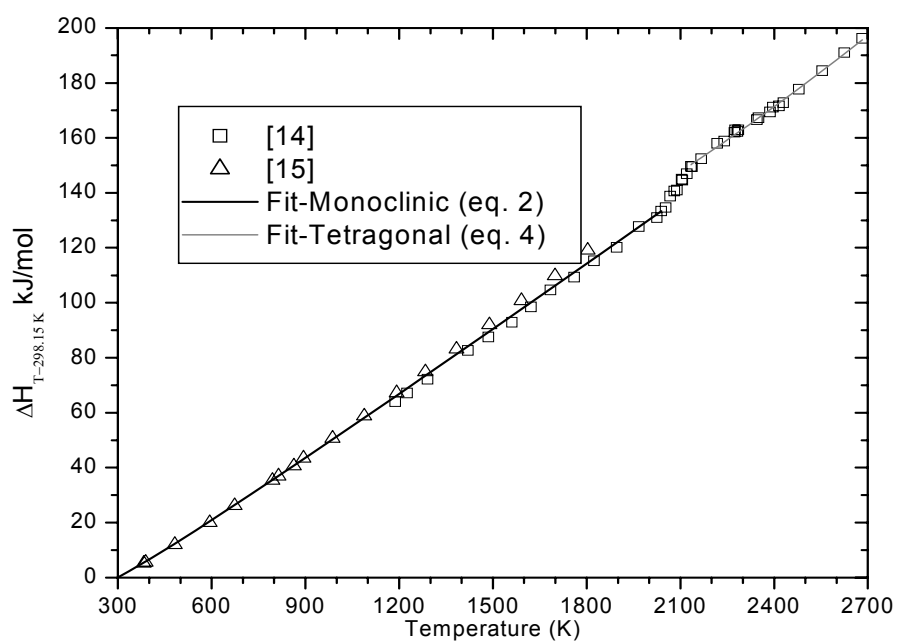


FIG. 2. A comparison of reported enthalpy increment data with present calculations.

The following heat capacity equation calculated by temperature differential of the above equation was used for calculating the heat capacity of tetragonal phase of HfO<sub>2</sub>. The values are plotted in the Fig. 1. It can be seen that in the case of HfO<sub>2</sub> there is a decrease in heat capacity for the high temperature tetragonal phase compared to low temperature monoclinic phase. This is a trend similar to the one observed by Curtis et al. [1] during lattice studies using XRD and by Ohnysty and Rose [2] during linear thermal expansion measurement. This may be due to difference in bond strength, causing inversion transition.

$$C_p \text{ (J/mol.K)} = 19.89111 + 0.02618 T \quad (5)$$

The mean heat capacity values given by Fortov et al. [14], were calculated by them from the enthalpy increment data, using the following relation:

$$C_p^{\text{mean}} = \Delta H_{298.15K}^T / (T - 298.15) \quad (6)$$

The mean heat capacity values calculated using this relation at such high temperatures are very unreliable. Heat capacity is a differential value,  $dH/dT$ , which can be taken as  $\Delta H/\Delta T$  only over a narrow temperature range. The calculation using,  $(H_T - H_{298.15})/(T - 298.15)$ , assumes that  $C_p$  is linear in the temperature range, 298.15 K to  $T$ . Then using a polynomial equation to express the  $C_p$  values is contradictory in itself. Therefore, the best method to calculate heat capacity values from enthalpy increment data is to find out a most suitable polynomial fit for the enthalpy increment data and then calculate a temperature differential of the equation to get a  $c_p$  polynomial. Particularly, during and after the first order transition, use of equation (6) for the calculation of heat capacity is equivalent to ignoring the fact that heat capacity equation is discontinuous at transition temperature. In other words, heat of transition cannot be included in the calculation of heat capacity. The effect of this is seen clearly in the heat capacity values given by Fortov et al., during the temperature range of transition, monoclinic→tetragonal (2039–2134 K). Even at temperatures higher than 2134 K, when the transition is complete, the heat capacity values calculated using equation (6) are expected to be much higher than the actual value, as they include the heat change due to transition as well.

Using the equations (2) and (4) for the enthalpy increments of monoclinic and tetragonal phases, respectively, and implementing the following relation, experimentally determined enthalpy increment values of Fortov et al. were used to estimate the percentage transition in the temperature range 2039–2134 K.

$$\begin{aligned} \% \text{ transition at } T &= 100 \{ \Delta H_{298.15K}^T(\text{exp}) - \Delta H_{298.15K}^T(\text{mono}) \} / \{ \Delta H_{298.15K}^T(\text{tetra}) - \Delta H_{298.15K}^T(\text{mono}) \} \\ &= 100 \{ \Delta H_{298.15K}^T(\text{exp}) - \Delta H_{298.15K}^T(\text{eq.2}) \} / \{ \Delta H_{298.15K}^T(\text{eq. 4}) - \Delta H_{298.15K}^T(\text{eq. 2}) \} \quad (7) \end{aligned}$$

The % transition values calculated using the above relation are given in table 4. By extrapolating enthalpy increment values to the accepted temperature of transition for monoclinic→tetragonal, 1973 K, the enthalpy of transition is calculated as 10.38 kJ/mol.

Table 1. A comparison of low temperature heat capacity values reported by Todd [12] with calculated values.

T(K)	Cp (J/mol.K)	
	Todd [[12]]	Fit (eq. 1)
52.47	9.27174	9.27123
56.55	10.45582	10.5277
60.7	11.79051	11.8036
65.29	13.29257	13.2082
70.13	14.7486	14.6782
74.9	16.12095	16.113
80.36	17.72761	17.7361
85.12	19.08741	19.1328
94.99	21.84048	21.9706
104.57	24.45548	24.6456
114.6	27.22529	27.3589
124.63	29.92815	29.9807
136.02	32.81511	32.8451
146.13	35.29204	35.2861
156.02	37.656	37.5809
166.07	39.84423	39.8181
176.11	42.00736	41.9574
187.91	44.39224	44.3491
196.35	45.94032	45.9784
206.35	47.78128	47.8208
216.37	49.45488	49.5711
226.34	51.08664	51.2174
236.13	52.42552	52.7415
245.94	53.93176	54.1766
256.36	55.27064	55.6001
266.38	56.52584	56.8708
276.25	57.78104	58.0284
286.5	59.03624	59.1317
296.34	59.95672	60.0961
298.16	60.2496	60.2643

Table 2. A comparison of measured enthalpy increment values and the average heat capacity values calculated reported by Fortov et al [14] with calculated values.

T(K)	$\Delta H_{298.15\text{ K}}^{\text{T}}$ (J/mol)			Cp (J/mol.K)		
	Exp. [[14]]	(eq 2)	(eq 4)	[[14]]	(eq 3)	(eq 5)
1187	63975	65853		71.9754	78.0718	
1226	67187	68900		72.4118	78.2026	
1291	72126	73990		72.6457	78.4069	
1420	82655	84128		73.6776	78.7726	
1486	87515	89333		73.6751	78.9439	
1561	92877	95261		73.5455	79.1285	
1622	98435	100092		74.3549	79.2720	
1685	104639	105091		75.4509	79.4150	
1760	109277	111053		74.7526	79.5792	
1824	115239	116151		75.5243	79.7149	
1897	120136	121975		75.1388	79.8656	
1967	127752	127571		76.5507	80.0064	
2025	130931	132215		75.8207	80.1207	
2039	133346	133336		76.5982	80.1481	
2053	134633	-		76.7205	-	
2067	138774	-		78.4545	-	
2081	140595	-		78.8599	-	
2089	140982	-		78.7233	-	
2105	144925	-		80.2086	-	
2107	144553	-		79.9144	-	
2121	146905	-		80.5908	-	
2134	149613		150286	81.4952		75.759
2138	149504		150589	81.2588		75.864
2167	152452		152800	81.5754		76.623
2218	158022		156742	82.3098		77.958
2241	158748		158542	81.7091		78.56
2274	161978		161149	81.979		79.424
2275	162904		161228	82.4057		79.451
2283	162285		161865	81.7617		79.66
2286	162879		162104	81.9374		79.739
2345	166623		166854	81.4046		81.283
2350	167354		167261	81.5624		81.414
2387	169415		170291	81.1044		82.383
2397	171140		171116	81.54		82.645
2416	171617		172691	81.0335		83.142
2430	172790		173858	81.0516		83.509
2479	177666		177981	81.4665		84.791
2554	184480		184414	81.7787		86.755
2625	190992		190640	82.0817		88.614
2682	196172		195733	82.2921		90.106

Table 3. A comparison experimentally determined enthalpy increment values, reported by Orr [[15]], with calculated values.

T(K)	$\Delta H^T_{298.15\text{ K}}$ (J/mol)		Cp (eq 3) J/mol.K
	Exp. [15]	Fit (eq. 2)	
382.7	5230	5437	67.281
388.6	5565	5835	67.611
481.5	12008	12308	71.350
593.7	20020	20465	73.824
673.3	26171	26388	74.932
794.4	35397	35538	76.090
814.1	36945	37038	76.239
862.5	40585	40736	76.572
894.3	43472	43174	76.768
986.5	50668	50276	77.260
1088	58785	58141	77.705
1192.5	67237	66282	78.091
1283.9	74810	73433	78.385
1383.4	83136	81247	78.673
1488.6	91964	89538	78.950
1591.2	100751	97652	79.200
1698.3	109830	106147	79.445
1803.6	119118	114525	79.672

Table 4. Estimation of percentage transition (monoclinic→tetragonal) from the enthalpy increment values.

T (K)	$\Delta H^T_{298.15\text{ K}}$ (J/mol)			% transition
	Fortov et al. [14]	Monoclinic (eq 2)	Tetragonal (eq 4)	
2039	133346	133336	143207	0.097
2053	134633	134459	144235	1.78
2067	138774	135581	145269	32.96
2081	140595	136704	146308	40.51
2089	140982	137346	146903	38.04
2105	144925	138630	148100	66.47
2107	144553	138791	148250	60.915
2121	146905	139915	149303	74.45
2134	149613	140959	150286	92.79



## REFERENCES TO SECTION 6.3.2

- [1] CURTIS, C.E., DONEY, L.M. and JOHNSON, J.R., J. American Ceramic Society, Vol. 37, No. 10 (1954) 458-465.
- [2] OHNYSTY, B. and ROSE, F.K., J. Am. Ceramic Soc., 47, 8 (1964) 398-400.
- [3] RUH, R., GARRETT, H.J., DOMAGALA, R.F. and TALLAN, N.M., J. Am. Ceramic Soc., 51, 1 (1968) 23-27.
- [4] BOGANOV, A.G., RUDENKA, V.S. and MAKAROV, L.P., Dokl. Akad. Nauk SSSR, 160, 5 (1965) 1065-1068.
- [5] BOCQUILLON, G., SUSSE, C., VODAR, B., Rev. Int. Hautes Temp. Refract., 5 (1968) 24, quoted in JCPDS-ICDD, X-ray diffraction file (1995), Card No. (21-904).
- [6] ROTH, W.A. and BECKER, G., Z. Phys. Chem., 159 A (1932) 1.
- [7] HUMPHREY, G.L., J. Am. Chem. Soc., 75 (1953) 2806.
- [8] PAPUTSKIY, YU.N., KRZHIZHANOVSKAYA, V.A., GLUSHKOVA, V.B., Izv. Akad. Nauk SSSR, Neorg. Mater., 10 (1974) 1551.
- [9] HUBER, E.J., JR. and HOLLEY, C.E., JR., J. Chem. Eng. Data, 13 (1968) 252.
- [10] KORNILOV, A.N. and USHAKOVA, I.M., Dokl. Akad. Nauk SSSR, 200 (1971) 1382.
- [11] KORNILOV, A.N., USHAKOVA, I.M., HUBER, E.J., JR. and HOLLEY, C.E., JR., J. Chem. Thermodynamics, 7 (1975) 21-26.
- [12] TODD, S.S., J. Am. Chemical Soc., 75 (1953) 3035-3036.
- [13] KELLEY, K.K., U.S. Bur. Mines Bulletin 477 (1950).
- [14] FORTOV, V., ONUFRIEV, S., PELETSKY, V., PESOCHIN, V., PETUKHOV, V. and TARASOV, V., Private Communication.
- [15] ORR, R.L., J. Am. Chem. Soc., 75 (1953) 1231-1232.
- [16] SHOMATE, C.H., J. Phys. Chem. 58 (1954) 368.

## 6.4. Structural materials

This chapter contains data on some Russian steels provided by IPPE and recommendations and measured data on the steam generator tubing alloys I600 and I800, which were provided by AECL.

Section 6.4.1 contains the Russian steel data and Section 6.4.2 contains the AECL assessment.

### 6.4.1. Russian steels

In the database of IPPE four “types” of data are generally stored:

- experimental (E-data),
- evaluated (V-data) – any data that are not the primary experimental ones,
- recommended (R-data) – the data chosen by the expert group as the most reliable ones,
- standard (S-data) – official standard (reference) data in Russia, prepared by the State Committee of Standards.

The purpose of this investigation was to recommend the most reliable data. The available data for a number of steels were examined in this study. Table 1 contains a summary listing of the examined steel types and their properties. The table also identifies the type of data (E, V, R or S) available for this examination. When S- or R-data were unavailable the V-data were presented to the experts for consideration. In the absence of any information, the goal was to use the properties of steels with similar chemical composition (“Steel Analogues”) as recommendations. When examining the chemical composition of the steels for “similarity”, special attention should be given to minor concentration of doping elements, which may affect the property under consideration. In this chapter, the “phonetic” translation for Russian steels names was used.

Information about foreign steels-analogues was taken from “Database of metals and alloys” of the Information and Marketing Center of Moscow State Institute of Steels and Alloys (<http://imc.misa.ac.ru/English/index.htm>).

The data presented in Table 1 were collected from 36 references. The notations of the various properties are:  $\rho$  - density,  $H$  – enthalpy,  $C_p$  – heat capacity,  $\lambda$  - thermal conductivity,  $a$  – thermal diffusivity,  $\alpha$  - thermal linear expansion coefficient,  $\rho_{el}$  – electrical resistance,  $L$  – Lorenz number. The maximum temperature for the property under consideration and the “type” of data referred to above are noted in the table. The additional notations are: PT – phase transition,  $T_l$  and  $T_s$  – liquidus/solidus temperatures.

Table 1. Available data on thermo-physical properties of Russian reactor steels

STEEL	PT	$\rho$	H	$C_p$	$\lambda$	a	$\alpha$	$\rho_{el}$	L
22K	-	1100°C (V)	943 K (E)	500°C (V)	1200°C (V)	-	1200°C (V)	1200°C (V)	-
VSt3sp	-	-	-	-	700°C (V)	-	600°C (V)	-	-
10KhSND	-	-	-	-	600°C (V)	-	600°C (V)	-	-
10KhN1M	-	-	-	-	-	-	600°C (V)	-	-
10KhN2MA	-	-	-	-	-	-	600°C (V)	-	-
10N3MFA	-	-	-	-	-	-	-	-	-
10GN2MFA	-	-	1256 K (E)	-	-	-	600°C V()	-	-
15Kh2MFA	-	-	-	-	-	-	600°C (V)	-	-
15Kh2NM1FA	-	-	-	-	-	-	-	-	-
15Kh2NMFA	-	-	1050 K (E)	-	1300°C (E)	-	600°C (V)	-	-
15Kh3NMFA	-	-	-	-	-	-	600 °C V	-	-
25Kh3MFA	-	-	-	-	-	-	-	-	-
12Kh1MF	-	1200 K (V)	-	1000C (V)	900°C (V)	900°C (V)	1200 K (V)	900°C (V)	900°C (V)
12Kh2MFB	-	-	-	-	900°C (V)	-	900°C (V)	800°C (V)	-
15Kh1M1F	-	600°C (V)	-	-	600°C (V)	-	600°C (V)	700°C (V)	-
25Kh1MF	-	600°C (V)	-	1200°C (E)	1200 K (V)	-	1200 K (V)	700°C (V)	600°C (V)
25Kh2M1F	-	600°C (V)	-	600°C (V)	714°C (VE)	-	600°C (V)	714°C (VE)	-
08Kh18N10T	T <sub>L</sub> , T <sub>S</sub> , etc	-	970 K (E)	-	300°C (V)	-	700°C (V)	-	-
08Kh18N12T	-	-	-	-	-	-	600°C (V)	-	-
12Kh18N10T	T <sub>L</sub> , T <sub>S</sub>	-	1380 K (S)	1380 K (S)	1100°C (VE)	1100°C (E)	1650 K (S)	700°C (V)	-
12Kh18N12T	-	900°C (V)	-	1200°C (V)	1200°C (V)	1200°C (V)	900°C (V)	1200°C (V)	-
12Kh18N9TL	-	-	-	900°C (V)	-	900°C (V)	900°C (V)	900°C (V)	-
08Kh18N9T	-	-	-	900°C (V)	900°C (V)	900°C (V)	900°C (V)	900°C (V)	900°C (V)
12Kh18N9T	T <sub>int</sub>	1400 K (V)	-	1200°C (V)	1200°C (V)	1200°C (V)	1400 K (V)	1200°C (V)	-
18Kh12VMBFR	-	1400 K (V)	-	1400 K (V)	1400 K (V)	-	1400 K (V)	700°C (V)	-
10Kh11N20T3R	T <sub>L</sub> , T <sub>S</sub>	700°C (V)	-	800°C (V)	900°C (V)	-	700°C (V)	-	-
KhN35VT	-	800°C (V)	-	1300°C (V)	1400 K (V)	800°C (V)	1200 K (V)	850°C (V)	850°C (V)
KhN35VTYu	-	900°C (V)	-	-	900°C (V)	-	900°C (V)	-	-

#### 6.4.1.1. Review of data analysis procedure

The regression data analysis used to obtain the recommendations is based on the least squares method (LSM) and includes estimation of covariance matrices of regression parameters. The fundamentals of statistical procedures can be found in [1], the practice of covariance matrices generation is reviewed in [2–5] and the practice of covariance matrices using is discussed in [6]. Here, the linear regression models are considered; the same results are valid for nonlinear models as linear approximation (see references).

LSM task is:

$$M = \sum_1^N [F_i - F(t; \theta)]^2 / W_i^2 \Rightarrow \min = (N-L) \cdot s^2$$

$$F(t; \theta) = \sum_{i=1}^L \theta_i x^{i-1} \quad (1)$$

$$\partial M / \partial \theta_j |_{\min} = 0$$

Here  $N$  is the number of experimental points,  $L$  is the number of parameters  $\theta$ ,  $W_i$  are statistical weights for each experimental point connected with prior information about experimental errors distribution. In the case of normal distribution of errors,  $(M/s^2)$  has the  $\chi^2$ -distribution with  $(N-L)$  degrees of freedom.

After defining

$$C_{ij} = \frac{1}{2} \frac{\partial^2 M}{\partial \theta_i \partial \theta_j}, \quad (2)$$

we have for the covariance matrix ( $L \times L$ ) of parameters  $\theta$ :

$$\mathbf{D}(\theta) = s^2 \cdot \mathbf{C}^{-1} / (N-L) \quad (3)$$

and for the covariance matrix ( $N \times N$ ) of *mean* values of  $F(t; \theta)$

$$D_{mn}[F(t; \theta)] = \sum_{i,j=1}^L \frac{\partial F(t; \theta)}{\partial \theta_i} \Big|_{t=t_m} D_{ij}(\theta) \frac{\partial F(t_n; \theta)}{\partial \theta_j} \Big|_{t=t_n} \quad (4)$$

The diagonal elements  $D_{mm}[F(t_m; \theta)]$  are the estimates of squares of  $F(t_m; \theta)$  standard errors and the "errors band" for the *mean values* of regression  $F(t; \theta)$  can be defined as

$$\Delta^2[F(t_m; \theta)] = t_{N-L; \alpha/2}^2 \cdot D_{mm}[F(t; \theta)], \quad (5)$$

where  $t_{N-L; \alpha/2}$  is the  $\alpha$ -quantile of  $t$ -distribution.

The covariance matrix  $\mathbf{D}(\theta)$  can be used within usual procedure of errors propagation when the regression  $F(t; \theta)$  is used for calculation as the estimate of a property value.

#### 6.4.1.2. Properties of austenitic steels

The most important austenitic Russian steels are: 08Kh18N10T, 08Kh18N12T, 12Kh18N10T and 12Kh18N12T. They are used for manufacturing core elements of Russian WWER-type reactors, such as fuel assemblies, spacer grids, reactor vault, shroud, protective piping, primary pipelines.

##### **Properties of steel: 08Kh18N10T**

The chemical composition of the steel is given below.

Element	C	Si	Mn	Cr	Ni	Ti	S	P
Content, %	≤0.08	≤0.8	1.5-2.0	17-19	9-11	5·C≤0.7 (0.4-0.6)	≤0.02	≤0.035

The foreign analogues are: Germany – X8CrNiTi18-10 (DIN 17460), USA – AISI 321 and S32100, Japan – SUS Y 321. The properties of foreign steels-analogues are not available.

#### *Solidus/liquidus temperature*

$T_L = 1446^\circ\text{C}$ ;  $T_S = 1416^\circ\text{C}$ ; over the range  $1200^\circ\text{C} - T_S$   $c_p = 0.622 \text{ kJ}/(\text{kg}\cdot\text{K})$ ; over the range  $1550^\circ\text{C} - T_L$   $c_p = 0.756 \text{ kJ}/(\text{kg}\cdot\text{K})$ ;  $q = 287 \text{ kJ/kg}$  ( $q$  – crystallization heat) [7].

#### *Enthalpy*

The recommended formula has been obtained using the experimental data [8].

$$H_T - H_{273} = -136.335 + 466.01 \cdot t + 67.3146 \cdot t^2, \quad (6)$$

where enthalpy in kJ/kg,  $t = 0.001T$  in K,  $406 \text{ K} \leq T \leq 969 \text{ K}$ . The mean square root error is 0.3%, the parameter covariance matrix is:

	Intercept	t	t <sup>2</sup>
Intercept	12.3055	-43.18295	34.40955
T	-43.18295	153.8046	-124.5734
t <sup>2</sup>	34.40955	-124.5734	103.2964

*Note:* In [9], the standard data for enthalpy of the steels 12Kh18N9T and 12Kh18N10T are presented. The actual composition of the steels is similar to that of the steel under consideration. In relation to enthalpy, these steels are analogues, so the data from [9] can be used for  $1380 \geq T$ ,  $K > 969$ .

#### *Density*

$\rho = 7900 \text{ kg/m}^3$  at  $T=293\text{K}$ .

#### *Coefficient of linear thermal expansion*

The recommended formula has been obtained using the evaluated data [10] for interval values ( $T-293$ ), K:

$$\alpha \cdot 10^6 = 14.3675 + 4.9497 \cdot t, \quad (7)$$

where  $\alpha$  is in  $1/\text{K}$ ,  $t = 0.001 \cdot T$  in K, where  $373 \text{ K} \leq T \leq 973 \text{ K}$ . The mean square root error is 0.8%, the parameter covariance matrix is:

	Intercept	T
Intercept	0.070753	-0.09793
t	-0.09793	0.15185

*Note:* In [11], the standard data on the coefficient of linear thermal expansion for the steel 12Kh18N10T are presented. The real composition of steel is similar to that of the steel under consideration. With respect to the linear thermal expansion, this two steels are analogues, so the data from [11] can be used for  $1650 \geq T$ ,  $K > 973$ .

#### *Coefficient of thermal conductivity*

The recommended formula has been obtained using the evaluated data [10].

$$\lambda = 10.436 + 15.274 \cdot t, \quad (8)$$

where  $\lambda$  is in  $\text{W}/(\text{m}\cdot\text{K})$ ,  $t = 0.001T$  in K, where  $373 \leq T \leq 573$ . The mean square root error is 1.6%, the parameter covariance matrix is

	Intercept	T
Intercept	1.7538	-3.6853
T	-3.6853	7.9879

**Properties of steel: 08Kh18N12T**

The chemical composition is given below:

Element	C	Si	Mn	Cr	Ni	Ti	S	P	Cu
Content, %	≤0.08	≤0.8	1.5-2.0	17-19	11-13	5·C ≤0.6	≤0.02	≤0.035	≤0.30

The foreign analogues are: Germany - X8CrNiTi18-10 (DIN 17460), USA – AISI 321 and S32100, France – Z 6 CNT 18-12. The properties of foreign steels-analogues are not available.

No information is available.

**Properties of steel: 12Kh18N10T**

The chemical composition is given below:

Element	C	Si	Mn	Cr	Ni	Ti	S	P	Cu
Content, %	≤0.12	≤0.8	≤2.0	17-19	9-11	5·C ≤0.8	≤0.02	≤0.035	≤0.30

Foreign analogues are: Germany - X12CrNiTi18-9 (SEW 470), USA - 321H (AISI 321H), France - Z 10 CNT 18.11 (NF).

*Solidus/liquidus*

$T_L = 1459^\circ\text{C}$ ;  $T_S = 1403^\circ\text{C}$  [7].

Melting temperature -  $1400^\circ\text{C}$ , [12].

*Enthalpy*

The standard data are presented in [9] in a table form. It was declared that for 95% confidence level the error is less than 1%. These data have been approximated with the equation

$$H_T - H_{298.15} = 12.32651182 + 852.18459835 \cdot t - 476.10633309 \cdot t^{1/2}, \quad (9)$$

where the enthalpy is in kJ/kg,  $t = 0.001 \cdot T$  in K,  $400 \text{ K} \leq T \leq 1380 \text{ K}$ . Because the fitting error is less than 1%, this equation is statistically equivalent to the standard table data. A covariance matrix cannot be obtained because the statistical properties of data used to get the equation (4) are rather complicated and are not well known.

*Coefficient of linear thermal expansion*

The recommended equation for mean values presented in [11] as the standard data is

$$\alpha_m \cdot 10^6 = -377.2/T + 16.305 + 3.096 \cdot 10^{-3} \cdot T, \quad (10)$$

where  $\alpha_m$  is in  $1/\text{K}$ . The temperature range is  $400 \text{ K} \leq T \leq 1650 \text{ K}$  and the mean square root error is  $5 \cdot 10^{-8} \text{ 1/K}$ . The estimated error for 95% confidence varies from  $3 \cdot 10^{-8}$  for low temperatures to  $10 \cdot 10^{-8}$  for the highest temperature.

*Coefficient of thermal conductivity*

The recommended formula has been obtained using the evaluated data [10, 13, 14].

$$\lambda = 10.466 + 15.4145 \cdot t, \quad (11)$$

where  $\lambda$  is in  $\text{W}/(\text{m} \cdot \text{K})$ ,  $t = 0.001 \cdot T$  in K. The temperature range is  $293 \text{ K} \leq T \leq 1173 \text{ K}$  and the mean square root error is 2.65%. The experimental data from [15] are more than 15% lower than those used for the analysis, so they were not used. The parameter covariance matrix is

	Intercept	t
Intercept	0.0763	-0.1071
T	-0.1071	0.1759

### *Coefficient of electrical resistance*

The recommended formula has been obtained using the evaluated data [10, 14].

$$\rho_{el} = 0.792413 + 0.404657 \cdot t - 0.0548338 \cdot t^{1/2}, \quad (12)$$

where  $\rho_{el}$  is in  $\mu\Omega/m$ ,  $t = 0.001 \cdot T$  in K. The temperature range is  $293 \text{ K} \leq T \leq 973 \text{ K}$  and the mean square root error is 0.88%. It should be noted that the data from [10] are systematically higher than the data from [14] by approximately 1.4%. The parameter covariance matrix is:

	Intercept	t	$t^{1/2}$
Intercept	0.00136385	-0.001179926	-0.000339381
t	-0.001179926	0.0010521944	0.0002864339
$t^{1/2}$	-0.000339381	0.0002864339	0.0000872806

### *Thermal diffusivity*

The data used were experimental data [15] after heat treatment: heating up to 1200°C, hold-up 0.5 hours, cooling in the air. Error band: 2–5%. The chemical composition is given below.

Element	C	Mn	Si	P	S	Ni	Cr	Mo	Cu	V	Ti
%	0.12	1.7	0.75	0.03	0.02	9	17	0.3	0.3	0.2	0.8

The recommended formula is as follows:

$$a \cdot 10^6 = 2.735047 + 1.319441 \cdot t, \quad (13)$$

where  $a$  is in  $m^2/s$ ,  $t = 0.001 \cdot T$  in K, where  $373 \text{ K} \leq T \leq 1373 \text{ K}$ , the mean square root error is 0.89%. The parameter covariance matrix is:

	Intercept	t
Intercept	0.0008556135	-0.000915404
t	-0.000915404	0.0011054555

### ***Properties of steel: 12Kh18N12T***

The chemical composition is given below:

Element	C	Si	Mn	Cr	Ni	Ti	S	P	Cu
Content, %	$\leq 0.12$	$\leq 0.8$	$\leq 2.0$	17-19	11-13	$5 \cdot C \leq 0.7$	$\leq 0.02$	$\leq 0.035$	$\leq 0.30$

Foreign steel-analogues were not found.

### *Density*

The recommended formula has been obtained using the evaluated data [10, 16].

$$\rho \cdot 10^{-3} = 8.019696 - 0.40955 \cdot t - 0.017589 \cdot t^3. \quad (14)$$

where  $\rho$  is in  $kg/m^3$ ,  $t = 0.001 \cdot T$ , K. The temperature range is  $293 \text{ K} \leq T \leq 1173 \text{ K}$  and the mean square root error is 0.05%. The parameter covariance matrix is

	Intercept	T	$t^3$
Intercept	0.0000222914	-0.00004844	0.0000250534
T	-0.00004844	0.0001138591	-0.000063252
$t^3$	0.0000250534	-0.000063252	0.0000390561

### *Coefficient of linear thermal expansion*

In [17], the evaluated data are presented for the *true coefficient of thermal expansion*; heat treatment conditions are water hardening from 1100°C.

$t, ^\circ\text{C}$	773	873	973
$\alpha \cdot 10^6, 1/\text{K}$	21.2	21.3	21.95

The recommended formula has been obtained using the evaluated data for *mean values* in interval (293 K-T) [10].

$$\alpha_m \cdot 10^6 = 16.4246 + 4.871 \cdot t - 2.6314 \cdot t^{1/2}, \quad (15)$$

where  $\alpha$  is in  $1/\text{K}$ ,  $t = 0.001 \cdot T$  in K. The temperature range is  $373 \text{ K} \leq T \leq 1173 \text{ K}$  and the mean square root error is 0.2%. The experimental data from [17] are 4.6% higher than those from [10] and were not used. The parameter covariance matrix is:

	Intercept	$t$	$t^{1/2}$
Intercept	0.29701	0.41841	-0.71611
$T$	0.41841	0.60632	-1.02408
$t^{1/2}$	-0.71611	-1.02408	1.74074

### *Specific heat*

The recommended formula has been obtained using the data from [10, 16].

$$c_p = 286.9706 + 293.4695 \cdot t^{1/2}, \quad (16)$$

where  $c_p$  is in  $\text{J}/(\text{kg} \cdot \text{K})$ ,  $t = 0.001 \cdot T$  in K. The temperature range is  $373 \text{ K} \leq T \leq 1473 \text{ K}$  and the mean square root error is 0.95%. The parameter covariance matrix is:

	Intercept	$t^{1/2}$
Intercept	35.4281	-39.218
$t^{1/2}$	-39.218	45.219

### *Coefficient of thermal conductivity*

The recommended formula has been obtained using the evaluated data [10, 16].

$$\lambda = 10.466 + 15.4145 \cdot t, \quad (17)$$

where  $\lambda$  is in  $\text{W}/(\text{m} \cdot \text{K})$ ,  $t = 0.001 \cdot T$  in K. The temperature range is  $293 \text{ K} \leq T \leq 1473 \text{ K}$  and the mean square root error is 1.85%. The parameter covariance matrix is:

	Intercept	$T$
Intercept	0.0763034	-0.1071
$T$	-0.1071	0.1759

### *Thermal diffusivity*

The recommended formula has been obtained using the evaluated data [16].

$$a \cdot 10^6 = 3.1395 + 2.8019 \cdot t, \quad (18)$$

where  $a$  is in  $\text{m}^2/\text{s}$ ,  $t = 0.001 \cdot T$  in K. The temperature range is  $293 \text{ K} \leq T \leq 1473 \text{ K}$ , the mean square root error is 0.17%. The parameter covariance matrix is:

	Intercept	$t$
Intercept	0.000050366	-0.00005328
$T$	-0.00005328	0.00006623



### *Coefficient of electrical resistance*

The recommended formula has been obtained using the evaluated data [10, 16].

$$\rho_e \cdot 10^9 = 277.25 + 854.332 \cdot t^{1/2}, \quad (19)$$

where  $\rho_e$  is in  $\Omega \cdot m$ ,  $t = 0.001 \cdot T$  in K, the range is  $293 \text{ K} \leq T \leq 1473 \text{ K}$ , the mean square root error is 0.89%. The parameter covariance matrix is :

	Intercept	$t^{1/2}$
Intercept	66.097	-78.68
$t^{1/2}$	-78.68	99.27

### *6.4.1.3. Properties of perlitic and carbon steels*

Here under consideration are the steels used to fabricate pressure vessel of WWER-type reactors and other equipment.

#### ***Properties of steel: 15Kh2NMFA***

The chemical composition of the steel is given below.

Element	C	Si	Mn	Cr	Ni	Mo	V	S	P	Cu
Content, %	0.13-0.18	0.17-0.37	0.3-0.6	1.8-2.3	1.0-1.5	0.5-0.7	0.10-0.12	$\leq 0.02$	$\leq 0.02$	$\leq 0.3$

Foreign analogues of this steel are unknown.

### *Coefficient of linear thermal expansion*

The recommended formula has been obtained using the evaluated data for the group of steels [19], which can be considered as the recommendations of MinAtom of Russia.

$$\alpha \cdot 10^6 = 6.450979 - 0.609934 \cdot t^3 + 8.928218 \cdot t^{1/2}, \quad (20)$$

where  $\alpha$  is in  $1/\text{K}$ ,  $t = 0.001 \cdot T$  in K. The temperature range is  $323 \text{ K} \leq T \leq 873 \text{ K}$  and the mean square root error is 0.17%. The parameter covariance matrix is:

	Intercept	$t^3$	$t^{1/2}$
Intercept	0.0153275778	0.0136719436	-0.024813799
$t^3$	0.0136719436	0.0142046658	-0.022841317
$t^{1/2}$	-0.024813799	-0.022841317	0.0405080211

#### ***Properties of steel: 15Kh2N1MFA (VK-2M)***

The chemical composition of the steel is given below:

Element	C	Si	Mn	Cr	Ni	Mo	V	S	P	Cu
Content, %	0.12-0.16	0.17-0.37	0.3-0.6	1.7-2.2	0.8-1.5	0.8-1.1	0.08-0.15	$\leq 0.02$	$\leq 0.02$	$\leq 0.15$

Foreign analogues are unknown.

No information available.

#### ***Properties of steel: 15Kh3NMFA (VK-2)***

The chemical composition is given below:

Element	C	Si	Mn	Cr	Ni	Mo	V	S	P	Cu
Content, %	0.12-0.16	0.17-0.37	0.3-0.6	2.2-2.7	0.8-1.3	0.5-0.8	0.08-0.15	$\leq 0.02$	$\leq 0.02$	$\leq 0.15$

Foreign analogues are unknown.

*Coefficient of linear thermal expansion*

See recommendation for the steel 15Kh2NMFA.

**Properties of steel: 15Kh2MFA (TS-3-40)**

The chemical composition is given below:

Element	C	Si	Mn	Cr	Ni	Mo	V	S	P	Cu
Content, %	0.13-0.18	0.17-0.37	0.3-0.6	2.5-3.0	≤0.4	0.6-0.8	0.25-0.35	≤0.025	≤0.025	≤0.025

Foreign analogues are unknown.

*Coefficient of linear thermal expansion*

See recommendation for the steel 15Kh2NMFA.

**Properties of steel: 25Kh3MFA (TS-4)**

The chemical composition is given below:

Element	C	Si	Mn	Cr	Ni	Mo	V	S	P	Cu
Content, %	0.22-0.27	0.17-0.37	0.3-0.6	2.8-3.3	≤0.4	0.6-0.8	0.25-0.35	≤0.025	≤0.025	≤0.025

Foreign analogues are unknown.

*Coefficient of linear thermal expansion*

See recommendation for the steel 15Kh2NMFA.

**Properties of steel: VSt3sp (Stsp)**

This carbon steel is used to fabricate the upper unit of WWER-1000 reactor. The chemical composition is given below.

Element	C	Si	Mn	Cr	Ni	S	P	Cu
Content, %	0.14-0.22	0.12-0.3	0.4-0.65	≤0.3	≤0.3	≤0.05	≤0.04	≤0.3

The German analogue is C22.3 (DIN 2528) of such composition:

Element	C	Si	Mn	Cr	Ni	S	P	Cu
Content, %	0.18-0.23	0.15-0.35	0.3-0.6	≤0.3	-	≤0.045	≤0.045	≤0.3

*Coefficient of linear thermal expansion*

See recommendation for the steel 15Kh2NMFA.

*Coefficient of thermal conductivity*

The recommended formula has been obtained using the evaluated data [10].

$$\lambda = 60.0799 - 32.9453 \cdot t^2, \quad (21)$$

where  $\lambda$  is in W/(m·K),  $t = 0.001 \cdot T$  in K, where  $393 \text{ K} \leq T \leq 973 \text{ K}$ , the mean square root error is 2.69%. The parameter covariance matrix is:

	Intercept	$t^2$
Intercept	0.9860078865	-1.423741703
$t^2$	-1.423741703	2.5714338285

### 6.4.2 Thermal conductivity of alloy 600 and 800

Alloy 800 and alloy 600 are materials used to fabricate steam generator tubes. These alloys generally follow the ASTM specifications for UNS N0800 and UNS N0600 with minor differences in the chemical composition, which are not expected to have a significant effect on the thermal conductivity. The ASTM specifications for the alloys UNS N0800 and UNS N0600 are given in Table 2. Depending on the manufacturer of these alloys, the alloy 800 is called Inconel 800 (I800) or Sanicro 30 (S30). The alloy 600 is called I600, INCO 600 or Sanicro 70 (S70). This report gives an assessment of the alloy 800 and 600 materials based on available data from the literature.

Table 2. ASTM specifications for UNS N08800 and UNS N06600 Alloys

ELEMENT	UNS N08800	UNS N06600
Nickel	30.0 – 35.0	72.0 min
Chromium	19.0 – 23.0	14.0 – 17.0
Iron	39.5 min.	6.0 – 10.0
Carbon	0.10 max.	0.15 max.
Manganese	1.5 max.	1.0 max.
Sulphur	0.015 max.	0.015 max.
Phosphorus	0.015 max.	0.015 max.
Nitrogen	0.03 max.	0.03 max.
Copper	0.75 max.	0.5 max.
Aluminium	0.15 – 0.60	0.15 – 0.60
Cobalt Average/steam generator	0.015 max.	-
Cobalt absolute/ heat	0.020 max.	-
Titanium	0.15 – 0.60	-
Silicon	1.0 max.	0.5 max.

#### Recommendation

For the thermal conductivity of alloy 800 the following equation is recommended for the temperature range from 375 to 675 K.

$$K = 8.704 + 0.0138 T, \quad (1)$$

where the temperature  $T$  is in [K] and the thermal conductivity  $K$  is in [W/m K]. The standard deviation is 0.305 [W/m K].

For the thermal conductivity of alloy 600 the following equation is recommended for the temperature range from 360 to 900 K.

$$K = 8.116 + 0.0176 T, \quad (2)$$

where the temperature  $T$  is in [K] and the thermal conductivity  $K$  is in [W/m K]. The standard deviation is 0.319 [W/m K].

#### Uncertainty

The uncertainty in the above recommendation is  $\pm 3\%$ .

#### Discussion

##### *Review of measurement techniques and recommendations*

In 1976 Atomic Energy of Canada Ltd. (AECL) sponsored experiments at the Purdue Properties Research Laboratories, at Dynatech and at the AECL Whiteshell Laboratories (Previous WNRE) to measure the thermal conductivity of alloy 800 and 600 materials in the temperature range from 450 to 650 K. The Purdue laboratory used a steady state experimental technique, called the Kohlrausch method, to determine the thermal conductivity of alloy 800 (I800 and S30) and alloy 600 (I600 and

S70) in the axial direction. This method consists of electrically heating a tubular specimen while the ends are cooled. From the temperature gradients in the specimen and power measurements the thermal conductivity was calculated. The same laboratory also measured the thermal conductivity of the same materials in the radial direction using Flash Technique. In this technique one side of the sample disc material is heated by a laser pulse and the temperature rise on the other side is recorded. From the temperature rise the thermal diffusivity is calculated. The thermal conductivity is calculated from known density, specific heat and diffusivity. Dynatech used a heat flow technique to measure the temperature gradient along a tube length, which was heated on one end while the other end was attached to a heat sink. To minimize heat losses, the sample was surrounded with heating elements with a matching temperature gradient. Using this method, the thermal conductivity of S30 and S70 in the axial direction was determined. Also, AECL measured the thermal conductivity of S30, S70 and I800 and I600 in the radial direction using the Flash technique in 1976. The laboratories claim that the uncertainty associated with the above measurements is not greater than  $\pm 3\%$ .

In 1997 AECL measured the thermal conductivity of alloy 800 and alloy 600 steam generator tubes in the axial direction. A steady state experimental technique was used, in which an axial temperature gradient along the tube length was established by supplying heat to one end of the tube, while the other end was cooled. The tube specimen was sandwiched between Armco iron standard tubes of known thermal conductivity. The set up was thermally insulated to minimize radial heat losses. A numerical technique, which accounted for the heat-losses from the test specimens, was developed to evaluate the experimental data and to determine the thermal conductivity of the tube specimen. The numerical technique was applied to an experimental set up in which the test specimen was replaced by an Armco iron standard tube of the same dimensions. The thermal conductivity of the Armco iron standard was reproduced by the same experimental and analytical techniques. The measured data were within  $\pm 2\%$  of the reference standard. The same techniques were applied to determine the thermal conductivity of alloy 800 and alloy 600 materials. The uncertainty for this technique is estimated at  $\pm 2\%$  based on the reference standard measurements. In addition to the measurements conducted by AECL in 1997, AECL sponsored the radial and axial thermal conductivity measurements of I800, S30 and I600 samples at the Anter Laboratories. The axial measurements used a steady state technique similar to Dynatech; the radial measurements used the Flash method. The uncertainty in the Anter data was  $\pm 15\%$  for the axial measurements and  $\pm 5\%$  for the radial measurements.

#### *Thermal conductivity of alloy 800*

In 1997 AECL conducted a rigorous statistical analysis of all the data from Purdue Laboratories, Dynatech, Anter Laboratories and AECL data, which was based on the covariance of temperature versus thermal conductivity of alloy 800 materials of all the data received in 1976 and 1997 [20]. The analysis showed that there was significant difference among the results from the different testers. When the AECL data of 1997 and the Purdue data of 1976 were considered, the difference between the testers was no longer evident. The analysis also showed that there was no evidence to suggest that the thermal conductivity was different in axial and radial directions. There was no strong evidence to suggest that the thermal conductivity of S30 and I800 is different. A strong linear relationship between temperature and thermal conductivity was also derived.

Based on the covariance analysis mentioned above, 88 data points from the 1997 AECL tests and the 1976 Purdue Laboratories for alloy 800 are further analysed and plotted in Figure 1. A linear regression analysis was conducted and the following equation was obtained for the temperature range from 375 to 675 K.

$$K = 8.704 + 0.0138 T, \quad (1)$$

where the temperature  $T$  is in [K] and the thermal conductivity  $K$  is in [W/m K]. The standard deviation is 0.305 [W/m K]. The uncertainty is estimated at  $\pm 3\%$  based on the scatter in the data.

Inco Alloys International Inc. published in 1987 the thermal conductivity data for their alloys [21]. The manufacturer's data for Incoloy 800 are plotted as a dashed line in Figure 1, which shows a small negative deviation from the above results; the slope of the dashed line is slightly higher than prescribed by equation (1). No details are available from the manufacturer on the measurements and analysis techniques used to obtain the data.

For the steam generator operating conditions, in the range from 575 to 600 K, the Incoloy 800 data are within the uncertainty band of  $\pm 2\%$  specified for equation (1).

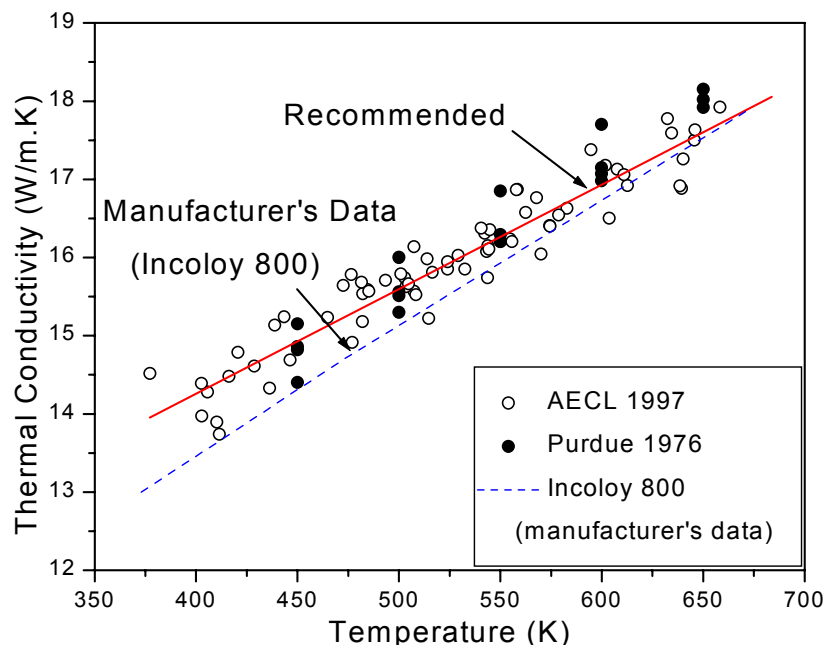


FIG. 1. Thermal conductivity of alloy 800 steam generator tube materials.

#### Thermal conductivity of alloy 600

In 1976 a number of measurements were sponsored by AECL in various Laboratories to measure the thermal conductivity of alloy 600 materials. Additional measurements were conducted in 1997 by AECL. An analysis of the Purdue Laboratories data of 1976 and the 1997 data of AECL [20] was conducted. The Purdue Laboratories data were for I600 and S70 for both the radial and axial directions, whereas the 1997 AECL data were for I600 in the axial direction.

L Filoni and G. Rocchini [22] measured the thermal conductivity of I600 using the axial heat flow method, which is similar to the method used by Dynatech. The technique in reference [22] used computer controls to compensate for the heat losses from the test set up. The published experimental data covered a wide temperature range from 360 to 900 K.

In Figure 2 all the data from Filoni et al., from AECL and from Purdue Laboratories are plotted (77 data points). Figure 2 shows that the AECL and the Purdue data are in good agreement with the data from Filoni et al. A linear regression analysis was conducted and the following equation was obtained for the temperature range from 360 to 900 K.

$$K = 8.116 + 0.0176 T, \quad (2)$$

where the temperature  $T$  is in [K] and the thermal conductivity  $K$  is in [W/m K]. The standard deviation is 0.319 [W/m K]. The uncertainty is estimated at  $\pm 3\%$  based on the scatter in the data.

Inco Alloys International Inc. published in 1987 thermal conductivity data for Inconel 600 [21]. Their data are shown as a dotted curve in Figure 2. The manufacturer's data are slightly above the recommended data for alloy 600. No details are available from the manufacturer on the measurements and analysis techniques used to obtain the data. For the steam generator operating conditions, in the range from 575 to 600 K, the Inconel 600 data by the manufacturer are about 4% higher than equation (2).

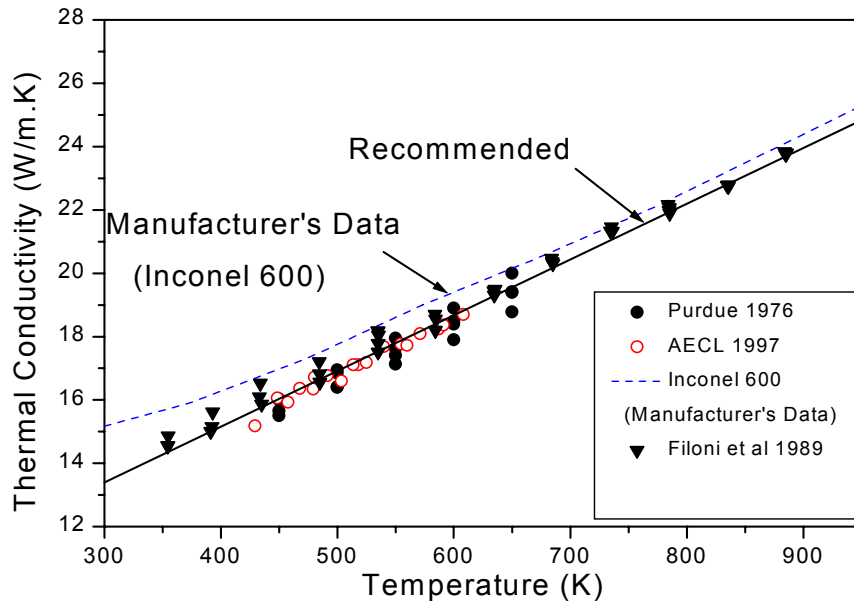


FIG. 2. Thermal conductivity of alloy 600 steam generator tube materials.

#### REFERENCES TO SECTION 6.4

- [1] ZACKS, S., The theory of statistical inference, J. Wiley & Sons, Inc., N.-Y – London – Sidney – Toronto (1971).
- [2] DRAPER, N.R., SMITH, H., Applied regression analysis, 2<sup>nd</sup> ed. J. Wiley & Sons, Inc., N.-Y – Chichester – Brisbane – Toronto – Singapore (1981).
- [3] MAINDONALD, J.H., Statistical computation, J. Wiley & Sons, Inc., N.-Y – Chichester – Brisbane – Toronto – Singapore (1984).
- [4] LEDERMAN, W. (Chief ed.), Handbook of Applicable Mathematics, V.1: Statistics, Part A. J. Wiley & Sons (1984).
- [5] HUDSON, D.J., Statistics, lectures on elementary statistics and probability, CERN, Geneva, 1964, and High Energy and Nuclear Physics Data Handbook, Ed. By W. Galbraith, W.S.C. Williams, Chilton (1963).
- [6] DUNFORD, C.L. (ed.), Int. Symposium on Nuclear Data Evaluation Methodology, BNL, Upton, N.-Y., USA, Oct. 1992, World Scientific Publ. Co., Singapore – New Jersey – London – Hong Kong (1992).
- [7] OSTROVSKY, O.I., GRIGORJAN, V.A., VYSHKAREV, A.F., Properties of metal melts. M., Metallurgia (1988).
- [8] ROSHUPKIN, V.V., FORDEEVA, L.K., Specific Enthalpy and heat capacity of steels 22K, 08Kh18N10T, 15Kh2NMFA and 10GN2MFA, Thermal Physics of High Temperatures, (1988), vol. 25, №5, p. 1016-1020.
- [9] The USSR Standard Reference Data Service. Stainless steels 12Kh18N9T nad 12Kh18N10T. Enthalpy and heat capacity at temperatures from 400 to 1380 K and atmospheric pressure. GSSSD 32-82. Moscow, State Committee of USSR on Standards (1983).
- [10] SOROKIN, V.G., VOLOSNIKOVA, A.V., et al., Steel and Alloy Grades Register. M., Mashinostroenie (1989).
- [11] The USSR Standard Reference Data Service. Molibdenum, monocrystal aluminium oxide, steel 12Kh18N10T. Thermal coefficient of linear expansion. GSSSD 59-83. Moscow, State Committee of USSR on Standards (1983).

- [12] SHEDROV, K.P., GAKMAN, E.L., Heat-Resistant Materials, Handbook. M., Mashinostroenie, (1965).
- [13] Register of Steel and Alloy Grades. Ed. by I.R. Krjanin, A.A. Astafiev, E.P. Mogilevsky. M.: TsNIITMASH, (1971).
- [14] ULYANIN, E.A., SOROKINA, N.A., Steels and alloys for cryogenic technology. Book of References. M., Metallurgia (1984).
- [15] KAZANTSEVA, N.M., TELEGIN, A.S., FEDJAEVA, L.A., Thermo-physical Properties of some grades of steel /Universities' Bulletin. Chernaya Metallurgia, N7 (1991), p. 86-88.
- [16] MASLENKOV, S.B., MASLENKOVA, E.A., Steels and alloys for high temperature applications. Book of References (agreed with SSRDA). Book 1. M., Metallurgia (1991).
- [17] NEIMARK, B.E. (Ed.), Physical properties of steels and alloys used in power engineering. Book of References, M., Energiya (1967).
- [18] Register of Steels for Machine Building. Research Institute for Machine Building Information, Moscow (1969).
- [19] Strength Calculation Norms for Equipment and Pipelines of Nuclear Power Facilities (PNAE G-7-002-86) (Gosatomenergondzor USSR). M.: Energoatomizdat (1989), 525 pages.
- [20] MATHEW, P.M., HUGHES, F.J., KRAUSE, M. and CHIN, Y.S., Thermal conductivity of steam generator tubing alloys, Atomic Energy of Canada Ltd. report, COG-97-101, (June 1997).
- [21] Inco Alloys International, "Properties of Inco Alloys", 7<sup>th</sup> Edition (1987).
- [22] FILONI, L. and ROCCHINI, G., Thermal conductivity of Inconel 600 and Ti-6Al-4V from 360 K to 900 K, High Temperatures – High Pressures (1989), Vol.21, pages 373-376.

## 6.5. Zirconium

### 6.5.1. *Enthalpy and heat capacity*

In the 1999 assessment of the enthalpy and heat capacity of liquid zirconium, Fink [1] pointed out contradictions in assessments and recommendations because there were significant differences between data from older and newer measurements. Consequently, as part of this CRP, the available data on  $C_p$  of liquid zirconium were extended by new measurements made at our institute in 2001 by Savvatimsky and Korobenko [2]. Because these new data show reasonable agreement with the 1972 measurements of Bonnel [3], the 1985 data of Kats [4], and the 1999 data of Paradis and Rhim [5] and indicate that the older data, which were discussed in some detail by Fink [1], are inconsistent, this review and recommendations are based on the experimental results of [2–5] only. All of these results are given on Table 1. Table 1 shows the method and the conditions of investigation for the measurement of enthalpy and heat capacity of liquid zirconium. It represents the investigation temperature ranges and the most relevant information: atmosphere, impurity, sample size and testing time, when possible.

Zirconium possesses a high affinity to oxygen. Therefore in the measurements of thermo- physical properties of liquid zirconium attention should be paid to prevention of zirconium oxidation.

In [2] the measurements were performed in air with duration of the experiment  $\sim 2\text{--}3\mu\text{s}$ . It seems reasonable to say that the chemical interaction between air and liquid zirconium was negligible during that short. The agreement of the data of [2] and the data obtained by stationary methods is indirect confirmation of this statement. The rough estimations show that in [2] the mass of oxidized material during the experiment was about  $10^{-2}\%$  of the initial mass of the sample and the oxygen penetration into the liquid sample (due to molecular diffusion) was about  $4\cdot 10^{-4}\mu\text{m}$ . Therefore oxidation and contamination of the sample with gas impurities in [2] was negligible.

Table 1. Investigation of enthalpy and heat capacity of liquid zirconium

AUTHOR	METHOD, MEASURED VALUE	$T$ , K	ATMOSPHERE	IMPURITIES Wt. %	SAMPLE	REMARKS
Bonnell, 1972	<b>LDC</b>	2233-3048	inert gas	-	-	Error 2 %
Catz, 1985	<b>LDC</b>	2130-2323	inert gas	Zr - 99.9 %	~10 g	Error $\approx$ 1 %
Paradis, 1999	<b>ESL</b>	2125-2200	Vacuum $10^{-8}$ mm Hg	Zr - 99.95%	2.5 mm diameter	-
Savvatimskii, 2001	<b>EFF</b>	2400-4100	Air	-	two strip of the thick 50 $\mu$ m-	Er. 7-8 %, Time of heating 2-3 $\mu$ s. Two-strip blackbody model

LDC - Levitation, drop calorimeter, (HT-HT0); ESL - Electrostatic levitation,  $C_p$ ; EFF - Electric firing of foil,  $C_p$

In [4] the measurements were carried out in argon, which was additionally purified before the experiment by heating in it up to 1500–1600K a foil of titanium (getter). After the experiment the mass of a hafnium specimen increased not more than 0.01%. It can be suggested that the increase in the mass of Zr samples after the experiment should be about the same. Thus the contamination and oxidation of the Zr samples in [4] should have been negligible.

In [5] the measurements were performed by a containerless method at high vacuum conditions ( $10^{-8}$  mm Hg). After the experiment the chemical and phase analysis of the sample were not conducted but taking into account high vacuum condition it may be concluded that contamination of the specimen during the experiment was negligible.

Bonnell [3] and Kats [4] investigated enthalpy. Their results are presented on Fig. 1 in the form of mean specific heat capacity  $c_p^m = (H_T - H_{298})/(T - 298)$ . The data of Savvatimsky [2] and Paradis [5] are presented in the form of heat capacity  $C_p$ . Without further analysis of the data in Fig.1 it is impossible to make any judgement about the agreement of the results of the different authors.



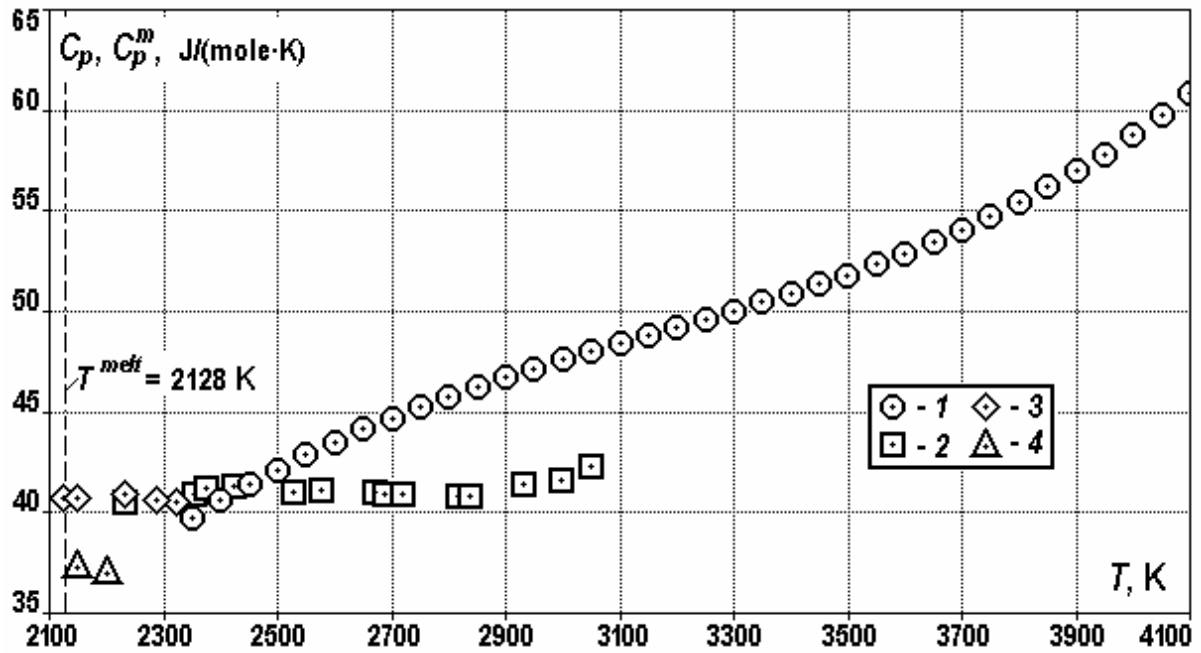


FIG. 1. True and mean heat capacity of liquid Zr:

1 - Korobenko and Savvatimskii (2001), 2 - Bonnell (1972),  
3 - Kats et al (1985), 4 - Paradis and Rhim (1999).

The results on enthalpy and heat capacity of liquid zirconium were co-processed by the least square method to obtain consistent recommended values using the unified linear (relative to the coefficients) equations. In this calculation procedure, we minimized the sum of the squares of deviations of the measured values of true and mean heat capacities (the latter were calculated from the measured values of enthalpy) from their regressions.

The temperature dependence of heat capacity was described by the equation

$$c_p = a_1 + a_2T + a_3T^2 + a_4T^3 \quad (1)$$

where  $a_j$ , denotes the coefficients of the equation to be calculated;

The temperature dependences of enthalpy and mean heat capacity were described by the equations

$$H_T - H_{T_0} = a_1(T - T_0) + a_2(T^2 - T_0^2)/2 + a_3(T^3 - T_0^3)/3 + a_4(T^4 - T_0^4)/4, \quad (2)$$

$T_0 = 298.15$  K,

$$c_p^m = a_1 + a_2(T^2 - T_0^2)/(T - T_0)/2 + a_3(T^3 - T_0^3)/(T - T_0)/3 + a_4(T^4 - T_0^4)/(T - T_0)/4. \quad (3)$$

We find the sum of squares of deviations,

$$R = \sum_{i=1}^N \varepsilon_i^2 = \sum_{i=1}^N [C_i - \alpha c_i - (1 - \alpha)c_i^m]^2$$

Here,  $\alpha = 1$  if  $C_i$  is the measured value of heat capacity and  $\alpha = 0$  if  $C_i$  is the measured value of mean heat capacity;  $c_i$  and  $c_i^m$  are the investigated regressions of respective heat capacities;  $\varepsilon_i$  is a deviation of the measured value from the value of its regression at point  $i$ ; and  $N$  is the total number of the points being processed.

We minimize the sum of squares of deviations relative to the coefficients of the selected model in view of equations (1) and (3) to derive the system of equations

$$\partial R / \partial a_j = \sum 2[C_i - \alpha c_i - (1 - \alpha)c_i^m] \partial \{ \sum [C_i - \alpha c_i - (1 - \alpha)c_i^m] \} / \partial a_j = 0,$$

whose solution enables us to determine the coefficients of the sought equations and obtain the information for analysing the selected model. The estimations of equations parameters are shown in Table 2.

The smoothed values of enthalpy, the mean and true heat capacity calculated by equations (2.1)–(2.3) of [6] in temperature range from 2125 to 4200 K are shown in Table 3 or on Fig. 2 and Fig. 3. Residuals and confidence bands at 0.95 level are presented on Fig. 4.

Table 2. Parameters of approximating equations (1) – (3)

CHARACTERISTIC	VALUES	CHARACTERISTIC	VALUES
$T_{\text{st}} - T_{\text{fin}}, \text{K}$	2128 - 4100	$r_{a1,a2}$	-0,992
$N$	55	$r_{a1,a3}$	0,979
$a_1$	$5.2389 \times 10$	$r_{a1,a4}$	0,964
$a_2$	$-1.912661 \times 10^{-2}$	$r_{a2,a3}$	-0,996
$a_3$	$7,5995 \times 10^{-6}$	$r_{a2,a4}$	0,988
$a_4$	$-6,1042 \times 10^{-10}$	$r_{a3,a4}$	-0,997
$S_{a1}^2$	4,28438	$\nu$	4
$S_{a2}^2$	$1,05847 \times 10^{-5}$	$t$	2
$S_{a3}^2$	$1,98331 \times 10^{-12}$	$R$	16.3608
$S_{a4}^2$	$3,35754 \times 10^{-20}$	$S_0^2$	0.3208

*Comments:*

$T_{\text{st}} - T_{\text{fin}}$  - temperature interval, K;  $a_1, a_2, a_3, a_4$  – coefficients of approximation equation;  $S_{a1}^2, S_{a2}^2, S_{a3}^2, S_{a4}^2$  – dispersions of equations coefficients;  $r_{a1,a2}, r_{a1,a3}, r_{a1,a4}, r_{a2,a3}, r_{a2,a4}, r_{a3,a4}$  – correlation coefficient of equations parameters;  $N$  - number of points;  $\nu$  - number of degrees of freedom;  $t$  - Student's coefficient;  $R = \sum [C_i^{\text{exp}} - C_i^{\text{calc}}]^2$  - sum of deviations squares of experimental and calculated enthalpy values in  $i$ -point of fetching,  $[\text{kJ/mole}]^2$ ;  $S_0^2 = R/\nu$  - dispersion of the result of measurement,  $[\text{kJ/mole}]^2$

Table 3. The rounded values of enthalpy, the mean specific heat and the heat capacity for liquid zirconium

$T$ , K	$H_T-H_{T_0}$ , J/mole	$C_p^m$ , J/(mole K)	$C_p$ , J/(mole K)	$T$ , K	$H_T-H_{T_0}$ , J/mole	$C_p^m$ , J/(mole K)	$C_p$ , J/(mole K)
2125	74503	40.78	40.20	3200	121887	42.00	49.00
2150	75510	40.78	40.33	3250	124350	42.13	49.54
2200	77533	40.77	40.59	3300	126841	42.25	50.09
2250	79569	40.77	40.87	3350	129360	42.39	50.65
2300	81620	40.77	41.17	3400	131907	42.53	51.22
2350	83687	40.79	41.49	3450	134482	42.67	51.79
2400	85769	40.81	41.82	3500	137086	42.81	52.37
2450	87869	40.83	42.17	3550	139719	42.97	52.95
2500	89987	40.87	42.53	3600	142381	43.12	53.54
2550	92123	40.91	42.91	3650	145073	43.28	54.14
2600	94278	40.96	43.30	3700	147795	43.45	54.74
2650	96453	41.01	43.71	3750	150547	43.61	55.34
2700	98649	41.07	44.13	3800	153329	43.79	55.95
2750	100867	41.14	44.57	3850	156142	43.96	56.56
2800	103106	41.21	45.01	3900	158985	44.14	57.17
2850	105368	41.29	45.47	3950	161859	44.32	57.79
2900	107654	41.38	45.95	4000	164764	44.51	58.41
2950	109963	41.47	46.43	4050	167700	44.70	59.03
3000	112297	41.56	46.92	4100	170667	44.89	59.65
3050	114656	41.66	47.43	4150	173665	45.09	60.27
3100	117040	41.77	47.94	4200	176694	45.28	60.89
3150	119450	41.89	48.47				

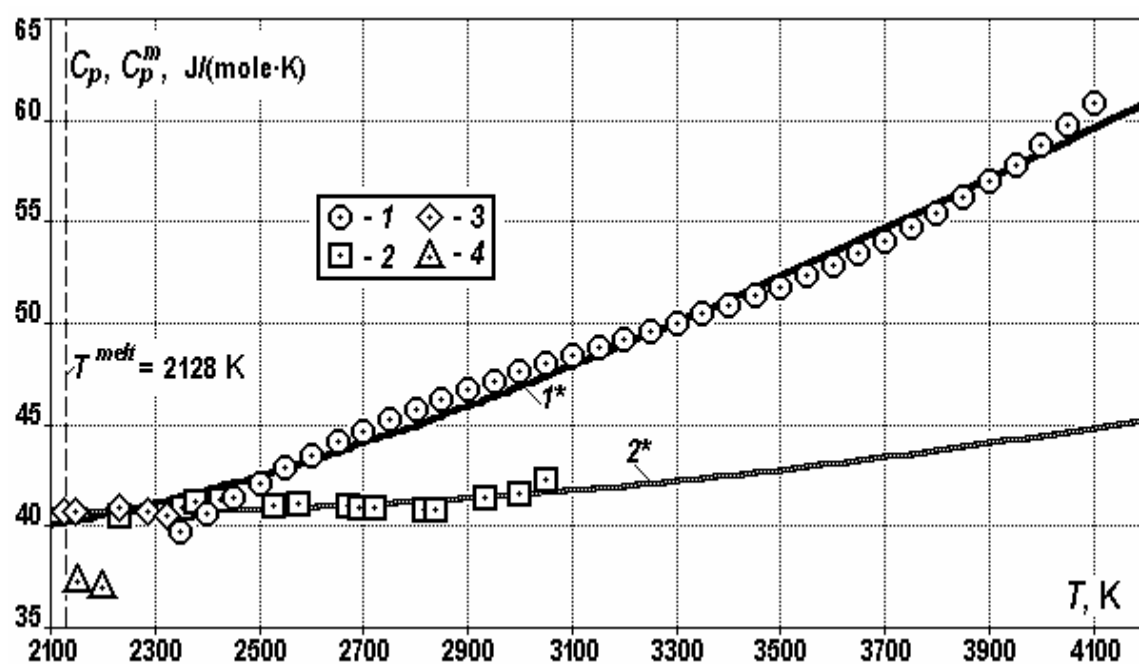


FIG. 2. True and mean heat capacity of liquid Zr:

1 - Korobenko and Savvatimskii (2001), 2 - Bonnell (1972),  
3 - Kats et al (1985), 4 - Paradis and Rhim (1999.)

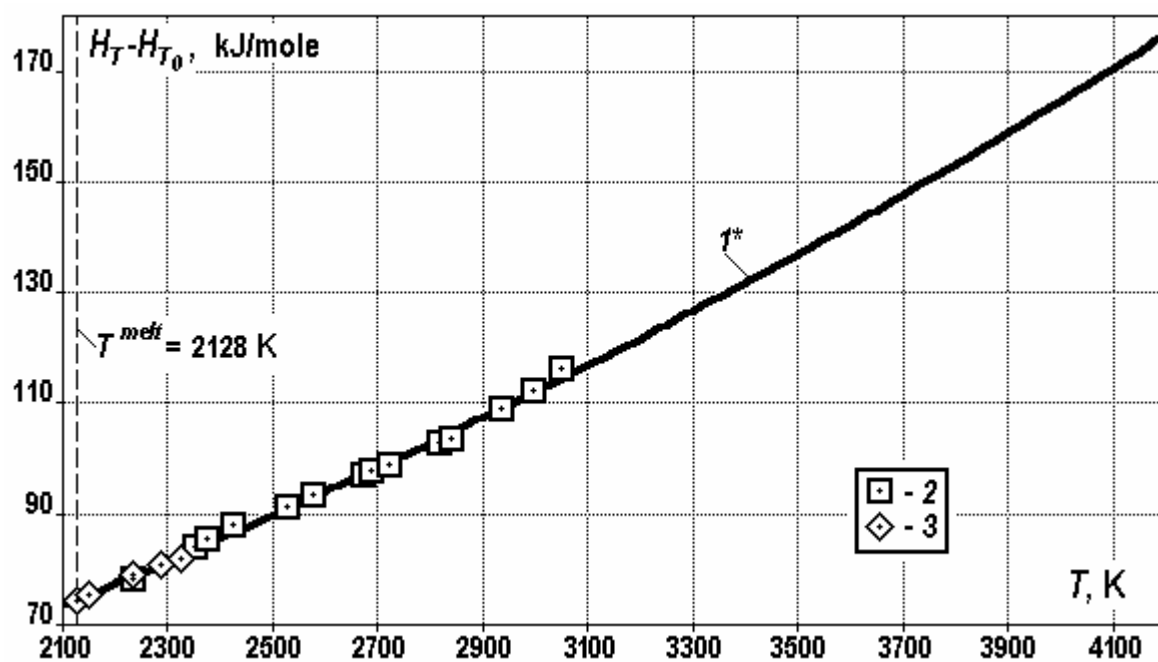


FIG. 3. Enthalpy of liquid Zr:

2 - Bonnell (1972), 3 - Kats et al (1985).

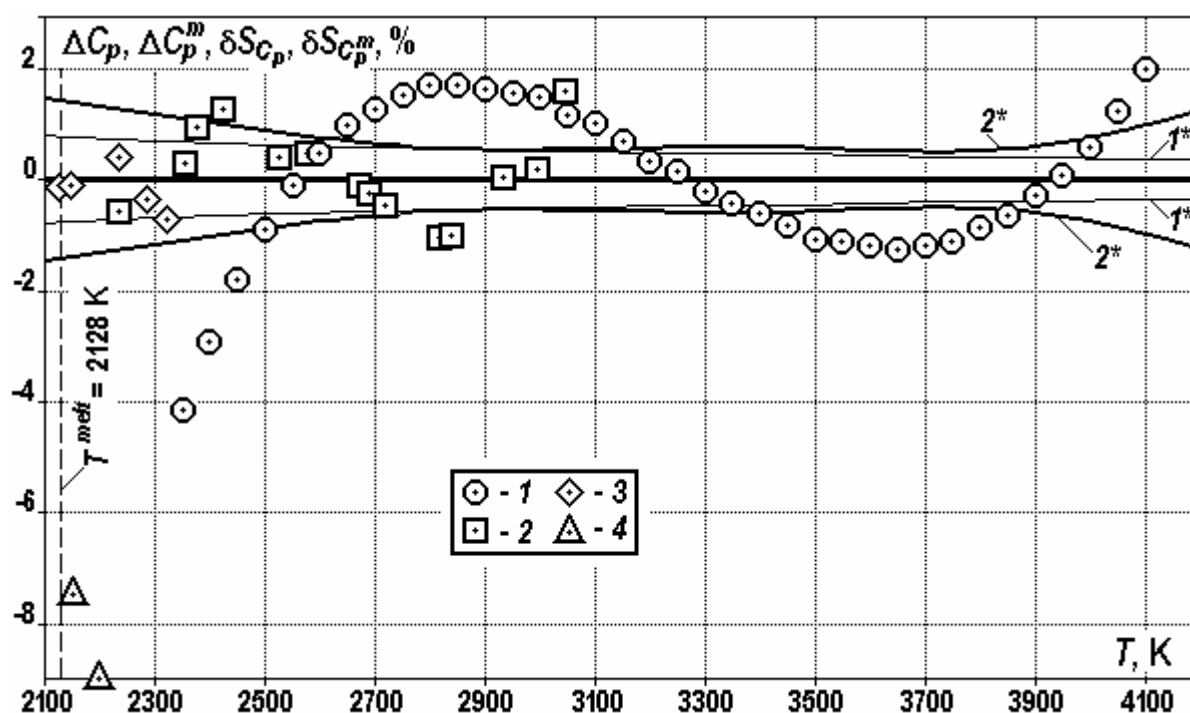


FIG.4. Relative deviations of data on heat capacity and confidence limits:

1 - Korobenko and Savvatimskii (2001), 2 - Bonnell (1972),  
3 - Kats et al (1985), 4- Paradis and Rhim (1999).

## REFERENCES TO SECTION 6.5.1

- [1] FINK, J.K., <http://www.insc.anl.gov/matprop/cladding/zirconium>. Enthalpy and heat capacity of liquid zirconium (1999).
- [2] KOROBENKO, V.N. and SAVVATIMSKII, A.I., Heat capacity of liquid zirconium, *Teplofiz. Vys. Temp.* V. 39, No. 5 (2001), p. 712-719, (in Russian).
- [3] BONNELL, D.W., Property measurements at high temperatures, *Levitation Calorimetry Studies of Liquid Metals*. Ph. D Thesis Rice University, Houston, TX (1972).
- [4] KATS, S.A., CHEKHOVSKOI, V.YA. and KOVALENKO, M.D., *Teplofiz. Vys. Temp.* V. 23, No. 2 (1985), p.395 (in Russian).
- [5] PARADIS, P.F., RHIM, W.-K., *J. Mater. Res.*, Vol 14, №9, (1999), p. 3113-3119.

## 6.5.2. Thermal conductivity

### Preliminary recommendation

The preliminary recommendation for the thermal conductivity of liquid zirconium is the value for the liquid at the melting point recommended by Mills et al. [1] in their recent review of thermal conductivities of liquid metals. Mills et al. recommend:

where  $\lambda(l, m)$  is the thermal conductivity of liquid zirconium at the melting point. Mills et al. used the

$$\lambda(l, m) = 36.5 \text{ W} \cdot \text{m}^{-1} \cdot \text{K}^{-1}$$

Weideman Franz Lorentz rule to calculate this value from the melting point electrical resistivity measurements of Korobenko and Savvatimskii [2] because no data exist for the thermal conductivity of liquid zirconium. No data on the temperature dependence for the thermal conductivity in the molten state are available.

### ***Uncertainty***

The uncertainty is estimated as 10%. This uncertainty was determined by comparing values of the thermal conductivity of solid zirconium at the melting point calculated from electrical resistivity measurements with values obtained from analysis of thermal conductivity and thermal diffusivity measurements.

### ***Discussion***

Measurements of the electrical resistivity of liquid zirconium are being carried out at the United Institute of High Temperature, Russian Academy of Sciences under the leadership of A. Savvatimskii. Those measurements will provide the temperature dependence of the electrical resistivity of liquid zirconium near the melting point, which may be used to determine the temperature dependence of the thermal conductivity. The above recommendation will be reassessed when results of these measurements are available.

In their review of thermal conductivities of liquid metals, Mills et al. also provide a recommendation for the thermal conductivity of the solid at the melting point. For zirconium, they recommend:

$$\lambda(s, m) = 38 \text{ W} \cdot \text{m}^{-1} \cdot \text{K}^{-1};$$

where  $\lambda(s, m)$  is the thermal conductivity of solid zirconium at the melting point. This value was also calculated from electrical resistivity measurements using the Weideman Franz Lorentz rule.

The electrical resistivity measurements by Desai et al. [3] and by Korobenko and Savvatimskii [2] at the melting point gave 39.5 and 37.7  $\text{Wm}^{-1}\text{K}^{-1}$ , respectively, for the thermal conductivity. Mills et al. [1] note that these values are in good agreement with the value (37.5  $\text{Wm}^{-1}\text{K}^{-1}$ ) obtained from extrapolation of the 1973 high-temperature zirconium thermal diffusivity data of Filippov [4].

Measurements of the thermal conductivity of solid zirconium from 1951 through 1992 have been reviewed by Fink and Leibowitz [5]. From their analysis of these data, they recommend an equation for the temperature range 298 through 2000 K. Extrapolation of their equation to 2128 K, the melting point of zirconium, gives 36.8  $\text{W} \cdot \text{m}^{-1} \cdot \text{K}^{-1}$ . Fink and Leibowitz comment the standard deviation is 9.5% at high temperatures because of large scatter in the data. The value of the solid thermal conductivity at the melting point calculated by Mills et al. is only 3% higher than the value obtained from the equation of Fink and Leibowitz. Thus, it is well within the standard deviation of thermal conductivity data.

## **REFERENCES TO SECTION 6.5.2**

- [1] MILLS, K.C., MONAGHAN, B.J. and KEENE, B.J., Thermal conductivities of molten metals: Part 1 pure metals, International Material Reviews 41, 209-242 (1996).
- [2] KOROBENKO, V.N. and SAVVATIMSKII, A.I., Properties of solid and liquid zirconium, Teplofiz. Vys. Temp. 29, No. 5, 883-886 (1991) [in Russian], High Temperature 29, 693-696 (1991) [English translation].
- [3] DESAI, P.O., JAMES, H.M. and HO, C.Y., Electrical resistivity of vanadium and zirconium, J. Phys. Chem. Ref. Data 13, 1097-1130 (1984).
- [4] FILIPPOV, L.P., Untersuchung der thermischen Eigenschaften im Stoff an der Moskauer Universität, Int. J. Heat Mass Transfer. 16, 865-885 (1973).
- [5] FINK, J.K. and LEIBOWITZ, L., Thermal conductivity of zirconium, J. Nucl. Mater. 226, 44-50 (1995).

### 6.5.3. *Enthalpy of fusion*

#### *Recommendation*

The recommendation for the enthalpy of fusion of zirconium is

$$153 \pm 4 \text{ J/g} = 13.96 \pm 0.36 \text{ kJ/mol}$$

This value for the enthalpy of fusion is an average enthalpy of fusion obtained by Korobenko, Savvatimskii and Sevostjanov [1, 2] from ten precise pulse heating experiments that simultaneously measured the temperature, enthalpy, heat capacity, and electrical resistivity of zirconium foils in the solid and liquid states up to 2350 K. Simultaneous measurement of the temperature, enthalpy and electrical resistivity made it possible to precisely determine the end of melting.

#### *Uncertainty*

The uncertainty in this recommendation for the enthalpy of fusion of zirconium is  $\pm 4\%$ , the uncertainty given by Korobenko, Savvatimskii and Sevostjanov [1, 2]. It is based on the deviations from the average values calculated using standard statistics for a reliability of 0.95. It does not include an uncertainty for identification of the instant of the start and end of melting in the graphical data.

#### *Discussion*

##### *Review of measurements and recommendations*

Table 1 lists the experimental values and recommended values for the enthalpy of fusion of zirconium available in both the Russian and western literature in chronological order. In 1963, Hultgren et al. [3] recommended 225 J/g (20.5 kJ/mol) for the enthalpy of fusion based on estimates using Richard's rule. In 1967, Elyutin et al. [4] recommended 229 J/g (20.9 kJ/mol) from their three measurements of 230 J/g, 224 J/g and 239 J/g that were obtained using the method of mixing in a liquid magnesium calorimeter. In reviewing the data, Korobenko and Savvatimskii [14] commented that the heat of mixing of the liquid zirconium and magnesium were neglected in the analysis of the experimental data. The 7% error, reported by Elyutin et al., is the uncertainty in the data analysis and does not include the total experimental error.

In his thesis, Bonnell [5] estimated the enthalpy of fusion of zirconium as 156 J/g from extrapolation of the enthalpies and heat capacities measured at 2233–2839 K using magnetic levitation in an adiabatic calorimeter. In 1973, Hultgren et al. [6] gave 185 J/g as an estimate of the enthalpy of fusion of zirconium. This value, which is considerably lower than their previous estimate, appears to take into account the data of Bonnell.

Martynyuk et al. measured the enthalpy of fusion using electrical resistive heating with 20  $\mu$  sec [16] and 400  $\mu$  sec pulses [7]. Their early measurements with 20  $\mu$  sec pulses gave 285 J/g with a 15% uncertainty. This value, reported only in a university publication [16], was not included in their subsequent journal publication. In 1974, Martynyuk and Tsapkov [7] reported a heat of fusion of 236 J/g with a 6% uncertainty from 400  $\mu$  sec pulse heating experiments. This value, obtained by dynamic methods, was in good agreement with the earlier drop calorimetry value [4] and the calculated enthalpy of fusion [3] and widely accepted. In their review of these measurements, Korobenko and Savvatimskii [14] question the accuracy of these measurements because the experimenters did not record an inflection in the resistivity that designates the onset of melting, the luminescence, nor the temperature. In addition, Korobenko and Savvatimskii [14] found that heating with long 400  $\mu$  sec pulses led to sample deformation at the onset of melting due to non-uniform heating.

In the 1976, IAEA special volume on zirconium, Alcock et al. [8] recommended 206 J/g (18.8 kJ/mol) by combining the new estimate of Hultgren [6] with the value recommended by Elyutin et al. [4] from their calorimetry measurements. Korobenko et al. [1] report that Regel and Glazov [9] recommended 158 J/g with a 2.3% uncertainty from review of the literature data and analysis of all the related properties of zirconium, taking into account the information from the periodical table of Mendeleev. The reference compilation by Glushko, ed. [10] gave the enthalpy of fusion as 150 J/g with an uncertainty of 29%. Although this recommendation is consistent with the enthalpy of fusion obtained from measurements by Bonnell, the large uncertainty was reflected the inconsistencies in the data.

In 1985, Kats et al. [11] made magnetic-levitation measurements that confirmed measurements of the enthalpy of the solid at the melting point and showed that the earlier measurements of the liquid enthalpy by Elyutin et al. and by Martynyuk and Tsapkov are inaccurate. However, the results of Kats et al., which confirmed the extrapolated value of Bonnell, were published only in the Russian edition of “*Teplofizika Vysokikh Temperatur*” and were not included in the English translation of the journal. Therefore, these results were not readily known outside Russia.

In his thorough review of zirconium properties, Guillermet [12] rejected Bonnell’s data because he believed they had a systematic error due to their disagreement with the data of Elyutin et al. [4] and the data of Martynyuk and Tsapkov [7]. Guillermet stated that the enthalpy measurements of Bonnell appear to have a systematic error but their slope seems reasonable and may be used to obtain a constant liquid heat capacity. He recommended 230 J/g (21 kJ/mol) based on the drop-calorimetric data of Elyutin et al. [4] because this value was supported by measurements by Martynyuk and Tsapkov [7] by a dynamic method. The assessment and recommendations of Guillermet [12] were also recommended by the Scientific Group Thermodata Europe [13] for use in phase diagram calculations.

Because of the inconsistency in the published zirconium enthalpy of fusion data and recommendations, Korobenko and Savvatimskii [14] performed two series of electric current pulsed heating experiments of zirconium at 20 and 100  $\mu$  sec. They performed no experiments with a longer pulse (400  $\mu$ sec) because they found that for longer pulses the surface tension and electromagnetic forces cause the conductor to deform from the onset of melting, indicating non-uniform heating and making property measurements meaningless. From these two measurements, they obtained 141 J/g and 138 J/g for the enthalpy of fusion, which gave an average value of 140 J/g with an uncertainty of 10%. They made additional measurements to make certain that their results are reliable. Their enthalpy of fusion at the melting point is consistent with the values obtained by magnetic levitation of Bonnell [5] and of Kats et al. [11] and is significantly lower than the values obtained by Martynyuk and Tsapkov [7]. They commented that the enthalpy of copper near the melting point determined by Martynyuk and Tsapkov [7] was high by about 70% and later refuted by subsequent pulsed heating experiments.

Despite the availability of these new data, the enthalpy of fusion given in the most recent version of MATPRO [15] remains at 225 J/g, the value recommended in 1981 [17], which was based on a 1968 recommendation by Brassfield [18].

Recently, Korobenko, Savvatimski, and Sevostjanov [1, 2] obtained an average enthalpy of fusion of  $153 \pm 4$  J/g from ten precise measurements on zirconium foils

#### *Measurements by Korobenko, Savvatimski, and Sevostjanov*

Because of the disagreements in the available data for the enthalpy of fusion, Korobenko, Savvatimski, and Sevostjanov [1, 2] used state-of-the art techniques to precisely determine the enthalpy, heat capacity, and electrical resistivity of zirconium in the melting region. An electrical pulse current of 3–5 kA for 3–5 microseconds heated zirconium strips of foils of 1–2 mm in width and 30–40 mm in length that had been obtained from three different manufacturers. The enthalpy, resistivity, temperature, and heat capacity in the solid and liquid states up to 2350 K were measured simultaneously. Temperature was measured from 1800 to 2350 K using a fast optical pyrometer through a quartz guide. The established melting point, 2128 K, served as a calibration point of the temperature at the plateau of melting. Simultaneous measurement of the temperature, enthalpy, and electrical resistivity provided precise determination of the end of melting. Foil thicknesses, density, and dimensions were precisely determined prior to each measurement. Density was determined by weighing the foils in air and in boiled water.

Following control experiments to determine the effects of surface treatment and surface quality on the precise determination of the beginning and the end of melting, three series of measurements were made using zirconium foils from three different manufacturers. The first series of measurements were made using an annealed foil of zirconium that was 24 microns thick, with a density of 6.53 g/cm<sup>3</sup>, from GIREDMET (Russia). In the first series of experiments, some non-coincidence of the moments of the start and finish of melting indicated non-homogeneity of the surface of this material. Therefore, a second series of measurements were made using a 44.6 micron thick, high-quality zirconium foil,



with a density of  $6.49 \text{ g/cm}^3$ , from Sundwig (Germany) that had very smooth surface with no apparent traces of rollers. Results from this series are more certain than those of the first series as indicated by the (1) smooth temperature plateau, (2) greater precision of fixing the beginning and ending of melting, and (3) coincidence of the finish of melting as indicated by the temperature plateau and by the electric resistivity. Because a thicker sample has a more uniform cross-section and produces more homogeneous heating and surface temperature, a third series of measurements was conducted with a thicker foil. This 95.45 microns thick foil with a density of  $6.54 \text{ g/cm}^3$ , was made of iodide zirconium and manufactured in Russia. It had a very smooth surface (almost unruffled) with only a slight strip-type structure of the surface in the rolling direction. The enthalpy of fusion results from these ten measurements are shown in Table 2. Additional data such as the enthalpy of transition from the  $\alpha$ -phase to the  $\beta$ -phase and the enthalpies of each phase at the phase transition are available in their paper [1] and data report [2]. Both the liquid enthalpy at the melting point based on the pyrometer and based on the electrical resistivity are shown in Table 2. Best agreement between these measurements was obtained for the high quality foil from Sudwig Germany. The last row of Table 2 gives the average values for the solid and liquid enthalpy determined using the pyrometer temperatures and the average enthalpy of fusion. Included with the average values are the statistically determined deviations from the average for a 0.95 confidence level. These deviations for the solid and liquid enthalpies and the enthalpy of fusion expressed as percentages are respectively, 1.7%, 1.4%, and 2.6%. Deviations from the average solid enthalpy range from a minimum of 0.3% to a maximum of 3.3%. Deviations from the average liquid enthalpy range from 0.5% to 3.0%. Deviations from the average enthalpy of fusion range from 1.3% to 5.2%. The recommended value for the enthalpy of fusion of zirconium,  $153 \pm 4 \text{ J/g}$ , is the average value obtained from these precise measurements.

Table 1. Measurements and recommendations of the enthalpy of fusion of zirconium

$\Delta H_f$ J/g	$H_l$ J/g	$H_s$ J/g	METHOD	REFERENCE	YEAR
225			estimated – Richard's rule	Hultgren et al. [3]	1963
$229 \pm 7\%$			Method of mixing in liquid Mg calorimeter- based on 3 measurements (230, 224, 239 J/g)	Elyutin et al. [4]	1967
156			Magnetic levitation in adiabatic calorimeter extrapolated from liquid at 2233-2839 K	Bonnell (Rice University thesis) [5]	1972
185			Recommended	Hultgren et al. [6]	1973
$236 \pm 6\%$	658	893	Pulse heating, heating rate: $5 \times 10^6 \text{ K/s}$ , onset of melting & luminescence not recorded	Martynyuk & Tsapkov [7]	1974
$206 \pm 11\%$			Recommended - average of Hultgren 1973 & Elyutin et al. 1967	Alcock (IAEA publication) [8]	1976
$158 \pm 2.3\%$			Recommended	Regel & Glazov (Russian only) [9]	1978
$150 \pm 29\%$			Recommended	Glushko, ed. [10]	1982
$161 \pm 6\%$	658	819	Magnetic levitation	Kats et al. (Russian only) [11]	1985
230			Recommended	Guillermet [12]	1987
				Dinsdale (SGTE) [13]	1991
$140 \pm 10\%$	640	780	2 pulse heating measurements (141, 138), rates: $2 \times 10^7 \text{ K/s}$ , $1 \times 10^8 \text{ K/s}$	Korobenko & Savvatimskii [14]	1991
225			Recommended	MATPRO, Hagerman [15]	1995
$153 \pm 3\%$	703	856	10 pulse heating measurements, heating rate: $3 \times 10^8 \text{ K/s}$	Korobenko, Savvatimskii, & Sevostjanov [1, 2]	1999

Table 2. Zirconium enthalpy of fusion results for 3 series of measurements

RUN	FOIL SOURCE, THICKNESS, DENSITY	H(s) from pyrometer, J/g	H(l) from pyrometer, J/g	H(l)from electrical resistivity, J/g	H(l)-H(s) from pyrometer, J/g
1	Russian annealed, 24 $\mu\text{m}$ , 6.53 g/cm <sup>3</sup>	695	840	830	145
2	Russian annealed, 24 $\mu\text{m}$ , 6.53 g/cm <sup>3</sup>	690	840	860-880	150
3	Sudwig Germany, 44.6 $\mu\text{m}$ , 6.49 g/cm <sup>3</sup>	710	860	850	150
4	Sudwig Germany, 44.6 $\mu\text{m}$ , 6.49 g/cm <sup>3</sup>	680	830	835	150
5	Sudwig Germany, 44.6 $\mu\text{m}$ , 6.49 g/cm <sup>3</sup>	700	860	860	160
6	Sudwig Germany, 44.6 $\mu\text{m}$ , 6.49 g/cm <sup>3</sup>	700	850	820-860	150
7	Russian, iodide Zr, 95.45 $\mu\text{m}$ , 6.54 g/cm <sup>3</sup>	710	860	840	150
8	Russian, iodide Zr, 95.45 $\mu\text{m}$ , 6.54 g/cm <sup>3</sup>	725	880	860	155
9	Russian, iodide Zr, 95.45 $\mu\text{m}$ , 6.54 g/cm <sup>3</sup>	705	860	840	155
10	Russian, iodide Zr, 95.45 $\mu\text{m}$ , 6.54 g/cm <sup>3</sup>	720	880	850	160
<b>Average</b>	-	<b>703 <math>\pm</math> 12</b>	<b>856 <math>\pm</math> 12</b>	-	<b>153 <math>\pm</math> 4</b>

## REFERENCES TO SECTION 6.5.3

- [1] KOROBENKO, V.N., SAVVATIMSKI, A.I. and SEVOSTJANOV, K.K., Experimental investigation of solid and liquid zirconium, paper presented at the 15<sup>th</sup> European Conference on Thermo-physical Properties, Würzburg, Germany, Sept 5-9, 1999, (to be published in High Temperature-High Pressures).
- [2] SAVVATIMSKIY, A.I., KOROBENKO, V.N., KRAEV, A.G. and KABANOV, L.P., Experimental research of thermo-physical properties of zirconium near melting point, INSC Report for Task 7-2 of Joint Project 10 Phase 2 A Measurement and Assessment of Material Properties for Databases of RINSC and USINSC, □ Moscow, Russia (1998).
- [3] HULTGREN, R., ORR, R.L., ANDERSON, P.D. and KELLEY, K.K., Selected values of thermodynamic properties of metals and alloys, John Wiley, New York (1963) pp. 326-330.
- [4] ELYUTIN, V.P., MAURAKH, M.A. and SVERDLOV, G.M., IZV. VYSSH. UCHEB. ZAVED., TSVET., Metall. 2, 87-88 (1967).
- [5] BONELL, D.W., Property measurements at high temperatures, levitation calorimetry studies of liquid metals, Ph. D Thesis Rice University, Houston, TX (May 1972).
- [6] HULTGREN, R., et al., Selected values of the thermodynamic properties of the elements, American Society for Metals, Metals Park, OH (1973) pp. 575-581.
- [7] MARTYNYUK, M.M., TSAPKOV, V.I., Izv. Akad. Nauk SSSR, Metall. 2, 181 (1974) [in Russian], Russ. Metall. 2, 108-112 (March 1974) [English translation].
- [8] ALCOCK, C.B., JAKOB, K.T. and ZADOR, S., Thermo-chemical properties, Chapter 1 of Zirconium: physico-chemical properties of its compounds and alloys, O. Kubaschewski ed., Atomic Energy Review Special Issue No. 6, International Atomic Energy Agency, Vienna (1976) pp. 5-65.
- [9] REGEL, A.R. and GLAZOV, V.M., Periodichesky Zakon i elektronnye svojstva elektronnyh rasplavov (Periodical law and physical properties of electronic fusions), Moscow: Nauka (1978)

- [Russian only]; as referenced by V. N. Korobenko, A. I. Savvatimski, and K. K. Sevostjanov, □ Experimental Investigation of Solid and Liquid Zirconium, □ paper presented at the 15<sup>th</sup> European Conference on Thermo-physical Properties, Würzburg, Germany, Sept 5-9, 1999, (to be published in High Temperature-High Pressures).
- [10] GLUSHKO, V.P. (ed.), Handbook of the Thermodynamic Properties of Individual Substances, Vol. 4 [in Russian], Nauka, Moscow (1982), p. 114.
  - [11] KATS, S.A., CHEKHOVSKOI, V.YA. and KOVALENKO, M.D., Teplofiz. Vys. Temp. 23, No. 2, 395 (1985), [in Russian]; this paper is not included in AHigh Temperatures, □ the English translation of Teplofiz. Vys. Temp.
  - [12] GUILLERMET, A.F., Critical evaluation of the thermodynamic properties of zirconium, High Temp.-High Pressures 19 119-160 (1987).
  - [13] DINSDALE, T., SGTE data for pure elements, CALPHAD 15, No. 4, 317-425 (1991).
  - [14] KOROBENKO, V.N. and SAVVATIMSKII, A.I., Properties of solid and liquid zirconium, Teplofiz. Vys. Temp. 29, No. 5, 883-886 (1991) [in Russian], High Temperatures 29, 693-696 (1991) [English translation]..
  - [15] HAGRMAN, D.T. (ed.), SCADAP/RELAP5/MOD3.1 Code Manual MATPRO- A Library of materials properties for light-water-reactor accident analysis, NUREG/CR-6150, EGG-2720 Vol. 4 (June 1995), p 16-6.
  - [16] MARTYNYUK, M.M., TSAPKOV, V.I., PANTELEICHUK, O.G. and KARIMKHODZHEV, I., Investigation of the physical properties of metals by the method of pulsed heating, [in Russian] Univ. Drzhby, Moscow (1972) as referenced by V. N. Korobenk and A. I. Savvatimskii (1991) [14].
  - [17] HAGRMAN, D.T., REYMANN, G.A. and MASON, R.E. (ed.), MATPRO- Version 11 (Revision 2) A Handbook of material properties for use in the analysis of light water reactor fuel rod behavior, Appendix D, Supporting material for MATPRO, NUREG/CR-0497 Rev. 2, TREE-1280 Rev.2 (August 1981) p 508.
  - [18] H. C. BRASSFIELD et al., Recommended property and reactor kinetics data for use in evaluating a light-water-coolant reactor loss-of-coolant incident involving Zircaloy-4 or 304-SS-Clad UO<sub>2</sub>, GEMP-482 (April 1968), as referenced by D. T. Hagrman, et al.(1981) [17].

#### 6.5.4. Surface tension

##### *Preliminary recommendation*

The preliminary recommendation for the surface tension of liquid zirconium, at its melting point is

$$1455 \pm 50 \text{ mN m}^{-1}$$

This is the mean of the melting point surface tensions obtained from measurements by Allen [1], Arkhipkin et al.[2], Vinet et al. [3] and Thiessen and Man [4]. No temperature dependence is available for the surface tension of liquid zirconium because measurements have been made only at the melting point.

##### *Uncertainty*

The 4% uncertainty is based on the uncertainty in the liquid density, which is used in the calculation of the surface tension from the measured parameters. This uncertainty is a factor of two higher than the 2% spread in the values that were used to obtain the recommendation. Although, the experimental uncertainty reported by Allen [1] is 2%, it does not include the uncertainty in the liquid density that Allen used in the data reduction. The greatest contribution to the surface tension uncertainty is in the value for the density of liquid zirconium at the melting point because no reliable data for the density of liquid zirconium have been published in the open literature. Estimated values for liquid densities were used in the reduction of the experimental data from early surface tension measurements. Their uncertainty was assumed to be about 10%. Liquid densities are now available for many transition metals and Vinet et al.[3] report that the densities they used in their data reduction are from recent measurements. Their density for liquid zirconium differs by 4% from the density used in the earlier measurements of Allen [1]. Because of this range in values for the density of liquid zirconium and the

lack of experimental liquid density data, the larger uncertainty than that reported by Allen and that obtained from the deviation from the mean is warranted.

## Discussion

Table 1 orders the available data on the surface tension of zirconium near the melting point according to year. Surface tension values are given in  $\text{mN m}^{-1} = \text{mJ m}^{-2}$ . The best value reported by each experimental group has been included in the table. Because Allen made measurements using two different methods, his best value for each method has been included in Table 1.

The most recent review of data on the surface tension of zirconium was done by Keene [7] in 1993. At that time, only measurements by four experimental groups were available [1, 2, 5, 6]. Keene recommended  $1430 \text{ mN m}^{-1}$ , which is the mean of the four highest values for the zirconium surface tension that were obtained by each of the experimental groups. In his review, Keene pointed out the scarcity in the data and the lack of any data on temperature dependence. Since the review by Keene [7], the surface tension of zirconium was measured by Vinet et al. using the drop weight method [3] and by Thiessen and Man [4] using a quasi-containerless pendant drop method.

Prior to the 1990s, the definitive surface tension measurements on transition metals were those done by Allen [1]. Allen measured the surface tension of 18 transition metals using both dynamic drop-weight and static pendant-drop techniques on samples from the same material heated by electron bombardment in a high vacuum ( $10^{-5}$  to  $10^{-7}$  Torr). The zirconium sample was from a high-purity crystalline bar. The surface tension given in Table 1 from the pendant drop measurements is the average of 30 photographs of drops. Allen [1] attributed the differences between his values for drop-weight measurements and those of earlier drop-weight measurements to differences in purity of the sample, outgassing in high vacuum prior to measurements, gas eruptions, the effect of rod diameter on oscillation of the drop prior to separation, and density differences. He commented that the largest uncertainty in the determination of surface tension comes from the uncertainty in the liquid density.

Vinet et al. [3] used the pendant-drop method in an ultrahigh vacuum ( $10^{-9}$  Torr) to determine the surface tension of rhenium, tungsten, niobium, iridium and zirconium. They used a range of wire diameters including very thin wire (0.3 mm in diameter) to study the process of detachment of the drop from the wire. During the growth of the drop, the refractory metal is purified. The drop falls when the surface tension can no longer balance the weight of the drop. They observed that poorly released drops have lower mass. From their measurements, they concluded that drops released from poorly outgassed wires or rods are statistically smaller and give an underestimation in the surface tension. Vinet et al. obtained a surface tension of  $1435 \text{ mN m}^{-1}$  from ten measurements on zirconium wires with diameters equal to 1 mm and 0.76 mm.

In their data reduction, Vinet et al. used liquid densities from sub-millimetric resistive heating experiments, which are more accurate than calculated values used in earlier surface tension measurements. However, none of the references given by Vinet et al. are for measurements of the density of liquid zirconium. Thus, the source of the value they used for density of liquid zirconium is not clear. The density of liquid zirconium that was used by Vinet et al. is  $6.05 \text{ g m}^{-3}$ , which is 4% higher than the estimated density,  $5.8 \text{ g m}^{-3}$ , used by Allen [1]. If the surface tensions obtained by Allen in his drop-weight and pendant-drop measurements are adjusted for this higher density, Allen's zirconium surface tensions would be respectively,  $1540 \text{ mN m}^{-1}$  and  $1530 \text{ mN m}^{-1}$ . These values are significantly higher than the value obtained by Vinet et al. Vinet et al. could not explain this disagreement. For W, Nb, Ta, and Re, the surface tension values determined by Vinet et al. showed good agreement with the values determined from measurements by Allen after these values were corrected for the liquid densities obtained from resistive heating experiments.

Consistent with the observation of Vinet et al., Thiessen and Man [4] found that measurements done over a four hour period showed an increase in surface tension with time as contaminants were gradually removed from the drop's surface by evaporation. The mean surface tensions that they obtained from three sets of measurements made on three separate days are  $1435 \pm 25$ ,  $1445 \pm 14$ , and  $1346 \pm 18 \text{ mN m}^{-1}$ . The first two values were obtained on samples that were thoroughly outgassed until the pressure was in the low  $10^{-7}$  Torr range.

The last value was obtained on a sample kept at room atmosphere for more than 1.5 hr followed by image capture at  $2 \times 10^{-6}$  Torr. These results indicate the sensitivity of the surface tension

measurements to sample preparation and vacuum conditions. The surface tension values obtained by Thiessen and Man are lower than the highest value obtained by Allen [1] using a drop-weight method. However, the best value reported by Thiessen and Man,  $1463 \pm 12 \text{ mN m}^{-1}$ , agrees well with the value,  $1469 \pm 4 \text{ mN m}^{-1}$ , obtained by Allen using a similar pendent-drop method.

The recommended value for the surface tension of liquid zirconium is  $1455 \pm 50 \text{ mN m}^{-1}$ . This value is the mean of the last five values given in Table 1, which are the values from the measurements by Allen, Arkhipkin et al., Vinet et al., and Thiessen and Man. The values given in Table 1 are considered to be the best values obtained by each experimental group using each measurement method. Two values reported by Allen have been included in the determination of this recommendation because they are the best values obtained by two different experimental techniques. The values reported by Peterson et al. and by Shunk and Burr have not been included in the average because they are significantly lower than the more recent measurements under high vacuum. The 4% uncertainty in the recommendation has been chosen to include not only the statistical variation in reported values but also the uncertainty in the liquid density. Measurements are needed to determine the density of liquid zirconium at the melting point and its variation with temperature. Surface tension measurements are needed to determine the temperature dependence.

Table 1. Measurements of the surface tension of zirconium near the melting point

SURFACE TENSION, $\text{mN m}^{-1}$	METHOD	EXPERIMENTER	YEAR
1400	Drop weight	Peterson et al. [5]	1958
1411	Drop weight	Shunk and Burr [6]	1962
1480	Drop weight	Allen [1]	1963
$1469 \pm 4$	Pendant drop		
1430	Detachment of a cylinder	Arkhipkin et al. [2]	1973
1435	Pendant drop	Vinet et al. [3]	1993
$1463 \pm 12$	Quasi-containerless pendant drop	Thiessen and Man [4]	1995

#### REFERENCES TO SECTION 6.5.4

- [1] ALLEN, B.C., The surface tension of liquid transition metals at their melting points, Trans of Met. Soc. Of AIME 227, 1175 (1963).
- [2] ARKHIPKIN, V.I., AGAEV, A.D., GIRGORIEV, G.A. and KOTKIKOV, V.I., Ind. Lab (USSR) 39 (8), 1340, (1973), as referenced by Keene.
- [3] VINET, B., GARANDET, J. P. and CORTELLA, L., J. Appli. Phys. 73, 3830 (1993).
- [4] THIESSEN, D.B. and MAN, K.F., A quasi-containerless pendant drop method for surface tension measurements on molten metals and alloys, Int=I J. of Thermo-physics 16, 245-255 (1995).
- [5] KEENE, B.J., A review of data for the surface tension of pure metals, International Materials Reviews 38, 157-192 (1993).
- [6] PETERSON, A.W., KEDES DY, H., PH. Keck, and E. Schwartz, J. Appl. Phys. 29, (2) 213 (1958).
- [7] SHUNK, F. and BURR, A.A., Trans. ASM. 55, 786 (1962).

### 6.5.5. Viscosity

#### *Preliminary recommendation*

The preliminary recommendation for the viscosity of molten zirconium at the melting point is:

$$8_{-2}^{+7} \text{ mPa} \cdot \text{s}$$

This value was reported by Yelvutin et al. [1] from measurements using a graphite crucible. A large positive uncertainty is warranted because this value reported for zirconium differs significantly from the viscosity of Zircaloy-2 measured by Bunnell and Prater [2]. Iida and Guthrie [3] report small differences between viscosities of dilute alloys and pure metals (1–5%). Thus, the viscosity of Zircaloy-2 (98 wt% Zr, 1.2–1.7 wt% Sn, 0.18–0.38 wt% Fe+Cr+Ni) is expected to be similar to that of zirconium. The negative uncertainty is based on differences between the value reported by Yelvutin et al. [1] and viscosities reported in the literature for similar metals.

#### *Discussion*

The viscosity of Zircaloy-2 was measured by Bunnell and Prater [2] as a function of temperature from 2075 to 2175 K. They found that, in this temperature range, the viscosity of Zircaloy-2 is a constant equal to 15 mPa · s. Bunnell and Prater comment that the different viscosities obtained for zirconium and Zircaloy-2 may be due either to differences in viscosity of Zircaloy-2 and zirconium or to impurity effects introduced by the crucible used in the measurements. Yelvutin et al. used a graphite crucible whereas Bunnell and Prater used a less reactive thoria crucible. At high temperatures, zirconium reacts with graphite to form ZrC. No data are available on the post-test analysis of the solidified liquid from the viscosity measurements of Yelvutin et al. Thus, it is possible that their reported viscosity is that of a liquid mixture of ZrC + Zr or of zirconium with carbon in solution, not pure zirconium.

In order to rule out contamination of their sample from interaction with the thoria crucible, Bunnell and Prater [2] repeated their measurements after holding the sample at temperature for 2 hr. They obtained the same viscosities. Metallographic examination of the sample after these 2 hr experiments showed metallic thorium precipitates. X-ray fluorescence measurements indicated 2 mol% thorium in the Zircaloy. Bunnell and Prater also measured the viscosity of Zr-UO<sub>2</sub> mixtures containing 70 to 94.9 mol% zirconium. Analysis of the samples of these mixtures after the viscosity measurements showed that thorium contamination was less than 1 mol%. These measurements indicate that the mixture viscosity increases with increasing zirconium content from 10 mPa · s for 70 mol% Zr to 17 mPa · s for 94.9 mol% zirconium. These results are consistent with the viscosity measured for Zircaloy-2 and with other viscosity measurements of UO<sub>2</sub>-Zr mixtures.

Although Bunnell and Prater report an abrupt change in viscosity when the sample became molten, it is possible that their measurements were made just as the sample began to flow. Liquidus temperatures of Zircaloy are a function of the amount of oxygen in the Zircaloy and range from 2136 to 2243 K for oxygen atom fractions of 0.007 to 0.19 [4]. The measurement by Yelvutin et al. was most likely made on a completely liquid sample since, unlike the alloy, the pure metal has a sharp melting point.

Based on the above data and considerations, it is clear that additional viscosity measurements are needed under well controlled atmospheres without contamination from containers. Until such data are available, a viscosity of 15 mPa · s is suggested for modeling the beginning of melting of Zircaloy, a Zr-Nb alloy, or zirconium with an oxide coating in an oxidizing atmosphere when the material begins to flow. However, for modeling the viscosity of zirconium in an inert or reducing atmosphere, a viscosity of 8 mPa · s is preferred.

## REFERENCES TO SECTION 6.5.5

- [1] YELVUTIN, V.P. et al., Chernage Met 7 (128) (1965); as referenced by Bunnell and Prater (Reference 2).
- [2] BUNNELL, L.R. and PRATER, J.T., Viscosity of zirconium-uranium oxide ( $\text{Zr-UO}_2$ ) mixtures at 1800 to 2100°C, U.S. Nuclear Regulatory Commission Report NUREG/CR-4495 (1986); Viscosity of zirconium uranium oxide ( $\text{Zr-UO}_2$ ) mixtures at 2075 to 2375 K, Pacific Northwest Laboratory Report PNL-SA-15644 (1988).
- [3] IIDA, T. and GUTHRIE, R.I.L., The physical properties of liquid metals, Clarendon Press, Oxford (1993).
- [4] HAGRMAN, D.T. (ed.), SCADAP/RELAP5/MOD3.1 Code Manual MATPRO- A library of materials properties for light-water-reactor accident analysis, NUREG/CR-6150, EGG-2720 Vol. 4 (1995), p 4-1 to 4-5.

## 7. THERMO-PHYSICAL PROPERTIES OF LIGHT AND HEAVY WATER

### 7.1. Introduction

This Chapter provides information on the current internationally accepted formulations for thermo-physical properties for ordinary (light) and heavy water substance with regard to their applications in power engineering and related fields. It includes all up-to-date changes of the formulations mentioned above.

Presentation of full wording of all the current formulations, as was done in the IAEA-TECDOC-949, June 1997 [1], is now practically impossible because it is extensive and too detailed. They can be found on the homepage of the International Association for the property of Water and Steam (IAPWS<sup>i</sup>) <http://www.iapws.org> under the item “Releases and Guidelines”. All the documents (Releases, Supplementary Releases, Guidelines and Advisory Notes) are downloadable as PDF files.

A survey of current IAPWS Releases, Supplementary Releases, Guidelines and Advisory Notes is in the attached **Supplement 1**. The survey was taken from the IAPWS homepage. In some releases the abbreviation IAPS is used. It comes from the former name of the association: “International Association for the Properties of Steam”.

A prospective user can find the formulations/equations in original documents or articles in journals, which are specified in the part “References” in this chapter. Some of the formulations presented in IAEA-TECDOC-949 are still valid and they are also referred to in this chapter.

However, the formulation for thermodynamic properties of water and steam, IAPS-84 [2], recommended in the IAEA-TECDOC-949, is obsolete. Moreover, it has never been accepted by the industry. Therefore we decided to present all the main equations and all coefficients of the recent standard for industrial calculations: “The IAPWS Industrial Formulation 1997 for the Thermodynamic Properties of Water and Steam” [3] in **Supplement 2**.

Today the software for thermo-physical properties of water and steam is available. A survey is given in paragraph 7.2.4.2. Besides the executable code, the professional version of programs contains also the source code. For correct usage of the source code of the industrial formulation mentioned above it is recommended to read related documents, or at least, Supplement 2.

### 7.2. Thermo-physical properties of light water

Extremely precise, based on large number of experimental values of different properties, but unsuitable for industrial calculations is The IAPWS Formulation 1995 for the Thermodynamic Properties of Ordinary Water Substance for General and Scientific Use [4, 5], abbreviated as “IAPWS-95”.

The extraordinary quality of IAPWS-95 is the reason why it has been placed at the beginning of this section. However, since density is one of the independent variables of this formulation, computing times for industrial applications may be excessive and therefore a new formulation has been developed for this purpose.

The IAPWS-95 formulation is in the form of a fundamental equation explicit in the Helmholtz free energy,  $f = f(T, \rho)$ , which yields other thermodynamic properties by differentiation and algebraic operations without use of any other information. The new formulation defines accurately the thermodynamic properties of ordinary water substance with complete thermodynamic consistency between these properties. It is valid for temperatures from the melting line (lowest temperature 251.2 K at 209.9 MPa) to 1273 K and pressures up to 1000 MPa, including the liquid–vapor

---

<sup>i</sup> IAPWS is an international non-profit association of national organizations concerned with the properties of water and steam, particularly thermo-physical properties and other aspects of high-temperature steam, water and aqueous mixtures that are relevant to thermal power cycles and other industrial applications.



equilibrium line. In this range IAPWS-95 represents the most accurate data. The equation extrapolates reasonably well to higher pressures and temperatures.

The IAPWS-95 formulation superseded the previous formulations IFC-68 [6] and IAPWS-84 [2]. Data calculated from the IAPWS-95 served as a source for the new industrial formulation.

The software implementing the IAPWS-95 formulation is available from NIST ([srdata@nist.gov](mailto:srdata@nist.gov)) as NIST Standard Reference Database 10 and from the Ruhr University Bochum, Germany (<http://www.ruhr-uni-boch.de/thermo>) as Software FLUIDCALC, version Grundpaket für Stoff Wasser.

### ***7.2.1. The IAPWS formulation 1997 for the thermodynamic properties of water and steam for industrial use***

In 1997 the International Association for the Properties of Water and Steam adopted a new formulation for industrial calculations under the title IAPWS Industrial Formulation 1997 for the Thermodynamic Properties of Water and Steam abbreviated to IAPWS-IF97.

The full wording of the equations is in the IAPWS document under the title Release on the IAPWS Release on the IAPWS Formulation 1997 for the Thermodynamic Properties of Water and Steam for Industrial Use [7]. A very detailed description of the IAPWS-IF97 was published in [3].

The description of IAPWS-IF97 is given in Supplement 2, the survey of available software in paragraph 7.2.4.2.

The formulation IAPWS-IF97 entirely replaces the previous standard for industrial calculations known under the abbreviation IFC-67 [8] used since the end of the sixties in power engineering and other industrial applications.

This new formulation is in the new temperature scale ITS-90 [9]. It is consistent with the scientific formulation IAPWS-95 [4], more accurate than IFC-67 and has better thermodynamic consistency on the region boundaries. The average computation time is five times shorter and additionally it involves a high-temperature region.

Its range of validity is the same as for IFC-67 i.e.:  $0^{\circ}\text{C} < t \leq 800^{\circ}\text{C}$  and  $p \leq 100 \text{ MPa}$ , which for high-temperature applications has been extended with the range  $800^{\circ}\text{C} \leq t \leq 2000^{\circ}\text{C}$  for  $p \leq 10 \text{ MPa}$ . The whole region is described with a set of equations for five sub-regions (see Fig. 1 in Supplement 2) to give accurate thermodynamic properties with short computing times. The equations have been fitted to properties calculated from IAPWS-95. The basic equations, are in specific Gibbs free energy  $g(p, T)$ . Only for the critical region the specific Helmholtz free energy  $f(\rho, T)$  has been used.

In order to achieve an increase in the computation speed the structure of the basic equations has been optimized. Further increase in the computation speed has been obtained by the development of backward equations to the basic equation. These backward equations may give a required property directly with the independent variables  $(p, h)$  and  $(p, s)$  and a number of properties can be calculated without any iteration. They could be used for the initial value calculations for iterative solutions with the basic equations. Between the backward and the basic equations there is an extremely good numerical consistency.

The new industrial formulation IAPWS-IF97 has been verified several times and its impact on the transition from the former standard IFC-67 to IAPWS-IF97 investigated. After very detailed tests the IAPWS-IF97 formulation has been adopted as a new international standard for computation in power engineering and for related industrial applications. It is highly recommended to introduce the IAPWS-IF97 formulation as a standard in nuclear power engineering.

#### ***7.2.1.1. Supplementary backward equations***

The most frequent backward equations are part of the formulation IAPWS-IF97, as mentioned above. Besides that, several supplementary backward equations to the IAPWS-IF97 have been developed and

the development of others continues. Using these backward equations time-consuming iterations in basic equations can be avoided.

Between the backward and the basic equations there is extremely good numerical consistency. The tolerable numerical inconsistency has to be about one order of magnitude smaller than the uncertainties of the corresponding equations. However, numerical problems would arise in the transition from backward to basic equations and vice versa.

A supplementary equation  $v(p,T)$  [10] has been developed for the critical and the supercritical region. However, for its complex form (7 subregions) it was not accepted by IAPWS as a Supplementary Release.

In 2001 IAPWS adopted the Supplementary Release on Backward Equations for Pressure as Function of Enthalpy and Entropy  $p(h,s)$  to the IAPWS Industrial Formulation 1997 for the Thermodynamic Properties of water and Steam [11]. These backward equations were developed for the liquid phase and for the superheated steam. Together with the backward equation  $T(p,h)$  of IAPWS-IF97 [7] it is possible to determine  $T$  from  $h$  and  $s$  without any iteration.

The backward equations should not be used for determining any thermodynamic derivatives. In the IAPWS document [11] the equations, their coefficients and exponents, numerical consistency with basic equations and computing times are given. Further details about equations  $p(h,s)$  can be found in [12].

In 2003 another supplementary release on backward equations for the functions  $T(p,h)$ ,  $v(p,h)$  and  $T(p,s)$ ,  $v(p,s)$  valid in the critical region [13] has been accepted (see Fig. 1 in Supplement 2).

At the IAPWS Meeting 2003 a draft on a Supplementary release on backward equations  $p(h,s)$  for the critical region, equations as a function of enthalpy and entropy for the region boundaries, and an equation  $T_{sat}(h,s)$  for wet steam was submitted [14]. It is very likely that the draft will be accepted in 2004 as an official supplementary release of IAPWS.

A list of the supplementary backward equations is included in the Supplement 1.

#### *7.2.1.2. Tabular Taylor Series expansion method*

The method employs a two-dimensional six-term Taylor Series expansion (TTSE) around selected grid points on a suitable plane of independent variables. The calculations are fast due to the small number of numerical operations required when using a table of stored properties and their derivatives. The stored primitives and their derivatives are precisely determined from a fundamental equation with modest requirements on computer memory. The accuracy of the TTSE method depends thus only on the grid spacing of the storage table.

The method was described in [15], [16], [17], [18]. The principle of the method, grid and cell structure, cell-finding strategy, accuracy and computing time were explained in the guideline [19].

This method is very suitable and effective for fast calculations but it does not replace the industrial formulation in any case. It is well suited to provide properties for use in CFD finite element calculations and could also be used for other fluids. The software and related data for this method can be obtained at <http://www.iapws.jap>.

In 2003 a paper on the application of the TTSE method for fast and accurate calculation of transport properties of water and steam was presented [20].

### **7.2.2. Transport properties**

#### *7.2.2.1. Viscosity*

The formulation for the viscosity of ordinary water substance, IAPS 1985, [21] was modified in 1997 [22] only to conform to the release on the scientific formulation IAPWS-95 and the recent temperature scale ITS-90. In 2003 an amended release has been adopted [23], which in addition modifies the near-critical term to remove a small discontinuity. The explanation of the correction was given in [24].

In the Revised release [23] the reference temperature has been changed. The new value, which is different from that in [1], is

$$T^* = 647.226 \text{ K}$$

The second change relates to the range of temperature and density where the only thermodynamically stable points for which  $\bar{\mu}_2 > 1$  lie. The range is specified by the inequalities:

$$0.996 \leq \bar{T} \leq 1.01$$

$$0.71 \leq \bar{\rho} \leq 1.36$$

It was shown that for industrial use, the density may be calculated from the industrial formulation IAPWS-IF97 and then viscosity from the interpolation equation presented in [22]. But it should be taken into account that if another density formulation than IAPWS-95 is used, a relative departure of  $\Delta\rho/\rho$  induces, at most, a relative departure  $\pm\mu/\mu = 2.5 \Delta\rho/\rho$  in viscosity.

The above-mentioned formulation of viscosity of ordinary water is the provisional one. Under way is the development of a new one. It is expected that the new viscosity formulation will be submitted in 2004.

#### 7.2.2.2. *Thermal conductivity*

In 1997 the thermal conductivity formulation IAPS 1985 [25] has been modified to conform to the releases on the scientific formulation IAPWS-95 for scientific equations for thermal conductivity, and to conform to the industrial formulation IAPWS-IF97 for the industrial equation for conductivity. In both cases it should also conform to the recent temperature scale ITS-90. The revised release on thermal conductivity [26], adopted by IAPWS in 1998, presents again two interpolating equations, for industrial and for general and scientific use.

Both equations were presented in the IAEA-TECDOC-949 [1], but the reference temperature was changed in both the scientific and industrial interpolating equations. In the equation for general and scientific use the reference temperature is  $T^* = 647.226 \text{ K}$ , and in the equation for industrial use  $T^* = 647.26 \text{ K}$ .

The revised IAPWS release on thermal conductivity [26] is still in force. The revision of thermal conductivity formulation will continue when the new formulation for viscosity is finished.

#### 7.2.3. *Other properties*

##### 7.2.3.1. *Dielectric constant*

A new release on static dielectric constant of ordinary water substance for temperatures from 238 K to 873 K and pressures up to 1000 MPa [27] has been authorized by IAPWS in 1997. It replaces that of 1977 [28], which was based on the old temperature scale IPTS-68.

The formulation is based on the dipole correlation or g-factor of Alder and Harris, and formulates this factor with 10 adjustable coefficients and associated powers of reduced density and inverse reduced temperature. The survey of available experimental data is given in [29]. Details about the equation presented in the release [27] can be found in the article [30].

The equation is valid in the temperature range 238 to 273 K in the metastable liquid at atmospheric pressure (0.101325 MPa), 273 to 323 K at pressures up to the lower melting pressure of the ice VI or 1000 MPa and above 323 K up to 600 MPa. The formulation extrapolates smoothly up to at least 1200 K and 1200 MPa.

The release [27] includes the equation, values of coefficients and exponents, estimated uncertainty and values for program verification.

### 7.2.3.2. *Refractive index*

A new release on the refractivity index of ordinary water substance as a function of wavelength, temperature and pressure [31] has been authorized by the IAPWS in 1997. Details on the previous formulation, used data and their evaluation are given in [32].

In the new document the related values were converted into the new temperature scale ITS-90 and the former previous equation of state was replaced by the IAPWS-95 [4]. Data on the refractivity index has been refitted to the original functional form, but in a reduced wavelength range.

IAPWS adopted the new formulation of the refractivity index in the range

Temperature	$-12\text{ }^{\circ}\text{C} \leq t \leq 500^{\circ}\text{C}$
Density	$0\text{ kg/m}^3 \leq \rho \leq 1060\text{ kg/m}^3$
Wavelength	$0.2\text{ }\mu\text{m} \leq \lambda \leq 1.1\text{ }\mu\text{m}$

Extrapolation of the formulation to longer wavelength has been tested. The formulation is in a good agreement with the results in [33] in liquid water at wavelengths up to 1.9  $\mu\text{m}$ .

The Release [31] includes the formulation, its coefficients, estimates of uncertainty and values for program verification. It can be used both with the scientific formulation IAPWS-95 and industrial formulation IAPWS-IF97. It replaces all documents presented before 1994 including the formulation given in Proceedings 12th ICPWS [34].

### 7.2.3.3. *Surface tension*

The new release on surface tension of ordinary water substance authorized by IAPWS in 1994 [35] replaces that of 1976 [36], which used the temperature scale IPTS-68.

The experimental results of surface tension have been examined and the values adjusted for the temperature change from IPTS-68 to ITS-90. The interpolation equation for the surface tension is the same as in the release from 1976, but the critical temperature was taken from the IAPWS release [37].

The equation is valid from the triple point temperature (273.16 K) to the critical point temperature (647.096 K).

## 7.2.4. *Steam tables and software based on the IAPWS-IF97*

### 7.2.4.1. *Steam tables based on the IAPWS-IF97*

Details on the contents of particular tables of properties of water and steam based on IAPWS-IF97 and on the Mollier charts are given below:

Steam tables published in Germany [38] include all equations of IAPWS-IF97, revised formulations for viscosity, thermal conductivity, surface tension, static dielectric constant, and refractive index. The tables comprise thermodynamic, transport and other properties including the Prandtl number along the saturation curve and in the single-phase region. Large-scale  $h$ - $s$  and  $T$ - $s$  diagrams are attached to the book. The book is bilingual – English-German.

A large-scale Mollier  $h$ - $s$  chart [39] was published in the Publishing House Springer.

The Czech National Committee for the Properties of Water and Steam prepared steam tables [40]. They are also bilingual – Czech-English. Included are detailed tables of saturation properties as function of temperature, and pressure,  $c_p$ ,  $k$ ,  $w$  and  $\sigma$  along the saturation curve, tables of compressed water and superheated steam (0–800°C, 0.001–100 MPa), critical region (compressed water and superheated steam 350–390°C, 18.5–26 MPa, specific heat capacity at constant pressure, isentropic exponent, speed of sound as function of  $(p, T)$ , properties of undissociated water at high temperatures (800–2000°C, 0.001–10 MPa), ideal-gas properties, thermal conductivity, and dynamic viscosity. Attached is a Mollier  $h$ - $s$  diagram. The large scale Mollier diagram [41] is also available separately.

By the end of 1999 the Japan Society of Mechanical Engineers published JSME Steam Tables (bilingual Japanese-English) [42]. Tables of saturation properties as functions of temperature and pressure, properties of compressed liquid and superheated steam, properties at high temperatures with a dense net of pressures, tables of  $v$ ,  $h$ ,  $s$  for the region of metastable subcooled steam, state values for the critical region, specific heat capacities at constant pressure and constant volume, speed of sound, isentropic exponent, surface tension, Laplace constant, refractive index for  $\lambda = 0.589$  nm, static dielectric constant, thermal conductivity, dynamic and kinematic viscosity, Prandtl Number, ion product, pH, and thermo-physical properties at saturation are presented on 201 pages. All computation relations and graphs of individual quantities are given without comments. Large-scale  $h$ - $s$ ,  $T$ - $s$  and  $h$ - $p$  charts are included. A CD-ROM with a FORTRAN program of IAPWS-IF97 and other recommended equations by IAPWS for thermo-physical properties of water and steam is part of the publication. In our opinion JSME Steam Tables are the most detailed tables.

Publishing House of Moscow Power Institute brought out Steam Tables [43]. The tables include equations for IAPWS-IF97, dynamic viscosity, thermal conductivity and surface tension. Tabulated are properties at saturation as functions of temperature and pressure,  $v, h, s$  for compressed liquid and superheated steam, isobaric heat capacity, speed of sound, dynamic viscosity, thermal conductivity and Prandtl number in the single-phase region as function of  $(p, T)$  and along the saturation curve. Attached are small-scale diagrams of selected quantities. The book was published for the 100<sup>th</sup> birthday anniversary of Prof. M.P. Vukalovitch.

At the beginning of 2000, the ASME International Steam Tables for Industrial Use [44] were published. They include thermodynamic, transport and other properties inclusive formulations. Tables in SI and U.S. customary units, and lot of small-scale diagrams of thermo-physical quantities for quick and easy reference are presented on 292 pages.

#### *7.2.4.2. Software for thermodynamic properties of water and steam based on the industrial formulation IAPWS-IF97*

Software for computation of thermodynamic properties of water and steam based on industrial formulation IAPWS-IF97 developed at the University Bochum, Germany, was published on CD-ROM by Springer [45]. Besides thermodynamic quantities it makes possible to compute viscosity, thermal conductivity and surface tension, refractive index and dielectric constant according to the recent international standards. The software enables to calculate more than 25 thermodynamic quantities in dependence on  $T$ ,  $p$ ,  $v$ ,  $h$ ,  $s$ ,  $g$ ,  $f$ , and  $x$  or for individual points, or along iso-lines. The software includes a graphic module for generation of  $h$ - $s$ ,  $T$ - $s$ ,  $p$ - $h$ , and  $p$ - $\rho$  graphs. For the most important quantities source codes (Fortran 77) or Dynamic Link Library files (DLL) are added. Further information is available on e-mail [wagner @ thermo.ruhr-uni-bochum.de](mailto:wagner@thermo.ruhr-uni-bochum.de).

The ASME Properties of Steam Subcommittee prepared computer software implementing the new industrial formulation IAPWS-IF97 in two versions. The professional version contains full source code and executable programs with accompanying documentation, and a student version contains the executable programs only. For further information or where to place an order contact ASME Information Central fax: 973-882-1717 or 973-882-5155, e-mail: [infocentral@asme.org](mailto:infocentral@asme.org).

The JSME CD-ROM, distributed with the tables [42], contains all IAPWS publications (Releases, Guidelines and IAPWS Certified Research Needs). The software part contains Fortran source codes and executable programs. In addition to the programs developed by JSME (not optimized in the computing speed), the subdirectory IAPWSscr contains codes of function subprograms for thermodynamic properties, developed by IAPWS WG for the development of IAPWS-IF97. They are optimized in computing speed. Directories with source codes contain files in three levels: source codes based on IAPWS-IF97 equations, auxiliary routines to develop applications and main programs. Executable programs enable users to calculate thermodynamic properties at a single point. They were prepared in two sets: for 16-bit environment (Windows and MS-DOS) and for 32-bit environment (Windows 95 or later).

The diskette attached to the proceedings [46] prepared by the Czech National Committee on the Properties of Water and Steam contains the set of optimized subroutines of IAPWS-IF97, which were

developed by IAPWS WG for the development of IAPWS-IF97, and a demonstration program. Later on, software for computation of thermodynamic, transport and other properties has been completed.

Software for thermodynamic charts, FluidEXL<sup>Graphics</sup>, based on the new industrial formulation IAPWS-IF97 [47] was developed at the University of Applied Sciences Zittau/Görlitz. It allows the users to represent calculated properties in 11 types of thermodynamic charts. Further information is available at e-mail [hj.kretzschmar@hs-zigr.de](mailto:hj.kretzschmar@hs-zigr.de).

### **7.3. Thermo-physical properties of heavy water**

In this field no significant changes occurred up to now. The only exception is the change of critical parameters [37] and innovation of the release on the surface tension [48].

It may be assumed that the application of the current documents both on the thermodynamic and transport properties in temperature scale IPTS-68, containing old values of reference constants, will not cause problems in current industrial calculations.

#### **7.3.1. Thermodynamic properties**

In this field no significant changes occurred up to now. The formulation for thermodynamic properties for heavy water adopted by IAPS as an international standard in 1984 has not been changed up to now. Thermodynamic properties of heavy water should be calculated from the *IAPS Formulation 1984 for the Thermodynamic Properties of Heavy Water Substance* [49] based on the paper [50]. This formulation is also presented in IAEA-TACDOC-949 [1].

The only change, which relates to the thermodynamic properties of heavy water is the change of the critical parameters [37], but the reference values in the release [49] remained the same.

Revision of thermodynamic properties of heavy water is under way. At the IAPWS Meeting 2003 a revised release on the IAPWS formulation 1984 for the thermodynamic properties of heavy water reflecting the change in the temperature scale has been submitted. Some discrepancies with new measurements along the saturation curve appeared and the problem is being under study now.

#### **7.3.2. Transport properties**

##### **7.3.2.1. Viscosity**

No significant improvements occurred up to now. The formulations for transport properties of heavy water were adopted by IAPS as international standards in 1984 [51]. They have not been changed up to now. These formulations agree with those presented in the IAEA-TECDOC-949 [1].

##### **7.3.2.2. Thermal conductivity**

Formulations for thermal conductivity of heavy water are presented in the same release [51]. The current formulation [51] agrees with that presented in the IAEA-TECDOC-949 [1].

It may be supposed that use of the documents [49] and [51] in the temperature scale IPTS-68 and old values of reference constants will not cause problems in current industrial calculations. (The values of the reference constants have not been affected by the change of critical parameters [37]).

#### **7.3.3. Other properties of heavy water**

##### **7.3.3.1. Equations for the saturated properties**

Equations for saturated properties  $p_s$ ,  $\rho'$ ,  $\rho''$ ,  $h'$ ,  $h''$ , and  $s'$ ,  $s''$  (saturated liquid and saturated vapour) [52] are expressed in polynomial form with fractional exponents. They were published in 1990. The paper [52] has not been accepted by IAPWS as a release.

### 7.3.3.2. Critical parameters

The critical parameters used in releases mentioned above were taken from the outdated document [53]. The new critical parameters conform to the ITS-90 [9]. They were presented in the revised release on the critical parameters [37]. Their numerical values are:

$$T_c = 643.847 \text{ K} \quad p_c = 21.671 \text{ MPa} \quad \rho_c = 356 \text{ kg.m}^{-3}$$

### 7.3.3.3. Surface tension

The Release on surface tension of heavy water 1985 [48] based on the International Practical Temperature Scale IPTS-68 has been revised to provide the values conforming to the International Temperature Scale of 1990 (ITS-90) [54]. The form of the interpolation equation, constants and exponent were kept the same. The equation is valid between the triple point (3.8°C) and reference temperature  $T_c = 643.847 \text{ K}$ .

Adjustment of the reference temperature produces values of surface tension from the equation for ITS-90 temperatures with improved root mean square deviations compared with the original equation and surface tension values for the IPTS-68 temperatures in the release of 1985. Deviations of the calculated values from experimental data are within -0.05 to +0.04 mN/m between 3.8 and 160°C, within -0.05 and -0.10 mN/m between 165 and 225°C and within -0.03 and +0.06 mN/m between 230 °C and  $T_c$ .

## REFERENCES TO SECTION 7

- [1] INTERNATIONAL ATOMIC ENERGY AGENCY, Thermo-physical properties of materials for water-cooled reactors. IAEA-TECDOC-949, Vienna (1997).
- [2] The IAPS Formulation 1984 for the Thermodynamic Properties of Ordinary Water Substance for Scientific and General Use. IAPS Secretariat (1984).
- [3] WAGNER, W., et al, The IAPWS Industrial Formulation 1997 for the Thermodynamic Properties of Water and Steam. Journal of Engineering for Gas Turbines and Power 122, 1 (2000) 150-182.
- [4] Release on the IAPWS Formulation 1995 for the Thermodynamic Properties of Ordinary Water Substance for General and Scientific Use. IAPWS Secretariat, Fredericia, Denmark (1996).
- [5] WAGNER, W., PRUSS, A., The IAPWS Formulation 1995 for the Thermodynamic Properties of Ordinary Water Substance for General and Scientific Use. J. Phys. Chem. Ref. Data Vol. 31, No.2 387-535, (2002).
- [6] The 1968 IFC Formulation for Scientific and General Use: A Formulation of the Thermodynamic Properties of Ordinary Water Substance. April 1968. Secretariat of IAPS, ASME United Engineering Center, NY, USA (1968).
- [7] IAPWS Release on the IAPWS Formulation 1997 for the Thermodynamic Properties of Water and Steam for Industrial Use. IAPWS Secretariat, Erlangen Germany (1997).
- [8] The 1967 IFC Formulation for Industrial Use, issued by the International Formulation Committee of the 6th International Conference on the Properties of Steam, VDI, Düsseldorf (1967).
- [9] PRESTON-THOMAS, H., The International Temperature Scale of 1990 (ITS-90), Metrologia 27, 3-10, (1990).
- [10] KRETZSCHMAR, H.-J., et al., Supplementary Equation  $v(p,T)$  for the Critical Region to the New Industrial Formulation IAPWS-IF97. In: Proceedings of the 13<sup>th</sup> ICPWS Steam, Water, and Hydrothermal Systems: Physics and Chemistry Meeting the Needs of Industry. Eds. P.R. Tremaine et al. NCR-CNRC NCR Research Press, Ottawa, Canada. pgs 255-264. (ISBN 0-660-17778-1).
- [11] Supplementary Release on Backward Equations for Pressure as Function of Enthalpy and Entropy  $p(h,s)$  to the IAPWS Industrial Formulation 1997 for the Thermodynamic Properties of Water and Steam. IAPWS Secretariat (2001).

- [12] KRETZSCHMAR, H.J., et al., Supplementary Backward Equations for Pressure as Function of Enthalpy and Entropy  $p(h,s)$  to the IAPWS Industrial Formulation 1997 for the Thermodynamic Properties of water and Steam. Submitted to Jour. of Engineering for Gas Turbines and Power.
- [13] Supplementary Release on Backward Equations for the functions  $T(p,h)$ ,  $v(p,h)$  and  $T(p,s)$ ,  $v(p,s)$  for Region 3 to the IAPWS Industrial Formulation 1997 for the Thermodynamic Properties of Water and Steam. IAPWS Secretariat, August 2003. Jour. of Eng. for Gas Turbines and Power. In preparation.
- [14] Supplementary release on backward equations  $p(h,s)$  for region 3, equations as a function of  $h$  and  $s$  for the region boundaries, and an equation  $T_{sat}(h,s)$  for wet steam of the IAPWS industrial formulation 1997 for the thermodynamic properties of water and steam. Draft. IAPWS Meeting Vejle, DK (2003).
- [15] MIYAGAWA, K., HILL, P.G., Application of the Taylor Series Expansion Method (TTSE) to the Mollier State Plane for Rapid and Accurate Calculation of Water and Steam Properties. In: Proceedings of the 13<sup>th</sup> ICPWS, Steam, Water, and Hydrothermal Systems: Physics and Chemistry Meeting the Needs of Industry. Eds P.R. Tremaine et al. NCR-CNRC, NCR Research Press, Ottawa, Canada. ISBN 0-660-17778-1. pp 229-237.
- [16] MIYAGAWA, K., HILL, P.G., A Tabular Taylor Series Expansion Method for Fast Calculation of Water and Steam Properties. Trans. ASME Jour. of Eng. for Gas Turbine and Power 119, 485-491 (1997).
- [17] HILL, P.G., MIYAGAWA, K., DENTON, J.D., Fast and Accurate Inclusion of Steam Properties in Two- and Three-dimensional CFD Calculations. J. Mech. Eng. Sci., Proc. Inst. Mech. Eng. 214, 903-919 (2000).
- [18] MIYAGAWA, K., HILL, P.G., Rapid and Accurate Calculation of Water and Steam Properties using the Taylor Series Expansion Method. Trans. ASME, Jour. of Eng. for Gas Turbine and Power 123, 707-712 (2001).
- [19] Guideline on the Tabular Taylor Series Expansion (TTSE) Method for Calculation of Thermodynamic Properties of Water and Steam Applied to IAPWS-95 as an Example IAPWS Secretariat, Vejle, DK (2003).
- [20] MIYAGAWA, K., Fast and accurate calculation of transport properties of water and steam using tabular Taylor Series expansion (TTSE) method (TTSEtrans). Presented on the IAPWS Meeting (2003), Vejle Denmark.
- [21] The IAPS Formulation 1985 for the Viscosity of Ordinary Water Substance. IAPS Secretariat Moscow, USSR (1985).
- [22] Revised Release on the IAPS Formulation 1985 for the Viscosity of Ordinary Water Substance. IAPWS Secretariat Erlangen, Germany (1997), Draft 7/24/ 97.
- [23] Revised Release on the IAPS Formulation 1985 for the Viscosity of Ordinary Water Substance. IAPWS Secretariat, Vejle, Denmark (2003).
- [24] Harvey A.: Defect in IAPWS Viscosity Release and Suggested Correction. Report to IAPWS/IATP Task Group on Transport Properties of Water (2003).
- [25] The IAPS Formulation 1985 for the Thermal Conductivity of Ordinary Water Substance. IAPS Secretariat, Moscow, USSR (1985).
- [26] Revised Release on the IAPS Formulation 1985 for the Thermal Conductivity of ordinary Water Substance. IAPWS Secretariat, London, England (1998).
- [27] Release on Dielectric Constant of Water and Steam from 238 K to 873 K, and up to 1000 MPa. IAPWS Secretariat (1997).
- [28] Release on Static Dielectric Constant of Water and Steam. IAPS Secretariat (1977).
- [29] FERNÁNDES, D.P. et al., A database for the static dielectric constant of water and steam. J. Phys. Chem. Ref. Data 24, 1 (1995) 33-69.
- [30] FERNÁNDES, D.P., GOODWIN, A.R.H., LEMMON, E.W., LEVELT SENGERS, J.M.H., WILLIAMS, R.C., A formulation for the static permittivity of water and steam at temperatures from 238 K to 873 K at pressures up to 12000 MPa including derivatives and Debye-Hueckel coefficients. J. Phys. Chem. Ref. Data 26, 4 (1997) 1125-1166.
- [31] Release on the Refractive Index of Ordinary Water Substance as a Function of Wavelength, Temperature and Pressure. IAPWS Secretariat, Erlangen Germany (1997).



- [32] SCHIEBENER, P., STRAUB, J., LEVELT SENGERS, J.M.H., GALLAGHER, J.S., Refractive Index of Water and Steam as Function of Wavelength, Temperature and Pressure. J. Phys. Chem. Ref. Data 19, 677-715 (1990).
- [33] BERTIE, J.E., LAN, Y., Appl. Spectrosc. 50, 1074 (1996).
- [34] Refractive index of water and steam as a function of wavelength, temperature and pressure. Release issued Sept. 1991 (5 pgs.). In: Physical Chemistry of Aqueous systems. Proc.12th ICPWS. Eds: White Jr. H.J., Sengers J.V., Neuman D.B., Bellows J.C.: Appendix 1: IAPWS Releases and Guidelines, A2.
- [35] IAPWS Release on Surface Tension of Ordinary Water Substance. IAPWS Secretariat, (1994).
- [36] Release on the Surface Tension of Ordinary Water Substance. IAPS Secretariat, (1977).
- [37] Release on the Values of Temperature, Pressure and Density of Ordinary and Heavy Water Substances at their Respective Critical Points. (Revision of the 1983 Release). IAPWS Secretariat (1992).
- [38] WAGNER, W., KRUSE, A., Properties of Water and Steam / Zustandsgrößen von Wasser und Wasserdampf. Springer-Verlag, Berlin (ISBN 3-540-64339-7) (1998).
- [39] KRETZSCHMAR, H.-J., Mollier  $h,s$ -Diagram for Water and Steam; IAPWS Industrial formulation 1997 for the Thermodynamic Properties of Water and Steam. Springer-Verlag, Berlin (ISBN 3-540- 64375-3) (1998).
- [40] MARES, R., SIFNER, O., KADRNOZKA, J.: PARNI TABULKY / Steam Tables - IAPWS-IF97. VUT Brno, VUTIUM Press, Brno. (ISBN 80-214-1316-6) (1999).
- [41] MARES, R., CERVENÝ, P., Mollieruv  $h-s$  diagram vody a vodní páry / Mollier  $h,s$  Diagram for Water and Steam – IAPWS-IF97. VUT Brno, VUTIUM Press. (ISBN 80-214-1266-6).
- [42] 1999 JSME Steam Tables. The Japan Society of Mechanical Engineers, Tokyo. (ISBN4-88898-093-4 C3053) (1999).
- [43] ALEKSANDROV, A.A., GRIGOREV, B.A., Tablicy Teplofizicheskikh svoystv vody a vodjanogo para. Spravochnik. Izdatelstvo MEI, Moscow. (ISBN 5-7046-0397-1) (1999).
- [44] PARRY, W.T., BELLOWES, J.C., GALLAGHER, J.S., HARVEY, A.H., ASME Steam Tables based on IAPWS-IF97. ASME International, New York. (ISBN 0791801543) (2000).
- [45] WAGNER, W., SPAN, R., BONSEN, C., WASSER und Wasserdampf. Interaktive Software zur Berechnung der thermodynamischen Zustandgrößen auf der Basis des Industriestandard IAPWS-IF97. Windows Version. CD-ROM mit Handbuch. Springer Verlag Berlin, (ISBN 3-540-14797-7) (2000.).
- [46] Proceedings: New International Formulation for Thermodynamic Properties of Water and Steam IAPWS-IF97. January 1998. CZ NC PWS, Institute of Thermo-mechanics, Academy of Sciences of the Czech Republic. (in Czech.)
- [47] KRETZSCHMAR, H.-J., STÖCKER, I., JÄHNE, I., Software for the new Industrial Formulation IAPWS-IF97 for water and steam including DLL and Add-In Fluid for MS-Excel EXL<sup>Graphics</sup> LibIF97. University of Applied Sciences, Department of Technical Thermodynamics. Zittau and Görlitz Germany. (1999).
- [48] IAPS Release on Surface Tension of Heavy Water Substance (D<sub>2</sub>O). IAPS Secretariat (1985).
- [49] Release on the IAPS Formulation 1984 for the Thermodynamic Properties of Heavy Water Substance. IAPS Secretariat, Moscow (1984).
- [50] HILL, P.G., MACMILLAN, R.D.CH., A Fundamental Equation of State for Heavy Water. J. Phys. Chem. Ref. Data 11 (1982) 1-14.
- [51] Release on the Viscosity and Thermal Conductivity of Heavy Water Substance. Sept. 1982, Revised 1984. IAPS Secretariat (1984).
- [52] MACMILLAN, R.D.CH., HILL, P.G., Equations for the saturation properties of heavy water. In: Properties of Water and Steam. Proc. 11<sup>th</sup> International Conference, Ed.: Pichal, M., Šifner, O., Hemisphere Publishing Corporation, New York 1990, pp. 57-68.
- [53] Release on the Values of Temperature, Pressure and Density of Ordinary and Heavy Water Substances at their Respective Critical Points. IAPS Secretariat (1983).
- [54] IAPWS Release on Surface Tension of Heavy Water Substance. IAPWS Secretariat (1994) (Revised Release of 1985).

## SUPPLEMENT 1

### IAPWS RELEASES, GUIDELINES AND OTHER DOCUMENTS<sup>1</sup>

---

IAPWS provides recommended formulations for numerous properties of water, steam, and aqueous solutions. These fall in several categories:

**Releases** provide carefully evaluated, internationally agreed-upon data and formulations of properties for which measurements of high quality exist over a wide range of states. They are intended to embody the state of the art for representation of the property at the time of the Release.

**Supplementary Releases** provide supplementary material to an existing Release, or provide specific (perhaps simpler) formulations for a subset of the material in an existing Release. They are intended to be of the same quality as Releases. *Guidelines* are similar, but for properties where the quality or range of the available data is limited. They are therefore not expected to provide as definitive a representation as Releases.

**Guidelines** are expected to require revision when new information is available.

**Advisory Notes** are documents that give additional information and guidance that is intended to be useful for users of IAPWS property formulations.

*A different type of IAPWS document is the IAPWS Certified Research Need (ICRN), which is a statement of the need for research on a specific topic.*

All current IAPWS Releases, Supplementary Releases, Guidelines and Advisory Notes are listed below (with the most recent at the top of each list) and are downloadable as PDF files.

#### Releases

- Revised Release on the IAPS Formulation 1985 for the Viscosity of Ordinary Water Substance (August 2003) (This is a revision of the 1997 release, which was a revision of the 1985 release).
- Revised Release on the IAPS Formulation 1985 for the Thermal Conductivity of Ordinary Water Substance (September 1998) (This is a revision of the 1985 release).
- Release on the Refractive Index of Ordinary Water Substance as a Function of Wavelength, Temperature and Pressure (September 1997) (This release replaces the corresponding release of 1991).

---

<sup>1</sup> Taken from the IAPWS homepage <http://www.iapws.org/release.htm>.

- Release on the Static Dielectric Constant of Ordinary Water Substance for Temperatures from 238 K to 873 K and Pressures up to 1000 MPa (September 1997) (This release replaces the corresponding release of 1977).
- Release on the IAPWS Industrial Formulation 1997 for the Thermodynamic Properties of Water and Steam (September 1997) (This release replaces the corresponding release of 1967). NOTE: This release has been supplemented by additional “backward” equations for  $p(h,s)$  in Regions 1 and 2 and  $T(p,h)$ ,  $v(p,h)$ ,  $T(p,s)$ ,  $v(p,s)$  in Region 3.
- Release on the IAPWS Formulation 1995 for the Thermodynamic Properties of Ordinary Water Substance for General and Scientific Use (September 1996) (This release replaces the corresponding release of 1984).
- Release: “Surface Tension of Heavy Water Substance” (September 1994) (This is a revision of the 1985 Release).
- Release: “Surface Tension of Ordinary Water Substance” (September 1994) (This is a revision of the 1976 Release).
- Release on the Pressure along the Melting and Sublimation Curves of Ordinary Water Substance (September 1993) (This is a revision of the 1989 Release)
- Release: “Values of Temperature, Pressure and Density of Ordinary and Heavy Water Substances at their Respective Critical Points” (September 1992) (This is a revision of the 1983 Release).
- Release: “IAPS Formulation 1984 for the Thermodynamic Properties of Heavy Water Substance” (December 1984).
- Release: “Viscosity and Thermal Conductivity of Heavy Water Substance” (February 1984).
- Release: “Ion Product of Water Substance” (May 1980).

### Supplementary Releases

- Supplementary Release on Backward Equations for the Functions  $T(p,h)$ ,  $v(p,h)$ , and  $T(p,s)$ ,  $v(p,s)$  for Region 3 of the IAPWS Industrial Formulation 1997 for the Thermodynamic Properties of Water and Steam (August 2003) *NOTE: This Supplementary Release provides additional “backward” equations designed to accompany the IAPWS Industrial Formulation 1997.*
- Supplementary Release on Backward Equations for Pressure as a Function of Enthalpy and Entropy  $p(h,s)$  to the IAPWS Industrial Formulation 1997 for the Thermodynamic Properties of Water and Steam (September 2001). *NOTE: This Supplementary Release provides additional “backward” equations designed to accompany the IAPWS Industrial Formulation 1997.*
- Supplementary Release: “Saturation Properties of Ordinary Water Substance” (September 1992) (This is a revision of the 1986 Release)

## Guidelines

- Guideline on the Tabular Taylor Series Expansion (TTSE) Method for Calculation of Thermodynamic Properties of Water and Steam Applied to IAPWS-95 as an Example (August 2003).
- Guideline on the Use of Fundamental Physical Constants and Basic Constants of Water (September 2001) *NOTE: This Guideline is reviewed annually and updated as necessary. Latest revision July 2002.*
- Guideline on the IAPWS Formulation 2001 for the Thermodynamic Properties of Ammonia-Water Mixtures (September 2001).
- Guideline on the Critical Locus of Aqueous Solutions of Sodium Chloride (September 2000).
- Guideline on the Equilibrium Constant for the Distribution of Gaseous Solutes between Steam and Water (September 1998).
- Guideline: “Solubility of Sodium Sulfate in Aqueous Mixtures of Sodium Chloride and Sulfuric Acid from Water to Concentrated Solutions, from 250°C to 350°C” (September 1994) (This is a revision of the 1990 Guideline).
- Guideline: Solubility of Simple Apolar Gases in Light and Heavy Water at High Temperature (September 1993).
- Guideline: “Electrolytic Conductivity (Specific Conductance) of Liquid and Dense Supercritical Water from 0°C to 800°C and Pressures up to 1000 MPa” (May 1990).

## Advisory Notes

- Advisory Note No. 1: Uncertainties in Enthalpy for the IAPWS Formulation 1995 for the Thermodynamic Properties of Ordinary Water Substance for General and Scientific Use (IAPWS-95) and the IAPWS Industrial Formulation 1997 for the Thermodynamic Properties of Water and Steam (IAPWS-IF97) (August 2003).

**Source for paper copies:** Paper copies of IAPWS Releases and Guidelines are available from the Executive Secretary, Barry Dooley, [bdooley@epri.com](mailto:bdooley@epri.com). Please include the full title from the list in any request.

This page updated September 10, 2003

## SUPPLEMENT 2

### THE IAPWS INDUSTRIAL FORMULATION 1997 FOR THE THERMODYNAMIC PROPERTIES OF WATER AND STEAM

(1)

---

#### 1. INTRODUCTION

In 1997 the International Association for the Properties of Water and Steam (IAPWS) adopted a new formulation for industrial calculations under the name “IAPWS Industrial Formulation 1997 for the Thermodynamic Properties of Water and Steam” abbreviated to “Industrial Formulation IAPWS-IF97” or even shorter “IAPWS-IF97”. This formulation entirely replaces the previous standard for industrial calculations IFC-67 [12].

The new formulation IAPWS-IF97 [10], [11] is in the new temperature scale ITS-90 [1], is more accurate than IFC-67, has better thermodynamic consistency on the region boundaries and involves the high-temperature region. The average computation speed is five times higher in comparison with IFC-67.

A brief description of the formulation IAPWS-IF97 is given below. The details as estimated uncertainties, deviations of the backward equations from the basic equations, inconsistencies between equations along region boundaries, values for verification of user computer-programs, information about computing time in relation to IFC-67, etc. are presented in [10] and [11].

#### 2. STRUCTURE OF FORMULATION IAPWS-IF97

IAPWS-IF97 formulation consists of a set of equations for five regions, as can be seen on the p-t graph, Fig.1. They cover the range of validity

$$273.15 \text{ K} \leq T \leq 1073.15 \text{ K} \quad p \leq 100 \text{ MPa}$$

$$1073.15 \text{ K} < T \leq 2273.15 \text{ K} \quad p \leq 10 \text{ MPa}.$$

The basic equations, framed in Fig.1, are in specific Gibbs free energy  $g(p, T)$ , for the regions 1, 2 and 5, in specific Helmholtz free energy  $f(\rho, T)$  for region 3, and in a saturation pressure equation  $p_s(T)$  for the saturation curve, region 4.

All the rest thermodynamic properties can be derived from the basic equations by appropriate combinations of the Gibbs functions (for regions 1, 2 and 5) or Helmholtz function (for region 3) and their derivatives. The relations are given in **Attachment 1**.

Numerical values of all coefficients are listed in **Attachment 2**.

The boundary between regions 2 and 3 is defined by a quadratic equation, the B23 function, describing roughly an isentropic line with values of entropy between 5.047 kJ/kg.K and 5.261 kJ/kg.K. It reads:

$$\pi = n_1 + n_2\theta + n_3\theta^2 \quad (1)$$

or alternatively expressed explicitly in temperature

$$\theta = n_4 + [(\pi - n_5) / n_3]^{0.5}. \quad (2)$$

where  $\pi = p/p^*$  and  $\theta = T^*/T$  with  $p^* = 1 \text{ MPa}$ ,  $T^* = 1 \text{ K}$ .

Equations (1) and (2) cover the range from 623.15 K at 16.5292 MPa up to 863.15 K at 100 MPa.

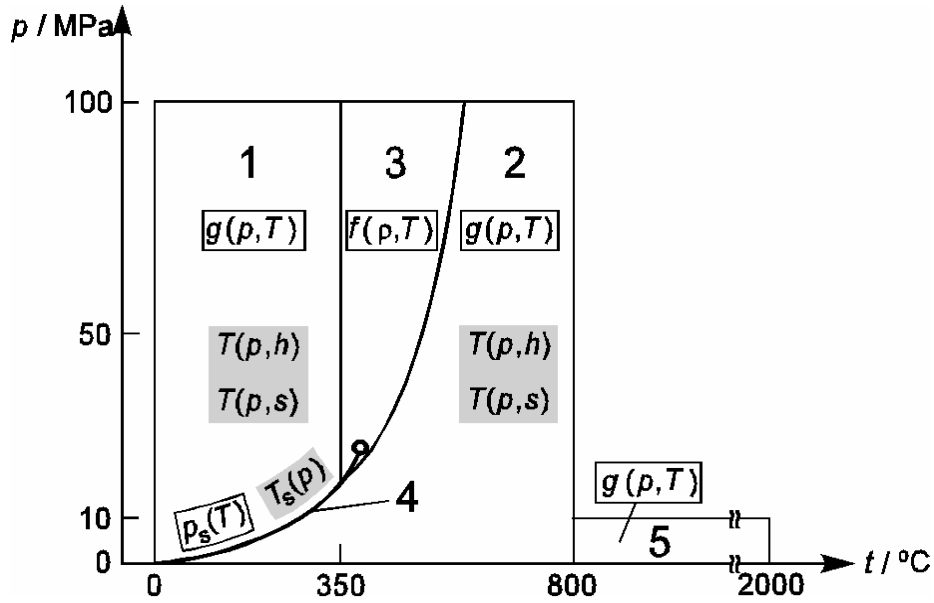


FIG. 1. Regions and equations of the IAPWS-IF97. Basic equations.

The specific gas constant of ordinary water is

$$R = 0.461\,526 \text{ kJ} \cdot \text{kg}^{-1} \cdot \text{K}^{-1}.$$

## 2.1. Region 1 – compressed liquid

$$\frac{g(p, T)}{RT} = \gamma(\pi, \tau) = \sum_{i=1}^{34} n_i (7, 1 - \pi)^{I_i} (\tau - 1.222)^{J_i}, \quad (3)$$

where  $\pi = p/p^*$  and  $\tau = T^*/T$  with  $p^* = 16.53 \text{ MPa}$ ,  $T^* = 1386 \text{ K}$ .

Equation (3) covers the region 1 defined with following parameters:

$$273.15 \text{ K} \leq T \leq 623.15 \text{ K}, \quad p_s(T) \leq p \leq 100 \text{ MPa}, \quad \text{where } p_s(T) \text{ is the saturation pressure.}$$

## 2.2. Region 2 – superheated steam

$$\frac{g(p, T)}{RT} = \gamma(\pi, \tau) = \gamma^0(\pi, \tau) + \gamma^r(\pi, \tau), \quad (4)$$

$$\gamma^0 = \ln \pi + \sum_{i=1}^9 n_i^0 \tau^{J_i^0}, \quad (5)$$

$$\gamma^r = \sum_{i=1}^{43} n_i \pi^{I_i} (\tau - 0.5)^{J_i} \quad (6)$$

In Eqs. (5) and (6)  $\pi = p/p^*$  and  $\tau = T^*/T$  with  $p^* = 1 \text{ MPa}$ ,  $T^* = 540 \text{ K}$ .

Equation (4) covers the region 2 defined with following parameters:

$$\begin{array}{lll} 273.15 \text{ K} \leq T \leq 623.15 \text{ K} & 0 < p \leq p_s(T)_{Eq(9)} \\ 623.15 \text{ K} < T \leq 863.15 \text{ K} & 0 < p \leq p(T)_{Eq(1)} \\ 863.15 \text{ K} < T \leq 1073.15 \text{ K} & 0 < p \leq 100 \text{ MPa} \end{array}$$

### 2.3. Region 3 – critical and supercritical

$$\frac{f(\rho, T)}{RT} = \Phi(\delta, T) = n_1 \ln \delta + \sum_{i=2}^{40} n_i \delta^{I_i} \tau^{J_i}, \quad (7)$$

where  $\delta = \rho / \rho^*$  and  $\tau = T^* / T$  with  $\rho^* = \rho_c = 322 \text{ kg} \cdot \text{m}^{-3}$ ,  $T^* = T_c = 647.096 \text{ K}$ .

Equation (7) covers the region 3 defined with following parameters:

Besides representing the thermodynamic properties in the single-phase region, Eq. (7) also meets the phase-equilibrium condition along the saturation line for  $T \geq 623.15 \text{ K}$  to the critical temperature  $T_c$ . Moreover, Eq. (5) meets exactly the critical parameters and yields zero for the first two pressure derivatives with respect to density at the critical point.

### 2.4. Region 4 – Saturation-pressure equation

It is an implicit quadratic equation, which can be solved with regard to both saturation pressure  $p_s$  and saturation temperature  $T_s$ . It reads:

$$\beta^2 \mathcal{G}^2 + n_1 \beta^2 \mathcal{G} + n_2 \beta^2 + n_3 \beta \mathcal{G}^2 + n_4 \beta \mathcal{G} + n_5 \beta + n_5 \mathcal{G}^2 + n_7 \mathcal{G} + n_8 = 0, \quad (8)$$

where  $\beta = (p_s / 1 \text{ MPa})^{0.25}$  and  $\mathcal{G} = T_s / 1 \text{ K} + [n_9 / (T_s / T^*) - n_{10}]$

Saturation pressure follows from

$$p_s / 1 \text{ MPa} = [2C / (-B + (B^2 - 4AC)^{0.5})]^4, \quad (9)$$

where  $A = \mathcal{G}^2 + n_1 \mathcal{G} + n_2$ ,  $B = n_3 \mathcal{G}^2 + n_4 \mathcal{G} + n_5$ , and  $C = n_6 \mathcal{G}^2 + n_7 \mathcal{G} + n_8$ .

(2) Saturation temperature follows from

$$T_s / 1 \text{ K} = \{n_{10} + D - [(n_{10} + D)^2 - 4(n_9 + n_{10} D)]^{0.5}\} / 2 \quad (10)$$

where  $D = 2G / [-F - (F^2 - 4EG)^{0.5}]$ ;  $E = \beta^2 + n_3 \beta + n_6$ ;

$$F = n_1 \beta^2 + n_4 \beta + n_7 \quad \text{and} \quad G = n_2 \beta^2 + n_5 \beta + n_8.$$

Equations (8) through (10) are valid along the entire vapor-liquid saturation curve from the triple-point temperature to the critical point temperature (647.096 K), can be simply extrapolated to 273.15 K, and from the 611.231 Pa (pressure extrapolated to  $T = 273.15 \text{ K}$ ) to the critical pressure 22.064 MPa, respectively.

### 2.5. Region 5 – high temperatures

$$\frac{g(p, T)}{RT} = \gamma(\pi, \tau) = \gamma^0(\pi, \tau) + \gamma^r(\pi, \tau), \quad (11)$$

$$\gamma^0 = \ln \pi + \sum_{i=1}^6 n_i^0 \tau^{J_i^0}, \quad (12)$$

$$\gamma^r = \sum_{i=1}^5 n_i \pi^{I_i} \tau^{J_i}, \quad (13)$$

In Equations (11) up to (13)  $\pi = p / p^*$  and  $\tau = T^* / T$ , where  $p^* = 1 \text{ MPa}$  and  $T^* = 1000 \text{ K}$ .

Equation (11) covers the region 5 defined with following parameters:

$$1073.15 \text{ K} \leq T \leq 2273.15 \quad 0 < p \leq 10 \text{ MPa}.$$

Equations in regions 1, and 3, Eqs. (3) and (7), yield reliable values for the metastable states close to the stable regions. For the region 2 a special equation for the metastable region is given.

## 2.6. Supplementary equation for the metastable-steam region 2

It reads

$$\frac{g(p, T)}{RT} = \gamma(\pi, \tau) = \gamma^0(\pi, \tau) + \gamma^r(\pi, \tau), \quad (16)$$

The equation for the ideal-gas part  $\gamma^0$  is identical with Eq. (5) except for the values of the coefficients  $n_1^0$  and  $n_2^0$ , which have following values:

$$n_1^0 = -0.969\,327\,683\,930\,49 \times 10^1 \quad n_2^0 = 0.100\,872\,759\,700\,06 \times 10^2,$$

The other values of coefficients are as given for Eq. (5).

The residual part is

$$\gamma^r = \sum_{i=1}^{13} n_i \pi^{I_i} (\tau - 0.5)^{J_i}, \quad (15)$$

where  $\pi = p/p^*$  and  $\tau = T^*/T$  with  $p^* = 1$  MPa, and  $T^* = 540$  K as well as for relations between the relevant thermodynamic properties of  $\gamma^0$  and  $\gamma^r$  of the dimensionless Gibbs function and its derivatives are summarized in Attachment 1.

The range of validity of Eq. (16) in the metastable-steam region is from the saturation vapor line to 5% equilibrium moisture line (determined from the equilibrium  $h'$  and  $h''$  values) at pressures from the triple-point pressure up to 10 MPa. Values for the computer-program verification are also given.

## 2.6. Backward equations

In order to achieve a further increase in the computation speed backward equations  $T(p, h)$  and  $T(p, s)$  for regions 1 and 2, and  $T(p_s)$  for the saturation curve, region 4, were developed.

Between the backward and basic equations an extremely good numerical consistency is required. Otherwise numerical problems would arise in transition from backward to basic equations and vice versa. The tolerable numerical inconsistency has to be about one order of magnitude smaller than the uncertainties of the corresponding equations. The boundary between the sub-regions 2a and 2b is the isobar  $p = 4$  MPa. The boundary between sub-region 2b and 2c corresponds to the entropy line  $s = 5.85 \text{ kJ} \cdot \text{kg}^{-1} \cdot \text{K}^{-1}$ .

## 2.7. Region 1:

The backward equation  $T(p, h)$  and  $T(p, s)$  have the following dimensionless form:

$$T(p, h)/T^* = \theta(\pi, \tau) = \sum_{i=1}^{20} n_i \pi^{I_i} (\eta + 1)^{J_i}, \quad (18)$$

where  $\theta = T/T^*$ ,  $\pi = p/p^*$ , and  $\eta = h/h^*$  with  $T^* = 1$  K,  $p^* = 1$  MPa, and  $h^* = 2500 \text{ kJ} \cdot \text{kg}^{-1}$ .

$$T(p, s)/T^* = \theta(\pi, \sigma) = \sum_{i=1}^{20} n_i \pi^{I_i} (\sigma + 2)^{J_i} \quad (19)$$



where,  $\theta = T / T^*$ ,  $\pi = p / p^*$ , and  $\sigma = s / s^*$  with  $T^* = 1 \text{ K}$ ,  $p^* = 1 \text{ MPa}$ , and  $s^* = 1 \text{ kJ} \cdot \text{kg}^{-1} \cdot \text{K}^{-1}$ .

Both equations, Eq. (16) and (19), have the same range of validity as the equation, Eq. (3), except for the metastable region (superheated water).

## 2.8. Region 2: $T(p, h)$ equations:

Region 2 is covered by three equations  $T(p, h)$  and three equations  $T(p, s)$ .

*Sub-region 2a*

$$T_{2a}(p, h) / T^* = \theta_{2a}(\pi, \eta) = \sum_{i=1}^{34} n_i \pi^{I_i} (\eta - 2.1)^{J_i} \quad (20)$$

*Sub-region 2b*

$$T_{2b}(p, h) / T^* = \theta_{2b}(\pi, \eta) = \sum_{i=1}^{38} n_i (\pi - 2)^{I_i} (\eta - 2.6)^{J_i} \quad (21)$$

*Sub-region 2c*

$$T_{2c}(p, h) / T^* = \theta_{2c}(\pi, \eta) = \sum_{i=1}^{23} n_i (\pi + 25)^{I_i} (\eta - 2.1.8)^{J_i} \quad (22)$$

In Eq. (20) through (22) is  $\theta = T / T^*$ ,  $\pi = p / p^*$ , and  $\eta = h / h^*$  with  $T^* = 1 \text{ K}$ ,  $p^* = 1 \text{ MPa}$ , and  $h^* = 2000 \text{ kJ} \cdot \text{kg}^{-1}$ .

For the  $T(p, h)$  functions a special correlation equation, between sub-regions 2b and 2c has been developed in order to know whether the  $T(p, h)$  equation for sub-region 2b or for sub-region 2c has to be used for given values  $p$  and  $h$ . It is so called

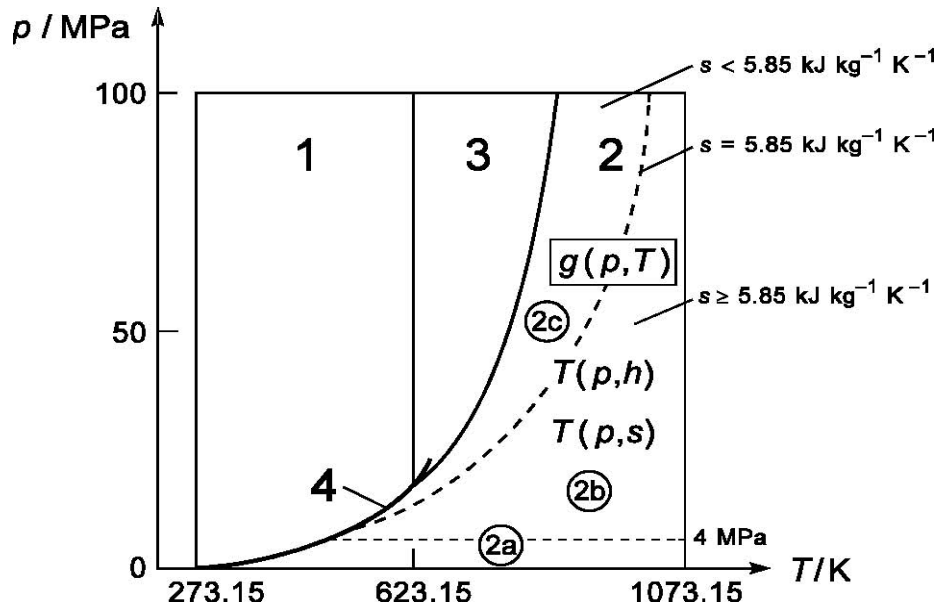


FIG. 2. Division of region 2 of IAPWS-IF97 into the subregions 2a, 2b, and 2c for the backward equations  $T(p, h)$  and  $T(p, s)$ .

Equation B2bc, which makes possible to determine if  $(p, h)$ , is in the sub-region 2b or 2c. It is a simple quadratic pressure-enthalpy relation, which reads

$$\pi = n_1 + n_2 \eta + n_3 \eta^2, \quad (23)$$

where  $\pi = p / p^*$ , and  $\eta = h / h^*$  with  $p^* = 1 \text{ MPa}$ , and  $h^* = 1 \text{ kJ} \cdot \text{kg}^{-1}$ .

The enthalpy-explicit form of Eq. (21) is as follows

$$\eta = n_4 + [(\pi - n_5) / n_3]^{1/2} \quad (24)$$

Equations (23) and (24) cover the boundary line between sub-regions 2b and 2c from the saturation state at  $T = 554.485 \text{ K}$  and  $p_s = 6.546 \text{ MPa}$  to  $T = 1019.32 \text{ K}$  and  $p = 100 \text{ MPa}$ .

## 2.9. Region 2: $T(p, s)$ equations:

For this backward equations the boundary between subregions 2(b) and 2(c) corresponds directly to the isentropic line  $s = 5.85 \text{ kJ} \cdot \text{kg}^{-1} \cdot \text{K}^{-1}$ .

*Sub-region 2a:*

$$T_{2a}(p, s) / T^* = \theta_{2a}(\pi, \sigma) = \sum_{i=1}^{46} n_i \pi^{I_i} (\sigma - 2)^{J_i}, \quad (25)$$

where  $\theta = T / T^*$ ,  $\pi = p / p^*$ , and  $\sigma = s / s^*$  with  $T^* = 1 \text{ K}$ ,  $p^* = 1 \text{ MPa}$ , and  $s^* = 2 \text{ kJ} \cdot \text{kg}^{-1} \cdot \text{K}^{-1}$ .

*Sub-region 2b:*

$$T_{2b}(p, s) / T^* = \theta_{2b}(\pi, \sigma) = \sum_{i=1}^{44} n_i \pi^{I_i} (10 - \sigma)^{J_i}, \quad (26)$$

where  $\theta = T / T^*$ ,  $\pi = p / p^*$ , and  $\sigma = s / s^*$  with  $p^* = 1 \text{ MPa}$ , and  $s^* = 0.7853 \text{ kJ} \cdot \text{kg}^{-1} \cdot \text{K}^{-1}$ .

*Sub-region 2c:*

$$T_{2c}(p, s) / T^* = \theta_{2c}(\pi, \sigma) = \sum_{i=1}^{30} n_i \pi^{I_i} (2 - \sigma)^{J_i}, \quad (27)$$

where  $\theta = T / T^*$ ,  $\pi = p / p^*$ , and  $\sigma = s / s^*$  with  $p^* = 1 \text{ MPa}$ , and  $s^* = 2.9251 \text{ kJ} \cdot \text{kg}^{-1} \cdot \text{K}^{-1}$ .

Equations (25) through (27) are only valid in the respective sub-region 2a, 2b, and 2c, which do not include the metastable-steam region. The lowest permissible pressure for Eq. (25) amounts to 611.153 Pa corresponding to the sublimation pressure at 273.15 K.

# ATTACHMENT 1

Table 1. Relations of thermodynamic properties to the dimensionless Gibbs free energy  $g$  and its derivatives  $a$  when using Eq. (3)

	$v = (\partial g / \partial p)_T$	$v(\pi, \tau) \frac{p}{RT} = \pi \gamma_\pi$
Specific internal energy	$u = g - T(\partial g / \partial T)_p - p(\partial g / \partial p)_T$	$\frac{u(\pi, \tau)}{RT} = \tau \gamma_\tau - \pi \gamma_\pi$
Specific entropy	$s = -(\partial g / \partial T)_p$	$\frac{s(\pi, \tau)}{R} = \tau \gamma_\tau - \gamma$
Specific enthalpy	$h = g - T(\partial g / \partial T)_p$	$\frac{h(\pi, \tau)}{RT} = \tau \gamma_\tau$
Specific isobaric heat capacity	$c_p = (\partial h / \partial T)_p$	$\frac{c_p(\pi, \tau)}{R} = -\tau^2 \gamma_{\tau\tau}$
Specific isochoric heat capacity	$c_v = (\partial u / \partial T)_v$	$\frac{c_v(\pi, \tau)}{R} = -\tau^2 \gamma_{\tau\tau} + \frac{(\gamma_\pi - \tau \gamma_{\pi\tau})^2}{\gamma_{\pi\pi}}$
Speed of sound	$w = v[-(\partial p / \partial v)_s]^{1/2}$	$\frac{w^2(\pi, \tau)}{RT} = \frac{\gamma_\pi^2}{\frac{(\gamma_\pi - \tau \gamma_{\pi\tau})^2}{\tau^2 \gamma_{\tau\tau}} - \gamma_{\pi\pi}}$
	$\gamma_\pi = \left[ \frac{\partial \gamma}{\partial \pi} \right]_\tau, \quad \gamma_{\pi\pi} = \left[ \frac{\partial^2 \gamma}{\partial \pi^2} \right]_\tau, \quad \gamma_\tau = \left[ \frac{\partial \gamma}{\partial \tau} \right]_\pi, \quad \gamma_{\tau\tau} = \left[ \frac{\partial^2 \gamma}{\partial \tau^2} \right]_\pi, \quad \gamma_{\pi\tau} = \left[ \frac{\partial^2 \gamma}{\partial \pi \partial \tau} \right]$	

Table 2. The dimensionless Gibbs free energy  $g$  and its derivatives  $a$  according to Eq. (3)

$$\begin{aligned}
 \gamma &= \sum_{i=1}^{34} n_i (7.1 - \pi)^{I_i} (\tau - 1.222)^{J_i} \\
 \gamma_\pi &= \sum_{i=1}^{34} -n_i I_i (7.1 - \pi)^{I_i-1} (\tau - 1.222)^{J_i} & \gamma_{\pi\pi} &= \sum_{i=1}^{34} n_i I_i (I_i - 1) (7.1 - \pi)^{I_i-2} (\tau - 1.222)^{J_i} \\
 \gamma_\tau &= \sum_{i=1}^{34} n_i (7.1 - \pi)^{I_i} J_i (\tau - 1.222)^{J_i-1} & \gamma_{\tau\tau} &= \sum_{i=1}^{34} n_i (7.1 - \pi)^{I_i} J_i (J_i - 1) (\tau - 1.222)^{J_i-2} \\
 \gamma_{\pi\tau} &= \sum_{i=1}^{34} -n_i I_i (7.1 - \pi)^{I_i-1} J_i (\tau - 1.222)^{J_i-1} \\
 \gamma_\pi &= \left[ \frac{\partial \gamma}{\partial \pi} \right]_\tau, & \gamma_{\pi\pi} &= \left[ \frac{\partial^2 \gamma}{\partial \pi^2} \right]_\tau, & \gamma_\tau &= \left[ \frac{\partial \gamma}{\partial \tau} \right]_\pi, & \gamma_{\tau\tau} &= \left[ \frac{\partial^2 \gamma}{\partial \tau^2} \right]_\pi, & \gamma_{\pi\tau} &= \left[ \frac{\partial^2 \gamma}{\partial \pi \partial \tau} \right]
 \end{aligned}$$

Table 3. Relations of thermodynamic properties to the ideal-gas part  $\gamma^0$  and the residual part  $\gamma^r$  of the dimensionless Gibbs free energy and their derivatives a when using Eq. (4) or Eq. (16)

Specific volume

$$v = (\partial g / \partial p)_T \quad v(\pi, \tau) \frac{P}{RT} = \pi(\gamma_\pi^0 + \gamma_\pi^r)$$

Specific internal energy

$$u = g - T(\partial g / \partial T)_p - p(\partial g / \partial p)_T \quad \frac{u(\pi, \tau)}{RT} = \tau(\gamma_\tau^0 + \gamma_\tau^r) - \pi(\gamma_\pi^0 + \gamma_\pi^r)$$

Specific entropy

$$s = -(\partial g / \partial T)_p \quad \frac{s(\pi, \tau)}{R} = \tau(\gamma_\tau^0 + \gamma_\tau^r) - (\gamma^0 + \gamma^r)$$

Specific enthalpy

$$h = g - T(\partial g / \partial T)_p \quad \frac{h(\pi, \tau)}{RT} = \tau(\gamma_\tau^0 + \gamma_\tau^r)$$

Specific isobaric heat capacity

$$c_p = (\partial h / \partial T)_p \quad \frac{c_p(\pi, \tau)}{R} = -\tau^2(\gamma_{\tau\tau}^0 + \gamma_{\tau\tau}^r)$$

Specific isochoric heat capacity

$$c_v = (\partial u / \partial T)_v \quad \frac{c_v(\pi, \tau)}{R} = -\tau^2(\gamma_{\tau\tau}^0 + \gamma_{\tau\tau}^r) - \frac{(1 + \pi\gamma_\pi^r - \tau\pi\gamma_{\pi\tau}^r)^2}{1 - \pi^2\gamma_{\pi\pi}^r}$$

Speed of sound

$$w = v[-(\partial p / \partial v)_s]^{1/2} \quad \frac{w^2(\pi, \tau)}{RT} = \frac{1 + 2\pi\gamma_\pi^r + \pi^2\gamma_\pi^{r^2}}{(1 - \pi^2\gamma_{\pi\pi}^r) + \frac{(1 + \pi\gamma_\pi^r - \tau\pi\gamma_{\pi\tau}^r)^2}{\tau^2(\gamma_{\tau\tau}^0 + \gamma_{\tau\tau}^r)}}$$

$$\gamma_\pi^r = \left[ \frac{\partial \gamma^r}{\partial \pi} \right]_\tau, \quad \gamma_{\pi\pi}^r = \left[ \frac{\partial^2 \gamma^r}{\partial \pi^2} \right]_\tau, \quad \gamma_\tau^r = \left[ \frac{\partial \gamma^r}{\partial \tau} \right]_\pi, \quad \gamma_{\tau\tau}^r = \left[ \frac{\partial^2 \gamma^r}{\partial \tau^2} \right]_\pi, \quad \gamma_{\pi\tau}^r = \left[ \frac{\partial^2 \gamma^r}{\partial \pi \partial \tau} \right],$$

$$\gamma_\tau^0 = \left[ \frac{\partial \gamma^0}{\partial \tau} \right]_\pi, \quad \gamma_{\tau\tau}^0 = \left[ \frac{\partial^2 \gamma^0}{\partial \tau^2} \right]_\pi,$$

Table 4. The ideal-gas part  $\gamma^0$  of the dimensionless Gibbs free energy and its derivatives according to Eq. (5)

$$\gamma^0 = \ln \pi + \sum_{i=1}^9 n_i^0 \tau^{J_i^0}$$

$$\gamma_\pi^0 = 1/\pi + 0 \quad \gamma_{\pi\pi}^0 = -1/\pi^2 + 0$$

$$\gamma_\tau^0 = 0 + \sum_{i=1}^9 n_i^0 J_i^0 \tau^{J_i^0-1} \quad \gamma_{\tau\tau}^0 = 0 + \sum_{i=1}^9 n_i^0 J_i^0 (J_i^0 - 1) \tau^{J_i^0-2}$$

$$\gamma_{\pi\tau}^0 = 0 + 0$$

$$\gamma_\pi^0 = \left[ \frac{\partial \gamma^0}{\partial \pi} \right]_\tau, \quad \gamma_{\pi\pi}^0 = \left[ \frac{\partial^2 \gamma^0}{\partial \pi^2} \right]_\tau, \quad \gamma_\tau^0 = \left[ \frac{\partial \gamma^0}{\partial \tau} \right]_\pi, \quad \gamma_{\tau\tau}^0 = \left[ \frac{\partial^2 \gamma^0}{\partial \tau^2} \right]_\pi, \quad \gamma_{\pi\tau}^0 = \left[ \frac{\partial^2 \gamma^0}{\partial \pi \partial \tau} \right]$$

Table 5. The residual part  $\gamma^r$  of the dimensionless Gibbs free energy and its derivatives according  $\gamma^r$  Eq. (6)

$$\begin{aligned}
 \gamma^r &= \sum_{i=1}^{43} n_i \pi^{I_i} (\tau - 0.5)^{J_i} \\
 \gamma_{\pi}^r &= \sum_{i=1}^{43} n_i I_i \pi^{I_i-1} (\tau - 0.5)^{J_i} & \gamma_{\pi\pi}^r &= \sum_{i=1}^{43} n_i I_i (I_i - 1) \pi^{I_i-2} (\tau - 0.5)^{J_i} \\
 \gamma_{\tau}^r &= \sum_{i=1}^{43} n_i \pi^{I_i} J_i (\tau - 0.5)^{J_i-1} & \gamma_{\tau\tau}^r &= \sum_{i=1}^{43} n_i \pi^{I_i} J_i (J_i - 1) (\tau - 0.5)^{J_i-2} \\
 \gamma_{\pi\tau}^r &= \sum_{i=1}^{43} n_i I_i \pi^{I_i-1} J_i (\tau - 0.5)^{J_i-1} \\
 \gamma_{\pi}^r &= \left[ \frac{\partial \gamma^r}{\partial \pi} \right]_{\tau}, & \gamma_{\pi\pi}^r &= \left[ \frac{\partial^2 \gamma^r}{\partial \pi^2} \right]_{\tau}, & \gamma_{\tau}^r &= \left[ \frac{\partial \gamma^r}{\partial \tau} \right]_{\pi}, & \gamma_{\tau\tau}^r &= \left[ \frac{\partial^2 \gamma^r}{\partial \tau^2} \right]_{\pi}, & \gamma_{\pi\tau}^r &= \left[ \frac{\partial^2 \gamma^r}{\partial \pi \partial \tau} \right]
 \end{aligned}$$

Table 6. Relations of thermodynamic properties to the dimensionless Helmholtz free energy  $f$  and its derivatives a when using Eq. (7)

Pressure

$$p = \rho^2 (\partial f / \partial \rho)_T \quad \frac{p(\delta, \tau)}{\rho RT} = \delta \phi_{\delta}$$

Specific internal energy

$$u = f - T (\partial f / \partial T)_{\rho} \quad \frac{u(\delta, \tau)}{RT} = \tau \phi_{\tau}$$

Specific entropy

$$s = -(\partial f / \partial T)_{\rho} \quad \frac{s(\delta, \tau)}{R} = \tau \phi_{\tau} - \phi$$

Specific enthalpy

$$h = f - T (\partial f / \partial T)_{\rho} + \rho (\partial f / \partial \rho)_T \quad \frac{h(\delta, \tau)}{RT} = \tau \phi_{\tau} + \delta \phi_{\delta}$$

Specific isochoric heat capacity

$$c_v = (\partial u / \partial T)_{\rho} \quad \frac{c_v(\delta, \tau)}{R} = -\tau^2 \phi_{\tau\tau}$$

Specific isobaric heat capacity

$$c_p = (\partial h / \partial T)_{\rho} \quad \frac{c_p(\delta, \tau)}{R} = -\tau^2 \phi_{\tau\tau} + \frac{(\delta \phi_{\delta} - \delta \tau \phi_{\delta\tau})^2}{2\delta \phi_{\delta} + \delta^2 \phi_{\delta\delta}}$$

Speed of sound

$$w = (\partial p / \partial \rho)_s^{1/2} \quad \frac{w^2(\delta, \tau)}{RT} = 2\delta \phi_{\delta} + \delta^2 \phi_{\delta\delta} - \frac{(\delta \phi_{\delta} - \delta \tau \phi_{\delta\tau})^2}{\tau^2 \phi_{\tau\tau}}$$

Phase-equilibrium condition

$$\begin{aligned}
 &(\text{Maxwell criterion}) \\
 &\frac{p_s}{RT\rho'} = \delta' \phi_{\delta}(\delta', \tau); \quad \frac{p_s}{RT\rho''} = \delta'' \phi_{\delta}(\delta'', \tau) \\
 &\frac{p_s}{RT} \left( \frac{1}{\rho''} - \frac{1}{\rho'} \right) = \phi(\delta', \tau) - \phi(\delta'', \tau)
 \end{aligned}$$

$$\phi_\delta = \left[ \frac{\partial \phi}{\partial \delta} \right]_\tau, \quad \phi_{\delta\delta} = \left[ \frac{\partial^2 \phi}{\partial \delta^2} \right]_\tau, \quad \phi_\tau = \left[ \frac{\partial \phi}{\partial \tau} \right]_\delta, \quad \phi_{\tau\tau} = \left[ \frac{\partial^2 \phi}{\partial \tau^2} \right]_\delta, \quad \phi_{\delta\tau} = \left[ \frac{\partial^2 \phi}{\partial \delta \partial \tau} \right]$$

Table 7. The dimensionless Helmholtz free energy equation and its derivatives according to Eq. (7)

$$\begin{aligned} \phi &= n_1 \ln \delta + \sum_{i=2}^{40} n_i \delta^{I_i} \tau^{J_i} \\ \phi_\delta &= n_1 / \delta + \sum_{i=2}^{40} n_i I_i \delta^{I_i-1} \tau^{J_i} & \phi_{\delta\delta} &= -n_1 / \delta^2 + \sum_{i=2}^{40} n_i I_i (I_i - 1) \delta^{I_i-2} \tau^{J_i} \\ \phi_\tau &= 0 + \sum_{i=2}^{40} n_i \delta^{I_i} J_i \tau^{J_i-1} & \phi_{\tau\tau} &= 0 + \sum_{i=2}^{40} n_i \delta^{I_i} J_i (J_i - 1) \tau^{J_i-2} \\ \phi_{\delta\tau} &= 0 + \sum_{i=2}^{40} n_i I_i \delta^{I_i-1} J_i \tau^{J_i-1} \\ \phi_\delta &= \left[ \frac{\partial \phi}{\partial \delta} \right]_\tau, \quad \phi_{\delta\delta} = \left[ \frac{\partial^2 \phi}{\partial \delta^2} \right]_\tau, \quad \phi_\tau = \left[ \frac{\partial \phi}{\partial \tau} \right]_\delta, \quad \phi_{\tau\tau} = \left[ \frac{\partial^2 \phi}{\partial \tau^2} \right]_\delta, \quad \phi_{\delta\tau} = \left[ \frac{\partial^2 \phi}{\partial \delta \partial \tau} \right] \end{aligned}$$

Table 8. Relations of thermodynamic properties to the ideal-gas part  $g^0$  and the residual part  $g^r$  of the dimensionless Gibbs free energy and their derivatives when using Eq. (11)

Specific volume

$$v = (\partial g / \partial p)_T \quad v(\pi, \tau) \frac{P}{RT} = \pi (\gamma_\pi^0 + \gamma_\pi^r)$$

Specific internal energy

$$u = g - T(\partial g / \partial T)_p - p(\partial g / \partial p)_T \quad \frac{u(\pi, \tau)}{RT} = \tau (\gamma_\tau^0 + \gamma_\tau^r) - \pi (\gamma_\pi^0 + \gamma_\pi^r)$$

Specific entropy

$$s = -(\partial g / \partial T)_p \quad \frac{s(\pi, \tau)}{R} = \tau (\gamma_\tau^0 + \gamma_\tau^r) - (\gamma^0 + \gamma^r)$$

Specific enthalpy

$$h = g - T(\partial g / \partial T)_p \quad \frac{h(\pi, \tau)}{RT} = \tau (\gamma_\tau^0 + \gamma_\tau^r)$$

Specific isobaric heat capacity

$$c_p = (\partial h / \partial T)_p \quad \frac{c_p(\pi, \tau)}{R} = -\tau^2 (\gamma_{\tau\tau}^0 + \gamma_{\tau\tau}^r)$$

Specific isochoric heat capacity

$$c_v = (\partial u / \partial T)_v \quad \frac{c_v(\pi, \tau)}{R} = -\tau^2 (\gamma_{\tau\tau}^0 + \gamma_{\tau\tau}^r) - \frac{(1 + \pi \gamma_\pi^r - \tau \pi \gamma_{\pi\tau}^r)^2}{1 - \pi^2 \gamma_{\pi\pi}^r}$$

Speed of sound

$$w = v [ -(\partial p / \partial v)_s ]^{1/2} \quad \frac{w^2(\pi, \tau)}{RT} = \frac{1 + 2\pi \gamma_\pi^r + \pi^2 \gamma_\pi^{r^2}}{(1 - \pi^2 \gamma_{\pi\pi}^r) + \frac{(1 + \pi \gamma_\pi^r - \tau \pi \gamma_{\pi\tau}^r)^2}{\tau^2 (\gamma_{\tau\tau}^0 + \gamma_{\tau\tau}^r)}}$$

$$\gamma_{\pi}^r = \left[ \frac{\partial \gamma^r}{\partial \pi} \right]_{\tau}, \quad \gamma_{\pi\pi}^r = \left[ \frac{\partial^2 \gamma^r}{\partial \pi^2} \right]_{\tau}, \quad \gamma_{\tau}^r = \left[ \frac{\partial \gamma^r}{\partial \tau} \right]_{\pi}, \quad \gamma_{\tau\tau}^r = \left[ \frac{\partial^2 \gamma^r}{\partial \tau^2} \right]_{\pi}, \quad \gamma_{\pi\tau}^r = \left[ \frac{\partial^2 \gamma^r}{\partial \pi \partial \tau} \right],$$

$$\gamma_{\pi}^0 = \left[ \frac{\partial \gamma^0}{\partial \pi} \right]_{\tau}, \quad \gamma_{\pi\pi}^0 = \left[ \frac{\partial^2 \gamma^0}{\partial \pi^2} \right]_{\tau}$$

Table 9. The ideal-gas part  $\gamma^0$  the dimensionless Gibbs free energy and its derivatives according to Eq. (12)

$$\gamma^0 = \ln \pi + \sum_{i=1}^6 n_i^0 \tau^{J_i^0}$$

$$\gamma_{\pi}^0 = 1/\pi + 0 \quad \gamma_{\pi\pi}^0 = -1/\pi^2 + 0$$

$$\gamma_{\tau}^0 = 0 + \sum_{i=1}^6 n_i^0 J_i^0 \tau^{J_i^0-1} \quad \gamma_{\tau\tau}^0 = 0 + \sum_{i=1}^6 n_i^0 J_i^0 (J_i^0 - 1) \tau^{J_i^0-2}$$

$$\gamma_{\pi\tau}^0 = 0 + 0$$

$$\gamma_{\pi}^0 = \left[ \frac{\partial \gamma^0}{\partial \pi} \right]_{\tau}, \quad \gamma_{\pi\pi}^0 = \left[ \frac{\partial^2 \gamma^0}{\partial \pi^2} \right]_{\tau}, \quad \gamma_{\tau}^0 = \left[ \frac{\partial \gamma^0}{\partial \tau} \right]_{\pi}, \quad \gamma_{\tau\tau}^0 = \left[ \frac{\partial^2 \gamma^0}{\partial \tau^2} \right]_{\pi}, \quad \gamma_{\pi\tau}^0 = \left[ \frac{\partial^2 \gamma^0}{\partial \pi \partial \tau} \right]$$

Table 10. The residual part  $\gamma^r$  of the dimensionless Gibbs free energy and its derivatives according to Eq. (13)

$$\gamma^r = \sum_{i=1}^5 n_i \pi^{I_i} \tau^{J_i}$$

$$\gamma_{\pi}^r = \sum_{i=1}^5 n_i I_i \pi^{I_i-1} \tau^{J_i} \quad \gamma_{\pi\pi}^r = \sum_{i=1}^5 n_i I_i (I_i - 1) \pi^{I_i-2} \tau^{J_i}$$

$$\gamma_{\tau}^r = \sum_{i=1}^5 n_i \pi^{I_i} J_i \tau^{J_i-1} \quad \gamma_{\tau\tau}^r = \sum_{i=1}^5 n_i \pi^{I_i} J_i (J_i - 1) \tau^{J_i-2}$$

$$\gamma_{\pi\tau}^r = \sum_{i=1}^5 n_i I_i \pi^{I_i-1} J_i \tau^{J_i-1}$$

Table 11. The residual part  $g^r$  of the dimensionless Gibbs free energy and its derivatives according to Eq. (15)

$$\gamma^r = \sum_{i=1}^{13} n_i \pi^{I_i} (\tau - 0.5)^{J_i}$$

$$\gamma_{\pi}^r = \sum_{i=1}^{13} n_i I_i \pi^{I_i-1} (\tau - 0.5)^{J_i} \quad \gamma_{\pi\pi}^r = \sum_{i=1}^{13} n_i I_i (I_i - 1) \pi^{I_i-2} (\tau - 0.5)^{J_i}$$

$$\gamma_{\tau}^r = \sum_{i=1}^{13} n_i \pi^{I_i} J_i (\tau - 0.5)^{J_i-1} \quad \gamma_{\tau\tau}^r = \sum_{i=1}^{13} n_i \pi^{I_i} J_i (J_i - 1) (\tau - 0.5)^{J_i-2}$$

$$\gamma_{\pi\tau}^r = \sum_{i=1}^{13} n_i I_i \pi^{I_i-1} J_i (\tau - 0.5)^{J_i-1}$$

$$\gamma_{\pi}^r = \left[ \frac{\partial \gamma^r}{\partial \pi} \right]_{\tau}, \quad \gamma_{\pi\pi}^r = \left[ \frac{\partial^2 \gamma^r}{\partial \pi^2} \right]_{\tau}, \quad \gamma_{\tau}^r = \left[ \frac{\partial \gamma^r}{\partial \tau} \right]_{\pi}, \quad \gamma_{\tau\tau}^r = \left[ \frac{\partial^2 \gamma^r}{\partial \tau^2} \right]_{\pi}, \quad \gamma_{\pi\tau}^r = \left[ \frac{\partial^2 \gamma^r}{\partial \pi \partial \tau} \right]$$

## APPENDIX 1.ATTACHMENT 2

Table C1. Coefficients of Equation (1) and (2)

$i$	$n_i$	$i$	$n_i$
1	0.34805185628969E+03	4	0.57254459862746E+03
2	-0.11671859879975E+01	5	0.13918839778870E+02
3	0.10192970039326E-02		

Table C2. Coefficients and exponents of Equation (3)

$i$	$I_i$	$J_i$	$n_i$	$i$	$I_i$	$J_i$	$n_i$
1	0	-2	0.14632971213167E+00	18	2	3	-0.44141845330846E-05
2	0	-1	-0.84548187169114E+00	19	2	17	-0.72694996297594E-15
3	0	0	-0.37563603672040E+01	20	3	-4	-0.31679644845054E-04
4	0	1	0.33855169168385E+01	21	3	0	-0.28270797985312E-05
5	0	2	-0.95791963387872E+00	22	3	6	-0.85205128120103E-09
6	0	3	0.15772038513228E+00	23	4	-5	-0.22425281908000E-05
7	0	4	-0.16616417199501E-01	24	4	-2	-0.65171222895601E-06
8	0	5	0.81214629983568E-03	25	4	10	-0.14341729937924E-12
9	1	-9	0.28319080123804E-03	26	5	-8	-0.40516996860117E-06
10	1	-7	-0.60706301565874E-03	27	8	-11	-0.12734301741641E-08
11	1	-1	-0.18990068218419E-01	28	8	-6	-0.17424871230634E-09
12	1	0	-0.32529748770505E-01	28	21	-29	-0.68762131295531E-18
13	1	1	-0.21841717175414E-013	30	23	-31	0.14478307828521E-19
14	1	3	-0.52838357969930E-04	31	29	-38	0.26335781662795E-22
15	2	-3	-0.47184321073267E-03	32	30	-39	-0.11947622640071E-22
16	2	0	-0.30001780793026E-03	33	31	-40	0.18228094581404E-23
17	2	1	0.47661393906987E-04	34	32	-41	-0.93537087292458E-25

Table C3. Coefficients and exponents of Equation (5)

$i$	$J_i^0$	$n_i$	$i$	$J_i^0$	$n_i$
1	0	-0.96927686500217E+01	6	-2	0.14240819171444E+01
2	1	0.10086655968018E+02	7	-1	-0.43839511319450E+01
3	-5	-0.56087911283020E-02	8	2	-0.28408632460772E+00
4	-4	0.71452738081455E-01	9	3	0.21268463753307E-01
5	-3	-0.40710498223928E+00			



Table C4. Coefficients and exponents of Equation (6)

$i$	$I_i$	$J_i$	$n_i$	$i$	$I_i$	$J_i$	$n_i$
1	1	0	-0.17731742473213E-02	23	7	0	-0.59059564324270E-17
2	1	1	-0.17834862292358E-01	24	7	11	-0.12621808899101E-05
3	1	2	-0.45996013696365E-01	25	7	25	-0.38946842435739E-01
4	1	3	-0.57581259083432E-01	26	8	8	0.11256211360459E-10
5	1	6	-0.50325278727930E-01	27	8	36	-0.82311340897998E+01
6	2	1	-0.33032641670203E-04	28	9	13	0.19809712802088E-07
7	2	2	-0.18948987516315E-03	29	10	14	0.10406965210174E-18
8	2	4	-0.39392777243355E-02	30	10	10	-0.10234747095929E-12
9	2	7	-0.43797295650573E-01	31	10	14	-0.10018179379511E-08
10	2	36	-0.26674547914087E-04	32	16	29	-0.80882908646985E-10
11	3	0	0.20481737692309E-07	33	16	50	0.10693031879409E+00
12	3	1	0.43870667284435E-06	34	18	57	-0.33662250574171E+00
13	3	3	-0.32277677238570E-04	35	20	20	0.89185845355421E-24
14	3	6	-0.15033924542148E-02	36	20	35	0.30629316876232E-12
15	3	35	-0.40668253562649E-01	37	20	48	-0.42002467698208E-05
16	4	1	-0.78847309559367E-09	38	21	21	-0.59056029685639E-25
17	4	2	0.12790717852285E-07	39	22	53	0.37826947613457E-05
18	4	3	0.48225372718507E-06	40	23	39	-0.12768608934681E-14
19	5	7	0.22922076337661E-05	41	24	26	0.73087610595061E-28
20	6	3	-0.16714766451061E-10	42	24	40	0.55414715350778E-16
21	6	16	-0.21171472321355E-02	43	24	58	-0.94369707241210E-06
22	6	35	-0.23895741934104E+02				

Table C5. Coefficients and exponents of Equation (7)

$i$	$I_i$	$J_i$	$n_i$	$i$	$I_i$	$J_i$	$n_i$
1	0	0	0.10658070028513E+01	21	3	4	-0.20189915023570E+01
2	0	0	-0.15732845290239E+02	22	3	16	-0.82147637173963E-02
3	0	1	0.20944396974307E+02	23	3	26	-0.47596035734923E+00
4	0	2	-0.76867707878716E+01	24	4	0	0.43984074473500E-01
5	0	7	0.26185947787954E+01	25	4	2	-0.44476435428739E+00
6	0	10	-0.28080781148620E+01	26	4	4	0.90572070719733E+00
7	0	12	0.12053369696517E+01	27	4	26	0.70522450087967E+00
8	0	23	-0.84566812812502E-02	28	5	1	0.10770512626332E+00
9	1	2	-0.12654315477714E+01	29	5	3	-0.32913623258954E+00
10	1	6	-0.11524407806681E+01	30	5	26	-0.50871062041158E+00
11	1	15	0.88521043984318E+00	31	6	0	-0.22175400873096E-01
12	1	17	-0.64207765181607E+00	32	6	2	0.94260751665092E-01
13	2	0	0.38493460186671E+00	33	6	26	0.16436278447961E+00
14	2	2	-0.85214708824206E+00	34	7	2	-0.13503372241348E-01
15	2	6	0.48972281541877E+01	35	8	26	-0.14834345352472E-01
16	2	7	-0.30502617256965E+01	36	9	2	0.57922953628084E-03
17	2	22	0.39420536879154E-01	37	9	26	0.32308904703711E-02
18	2	26	0.12558408424308E+00	38	10	0	0.80964802996215E-04
19	3	0	-0.27999329698710E+00	39	10	1	-0.16557679795037E-03
20	3	2	0.13899799569460E+01	40	11	26	-0.44923899061815E-04

Table C6. Coefficients of Equation (8), (9), (10)

$i$	$n_i$	$i$	$n_i$
1	0.11670521452767E+04	6	0.14915108613530E+02
2	-0.72421316703206E+06	7	-0.48232657361591E+04
3	-0.17073846940092E+02	8	0.40511340542057E+06
4	0.12020824702470E+05	9	-0.23855557567849E+00
5	-0.32325550322333E+07	10	0.65017534844798E+03

Table C7. Coefficients and exponents of Equation (12)

$i$	$J_i^0$	$n_i^0$	$i$	$J_i^0$	$n_i^0$
1	0	-0.13179983674201E+02	4	-2	0.36901534980333E+00
2	1	0.68540841634434E+01	5	-1	-0.31161318213925E+01
3	-3	-0.24805148933466E-01	6	2	-0.32961626538917E+00

Table C8. Coefficients and exponents of Equation (13)

$i$	$I_i$	$J_i$	$n_i$	$i$	$I_i$	$J_i$	$n_i$
1	1	0	-0.12563183589592E-03	4	2	9	-0.39724828359569E-05
2	1	1	0.21774678714571E-02	5	3	3	0.12919228289784E-06
3	1	3	-0.45942820899910E-02				

Table C9. Coefficients and exponents of Equation (15)

$i$	$I_i$	$J_i$	$n_i$	$i$	$I_i$	$J_i$	$n_i$
1	1	0	-0.73362260186506E-02	8	3	4	-0.63498037657313E-02
2	1	2	-0.88223831943146E-01	9	3	16	-0.86043093028588E-01
3	1	5	-0.72334555213245E-01	10	4	7	0.75321581522770E-02
4	1	11	-0.40813178534455E-02	11	4	10	-0.79238375446139E-02
5	2	1	0.20097803380207E-02	12	5	9	-0.22888160778447E-03
6	2	7	-0.53045921898642E-01	13	5	10	-0.26456501482810E-02
7	2	16	-0.76190409086970E-02				

Table C10. Coefficients and exponents of Equation (18)

$i$	$I_i$	$J_i$	$n_i$	$i$	$I_i$	$J_i$	$n_i$
1	0	0	-0.23872489924521E+03	11	1	4	-0.65964749423638E+01
2	0	1	0.40421188637945E+03	12	1	10	0.93965400878363E-02
3	0	2	0.11349746881718E+03	13	1	32	0.11573647505340E-06
4	0	6	-0.58457616048039E+01	14	2	10	-0.25858641282073E-04
5	0	22	-0.15285482413140E-03	15	2	32	-0.40644363084799E-08
6	0	32	-0.10866707695377E-05	16	3	10	0.66456186191635E-07
7	1	0	-0.13391744872602E+02	17	3	32	0.80670734103027E-10
8	1	1	0.43211039183559E+02	18	4	32	-0.93477771213947E-12
9	1	2	-0.54010067170506E+02	19	5	32	0.58265442020601E-14
10	1	3	0.30535892203916E+02	20	6	32	-0.15020185953503E-16

Table C11. Coefficients and exponents of Equation (19)

$i$	$I_i$	$J_i$	$n_i$	$i$	$I_i$	$J_i$	$n_i$
1	0	0	0.17478268058307E+03	11	1	12	0.35672110607366E-09
2	0	1	0.34806930892873E+02	12	1	31	0.17332496994895E-23
3	0	2	0.65292584978455E+01	13	2	0	0.56608900654837E-03
4	0	3	0.33039981775489E+00	14	2	1	-0.32635483139717E-03
5	0	11	-0.19281382923196E-06	15	2	2	0.44778286690632E-04
6	0	31	-0.24909197244573E-22	16	2	9	-0.51322156908507E-09
7	1	0	-0.26107636489332E+00	17	2	31	-0.42522657042207E-25
8	1	1	0.22592965981586E+00	18	3	10	0.26400441360689E-12
9	1	2	-0.64256463395226E-01	19	3	32	0.78124600459723E-28
10	1	3	0.78876289270526E-02	20	4	32	-0.30732199903668E-30

Table C12. Coefficients and exponents of Equation (20)

$i$	$I_i$	$J_i$	$n_i$	$i$	$I_i$	$J_i$	$n_i$
1	0	0	0.10898952318288E+04	18	2	7	0.11670873077107E+02
2	0	1	0.84951654495535E+03	19	2	36	0.12812798404046E+09
3	0	2	-0.10781748091826E+03	20	2	36	-0.98554909623276E+09
4	0	3	0.33153654801263E+02	21	2	40	0.28224546973002E+10
5	0	7	-0.74232016790248E+01	22	2	42	-0.35948971410703E+10
6	0	20	0.11765048724356E+02	23	2	44	0.17227349913197E+10
7	1	0	0.18445749355790E+01	24	3	24	-0.13551334240775E+05
8	1	1	-0.41792700549624E+01	25	3	44	0.12848734664650E+08
9	1	2	0.62478196935812E+01	26	4	12	0.13865724283226E+01
10	1	3	-0.17344563108114E+02	27	4	32	0.23598832556514E+06
11	1	7	-0.20058176862096E+03	28	4	44	-0.13105236545054E+08
12	1	9	0.27196065473796E+03	29	5	32	0.73999835474766E+04
13	1	11	-0.45511318285818E+03	30	5	36	-0.55196697030060E+06
14	1	18	0.30919688604755E+04	31	5	42	0.37154085996233E+07
15	1	44	0.25226640357872E+06	32	6	34	0.19127729239660E+05
16	2	0	-0.61707422868339E-02	33	6	44	-0.41535164835634E+06
17	2	2	-0.31078046629583E+00	34	7	28	-0.62459855192507E+02

Table C13. Coefficients and exponents of Equation (21)

$i$	$I_i$	$J_i$	$n_i$	$i$	$I_i$	$J_i$	$n_i$
1	0	0	0.14895041079516E+04	20	2	40	0.71280351959551E-04
2	0	1	0.74307798314034E+03	21	3	1	0.11032831789999E-03
3	0	2	-0.97708318797837E+02	22	3	2	0.18955248387902E-03
4	0	12	0.24742464705674E+01	23	3	12	0.30891541160537E-02
5	0	18	-0.63281320016026E+00	24	3	24	0.13555504554949E-02
6	0	24	0.11385952129658E+01	25	4	2	0.28640237477456E-06
7	0	28	-0.47811863648625E+00	26	4	12	-0.10779857357512E-04
8	0	40	0.85208123431544E-02	27	4	18	-0.76462712454814E-04
9	1	0	0.93747147377932E+00	28	4	24	0.14052392818316E-04
10	1	2	0.33593118604916E+01	29	4	28	-0.31083814331434E-04
11	1	6	0.33809355601454E+01	30	4	40	-0.10302738212103E-05
12	1	12	0.16844539671904E+00	31	5	18	0.28217281635040E-06
13	1	18	0.73875745236695E+00	32	5	24	0.12704902271945E-05
14	1	24	-0.47128737436186E+00	33	5	40	0.73803353468292E-07
15	1	28	0.15020273139707E+00	34	6	28	-0.11030139238909E-07
16	1	40	-0.21764114219750E-02	35	7	2	-0.81456365207833E-13
17	2	2	-0.21810755324761E-01	36	7	28	-0.25180545682962E-10
18	2	8	-0.10829784403677E+00	37	9	1	-0.17565233969407E-17
19	2	18	-0.46333324635812E-01	38	9	40	0.86934156344163E-14

Table C14. Coefficients and exponents of Equation (22)

$i$	$I_i$	$J_i$	$n_i$	$i$	$I_i$	$J_i$	$n_i$
1	-7	0	-0.32368398555242E+13	13	1	4	0.37966001272486E+01
2	-7	4	0.73263350902181E+13	14	1	8	-0.10842984880077E+02
3	-6	0	0.35825089945447E+12	15	2	4	-0.45364172676660E-01
4	-6	2	-0.58340131851590E+12	16	6	0	0.14559115658698E-12
5	-5	0	-0.10783068217470E+11	17	6	1	0.11261597407230E-11
6	-5	2	0.20825544563171E+11	18	6	4	-0.17804982240686E-10
7	-2	0	0.61074783564516E+06	19	6	10	0.12324579690832E-06
8	-2	1	0.85977722535580E+06	20	6	12	-0.11606921130984E-05
9	-1	0	-0.25745723604170E+05	21	6	16	0.27846367088554E-04
10	-1	2	0.31081088422714E+05	22	6	20	-0.59270038474176E-03
11	0	0	0.12082315865936E+04	23	6	22	0.12918582991878E-02
12	0	1	0.48219755109255E+03				

Table C15. Coefficients of Equation (23), (24)

$i$	$n_i$	$i$	$n_i$
1	0.90584278514723E+03	4	0.26526571908428E+04
2	- 0.67955786399241	5	0.45257578905948E+01
3	0.12809002730136E-03		

Table C16. Coefficients and exponents of Equation (25)

$i$	$I_i$	$J_i$	$n_i$	$i$	$I_i$	$J_i$	$n_i$
1	-1.50	-24	-0.39235983861984E+06	24	-0.25	-11	-0.59780638872718E+04
2	-1.50	-23	0.51526573827270E+06	25	-0.25	-6	-0.70401463926862E+03
3	-1.50	-19	0.40482443161048E+05	26	0.25	1	0.33836784107553E+03
4	-1.50	-13	-0.32193790923902E+03	27	0.25	4	0.20862786635187E+02
5	-1.50	-11	0.96961424218694E+02	28	0.25	8	0.33834172656196E-01
6	-1.50	-10	-0.22867846371773E+02	29	0.25	11	-0.43124428414893E-04
7	-1.25	-19	-0.44942914124357E+06	30	0.50	0	0.16653791356412E+03
8	-1.25	-15	-0.50118336020166E+04	31	0.50	1	-0.13986292055898E+03
9	-1.25	-6	0.35684463560015E+00	32	0.50	5	-0.78849547999872E+00
10	-1.00	-26	0.44235335848190E+05	33	0.50	6	0.72132411753872E-01
11	-1.00	-21	-0.13673388811708E+05	34	0.50	10	-0.59754839398283E-02
12	-1.00	-17	0.42163260207864E+06	35	0.50	14	-0.12141358953904E-04
13	-1.00	-16	0.22516925837475E+05	36	0.50	16	0.23227096733871E-06
14	-1.00	-9	0.47442144865646E+03	37	0.75	0	-0.10538463566194E+02
15	-1.00	-8	-0.14931130797647E+03	38	0.75	4	0.20718925496502E+01
16	-0.75	-15	-0.19781126320452E+06	39	0.75	9	-0.72193155260427E-01
17	-0.75	-14	-0.23554399470760E+05	40	0.75	17	0.20749887081120E-06
18	-0.50	-26	-0.19070616302076E+05	41	1.00	7	-0.18340657911379E-01
19	-0.50	-13	0.55375669883164E+05	42	1.00	18	0.29036272348696E-06
20	-0.50	-9	0.38293691437363E+04	43	1.25	3	0.21037527893619E+00
21	-0.50	-7	-0.60391860580567E+03	44	1.25	15	0.25681239729999E-03
22	-0.25	-27	0.19363102620331E+04	45	1.50	5	-0.12799002933781E-01
23	-0.25	-25	0.42660643698610E+04	46	1.50	18	-0.82198102652018E-05

Table C17. Coefficients and exponents of Equation (26)

$i$	$I_i$	$J_i$	$n_i$	$i$	$I_i$	$J_i$	$n_i$
1	-6	0	0.31687665083497E+06	23	0	2	0.41727347159610E+02
2	-6	11	0.20864175881858E+02	24	0	4	0.21932549434532E+01
3	-5	0	-0.39859399803599E+06	25	0	5	-0.10320050009077E+01
4	-5	11	-0.21816058518877E+02	26	0	6	0.35882943516703E+00
5	-4	0	0.22369785194242E+06	27	0	9	0.52511453726066E-02
6	-4	1	-0.27841703445817E+04	28	1	0	0.12838916450705E+02
7	-4	11	0.99207436071480E+01	29	1	1	-0.28642437219381E+01
8	-3	0	-0.75197512299157E+05	30	1	2	0.56912683664855E+00
9	-3	1	0.29708605951158E+04	31	1	3	-0.99962954584931E-01
10	-3	11	-0.34406878548526E+01	32	1	7	-0.32632037778459E-02
11	-3	12	0.38815564249115E+00	33	1	8	0.23320922576723E-03
12	-2	0	0.17511295085750E+05	34	2	0	-0.15334809857450E+00
13	-2	1	-0.14237112854449E+04	35	2	1	0.29072288239902E-01
14	-2	6	0.10943803364167E+01	36	2	5	0.37534702741167E-03
15	-2	10	0.89971619308495E+00	37	3	0	0.17296691702411E-02
16	-1	0	-0.33759740098958E+04	38	3	1	-0.38556050844504E-03
17	1	1	0.47162885818355E+03	39	3	3	-0.35017712292608E-04
18	-1	1	-0.19188241993679E+01	40	4	0	-0.14566393631492E-04
19	-1	8	0.41078580492196E+00	41	4	1	0.56420857267269E-05
20	-1	9	-0.33465378172097E+00	42	5	0	0.41286150074605E-07
21	0	0	0.13870034777505E+04	43	5	1	-0.20684671118824E-07
22	0	1	-0.40663326195838E+03	44	5	2	0.16409393674725E-08

Table C18. Coefficients and exponents of Equation (27)

$i$	$I_i$	$J_i$	$n_i$	$i$	$I_i$	$J_i$	$n_i$
1	-2	0	0.90968501005365E+03	16	3	1	-0.14597008284753E-01
2	-2	1	0.24045667088420E+04	17	3	5	0.56631175631027E-02
3	-1	0	-0.59162326387130E+03	18	4	0	-0.76155864584577E-04
4	0	0	0.54145404128074E+03	19	4	1	0.22440342919332E-03
5	0	1	-0.27098308411192E+03	20	4	4	-0.12561095013413E-04
6	0	2	0.97976525097926E+03	21	5	0	0.63323132660934E-06
7	0	3	-0.46966772959435E+03	22	5	1	-0.20541989675375E-05
8	1	0	0.14399274604723E+02	23	5	2	0.36405370390082E-07
9	1	1	-0.19104204230429E+02	24	6	0	-0.29759897789215E-08
10	1	3	0.53299167111971E+01	25	6	1	0.10136618529763E-07
11	1	4	-0.21252975375934E+02	26	7	0	0.59925719692351E-11
12	2	0	-0.31147334413760E+00	27	7	1	-0.20677870105164E-10
13	2	1	0.60334840894623E+00	28	7	3	-0.20874278181886E-10
14	2	2	-0.42764839702509E-01	29	7	4	0.10162166825089E-09
15	3	0	0.58185597255259E-02	30	7	5	-0.16429828281347E-09

## 8. THERMO-PHYSICAL PROPERTIES OF CORIUM UNDER SEVERE ACCIDENT CONDITIONS (CEA, CADARACHE )

### 8.1. Thermo-physical properties for severe accident analysis

Safety studies are required under accident and severe accident conditions for current and future water-cooled reactors. In a hypothetical severe accident, very high temperatures of around 3300 K could be reached. The materials of the nuclear reactor, such as fuel and fission products, cladding, metallic alloys, moderator, absorbers, structural materials, coolants, concrete, etc...- could melt to form complex, multi-phases, and aggressive mixtures called under the general appellation “corium”.

In the framework of severe accident studies, accurate data for the thermo-physical properties [1,2] are necessary to model the corium behaviour (thermal-hydraulics, physico-chemistry, etc...) at different steps during the various stages of severe accident progression (steam explosion, in-vessel interaction, corium concrete interaction, corium spreading,...) and for use in severe accidents codes (see FIG. 1).

For experimental interpretation, modelling or code calculations of severe accident progression in a reactor, it is necessary to estimate the corium physical properties as a function of composition and temperature.

*Several approaches can be used to estimate the thermo-physical properties of corium:*

- Experimental approach
- Database approach
- Theoretical approach

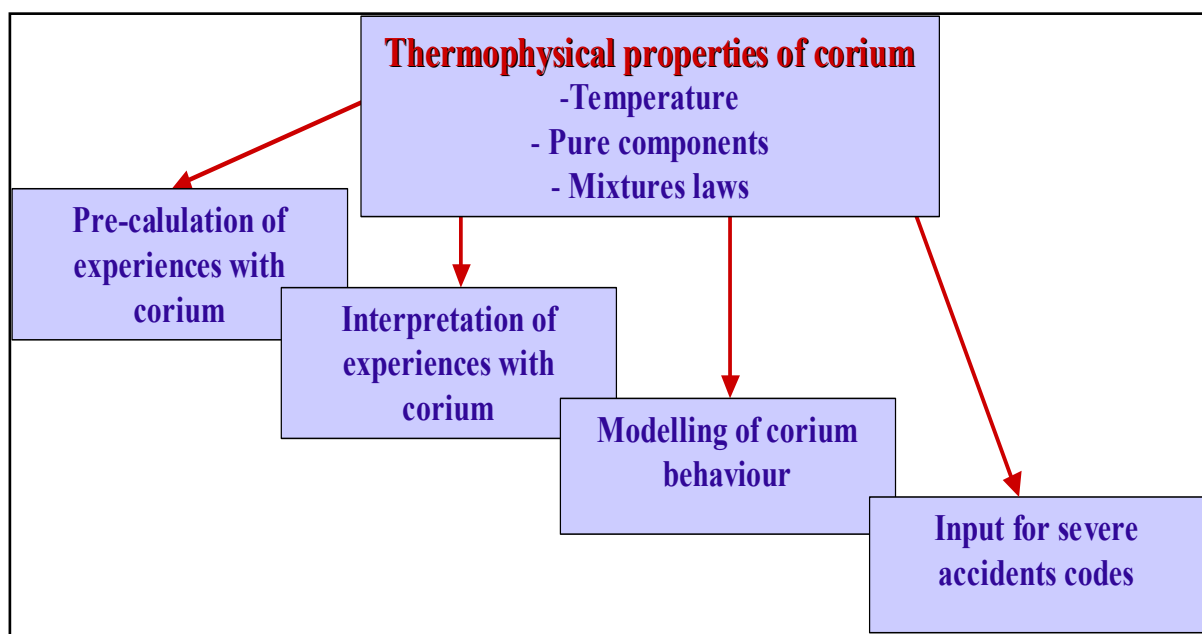


FIG. 1. Use of thermo-physical properties for severe accidents analysis.

#### 8.1.1. Experimental approach

High temperature (>2300 K) thermo-physical properties measurements of molten oxides and/or metallic mixtures are constrained by difficulties in achieving and controlling high temperatures, and in ensuring physical and chemical inertness between the oxides and the environment. For example, one of the possible constituents of corium,  $\text{FeO}_x$  is highly corrosive at liquid state and dissolves a number of other materials.

A few characterization techniques are under development to measure the high temperature thermo-physical properties of corrosive materials such as corium. For example, contact-less measurements avoid these technological problems, especially the levitation techniques. Among the levitation techniques, the gas-film levitation technique is well adapted to insulating liquid materials, such as corium [3, 4]. At CEA-Cadarache, an installation, called **VITI** (**V**iscosity **T**emperature **I**nstallation), has been developed to perform viscosity measurements on corium (mixture with uranium dioxide) using the levitation method [1].

Measurements of thermo-physical properties of corium components at liquid state are difficult to carry out and in some cases, the results are even questionable. For example, the measurement of thermal conductivity of  $\text{UO}_2$  have been performed in the 1980s [5, 6, 7] but the results have been contested later [8, 9].

A last point concerns the temperature range of interest. The experimental measurements of some of the corium constituents during the past 50 years were mainly carried out at a relatively “low” temperature ( $T < 2000\text{K}$ ). It must be stressed that there is also limited economic interest to measure the thermo-physical properties of corium melt mixtures under severe accident conditions.

### **8.1.2. Database approach**

Different databases have been developed for chemical and physical properties of the compounds.

In the field of severe accidents, we can mainly quote:

- The Nuclear data bases for thermo-physical properties
  - MATPRO
  - INSC
  - AIEA/THERSYST: Thermo-physical Properties data for LWRs and HWRs
  - HEMATIC and

- Commercial data base for thermo-physical properties:

The main web site addresses are:

-INSC /MATPRO/ :

<http://www.insc.anl.gov/matprop/#comp>

IAEA : general database web-site:

<http://www.iaea.org/inis/inisdb.htm> (International Nuclear Information System)

For the severe accidents analysis needs, we can give some comments about the existing thermo-physical databases:

#### **For nuclear data-bases,**

- the majority of the data are given at solid state and mainly under normal conditions,
- there are no or few data for liquid state,
- there are no or few for temperature greater than 2000K,
- there are no or few data for mixtures,
- some data are given, but they do not contain the proposed information,
- there are problems of maintenance.

#### **For commercial data bases,**

- all properties of interest to severe accidents needs are not included
- there are few or no data about nuclear materials and fission products
- there are few or no data about mixtures



### 8.1.3. Theoretical approach

Modeling or code calculation of severe accident phenomena requires reliable thermo-physical properties. As discussed in sections 8.1.1 and 8.1.2, very few data exist at temperatures greater than 2000K.

Corium being a multi-phases and multi-components mixture, special attention has been given at CEA to the mixing laws. The estimation of corium thermo-physical properties is therefore based on both a review of individual constituents and the development of mixing laws as well as the use of validity criteria for various applications.

In practice, the following steps are involved in the determination of a corium thermo-physical property [2]:

- Estimation of the physical property of all the phases present in a given corium (These phases can be either pure substance or solutions; in the latter case, the property of the solution is estimated by taking into account the contributions of the solution constituents);
- Estimation of the corium apparent property, by using mixing laws applicable to the given topological configuration of the phases.

In the next section recommendations are provided on the following thermo-physical properties:

- Density,
- Thermal conductivity,
- Viscosity.

## 8.2. Modelling of corium properties

### 8.2.1. Density

Three properties are linked by the following equations :

- The molar volume  $V_{\text{molar}}$  is the volume occupied by one mole of the species (note that it depends of the definition of the species, e.g. one mole of  $\text{FeO}_{1.5}$  occupies half the volume of 1 mole of  $\text{Fe}_2\text{O}_3$ .)

$$V_{\text{molar}} = \frac{M}{\rho} \quad ; \quad M : \text{molar mass} \quad \rho : \text{density} \quad (1)$$

- The coefficient of volume expansion is defined as the ratio of the temperature derivative of the molar volume by the molar volume.

$$\alpha_V = \frac{1}{V_{\text{molar}}} \cdot \left( \frac{\partial V_{\text{molar}}}{\partial T} \right) \quad ; \quad T \text{ temperature} \quad (2)$$

- Volume expansion is the driving force for natural convection. Therefore a good knowledge of this derivative is necessary.
- The linear thermal expansion  $\alpha$  in the x,y,z directions is related to the coefficient of volume expansion by :

$$(1 + \int \alpha_x dT)(1 + \int \alpha_y dT)(1 + \int \alpha_z dT) = 1 + \int \alpha_V dT \quad (3)$$

#### 8.2.1.1. Density – molar volume of solutions

For solutions (either solid or liquid), the independence of partial molar volumes of each constituent from bulk composition and ideal mixing is assumed. Nelson & Carmichael [12] have verified on silicate liquids that the above assumption could lead to errors of the order of 1% or less. For solid-state

compound oxides, Kamigaito [13] showed that assuming ideal mixing of the single oxides gives also generally a good estimate. Harmathy [14] also adopted this approach for solid concrete. This also has been promoted for metallic alloys with errors of less than 4% [15].

Nevertheless, some metallic alloys are non ideal [16], such as Na-Pb, Na-Bi, Na-In, Fe-Si. The maximum non-ideal behaviour is observed at compositions generally corresponding to the solid state to inter-metallic compounds. It must be noted that Crawley [16] proved a lack of correlation between the excess volumes (and even the sign of excess volume) and excess enthalpies or entropies where the excess parameter ( $X^{ex}$ ) is defined as the difference between the actual value of magnitude and the value for an ideal system:

$$X^{ex} = X(\text{actual}) - X(\text{ideal}) \quad (4)$$

Nevertheless, in the absence of pertinent data, the excess volumes are assumed to be negligible.

Neglecting excess volumes, the volume of one mole of solution is given by:

$$V = \sum_i y_i \cdot V_i \quad (5)$$

where  $y_i$  is the molar fraction of species  $i$  (having a “partial” molar volume  $V_i$  and a molar mass  $M_i$ ) in the solution. The site fractions are used as estimators of the species molar fraction  $y_i$ , the site fractions are calculated by a thermodynamic code (Gibbs energy minimizer) such as GEMINI2 software using the thermodynamic database (e.g. the TDBCR or NUCLEA databases [17]). In this modelling, for the solid and liquid solution phases, a general multi-sub-lattice model has been used:

$$G^{ref} = \sum_i P_i(Y) \cdot G_i \quad (6)$$

where  $G_r$  represents the Gibbs Energy of all reference substances,  $P_i(Y)$  is the corresponding product of site fractions from the matrix:  $Y = y_i^{sl}$ , atomic fraction of the component  $i$  (pure or associate species) on the sub-lattice  $sl$ .

The density of the solution is then given by:

$$\rho = \frac{\sum_i y_i \cdot M_i}{\sum_i y_i \cdot V_i} \quad (7)$$

The values for pure species can be calculated adding partial molar volumes to the data- on pure species molar volumes and densities. The value of density or molar volume, which must be taken for liquid components in mixtures that are liquid at temperatures below the melting temperature of the pure component, is an important factor. For the density calculations, we recommend that the expansion coefficient be taken as a constant below the melting point.

The assumption of ideal mixing and constant thermal expansion below pure substance melting point, was validated for the U-Fe binary system [18] using measured densities of the U-Fe binary system (see FIG. 2). The ideal mixing law (extrapolated to the superheated region the measured values for pure uranium and pure iron) is within 3% of the experimental data, which is acceptable (see FIG. 3).

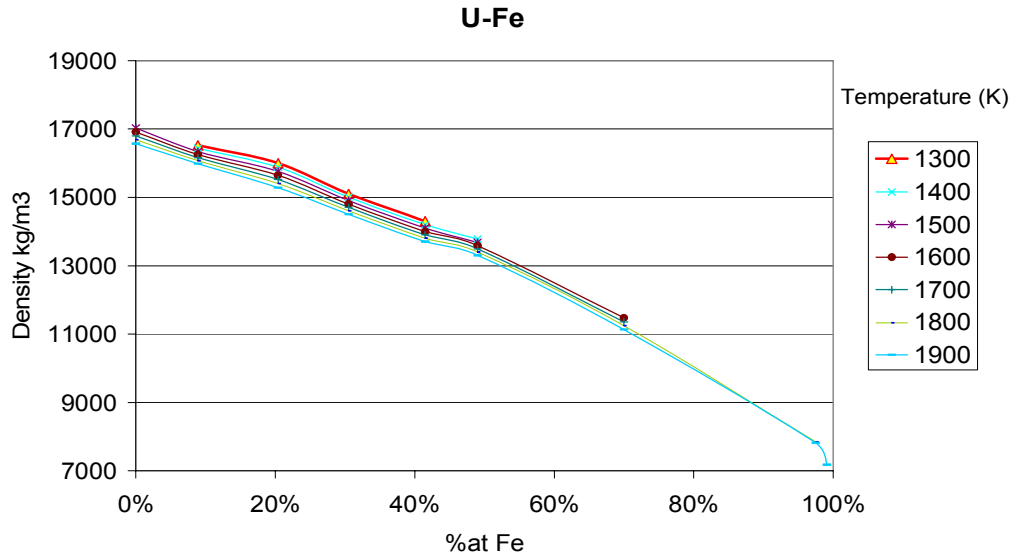


FIG. 2. Experimental U-Fe densities [18].

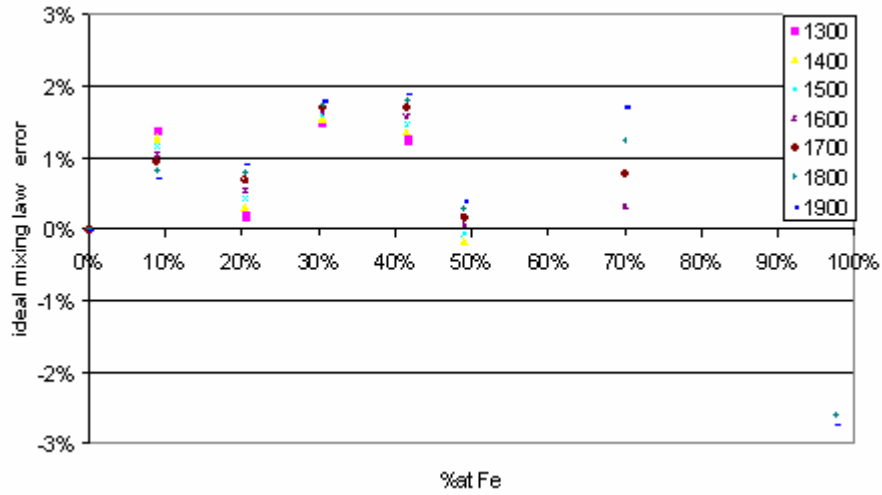


FIG. 3. Density difference between experimental data and ideal mixing law in U-Fe binary.

For a mixture of different condensed phases (liquid(s), solid solutions), the following mixing law is used. The volume of one mole of a mixture made of phases having molar fractions  $x_j$  and molar volumes  $V_j$  is given by :

$$V = \sum_j x_j \cdot V_j \quad (8)$$

The above approach is, for instance, proposed for multiphase solids such as concretes [14].

In case of gaseous inclusions, the major effect is an increase in the global molar volume. If the volume fraction of gases is  $P$  and the density of the condensed phases is  $\rho$ , then the global density taking into account of porosity is :

$$\rho_{global} = (1 - P) \rho_{condensed} \quad (9)$$

### 8.2.2. Thermal conductivity

The recommendations on corium thermal conductivity included a review of the available experimental data by an expert panel [19].

For the pure constituents of corium, the panel recommendation differentiated between experimental data, calculated data and extrapolated data. In the absence of any/or reliable data (for example non reliable techniques used for measurements, too large uncertainties on temperature measurements,...), another approach was developed. In that approach, some physical models were developed based on analogies of physical properties.

On a macroscopic scale, the thermal conductivity is described by the following equation:

$$\lambda = \alpha \rho C_p \quad (10)$$

The thermal conductivity is described by the following equation on a microscopic scale with 3 contributions (lattice vibration, electronic, radiation):

$$\lambda = \lambda_L + \lambda_e + \lambda_r \quad (11)$$

Below 1800 K, the thermal conductivity is essentially governed by the lattice vibration (phonons). Thus, the following general law can describe the thermal conductivity due to the lattice vibration [20]:

$$\lambda_L = (a + bT)^{-1} \quad (12)$$

Above 1800 K, the radiation component becomes important. Therefore, the radiation contribution is as follows (knowing that this phenomena starts being appreciable at 1000K):

$$\lambda_r = \frac{16}{3} \sigma n^2 T^3 l_r \quad (13)$$

For metals such as U, Zr or Fe at high temperatures, the thermal conductivity is governed by the electronic contribution [21]:

$$\lambda_e = \frac{2m^{*1/2}}{3^{1/2} E_g e} (kT)^{3/2} \mu^* \frac{\left(2 + \frac{E_g}{kT}\right)^2}{\frac{3}{2} + \frac{E_g}{kT}} \quad (14)$$

For oxides at very high temperatures, another contribution has been recently identified: the polaron contribution (ion-electron contribution). This component contributes to the increase of the thermal conductivity at temperature above 2000 K. Macroscopically, it means that the thermal diffusivity remains constant, whereas the heat capacity increases [22].

Applying this approach to oxides present in corium, it is possible to propose a new general law for the macroscopic evolution of the thermal conductivity, applicable to oxides such a zirconia or iron oxide [19, 23].

$$\lambda = \frac{1}{a + bT} + c(n) T^3 + \frac{d(\sigma)}{T} \quad (15)$$

$d(\sigma)$  is a function of the electrical conductivity.

For example, for zirconium dioxide, we recommend the general variation law:

$$\lambda = \frac{1}{0,0893 + 0,0002 * T} + 1,3 \cdot 10^{-10} * T^3 \quad (16)$$

for  $300 < T < 2982$  K

For the thermal conductivity of  $\text{UO}_2$  ceramic dioxide, many data are available up to 2500K [20, 22–28]. Some authors re-calculated experimental data of other researchers and proposed different models (see Fig. 4). We recommend, J. Fink's [8] analysis as most complete, who recommends the following equation for the  $\text{UO}_2$  thermal conductivity (see FIG. 4):

$$\lambda = \frac{1}{0.95} * \left( \frac{100}{6,548 + 23,533 * (T \cdot 10^{-3})} + \frac{6400 \exp\left(\frac{-16,35}{T \cdot 10^{-3}}\right)}{(T \cdot 10^{-3})^{5/2}} \right) \quad (17)$$

for  $300 \text{ K} < T < 3100 \text{ K}$ .

The first part of the equation can be attributed to phonon conduction and the second to the ambipolar conduction. This model describes the best experimental values in a large range of temperature in comparison to Hyland [20] analysis. Note that Figure 4 shows both the calculated data [20, 22, 29–33] and the recommended data [23].

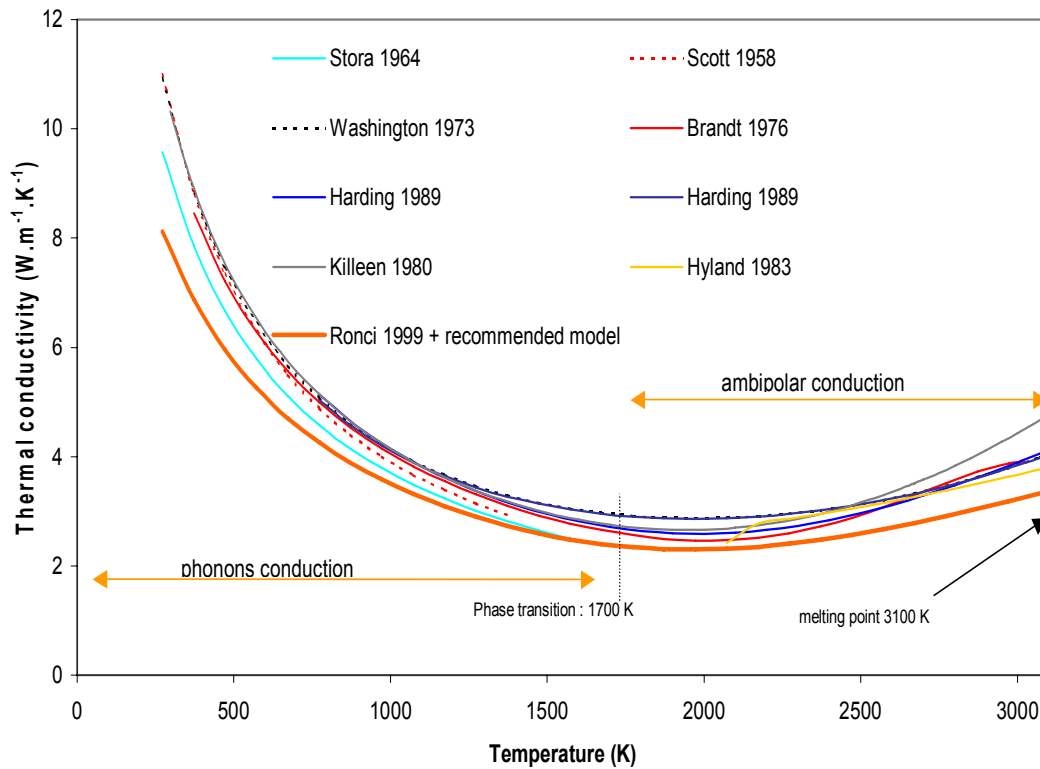


FIG. 4. Thermal conductivity ( $\lambda$ ) of  $\text{UO}_{2.00}$  : calculated and recommended data.

### Thermal conductivity at liquid state

For very high temperatures, especially for oxides (except for  $\text{UO}_2$  [8, 9]), only very few experimental or calculated data are available for the constituents of corium at liquid state. Usually, severe accident researchers use, for the thermal conductivity in the liquid state, the value recommended for the solid state, which is an extrapolation without any scientific justification. A different empirical approach was used by us to calculate the thermal conductivity in the liquid state using an analogy of the relationship between the thermal conductivity in the solid and the liquid states at the melting point.

$$\lambda_{\text{liquid}} = \alpha_{\text{solid}} \cdot \rho_{\text{liquid}} \cdot C_{v\text{liquid}} \quad (18)$$

We can make the following two hypothesis:

- 1) Continuity of the thermal diffusivity at the melting point ( $\alpha_{\text{liquid}} = \alpha_{\text{solid}}$ ) and
- 2) For liquid state, we must consider  $C_v$  as heat capacity. But, there are no data available for  $C_v$  of liquid oxides.

For  $\text{UO}_2$ , Ronchi [9] proposes that  $\rho.C_v$  at solid state is about 40% lower than the liquid state. With this assumption for the liquids and extending the relationship to all the oxides, we get the following relationship:

$$\rho_{\text{liquid}}(T).C_{v\text{liquid}} = 0.4\rho_{\text{solid}}.C_{p\text{solid}} \quad (19)$$

### Thermal conductivity of 2 phases: solid and gas

For mixtures including a solid phase and a gas phase, the general thermal conductivity laws will depend on their volume fractions. We recommend the following general physical laws depending on the void fraction (gas phase) and neglecting the radiation contribution:

- Void fraction < 5%, Loeb's modelling [34]:

$$\lambda_t = (1-V)\lambda_{\text{dense}} \quad (20)$$

- 5% < Void fraction < 25%, Maxwell-Eucken's model [35]:

$$\lambda_t = \frac{2\lambda_d + \lambda_g + 2V(\lambda_g - \lambda_d)}{2\lambda_d + \lambda_g - V(\lambda_g - \lambda_d)} \lambda_d \quad (21)$$

- $\lambda_g = 0.024 \text{ W.m}^{-1}.\text{K}^{-1}$  at  $20^\circ\text{C}$  [35]
- 25% < Void fraction < 35%, Percolation model [37]:

$$\lambda_t = \frac{1}{4} \left( \lambda_g(3V-1) + \lambda_d(2-3V) + \left[ (\lambda_g(3V-1) + \lambda_d(2-3V))^2 \right]^{1/2} \right) \quad (22)$$

### 8.2.3. Viscosity

#### Viscosity of non-silicate liquid phases

For corium with less than 5% mol of silica, it is recommended [38] to use the Andrade [39] relationship:

$$\eta = K \cdot \frac{(M \cdot T_m)^{1/2}}{V^{2/3}} \cdot \exp \left[ \frac{Q}{R} \cdot \left( \frac{1}{T} - \frac{1}{T_m} \right) \right] \quad (23)$$

where the coefficient  $K$  recommended for corium is the value proposed by Nazaré [40]. The activation energies [38] are 35 kJ/mol for  $\text{UO}_2$  and 247 kJ/mol for  $\text{ZrO}_2$ . For the other materials, the following empirical relationship is recommended (although it was derived for metals) [41]:

$$Q \sim 1.8 T_m^{1.348} \quad (24)$$

This approach was validated [38] against experimental data obtained from the RASPLAV project [42].

#### Viscosity of silicate liquids

For silicate melts, the presence of silicate chains significantly increases the viscosity. Andrade [39] model is no more valid and we recommend the approach of Urbain [43], which has been extended to corium [44].

The viscosity is described by the Weymann relationship:

$$\eta = 0.1 A T \exp \left( \frac{1000 B}{T} \right) \quad (25)$$

where  $A$  and  $B$  are linked by the empirical relationship:

$$-\ln A = 0.29 B + 11.57 \quad (26)$$

The molten silicate melt constituents are divided into three families: glass formers ( $\text{SiO}_2$  and complex silicate molecules), modifiers ( $\text{CaO}$ ,  $\text{MgO}$ ,  $\text{FeO}$ ,  $\text{U}_{1/2}\text{O}$ ,  $\text{Zr}_{1/2}\text{O}$ ) and amphoteric ( $\text{Al}_2\text{O}_3$ ,  $\text{Fe}_2\text{O}_3$ ). The parameter  $B$  in equation (26) is obtained from the molar fractions of glass formers and modifiers using the nomogram in FIG. 5. Ramacciotti [44] validated this approach against experimental data both without and with uranium dioxide.

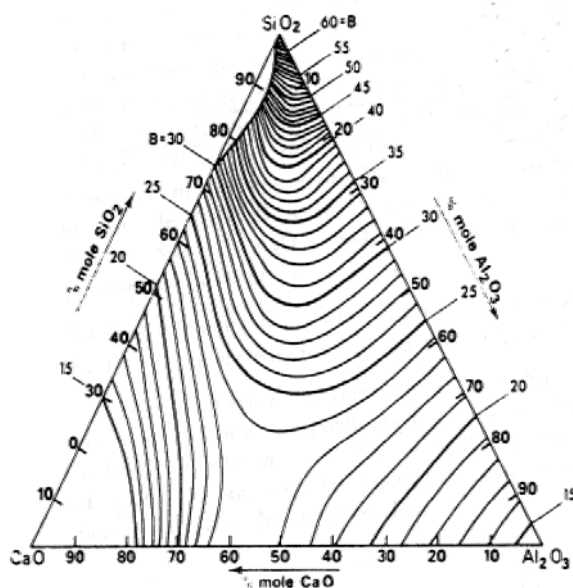


FIG. 5. Nomogram linking  $B$  to the former, modifier and amphoteric mole fractions in molten silicate melts.

### Viscosity of suspensions

Viscosity is strongly affected by the presence of solid particles. This property is important during some solidification processes as those of spreading or rapid cooling. For a semi-solid configuration, Ramacciotti [44] recommends the following equation to estimate the mixture viscosity from the actual-liquid viscosity and the solid volume fraction (estimated from thermodynamics) as follows:

$$\eta = \eta_{\text{liquid}} e^{2.5C\phi} \quad (27)$$

where the constant  $C$  is approximately 6.

This relationship was validated using data from corium viscosity measurements and data from corium spreading calculations of prototypic material experiments [45].

### Viscosity of emulsions

Another phenomenon, to take into account in corium behaviour, is the emulsion of a liquid phase in another liquid. In this case, we propose the Taylor [46] model:

$$\eta_r = \frac{\eta}{\eta_c} = 1 + \frac{5K+2}{2(K+1)}\phi \quad (28)$$

It must be noted that for the solidification of corium with a miscibility gap, the viscosity calculation leads to different results depending on whether one considers an emulsion of metal in a semi-solid oxide or a suspension of oxide crystals in an oxide-metal emulsion. The choice of the pertinent configuration is thus crucial. For spreading, experiments [45] show that the first assumption is true.

### Viscosity of bubbly flows

Another phenomenon of interest is an emulsion of gas bubbles in corium. In this case, we recommend, the following Llewellyn [47] relationship:

$$\eta = \eta_0 (1+9\phi), \quad (29)$$

which was established for stationary flows. For rapid transients [48] in the shear rates, the viscosity decreases to:

$$\eta = \eta_0 \left(1 - \frac{5}{3}\phi\right) \quad (30)$$

### Nomenclature

- a: parameter linked to the purity of the materials
- A: Urbain's model parameter [Pa.s.K<sup>-1</sup>]
- a1, a2, a3, a4 : model coefficients
- b: parameter linked to the phonon-phonon coupling (Umklapp)
- B: Urbain's model parameter [K]
- c: constant including the refraction index n
- C=6, Ramacciotti's model parameter
- C<sub>j</sub> : concentration in species j
- C<sub>p</sub>: heat capacity at constant pressure [J.kg<sup>-1</sup>.K<sup>-1</sup>]
- C<sub>v</sub>: heat capacity at constant volume [J.kg<sup>-1</sup>.K<sup>-1</sup>]
- d: constant including the electrical conductivity σ<sub>e</sub>
- E<sub>g</sub>: electron-hole pair formation energy [[J.mol<sup>-1</sup>]
- K= 0.194.10<sup>-6</sup> m.kg<sup>1/2</sup>.K<sup>-1/2</sup>.s<sup>-1</sup>, Nazare parameter
- l<sub>l</sub>: mean free path of photons in the material
- m<sup>\*</sup>: ambipolar mass [kg]
- M<sub>i</sub> molar mass of species i [kg.mol<sup>-1</sup>]
- n: refraction index
- Q: activation energy [J.mol<sup>-1</sup>]
- T: temperature [K]
- V: void faction
- V<sub>i</sub>: molar volume of the solution [m<sup>3</sup>.mol<sup>-1</sup>]
- y<sub>i</sub>: molar fraction of species i
- Z: ionic charge

### Greek letters

- α: thermal diffusivity [m<sup>2</sup>.s<sup>-1</sup>]
- φ : volume fraction
- λ: thermal conductivity [W.m<sup>-1</sup>.K<sup>-1</sup>]
- μ<sup>\*</sup>: ambipolar mobility
- η: viscosity [Pa.s]
- ρ: density [kg.m<sup>-3</sup>]
- σ: Stefan constant

### Indices

- c: continuous phase
- d: dense
- e: electron component
- g: gas
- i: species index in a solution
- L: lattice
- L: lattice vibration
- liquid: liquid phase
- m: melting
- r: radiation component
- t: total



## REFERENCES TO SECTION 8

- [1] PILUSO, P., MONERRIS, J., JOURNEAU, C. and COGNET, G., Viscosity measurements of ceramic oxides by aerodynamic levitation, *International Journal of Thermophysics* (2002).
- [2] JOURNEAU, C., PILUSO, P., FROLOV, K.N., Corium Physical Properties for Severe Accident R&D, Intern. Cong. on Advanc. Nuclear Power Plant, to be published (2004).
- [3] GANDHI, A.S., SARAVAN, A., JAYARAM, V., Materials Science and Engineering, A221, 68 (1996).
- [4] PEREZ, M., SALVO, L., BRECHET, Y., PAPOULAR, M., *Matériaux et Techniques*, 9-10 (2000).
- [5] OTTER, C., DAMIEN, D., Mesure de la diffusivité thermique de UO<sub>2</sub> fondu, *High Temperatures-High Pressures*, 16, P.1-6 (1984).
- [6] TASMAN, H.A., PEL, D., RICHTER, J., SCHMIDT, H.-E., Measurement of the thermal conductivity of liquid UO<sub>2</sub>, *High Temperatures- High Pressures*, 15, P.419-431 (1983).
- [7] KIM, C.S. et al., Measurement of thermal diffusivity of Molten UO<sub>2</sub>, *Proceedings 7<sup>th</sup> Symposium on Thermophysical Properties*, Gaithersburg MD ( New York : ASME) P.338-343 (1977).
- [8] FINK, J.K., Thermophysical properties of uranium dioxide, *Journal of Nuclear Materials*, 279, P.1-18 (2000).
- [9] RONCHI, C., SHEINDLIN, M., MUSELLA, M., HYLAND, G.J., Thermal conductivity of uranium up to 2900K from simultaneous measurement of the heat capacity and thermal diffusivity, *Journal of Applied Physics*, 85 , N°2, P.776-789 (1999).
- [10] HOHORST, J. K., *SCDAP/RELAP5/MOD3 code Manual Volume 4: MATPRO – A Library of Materials Properties for Light Water Reactor Accident Analysis*, EG&G Idaho Report NUREG/CR 5273 (1990).
- [11] INTERNATIONAL ATOMIC ENERGY AGENCY, Thermophysical Properties of Materials for Water Cooled Reactors, IAEA-TECDOC-949, Vienna (1997).
- [12] NELSON, S.A., CARMICHAEL, I.S.E., Partial molar volume of oxide components in silicate liquid, *Contrib. Mineral. Petr.*, 71, 117-124 (1979).
- [13] KAMIGAITO, O., Density of compound oxides, *J Ceram Soc Jap.*, 108, 944-947 (2000).
- [14] HARMATHY, T.Z., Thermal properties of concrete at elevated temperatures, *J. Mater.* 5 (1), 47-74. (1970).
- [15] HULL, F.C., Estimating alloy densities, *Metal Progress*, Nov. 1969, pp. 139-140 (1969).
- [16] CRAWLEY, A.F., Densities of liquid Metals and Alloys”, *Int. Metal. Rev.*, 19: 32-48 (1974).
- [17] DE BREMAECKER, A. et al., “European Nuclear Thermodynamic Database validated and applicable in Severe Accidents Codes”, *Proc. FISA-2003*, 460-465, European Commission, Luxembourg (2003).
- [18] GARDIE, P., Contribution à l’étude thermodynamique des alliages U-Fe et U-Ga par spectrométrie de masse à haute température, et de la mouillabilité de l’oxyde d’yttrium par l’uranium”, PhD Thesis, Institut National Polytechnique, Grenoble (1992).
- [19] FAYETTE, S., PILUSO, P., SMITH, D., Conductivité thermique des oxydes à moyennes et haute températures, *Congrès « MFHT-1 » session propriétés physiques*, Aix-en-Provence, France (2002). HYLAND, G.J., Thermal conductivity of solid UO<sub>2</sub> : critique and recommendation”, *J. of Nucl. Mat.*, 113, 125-135 (1983).
- [21] WEILBACHER, J.C., Mésures de la diffusivité thermique des oxydes mixtes d'uranium et de plutonium, influence de la stoechiométrie et de la teneur en plutonium, Thèse de doctorat es sciences Physiques (1972).
- [22] KILLEEN, J.C., Measurement of electron-to-hole mobility ratio in UO<sub>2</sub> and its effect on thermal conductivity, *J. of Nucl. Mat.*, 92, 136-140 (1980).
- [23] PILUSO, P., Corium physical properties”, *Eurocourse*, Aix-en-Provence, France (2003).
- [24] HARDING, J.H., MARTIN, D.G., A recommendation for the thermal conductivity of UO<sub>2</sub>”, *J. of Nucl. Mat.*, 166, 223-226 (1989).
- [25] SCOTT, R.W., *UKAEA Report AERE-m/R 252* (1958).
- [26] BRANDT, R.E., NEUER, G., Thermal conductivity and thermal radiation properties of UO<sub>2</sub>”, *J. Non-equilib. Thermodyn.* , 1, 3-23 (1976).

**Korea, Republic of**

KINS Inc., Information Business Dept. Samho Bldg. 2nd Floor, 275-1 Yang Jae-dong SeoCho-G, Seoul 137-130  
Telephone: +02 589 1740 • Fax: +02 589 1746  
Email: sj8142@kins.co.kr • Web site: <http://www.kins.co.kr>

**Netherlands**

De Lindeboom Internationale Publicaties B.V., M.A. de Ruyterstraat 20A, NL-7482 BZ Haaksbergen  
Telephone: +31 (0) 53 5740004 • Fax: +31 (0) 53 5729296  
Email: [books@delindeboom.com](mailto:books@delindeboom.com) • Web site: <http://www.delindeboom.com>

Martinus Nijhoff International, Koraalrood 50, P.O. Box 1853, 2700 CZ Zoetermeer  
Telephone: +31 793 684 400 • Fax: +31 793 615 698 • Email: [info@nijhoff.nl](mailto:info@nijhoff.nl) • Web site: <http://www.nijhoff.nl>

Swets and Zeitlinger b.v., P.O. Box 830, 2160 SZ Lisse  
Telephone: +31 252 435 111 • Fax: +31 252 415 888 • Email: [infoho@swets.nl](mailto:infoho@swets.nl) • Web site: <http://www.swets.nl>

**New Zealand**

DA Information Services, 648 Whitehorse Road, MITCHAM 3132, Australia  
Telephone: +61 3 9210 7777 • Fax: +61 3 9210 7788  
Email: [service@dadirect.com.au](mailto:service@dadirect.com.au) • Web site: <http://www.dadirect.com.au>

**Slovenia**

Cankarjeva Založba d.d., Kopitarjeva 2, SI-1512 Ljubljana  
Telephone: +386 1 432 31 44 • Fax: +386 1 230 14 35  
Email: [import.books@cankarjeva-z.si](mailto:import.books@cankarjeva-z.si) • Web site: <http://www.cankarjeva-z.si/uvvoz>

**Spain**

Díaz de Santos, S.A., c/ Juan Bravo, 3A, E-28006 Madrid  
Telephone: +34 91 781 94 80 • Fax: +34 91 575 55 63 • Email: [compras@diazdesantos.es](mailto:compras@diazdesantos.es)  
[carmela@diazdesantos.es](mailto:carmela@diazdesantos.es) • [barcelona@diazdesantos.es](mailto:barcelona@diazdesantos.es) • [julio@diazdesantos.es](mailto:julio@diazdesantos.es)  
Web site: <http://www.diazdesantos.es>

**United Kingdom**

The Stationery Office Ltd, International Sales Agency, PO Box 29, Norwich, NR3 1 GN  
Telephone (orders): +44 870 600 5552 • (enquiries): +44 207 873 8372 • Fax: +44 207 873 8203  
Email (orders): [book.orders@tso.co.uk](mailto:book.orders@tso.co.uk) • (enquiries): [book.enquiries@tso.co.uk](mailto:book.enquiries@tso.co.uk) • Web site: <http://www.tso.co.uk>

**On-line orders:**

DELTA Int. Book Wholesalers Ltd., 39 Alexandra Road, Addlestone, Surrey, KT15 2PQ  
Email: [info@profbooks.com](mailto:info@profbooks.com) • Web site: <http://www.profbooks.com>

**Books on the Environment:**

Earthprint Ltd., P.O. Box 119, Stevenage SG1 4TP  
Telephone: +44 1438748111 • Fax: +44 1438748844  
Email: [orders@earthprint.com](mailto:orders@earthprint.com) • Web site: <http://www.earthprint.com>

**United Nations (UN)**

Dept. I004, Room DC2-0853, First Avenue at 46th Street, New York, N.Y. 10017, USA  
Telephone: +800 253-9646 or +212 963-8302 • Fax: +212 963-3489  
Email: [publications@un.org](mailto:publications@un.org) • Web site: <http://www.un.org>

**United States of America**

Bernan Associates, 4611-F Assembly Drive, Lanham, MD 20706-4391  
Telephone: 1-800-865-3457 • Fax: 1-800-865-3450  
Email: [order@bernan.com](mailto:order@bernan.com) • Web site: <http://www.bernan.com>

Renouf Publishing Company Ltd., 812 Proctor Ave., Ogdensburg, NY, 13669  
Telephone: +888 551 7470 (toll-free) • Fax: +888 568 8546 (toll-free)  
Email: [order.dept@renoufbooks.com](mailto:order.dept@renoufbooks.com) • Web site: <http://www.renoufbooks.com>

**Orders and requests for information** may also be addressed directly to:

**Sales and Promotion Unit, International Atomic Energy Agency**

Wagramer Strasse 5, P.O. Box 100, A-1400 Vienna, Austria  
Telephone: +43 1 2600 22529 (or 22530) • Fax: +43 1 2600 29302  
Email: [sales.publications@iaea.org](mailto:sales.publications@iaea.org) • Web site: <http://www.iaea.org/books>

## **9. THERPRO: ON-LINE NUCLEAR MATERIALS THERMO-PHYSICAL PROPERTIES DATABASE**

### **9.1. Introduction to THERPRO database**

Materials property data are an essential part of major disciplines in many engineering fields. In the field of nuclear engineering, fundamental understanding of thermo-physical-chemical-mechanical properties of nuclear materials is very important. For example, evaluation of nuclear reactor performance under normal operation or accident conditions is very critical in the design and analysis of current and future reactors. For such analyses, accurate and reliable data of materials properties under the relevant temperature, pressure and neutron irradiation conditions are necessary. Therefore collection and systematization of openly available thermo-physical properties data, as well as necessary new data measurements, have been conducted within IAEA's Coordinated Research Project on "Establishment of a Thermo-physical Properties Database of LWRs and HWRs".

Thanks to the great efforts of IKE (Institut für Kernenergie und Energiessysteme, University of Stuttgart, Germany), THERSYST, a thermo-physical properties database for solid materials was developed and internationally acknowledged as an outstanding database. Unfortunately, however, it has been inactively utilized due to several reasons. Thus acquisition and conversion of the DOS-based THERSYST database into a web-based database has been carried out as a part of the IAEA's third Coordinated Research Project. This work initially concentrated on the analysis of the database structure and means for the revitalization of the old database. Later, the database was redesigned and reconstructed into a modern web-based database using the contemporary information technologies. The name "THERPRO" was given to this new web-based database by the participants of IAEA's CRP. The conversion of the THERSYS database to the THERPRO database was carried out by the Nuclear Materials Lab., Hanyang University, Seoul, Republic of Korea under the supervision of the IAEA and the financial support of MOST (Ministry of Science and Technology) of Korean government.

The THERPRO database is an on-line database (<http://www.iaea.org/THERPRO>), providing various materials properties data to the registered/authorized users in the IAEA Member States. To date more than 13,000 thermo-physical properties data sets of more than 1,300 materials have been collected and compiled in THERPRO. Latest data published in the relevant technical journals are being collected and included.

THERPRO database is owned by IAEA and managed by the Agency's Designated Center for Nuclear Materials Properties Database Management located at Hanyang university, Seoul, Republic of Korea. Whereas data review and assessment for the update and the upgrade of THERPRO will be performed through IAEA activities, the registered users of the on-line database will be controlled by the Agency and served by the designated center under the supervision of Agency.

### **9.2. Structure of THERPRO database**

#### **9.2.1. Overall structure of database**

THERPRO home page (FIG. 1) provides the access to the main body of database for the registered/authorized users.



**IAEA THERPRO**  
Thermo-Physical Materials Properties Database

[Home](#) | [Index](#) | [Link](#) | [Registration](#) | [ContactUs](#) | [Bulletin](#) | [Help](#) | [Workgroup](#)



**IAEA Designated Center for Nuclear Materials Properties Database Management**

**Introduction to THERPRO Database**



Materials property data are an essential part of major disciplines in many engineering fields. To nuclear engineering, fundamental understanding of thermo-physical-chemical-mechanical properties of nuclear materials is very important. For example, evaluation of nuclear reactor performance under normal operation or accident conditions using accurate and reliable properties data is very critical in the design and analysis of current and future reactors. For such analyses, accurate data are necessary for materials properties under the relevant temperature, pressure and neutron irradiation conditions. Collection and systematization of, openly available thermo-physical properties data as well as necessary new data measurements have been conducted within IAEA's Coordinated Research Project on "Establishment of a Thermo-physical properties Database of LWRs and HWRs". ... [\(more\)](#)

**History of THERPRO Database**

THERSYST was originally developed for the modular reactor localization program RSYST as a combination of a factual solid materials thermo-physical properties database and a modular program system to handle the data base contents. Practically thermo-physical properties of solid materials are very sensitive to the manufacturing process of the materials as well as the experimental conditions of the measurements. They depend not only on their chemical composition but also on their micro- and macrostructure resulting from the subsequent treatment: mechanical, chemical, thermal, or irradiative. This means that thermo-physical properties data should be described by not only the measurement values but also supporting information such as material characterization and experimental techniques. Particularly for engineering materials, the situation is more complicated because they rarely have unique compositions and their properties are drastically affected by the materials production process. Due to the sensitivity and the complexity of the properties database, THERSYST was designed to be operated on the mainframe computer (VAX). Later it was transformed into a stand-alone PC-based database since personal computers became popular and widely available. ... [\(more\)](#)



**News**

- Welcome to THERPRO !!!
- THERPRO Homepage Update [NEW](#)
- New Data Added [NEW](#)
- DB Center Open [NEW](#)

**Bulletin**

- Welcome to THERPRO !!!
- THERPRO Homepage Update [NEW](#)
- New Data Added [NEW](#)
- DB Center Open [NEW](#)

**Announcement**

- Welcome to THERPRO !!!
- THERPRO Homepage Update [NEW](#)
- New Data Added [NEW](#)
- DB Center Open [NEW](#)


**MINISTRY OF SCIENCE & TECHNOLOGY**


**HANYANG UNIVERSITY**

FIG. 1. THERPRO database home page.

Once the access is approved, the registered user will be led to the entry level consisting of periodic table for easy access to target data set and supplementary features for convenient data retrieval.

THERPRO has a hierarchical structure consisting of several levels: home page, entry, element, compound, property, author, report, and bibliography level. All of the data sets in each level are interconnected using a network structure and thus every data can be easily retrieved including the bibliographical information by an appropriate query action. The internal structure is shown in Figure 2.

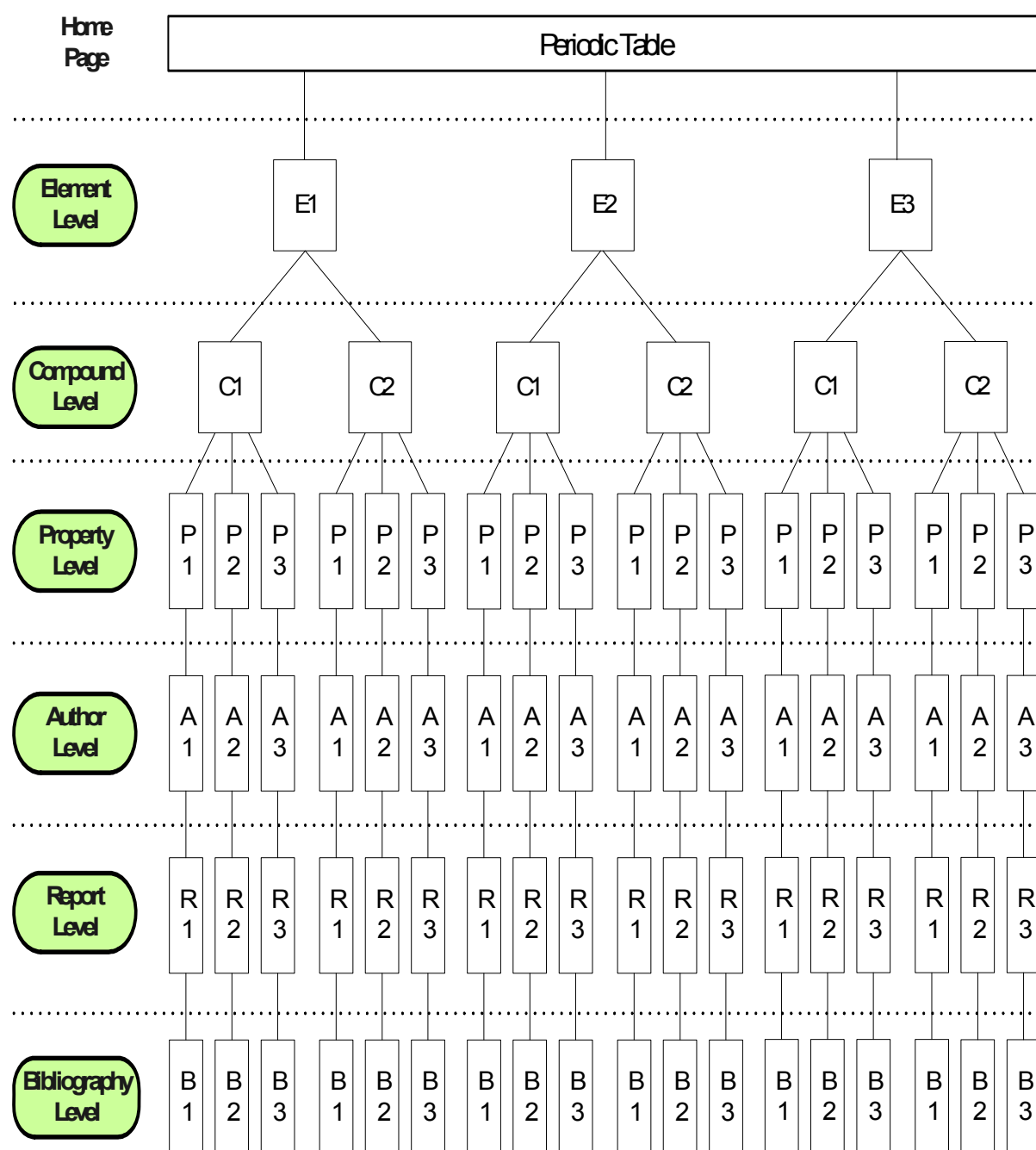


FIG. 2. Overall structure of THERPRO database.

Element level is the actual first level in the search of the target properties of the materials. In order to begin the search, the user has to click the symbol of the major element of the compound in the periodic table (Figure. 4) in the entry level. The user will be then taken to the element level, where all of the compounds of the element collected in THERPRO, are listed along with the general properties of the element. If the user makes a selection of the target compound using the “index search” in the THERPRO home page, it will guide the user directly to the compound level. There the user will find the list of thermo-physical properties of the compound.

The next level is the property level. This level belongs to the database platform in which collected properties data are sorted, classified, and stored. All of the properties data and information in this platform are linked to the corresponding compounds in the compound level.

Three levels, author, report, and bibliography level, constitute the platform; thus they are constructed in the common layer. When the user reaches the property level or the platform, he/she selects author

and then the authors' report from the document list right next to the author list. Within this platform the user can choose multiple authors and multiple reports. Once user selects the report, he/she can request to plot the retrieved data in a graphic form.

Bibliography level is the lowest level in the database structure. If the user wants the bibliographic information on the retrieved data, he/she can see the information including the numeric property data by clicking the report ID number in the screen. Since this information has been saved in a text file user can copy and paste it in his/her own document.

### **9.2.2. Structure of standard data set**

In order to keep the consistency of the collected information on the solid materials properties and to ease the comparison and the interpretation of the data, a standard data set has been developed for THERPRO database.

The standard format consists of five classes: material characterization, data characterization, measurement technique, bibliography, and numerical data. All of the data sets with this standard category scheme are sorted according to the materials name and/or chemical formula and then hierarchically ordered in the corresponding structural level of the database except the bibliography level. The user can trace back to the bibliographic information how the data were generated. Table 1 shows an example of the standard data set: thermal conductivity of  $\text{UO}_2$  reported by Lucuta P.G., Matzke H.J., and Verrall R.A. in Journal of Nuclear Materials (1995).

#### **Material Characterization**

=====

Material name: uranium dioxide                      Chemical formula:  $\text{UO}_2$   
Chemical composition [mole(s)]:  
                     $\text{UO}_2$  1.0000 (O/U ratio 2.0000 oxygen/metal ratio)  
Physical state: solid  
Material preparation: sintered  
                    temperature 1700.00 C                      atmosphere - 4% $\text{H}_2$ +Ar  
Molecular mass: 270.0 g  
Bulk density: 10.776 g/cm<sup>3</sup>

#### **Data Characterization**

=====

Classification: calculated from other measured properties  
Remarks: calculated from thermal diffusivity (E5002462) and specific heat capacity (E5002461)

#### **Measurement Technique**

=====

Property measurement method: DSC- technique  
Sample dimension: disc with dia = 6mm, l = 2-3mm

#### **Bibliography**

=====

Author: Lucuta P.G., Matzke H.J., Verrall R.A.  
Institution: AECL Chalk River Laboratories, Chalk River, Ontario, Canada  
Title: Thermal conductivity of hyper-stoichiometric SIMFUEL.  
Source: J. Nucl. Mater. 223 (1995) 51-60  
Year of publication: 1995  
Language: English

### Numerical Data

=====

Temp.[K]	Thermal Property [W/cm K]
2.9615E+02	8.5550E-02
3.7315E+02	8.1530E-02
4.7315E+02	7.2290E-02
5.7315E+02	6.3970E-02
6.7315E+02	5.7410E-02
7.7315E+02	5.1420E-02
8.7315E+02	4.7030E-02
9.7315E+02	4.2750E-02
1.0732E+03	3.9050E-02
1.1732E+03	3.5630E-02
1.2732E+03	3.2970E-02
1.4732E+03	2.8490E-02
1.6732E+03	2.5490E-02
1.7732E+03	2.3890E-02

Table 1. An example of the standard data set in THERPRO database

#### 9.2.3. *Data retrieval schemes*

THERPRO database provides three data searching schemes: hierarchical search, index search, and direct search. Hierarchical search is the basic and primary searching method. Two additional search methods were developed for more convenient and powerful data retrieval. Figure. 3 shows the sequential flows of the search scheme in the structural diagram.

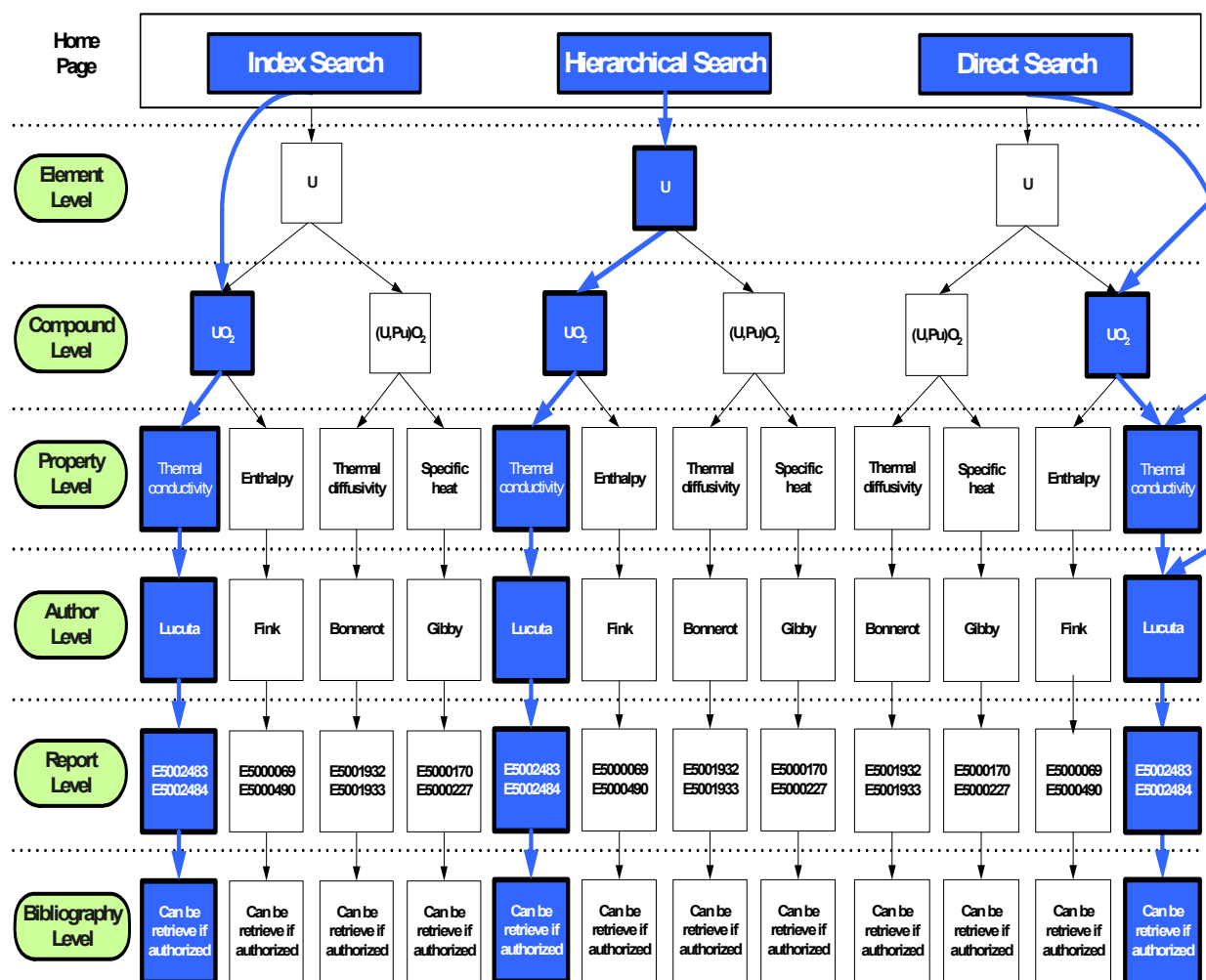


FIG. 3. Data retrieval schemes of THEKPRO database.

#### 9.2.3.1. Hierarchical search

Once registered user has visited the entry level, he/she is ready to begin the “hierarchical search” since the periodic table in this level is actually the entry gate for the data search. Selection and click of the major element of the target compound in the periodic table leads him/her to element level. The user then selects the compound of interest from the compound list. A scroll bar will guide the user to the compound level with the properties list. When the user selects a property in the list, he/she will be led to the properties database platform consisting of the three levels: author, report, and bibliography level. The user then selects the author and the report and can request to have the data plotted.

#### 9.2.3.2. Index search

THERPRO home page offers many features for the convenient data retrieval and satisfactory user support. The index search is one of them. The user can use the index for the search. First the user will find the “Index” button in the upper right corner of the home page. Clicking the index button will show three indices: symbol, compound, and author. When the user selects the symbol index, he/she



will find the list of compounds expressed in chemical formulas. If the user selects the compound index, he/she will see the list of compounds written in generic names. Clicking the compound of the user's interest in the index will lead him/her directly to the compound level. From this level on the user just follows the same procedure as described in the hierarchical search until he/she gets the information that he/she wants. Currently the author index search scheme is not available.

### 9.2.3.3. Direct search

A direct search scheme is provided for the power users who are familiar with THERPRO data base. The user will find boxes for compound name and property input in the top section of the entry level. The user can type the compound name of interest directly there and select the property of interest in the right next box. Then it will guide the user directly to the property level. From this level on the user just follows the same procedure as described in the hierarchical search until he/she gets the information that he/she wants. Currently the author index search scheme is not available.

**IAEA THERPRO**  
Thermo-Physical Materials Properties Database

Home | Index | Link | Registration | Contact Us | Bulletin | Help | Workgroup

Login ID: \_\_\_\_\_ Password: \_\_\_\_\_ Login NEW

Compound: \_\_\_\_\_ Property: --SELECT-- Author: --SELECT-- Year of pub.: \_\_\_\_\_ Search

**Periodic Table of the Elements**

Legend:  
 A: Solid   A: Gas   A: Liquid   A: Synthetic  
 : Alkali metals   : Alkali earth metals   : Transition metals   : Rare earth metals   : Other metals   : Nonmetals  
 : Halogens   : Noble gases

FIG. 4. Periodic Table of the Elements on THERPRO.

### 9.2.4. User registration/authorization and database security

Since THERPRO database has been developed as a common utility for engineers, researchers, and managers working in the nuclear laboratories and industries in all member states, this on-line database will be basically available to anyone of them once user registers. Nevertheless, the access to the source data files must be limited for the database protection and security. In practice, THERPRO offers three user groups category: group 1, group 2, and administrative group. This user group assignment will be made by the IAEA. Any user in any group is entitled to make suggestions and comments on the database and data modification/correction.

Group 1 user can visit any part of the THERPRO database except the bibliographical information on the retrieved data. Anyone can be this group user when he or she accepts the security notice, privacy policy, copyrights, and terms and conditions effectively required by IAEA, fill out the on-line registration form, and submit it. As stated in terms and conditions, IAEA has the right to cancel the user's registration for the future use if the user provides any fake information during the registration process.

Group 2 user is an authorized user who has the right to access any available source file or information including the bibliographical information. However, this group user has no rights to modify or correct the data. Group 1 user can apply for group 2 authorization. The application for the upgrade will be reviewed by IAEA.

Administrative group users are the users who have rights to modify or correct the data. Only a small number of people such as staffs in IAEA headquarter and staffs in the THERPRO management center will fall in this user group.

#### **9.2.5. *THERPRO database management: data update and upgrade***

The Nuclear Materials Lab. at Hanyang university, Seoul, Korea takes care of the routine maintenance of THERPRO database and the support required for the coordinated user and work group activities and registered users needs.

The database at the Hanyang University center will be managed by the staff at the center under the supervision of the IAEA, while new data collection/review/assessment for the update and upgrade of the database is carried out by the IAEA's work group or committee members. For coordinating the work on data collection, review, and assessment of the working group members an on-line communication tool is provided in the THERPRO homepage.



## CONTRIBUTORS TO DRAFTING AND REVIEW

Cognet, G.	Commissariat à l'énergie atomique (CEA), Cadarache, France
Efanov, A.	Institute of Physics and Power Engineering, Russian Federation
Fortov, V.	High Energy Density Research Centre, Institute for High Temperatures, Russian Federation
Fink, J.K.	Argonne National Laboratory, United States of America
Froment, K.	Commissariat à l'énergie atomique (CEA)/Grenoble, France
Gromov, G.	Ministry for Environmental Protection and Nuclear Safety, Ukraine
Hwang, I.S.	Seoul National University, Republic of Korea
Jaroma-Weiland, G.	Universität Stuttgart, Germany
Jeong, K.J.	Seoul National University, Republic of Korea
Jiang, Y.	Nuclear Power Institute of China, China
Kim, Y.S.	Hanyang University, Republic of Korea
Mares, R.	University of West Bohemia in Plzen, Czech Republic
Mathew, P.M.	AECL Whiteshell Laboratories, Canada
Petoukhov, V.	Institute for High Energy Densities, Russian Federation
Piluso, P.	CEA Cadarache, France
Sengupta, A.K.	Bhabha Atomic Research Centre, India
Venugopal, V.	Bhabha Atomic Research Centre, India
Vinogradov, V.	Institute of Physics and Power Engineering, Russian Federation